99

Structure & Bonding

VOLUME EDITOR: J.-P. SAUVAGE

Molecular Machines and Motors

Springer

99
Structure and Bonding

Springer
Berlin
Heidelberg
New York
Barcelona
Hong Kong
London
Milan
Paris
Singapore
Tokyo

Molecular Machines and Motors

Volume Editor: J.-P. Sauvage

With contributions by
V. Amendola, R. Ballardini, V. Balzani, A. Credi,
L. Fabbrizzi, M.T. Gandolfi, J.K. Gimzewski,
M. Gómez-Kaifer, C. Joachim, A.E. Kaifer, E. Katz,
T.R. Kelly, J. Liu, C. Mangano, P. Pallavicini,
A.R. Pease, L. Raehm, M. Sano, J.-P. Sauvage,
J.P. Sestelo, A.N. Shipway, J.-F. Stoddart,
M. Venturi, I. Willner

Springer

The series *Structure and Bonding* publishes critical reviews on topics of research concerned with chemical structure and bonding. The scope of the series spans the entire Periodic Table. It focuses attention on new and developing areas of modern structural and theoretical chemistry such as nanostructures, molecular electronics, designed molecular solids, surfaces, metal clusters and supramolecular structures. Physical and spectroscopic techniques used to determine, examine and model structures fall within the purview of Structure and Bonding to the extent that the focus is on the scientific results obtained and not on specialist information concerning the techniques themselves. Issues associated with the development of bonding models and generalizations that illuminate the reactivity pathways and rates of chemical processes are also relevant.

As a rule, contributions are specially commissioned. The editors and publishers will, however, always be pleased to receive suggestions and supplementary information. Papers are accepted for *Structure and Bonding* in English.

In references *Structure and Bonding* is abbreviated *Struct Bond* and is cited as a journal.

Springer WWW home page: http://www.springer.de

ISSN 0081-5993
ISBN 3-540-41382-0
Springer-Verlag Berlin Heidelberg New York

CIP Data applied for

Springer-Verlag Berlin Heidelberg New York a member of BertelsmannSpringer Science + Business Media GmbH
http://www.springer.de

Printed in Germany

Typesetting: Scientific Publishing Services (P) Ltd, Madras
Production editor: Christiane Messerschmidt, Rheinau
Cover: Medio V. Leins, Berlin
Printed on acid-free paper SPIN: 10702298 02/3020 - 5 4 3 2 1 0

Volume Editor

Professor Jean-Pierre Sauvage

Université Louis Pasteur
Faculté de Chimie
Laboratoire de Chimie Organo-Minérale
4, Rue Blaise Pascal
F-67070 Strasbourg Cedex, France
E-mail: sauvage@chimie.u-strasbg.fr

Editorial Board

Preface

The field of molecules in motion, for which movements and shape changes are triggered and controlled from outside, has been indisputably one of the most rapidly developing areas of the last decade.

Clearly, molecular chemists in general are able to elaborate more and more complex species, as beautifully demonstrated by the synthesis of amazingly complicated natural products. For instance, the total synthesis of compounds such as taxol and brevetoxin B represents a formidable tour de force, as does that of many other recent examples. However, most of the time, once the compound has been made, the target has been reached.

The synthesis of molecules for which given functions are to be expected and explored once sufficient amounts of the compounds are available, requires the interaction of several fields. The multidisciplinary aspect, involving various methodologies from synthesis to electro- and photochemistry, from surface science to spectroscopy and magnetic properties, allows the design and elaboration of molecular objects displaying new functions. Amongst the new functions that chemists want to introduce into their systems, motion is particularly important. In addition, a geometrical change will generally be accompanied by a modification of one or more properties (colour, luminescence, catalytic properties, etc...) which could be used as a testimony to the motion and also be of practical interest for future applications.

The machine-like molecular assemblies available today, in large part from the outstanding contributions of the groups whose work is collected in this volume, are nevertheless still primitive, sometimes slow to move and may also lack complete reversibility. However, new and important concepts have been proposed which introduce a new dimension to molecular sciences. For the future, an important step will be to transpose what has been performed on large collections of molecules in solution to ordered 2D- and 3D-arrays and single molecules on a surface.

The first three chapters of the present volume are focused on rotary motors. The first contribution discusses the possibility of elaborating single-molecule rotary machines, while the other two chapters deal with purely organic molecules or transition metal complexes in solution. Of particular note in the second chapter is the introduction by the authors of the important concept of directionality in rotary machines at the molecular level. Chapters 4 and 5 discuss recent examples of molecular systems in motion, based on transition

metal complexes. Two important notions are introduced: associating a light emission signal with a motion and performing molecular hysteresis by electrochemical reactions. In the sixth chapter, the authors use, in particular, rotaxanes to discuss in-depth practical problems which could be associated with single-molecule devices and possible ways circumventing them. Chapter 7 is related to molecular machines which are set into motion using a photoinduced redox process. The authors of this chapter made an important contribution to popularising the term "molecular machine" at an early stage. Chapter 8 describes some work done by the author's group in the field of logic gates. It also discusses recent literature reports in connection with futuristic "molecular computers". Finally, the ninth and last chapter is related to potential information storage and processing devices, either in solution or on surfaces. It will provide the reader with a detailed discussion of possible future applications.

Strasbourg, March 2001 Jean-Pierre Sauvage

Contents

Single Molecular Rotor at the Nanoscale
C. Joachim, J.K. Gimzewski 1

Rotary Motion in Single-Molecule Machines
T.R. Kelly, J.P. Sestelo 19

Molecular Machines and Motors Based on Transition Metal-Containing Catenanes and Rotaxanes
L. Raehm, J.-P. Sauvage 55

Molecular Movements and Translocations Controlled by Transition Metals and Signaled by Light Emission
V. Amendola, L. Fabbrizzi, C. Mangano, P. Pallavicini 79

Molecular Hysteresis by Linkage Isomerizations Induced by Electrochemical Processes
M. Sano 117

Switchable Molecular Devices: From Rotaxanes to Nanoparticles
J. Liu, M. Gómez-Kaifer, A.E. Kaifer 141

Molecular-Level Artificial Machines Based on Photoinduced Electron-Transfer Processes
R. Ballardini, V. Balzani, A. Credi, M.T. Gandolfi, M. Venturi 163

Computing at the Molecular Level
A.R. Pease, J.F. Stoddart 189

Molecular Memory and Processing Devices in Solution and on Surfaces
A.N. Shipway, E. Katz, I. Willner 237

Author Index Volumes 1–99 283

Contents of Volume 96

Molecular Self-Assembly Organic Versus Inorganic Approaches

Volume Editor: M. Fujita

Part I: Organic Assemblies

The Utilization of Persistent H-Bonding Motifs in the Self-Assembly of Supramolecular Architectures
M.J. Krische, J.-M. Lehn

Controlling Hydrogen Bonding: From Molecular Recognition to Organogelation
R.E. Meléndez, A.J. Carr, B.R. Linton, A.D. Hamilton

Heteroaromatic Modules for Self-Assembly Using Multiple Hydrogen Bonds
S.C. Zimmerman, P.S. Corbin

Hydrogen-Bonded Liquid Crystals: Molecular Self-Assembly for Dynamically Functional Materials
T. Kato

Part II: Inorganic Assemblies

Synergistic Effect of Serendipity and Rational Design in Supramolecular Chemistry
R.W. Saalfrank, E. Uller, B. Demleitner, I. Bernt

Molecular Paneling Through Metal-Directed Self-Assembly
M. Fujita

Pythagorean Harmony in the World of Metal $\{Mo_{11}\}$ Oxygen Clusters of the Type: Giant Wheels and Spheres both Based on a Pentagonal Type Unit
A. Müller, P. Kögerler, H. Bögge

Single Molecular Rotor at the Nanoscale

Christian Joachim[1], James Kazimiez Gimzewski[2]

[1] Centre d'Elaboration de Matériaux et d'Etudes Structurales-Centre National de la Recherche Scientifique (CEMES-CNRS), 29 rue J. Marvig, 31055 Toulouse Cedex, France
[2] IBM Research, Zurich Research Laboratory, 8803 Rüschlikon, Switzerland
E-mail: gim@zurich.ibm.com

The design of a monomolecular engine such as a rotating motor first requires the preparation of a semi-classical rotating motion of the rotor part of the engine. We show that this can be achieved either by a careful quantum control of the time evolution of an initially prepared rotating quantum wave packet or by controlling the interaction of the rotor (or stator) with a reservoir. This second alternative is illustrated experimentally through the realization of the rotary motion of a hexa-*tert*-butyl-decacyclene molecule self-assembled in an homomolecular cavity on an ultraclean Cu(100) surface. The conditions to transform such a molecular rotor into a motor with a given motive power are also discussed.

Keywords: Molecular rotor, Motive power, Decoherence, Classical motion, Quantum control, Nano-thermodynamics

1 Introduction 2

2 The Rotation of a Nanoscale Material Object 3

3 The Motive Power of a Quantum-State Superposition 5

4 Decoherence and Classical Motion 8

5 Observation of the Semi-Classical Rotation of a Single Molecular Rotor 11

6 Towards Nano-Thermodynamics 15

7 Conclusion 16

8 References 17

List of Abbreviations

STM	scanning tunneling microscope
ESQC	elastic scattering quantum chemistry
AFM	atomic force microscope
HBDC	hexa-*tert*-butyl-decacyclene molecule
UHV	ultrahigh vacuum

Structure and Bonding, Vol. 99

1 Introduction

Machines essentially are arrays of functional components that transform energy (or information) and use this transformation. Their miniaturization is often required for convenience and performance, for example, to build computing machines or large memories by assembling or integrating molecules at the nanoscale [1]. Here, we are interested by the ultimate limits of miniaturization of another type of machine: mechanical machines able to create motion, produce work, pump heat, or perform other useful functions. To generate motion, a machine has to consist of moving parts and requires a least one source of energy. In macroscopic machines whose components are typically much larger than 100 microns, the motion of the parts is governed by classical mechanics [2]. Rotors and motors down to a few microns can also be integrated on a silicon wafer [3]. These micro-machines are simply scaled-down versions of machines in our daily life, using the same working principles such as, for instance, a steam engine. Even smaller are biological motors, which do not function directly along the lines of established engineering concepts or even perhaps human intuition [4]. They are supramolecular assemblies of proteins capable of maintaining a linear or rotating motion when fueled by a chemical reaction [5, 6]. These "meso"-machines have dimensions on the scale of a few tens of nanometers. Their working principle is still under debate but appears to depend on a subtle equilibrium between the noise spectrum of the excitation and the asymmetric potential profile of the moving parts relative to the static ones [7]. In layman's terms, biological machines maintain operation within an environment where fluctuations and vibrations exceed the actual motions of the machines and they may actually use or rectify such fluctuations as an operational principle. In such a supramolecular assembly there are so many degrees of freedom that the classical concept of diffusive motion still applies, and has indeed been observed [8]. Below these "evolution-selected" or "non-intuitive" machines are nanoscale devices made of several fairly small molecules [9]. Under such conditions, human expectation is to find definite molecular structures that are capable of transforming electrical, optical, or chemical forces into observable motion of a part of the molecule on a single-molecule basis. To follow this transformation, kinetic observations are generally performed in solution averaged over billions of molecules [10–12]. Therefore, what is mainly observed is the statistical occupation of what may be independent "stations" of moving parts but with no actual insight into the actual spatial motion between stations. While the working principle of micro- and meso-machines is to all extents and purposes resolved, a new horizon of nanotechnology is to learn about and realize the limits imposed by the laws of physics on the design of molecular rotors and motors on the nanometer scale [9].

As a model example of a nanoscale machine, we discuss here the physics of a single-molecular rotor capable of transforming surface thermal energy into random rotational fluctuations. A motor will result if this rotor is capable of permanently driving the motion of another rotor or the linear displacement of

a molecular rod. In Sect. 2, we discuss the concept of motion on the nanoscale recalling that classical motion such as a unidirectional rotation is unnatural for a molecular wheel. In Sect. 3, we describe how to use the motive power of a non-stationary-state superposition to create and control such a motion. The problem is that to use the energy of a rotational wave packet requires that the rotor be in interaction with at least one energy source. Among the various possibilities for a molecule to interact with such a source, we describe in Sect. 4 how coupling of the rotor with a thermal bath may restore semi-classical motion. The example of a 1.5-nm diameter molecular wheel whose rotation is stabilized by a supramolecular stator assembled on a surface is presented in Sect. 5. Here, the scanning tunneling microscope (STM) is able to follow molecular motion at the nanoscale as a time-averaged effect in the image. Sect. 6 deals with an extension of this approach to produce work using controlled motion.

2
The Rotation of a Nanoscale Material Object

The motion of a material object is governed by mechanics. Down to the micron scale, classical mechanics describes the relation between forces and motion. The movement of the mobile parts follows Newton's equations of motion, which determine the coordinates and speed of each part of the machine relative to a given origin. In contrast, on the nanoscale, only a correspondence between forces and quantum eigenstates of a nanomachine is available through the Schrödinger equation of motion. Therefore, the concept of movement is not as immediately intuitive as it is at the macroscopic scale [13].

To discuss this point, let us consider an isolated molecular rotor, Fig. 1. Relative to its center of mass and by freezing its translation along the X-X′

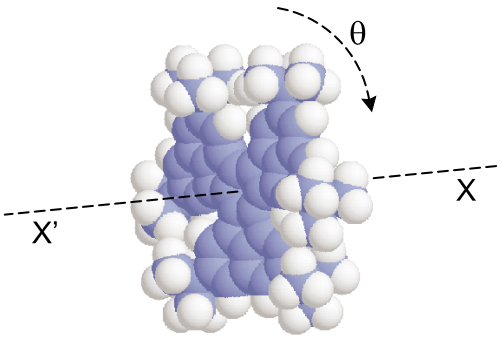

Fig. 1. Example of a hexa-*tert*-butyldecacyclene (HBDC) molecular rotor, which is supposed to rotate around the X-X′ axis. Isolated in the gas phase, the quantum state of this molecule can be prepared in a rotational wave packet to start the described rotation before quantum dilution of the wave packet

virtual rotation axis, the standard Schrödinger equation of this molecule prepared in any initial angular state $\chi(\theta, 0)$ is written as

$$-\frac{\hbar^2}{2I}\frac{\delta^2}{\delta\theta^2}\chi(\theta,t) + V(\theta)\chi(\theta,t) = i\hbar\frac{\delta}{\delta t}\chi(\theta,t), \tag{1}$$

where $V(\theta)$ is an external periodic potential energy profile determining the multiple equilibrium positions (hereafter called stations) of the molecule when the rotation is defined in reference to the X-X′ axis, and I is the inertia momentum of the rotor.

For this molecule to be a rotor, its atoms must turn around the X-X′ axis in real space starting from one of the $V(\theta)$ stations and reaching all the other stations in always the same sequential time order. Therefore, the time-dependent average value $\langle\theta(t)\rangle = \langle\chi(\theta,t)|\Theta|\chi(\theta,t)\rangle$ of the quantum angular momentum Θ must satisfy the classical equation of motion:

$$I\frac{\mathrm{d}^2}{\mathrm{d}t^2}\langle\theta(t)\rangle = -\frac{\mathrm{d}V(\langle(\theta,t)\rangle)}{\mathrm{d}\langle(\theta,t)\rangle}. \tag{2}$$

If this equation is satisfied, a unidirectional rotation occurs when the kinetic energy of the rotor is greater than $\max_\theta V(\theta)$. A given atom of the molecule shown in Fig. 1 will follow an $x(t) = \mathrm{d}\cos\langle\theta(t)\rangle$ and $y(t) = \mathrm{d}\sin\langle\theta(t)\rangle$ motion in a Cartesian frame.

Unfortunately, $\langle\theta(t)\rangle$ is not a solution of Eq. (2) but satisfies the time-dependent equation

$$I\frac{\mathrm{d}^2\langle\theta(t)\rangle}{\mathrm{d}t^2} = -\left\langle\chi(\theta,t)\left|\frac{\mathrm{d}V(\theta)}{\mathrm{d}\theta}\right|\chi(\theta,t)\right\rangle \tag{3}$$

obtained exactly using the Ehrenfest theorem [14]. The transformation of Eq. (3) into Eq. (2) would require the permutation of the summation and derivative in Eq. (3), which is not possible for an equation describing the quantum dynamics of a single molecule. The intuitive relation between the initial preparation of motion and the real ($x(t)$, $y(t)$) movement of the rotor deduced from Eq. (2) is lost on the nanoscale based a single-molecule basis. For example, when the molecule is prepared a $t = 0$ in one of its $\chi_n(\theta)$ rotor eigenstates, there will be no average ($x(t)$, $y(t)$) motion because in this case $\mathrm{d}/\mathrm{d}t\langle\theta(t)\rangle = 0$ even for an eigenstate whose eigenvalue $E_n > \max_\theta V(\theta)$. This introduces a new problem compared to classical machines. This implies that, before controlling the internal dynamics of a molecular engine and using it to produce work, the mobile parts of this engine have to be prepared in a classical sense.

Note that with a large population of N molecules of the type shown in Fig. 1 a reasonable assumption is often that the average angle $\theta(t) = 1/N\sum_k\langle\theta_k(t)\rangle$ sequentially explores the correct order of motion through the $V(\theta)$ stations. In this case, the motion of each molecule taken individually in the ensemble will be the appropriate solution of Eq. (2). This is also the starting hypothesis of molecular mechanics and molecular dynamics calculations, assuming that an equivalence class of molecules represents an individual molecule [15]. This

assumption simplifies the design procedure for a molecular rotor. The potential function $V(\theta)$ can be calculated for a variety of molecules until one with the appropriate $V(\theta)$ profile has been found. Experimentally, the kinetics of the molecular assembly is followed by measuring the statistical occupation in time of each $V(\theta)$ station when their rotation is driven by an external excitation [10, 11, 16]. Nevertheless, this does not imply that each molecule in the ensemble follows exactly the sequence in time observed over the ensemble nor that the motion of each molecule between two stations is a classical rotation following Eq. (2).

To construct, on a single-molecule basis, an $(x(t), y(t))$ motion of rotation in the classical sense, the only solution is to find a superposition of $\chi_n(\theta)$ rotor eigenstates for $\langle\theta(t)\rangle$, which is almost a solution of Eq. (2) in the time interval of interest. Furthermore, $\langle\theta(t)\rangle$ cannot be an exact solution of Eq. (2) for all times. This is again a manifestation that a classical motion such as a unidirectional rotation is not a natural movement for an isolated quantum object. Only a simple quantum harmonic oscillator is able to perform classical motion when correctly prepared [17].

A standard way to mix the $\chi_n(\theta)$ eigenstates is to let the rotor (its axis or its stator) interact with at least one source of energy. There are several possible choices for these sources and interactions. As presented in the next section, the rotor can initially be in interaction with an electromagnetic field to prepare an initial $\chi(\theta, 0)$ wave packet, pumping at $t = 0$ many $\chi_n(\theta)$ states starting from the $\chi_0(\theta)$ ground state. In this case, the rotor will be free to rotate unidirectionally with respect to this initial preparation for a short period of time before dilution of the wave packet occurs. The interaction with the field can be maintained for the duration of motion to control the dilution of the packet. This will ensure that the trajectory of the rotor in its quantum state space does not deviate from the required one. Finally, the rotor (its axis or its stator) can be maintained permanently in interaction with at least one reservoir at a given temperature T. The role of the reservoir is twofold. First, the mixing of the $\chi_n(\theta)$ states with the continuum states of the reservoir attenuates the quantum character of the molecular rotor as shown in Sect. 4. Second, this mixing provides the energy for rotation. The reservoir may be the surface of a solid as described experimentally in Sect. 5. However, the reservoir may also be intrinsic to the molecule itself. In this case, the use of an intramolecular vibrational manifold located for example in the stator would serve as reservoir. With the introduction of the reservoir to mix the $\chi_n(\theta)$ quantum states, we now face the consequences of the second law of thermodynamics, which classically requires that there be at least two reservoirs for the rotor to produce useful work. This is discussed in Sect. 6.

3 The Motive Power of a Quantum-State Superposition

Let us consider the preparation of an isolated quantum system in a non-stationary state where a wave packet initiates a permanent quantum motion (a coherent process) in this system. This situation is similar to, for example, the

simple case of oscillatory energy exchange in a two-site quantum system studied first by Heisenberg [18]. The motive power of this system will be measured by the efficiency of this motion in producing work (or information in the case of a computing nanomachine [19]). A cycle of preparation has to be introduced to compensate for the energy lost by the progressive relaxation of the system to its ground state (a decoherence process). As already noted by Carnot [20], the motive power of any engine can be estimated by its ability to lift a weight. Before addressing this point in Sect. 6, we have to discuss how to put a molecule into a classical motion and how to control this motion.

For this purpose, let us now consider the molecular wheel presented in Fig. 1, chemically bound to a "string" holding a nanoscale object of mass m (Fig. 2). The string of length l_0, $l_0 > 2\pi d$ could be realized using a conjugate polymer and we can let the nanoobject be a metallic cluster. Eq. (1) can be considered as a simplified state equation describing this system by supposing that the molecular string is capable of complex intramolecular motions to

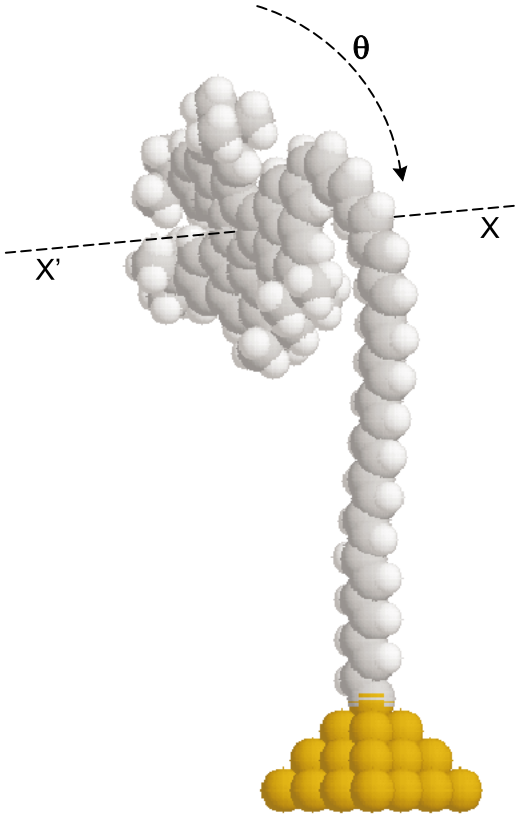

Fig. 2. Example of an HBDC molecular rotor chemically bound to a polyene chain holding a metal cluster. As in Fig. 1, X-X′ is the rotation axis. This molecule must be prepared in a quasi-classical state to ensure lifting of the cluster load using the polymer chain as a string

follow the movement of the rotor. In this case, $V(\theta) = m \cdot g \cdot d \cdot \cos(\theta)$, and the initial preparation of the rotor in any of its $\chi_n(\theta)$ eigenstates will not lead to a classical lifting of the cluster as already discussed in Sect. 2.

To obtain a classical lift of the weight, the system has to be prepared in a $\chi(\theta, 0)$ non-stationary state. For $\chi(\theta, 0)$ to drive classical rotation, the $C_n(0)$ complex-valued coefficients and the $\chi_n(\theta)$ eigenstates selected to form the $\chi(\theta, 0) = \sum_n C_n(0)\chi_n(\theta)$ initial wave packet have to make Eq. (3) almost equivalent to Eq. (2) on the time scale required for motion. Starting the cluster in a down position at $\theta = -\pi/2$, its motion is expected to follow an $l(t) = l_0 + 2\pi d \cos(\omega t)$ trajectory. This is an oscillatory motion in the same spirit as the original Heisenberg exchange studies. The process can be stopped by making all the $\chi_n(\theta)$ excited states of the rotor relax towards $\chi_0(\theta)$ on a time scale much greater than $2\pi/\omega$. The motive power of $\chi(\theta, 0)$ is determined by our ability to find a set of $C_n(0)$ complex-valued numbers in such that

$$\langle \chi(\theta, t) | \cos\theta | \chi(\theta, t) \rangle = \cos \omega t, \tag{4}$$

$$\langle \chi(\theta, t) | \sin\theta | \chi(\theta, t) \rangle = \sin \omega t, \tag{5}$$

with ω defined as

$$\omega = \left\langle \chi(\theta, t) \middle| \dot{\theta} \middle| \chi(\theta, t) \right\rangle. \tag{6}$$

If such a set $C_n(0)$ exists, the expectation value of the position operators X and Y of the rotor atoms where the molecular string is attached will follow an $\langle X(H) = d \cos \omega t \rangle$ and $\langle Y(H) = d \sin \omega t \rangle$ classical time dependence of a lift-up motion during half of the period. During this motion, the energy $E = 1/2 I\omega^2 + \langle V(\theta) \rangle$ of the system remains constant and equal to the initial preparation energy of the rotor. The available energy to drive up and down the motion of the cluster is $\Delta E = |E - E_0|$, where E_0 is the ground-state rotation energy of the system in Fig. 1b. Therefore, to be able to lift the mass, the wave-packet preparation of this system must be such that $\Delta E > 2\pi d \cdot m \cdot g$. The experimental preparation of the wave packet can result from the interaction of the rotor with a external microwave source. The profile of the microwave pulse will determine the amplitude and phase of $C_n(0)$ together with the dipolar moment of each $\chi_0(\theta) \rightarrow \chi_n(\theta)$ transition.

Unfortunately, it is not possible to find a set of $C_n(0)$ to solve simultaneously Eqs. (4), (5) and (6), with the total classical energy expression $E = (1/2) I\omega^2 + V(\langle\theta\rangle)$. As a consequence, the wave packet $\chi(\theta, t)$ will spread out owing to a progressive dephasing in time of the $C_n(t)$, resulting from the fact that the rotor eigenvalues are not equally spaced in energy. This introduces non-commensurable frequency components in the time evolution of the rotor [16, 20].

This inability to initiate rotational motion and to lift a weight by preparing a well-tailored wave packet associating all the system eigenstates confirms that such a classical motion is not very natural for quantum systems. The energy ΔE provided by the initial non-stationary superposition of the rotor states is not fully available to be directed into motion. Without control of the time

evolution of the wave packet, there is a spontaneous dilution of the energy on many of the $\chi_n(\theta)$ eigenstates, which would have to remain mainly inactive for the motion to become a classical rotation.

This analysis indicates that the motive power of a non-stationary-state superposition alone is very weak because it cannot generate a controlled motion even for $m = 0$. For a classical machine, the motive power is truly a measure of its ability to produce work, whereas, for a quantum machine, the motive power is firstly characteristic of its motion because a quantum system cannot be separated into parts. For example, the energy spectra of the molecules in Figs. 1 and 2 are totally different. Therefore, one solution to keep the initial wave packet in shape is to complement its preparation by a time-dependent control of dephasing each of its $C_n(t)$ during the time evolution period. This $C_n(t)$ phase control is only possible using a permanent interaction of the rotor with the driving microwave source as was recently proposed using well-tailored pulses [21]. A periodic field is very appealing because, if introduced into Eq. (1) as a perturbation, it dresses the eigenstates of the system and the resulting quasi-energies are then equally spaced. In this case, a coherent state of rotation will remain forever [21, 22]. Terminating the field will rapidly induce a dilution of the wave packet and a destruction of classical motion. The rotor will relax to its ground state with the cluster positioned downwards. This return to equilibrium occurs at random without a precise trajectory in space. This solution of controlling the quantum dynamics of a wave packet may not be totally appropriate to our objective. The rotor (with its stator) – not the time-dependent shape of the field interacting with the rotor – must have a defined structure and the resultant ability to transform the energy into unidirectional rotation.

4
Decoherence and Classical Motion

We now bring the molecular rotor, Fig. 1, into interaction with a surface (Fig. 3). In this case, the $\chi_n(\theta)$ states of the rotor mix with the quantum states $g_p(R_1, \ldots, R_m)$ of the surface, which constitutes a reservoir maintained at a given temperature T. The wave function of the rotor and surface system is written as

$$\Psi(\theta, R_1, \ldots, R_m, t) = \sum_n \sum_{P_1,\ldots,P_m} A_{n,P_1,\ldots,P_m}(t)\chi_n(\theta)g_p(R_1, \ldots, R_m) \tag{7}$$

This expression indicates that the motion of the rotor can no longer be described by a simple quantum movement driven by the preparation of the rotor in a pure rotation state. Several authors have shown that the interaction of a quantum system with a reservoir destroys the phase coherence of any wave packet prepared to profit from more semi-classical-like behavior [23, 24]. To demonstrate this below, we use the Madelung polar decomposition [25] of the wave function, Eq. (7). For these purposes, the density matrix technique is usually preferred [26, 27], however, the alternate route practiced here has the advantage of direct extraction of the equations of motion of the rotor alone.

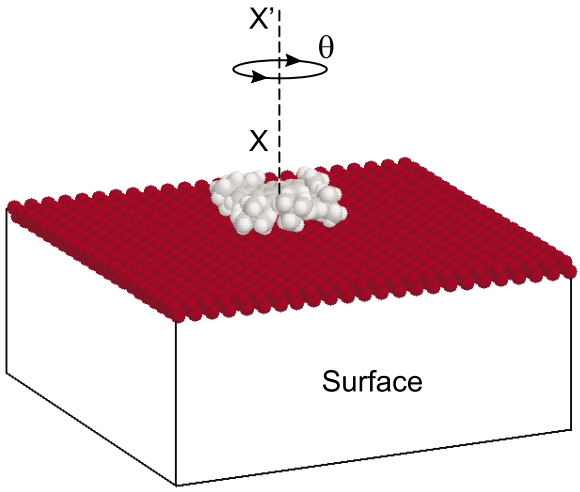

Fig. 3. Here the HBDC molecule is physisorbed on a metal surface to decrease the quantum character of its dynamic behavior. The molecular rotation axis is perpendicular to the surface. The surface temperature must be very low to freeze the lateral diffusion of the molecule on the surface

The wave function, Eq. (7), is a solution of the Schrödinger equation:

$$\left[-\frac{\hbar}{2I}\frac{\delta^2}{\delta\theta^2}-\sum_k\frac{-\hbar^2}{2mk}\Delta_{R_k}+V(\theta,R_1,\ldots,R_m,t)\right]\Psi(\theta,R_1,\ldots,R_m,t) = i\hbar\frac{\delta}{\delta t}\Psi(\theta,R_1,\ldots,R_m,t) \tag{8}$$

Like any complex-valued function [25, 28], Eq. (7) can be decomposed into a modulus and an argument component:

$$\Psi(\theta,R_1,\ldots,R_m,t)=\phi(\theta,R_1,\ldots,R_m,t)\exp\frac{i}{\hbar}\Omega(\theta,R_1,\ldots,R_m,t) \tag{9}$$

with $\Omega(\theta,R_1,\ldots,R_m,t)$ the total quantified action of the rotor and surface system, and $\rho(\theta,R_1,\ldots,R_m,t)=\phi(\theta,R_1,\ldots,R_m,t)^2$ the probability density of the system defined in configuration space with $\int\rho(\theta,R_1,\ldots,R_m,t)\mathrm{d}\theta\mathrm{d}\tau_1,\ldots,\mathrm{d}\tau_n=1$. By substituting Eq. (7) by Eq. (9) in Eq. (8), one obtains the standard probability conservation equation [27]:

$$\frac{\delta}{\delta t}\rho+Div(J)=0 \tag{10}$$

and a set of dynamic equations [27]:

$$I\frac{\delta}{\delta t}\nabla_\theta\Omega(\theta,R_1,\ldots,R_m,t)=-\nabla_\theta\left(\frac{\varepsilon}{\rho}\right), \tag{11}$$

$$m_k\frac{\delta}{\delta t}\nabla_k\Omega(\theta,R_1,\ldots,R_m,t)=-\nabla_k\left(\frac{\varepsilon}{\rho}\right)\Big|_{k=1,\ldots,m}, \tag{12}$$

where $J(\theta, R_1, \ldots, R_m, t) = \mathrm{Grad}(\Omega(\theta, R_1, \ldots, R_m, t))$ is the current density vector on the space configuration and $\varepsilon(\theta, R_1, \ldots, R_m, t)$ is the energy density of the system [27]. As Eq. (12) describes the reservoir, we focus on Eq. (11) and its transformation into a semi-classical equation of motion close to Eq. (3). For this purpose, Eq. (11) can be multiplied by $\rho(\theta, R_1, \ldots, R_m, t)$ and integrated over all space configurations. In this case, one obtains

$$I\frac{\delta\omega(t)}{\delta t} = -\int \nabla_\theta(\varepsilon)\,\mathrm{d}\theta\mathrm{d}\tau_1, \ldots, \mathrm{d}\tau_m - \int \frac{\varepsilon}{\rho}\nabla_\theta(\rho)\mathrm{d}\theta, \mathrm{d}\tau_1, \ldots, \mathrm{d}\tau_m \tag{13}$$

with $\omega(t)$ the average angular speed of the rotor. Obviously, Eq. (13) is still coupled to the infinite set of Eqs. (12), which represent the quantum states of the reservoir. But one can substitute a single thermodynamic equation to this set describing the statistical behavior of this reservoir. In this case, the interaction of the reservoir with the rotor and its rotational fluctuations resulting from local fluctuations of the reservoir have to be included in Eq. (13). However, the energy density term in Eq. (13) contains two contributions. One is the potential energy contribution, and the other is the loss in energy due to the interaction of the rotor with the surface. Therefore, the first right-hand term of Eq. (13) can be decomposed into the gradient of an effective potential energy profile $V_{\mathrm{eff}}(\theta)$ and into a friction term describing the change of $\omega(t)$ due to the molecule's interaction with the reservoir. Moreover, when the complete system is prepared in a purely stationary state, $\varepsilon(\theta, R_1, \ldots, R_m, t)$ is proportional to $\rho(\theta, R_1, \ldots, R_m, t)$ and the second right-hand term of Eq. (13) cancels. This second term then represents the random rotational fluctuations of the rotor introduced by the reservoir, which is active only for non-stationary states of the complete system. These fluctuations can be modeled by an effective random force acting on the rotor. Using this interpretation, Eq. (13) can now be rewritten as

$$I\frac{\delta\omega(t)}{\delta t} = -\frac{\mathrm{d}}{\mathrm{d}\theta}V_{\mathrm{eff}}(\theta) - \mu\omega(t) + \xi(T, t) \tag{14}$$

which represents the equation of motion of the rotor. Here the intervention of the reservoir is described by the stochastic process $\xi(T, t)$ and the friction coefficient μ. From Eq. (14) we now find that the behavior of the rotor is almost classical, i.e., unidirectional rotation is now not forbidden. To realize this state, lateral diffusive motion of the molecule on the surface must be frozen out while permitting rotational motion. One solution is to lower T below the diffusion barrier. The second solution is to surround the rotor by a supramolecular stator, which constrains it to only rotate. Next, the rotor has to be prepared in a undirectional rotational state. Whether a very specific $V_{\mathrm{eff}}(\theta)$ profile and a specific $\xi(T, t)$ stochastic process will do the job, as the $\xi(T, t)$ fluctuation term is the only source of energy, is now a relevant question discussed in Sect. 6.

It is important to note that the above demonstration is not restricted to a reservoir consisting of a surface with supporting bulk solid. A system with a large number of degrees of freedom such as the proteins involved in a biological motor may also be considered a reservoir. In this case, the equation

of motion of the rotation angle can also be extracted from the other variables of the system by using the Madelung decomposition system applied here for a surface at its bulk.

5 Observation of the Semi-Classical Rotation of a Single Molecular Rotor

To observe experimentally that a molecule interacting with a reservoir behaves almost semi-classically, the motion of this molecule should be observed on a single-molecule basis, which precludes all averaging experimental methods. For this purpose, a monolayer of the HBDC molecular rotors presented in Fig. 1 was prepared on an atomically clean Cu(100) metal surface. The conformations of the molecules together with the packing and ordering of the fabricated monolayer were studied in ultrahigh vacuum (UHV) using an STM. In the experiment, the Cu(100) metal surface plays the role of the reservoir and van der Waals interactions within the monolayer have the useful function of suppressing lateral diffusion of the molecules [9].

The HBDC molecules were deposited in UHV on an ultraclean Cu(100) surface using sublimation rate of 0.09 nm/min, at 350 °C [9]. At full monolayer coverage, the molecules form a regular two-dimensional van der Waals crystal [9], which freezes any motion of the molecules even at room temperature (Fig. 4). As a consequence, each molecule in the lattice can be imaged by STM with clear intramolecular contrast. Each molecule displays six lobes arranged in a hexagonal pattern. The distance between the lobes alternates between 0.6 and 0.8 nm, which corresponds well with the alternate

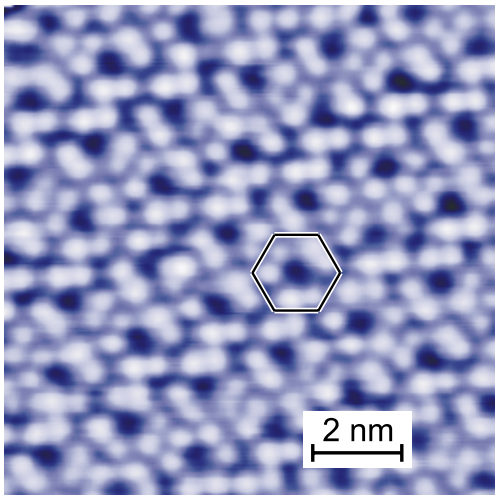

Fig. 4. Constant current STM image of an atomically clean Cu(100) surface after exposure to a full monolayer coverage of HBDC molecules (Fig. 1). Each molecule appears as a hexagonal six-lobed structure. Reprinted with permission from [9]. Copyright 1998 American Association for the Advancement of Science

interleg distances of the *tert*-butyl groups in the HBDC molecule. In this monolayer conformation, the intramolecular conformation of the HBDC molecules on the Cu(100) surface was extracted by making the calculated STM image converge toward the experimental one by including a detailed optimization of the corrugation (Fig. 5). Molecular mechanics optimizations were also necessary to find the appropriate intramolecular conformations of the six *tert*-butyl legs, the three polyaromatic connections and the central part of each HBDC. In its van der Waals lattice, the conformation extracted confirms that each HBDC molecule is imaged through the six lobes, which correspond to the six *tert*-butyl groups of the molecule. More importantly, at room temperature, this analysis shows that a given molecule is not moving laterally (or not rotating) in its van der Waals cavity formed by the six other surrounding molecules within a precision of a few tenths of an angstrom.

The dynamics of the HBDC molecules turned out to be very different for a surface coverage just below one monolayer. Although fairly large ordered 2D-domains of HBDC molecules remain, some molecules are now missing. These create nanometer-scale vacancies in the monolayer, which are sometimes very close to the size of a single HBDC molecule (Fig. 6). Such defects provide the

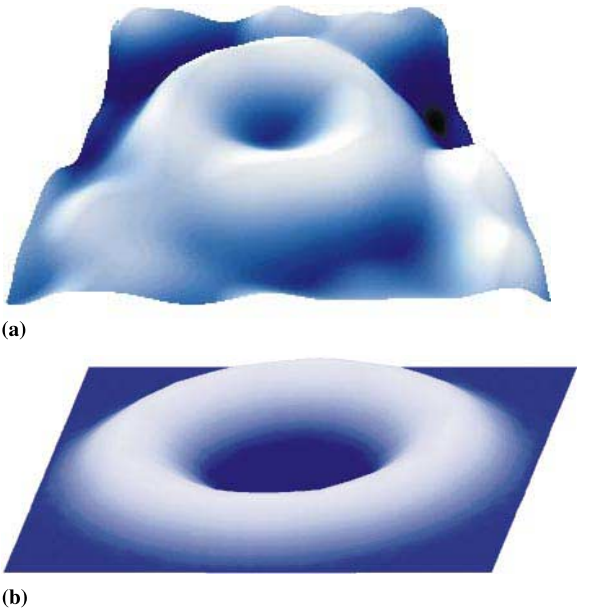

Fig. 5. A detailed comparison between STM experimental **(a)** and calculated constant current (**b**) images of HBDC molecules. The calculated image was obtained using the elastic scattering quantum chemistry (ESQC) technique with additional molecular mechanics optimization of the conformation on the surface to converge with the experimental image. Different heights in the images of the *tert*-butyl lobes are observed experimentally, corresponding to different propeller-like conformations of the HBDC molecules. The intramolecular conformation of each experimentally observed molecule can be accurately extracted using ESQC plus molecular mechanics calculations

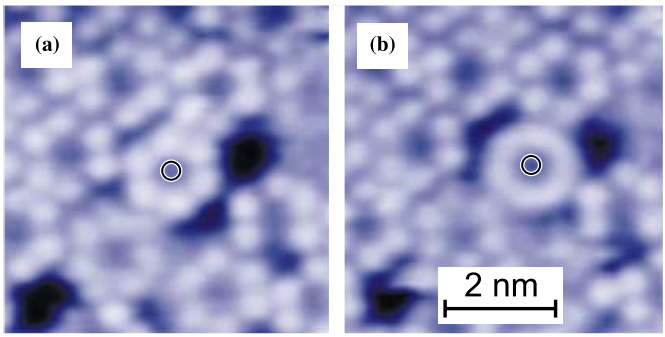

Fig. 6. Constant-current STM image of an atomically clean Cu(100) surface after exposure to a monolayer coverage of HBDC molecules just before the threshold of full coverage. Holes in the monolayers are readily observed, in which some HBDC molecules have been observed to rotate freely for some time. Note that the HBDC molecules at the border of these holes generally are not moving owing to their interaction with the surrounding ordered part of the corresponding monolayer island. In **A** the central molecule is fixed and in **B** after a translation of 0.25 nm the central molecule is observed to rotate. Reprinted with permission from [9]. Copyright 1998 American Association for the Advancement of Science

opportunity for a molecule to be in motion driven by the heat of the substrate. We focused on those defects, which form a cavity where a central HBDC molecule was surrounded by a network of other molecules belonging to an ordered part of the lattice. These external molecules cannot move because they are locked in their van der Waals lattice and form a stator (Fig. 6). In this case, the behavior of the central molecule was studied in detail. In some observations, the central molecule displays six lobes, indicating the absence of a large motion of its center of mass. Tip manipulation or other fluctuations in some images can cause the center of mass of the molecule to be shifted by a several atomic units of the Cu(100) surface. This was found to be accompanied by a distinct change in the intramolecular contrast of the STM image of the molecule (Fig. 7a). In these cases, we also performed a determination of one intramolecular conformation of the central HBDC molecule. We have first searched for specific new adsorption sites for the central molecule in its tiny cavity that could be responsible for this large change of the STM image. No such sites were found under the hypothesis that the underlying Cu(100) surface atomic configuration remains at rest and electronic changes resulting from adsorption can be ruled out. In this case, the most plausible interpretation of the change in STM contrast and the corrugation observed is that the molecule rotates at a speed that is must greater than the STM observation time (Fig. 7b).

Spontaneous changes from the non-rotating to the rotating state of this rotor observed from time to time can be interpreted by the low lateral diffusion barrier height in the cavity [9]. At room temperature, this also confirms our hypothesis that the Cu(100) surface atoms remains at rest. STM manipulation of the central molecule from a non-rotating to a rotating state is

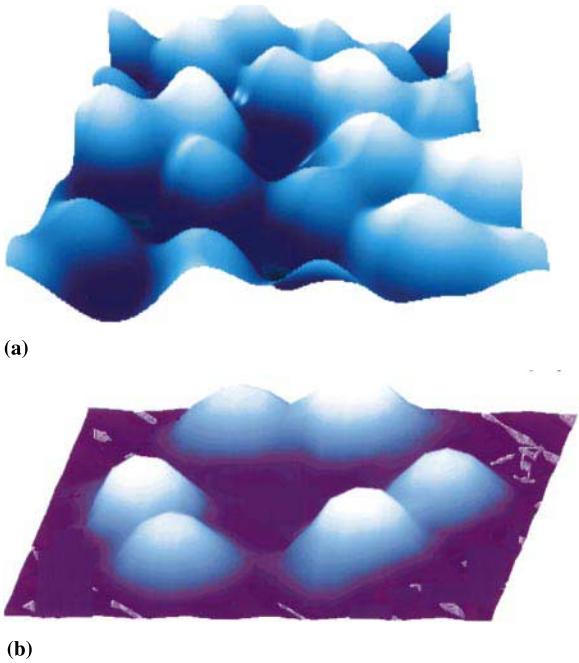

Fig. 7. **(a)** Constant-current 3D STM view of a single HBDC molecule in rotation in its HDBC-molecule stator. Note that the internal contrast reveals no lobe alternation. **(b)** Calculated constant-current STM images using the ESQC technique by supposing a rotation speed of the HBDC molecules larger than the STM image-recording time

very attractive because it opens the way for a more detailed analysis of the physics of the molecular rotation. During one experiment on molecular rotors we also recorded the noise of the tunneling current in the rotating and non-rotating states of the rotor. The limited bandwidth of the STM feedback loop limited the frequency range of our measurement to the kilo-Hertz range. In this case we observed structureless $1/f$ noise with the same characteristics in both the rotating and the non-rotating cases [9].

This experiment yields two insights regarding the problem of preparing a molecule in a semi-classical rotational state. Given the observation of a shift of the center of mass of a specific HBDC molecule in a cavity, the resulting motion of the molecule can be interpreted as rotation. This rotation is certainly at random because it is fueled by the heat of the Cu(100) surface. This is in excellent agreement with the motion governed by Eq. (14), which follows a $V(\theta)$ potential of rotation without residual lateral motion as would have resulted from quantum entanglement with the previous non-rotating state. Second, there is no sign of a dilution process of the rotating wave packet during the observed motion. The signature of this dilution would have been an immobilization during a short period of time of the rotor at random time intervals, and is characteristic of a pure quantum motion. Such behavior will have to be confirmed by low-temperature experiments on the same molecular

system or by designing new molecular rotors with different rotational energy barriers.

6 Towards Nano-Thermodynamics

The first difficulty in designing a molecular engine using a molecular wheel is to force the quantum system to behave almost classically. In the preceding sections, we have discussed two solutions for that problem: quantum control of the wave-packet trajectory in the state space and the use of a reservoir to randomize the phase of the rotor wave function. The former may be practicable to design flying or floating molecular nanorobots [29]. In the latter case, using a first reservoir to mix the $\chi_n(\theta)$ quantum states reintroduces the issue of producing useful work using only one reservoir (reservoir 1). However in this case, the second principle of thermodynamics still applies because this first reservoir has a defined temperature T. Therefore, on the macroscopic scale, a second reservoir (reservoir 2) at a different temperature is required for a rotor to become a motor [30]. In contrast, a macroscopic engine is too large to prevent exploration of local fluctuations in energy of a single reservoir to produce useful results.

At the nanoscale, the situation is quite different. First, the inertial momentum I is very small for a molecular rotor. Therefore, an inertial motion described by Eqs. (2) or (14) can be transformed into a diffusive motion by contact with a reservoir. In this case and for classical motion, it has been demonstrated that a colored-noise source exciting a system into a diffuse motion can play the role of a second source (reservoir 2) with an equivalent temperature different from that of reservoir 1 whose fluctuations are described by a white noise [7]. In this configuration, the rotor can rotate unidirectionally because it rectifies the colored noise. However, the torque of the engine is not very well characterized. Second, the reservoir can also be part of the molecule. For example, the intramolecular vibrational manifold of the stator can provide the quantum states required to mix the $\chi_n(\theta)$ rotor states. Heating this manifold A is possible by the process of intramolecular vibration relaxation [31], preparing the stator in an electronic excited state (Fig. 8). These excited states can be reached optically or by tunneling electrons. On its relaxation pathway to the ground state of the stator, this energy may drive the rotation of the coupled rotor. In this case, the intramolecular heat source is the vibrational manifold A, and the surface (support) provides the final spontaneous relaxation channel, i.e., the cold source (Fig. 8).

This situation is also encountered if one considers the coupling between two intramolecular manifolds A and B. Here, the energy that can be captured by B from A is of interest. On its transfer path from A to B, via a molecular coupling channel, the energy can be transformed by a molecular rotor into motion [30]. Lloyd concluded that "any quantum system that can obtain information (energy) about another quantum system can form the basis of a quantum demon" [32]. Problematic is that a non-invasive observer is required to measure this exchange of information energy between the two nanosystems

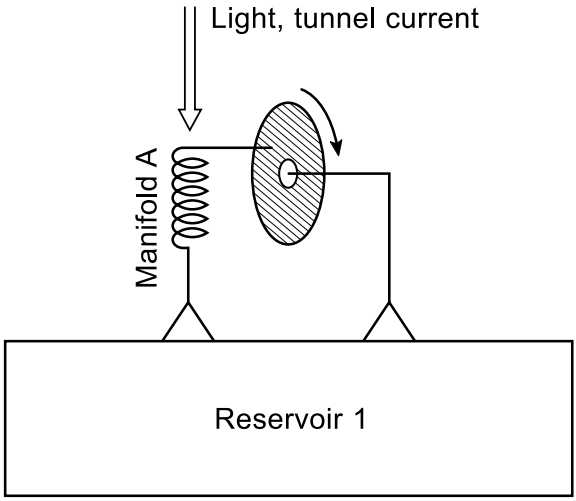

Fig. 8. Schematic of a molecular motor activated by intramolecular vibration energy relaxation of manifold A towards the rotor part of the motor. The rotor is positioned on an axis connected to reservoir 1 kept at a temperature T. Vibration manifold A is represented here by a simple molecular spring that can be excited by light or by the inelastic effect of a tunneling current passing through the molecular spring. Without such an excitation, manifold A is statistically populated by reservoir 1. A specific choice of a molecular structure equivalent to the spring may avoid its complete thermalization, for example by filtering the thermal noise giving rise to a unidirectional rotary motion

even if this exchange is secured by the molecular channel rather than being through space. In the case of a rotor, the amount of energy transferred from A to B will be measured by detecting the unidirectional rotation of the rotor using, for instance, an STM or an atomic force microscope (AFM) to estimate the torque. The A and the B manifolds are clearly chosen to play the role of the hot and the cold reservoirs, respectively. In both cases, manifold A controls the repartition of the driving energy on the $\chi_n(\theta)$ states intermixed with the manifold-A states. A few years ago, this situation would have been deemed experimentally unrealizable. Today, however, one can experimentally interface such nanosystems with an STM (or an AFM) tip in an almost non-invasive setup. This opens the exciting opportunity to actually investigate the role of the second law on the nanoscale in terms of the ultimate limits of energy exchange and transformation between nanosystems constituting a nano-engine.

7 Conclusion

On a single-molecule basis, a unidirectional molecular rotation requires careful preparation of the non-stationary quantum state of the rotor. The motive power of such rotating wave-packet states is weak and requires

permanent quantum control of the wave-packet dynamics using a time-dependent external excitation with the appropriate form. A semi-classical rotating motion is found in cases where the rotor interacts with a reservoir. Using the STM and a specifically designed molecule, we have verified experimentally this first preparation step. However, such an interaction reintroduces the second law of thermodynamics, which is absent in a purely coherent intramolecular evolution before the decoherence step. One benefit of the small dimensions of a molecular rotor is its sensitivity to local quantum fluctuations of the reservoir. This, for example, suggests that one should search for a molecular structure capable of avoiding thermalization in the stator and of inducing unidirectional rotation. This quest is a new design of machines using individual molecular components.

Acknowledgements. We thank the European Union and the Swiss Federal Office for Education and Science for financial support through the IST-FET project "Bottom-up Nanomachines (BUN)".

8 References

1. Joachim C, Gimzewski JK, Aviram A (2000) Nature 408: 541
2. Symon KR (1961) Mechanics, Addison-Wesley, London
3. Hawa RJ, Muller RS, Gabrieland KJ, Trimmer WSN (1990) IEEE Spectrum 27: 29
4. Schnapp BJ (1995) Nature 273: 655
5. Noji H, Yasuda R, Yoshida M, Kinosita K (1997) Nature 386: 299
6. Jankowsky E, Gross CH, Shuman S, Pyle AM (2000) Nature 403: 447
7. Astumian RD (1997) Science 276: 917
8. Sabbert D, Junge W (1997) Proc Natl Acad Sci USA 94: 2312
9. Gimzewski JK, Joachim C, Schlittler RR, Langlais V, Tang H, Johannson I (1998) Science 281: 531
10. Kelly TR, De Silva H, Silva RA (1999) Nature 401: 150
11. Koumura N et al. (1999) Nature 401: 152
12. Livoreil A, Dietrich-Buchecker CO, Sauvage JP (1994) J Am Chem Soc 116: 9399
13. Tang H, Cuberes MT, Joachim C, Gimzewski JK (1997) Surface Science 386: 115
14. Ehrenfest P (1927) Z Physik 45: 455
15. van Gunsteren WF, Weiner PK, Wilkinson AJ (eds) (1993) Computer Simulation of Biomolecular Systems: Theoretical and Experimental Applications, vol 2. ESCOM, Leiden
16. Kelly TR, Telliter I, Sestelo JP (1997) Angew Chem Int Ed Engl 36: 1866
17. Toyoda T, Wakayama S (1999) Phys Rev A 59: 1021
18. Heisenberg W (1926) Z Phys 40: 501
19. Feynman RP (1987) In: Metropolis N, Kerr DM, Rota G (eds) New Directions in Physics: The Los Alamos 40th Anniversary Volume. Academic Press, Boston, p 7
20. Carnot S (1963) The Laws of Thermodynamics. In: Feynman RP, Leighton RB, Sands M (eds) Chap 44 of The Feynman Lectures on Physics, vol 1. Addison-Wesley, New York
21. Ortigoso J (1998) Phys Rev A 57: 4592
22. Villeneuve DM, Aseyev SA, Dietrich P, Spanner M, Ivanov MY, Corkum PB (2000) Phys Rev Lett 85: 542
23. Zurek WH (1991) Physics Today, p 36
24. Myatt CJ, King BE, Turchette QA, Sackett CA, Kielpinski D, Itano WM, Monroe C, Wineland DJ (2000) Nature 403: 269

25. Madelung E (1926) Z Phys 40: 322
26. Calderia AO, Leggett AJ (1985) Phys Rev A 31: 1059
27. Unruh WG, Zurek WH (1989) Phys Rev D 40: 1071
28. Joachim C (1986) J Phys A 19: 2549
29. Pinske PWH, Fischer T, Maunz P, Rempe G (2000) Nature 404: 365
30. Allahverdyan AE, Nieuwenhuizen TM (2000) Phys Rev Lett 85: 232
31. Smalley RE (1982) J Phys Chem 86: 3504
32. Lloyd X (1997) Phys Rev A 56: 3374

Rotary Motion in Single-Molecule Machines

T. Ross Kelly[1], José Pérez Sestelo[2]

[1] Department of Chemistry, E.F. Merkert Chemistry Center, Boston College, Chestnut Hill, Massachusetts 02467, USA
E-mail: ross.kelly@bc.edu

[2] Departamento de Química Fundamental, Facultad de Ciencias, Universidade da Coruña, 15071A Coruña, Spain
E-mail: sestelo@udc.es

Molecular systems that exhibit controlled or coordinated rotary motion are discussed in this chapter. These systems represent a reproduction of a variety of macroscopic mechanical devices on the molecular scale. From gears to a motor, passing through a turnstile, a brake and a ratchet, we describe their design, synthesis and dynamic behavior. The importance of molecular motors in the biological realm and possible applications in nanotechnology are also discussed.

Keywords: Molecular devices, Motors, Nanostructures, Triptycenes

1 Introduction 19

2 Biological Molecular Motors 20

3 Molecular Gears 21

4 Molecular Turnstile 25

5 Molecular Brake 27

6 Molecular Ratchet 34

7 Molecular Rotary Motor 41

8 Conclusions 51

9 References 51

1 Introduction

The construction of molecular machines that mimic physical and biological systems has attracted the attention of many scientists over the past 30 years [1]. This interest stems in part from the ever-continuing effort to reduce the size of mechanical devices, because as one proceeds to smaller and smaller dimensions, one eventually arrives at the molecular scale. The miniaturization of motors has had a particular fascination. In 1959, the Nobel laureate physicist Richard Feynman offered a $1000 reward for the first "operating

Structure and Bonding, Vol. 99

electric motor [that] is only 1/64 inch cube" [2]. The reward was collected within a year [2]. More recently, microfabrication using photolithographic techniques has led to motors whose diameters are smaller than that of a human hair [3]. Physicists, bioengineers, mathematicians and others have given much theoretical attention to "molecular combustion motors" [4], "forced thermal ratchets" [5], "fluctuation driven ratchets" [6] and related conceptual devices [7]. In 1995 a New Jersey team experimentally demonstrated an "optical thermal ratchet" that harvests energy from Brownian motion [8, 9].

The design and synthesis of a molecular motor is the ultimate response to Richard Feynman's 40-year-old challenge and is, we believe, a major accomplishment in its own right [2]. In addition, however, the achievement has significant implications in the biological realm, because it would provide an atomic-scale model for the operation of a biological motor. The quest for such an atomic-level explanation has been the elusive Holy Grail of biophysicists, "despite being the subject of what may be described as the most extensive research effort in biophysics in the last forty years" [10]. Last, but far from least, the possibility of attaching millions of individual motor molecules to surfaces or to sides of individual particles and other micro-and nanoscale assemblies offers the potential for a host of new materials and devices.

For the past several years our research group has had as a long-term goal the rational design and construction of a molecular motor. In particular, we have focused our attention on achieving a rotary (as distinct from a linear or a two-state reciprocating) motor. Given the other contributions to this volume, in this chapter we will confine ourselves to discussing in chronological order a variety of molecular-scale devices that exhibit, in one form or another, various aspects of controlled or coordinated rotary motion. That discussion roughly follows the historical chronology, beginning with gears and turnstiles, before delineating our own efforts to add the control or power elements found in brakes, ratchets and motors. But before discussing molecular devices produced by chemists, by way of context, we first briefly examine Nature's molecular motors.

2
Biological Molecular Motors

The first evidence of the importance that molecular machines have in life is their presence in all living systems. Even very small biological units such as cells and bacteria are provided with molecular motors that allow their independent life and permit interaction with more complex living systems. As distinguished from macroscopic mechanical motors, these biological systems use chemical energy in the form of ATP or proton-motive forces, not electricity or petroleum.

Enormous effort has been expended attempting to fathom the operating principles of biological machines [10, 11]. How do muscles contract? How do bacteria "swim"? Biologists and biochemists have put forward crude models that attempt to show, in a superficial way, what is happening if one were to examine through a microscope a muscle contraction or the propulsion of a

bacterium by its flagella. Indeed, the most recent (1995) edition of Stryer's "Biochemistry" [12] now has an entire chapter, titled "Molecular Motors", devoted to this topic that offers various schematic depictions of how a muscle generates movement and how the chemical energy of the energy-rich biological fuel ATP is transformed into coordinated movement. Likewise, the latest (1995) edition of Voet and Voet's "Biochemistry" [13] contains a beautiful drawing that illustrates schematically what viewers might see, were they to look at a flagellum through a powerful microscope.

What is missing from both these books, however, is an answer to the question "how do the biological fuels (most commonly ATP and proton gradients) ultimately produce coordinated motion?" Even more conspicuously absent from those – and virtually [14] all other – depictions of biological motors is any atomic detail. That absence is due to lack of knowledge, not imprecise graphics.

In the past several decades, chemists have turned increasingly to biology for clues to design. Biochemists have provided atomic-scale resolution to the operation of enzymes, and brought crucial insights to the fields of catalysis, molecular recognition, self-assembly, regulation, and sensors, to name but a few. To date, however, biology has provided little atomic-level information on how to construct a molecular-scale motor. We hope that the synthesis of molecular devices capable of controlled movement will be helpful for the understanding of biological systems.

The molecular motors of biological systems can be classified into linear and rotary motors. Commonly, we associate the concept of movement with change of position (translation), which is indeed fundamental to the transport of particles in living systems. But rotary motion also plays an important role in biology; ATP synthase and flagella are the most well-known examples, but many allosteric enzymes are activated by a change of conformation through rotation. Figure 1 shows some of the most studied molecular motors, ATP synthase, the flagellum in bacteria, the kinesin motor, and DNA polymerase, classified by the type of movement.

All known biological motors use chemical energy to produce coordinated movement. In the case of ATP synthase, biology's smallest known motor [15], the energy is normally obtained from a proton gradient and the motor function is achieved by rotation [16, 17]. Run "in reverse" ATP synthase can use ATP to produce rotary motion. The flagellar rotary motor in bacteria also uses proton motive forces. This bacterial motor allows movement at a rate of 100 $\mu m\ s^{-1}$, a speed that, if the bacteria were resized to the weight of cars, they would supposedly break the sound barrier. ATP is used as an energy source by many other complex biological motors such as myosin (the motor component of muscle) and kinesin [18].

3 Molecular Gears

Molecular gearing systems are the first successful examples of rotary molecular devices engineered and synthesized using conventional chemistry. At the

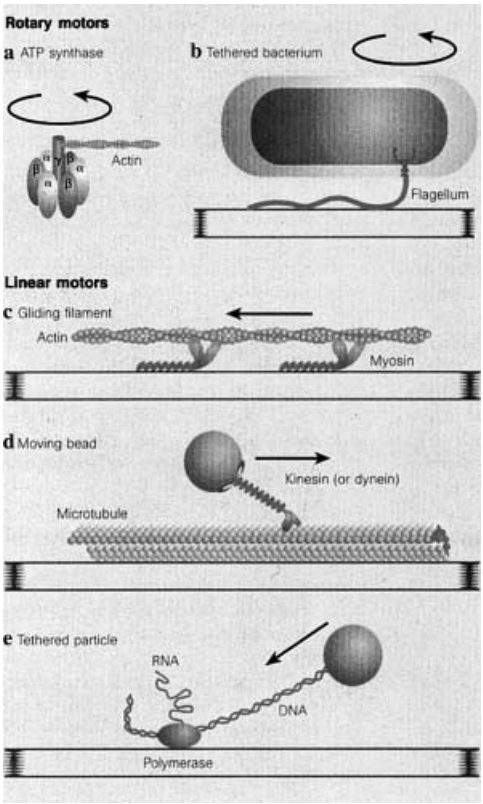

Fig. 1a–e. Biological examples of molecular motors. Motors shown in **a** and **b** are rotary motors and **c–e** are linear motors. Motion takes place in the direction indicated by the arrows, and diagrams are not drawn to scale (reproduced with permission from [15])

macroscopic scale mechanical gears are used to generate and control rotational movement and produce useful work in numerous mechanical devices including clocks, transmissions and drive trains [19]. At the molecular level, rotation around single bonds is the norm, so such bonds can serve as the molecular equivalent of axles. The design and synthesis of molecular systems that work as gears have engaged the interest of several research groups over the past three decades [20].

The major efforts aimed at synthesizing molecular gears have been focused on triptycene derivatives. Triptycene (Tp), a rigid molecular unit with three blades each composed of a benzene ring, represents a molecular mimic of a gearing element [21]. The use of triptycenes as molecular gears (Fig. 2) has been studied since the 1970s mostly by Mislow and Iwamura [20].

The simplest triptycene molecular gears were constructed by Oki [22] using two triptycene derivatives connected by an appropriate bridge (CH_2, NH, O, SiH_2, —C═C—). According to computational studies the gearing barrier in Tp_2X (X = CH_2, CO) and Tp_2O is only 1–2 kcal mol^{-1}; thus the Tp rotors are

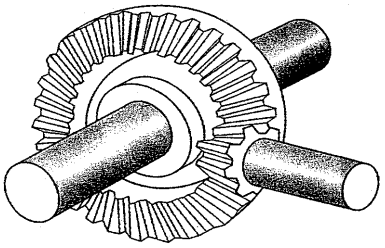

Fig. 2. Physical bevel gear (reproduced with permission from [20c])

highly mobile, almost frictionless, and tightly meshed and securely interlocked bevel gears. Indeed, NMR studies show that these molecular analogs of bevel gears exhibit very rapid correlated disrotation. The ^{1}H NMR spectra of Tp_2O and Tp_2CH_2 show no splitting of the benzene ring signals down to ca. −90 °C, consistent with an upper limit of 7–8 kcal mol^{-1} for the gearing barrier [23]. The energy barrier for gear slippage is much higher and highly dependent on the joint group; variable temperature ^{1}H NMR experiments show a barrier ranging from 20.4 ± 0.4 kcal mol^{-1} for the silane **5** to as high as 41.0 ± 0.5 kcal mol^{-1} for the ether **1** (Fig. 3) [24].

From the rotation of these systems there arises, in the absence of slippage, a particular case of stereoisomerism, which has been dubbed by Iwamura as "phase isomerism" [25]. If two blades, one in each wheel, are labeled, three stereoisomers are produced, a racemic pair and a *meso* form.

More complex triptycene molecular gears are those composed of more than two connected triptycenes. The use of mechanical gear trains is an idea of great antiquity used by the Greeks, inter alia, to compute planetary motions [26]. Over 2000 years later, Iwamura and co-workers succeeded in synthesizing a chemical gear train (see Fig. 4) [27], a system consisting of two labeled triptycenes connected by ether-type bonds (**7**). The movement is more complex in these systems. The rotation follows a rule, which is that the motion of the two terminal gears in a train is disrotarory if the number of gears is even and conrotatory if the number is odd. As with the *meso* and *d*/*l* forms of **1**–**6**, substituted derivatives of phase isomers **7** can be separated by HPLC and identified by NMR.

The synthesis of extended chemical gear trains opens an important door to the construction of macromolecular chains that can transfer information from

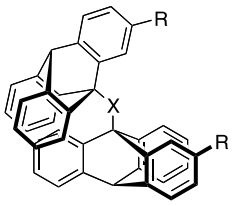

Gear	R	X	E (kcal mol^{-1})
1	Cl	O	42
2	Cl	S	29
3	Cl	NH	39
4	CH_3	CH_2	31
5	Cl	SiH_2	21
6	Cl	HC=CH	30

Fig. 3. Energy barriers to gear slippage in molecular bevel gears

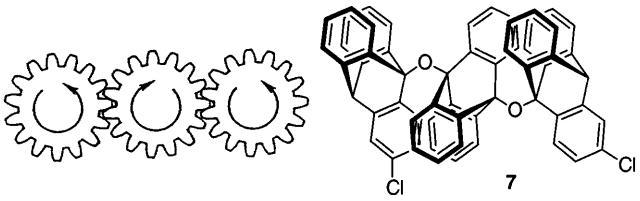

Fig. 4. Representation of a macroscopic drive train and *meso* form of molecular analog **7** (reproduced with permission from [20b])

one end of the molecule to the other via cooperative torsional motions along the chain. Realization of this idea has not yet been reported.

Other molecular gear-like constructs involving triptycene units are those containing a triptycene and an external ring linking the C-9 and C-10 positions (**8** and **9**). These devices were designed by Gakh et al. [20c] with the aim of studying the rotation of the triptycene and to explore their use as molecular containers. These systems have also included two triptycene units incorporated in a ring (see **10** and **11** in Scheme 1) [28].

The molecules were synthesized from 9,10-bis(chloromethyl)anthracene and poly(oxyethylene)glycols under basic conditions. The 9,10-anthraceno-

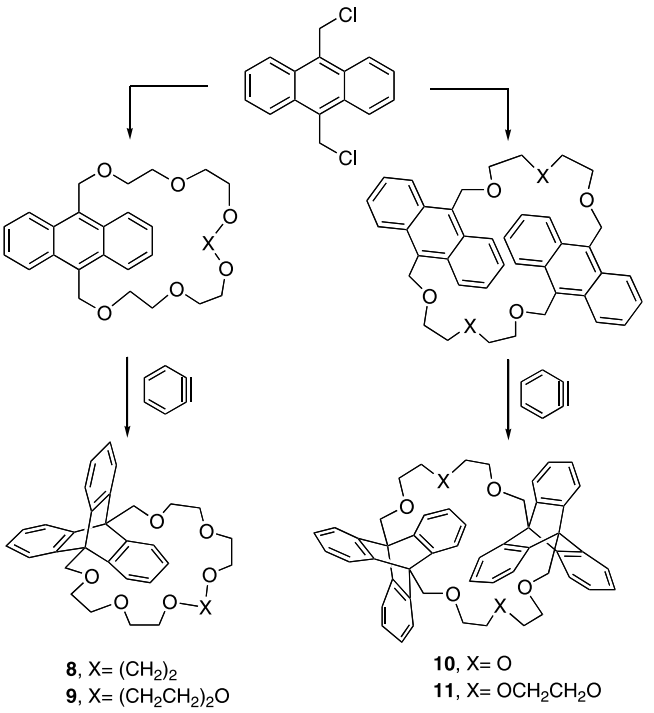

Scheme 1.

crown ethers were converted to triptycenocrown ethers **8–11** using benzyne addition. As one would expect, whether the triptycene rotates with respect to the external ring depends on the size of the ring, allowing for the triptycene either "rope skipping" or staying rotationally locked. With short bridges – $(CH_2)_6$, $(CH_2)_8$ or, as in **8** – the "rope-skipping" mode of the internal triptycene (gear) is not observed even at elevated temperatures [29]. Nevertheless, molecular systems having a larger polyoxyethylene-type external ring, analogous to crown ethers, such as **9**, allow the rotation of the triptycene. Experiments to determine if metal ion complexation would slow down the rotation of the triptycene in **9** indicate that the effect is small [20c]. Bis-triptycenocrown ethers such as **10** and **11** also showed internal rotation as determined by ^{1}H NMR studies. In these compounds, the triptycene gears undergo fast rotation (on the NMR time scale) at temperatures higher than 60 °C; lowering the temperature results in peak broadening with resolution into sets of individual signals (<−40 °C).

In summary, bevel gears and gear trains have been reproduced at the molecular scale using triptycene units. Studies towards more complex molecular systems with coordinated movement and applications in nanotechnology need to be further developed.

4 Molecular Turnstile

Another example of rotary motion in a molecular system is provided by the "molecular turnstile" prepared by Moore and Bedard [30]. The turnstile architecture consists of a hexa(phenylacetylene) macrocyclic frame with a

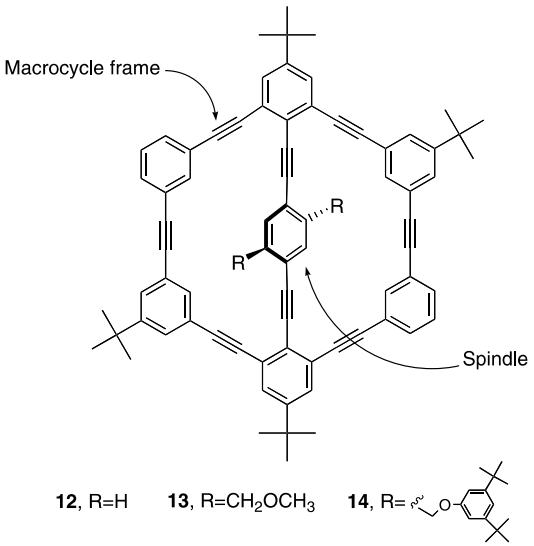

Fig. 5. Chemical structures of molecular turnstiles **12**, **13**, and **14**

diethynylarene bridge (Fig. 5). The bridging unit should exhibit rotation around its own axis and act as the "spindle" of a turnstile. The turnstile exhibits conformational bistability, a term which describes the double-well potential energy surface exhibited by a pair of isoenergetic rotational isomers [31].

The molecular turnstile was synthesized by regioselective and sequential palladium-catalyzed cross-coupling reactions between aryl halides and terminal alkynes [32]. The successful strategy incorporates the spindle in the first step of the synthesis and the last step is a macrocyclization. Three molecular systems (**12**–**14**) with different spindles have been prepared. The compounds, particularly **12** and **13**, show low solubility, perhaps due to their relative planarity.

The dynamic behavior of the systems was assayed by variable temperature ^{1}H NMR experiments based on the fact that the benzylic hydrogens in compounds **13** and **14** are diastereotopic (appearing as an AB system) in the absence of rotation, and enantiotopic (seen as a singlet) under free rotation. The ^{1}H NMR spectrum of **14** (Fig. 6) shows, at all temperatures studied (up to 150 °C), the benzylic hydrogens always appearing as an AB pattern, which indicates that the spindle does not rotate on the NMR time scale. In turnstile **13**, the benzylic hydrogens appear as an AB system only at low temperature; at −54 °C a chemical shift difference of 9 Hz is observed, which coalesces to a singlet at a temperature of approximately 0 °C (Fig. 7).

The results summarized in Figs. 6 and 7 are consistent with the idea that turnstile **14** is conformationally locked and cannot undergo spindle rotation while turnstile **13** exhibits spindle rotation on the NMR time scale at room temperature. The estimated barrier for spindle rotation of **13** is approximately

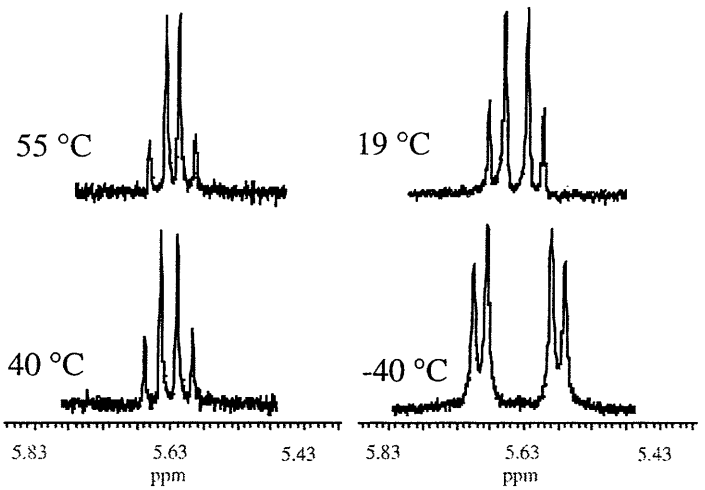

Fig. 6. Variable-temperature 500 MHz ^{1}H NMR spectra ($CDCl_3$) of **14** in the region of the spindle methylene resonance at the indicated temperatures (reproduced with permission from [32])

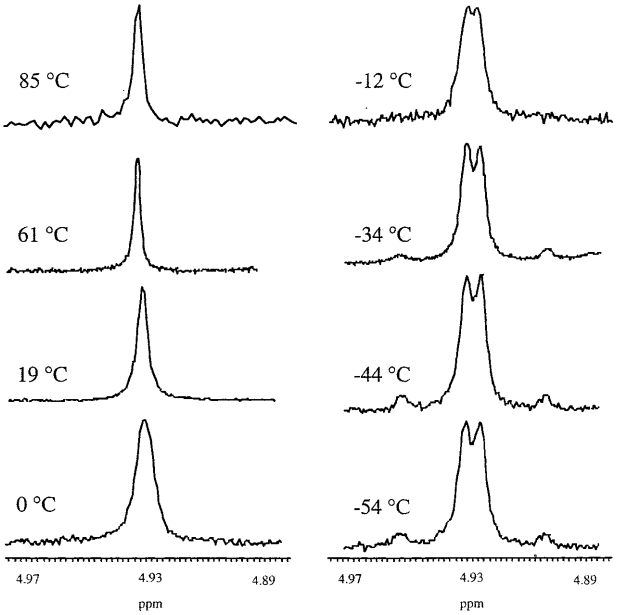

Fig. 7. Variable-temperature 500 MHz ^{1}H NMR spectra ($CDCl_3$) of **13** in the region of the spindle methylene resonance at the indicated temperatures (reproduced with permission from [32])

13.4 kcal mol^{-1} and somewhere in excess of 20.6 kcal mol^{-1} for **14** [33]. Examination of molecular models shows that rotation of the turnstile in **13** requires distortion of the macrocyclic framework from a planar conformation. The mechanism for rotation has not been established yet.

In summary, the turnstile represents a new example of rotation in a molecular system. The fact that phenylacetylene macrocycles form discotic liquid crystals suggests the possibility that turnstiles might function as discotic ferroelectric liquid crystals [34]. A dipole appropriately incorporated on the spindle might allow for its own rotation to be controlled rapidly and reversibly by an external field.

5
Molecular Brake

In 1994 we reported the first rotary molecular gearing system with a control element, a molecular brake [35]. On the molecular level, motion is the norm; spontaneous free rotation around single bonds is thus the rule, not the exception. Our long-term goal was to construct a molecular motor, but at that time we had not yet worked out how to do this. In undertaking a molecular brake we hoped that by developing a molecular device that stopped rotary motion, we would gain insights into designing a molecular system that created rotary motion, i.e., a motor.

In designing a molecular brake we envisioned the use of a triptycene as a three-toothed gear, and the brake being incorporated as a bipyridine attached to the triptycene through an axle. The brake would be activated by a change of conformation of the bipyridine unit (noncoplanar to coplanar) upon complexation of the bipyridine by a metal ion, thereby obstructing the rotation of the triptycene. Scheme 2 represents the concept in both general and specific terms.

Using space-filling (CPK) models we designed **15**, our first version of the molecular brake. The brake consists of a pyridine and a benzoisoquinoline, and the acetylene unit acts as the axle. It was expected that, after complexation with a metal ion, the carbocyclic rings of the benzoisoquinoline would insert between the blades of the triptycene, blocking rotation (**16**). The system as a whole was assembled (Scheme 3) using palladium-catalyzed cross-coupling reactions as key steps. The known triptycene unit **17**, with the axle installed, was prepared from commercial 9-anthracenecarboxaldehyde in a five-step synthetic sequence that involves protection of the aldehyde, benzyne addition, deprotection, and generation of the alkyne group via a Wittig reaction and a β-elimination [36]. Reaction of **17** with the bromo-aminopyridine **18**, prepared from commercial 6-amino-3-picoline, led to the intermediate system **19**. Transformation of the amino group into a triflate (**20**) and coupling with the 3-stannylbenzoisoquinoline **21** [37] afforded the desired molecular system **15**.

Once **15** was in hand, we proceeded to study the rotation of the triptycene unit and the ability of the benzoisoquinoline to function as a brake. That the triptycene unit in **15** spins rapidly is evident from the NMR spectrum wherein the three aromatic rings in the triptycene are equivalent due to rapid rotation. Addition of various metal ions (Zn^{2+}, Pd^{2+}, Pt^{2+}, Hg^{2+}, etc.) to solutions of **15**

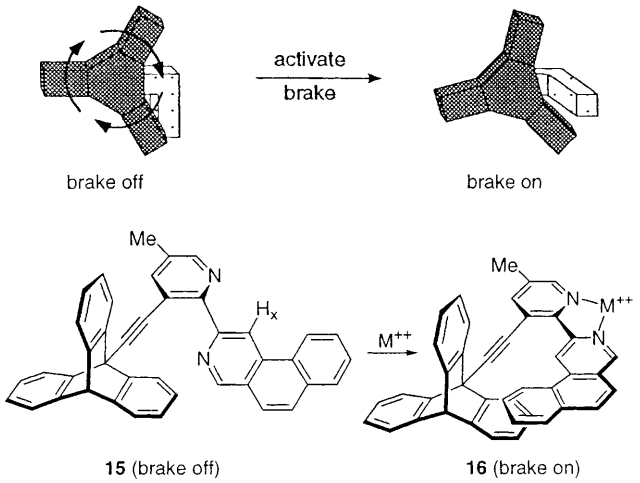

Scheme 2. Schematic and actual depiction of the concept of a molecular brake

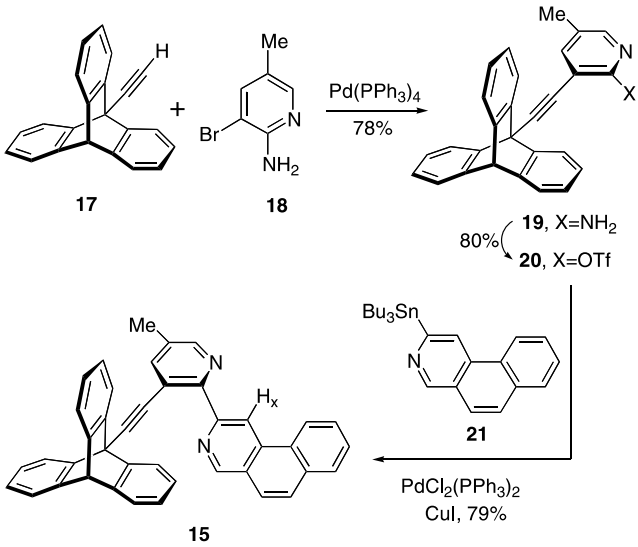

Scheme 3.

resulted in profound changes in the ^{1}H NMR spectrum consistent with formation of complex **16** (for example, the resonance for H_x is shifted 1.7 ppm downfield, consistent with H_x being forced into the deshielding region of the triple bond), but there was no evidence to indicate that rotation of the triptycene had been slowed (there was no peak broadening, let alone nonequivalence of the signals for the three triptycene rings), even at temperatures as low as −120 °C. Moreover, replacing the relatively weak nitrogen-metal coordination bonds with covalent bonds by reaction of **15** with 1,2-dibromoethane did not detectably hinder rotation of the triptycene.

In trying to understand why **15/16** did not function as intended, we reached the conclusion that the acetylenic axle was not sufficiently rigid, and the intended brake was behaving more like a playing card fastened to a wheel of a child's bicycle, being, in effect, continually dislodged by each passing spoke (probably a more accurate explanation is that the benzoisoquinoline/pyridine complex vibrates out of the way on its own, not because it is pushed aside by a spoke).

Based on our hypothesis that the acetylene was too flexible for **15/16** to function as a brake, we redesigned the system by deleting the acetylenic unit and connecting the pyridine directly to the triptycene as in **22**. Unfortunately, the synthesis of **22** proved unsuccessful, because the reaction of the anthracene of **23** with benzyne then failed (Scheme 4).

We speculated that the electron-withdrawing nature of the pyridine ring was responsible for the lack of reactivity of **23** toward benzyne. In troubleshooting the benzyne addition we examined the use of a methoxy group to offset the electron-withdrawing properties of the pyridine. Compounds **24**–**28** (Fig. 8) were prepared in the order indicated. As each was

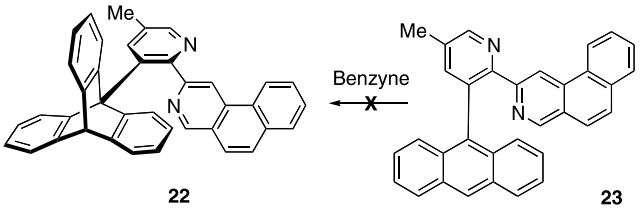

Scheme 4.

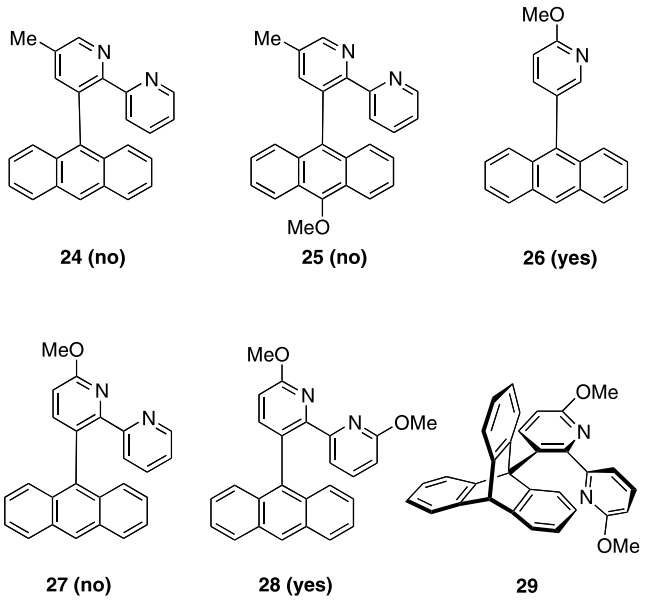

Fig. 8. Molecules studied to troubleshoot the failure of benzyne to add to the central ring of the anthracene in **23**. Whether benzyne adds is indicated in parentheses

synthesized, its susceptibility to benzyne addition was assayed. The results are indicated in parentheses in Fig. 8.

The positive outcome with **28**, giving **29**, suggested that **30** could be prepared analogously from **31** (Fig. 9), but the preparation of **31** proved unnecessary because, in the presence of Hg^{2+}, the bipyridine in **29** achieved braking action.

The synthesis of **29** (Scheme 5), despite the molecule's apparent complexity, was quite straightforward thanks again to the enlistment of two palladium-catalyzed biaryl coupling reactions [38]. Commercial 2,6-dibromopyridine (**32**) was transformed into the corresponding bromomethoxypyridine **33** and homocoupling of **33** afforded the bipyridine **34**. Bromination and a subsequent cross-coupling reaction with 9-(trimethylstannyl)anthracene led to **28**, the immediate precursor of **29** which, as noted above, was achieved using a benzyne addition.

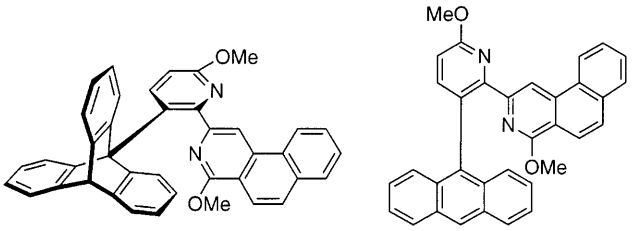

30 31

Fig. 9. Putative replacement (**30**) for **22** and anthracene precursor

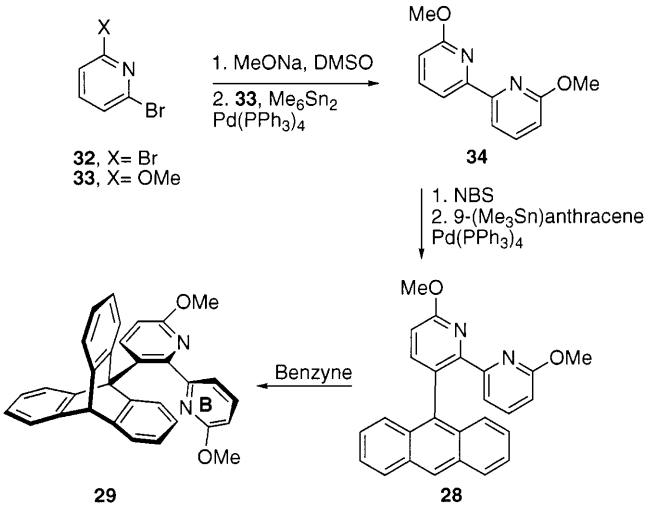

29 28

Scheme 5.

In the absence of Hg^{2+} (or other metal ions) the triptycene wheel in **29** (Scheme 6) spins rapidly at 30 °C, as evidenced by the simplicity of the ^1H NMR spectrum of **29** (Fig. 10) wherein, by virtue of C_3 symmetry arising from relatively rapid rotation, the 12 triptycene aromatic protons give rise to only

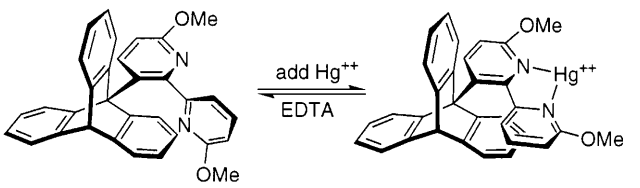

29 35

Scheme 6.

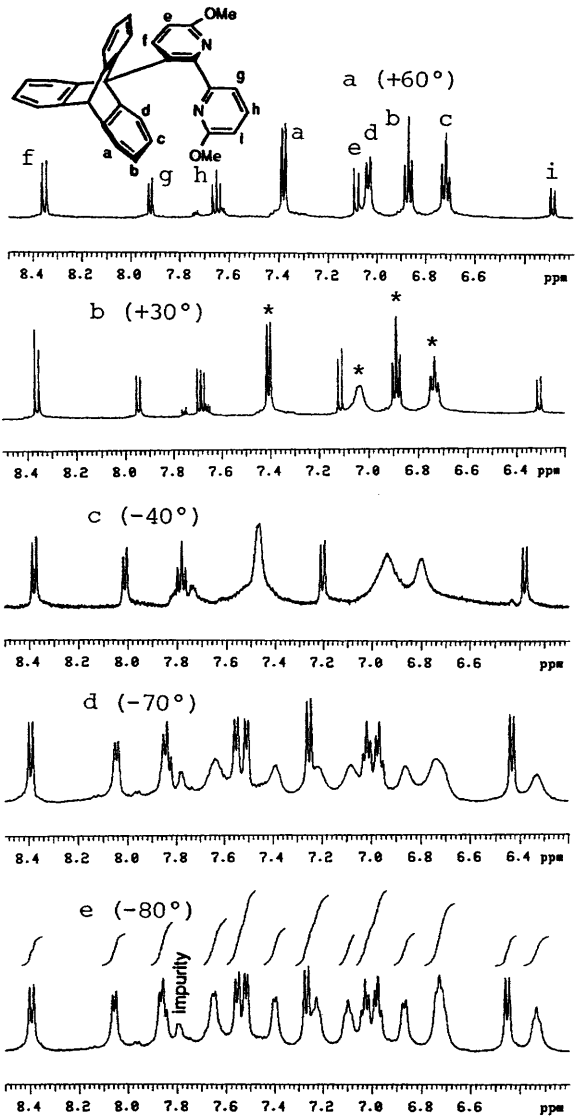

Fig. 10. Aromatic region of the 500 MHz ^{1}H NMR spectrum (acetone-d_6) of **29** at various temperatures. Note that at 30 °C the asterisked peaks for the 12 triptycene aromatic protons appear as four sets of resonances, indicating equivalence (due to the relatively rapid rotation). At −40 °C, peak broadening reflects slowed rotation but, even at −70 °C (**d**), the broadened peaks indicate that rotation has not stopped on the NMR time scale

four sets (asterisked) of resonances. Addition of $Hg(O_2CCF_3)_2$ to **29** results in profound changes in the 30 °C (and other) ^{1}H NMR spectrum (Figs. 10 and 11). Most noteworthy is the change in the chemical shift of the B-ring methoxy in **29**, which appears (not shown) at the extraordinary value of 2.11 ppm due

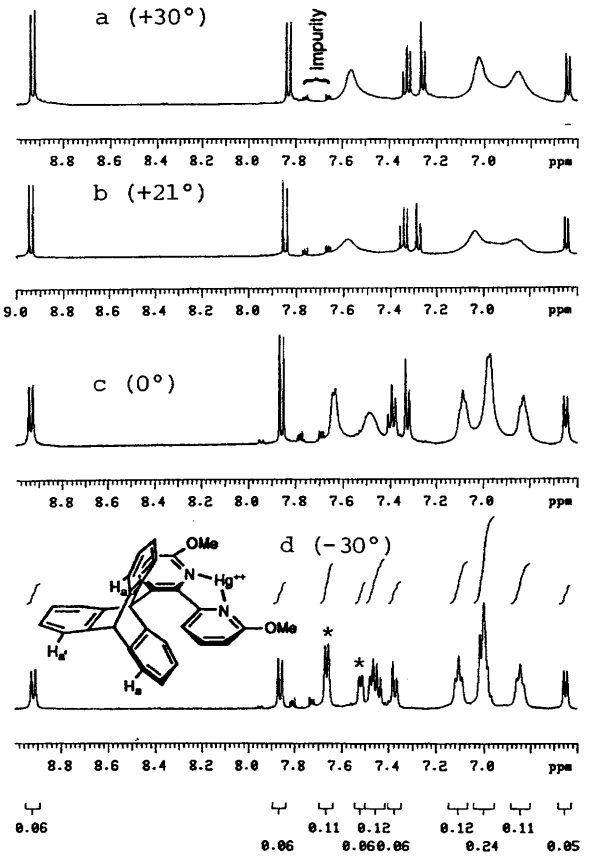

Fig. 11. Aromatic region of the 500 MHz ^{1}H NMR spectrum (acetone-d_6) of **35** (M = Hg^{2+}). Contrast the broad peaks at 30 °C with the sharp peaks at 30 °C in Fig. 10 and the sharp peaks at −30 °C in this figure (indicating frozen rotation) with the broad peaks at −40 °C and −70 °C in Fig. 10

to the shielding effect of the benzene rings of the triptycene, to a normal δ 4.13 value. At the same time we observed the broadening of the four resonances attributable to the hydrogens in the three benzo rings of the triptycene.

Variable-temperature ^{1}H NMR experiments (see Figs. 10 and 11) document the engagement of the brake. In particular, at −30 °C, and in contrast to the system without any metal ion, the three aromatic rings of the triptycene are no longer equivalent because of the arrest of rotation on the NMR time scale. That nonequivalence is most clearly seen (Fig. 11d) in the two asterisked doublets at δ 7.67 and 7.53 (in a 2:1 ratio) due to the two H_a and one $H_{a'}$ resonances in Fig. 11d indicating that engagement of the brake results in the plane of symmetry implied in **35**. By contrast, in the absence of metal, restricted rotation at a much lower temperature (ca. −80 °C) (Fig. 10e) renders all 12 triptycene protons nonequivalent. When the −30 °C solution of **35** with the

brake engaged is allowed to warm, the brake begins to slip, as evidenced by broadened peaks for H_a and $H_{a'}$ at 0 °C and their coalescence at 21 °C. As warming continues, the single peak for $H_a + H_{a'}$ begins to sharpen but the complex irreversibly decomposes (~70 °C) before the spectrum has sharpened sufficiently to indicate rapid rotation. To confirm the "reversibility" of the braking mechanism we added EDTA to molecular brake **35**; the experiments showed that the Hg^{2+} is removed and the brake is released [35].

In summary, we developed the first example of a molecular brake. The brake operates by coordination of a metal at a remote site, which brings about a conformational change that reversibly halts rotation of a molecular-scale gear.

6 Molecular Ratchet

Following our first effort to translate the principles of mechanical machines to the molecular scale by constructing a molecular brake, in 1996 we sought to prepare a molecular ratchet [39]. Commonly, ratchets are devices that allow motion in only one direction; in the simplest form they contain three components (Fig. 12): (a) a toothed ratchet wheel, (b) a pawl that prevents unintended rotation of the ratchet wheel, and (c) a spring that holds the pawl in place. Both the tension of the spring and the contours of the ratchet wheel and pawl determine the ease (and direction) of rotation. We thought a ratchet might well be an essential component of our long-term goal of a molecular motor.

In designing a molecular ratchet we envisioned continuing with a triptycene, which would act as the ratchet wheel, and using helicenes [40] to simultaneously serve as pawls and springs. The two molecular ratchets proposed are **36** and **37** (Fig. 13). Both systems have essentially the same components, but can be differentiated by the length of the helicene.

Examination of models, particularly of **37**, indicates a distinctly helical conformation to the [4]helicene unit; that asymmetry is evident in Fig. 14, which is a stereoview of an electron density surface map of the lowest energy conformation of **37b**. Manual rotation of the triptycene in models of **37** forces the helicene further and further out of planarity until the energy maximum is reached. That rotation is accomplished much more easily with a clockwise

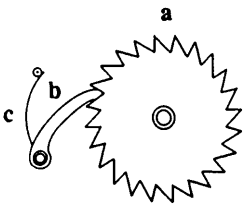

Fig. 12. A simple mechanical ratchet: **a** a ratchet wheel; **b** a pawl; **c** a spring that holds the pawl against the wheel

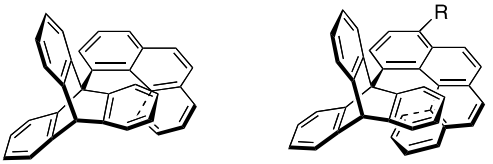

36 **37 a**, R= H
b, R= Me

Fig. 13. Proposed molecular ratchets

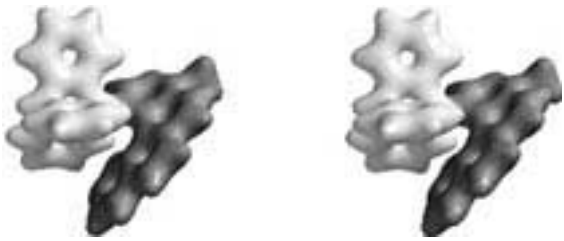

Fig. 14. Stereoview of an electron density surface map of the lowest energy conformation of **37b**

instead of a counterclockwise turning of the triptycene (for the enantiomer of structure **37** that is shown), as would be expected of a ratchet.

Helicenes are polycyclic aromatic compounds in which the helical structure is a consequence of a steric repulsion of the terminal aromatic nuclei. The conformation and chirality of helicenes have attracted the attention of many researchers over the years [39]. We chose to enlist helicenes as both pawls and springs because (1) they have an inherent helicity that we thought would favor the unidirectional rotation and (2) their relatively rigid structures resist deformation. That resistance to deformation is also a characteristic of springs.

An important parameter to investigate prior to the synthesis of the molecular targets is the energy barrier to rotation. In order to study rotation by NMR techniques, an energy barrier on the order of 18–27 kcal mol^{-1} is required. Molecular modeling calculations (AM1) using the coordinate drive feature of the Spartan program [41] indicated unexpectedly – at least to us – that the smaller [3]helicene in **36** presents a greater barrier to rotation (27 kcal mol^{-1}) than the larger [4]helicene in **37** (22 kcal mol^{-1}). Since the computed barriers (at least their relative magnitudes) were in due course borne out by experiments, we suggest that this difference in rotational barriers is due to the interaction between the one-ring-longer helicene in **37** and a blade of the triptycene, which prevents **37** from relaxing to as stable a ground state conformation (relative to the energy maximum) as is accessible to **36**.

Figure 15 is a plot of the calculated energy of **37a** as a function of rotation around the triptycene/helicene bond. The asymmetry of the peak is consistent with what might be expected if **37a** were to function as a ratchet. Figure 16

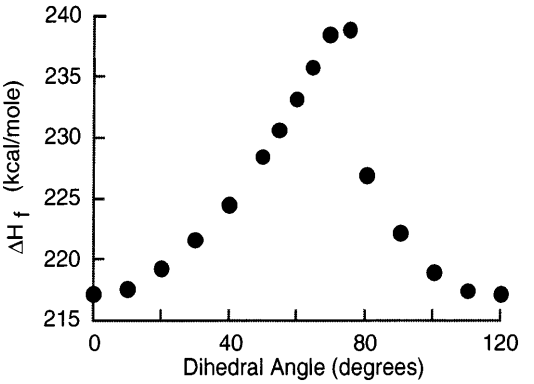

Fig. 15. Calculated (AM1) energetics for rotation around the triptycene/[4]helicene bond in **37a**. Clockwise rotation of the triptycene in **37a** corresponds to a left-to-right progression on the X-axis

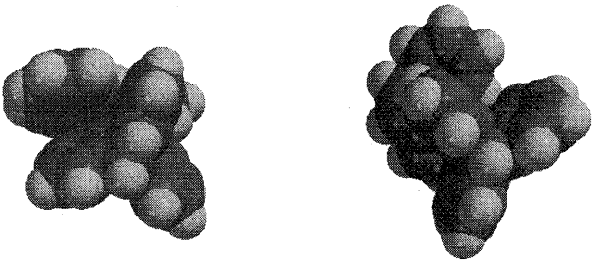

Fig. 16. Space-filling models of calculated minimum and maximum energy conformations of **37a**

depicts space-filling models corresponding to the minimum and maximum energy conformations of **37a**. Note the difference in the position of the helicene.

Based on the foregoing considerations we decided to first undertake the synthesis of the 1-triptycyl[4]helicenes **37**, whose anticipated barrier to rotation seemed most amenable to assessment by NMR. In order to study and compare the theoretical calculations, the synthesis of the 4-triptycylphenanthrene **36** was also carried out.

Compound **37b** was synthesized using a stilbene photocyclization approach; key steps in this route are the preparation of the aldehyde **40** and the final stilbene photocyclization (Scheme 7). The methyl group is incorporated to favor formation of the desired photocyclized product. The route is convergent and affords 1-triptycyl[4]helicene **37b** in 20% overall yield (4 steps).

Based on the experience obtained from the synthesis of the [4]helicene **37b**, we initially sought to prepare 4-(9-triptycyl)phenanthrene (**36**) also using a stilbene photocyclization strategy. Unfortunately, various photochemical approaches failed in the final photocyclization step. Given these results, we

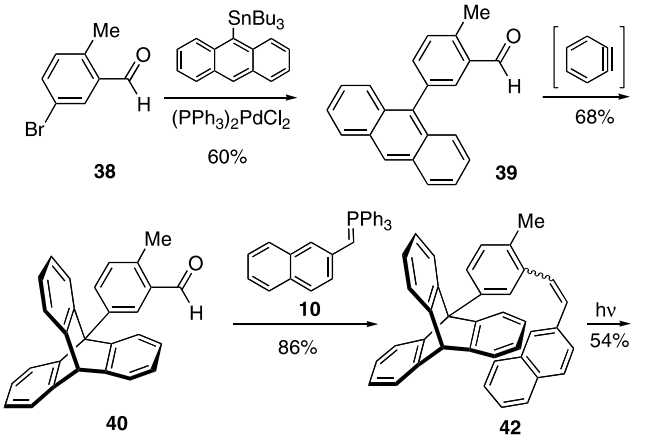

Scheme 7.

undertook the preparation of the 4-substituted phenanthrene using a non-photochemical route (Scheme 8). Starting from the known ketone **43** [42], the desired 4-(9-triptycyl)phenanthrene (**36**) was obtained in 23% overall yield (4 steps).

The dynamic behavior of **36** and **37b** was studied by analysis of NMR spectra recorded at various temperatures. The ^{1}H NMR spectra of **36** and **37b** indicate that at room temperature rotation around the triptycene/helicene bond is frozen in both compounds, but that the topology of the two is distinctly different. In particular, the ^{1}H NMR spectrum of **36** reveals a plane of symmetry (recall the engaged brake) since two (but not all three) of the rings of the triptycene unit are equivalent. The phenanthrene component of **36** is therefore either planar or exists as a rapidly racemizing mixture of two helicene enantiomers. Even at 160 °C, the upper temperature limit of our NMR

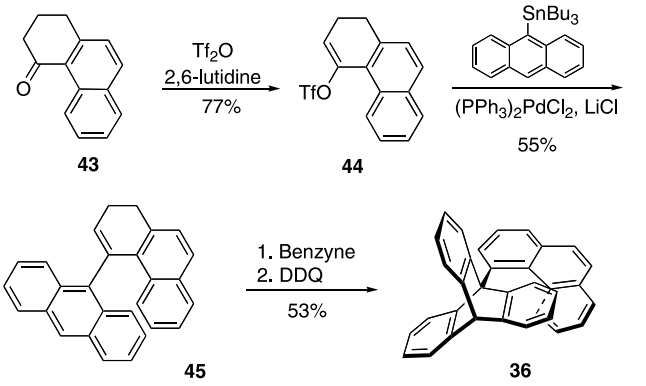

Scheme 8.

probe, ^{1}H NMR spin polarization transfer experiments (see below) reveal no detectable rotation of the triptycene in **36** within 2 s of polarization, which indicates a barrier ($\Delta G^{\ddagger}$) to rotation around the triptycene/phenanthrene bond in excess of 27 kcal mol^{-1}.

The ^{1}H NMR room temperature spectrum of **37b** reflects an absence of symmetry, where all three rings of the triptycene are nonequivalent. At 160 °C, but not at lower temperatures, however, some peak broadening of triptycene (but not helicene) resonances is observed, indicating somewhat less retarded rotation. Extrapolation, based on analogy to our earlier work with the molecular brake, suggests a coalescence temperature of about 220 °C, which corresponds to a $\Delta G^{\ddagger}$ of approximately 25 kcal mol^{-1}, a value that is corroborated by the studies described below and which is reassuringly close to the calculated barrier ($\Delta H^{\ddagger}$, not $\Delta G^{\ddagger}$) of 22 kcal mol^{-1}.

Given the above, it was of interest to establish the direction of rotation of the triptycene in **37b**. Preparation of isotopically labeled rotamers of **37b** should be possible, but would require extensive synthetic, rotamer-separation, and structure-determination efforts. Fortunately, the spin polarization transfer NMR technique [43] affords the same information at a small fraction of the effort. In short, if one has a system that is conformationally mobile, but that mobility is slow on the NMR time scale, then one can polarize the spin of a slowly conformationally mobile atom, wait an appropriate time, and assay where (if anywhere) that polarization has moved to.

In the present case, where the experimentally determined barrier ($\Delta G^{\ddagger}$) to rotation is approximately 24.5 kcal mol^{-1} [44], then at 160 °C a single rotamer has a half life of about 0.17 s. Thus, if one selectively polarizes one of the three H_a, H_b and H_c (see **46** in Fig. 17) protons and – after appropriate time delays – assays for the location of that polarization, a clearcut distinction between predominantly unidirectional rotation and bidirectional rotation is available. In the former case, a disproportionate share of the polarization that has moved should be transferred to a resonance for only one of the two other protons. In the latter case, the polarization that moves should be transferred equally to the remaining two resonances.

In the event, spin polarization of one (see **46**) of the three H_x protons in **37b** was achieved using a selective 180°-pulse-delay-observe sequence. As is evident from Fig. 17, the triptycene rotates clockwise and counterclockwise to the same extent. Control experiments polarizing the spin of each of the other two H_x protons give equivalent results.

The spin polarization transfer results demonstrate unequivocally that rotation occurs equally in both directions. That is, **37b** does not behave as a ratchet. (More subtle issues, such as how we distinguish between uni/bidirectional rotation and helicene racemization, and why it is not necessary to resolve racemic **37b** are addressed in the full paper [39b].)

The finding that the triptycene in **37b** rotates equally in both directions will come as no surprise to those who are fully aware of the more subtle consequences of the Second Law of Thermodynamics. But for many, especially those who have manipulated models of **37**, the finding is counterintuitive. And for those who have been seduced by the models, the

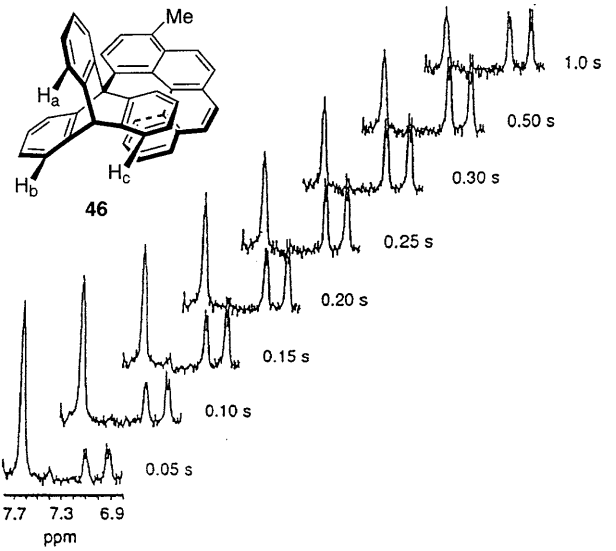

Fig. 17. Results of spin polarization transfer experiment at 160 °C (calibrated temperature). The resonances for H_a, H_b and H_c (see **46**) appear at δ 7.6, 7.1 and 6.9 ppm (not necessarily respectively). The spin of the proton resonating at δ 7.6 was polarized, and transfer of that polarization was monitored over time

substantial asymmetry of the energy curve (Fig. 15) for rotation around the triptycene/[4]helicene bond reinforces the expectation that rotation in one direction will be more facile than in the other. However, Fig. 15 contains a cautionary hint: the two energy minima flanking the energy maximum are equal in energy. More specifically, the expectation of a preferred direction of rotation overlooks an elementary consequence of energy diagrams which requires that, unlike mountain climbing, it is only the height of the summit, not the steepness of the ascent, that matters. Put another way, the principle of microscopic reversibility rules.

The finding that **37b** does not function as a ratchet is also reminiscent of the somewhat whimsical ratchet and pawl conundrum posed in 1962 by Nobel Laureate physicist Richard Feynman [45] and reiterated below.

"*Let us try to invent a device which will violate the Second Law of Thermodynamics, that is, a gadget which will generate work from a heat reservoir with everything at the same temperature. Let us say we have a box of gas at a certain temperature, and inside there is an axle with vanes in it (see Fig. 18 but take* $T_1 = T_2 = T$, *say). Because of the bombardments of gas molecules on the vane, the vane oscillates and jiggles. All we have to do is to hook onto the other end of the axle a wheel that can turn only one way – the ratchet and pawl. Then when the shaft tries to jiggle one way, it will not turn, and when it jiggles the other, it will turn. Then the wheel will slowly turn, and perhaps we might even tie a flea onto a string hanging from a drum on the shaft, and lift the flea! Now let us ask if this is possible. According to Carnot's*

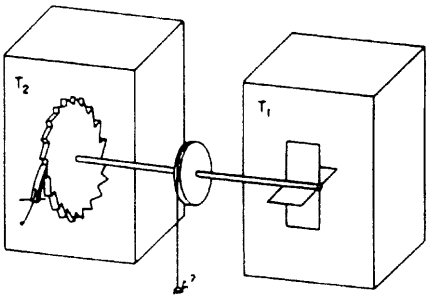

Fig. 18. The ratchet and pawl machine (reproduced from [45])

hypothesis, it is impossible. But if we just look at it, we see, prima facie, that it seems quite possible."

If one imagines taking Feynman's device (Fig. 18), shrinking the axle length to zero, and fusing the vanes to the ratchet wheel to give the assembly in Fig. 19, then **37b** is the functional equivalent of that assembly, except that in **37b** the triptycene functions simultaneously as the wheel and the vanes, and the helicene serves double duty as the pawl and the spring. The finding that **37b** rotates equally in both directions is contrary to the Feynman scenario excerpted above. But as Feynman recognized, his argument, while tantalizing, is specious. For Feynman's device, or our **37b**, to rotate unidirectionally without an input of energy would require the violation of the principle of microscopic reversibility and the Second Law of Thermodynamics.

In summary, the synthesis of triptycyl[4]helicene **37b** successfully incorporates into a single molecule the essential components of a simple ratchet: the asymmetric combination of a ratchet wheel, a pawl and a spring. Tantalizing as models of **37b** are, the experimental demonstration that **37b** rotates bidirectionally rather than unidirectionally illustrates the perils of extrapolating from macroscopic to molecular scales. It follows that molecular units such as **37** cannot be used to induce unidirectional rotation in an isothermal environment. Nonetheless, as becomes evident in the next section, their ability to modulate the barrier to free rotation makes them useful components of more complex systems such as molecular motors.

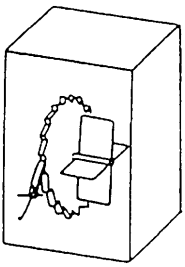

Fig. 19. Truncated version of Fig. 18

7
Molecular Rotary Motor

The design of a molecular system that functions as a motor has been one of the ultimate goals in our research group. After the earlier work on the design and synthesis of the molecular brake and "ratchet" devices, we conceived of a way to prepare a rotary molecular motor [46, 47]. The motor retains the components of the molecular "ratchet", but incorporates additional functionality. The energy to produce unidirectional rotation will in this case be obtained from phosgene, an energy-rich molecule. Chemical energy is the common fuel in biological motors, in the form of ATP or proton gradient force. To us, the double acid chloride phosgene is reminiscent of the energy-rich ATP.

As detailed in the preceding section, we previously established that the barrier to rotation of the triptycene rotor around the helicene bond in structure **37b** (Fig. 20) is approximately 25 kcal mol^{-1}, and that rotation occurs equally in both directions when thermal energy is applied to the system; that is, the molecular system works more as a brake than a ratchet. The essence of converting **37b** into a molecular motor involves continuing the friction-braking action to prevent counterclockwise rotation, while using the chemical energy of phosgene to harvest ambient thermal energy, thereby selectively fostering clockwise rotation of the triptycene rotor.

The basic strategy to produce the unidirectional rotation is presented in detail in Fig. 21. We start with a molecule related to **37b** whose rotational ground state is ca. 25 kcal mol^{-1} below the summit (see Fig. 21b), but which could be trapped (schematically represented by a brick wall in Fig. 21d; in actuality we use a tether) somewhat above that minimum by using a phosgene-powered chemical reaction. That trapping stations the trapped species in a "base camp" energetically closer to the summit, and within easier (relative to Fig. 21b) thermal reach of the mountaintop. Once the summit is achieved (Fig. 21e), descent down the other side of the E_{act} mountain then releases 25 kcal mol^{-1} of energy, which immediately diffuses through the system and thus is not directly available to drive the more energy-intensive reverse reaction (25 kcal mol^{-1} contrasted to the less demanding Fig. 21, **d** → **e** forward process). Put another way, states **b** and **f** in Fig. 21 are isoenergetic,

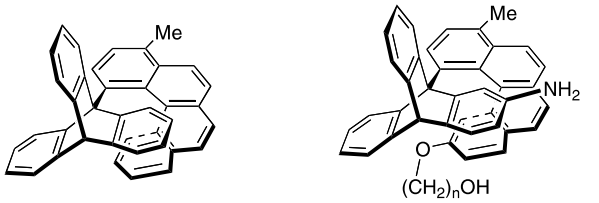

37b

47, n = 3 (as a mixture of atropisomers)
48, n = 2 (as a mixture of atropisomers)

Fig. 20. "Ratchet" and motor prototypes

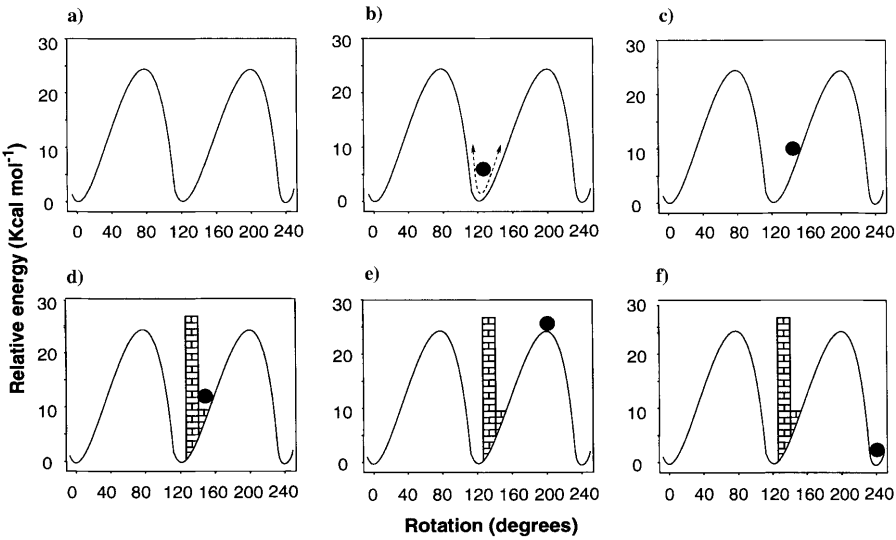

Fig. 21. Schematic representation of the concepts underlying the design of the system (see text)

and the rates of the **b** → **f** and **f** → **b** conversions will be identical; but by using the chemical energy of phosgene to trap **b** in the form of **c**, **c** → **f** is an exothermic transformation, and unidirectional rotation is driven by the negative value of ΔG for the **c** → **f** transformation.

The molecules chosen as prototypes for a molecular rotary motor are **47** and **48** (Fig. 20). Compounds **47** and **48** differ from each other only by the length of the hydroxyalkoxy tether (vide infra). They were selected for several reasons. First, we wanted to use molecules as close in structure to **37b** as possible, so that the knowledge acquired in the context of **37b** could be most directly brought to bear. In particular, we hoped that by making as few changes as possible, we would be able to maintain the close agreement between experiment and molecular modeling found with **37b** (the use of calculated $\Delta H^{\ddagger}$ values to predict experimentally determined $\Delta G^{\ddagger}$ values is not rigorous, but we have found it quite useful). Furthermore, we sought, by selecting **47** and **48** as targets, to make the synthetic component of the project no more difficult than necessary, by having the synthesis be as derivative of the synthesis of **37b** as possible.

Scheme 9 provides (using **47** for purposes of illustration) molecular detail for the concepts outlined in Fig. 21. In essence, the proof of principle for the molecular motor starts with **47a**. Compound **47a** is one of three low-energy rotational isomers (rotamers) about the axle connecting the triptycene and helicene components (**47b** is a second low-energy rotamer). Rotamer **47a** is activated by reaction with phosgene to give the isocyanate **49**. Isocyanate **49** is chemically "armed" to react with the OH group in the hydroxypropyl tether attached to the helicene, but, in the rotational ground state **49**, the isocyanate

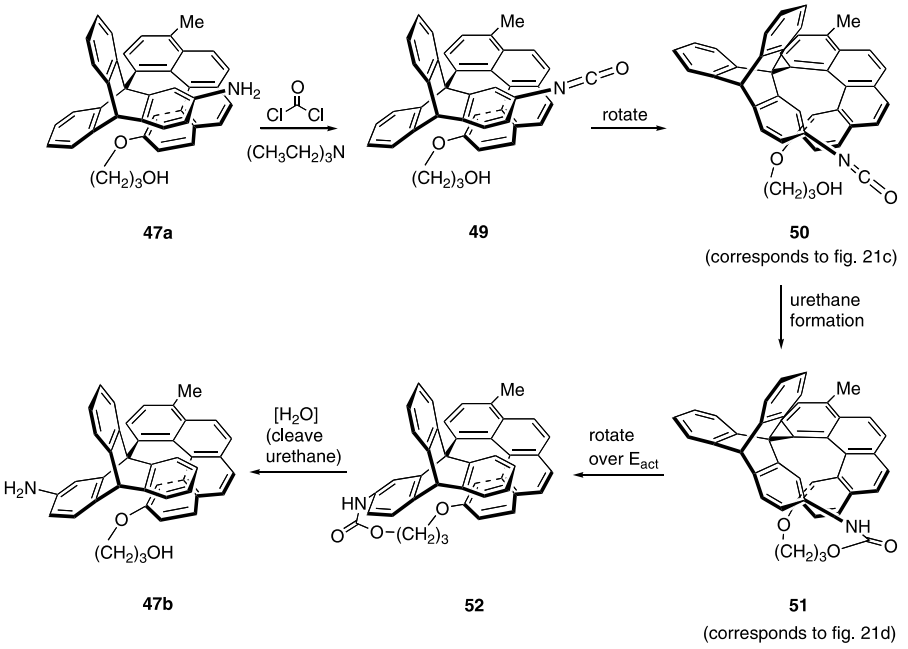

Scheme 9. Proposed sequence of events in the chemically powered rotation of **47a** to **47b**

and the OH group are too far apart to interact. However, at those instants when a clockwise rotation of the triptycene (not possible with a comparable counterclockwise rotation) brings the isocyanate and the OH group sufficiently close to react (see **50**), urethane formation (→**51**) can then result, irreversibly trapping the triptycene in a relatively high (compared to **49**; also see Fig. 21d vs. 21b) energy conformation around the triptycene/helicene axle. Ambient thermal energy would then drive the exoergic unidirectional rotation from **51** to **52**. Finally, **52** is cleaved to **47b**, thereby completing the chemically driven rotation of **47a** to **47b**.

The synthesis of **47** and **48** is more difficult than the synthesis of the nonfunctionalized system **37b**, in part because the lack of symmetry in the triptycene leads to a mixture of three interconvertible rotamers that must be isolated and identified. Nevertheless, the synthetic strategy developed is heavily based on the previous synthesis (see Sect. 6) of **37b**. As summarized retrosynthetically in Scheme 10, the key steps for the synthesis of **47** and **48** are the preparation and photocyclization of the stilbene **54** containing the triptycene unit. Stilbene **54** would be formed by a Wittig reaction between aldehyde **55** and the ylide **56**. Photocyclization and cleavage of the methyl ether would give phenol **53** which should allow the incorporation of tethers of variable length to give **47** or **48**.

Aldehyde **55** was prepared (see Scheme 11) from 2-aminoanthracene (**57**) in a five-step sequence which commenced with protection of the amino group,

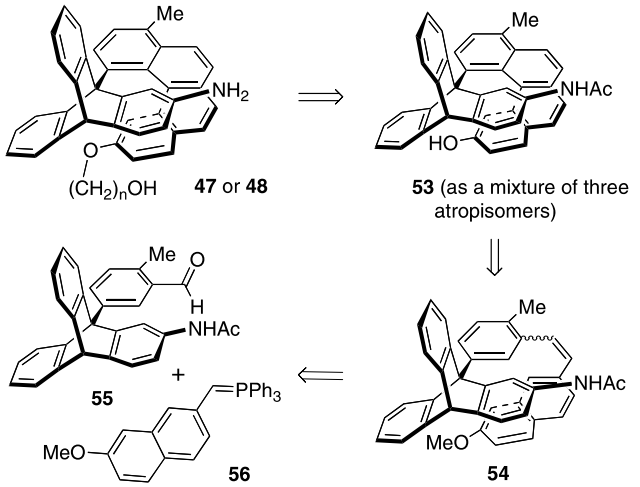

Scheme 10.

followed by bromination, and transformation to the boronic acid **60**. After Suzuki coupling of **60** with **61**, a regioselective Diels-Alder addition of benzyne across the central ring of the anthracene afforded the desired aldehyde **55**.

Wittig reaction (Scheme 12) between the aldehyde **55** and the ylide **56**, which was prepared from 7-methoxy-2-naphthol [47], gave stilbene **54** as a

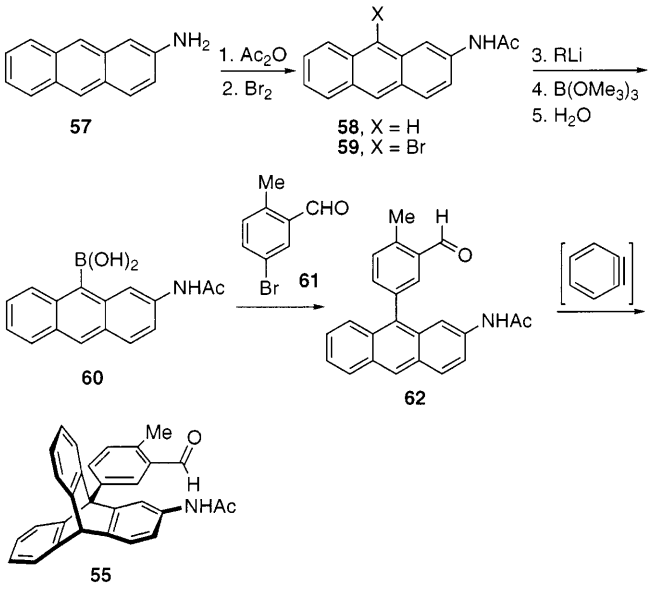

Scheme 11.

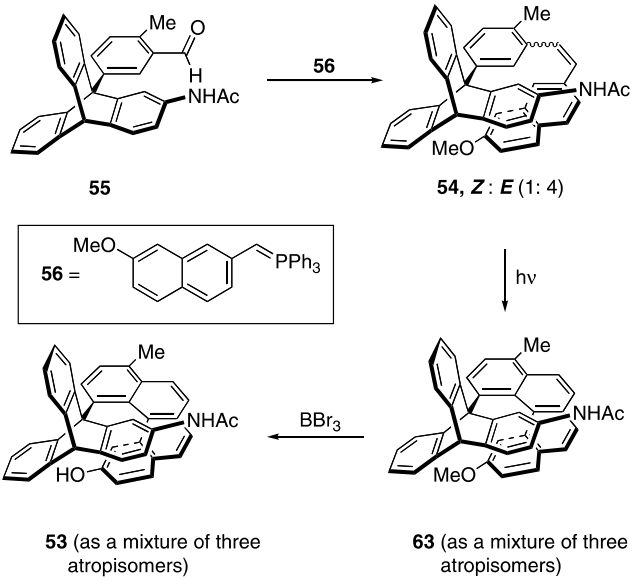

Scheme 12.

mixture of *cis*/*trans* isomers in a 1:4 ratio. Photocyclization of **54** led, after careful and protracted experimental studies, to the 1-triptycyl[4]helicene **63** in 40% yield as a mixture of atropisomers [48]. Treatment of **63** with BBr_3 afforded the desired phenol **53**.

With the basic skeleton of **47** and **48** in hand, we proceeded to incorporate the tethers (Scheme 13). The three-carbon tether was attached to the helicene unit by reacting the phenol of **53** with 3-bromo-1-propanol under basic conditions. Deprotection of the acetamide in **64** with KOH at reflux afforded the desired molecular rotary motor prototype **47** as a mixture of atropisomers. In an analogous way, the two-carbon tether was introduced by reaction of the phenol **53** with the methoxymethyl (MOM) ether of 2-bromoethanol. Deacetylation with KOH (→**66**) and removal of the MOM group under acidic conditions led to the two-carbon tether molecular motor prototype **48**, again as a mixture of three rotamers (Scheme 13).

With the two molecular systems in hand, we then set out to separate and identify each of the three atropisomers of **47** and **48**. After extensive attempts, we found that by using semipreparative thin layer chromatography plates (0.25 mm thick silica, 20 × 20 cm), the rotamers could be separated in excellent yield, although it was necessary to use cold solvents to avoid thermal interconversion of individual atropisomers during the isolation process. The conformations of individual atropisomers were initially tentatively assigned by use of 1- and 2-D low temperature ^{1}H NMR spectroscopy. The initial assignments were then confirmed by reaction with phosgene and triethylamine as discussed below.

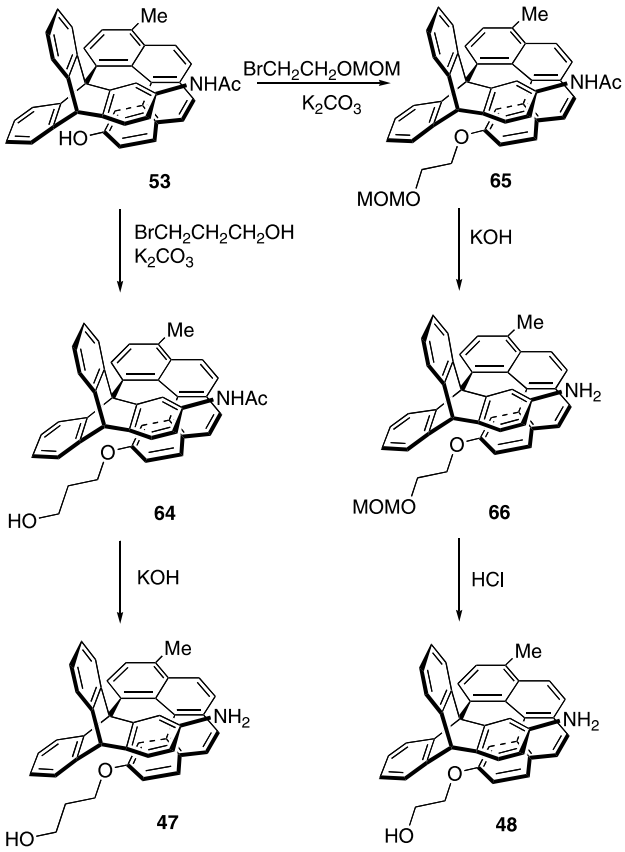

(All compounds shown are a mixture of three atropisomers around the triptycene/helicene bond.)

Scheme 13.

After separating and determining the structures of atropisomers **47a**, **b** and **c** (Fig. 22) by ^{1}H NMR spectroscopy, we evaluated whether it would be better to form urethane **49** from **47a** and phosgene by way of a carbamoyl chloride or an isocyanate. Semi-empirical calculations at the PM3 level carried out on the appropriate derivatives of structure **47a** indicated that formation of the corresponding carbamate from a carbamoyl chloride would be an endothermic process ($\Delta H = +1$ kcal mol^{-1}). However, formation of the carbamate from the corresponding isocyanate would be substantially exothermic ($\Delta H = -12$ kcal mol^{-1}). Accordingly, carbamate formation via isocyanate was chosen. In model studies with the simple triptyceneamine **67** and naphthol **68** (Fig. 22) we found that use of 5 equiv of triethylamine in the reaction of **67** with phosgene resulted in complete and rapid formation of isocyanate without accumulation of the carbamoyl chloride.

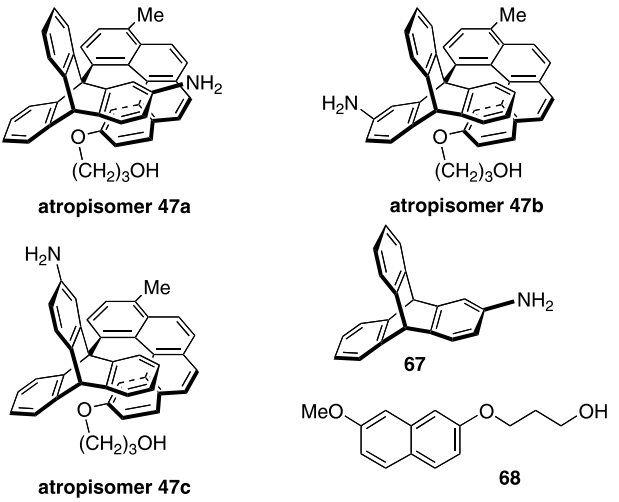

Fig. 22. Atropisomers of **47** and compounds for model studies

When atropisomer **47b** was treated with 1 equiv of phosgene (20% solution in toluene), followed by the addition of triethylamine (5 equiv), the rapid formation of carbamate **52** was seen (Scheme 14) but, importantly, **52** did not convert to **51**. In contrast, the reaction of atropisomer **47a** under the same conditions resulted, ultimately, in the formation of "post-barrier"

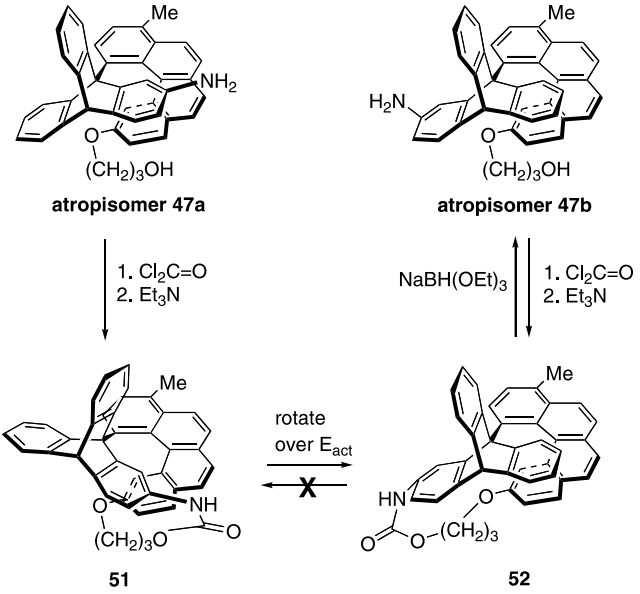

Scheme 14.

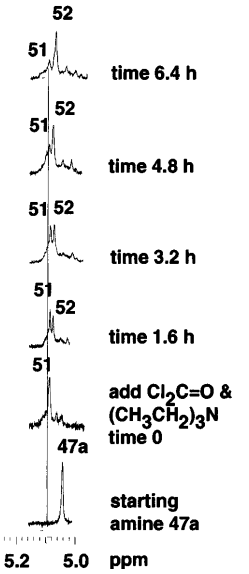

Fig. 23. ^{1}H NMR data (monitoring peaks for bridgehead protons) demonstrating the formation of **47a** to **51** and the conversion of **51** to **52** over time. Structural assignments were independently confirmed by ReactIR technology [49]

carbamate **52** via "pre-barrier" carbamate **51** (Fig. 23). Given the cleavage of **52** to **47b** mentioned above, *the unidirectional rotation of* **47a** *to* **47b** *had been achieved and a prototype of a molecular motor was in hand!*

The phosgene-promoted conversion of **47a** to **47b** constitutes the proof of principle of the first rationally designed, chemically powered molecular motor. Once the prototype molecular motor **47** had been shown to function as desired, we proceeded to study the rotation of the analogous molecular system **48**, where the tether contains only two carbons. Based on earlier considerations (Fig. 21 and Scheme 9), one would predict that use of a shorter tether should give a "pre-barrier" carbamate closer in energy to the summit. Such a situation should reduce the amount of time needed for rotation to the "post-barrier" carbamate **52** and therefore increase the speed of rotation.

When the rotamer **48a** was treated under the same reaction conditions [phosgene (1 equiv) and Et_3N (5 equiv)] as used with **47a**, a 3:1 mixture of isocyanate **69** and carbamate **70** (Fig. 24) was formed. Investigative studies showed that isocyanate **69** does not convert to carbamate **70** (apparently due to geometric constrains) and that formation of **70** occurs through the carbamoyl chloride **71** (Scheme 15).

Accordingly, experimental conditions [phosgene mixed with 2,6-di(*tert*-butyl)pyridine and addition of triethylamine (5 equiv)] that favor the formation of the carbamoyl chloride **71** rather than isocyanate **69** were chosen. The result is that the "post-barrier" carbamate **70** was formed from

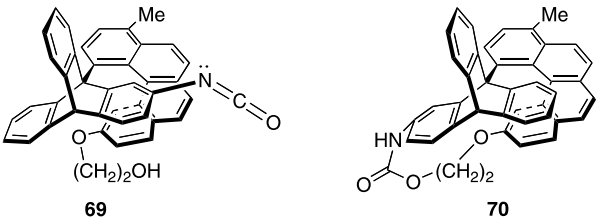

Fig. 24. Products from reaction of **48a** with phosgene under original reaction conditions

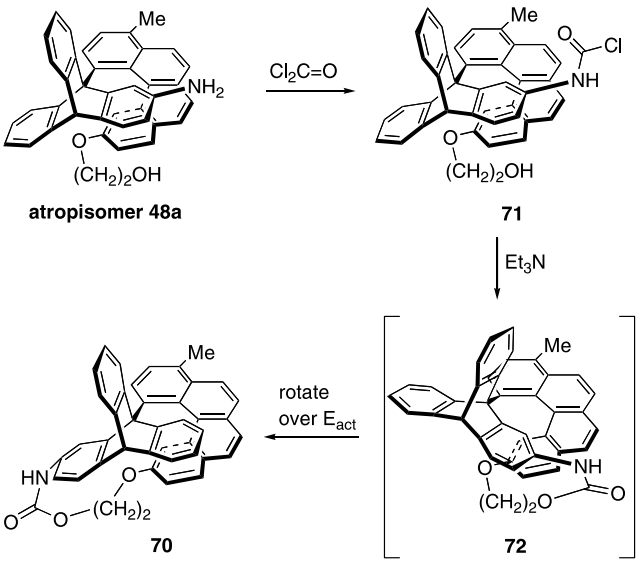

Scheme 15.

48a almost exclusively in a period of 80 min (see Fig. 25) without detection of "pre-barrier" carbamate **72**. Furthermore, treatment of **48a** and 2,6-di(*tert*-butyl)pyridine with phosgene and 14 equiv of triethylamine gave identical results but required only 15 min for reactions and rotation of **48a** to **70** to be completed.

The important conclusions from the study of **48a** (Fig. 25) rather than **47a** (Fig. 23) are that while the details (carbamoyl chloride rather than isocyanate) are different, the use of a shorter tether not only accelerates the speed of rotation, but also changes the rate-limiting step from rotation over the barrier to formation of the carbamate.

The chemically powered unidirectional rotation of **47a** to **47b** constitutes a proof of principle of the first rationally designed molecular motor. Much optimization remains to be done before we achieve a molecular system that rotates continuously and rivals the speed of its biological and mechanical counterparts. The next step, however, is now clear: To achieve repeated

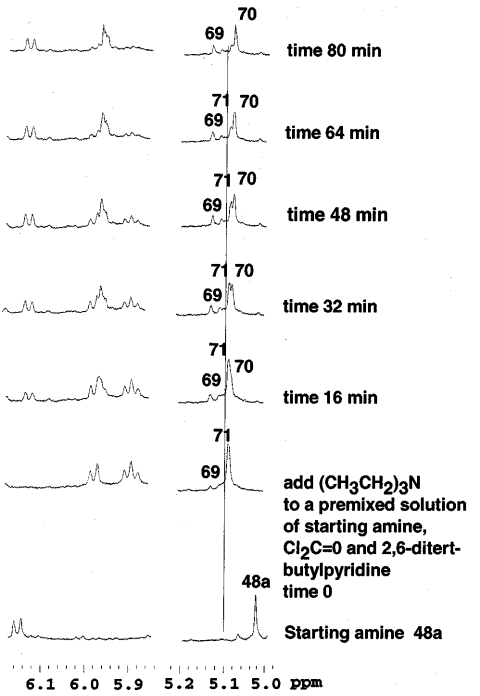

Fig. 25. ^{1}H NMR spectroscopic monitoring of the unidirectional conversion of **48a** to "post-barrier" carbamate **70** via carbamoyl chloride **71**. Isocyanate **69** does not participate

rotation by modifying **48a** so that each blade of the triptycene is ready to be selectively armed at the appropriate time, and to include in the system (probably by attachment to the helicene) units with the appropriate spatial positioning that can capture and deliver $Cl_2C{=}O$ and cleave the urethane, as represented schematically in Fig. 26. Efforts in that direction are now in progress. Meanwhile, the concepts underlying the present work should be of general application to the understanding of biological and other motors.

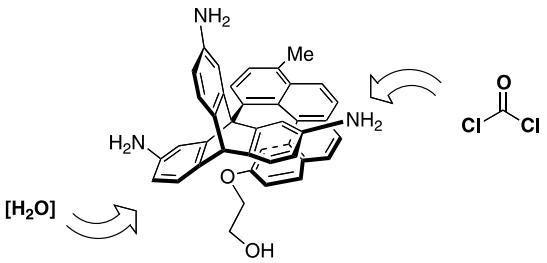

Fig. 26. Schematic representation of a continually operating molecular motor

8 Conclusions

Over the last 10 years, efforts of several groups have led to the synthesis of a variety of molecular devices that exhibit controlled or coordinated rotation. In our research group the ultimate achievement has been the synthesis of a molecular system that functions as a prototype of a motor. This work was possible thanks to the experience gained in preparing a molecular brake and "ratchet".

The utility of these systems in nanochemical engineering is still far in the future but their study has contributed to identifying some of the perils and promise of extrapolating macroscopic principles to the molecular level, and has provided conceptual insight into the operation of biological motors.

Acknowledgements. This work would not have been accomplished without the dedicated efforts of the coworkers named in the references. We thank them for their enormous contributions and the National Institutes of Health (grant GM56262) for partial support.

9 References

1. (a) Drexler KE (1992) Nanosystems: molecular machinery, manufacturing and computation. Wiley, New York; (b) Lehn J-M (1995) Supramolecular chemistry, VCH, Weinheim, Germany; (c) Dugas H (1996) Molecular devices. In: Canton CR (ed) Bioorganic chemistry, 3rd edn. Springer-Verlag, New York; (d) Balzani V, Gómez-López M, Stoddart JF (1998) Acc Chem Res 31: 405; (e) Sauvage J-P (1998) Acc Chem Res 31: 405
2. Feynman RP (1961) In: Gilbert HD (ed) Miniaturization. Reinhold Publishing Corp, New York, p 282. The article is also available on the Internet at http://nano.xerox.com/nanotech/feynman.html
3. Drexler KE (1991) Science and the future 1990. In: Encyclopedia Britannica, Chicago, p 162
4. Magnasco MO (1994) Phys Rev Lett 72: 2656
5. Magnasco MO (1993) Phys Rev Lett 71: 1477
6. Astumian RD, Bier M (1994) Phys Rev Lett 72: 1766
7. (a) Leibler S, Huse DA (1993) J Cell Biol 121: 1357; (b) Prost J, Chauwin JF, Peliti L, Ajdari A (1994) Phys Rev Lett 72: 2652; (c) Doering CR, Horsthemke W, Riordan J (1994) Phys Rev Lett 72: 2984
8. Faucheux LP, Bourdieu LS, Kaplan PD, Libchaber AJ (1995) Phys Rev Lett 74: 1504
9. For an overview, see Travis J (1995) Science 267: 1593
10. Vale RD, Oosawa F (1990) Adv Biophys 26: 97
11. Alberts B, Miake-Lye R (1992) Cell 68: 415
12. Stryer L (1995) Molecular motors. In: Biochemistry, 4th edn. WH Freeman and Co, New York, Ch 15
13. Voet D, Voet JG (1995) Biochemistry, 2nd edn. Wiley, New York
14. Only in very recent studies of ATP synthase, which is powered by a proton gradient, has an atomic-level explanation of function begun to emerge: (a) Boyer PD (1998) Angew Chem Int Ed Eng 37: 2296; (b) Walker JE (1998) Ibid 37: 2308; (c) Elston T, Wang H, Oster G (1998) Nature 391: 510
15. Block SM (1997) Nature 386: 217

16. Noji H, Yasuda R, Yoshida M, Kinosita K Jr (1997) Nature 386: 299
17. Mitchell P (1979) Science 206: 1148
18. Howard J (1997) Nature 389: 561
19. For a thought provoking collection of examples, see Brown HT (1984) 507 Mechanical movements, 17th edn. Lindsay Publications, Bradley, IL
20. For reviews on molecular gears, see (a) Iwamura H, Mislow K (1988) Acc Chem Res 21: 175; (b) Mislow K (1989) Chemtracts-Org Chem 2: 151; (c) Gakh A, Sachleben RA, Bryan JC (1997) Chemtech 27: 26
21. For a review on triptycenes, see Skvarchenko VR, Shalaev VK, Klabunovskii EI (1974) Russ Chem Rev 43: 951
22. (a) Oki M (1976) Angew Chem Int Ed Engl 15: 87; (b) Oki M (1983) Top Stereochem 14: 1
23. (a) Koga N, Iwamura H (1985) J Am Chem Soc 107: 1426; (b) Iwamura H (1985) J Mol Struct 126: 401; (c) Koga N, Iwamura H (1986) Chem Lett 247
24. (a) Guenzi A, Johnson CA, Cozzi F, Mislow K (1983) J Am Chem Soc 105: 1438; (b) Kawada Y, Iwamura H (1983) J Am Chem Soc 105: 1449
25. Kawada Y, Iwamura H (1981) Tetrahedron Lett 22: 1533
26. (a) Dudley DW (1969) The evolution of the gear art. American Gear Manufacturers Association, Washington, DC; (b) de Solla Price DJ (1959) Sci Am 200: 60
27. (a) Koga N, Kawada Y, Iwamura H (1983) J Am Chem Soc 105: 5498; (b) Koga N, Kawada Y, Iwamura H (1986) Tetrahedron 42: 1679
28. Gakh AA, Sachleben RA, Bryan JC, Moyer BA (1995) Tetrahedron Lett 36: 8163
29. Vogtle F, Mew PKT (1978) Angew Chem Int Ed Engl 17: 60
30. Bedard TC, Moore JS (1995) J Am Chem Soc 117: 10662
31. Zhang J, Moore JS (1994) J Am Chem Soc 116: 2655
32. (a) Zhang J, Moore JS, Xu Z, Aguirre RA (1992) J Am Chem Soc 114: 2273; (b) Moore JS, Zhang J (1992) Angew Chem Int Ed Engl 31: 922; (c) Zhang J, Pesak DJ, Ludwick JL, Moore JS (1994) J Am Chem Soc 116: 4227; (d) Wu Z, Lee S, Moore JS (1992) J Am Chem Soc 114: 8730
33. Sandstrom J (1982) Dynamic NMR spectroscopy, Academic Press, England
34. Goodby JW, Blinc R, Clark NA, Lagerwall ST, Osipov MA, Pikin SA, Sakurai T, Yoshino K, Zeks B (1991) Ferroelectric liquid crystals: principles, properties, and applications, Gordon and Breach Science Publishers, Amsterdam
35. Kelly TR, Bowyer MC, Bhaskar KV, Bebbington D, García A, Lang F, Kim MH, Jette MP (1994) J Am Chem Soc 116: 3657
36. See supplementary material of preceding reference
37. The isoquinoline was prepared from 1-naphthaleneacetic acid by a four-step sequence [36]
38. (a) Bringmann G, Walter R, Weirich R (1990) Angew Chem Int Ed Engl 29: 977; (b) Knight DW (1993) In: Trost BM, Fleming I (eds) Comprehensive organic synthesis, vol 3. Pergamon Press, Oxford, p 481
39. (a) Kelly TR, Tellitu I, Sestelo JP (1997) Angew Chem Int Ed Engl 36: 1866; (b) Kelly TR, Sestelo JP, Tellitu I (1998) J Org Chem 63: 3655
40. For reviews of helicene chemistry, see (a) Martin RH (1974) Angew Chem Int Ed Engl 13: 649; (b) Laarhoven WH, Prinsen WJC (1984) Top Curr Chem 125: 63; (c) Meurer KP, Vögtle F (1985) Top Curr Chem 127: 1. Some more recent papers; (d) Liu L, Katz TJ (1990) Tetrahedron Lett 31: 3983; (e) Willmore ND, Liu L, Katz TJ (1992) Angew Chem Int Ed Engl 31: 1093; (f) Janke RH, Haufe G, Würthwein E, Borkent JH (1996) J Am Chem Soc 118: 6031
41. Calculations (AM1) were carried out using the coordinate drive feature of the Spartan molecular modelling program (Wavefunction, Inc., Irvine, CA), Version 4.0, on a Silicon Graphics workstation
42. Huggenberg S, Hesse M (1980) Helv Chem Act 63: 2295
43. For leading references to the spin polarization transfer method, see (a) Dahlquist FW, Longmur KJ, Du Vernet RB (1975) J Magn Reson 17: 406; (b) Frim R, Zilber G,

Rabinovitz M (1991) J Chem Soc Chem Commun 1202; (c) Abdourazak AH, Sygula A, Rabideau PW (1993) J Am Chem Soc 115: 3010. For a more general review of the application of 2-D NMR spectroscopy to the kinetics of exchange processes, see Perrin CL, Dwyer TJ (1990) Chem Rev 90: 935
44. The value of $\Delta G^{\ddagger}$ is calculated from the half life obtained from the data in Fig. 17. See, for example, Scudder PH (1992) Electron flow in organic chemistry, Wiley, New York, p 38
45. Feynman RP, Leighton RB, Sands M (1963) The Feynman lectures on physics, vol 1. Addison-Wesley, Reading, MA, chap 46
46. Kelly TR, De Silva H, Silva RA (1999) Nature 401: 150
47. For a report of a light-powered molecular motor, see Koumura N, Zijlstra RWJ, van Delden RA, Harada N, Feringa BL (1999) Nature 401: 152
    Note added in press: We were under the misimpression that a chapter detailing that work would be included in this volume, so we did not discuss it. We regret the omission
48. Kelly TR, Silva RA, De Silva H, Jasmin S, Zhao Y (2000) J Am Chem Soc 122: 6935
49. ASI Applied Systems, Millersville, MD 21109, USA. For a bibliography of applications, see www.asirxn.com

Molecular Machines and Motors Based on Transition Metal-Containing Catenanes and Rotaxanes

Laurence Raehm, Jean-Pierre Sauvage

Laboratoire de Chimie Organo-Minérale, UMR 7513 du CNRS, Université Louis Pasteur, Faculté de Chimie, 4, rue Blaise Pascal, 67070 Strasbourg Cedex France
E-mail: sauvage@chimie.u-strasbg.fr

Molecular motors of various kind (linear, rotary) are very common in biology where they play an essential role. However, the number of synthetic molecular ensembles whose dynamic behavior is reminiscent of biological motors is presently very limited. In order for an object to be regarded as a motor, several basic requirements have to be fulfilled. Even without trying to apply a strict thermodynamic definition, the system will have to convert a certain type of energy into another form of energy, while undergoing some kind of continuous motion. Threaded or interlocked rings are ideally suited to the construction of fully artificial molecular motors. If a ring is threaded onto a rod, it can either rotate around the axle or undergo a translation movement. Similarly, in catenanes, a ring can glide at will within another ring. Several examples of such compounds have been elaborated and studied in recent years, using threaded and interlocked molecules either based on acceptor-donor and hydrogen-bonded complexes or on transition metal complexes.

Keywords: Molecular motions, Rotaxanes, Catenanes, Copper, Electrochemistry

1 Introduction 55

2 Molecular Motions in Transition Metal-Containing Rotaxanes . . 58

2.1 Electrochemically-Driven Translation of a Ring on the Molecular String on Which It Is Threaded 58
2.2 Pirouetting of a Wheel Around Its Axle: Towards Rotary Motors . 66

3 Electrochemically-Driven Ring Gliding Motion in Catenanes . . . 72

3.1 A Two-Geometry Catenane 72
3.2 A Three-Configuration Copper Catenane 74

4 Conclusion and Perspectives 75

5 References 77

1 Introduction

In biology, many "molecular motors" or "machines" play essential roles. These systems are multicomponent assemblies undergoing large amplitude geometrical changes or leading to the locomotion of one of the components,

Structure and Bonding, Vol. 99

either under the action of an external stimulus (pH change, redox process, light pulse, etc.) or of a chemical gradient. Many examples of proteins are known which undergo important shape modifications (folding-defolding) after a signal has been sent to the protein [1–5]. Real molecular motors consist of several units among which some parts will be considered as motionless and some others will move continuously while a "fuel" is "burnt", which translates, in biological systems, as: ATP is hydrolyzed. Linear motors such as myosin-actin [6–9] (from skeletal muscle) have been known for many years and knowledge about them has made considerable progress recently. By contrast, few rotary motors have been identified and investigated [10, 11]. The most spectacular example is that of ATPase [12–16], whose rotational motion was postulated long ago but which could be directly observed only recently. ATPase consists of a "stator", with 6 proteins ($\alpha_3\beta_3$) assembled to form a cylinder-like unit, a seventh, rod-like, protein (γ) being threaded in the hollow part of the $\alpha_3\beta_3$ unit to form the "rotor" (Fig. 1). The γ subunit rotates inside the $\alpha_3\beta_3$ assembly with concomitant hydrolysis of ATP, or ATP synthesis when a pH gradient is present.

The number of synthetic molecular ensembles whose dynamic behavior is reminiscent of biological motors is presently very limited. If a ring is threaded onto a rod, it can either rotate around the axle or undergo a translation movement. Similarly, in catenanes (i.e., compounds consisting of two interlocking rings), a ring can glide at will and spin within another ring. Recently, a new dimension has been added by moving components of these

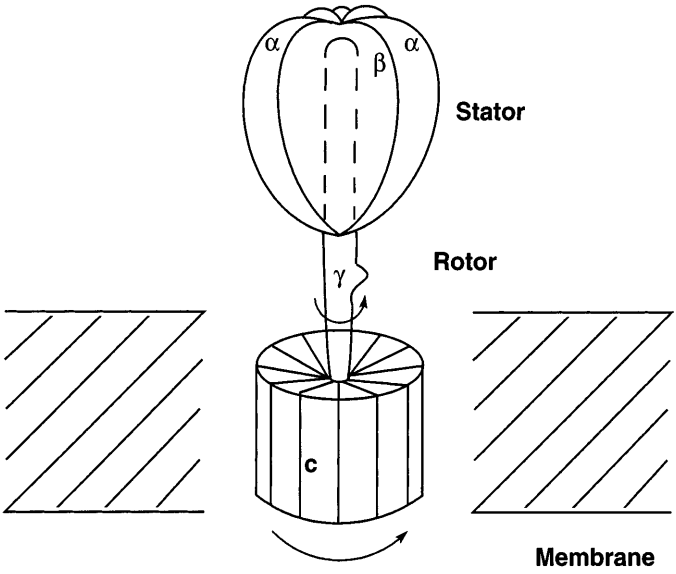

Fig. 1. A schematic representation of ATP synthase, a biological rotary motor: γ (and c) are mobile whereas the aggregate $\alpha_3\beta_3$ is fixed to the membrane and constitutes the stator of the motor

molecular systems at will, under the action of a photochemical or electrochemical signal. In fact, compounds containing interlocking rings or rings threaded onto an acyclic fragment are the ideal precursors to molecular machines, i.e., multi-component systems for which selected parts can be set in motion while the other fragments remain motionless. As schematically represented in Fig. 2, these topologies provide the working parts of the machines or motors to be elaborated.

Molecules whose shape is modified from the outside by sending a signal to the system are of course numerous. However, molecular machines tend to refer to *large amplitude* motions leading to real translocation of some parts of the compound, reversibility being of course an essential feature of the system. Several examples of such compounds have been elaborated and studied in recent years, using threaded and interlocked molecules either based on acceptor-donor and hydrogen-bonded complexes [17] or on transition metal complexes [18, 19]. In the purely organic systems, interesting processes have been evidenced, such as dethreading of an acyclic component from a ring under the action of light or translation of a ring between two distinct positions of a thread, induced by a redox signal. The group of Stoddart has recently created a vast and new family of interlocking and threaded compounds constructed on acceptor-donor aromatic complexes. This remarkable synthetic work has been sustained by very elegant photochemical and electrochemical studies carried out in Balzani's [20–23] and Kaifer's [24] groups, respectively. These authors have demonstrated that molecular movements can be induced in such systems, either by irradiating the compounds with visible light in the presence of other additional reagents acting as an electron donor or acceptor, or by using electrochemical reactions (Fig. 3).

Inorganic systems based on linkage isomerism induced by changing the metal oxidation state are also know [25–32]. For instance, a sulfoxide is

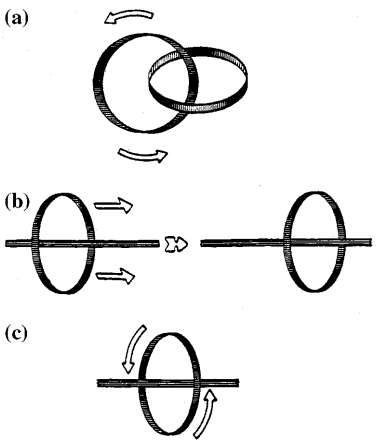

Fig. 2. Interlocking rings and threaded systems can be considered as elemental working parts of future molecular machines. (**a**) A [2]-catenane in motion. (**b**) Translation of a ring on an axle. (**c**) A wheel and axle in action

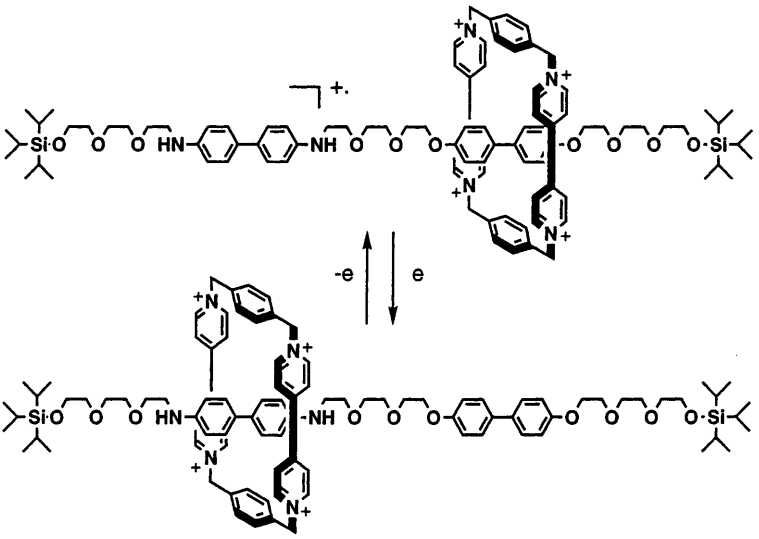

Fig. 3. A switchable rotaxane based on acceptor-donor complexes [24]. Before oxidation, the electron acceptor (ring) interacts preferentially with the benzidine nucleus (donor). After electrochemical oxidation of the latter, the ring is shifted towards the biphenol group. The process is reversible

O-bonded to ruthenium(III) in its stable form (Ru-OSR_2). By reducing the metal to the divalent state, the O-bonded species obtained at first rearranges to afford the stable S-bonded complex [Ru-$S(O)R_2$]. In an elegant study, Taube and Sano have shown that this principle can lead to molecular hysteresis [32–36]. Another pertinent example of redox-induced movement is based on a multifunctional system incorporating sets of ligands forming two distinct coordination sites, adapted to either Fe(II) or Fe(III) [37, 38]. By changing the iron oxidation state, translocation of the metal is observed (Fig. 4).

In a recent paper, Feringa and coworkers [11] have shown that it is possible to induce a repetitive, monodirectional rotation around a central carbon–carbon double bond in a chiral, helical alkene, with each 360° rotation involving four discrete isomerization steps activated by ultraviolet light or a change in the temperature of the system (Fig. 5).

2
Molecular Motions in Transition Metal-Containing Rotaxanes

2.1
Electrochemically-Driven Translation of a Ring on the Molecular String on Which It Is Threaded

The synthetic strategy developed in our group for making rotaxanes relies on the ability of copper(I) to gather the two constitutive organic fragments (a ring incorporating a bidentate chelate and an open-chain component) and to force

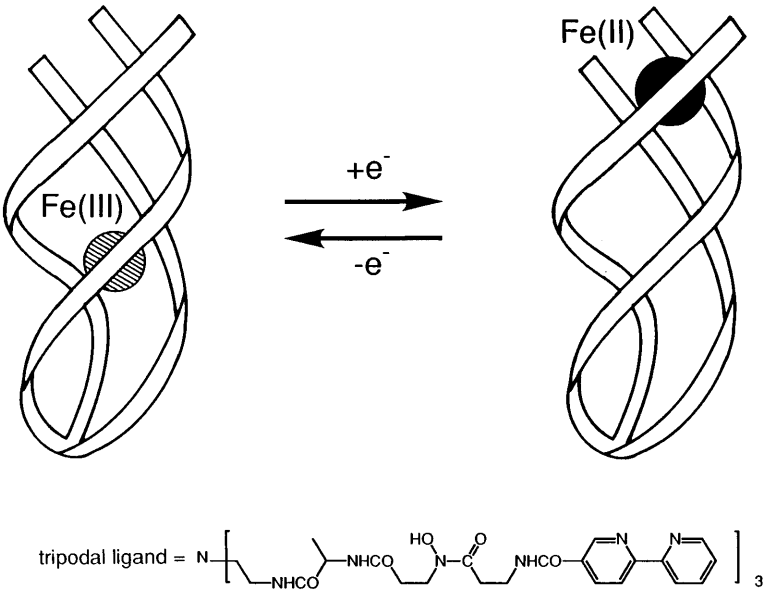

Fig. 4. Hopping of an iron center between two coordination sites. In the stable form of the Fe(II) complex, the metal is bound to three bipy ligands. After oxidation to Fe(III), the metal center moves to the anionic site [37]

the string to thread through the ring. This threading step is generally quantitative provided that the stoichiometry of the reaction is carefully respected, due to the selective formation of very stable tetrahedral copper(I) complexes (Fig. 6a). It can be extended to strings containing two identical coordination sites, thus permitting the threading of two identical rings (Fig. 6b) [39–41]. It can also be generalized to molecular strings containing two *different* sites, such as *bi*dentate and *ter*dentate coordinating units (Fig. 6c). In this case, again because of the very strong preference of copper(I) for 4-coordinate complexes (tetrahedral or distorted tetrahedral), the threading process will be very selective and lead to a situation in which the ring is exclusively associated with the bidentate chelate fragment of the string, in its coordination to copper(I), as indicated in Fig. 6c [42, 43].

It is of course this latter compound which will be prompted to undergo motions by changing the redox state. This particular system and most of the other "molecular machines" elaborated and studied in our group function on the same principle. Among the first row transition metal ions, copper displays unusual features related to the geometrical properties of its complexes: The stereoelectronic requirements of copper(I) and copper(II) are markedly different. This characteristic will provide the driving force for setting our systems in motion. Whereas a coordination number (CN) of 4, usually with a roughly tetrahedral arrangement of ligands, corresponds to stable monovalent systems, copper(II) requires higher coordination numbers. The most commonly encountered copper(II) complexes have a CN of 5 (square pyramidal or

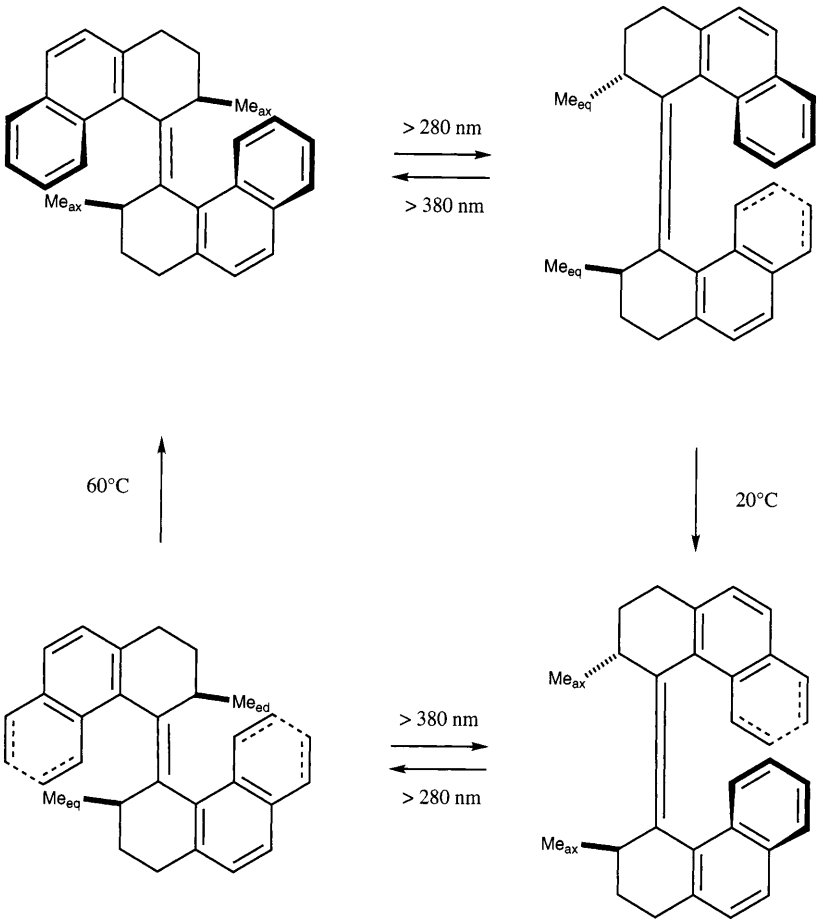

Fig. 5. Photochemical and thermal isomerization processes in a biphenanthrylene derivative [11]

trigonal bipyramidal geometries) or 6 (octahedral arrangement, with Jahn-Teller distortion). Thus, by switching alternatively from copper(I) to copper(II), one should be able to induce changes in the molecule so as to afford a coordination situation favorable to the corresponding oxidation state. The principle is illustrated in Fig. 7, [42, 43] using the threaded system of Fig. 6c.

Of course, if the acyclic molecular fragment which threads the ring does not bear blocking groups at its ends, dethreading may occur. This is indeed observed in polar solvents (CH_3CN), mostly at the 2+ stage, to afford a bis-terpy-like (terpy = 2, 2′, 6′, 2″-terpyridine) complex obtained when two strings are taken up by the same copper(II) center. The obvious improvement is to attach one or, better, two bulky groups at the extremities of the string in order to prevent unthreading [44]. These new systems are represented in Fig. 8.

The semi-rotaxane was simply obtained by mixing stoichiometric amounts of **8**, which is an improved version of **6** (Fig. 6), $Cu(CH_3CN)_4^+$, and **1** (Fig. 6). If, in **9**, the OCH_3 group borne by the phen unit of the string (phen = 1, 10-phenanthroline) is replaced by a phenolic function (**9**), threading will lead to a $\mathbf{10}^+$-type compound with a reactive end. Activation of the -OH function and covalent attachment of the blocking group affords the real rotaxane $\mathbf{11}^+$. It is real in the sense that demetallation furnishes a copper-free system (**12**) whose acyclic component will not dethread from the 30-membered ring.

The electrochemical behavior of $\mathbf{11}^+$ is particularly clean and interesting since only the 4- and the 5- coordinate geometries can be obtained by translating the metal complexed-ring from the phen site to the terpy site [44]. The electrochemically induced molecular motions (square scheme) similar to those represented in Fig. 7 but now involving stoppered compounds can be monitored by cyclic voltammetry (CV) and controlled potential electrolysis experiments [44].

From the CV measurements at different scan rates (from 0.005 to 2 $V \cdot s^{-1}$) both on the copper(I) and copper(II) species, it could be inferred that the chemical steps (motions of the ring from the phenanthroline to the terpyridine and *vice-versa*) are slow on the time scale of the experiments. As the two redox couples involved in these systems are separated by 0.7 V, the concentrations of the species in each environment (tetra- or penta-coordination) are directly deduced from the peak intensities of the redox signals. In Fig. 9 are displayed some voltammograms (curves a–e) obtained on different oxidation states of the rotaxane $\mathbf{11}^+$ and at different times.

Curve a) displays the voltammogram of a red solution of $\mathbf{11}^+$ in degassed acetonitrile. A reversible redox wave at 0.68 V (vs. SCE) attests to the tetrahedral environment around the copper(I) atom [18, 19, 45]. During the potential scan, for rates between 0.005 and $2 \times V \cdot s^{-1}$, no redox signal corresponding to the penta-coordination could be observed. This fact evidences the high kinetic stability of the 4-coordinate copper(II) rotaxane generated at the electrode. At this stage, a controlled potential electrolysis (applied potential = +1.0 V) was performed until one Faraday was exchanged per mole of complex. During the electrolysis the red color of the solution changed to light green. Immediately after the coulometry, the voltammogram on the copper(II) species (curve b) showed the same redox couple at +0.68 V and an additional small reversible couple at −0.03 V. These signals are characteristic of the $Cu(II)_{(4)}/Cu(I)_{(4)}$ and $Cu(II)_{(5)}/Cu(I)_{(5)}$ couples, respectively (the subscripts *4* and *5* indicate the coordination number of the copper center) [18, 19, 45]. After several hours at room temperature, without any visible color change, the progressive disappearance of the redox couple at +0.68 V (4-coordinate state) and the concomitant growth of the couple at −0.03 V (5-coordinate state) attest to the coordination change around the copper(II) ion (curves c and d). The analysis of the concentration of the two different copper(II) species with time leads to a first-order rate constant of 1.5×10^{-4} s^{-1} for the chemical reaction $Cu(II)_{(4)}$ giving $Cu(II)_{(5)}$. According to the invariant shape of the signals with the scan rate of the copper(II) solution, it can be inferred that the rate constant for the reaction $Cu(I)_{(5)}$ to $Cu(I)_{(4)}$

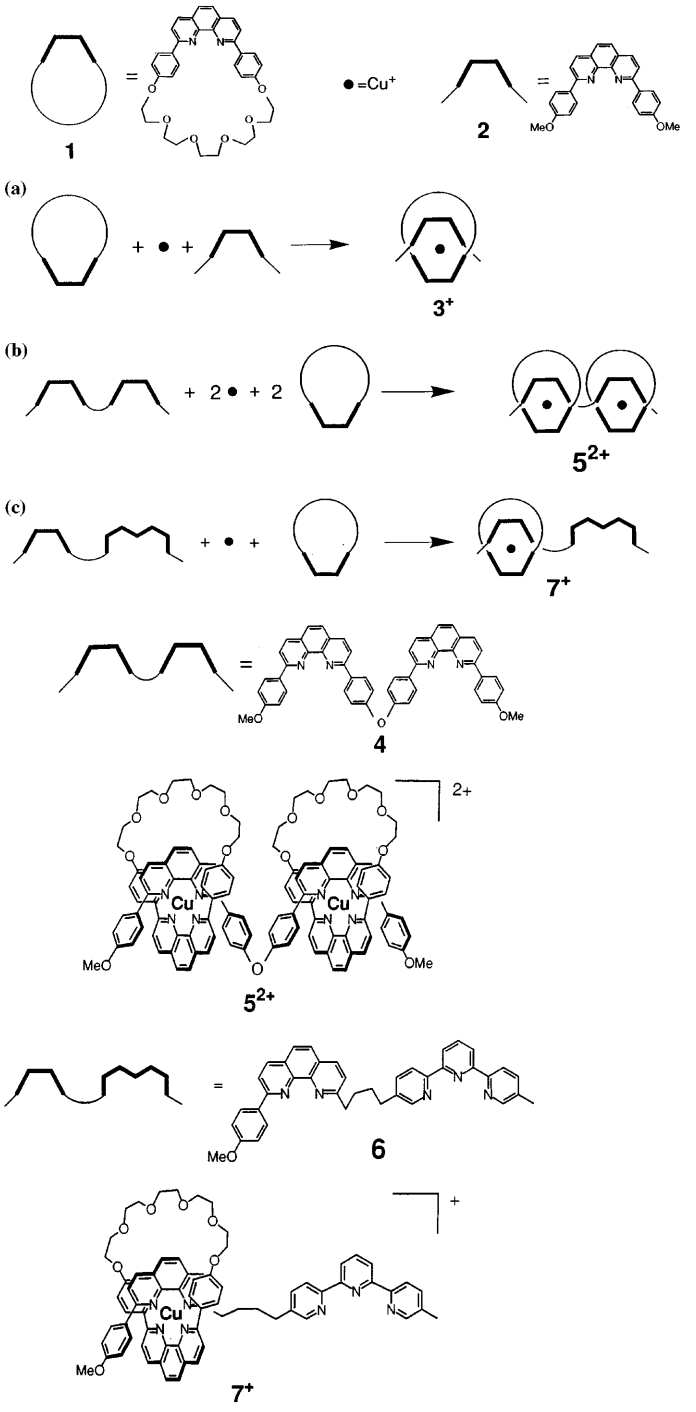
1
● =Cu+
2
MeO
OMe
(a)
3+
(b)
+ 2 ● + 2
5 2+
(c)
7+
4
MeO
OMe
2+
Cu
Cu
MeO
OMe
5 2+
6
MeO
+
Cu
MeO
7+

Fig. 6. Copper(I)-induced threading of one or two rings on a molecular string. **1** is a 30-membered ring, containing a bidentate ligand. (**a**) The acyclic fragment **2** is a simple phenanthroline derivative. This threading process has been used in our group since the early 1980s to make catenanes. (**b**) The string **4** now incorporates two identical bidentate units; like in (**a**), the process is quantitative. (**c**) A slightly more complex case. the acyclic component contains both a *bi*dentate ligand and a *ter*dentate coordinating unit (2, 2′, 6′, 2″-terpyridine). With copper(I) as gathering metal, exclusive formation of the 4-coordinate complex $\mathbf{7}^+$ is observed

is smaller than 10^{-2} s^{-1}. A second electrolysis at −0.3 V restores the initial red solution. The voltammogram (curve e) performed immediately after the reductive electrolysis displays the redox couple of $\mathbf{11}^+$ and is invariant with time. As all the $Cu(I)_{(5)}$ species formed electrochemically are quantitatively transformed into $Cu(I)_{(4)}$ species during the electrolysis, we can give a lower limit of 10^{-4} $s^{-1}$for the rate constant of the chemical reaction. The residual signal at −0.03 V simply reflects an incomplete electrolysis.

The behavior of the systems constituted by the semirotaxane $\mathbf{10}^+$ [42–44], is related to the fully blocked rotaxane $\mathbf{11}^+$, i.e., the same redox couple can be observed. Some variations of peak intensities with the scan rate also indicate an acceleration of the chemical processes as compared to $\mathbf{11}^+$. However, additional signals corresponding to the species $Cu(I)(MeCN)_4^+$ ($E_{1/2}$ = +1.02 V) and $Cu(II)_{(6)}$ (6-coordinate state, $E_{1/2}$ = −0.41 V) [45] reveal that the dethreading process becomes significant and occurs primarily with the copper(II) species. The 6-coordinate complex evidenced by CV originates from the dethreading and coordination of the two linear fragments via their terpy units to a copper center.

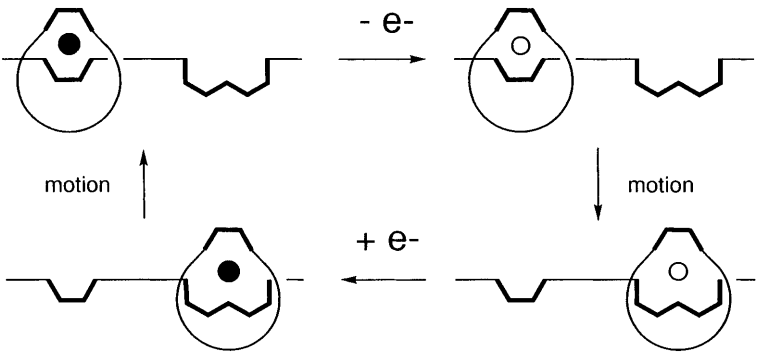

Fig. 7. Principle of the electrochemically induced molecular motions in a copper(I) complex pseudorotaxane. The stable four-coordinate monovalent complex is oxidized to an intermediate tetrahedral divalent species. This compound undergoes a rearrangement to afford the stable five-coordinate copper(II) complex. Upon reduction, the five-coordinate monovalent state is formed as transient. Finally, the latter undergoes the reorganization process that regenerates the starting complex [the black circle represents Cu(I) and the white circle represents Cu(II)]

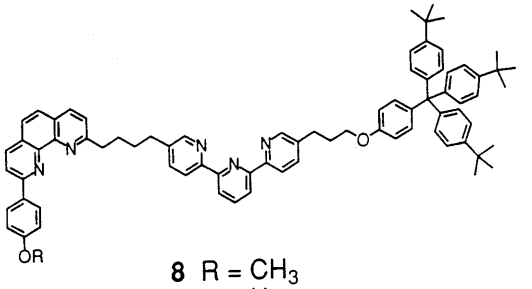

8 R = CH_3
9 R = H

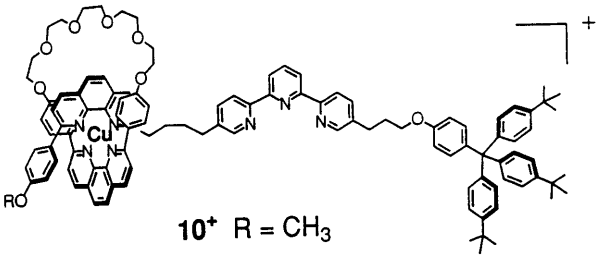

10^+ R = CH_3

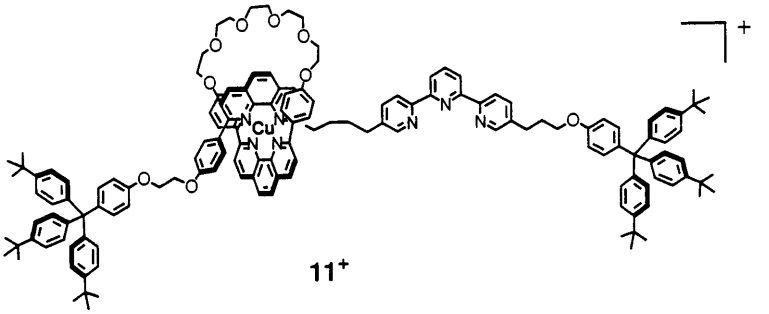

11^+

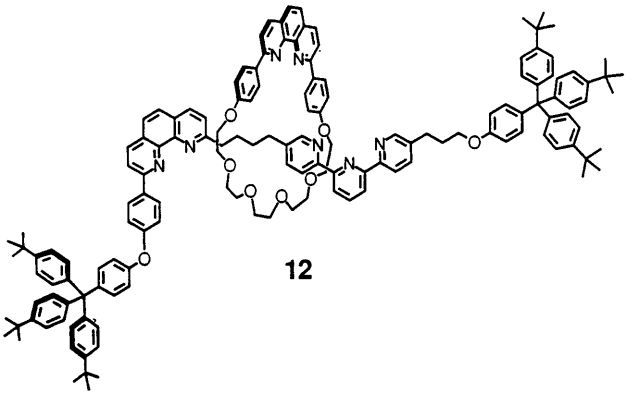

12

Fig. 8. The semi-rotaxane $\mathbf{10}^+$, the real copper-containing rotaxane $\mathbf{11}^+$ and the demetallated rotaxane **12**

It is noteworthy that oxidation of $\mathbf{11}^+$ to the divalent copper(II) state affords exclusively the 5-coordinate species after rearrangement of the system. The bis-terpy complex, which would be formed by decomplexation of the copper(II) center and recoordination to the terpy fragments of two different molecules of **12**, is not detected. This observation is important in relation with the general mechanism of the changeover step converting a 4-coordinate Cu(II) species $[Cu(II)_{(4)}]$ into the corresponding stable 5-coordinate complex

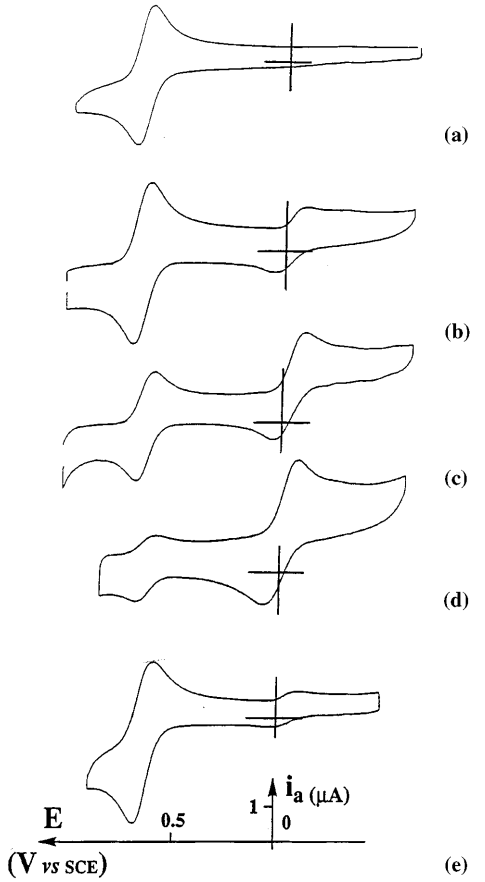

Fig. 9. (**a**) Cyclic voltammogram of $\mathbf{11}^+$; (**b**) after electrolysis during 1 h at +1.0 V; (**c**) and (**d**) evolution of $\mathbf{11}^{2+}$ solution with time after 2 h (**c**) and after 4 h (**d**). (**e**) Cyclic voltammogram immediately after electrolysis of $\mathbf{11}^{2+}$ solution at −0.3 V. Conditions: MeCN (0.1 M, *n*-Bu_4NBF_4), Pt electrode, v = 100 mV s^{-1}, 25 °C

[Cu(II)$_{(5)}$]. It tends to indicate that the conversion does not involve full demetallation of Cu(II)$_{(4)}$ followed by recomplexation but is rather an intramolecular reaction, probably consisting of several elemental dissociation-association steps involving the phen and terpy fragments of the string as well as solvent molecules and, possibly, counterions. The square scheme involving the fully blocked rotaxanes $\mathbf{11}^{n+}$ (n = 1 or 2) corresponds to the following sequence of reactions:

$$
\begin{array}{lll}
(1) & \mathbf{11}_{(4)}^{+} \xrightarrow{-e} \mathbf{11}_{(4)}^{2+} & E^\circ = +0.68 \text{ V (vs SCE in } CH_3CN) \\
(2) & \mathbf{11}_{(4)}^{2+} \xrightarrow{\text{gliding}} \mathbf{11}_{(5)}^{2+} & \\
(3) & \mathbf{11}_{(5)}^{2+} \xrightarrow{-e} \mathbf{11}_{(5)}^{+} & E^\circ = -0.03 \text{ V} \\
(4) & \mathbf{11}_{(5)}^{+} \xrightarrow{\text{gliding}} \mathbf{11}_{(4)}^{+} &
\end{array}
\qquad (1)
$$

It is noteworthy that the redox couples of reactions 1–3 [Eq. (1)] are perfectly reversible provided the scan rate is sufficient (>100 mV · s^{-1}). The gliding motions, either for the divalent or the monovalent complex, are slow on the time scale of the voltammetry measurements (lines 2 and 4).

2.2
Pirouetting of a Wheel Around Its Axle: Towards Rotary Motors

An other type of motion, pirouetting of a wheel around its axle (Fig. 10), can also be electrochemically triggered.

The driving force of this motion is again based on different geometrical preferences for Cu(I) and Cu(II). But in this case, the wheel of the rotaxane is a bis-coordinating macrocycle and the axle incorporates only one bidentate moiety.

The principle of the synthesis is the one described earlier, slightly modified by using an alternative strategy which consists in using a monostoppered species to form the prerotaxane intermediate and in adding the second stopper afterwards. The advantage of this method is to limit dethreading of the macrocycle during the stoppering reaction.

The rotaxane $\mathbf{13}_{(4)^+}$ [the nomenclature of the rotaxanes described here is $\mathbf{13}_{(N)^{n+}}$, where *N* refers to the coordination number of the metal (*4* or *5*) and n to its charge] synthesized herein is composed of two subunits: a macrocycle and a molecular thread (Fig. 11). The 33-membered macrocycle M_{t33} [18, 19] contains two different coordinating sites: a terpyridine moiety and a 1, 10-phenanthroline one.

The molecular thread contains the phenanthroline bidentate unit (dpp). The end-groups of the thread, i.e., the stoppers of the rotaxane, are tetraarylmethane derivatives. These last species were selected as blocking groups since they are large enough to prevent dethreading of the ring.

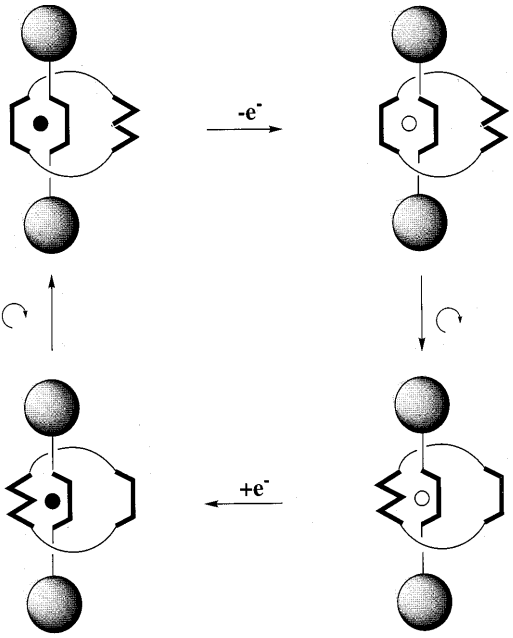

Fig. 10. Principle of the electrochemically induced molecular motions in a copper complex rotaxane. The stable 4-coordinate monovalent complex [*top left*, the black circle represents Cu(I)] is oxidized to an intermediate tetrahedral divalent species [*top right*, the white circle represents Cu(II)]. This compound undergoes a complete reorganization process to afford the stable 5-coordinate Cu(II) complex [*bottom right*]. Upon reduction, the 5-coordinate monovalent state is formed as a transient [*bottom left*]. Finally, the latter undergoes the conformational change which regenerates the starting complex

The rotaxane $\mathbf{13}^{+}_{(4)}$ is the exact counterpart of rotaxane $\mathbf{11}^{+}_{(4)}$ in the sense that the 2-chelate fragments are the ring for $\mathbf{13}^{+}$ and the string for $\mathbf{11}^{+}$, whereas the mono dpp components are the string and the ring, respectively. As will be discussed later, this structural analogy does not at all correspond to a dynamic analogy.

Cu(I) complex rotaxane $\mathbf{13}^{+}_{(4)}$ could be easily demetallated [46] by reaction with cyanide in mild conditions, leading to rotaxane **14**, with free coordination sites. Transformation of the free rotaxane **14** into the Cu(II) complex $\mathbf{13}^{2+}_{(5)}$ was quantitatively achieved by mixing **14** with a solution of $Cu(II)(BF_4)_2$.

The electrochemical behavior of tetracoordinated Cu(I) complexes, i.e., $Cu(dpp)_2$-based cores, is well established [47, 48]. The reversible redox potential for the Cu(II)/Cu(I) transition is around 0.6–0.7 V vs. SCE. Once again, this relatively high potential underlines the stability of the 4-coordinate Cu(I) complexes versus the corresponding Cu(II) ones. The redox potential of pentacoordinated copper complexes [18, 19, 44] is observed in a much more cathodic range. For example, for the 5-coordinate complex $Cu(M_{t33}, dap)^{2+/+}$ (dap = 2, 9-di-*p*-anisyl-1, 10-phenanthroline), in which the terpy fragment of the ring is bound to the metal, the redox potential is −0.035 V. This potential

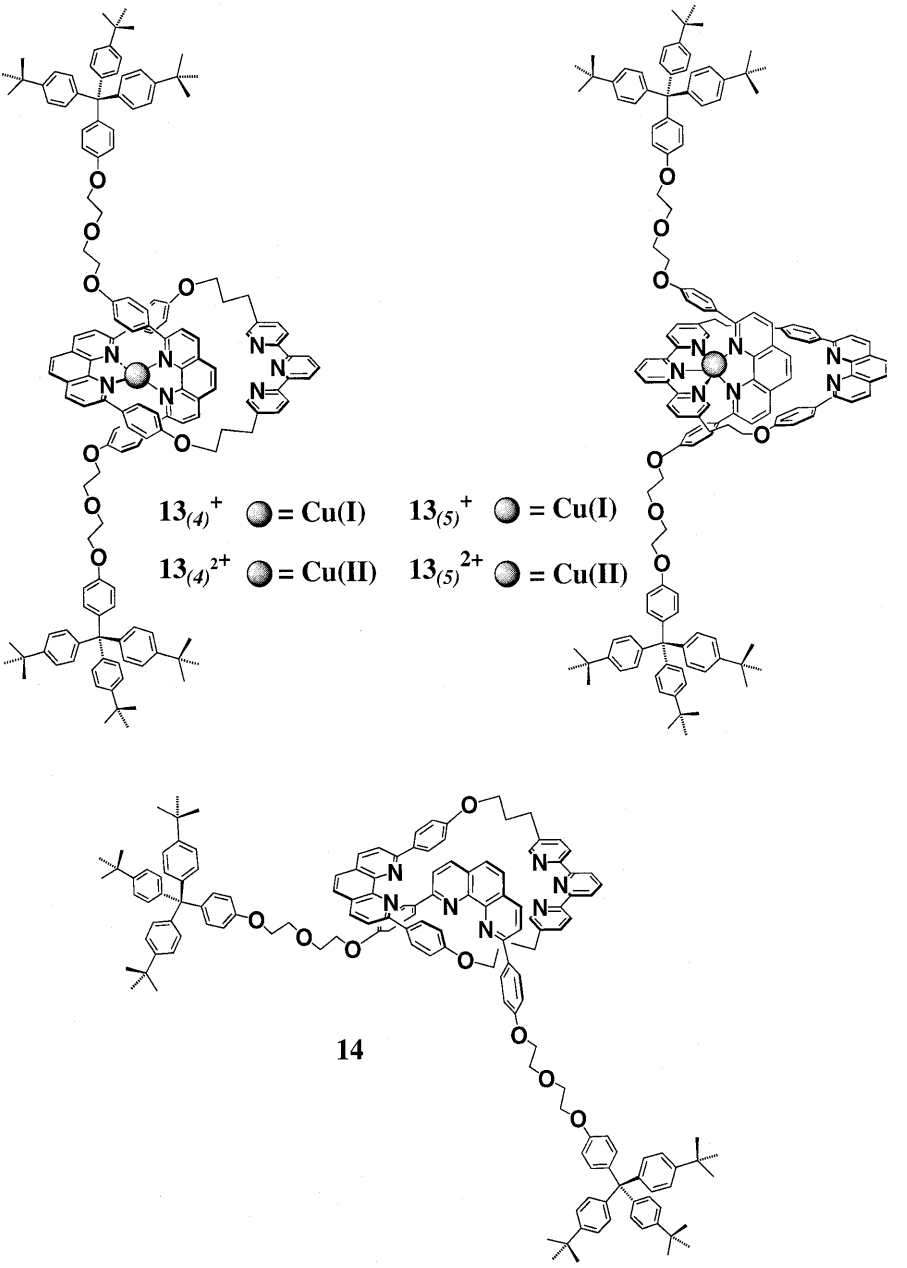

Fig. 11. Molecular representation of the metallated rotaxanes $\mathbf{13}^{+}_{(4)}$, $\mathbf{13}^{+}_{(5)}$, $\mathbf{13}^{2+}_{(4)}$, $\mathbf{13}^{2+}_{(5)}$ and of the metal-free rotaxane **14**

shift when going from tetracoordinated to pentacoordinated copper systems is due to the better stabilization of the Cu(II) state thanks to the presence in the coordination sphere of five donor atoms.

The electrochemical behavior of $\mathbf{13}^{+}_{(4)}$ in an CH_2Cl_2-CH_3CN solution has been studied by cyclic voltammetry (CV) and is represented Fig. 12a. A reversible signal appears at 0.545 V.

In the rotaxane $\mathbf{13}^{+}_{(4)}$, where the metal is tetracoordinated, the signal occurring at 0.54 V corresponds to the tetracoordinated Cu(II)/Cu(I) couple. The ratio of the intensities of the anodic and cathodic peaks ipc/ipa is 0.95 (ipc

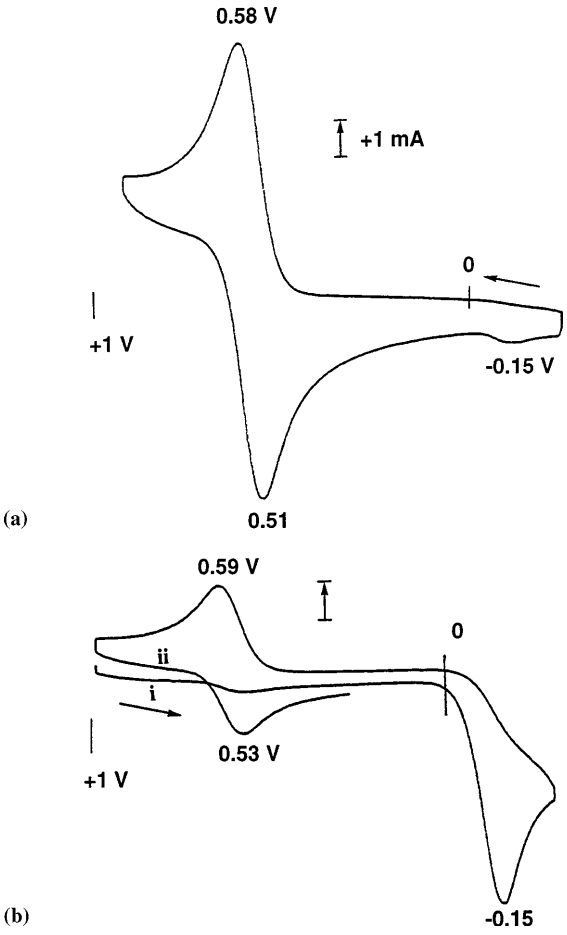

Fig. 12. Cyclic voltammetry curves recorded using a Pt working electrode at a 100 mV · s^{-1} sweep rate (CH_3CN-CH_2Cl_2, 4:1, supporting electrolyte: tetrabutylammonium tetrafluoroborate, 0.1 mol L^{-1}, Ag wire pseudo-reference). (**a**) Compound $\mathbf{13}^{+}_{(4)}$ (**b**) Chemically prepared $\mathbf{13}^{2+}_{(5)}$. Curve (ii) refers to a second potential sweep following immediately the first one (i)

and ipa being, respectively, the intensity of the cathodic and anodic peaks), showing that no transformation or reorganization of the coordination sphere of the tetracoordinated Cu(II) complex occurs in the time scale of the measurements (sweep rate of the potential: 100 mV × s^{-1}). The weak signal at −0.15 V is due to the presence of small amounts of $\mathbf{13}^{2+}_{(5)}$.

The cyclic voltammetry behavior of the Cu(II) rotaxane $\mathbf{13}^{2+}_{(5)}$ (Fig. 12b), is very different from that of $\mathbf{13}^{+}_{(4)}$. The potential sweep for the measurement was started at +0.9 V, a potential at which no electron transfer should occur, whatever the surrounding of the central Cu(II) is (penta- or tetracoordinated). Curve (i) (first scan, recorded at 100 mV × s^{-1}) shows two cathodic peaks: a very small one, located at +0.53 V followed by an intense one at −0.15 V. Only one anodic peak at 0.59 V appears during the reverse sweep. If a second scan (ii) follows immediately after the first one (i), the intensity of the cathodic peak at 0.53 V increases noticeably.

The weak peak at 0.53 V (i) is due to the presence of small quantities of $\mathbf{13}^{+}_{(4)}$. The main cathodic peak at −0.15 V is characteristic of pentacoordinated Cu(II). Thus, in $\mathbf{13}^{2+}_{(5)}$ prepared from the free rotaxane by metallation with Cu(II) ions, the central metal is coordinated to the terdentate terpyridine of the wheel and to the bidentate dpp of the axle. On the other hand, the irreversibility of this peak means that the pentacoordinated Cu(I) species formed in the diffusion layer, when sweeping cathodically, is transformed very rapidly and in any case before the electrode potential becomes again more anodic than the potential of the pentacoordinated Cu^{2+}/Cu^{+} redox system. The irreversible character of the wave at −0.15 V and the appearance of an anodic peak at the value of +0.53 V indicates that the transient species, formed by reduction of $\mathbf{13}^{2+}_{(5)}$, has undergone a complete reorganization, which leads to a tetracoordinated copper rotaxane. The second scan (ii) which follows immediately after the first one (i) confirms this assertion. Indeed, a cathodic peak (+0.53 V) has appeared, corresponding to the reduction of this tetracoordinated species.

These two complementary cyclic voltammetry experiments confirm that in this rotaxane, like in previously studied related systems, the tetracoordinated Cu(I) state is more stable than the pentacoordinated one and the pentacoordinated Cu(II) state is more stable than the tetracoordinated one. Moreover, it was observed that the rearrangement rates from the less to the most stable geometries are drastically different for the two oxidation states of the metal.

The irreversibility of the reduction peak of $\mathbf{13}^{2+}_{(5)}$, combined with the appearance of a reversible peak corresponding to tetracoordinated copper suggests that the reorganization of the rotaxane in its pentacoordinated form $\mathbf{13}^{+}_{(5)}$ (i.e., with the copper being coordinated to terpy and to dpp units), to its tetracoordinated form $\mathbf{13}^{+}_{(4)}$ (where the copper is surrounded by two dpp units) occurs within the time scale of the cyclic voltammetry. Indeed, the cyclic voltammetry response located at −0.15 V becomes progressively reversible when increasing the potential sweep rate, as expected for an electrochemical process where an electron transfer is followed by an irreversible chemical reaction (EC). Following the method of Nicholson and Shain [49], the rate constant value, k, of the chemical reaction, i.e., transformation of pentaco-

ordinated Cu(I) into tetracoordinated Cu(I) was determined. A value of 17 s^{-1} was found for k, which corresponds to a half-life time $t_{1/2}$ of 56 ms for the pentacoordinated Cu(I) complex.

On the other hand, Fig. 12a evidences the inertness of the reorganization of the tetracoordinated Cu(II) rotaxane. Thus, a total conversion of tetracoordinated $\mathbf{13}^{+}_{(4)}$ to tetracoordinated $\mathbf{13}^{2+}_{(4)}$ was performed by preparative electrolysis and the subsequent rearrangement of tetracoordinated $\mathbf{13}^{2+}_{(4)}$ into pentacoordinated $\mathbf{13}^{2+}_{(5)}$ was followed by monitoring the current (vs. time) flowing through a rotating disk electrode polarized at +0.3 V. Indeed, at that potential, the cathodic current observed is representative of the presence and concentration of $\mathbf{13}^{2+}_{(4)}$, the tetracoordinated Cu(II) complex only. This remains true even if the electrolytic solution contains tetracoordinated $\mathbf{13}^{+}_{(4)}$ which will be electrochemically silent in the potential range used.

Current versus time was recorded and an exponential decrease of the intensity of the current was observed. When the current was near to 0, a new cyclic voltammetry curve of the solution was measured, leading to a voltammogram similar to the one represented, Fig. 12b. This confirms that the electrogenerated tetracoordinated Cu(II) rotaxane has undergone a rearrangement to form the pentacoordinated Cu(II) rotaxane $\mathbf{13}^{2+}_{(5)}$.

The kinetic constant k′ of this rearrangement can be extracted from the variation of the cathodic current versus time and its average value is 0.007 ± 0.003 s^{-1}. In other words, the half-life time of tetracoordinated Cu(II) rotaxane is 120 ± 50 s.

These experiments underline the noticeable difference of the kinetic rate constants k and k′ for the reorganization processes leading respectively from $\mathbf{13}^{+}_{(5)}$ to $\mathbf{13}^{+}_{(4)}$ and from $\mathbf{13}^{2+}_{(4)}$ to $\mathbf{13}^{2+}_{(5)}$. Indeed, the ratio k/k′ is about 3000. In the analogous systems already studied [18, 19, 44], an important difference between the related rate constants had also been observed. Nevertheless, for the systems based on a copper [2]catenate [18, 19] (*vide infra*), where one of the macrocycles is monochelating and the other one hetero-bischelating, the two processes are much slower. For the rotaxane $\mathbf{11}^{+}$ [44] (*vide supra*) where the axle is a hetero-bischelating molecular thread and the wheel a monochelating macrocycle, the reorganization processes which imply a translation of the ring along the string, the values determined for k and k′ are also several order of magnitude smaller. It is thus clear that pirouetting of a macrocycle around its axle induced by changing the redox state of the central metal is a fast process as compared to the other related reactions.

These different types of molecular motion: gliding, translating, and pirouetting are possible thanks to the kinetic lability of copper complexes. As mentioned above, the k/k′ ratio is high in all the cases studied so far, which means that the reorganization process around Cu(I) is much faster than that around Cu(II). Both rearrangements require a decoordination step of one of the chelates, followed by recomplexation by the other chelate. The activation barrier of this decoordination step is higher for the tetracoordinated Cu(II) to pentacoordinated Cu(II) process one than for the pentacoordinated Cu(I) to tetracoordinated Cu(I) process, due to the higher electronic requirements of Cu(II). Thus, the difference of molecular motion

rates induced by changing the redox state of the metal could be partially attributed to the ligand field effect.

3
Electrochemically-Driven Ring Gliding Motion in Catenanes

3.1
A Two-Geometry Catenane

The first molecular motor elaborated and studied in our group was a catenane containing two different interlocking rings [18, 19]. Its principle is explained in Fig. 13.

The actual system and the full square-scheme are indicated in Fig. 13. The starting copper(I) complex $\mathbf{15}^{+}_{(4)}$ is a 4-coordinate species, whose high

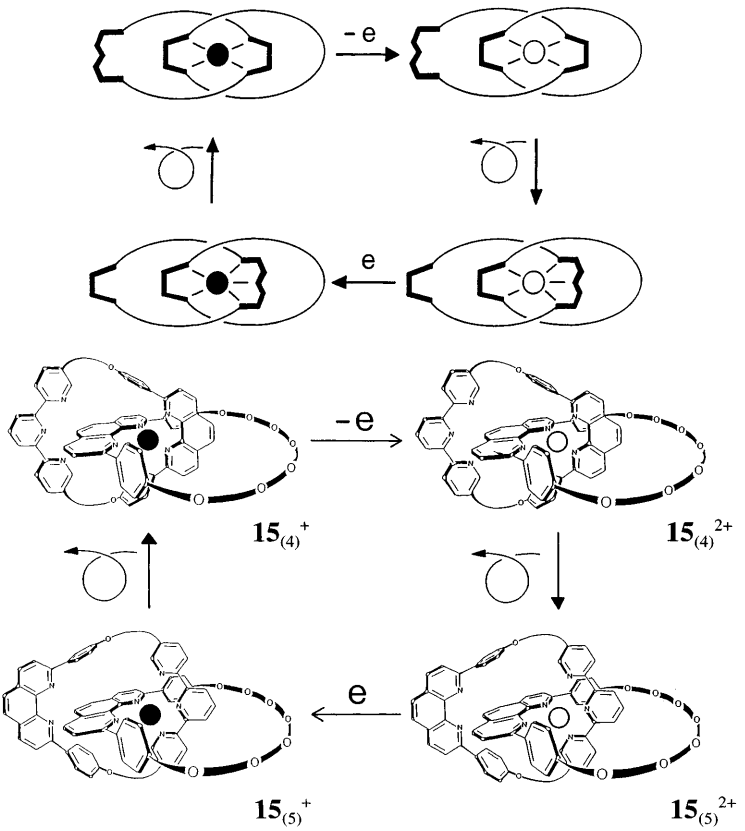

Fig. 13. Electrochemically triggered rearrangement of a [2]catenate containing two different rings. The principle is the same as the one described for the copper complex rotaxane (Fig. 10)

redox potential (+0.63 V vs. SCE in CH_3CN) clearly indicates that the geometry of the system (tetrahedral or distorted tetrahedral) is well adapted to copper(I). This redox state being very stable with the environment provided by $\mathbf{15}^{+}_{(4)}$, a relatively high redox potential will have to be applied for the monovalent copper center to be oxidized to the divalent state. Interestingly, the 4-coordinate Cu(II) complex $\mathbf{15}^{2+}_{(4)}$ is an intense green species, with an absorption band at 670 nm ($\varepsilon = 800$) in CH_3CN. This compound can be generated either by chemical (Br_2 or $NOBF_4$) or electrochemical oxidation.

The changeover reaction converting $\mathbf{15}^{2+}_{(4)}$ to the stable 5-coordinate species $\mathbf{15}^{2+}_{(5)}$ is quantitative. It is easily monitored by visible absorption spectroscopy since the product of the rearrangement reaction is only slightly colored (pale olive-green; $\lambda_{max} = 640$ nm; $\varepsilon = 125$). The geometry of the copper(II) catenate obtained via decomplexation and remetallation has been confirmed by comparison of its physical and chemical properties with those of the literature compounds, whose structures have already been established. Its redox potential is −0.07 V vs. SCE in acetonitrile, indicating a good stabilization of the copper(II) state. UV-visible absorption spectroscopy reveals a band centered at 636 nm ($\varepsilon = 125$) in acetonitrile, corresponding to a *d-d* transition, resulting in a pale olive-green solution. This value can be compared with the one obtained for the 5-coordinated complex Cu(II)(terpy)(bipy)$(ClO_4)_2$: 640 nm ($\varepsilon = 120$) [50, 51], as well as for the same complex present in a copper(II) helicate recently synthesized [52]. Both copper(II) complexes $\mathbf{15}^{2+}_{(4)}$ and $\mathbf{15}^{2+}_{(5)}$ have electronic spectra typical for 4- and 5-coordinated species, respectively, in accordance with previously reported complexes having analogous ligand sets [53–55]. The same conversion process can also be monitored by EPR [56]. It was demonstrated in an unambiguous fashion that $\mathbf{15}^{2+}_{(4)}$ is a distorted tetrahedral complex and that the product of the changeover, $\mathbf{15}^{2+}_{(5)}$, is a square pyramidal compound.

An interesting question concerns the rate of the ring gliding motion which transforms $\mathbf{15}^{2+}_{(4)}$ into $\mathbf{15}^{2+}_{(5)}$ or, after reduction of the latter, $\mathbf{15}^{+}_{(5)}$ into $\mathbf{15}^{+}_{(4)}$. It was observed that this last process, involving Cu(I), is fast (a few seconds at room temperature, regardless of the solvent) whereas the copper(II) complex rearrangement $\mathbf{15}^{2+}_{(4)} \rightarrow \mathbf{15}^{2+}_{(5)}$ is slow and depends enormously on the solvent and the nature of the counterion. The strong accelerating influence of CH_3CN (over CH_2Cl_2) or Cl^- (over $[PF_6]^-$) may give indications regarding the rearrangement mechanism. In the course of the changeover process, removal of a dpp unit (dpp = 2, 9-diphenyl-1, 10-phenanthroline) from the copper(II) coordination sphere has to proceed before any interaction between the metal center and the entering terpy ligand is possible. This implies that the copper(II) atom be "half-naked" at some stage. If coordinating ions or solvent molecules are present in the medium, they could interact with the metal in this coordinatively unsaturated complex, in a transitory fashion, and thus lower the activation barrier of the rearrangement by stabilizing intermediate states.

3.2
A Three-Configuration Copper Catenane

The last system which we will discuss is based on a [2]catenane which can adopt three distinct geometries [45] and contains two identical interlocking rings. Multistage systems seem to be uncommon, although they are particularly challenging and promising in relation to photo- and electrochemical devices aimed at important electronic functions and information storage. In particular, if molecules or molecular assemblies are to be utilized one day as information storage devices, it is obvious that the use of three-state systems will produce a great increase in information density as compared to bistable systems. For instance, an assembly of ten distinct molecules whose each individual molecular component can occupy two states (say, + or −) will lead to 2^{10} [57–59] different states (i.e., 1024 states) whereas, if the same collection of 10 distinct molecules is such that each compound can now occupy three states (+, 0, and −), the overall number of states is now 3^{10} [57–59] (i.e., 59049).

The principle of the three-situation electromediated catenate is represented in Fig. 14. Again, it relies on the drastic differences of stereochemical requirements for coordination of Cu(I) and Cu(II), the sequences of preferred coordination numbers (CN) being:

$$\mathrm{CN} = 4 > \mathrm{CN} = 5 > \mathrm{CN} = 6 \text{ for Cu(I)}$$

and

$$\mathrm{CN} = 6 > \mathrm{CN} = 5 > \mathrm{CN} = 4 \text{ for Cu(II)}.$$

Detailled electrochemical studies have been carried out on $\mathbf{16}^{+}_{(4)}$. Although we will not discuss them in the present chapter, they afford very conclusive data and, in particular, they demonstrate unambiguously that the compound undergoes the rearrangement reactions schematically represented in Fig. 14.

The sequence of electron-transfer steps and ring-gliding motions corresponding to the cyclic process of Fig. 14 can also be induced by using chemical reagents. For instance, when a dark red solution of $\mathbf{16}^{+}_{(4)}$ is oxidized by NO^{+} BF_4^{-} in CH_3CN, an intense green solution of $\mathbf{16}^{2+}_{(4)}$ is first obtained. As expected, the cyclic voltammogram (CV) of this species is the same as for the starting complex, which is in accordance with the 4-coordinate situation for both oxidized and reduced forms. The visible absorption spectrum shows a band at λ_{max} = 670 nm with a high extinction coefficient (ε = 810 mol^{-1} L cm^{-1} in CH_3CN), typical of tetrahedral complexes with nitrogen ligands. The ring-gliding step will subsequently lead to a hexa-coordinated complex, the 5-coordinated compound being characterized as a transient species by electrochemistry only.

Reversing the process, reduction of the stable species $\mathbf{16}^{2+}_{(6)}$ will afford $\mathbf{16}^{+}_{(6)}$ which rapidly rearranges to the stable monovalent complex $\mathbf{16}^{+}_{(4)}$. The intermediate $\mathbf{16}^{+}_{(5)}$ has not been isolated nor spectroscopically characterized, but its formation was clearly evidenced by cyclic voltammetry, due to its analogy with $\mathbf{15}^{+}_{(5)}$.

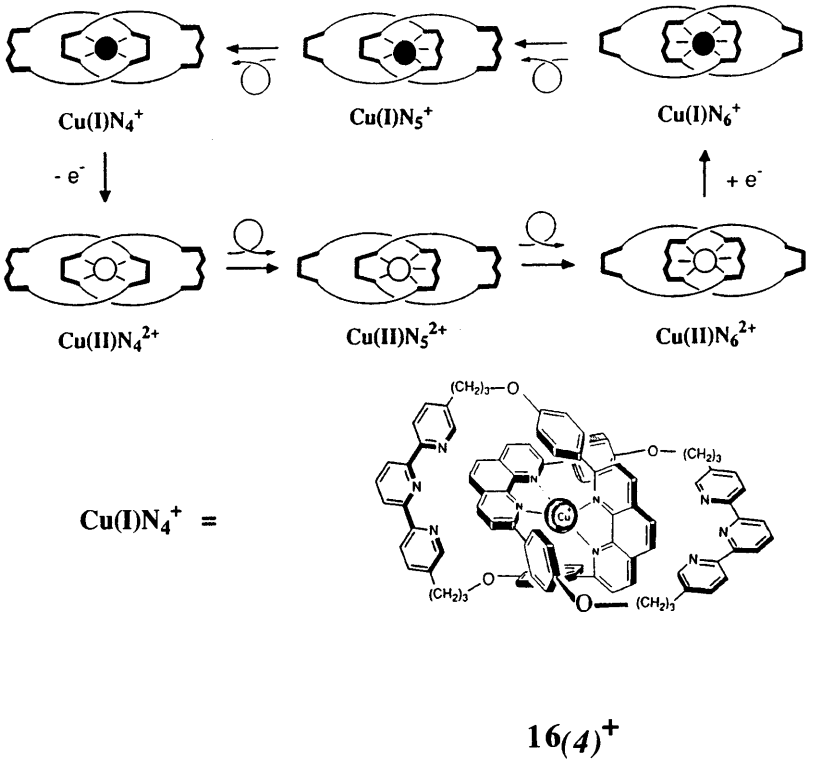

Fig. 14. A three-configuration Cu(I) catenate whose general molecular shape can be dramatically modified by oxidizing the central metal [Cu(I) to Cu(II)] or reducing it back to the monovalent state. Each ring of the [2]catenate incorporates two different coordinating units. a bidentate unit and a terdentate fragment. Starting from the tetracoordinated monovalent Cu complex [$Cu(I)N_4^+$; *top left*] and oxidizing it to the divalent state [$Cu(II)N_4^{2+}$], a thermodynamically unstable species is obtained which should first rearrange to the 5-coordinate complex $Cu(II)N_5^{2+}$ by gliding of one ring (*left*) within the other and, finally, to the hexacoordinate stage $Cu(II)N_6^{2+}$ by rotation of the second cycle (*right*) within the first one. $Cu(II)N_6^{2+}$ is expected to be the thermodynamically stable divalent complex. The double ring-gliding motion following oxidation of $Cu(I)N_4^+$ can be inverted by reducing $Cu(II)N_6^{2+}$ to the monovalent state [$Cu(I)N_6^+$; *top right*], as represented on the top line of the Figure

The three forms of the catenate are represented in Fig. 15.

The redox potentials for the three situations (CN = 4, 5, or 6) are in perfect agreement with those of similar systems with identical CNs. The pentacoordinated complexes were characterized as transient species only since the present system does not allow us to stop motions at this stage.

4 Conclusion and Perspectives

It is now more than 15 years ago that our group published the first templated synthesis of a catenane [60–62], following the elegant work previously reported

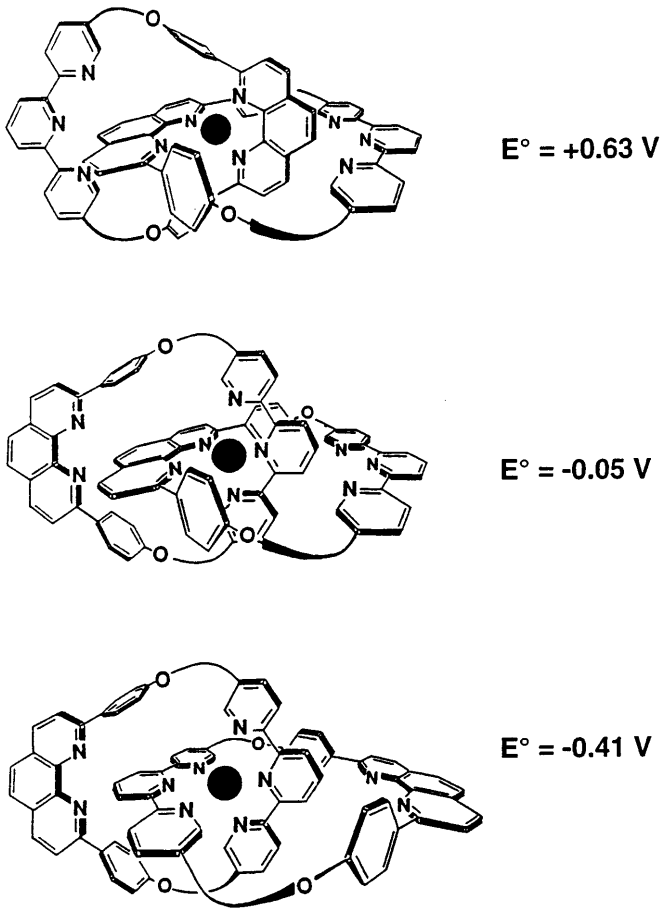

Fig. 15. The 4-, 5-, and 6- coordinate copper complexes involved. The corresponding Cu(II)/Cu(I) redox potentials are also indicated. They clearly show the sequence of preferred stabilities for copper(II) versus copper(I), the hexacoordinate complex leading to the most stable divalent complex

by others and based on pure organic chemistry [63–65]. Since the mid 1980s, the field has experienced a spectacular development, with the introduction of more and more complexity and functionality into the molecules. The use of transition metals as templates and of their complexes as electroactive and mobile components turned out to be particularly useful in the construction of *electromechanical molecular machines* and machines based on coordination compounds. Nanoscopic motors and machines might lead to practical applications in the future as molecular information storage devices, or as nanoscale components in electronics, making the search for such molecules or molecular assemblies particularly important.

The concepts discussed in the present paper can certainly be generalized to organized assemblies of molecules (liquid crystals) or to molecular compo-

nents attached to an electrode surface. The overall properties of the system (now, a "device") could be switched by just applying a given signal. The variety of impulses to be used is immense: redox, photonic, heat or pressure change, magnetic field variation, pH-change, chemical signal (recognition of a molecule), electric field, etc. The effect obtained is also multifarious and could lead to dramatic modifications of the bulk properties of the system. Since a simple signal can change the shape and the volume of a compound and of its assemblies, fascinating features related to mechanics (contraction or stretching) could be imagined, reminiscent of biological systems such as muscles.

5 References

1. Shenck HL, Dada GP, Gellman SH (1996) J Am Chem Soc 118: 12487
2. Dado GP, Gellman SH (1993) J Am Chem Soc 115: 12609
3. Bixler J, Bakker G, McLendon G (1992) J Am Chem Soc 114: 6938
4. Thirumalai D, Woodson SA (1996) Acc Chem Res 29: 433
5. Pascher T, Chesick JP, Winkler JR, Gray HB (1996) Science 271: 1858
6. Kitamura K, Tokunaga M, Iwane AH, Yanagida T (1999) Nature 397: 129
7. Rayment I, Holden HM, Whittaker M et al. (1993) Science 261: 58
8. Rayment I, Rypniewski WR, Schmidt-Bäse K et al. (1993) Science 261: 50
9. Dobbie I, Linari M, Piazzesi G et al. (1998) Nature 396: 383
10. Elston T, Wang H, Oster G (1998) Nature 391: 510
11. Koumura N, Ziljstra RWJ, Delden RAv, Harada N, Feringa BL (1999) Nature 401: 152
12. Abrahams JP, Leslie AGW, Lutter R, Walker JE (1994) Nature 370: 621
13. Noji H, Yasuda R, Yoshida M, Kinosita K (1997) Nature 386: 299
14. Walker JE (1998) Angew Chem Int Ed 37: 2308
15. Allison WS (1998) Acc Chem Res 31: 819
16. Boyer PD (1998) Angew Chem Int Ed 37: 2296
17. Philp D (1996) Angew Chem Int Ed Engl 35: 1154
18. Livoreil A, Dietrich-Buchecker C, Sauvage J-P (1994) J Am Chem Soc 116: 9399
19. Livoreil A, Sauvage J-P, Armaroli N, Balzani V, Flamigni L, Venturi B (1997) J Am Chem Soc 119: 12114
20. Ashton PR, Ballardini R, Balzani V et al. (1995) J Am Chem Soc 117: 11171
21. Ashton PR, Ballardini R, Balzani V et al. (1997) Chem Eur J 3: 152
22. Credi A, Balzani V, Langford SJ, Stoddart JF (1997) J Am Chem Soc 119: 2679
23. Ballardini R, Balzani V, Gandolfi MT et al. (1993) Angew Chem Int Ed Engl 32: 1301
24. Bissel RA, Crdova E, Kaifer AE, Stoddart JF (1994) Nature 369: 133
25. Geiger WE (1979) J Am Chem Soc 101: 3407
26. Bernardo MM, Robandt PV, Schroeder RR, Rorabacher DB (1989) J Am Chem Soc 111: 1224
27. Katz NE, Fagalde F (1993) Inorg Chem 32: 5391
28. Moraczewski J, Sassano CA, Mirkin CA (1995) J Am Chem Soc 117: 11379
29. Singewald ET, Mirkin CA, Stern CL (1995) Angew Chem Int Ed Engl 34: 1624
30. Wytko JA, Boudon C, Weiss J, Gross M (1996) Inorg Chem 35: 4469
31. Chin TT, Geiger WE, Rheingold AL (1996) J Am Chem Soc 118: 5002
32. Sano M, Taube H (1991) J Am Chem Soc 113: 2327
33. Sano M, Taube H (1994) Inorg Chem 33: 705
34. Sano M, Sago H, Tomita A (1996) Bull Chem Soc Jpn 69: 977
35. Tomita A, Sano M (1994) Inorg Chem 33: 5825
36. Tomita A, Sano M (1996) Chem Lett 981
37. Zelikovich L, Libman J, Shanzer A (1995) Nature 790

38. Canevet C, Libman J, Shanzer A (1996) Angew Chem Int Ed Engl 35: 2657
39. Chambron J-C, Dietrich-Buchecker CO, Nierengarten J-F, Sauvage J-P (1993) New J Chem 17: 331
40. Chambron J-C, Dietrich-Buchecker CO, Nierengarten J-F et al. (1995) New J Chem 19: 409
41. Amabilino DB, Dietrich-Buchecker CO, Sauvage J-P (1996) J Am Chem Soc 118: 3285
42. Gaviña P, Sauvage J-P (1997) Tetrahedron Lett 38: 3521
43. Collin J-P, Gaviña P, Sauvage J-P (1996) Chem Commun 2005
44. Collin J-P, Gaviña P, Sauvage J-P (1997) New J Chem 21: 525
45. Càrdenas DJ, Livoreil A, Sauvage J-P (1996) J Am Chem Soc 118: 11980
46. Dietrich-Buchecker C, Sauvage J-P (1990) Tetrahedron 46: 503
47. Dietrich-Buchecker C, Kern J-M, Sauvage J-P (1989) J Am Chem Soc 111: 7791
48. Federlin P, Kern J-M, Rastegar A, Dietrich-Buchecker C, Marnot PA, Sauvage J-P (1990) New J Chem 14: 9
49. Nicholson RS, Shain I (1964) Anal Chem 36: 706
50. Harris CM, Lockyer TN (1970) Aust J Chem 23: 673
51. Arena G, Bonmo RP, Musumeci S, Purello R, Rizarelli E, Sammartanos S (1983) J Chem Soc Dalton Trans 1279
52. Hasenknopf B, Lehn J-M, Baum G, Fenske D (1996) Proc Natl Acad Sci USA 93: 1397
53. Sanni SB, Behm HJ, Beurskens PT et al. (1988) J Chem Soc Dalton Trans 1429
54. Goodwin JA, Stanbury DM, Wilson LJ, Eigenbrot CW, Scheidt WR (1987) J Am Chem Soc 109: 2979
55. Goodwin JA, Bodager GA, Wilson LJ, Stanbury DM, Scheidt WR (1989) Inorg Chem 28: 35
56. Baumann F, Livoreil A, Kaim W, Sauvage J-P (1997) J Chem Soc Chem Commun 35
57. Drexler KE (1992) Nanosystems, molecular machinery, manufacturing and computation, Wiley, New York
58. Ikeda A, Tsudera T, Shinkai S (1997) J Org Chem 62: 3568
59. Urry DW (1993) Angew. Chem Int Ed Engl 32: 819
60. Dietrich-Buchecker C, Sauvage J-P (1983) Tetrahedron Lett 24: 5091
61. Dietrich-Buchecker C, Sauvage J-P, Kintzinger J-P (1983) Tetrahedron Lett 24: 5095
62. Dietrich-Buchecker C, Sauvage J-P, Kern J-M (1984) J Am Chem Soc 106: 3043
63. Wasserman E (1960) J Am Chem Soc 82: 4433
64. Schill G (1971) Catenanes, Rotaxanes and Knots, Academic Press, New York
65. Harrison IT, Harrison S (1967) J Am Chem Soc 89: 5723

Molecular Movements and Translocations Controlled by Transition Metals and Signaled by Light Emission

Valeria Amendola, Luigi Fabbrizzi, Carlo Mangano, Piersandro Pallavicini

Dipartimento di Chimica Generale, Università di Pavia, via Taramelli 12, 27100 Pavia, Italy
E-mail: fabbrizz@unipv.it

Transition metals can play a determining role in promoting oriented movements at the molecular level. Examples include the oscillation of a pendant arm in Ni(II) and Cu(II) scorpionate complexes (i.e., complexes of a tetraaza macrocycle containing a flexible coordinating side chain), which can be relocated either on the metal center or far away from it, by varying pH. Moreover, a transition metal itself can be reversibly translocated between the two defined compartments of a heteroditopic multidentate ligand, by taking profit (i) of a pH change (which modifies the binding tendencies of one compartment) or (ii) of a variation of the redox potential [which changes the oxidation state of the metal, e.g., Fe(III)/Fe(II), Cu(II)/Cu(I)]. Examples are given in which the molecular motion [the swinging of the pendant arm in an Ni(II) scorpionate complex; the pH-driven translocation of an Ni(II) ion within an acid-sensitive two-box system] is signaled to the outside through a net change of the fluorescent emission of a built-in anthracene fragment.

Keywords: Molecular movements, Metal translocation, Scorpionate complexes, Fluorescence switches, M(III)/M(II) and M(II)/M(I) redox couples

1 Introduction 79

2 pH- and Redox-Controlled Relocation of a Covalently Linked Pendant Arm 80

3 pH- and Redox-Controlled Translocation of Metal Ions within Two-Compartment Ligands 91

3.1 pH-Driven Translocation of Metal Ions 91
3.2 Redox-Driven Translocation of Metal Ions 102
3.3 Redox-Driven Anion Translocation Between Metal Centers 108

4 Perspectives 113

5 References 114

1 Introduction

There exist molecular systems made of mobile and fixed components, in which the position of the mobile fragment can be varied at will by means of an

Structure and Bonding, Vol. 99

external stimulus (in an aqueous medium: the variation of pH or the change of the redox potential). As a first prerequisite for the generation of a controlled movement, the mobile part should be able to bind the fixed molecular body according to a labile interaction: electrostatic (including hydrogen bonding), σ- and π-donor/acceptor, metal-ligand. Secondly, the fixed component should offer the mobile fragment two non-equivalent binding sites. In such circumstances, altering the binding tendencies of the two sites by the external input inverts the interaction priority, thus inducing the translocation of the mobile part to the site that has become energetically more favorable. The lability of the interaction ensures the occurrence of the reverse translocation process, following an input of the opposite nature (e.g., addition of base, if the original input was addition of acid; addition of a reducing agent, after the addition of an oxidizing agent). Stoddart's two-station rotaxanes (based on π-donor/acceptor interactions and driven by both acid-base and redox inputs [1]) and Sauvage's asymmetric 2-catenanes (based on metal-ligand interaction and driven by a redox input [2]) are among the first supramolecular systems deliberately designed to carry out controlled movements at the molecular level.

In the present chapter, we will focus our attention on motions occurring in systems containing one or more transition metal centers: in particular, the controlled movement will result from the alteration of the labile metal-ligand bonds. Examples will include the swinging of a pendant arm, which possesses a donor atom and is covalently linked to the ligand backbone of a macrocyclic complex; following a pH change or the variation of the redox potential, the pendant arm can be relocated either on the metal center or far away from it. Moreover, we will consider the case in which the oriented movement is generated by the displacement of an ionic particle between two definite and non-equivalent positions in the same molecular framework. When the particle is a transition metal, translocation from one position to the other can be induced by either a change of the oxidation state of the metal (which modifies its binding tendencies) or a variation of pH (which, under appropriate circumstances, may alter the binding priority of the two sites).

Special attention will be devoted to systems able to sharply signal to the outside the occurrence of the movement through the drastic change of a given molecular property. An especially suitable property for signaling purposes is luminescence, which can be visually perceived and instrumentally detected with extreme sensitivity. On the other hand, systems in which a chemical input induces the controlled and reversible relocation of a mobile part convert chemical energy into mechanical work and are therefore defined molecular machines [3, 4]. If the repeatable motion is accompanied by on/off switching of a luminescent signal, such devices can be defined as *light-emitting machines*.

2
pH- and Redox-Controlled Relocation of a Covalently Linked Pendant Arm

In 1977 Kaden reported on the intriguing solution behavior of the nickel(II) complex of the functionalized macrocycle **1** [5].

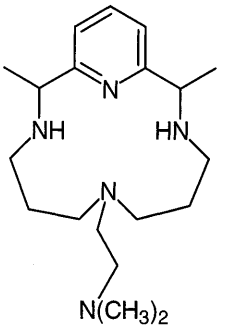

1

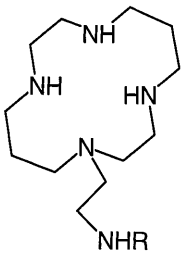

2 R = H

3 R = CH_2-

In the $[Ni(II)\text{-}(\mathbf{1})]^{2+}$ complex, the metal center is firmly incorporated by the tetraaza macrocyclic ring, according to a square stereochemical arrangement, in which the four nitrogen atoms of the ring are coplanar with the Ni(II) ion. In this situation, Ni(II) is especially resistant to the demetallation due to the so-called *kinetic macrocyclic effect* [6]. In particular, the tetraaza macrocyclic complex persists indefinitely in a strongly acidic solution, even if the processes of metal extrusion and protonation of the nitrogen atoms would be very favored from a thermodynamic point of view. The Ni(II)—N bond itself (with both amine and pyridine donor atoms) is intrinsically labile: thus, inertness must derive from the steric constraints imposed by the cyclic ligand. In particular, it has been observed that demetallation in tetraaza macrocyclic complexes would require the simultaneous breaking of two metal-nitrogen bonds, an event which is mechanically impeded and poorly favored from a probability point of view. On the other hand, ligand **1** contains a fifth binding site, the tertiary nitrogen atom belonging to the ethylamine side-chain covalently linked to the macrocycle. Ni(II) likes six-coordination, according to an octahedral stereochemistry: thus, the dimethylamine group of the pendant arm goes to occupy one of the axial positions of the octahedron, the other axial position being occupied, in an aqueous solution, by a water molecule (structure **I** in Fig. 1).

In an octahedral coordinative environment, the Ni(II) ion, electronic configuration d^8, possesses two unpaired electrons and displays three *d-d* optical transitions, which are formally symmetry forbidden and which are in any case responsible for the pale blue-violet color. Actually, a solution of $[Ni(II)\text{-}(\mathbf{1})]^{2+}$, adjusted to pH ≥ 7 exhibits a pale blue-violet color. The interaction of Ni(II) with the axially bound amine nitrogen atom does not suffer from any steric constraint and is therefore labile. Thus, it is expected that, on acidification, the amine group is quickly protonated and removed from coordination. Indeed, bringing pH from 7 to 5 causes the color of the solution to change from pale blue to yellow, while a relatively intense

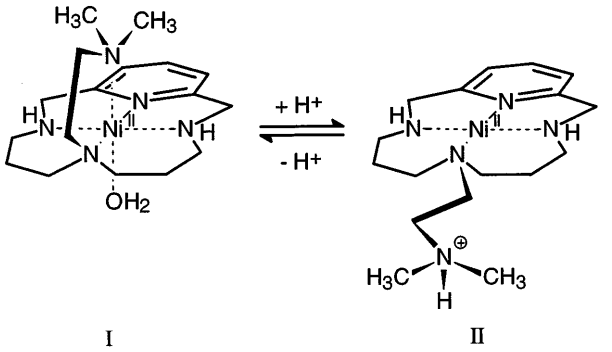

Fig. 1. The pH-controlled coordination of an amine pendant arm to a Ni(II) center encircled by a tetraaza macrocycle. When the pendant arm is apically bound, the Ni(II) complex has an elongated octahedral stereochemistry, the sixth coordination site being occupied by a water molecule (**I**, high-spin state, blue-violet color). On protonation, the pendant arm is detached, and a square-planar complex forms (**II**, low-spin state, yellow color)

absorption band develops at 480 nm. The latter band corresponds to a Ni(II) complex of square planar stereochemistry, in which the four nitrogen atoms of the macrocyclic ring remain coordinated to the metal and the ammonium group of the pendant arm stays far away from the coordination sphere (structure **II** in Fig. 1). The octahedral-to-square stereochemical rearrangement induces serious modifications of the bonding and electronic properties of the metal center: in particular, in-plane Ni(II)—N bond distances are shortened (from 2.05–2.10 Å to 1.85–1.90 Å) and the corresponding increase of the in-plane interactions causes electron pairing. Thus, a moderate change of pH (achieved through the addition of a fraction of drop of a standard acid solution) generates remarkable changes in the system $[\text{Ni(II)-(}\mathbf{1}\text{)}]^{2+}$: changes of the stereochemistry, of the color and of the magnetic properties (i.e., from a paramagnetic species, high-spin, to a diamagnetic species, low-spin). The change is quickly reversible and addition of standard base, enough to bring the pH back to 7, relocates the pendant arm on one of the axial positions of the octahedron, as indicated by the color change from yellow to pale blue. Notice that the pK_A value associated to the dissociation of the ammonium group in the Ni(II) complex of **1** is 6.29, a value remarkably lower than that typically observed for an uncoordinated tertiary amine group; for instance, the pK_A of trimethylamine is 9.81. The substantial difference of the pK_A values (which corresponds to a free energy change of 4.8 kcal · mol^{-1}) mainly reflects the exothermic formation of the Ni(II)—N(tertiary) axial bond. Varying the nature of the donating group of the pendant arm is expected to alter the intensity of the Ni(II)—N interaction and, consequently, to change the pK_A value.

For instance, in the functionalized macrocycle **2** the donor atom of the ethylamine pendant arm is a primary, rather than a tertiary, amine nitrogen atom, which gives rise to a stronger axial interaction with the metal. In fact, the pK_A of the pendant amine group in the $[\text{Ni(II)-(}\mathbf{2}\text{)}]^{2+}$ complex, 2.8, is much lower than observed for the corresponding complex of **1**. Noticeably, in the

$[Ni(II)\text{-}(\mathbf{2})]^{2+}$ complex the process of attack/detachment of the pendant arm at/from the metal center can also be induced by a redox input, in particular by carrying out the reversible Ni(II)/Ni(III) change. In this connection, it has to be noted that coordination by the cyclam-like tetramine ring of ligand **2** favors the access to the otherwise uncommon Ni(III) state. For instance, the potential of the Ni(III)/Ni(II) couple within the cyclam ring, in 1 M HCl, is 0.71 V. The easy access to the trivalent state essentially reflects the capability of the symmetric 14-membered tetramine macrocycle to establish especially strong in-plane interactions which raise the energy of the $d_{x^2-y^2}$ level from which the electron is abstracted in the $Ni(II)^{II}$-to-Ni(III) oxidation process. Moreover, Ni(III) has to be low-spin (d^7 electronic configuration, with an unpaired electron) and likes being six-coordinated, according to an axially distorted octahedral stereochemistry (distortion, e.g., elongation, is imposed by the Jahn-Teller effect). On carrying out an exhaustive electrolysis experiment on a solution of the Ni(II) complex of **2**, which is also 10^{-3} M in $HClO_4$ (yellow, pendant arm protonated) by setting the potential of the platinum gauze acting as a working electrode at 0.9 V vs. SCE, the color turns from yellow to bright green, due to the formation of the Ni(III) complex. There is evidence from the ESR spectrum (splitting of the g feature into three lines of equal intensity) that the pendant arm is axially bound to the metal. Thus, the Ni(II)-to-Ni(III) oxidation induces the deprotonation of the ammonium group of the pendant arm and its simultaneous relocation on the metal center; at the same time, a water molecule goes to occupy the other axial position to complete the octahedral coordination (see the **b** to **c** equilibrium in Fig. 2). This behavior reflects the greater affinity of Ni(III), compared to Ni(II), towards both amine donor atom binding and six coordination. However, it has to be noted that the binding tendency of the pendant arm towards Ni(III) is not able to resist H^+ competition at a higher concentration of acid. In particular, in a 0.2 M $HClO_4$ solution of the electrochemically generated Ni(III) complex of **2**, the g feature appears as a single line, indicating that the pendant nitrogen atom is no longer bound to the metal, but stays far away from the coordination sphere, as an ammonium group: in particular, a six-coordinate stereochemical arrangement is maintained around the Ni(III) center, but both axial positions are now

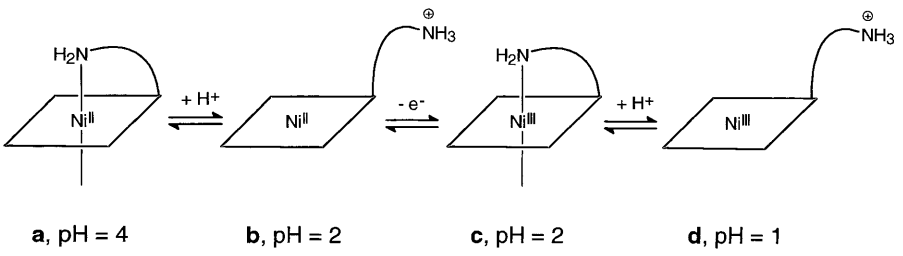

Fig. 2. pH- and redox-controlled relocation of the aminoethyl pendant arm in the nickel complex of **2**. The pendant arm can be sequentially bound to and detached from the metal center, by varying the pH and the oxidation state of the metal center (whether +2 or +3)

occupied by water molecules (structure **d** in Fig. 2). The multi-step equilibrium in Fig. 2 illustrates well the dynamic behavior of the nickel complex of **2** in solution: on alternating the external input (either $\pm H^+$ or $\pm e^-$), the pendant arm is relocated on and far away from the metal center.

Ligands **1** and **2** have been given the current name of *scorpionands*, by considering that they firmly chelate an individual (the metal ion in a given oxidation state), which can be further bitten from the top by an aggressive tail. Nickel scorpionate complexes are convenient systems for carrying out controlled molecular motions driven by either a pH change or a variation of the redox potential. The mobile part (the flexible side-chain) is covalently connected to its fixed counterpart (the rigid tetraaza ring). The mobile and the fixed components can further interact through a labile type of bond which involves the metal center: motion results from the competition of the metal center and of the hydrogen ion for the amine group of the pendant arm.

We were recently interested in associating the pH-controlled motion of the pendant arm in nickel(II) scorpionate complexes to the generation of a luminescent signal. In this perspective, an anthracene fragment (An) was covalently linked to the nitrogen donor atom of the ethylamine side-chain of scorpionand **2**, through a $-CH_2-$spacer, to give **3**, which will be indicated in the following as L [8]. The solution behavior of the Ni(II)-L system was investigated in an $MeCN/H_2O$ mixture (4:1 v/v): the non-aqueous solvent was used to provide solubility of the complex, which contains a definitely lipophilic portion, the An subunit. Potentiometric titration experiments assessed the presence of three distinct metal complex species over the 2–12 pH range, as shown in the distribution diagram of Fig. 3.

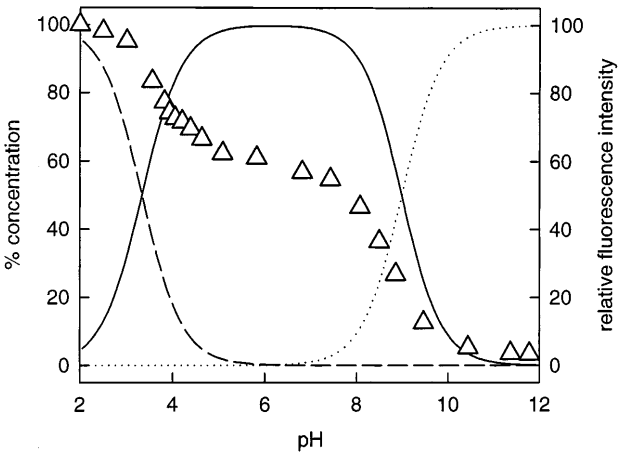

Fig. 3. The distribution curves of the species present at the equilibrium for the Ni(II)/**3** system in an $MeCN/H_2O$ mixture (4:1, v/v), % concentration in the left vertical axis:$[Ni(II)(LH)]^{3+}$, dashed line, structural formula **I** in Fig. 4; $[Ni(II)(L)]^{2+}$, solid line, structural formula **II** in Fig. 4; $[Ni(II)(L)(OH)]^{+}$, dotted line, structural formula **III** in Fig. 4. Open triangles indicate the intensity of the fluorescent emission of the anthracenyl fragment appended to the aminoethyl side chain of scorpionand **3** (right vertical axis)

At pH ≤ 3, a species of stoichiometry $[Ni(II)(LH)]^{3+}$ predominates, in which the secondary amine group of the pendant arm is protonated. In the 3–9 pH interval, the octahedral $[Ni(II)(L)]^{2+}$ complex is present, with the amine group of the pendant arm axially bound to the metal. At pH ≥ 9, a further acidic dissociation process is observed and the $[Ni(II)(L)(OH)]^{+}$ species forms: it has been suggested that hydrogen ion is released from the water molecule that occupies the other axial position of the coordination octahedron. Very beneficial for signaling purposes, pH variation from 2 to 12 induces remarkable changes in the fluorescent emission of the anthracene fragment. In Fig. 3, the intensity of the emission band, I_F, measured at varying pH, has been superimposed on the distribution diagram of the three species. It is seen that:

(i) I_F decreases with increasing pH according to a reversible three-level profile and
(ii) each level corresponds to one of the three species present at the equilibrium.

In particular, the highest fluorescent emission pertains to the $[Ni(II)(LH)]^{3+}$ complex, in which, due to the electrostatic repulsion between the ammonium group of the pendant arm and the Ni^{2+} ion, the fluorophore stays at the highest distance from the metal center: the stereochemical arrangement of the $[Ni(II)(LH)]^{3+}$ complex is sketched in Fig. 4 (structure **I**). The distance between the Ni(II) ion and the anthracene carbon atom connected to the linker, Ni(II)-C9, as calculated through molecular modeling, is 7.7 Å. It is possible that electrostatic repulsive effects minimize the dangling of the pendant arm which may bring the anthracene fragment to occasional Van der Waals contact with the Ni(II) center (which should quench, at least partially, the natural emission of the fluorophore). In this connection, it has to be noted

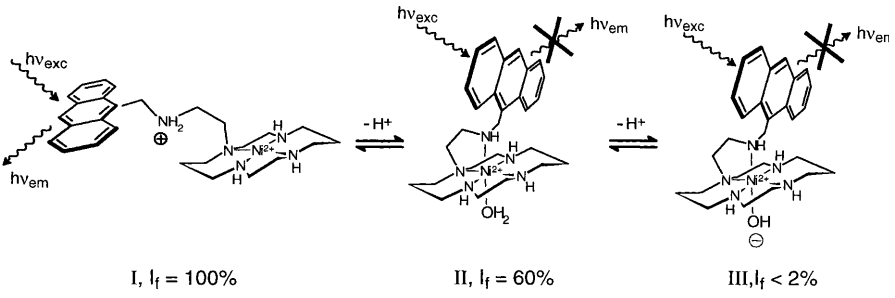

Fig. 4. The mechanism of the pH controlled variation of the fluorescent intensity of the anthracene subunit in the Ni(II)/**3** system. The molecular movement of the pendant arm (from **I** to **II**) is signaled by a partial quenching of the light-emission [due to an energy transfer process involving the Ni(II) center]. Complete quenching (step from **II** to **III**) is associated to the deprotonation of the water molecule axially bound to the metal [which promotes the occurrence of an electron transfer process from Ni(II) to the excited anthracene fragment]

that the quantum yield, Φ, for the $[Ni(II)(LH)]^{3+}$ is 0.083 in EtOH, to be compared to $\Phi = 0.27$ for plain anthracene, in the same medium.

At pH $\geq$ 3, following deprotonation, the secondary amine group of the side-chain goes to occupy one of the axial sites, an event which is accompanied by quenching of the fluorescent emission to 60% of the intensity measured in the strongly acidic region: pendant arm coordination brings the An fragment much closer to the metal center (see structure **II** in Fig. 4, for which the calculated distance between the C9 atom of the anthracene fragment and Ni(II) is 4.4 Å). This makes the occurrence of occasional metal-fluorophore contact and of an electronic energy transfer between An* and the high-spin Ni(II) ion more favorable, thus competing with the radiative decay of the excited fluorophore and causing partial quenching of the light emission. Deprotonation of the metal-bound water molecule (structure **III** in Fig. 4) activates a further mechanism which quenches An* emission almost completely. There is evidence for an electron transfer nature of this process. It has been hypothesized that the reduction of the electrical charge associated to OH^- binding favors the Ni(II)-to-Ni(III) oxidation process, thus making possible the occurrence of an especially efficient Ni(II)-to-An* electron transfer process.

In conclusion, the attack/detachment of the fifth nitrogen atom on the Ni(II) center, which is associated to the pH-controlled motion of the pendant arm, is signaled by partial quenching/full restoring of the emission of the An subunit. However, there exists a further important effect, which brings down the fluorescent emission almost completely (and partially restores it through an opposite input). This effect is not related to any drastic nuclear rearrangement, but results from the moderate electron reorganization on the metal center following OH^- binding.

Several molecular and supramolecular luminescent systems of varying complexity have been reported, whose emission can be turned on/off at will by means of an external input (either a pH or a redox potential change) and have been therefore considered as molecular level analogues of everyday life light switches [9–13]. The Ni(II)-**3** system is different in that it controls three levels of illumination: high-low-off, as switches operating car headlights do in the macroscopic world.

Other metal ions, e.g., Cu(II), can replace Ni(II) in scorpionate complexes, providing a similar dynamic behavior. When the side-chain is protonated, the Cu(II) complex exhibits a square stereochemistry. Following pendant arm deprotonation and metal binding, the complex adopts a square-pyramidal coordination geometry. The stereochemical rearrangement induces a red-violet to blue-violet color change, which corresponds to the shift of the Cu(II) *d-d* broad absorption band towards the higher wavelengths. For instance, in the case of the Cu(II)-**2** system, the $[Cu(II)(LH)]^{3+}$ complex presents an absorption band centered at 528 nm ($\varepsilon = 129\ M^{-1} \cdot cm^{-1}$), whereas $[Cu(II)(L)]^{+}$ absorbs at 580 nm ($\varepsilon = 180\ M^{-1} \cdot cm^{-1}$). In general, pendant arm coordination is less favored for Cu(II) than for Ni(II) complexes, as indicated by the higher value of pK_A [for the Cu(II)-**2** system $pK_A = 4.0$]; this results from the fact that the stereochemical change for Cu(II) scorpionate

complexes (from square to square-pyramid) is characterized by the formation of one more metal-nitrogen bond, whereas in the case of Ni(II) pendant arm coordination involves also the additional contribution which results from the binding of a water molecule (square to octahedron change).

Color signaling of pH-induced pendant arm relocation is less eye-catching for Cu(II) than for Ni(II), where axial binding induces a drastic change of the electronic structure of the d^8 cation (from low-spin to high-spin), a unique feature, which cannot be experienced by a d^9 center like Cu(II). On the other hand, fluorescence signaling for the Cu(II)-**3** system is as powerful and showy as observed with Ni(II)-**3**.

Figure 5 displays the distribution diagram of the species present at the equilibrium in the case of the Cu(II) scorpionate complex. They are the same as those observed in the case of the Ni(II) analogue, namely: $[Cu(II)(LH)]^{3+}$, $[Cu(II)(L)]^{2+}$, $[Cu(II)(L)(OH)]^{+}$. Also, the I_F vs. pH profile is similar to that shown by Ni(II), disclosing three well-defined plateaux. The first substantial decrease of the fluorescent emission intensity, observed in the acidic region (to about 40%) is associated to the ammonium group deprotonation and relocation of the pendant arm on the Cu(II) center ($pK_{A1} = 4.3$); quenching has to be ascribed to the occurrence of a rather efficient electronic energy transfer process involving An* and Cu(II). A second step is observed in the slightly alkaline region, pertinent to the $[Cu(II)(L)]^{2+} + H_2O = [Cu(II)(L)(OH)]^{+} + H^{+}$ equilibrium ($pK_{A2} = 8.5$), which brings I_F down to about 20% of the original value (Fig. 6). However, the stereochemical change promoting the latter quenching process cannot be the same as hypothesized

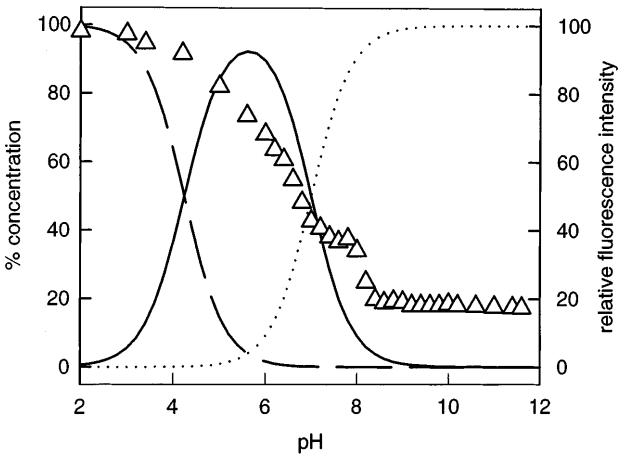

Fig. 5. The distribution curves of the species present at the equilibrium for the Cu(II)/**3** system in an $MeCN/H_2O$ mixture (4:1, v/v), % concentration in the left vertical axis: $[Cu(II)(LH)]^{3+}$, dashed line, structural formula **I** in Fig. 6; $[Cu(II)(L)]^{2+}$, solid line, structural formula **II** in Fig. 6; $[Ni(II)(L)(OH)]^{+}$, dotted line, structural formula **III** in Fig. 6. Open triangles indicate the intensity of the fluorescent emission of the anthracenyl fragment appended to the aminoethyl side chain of scorpionand **3** (right vertical axis)

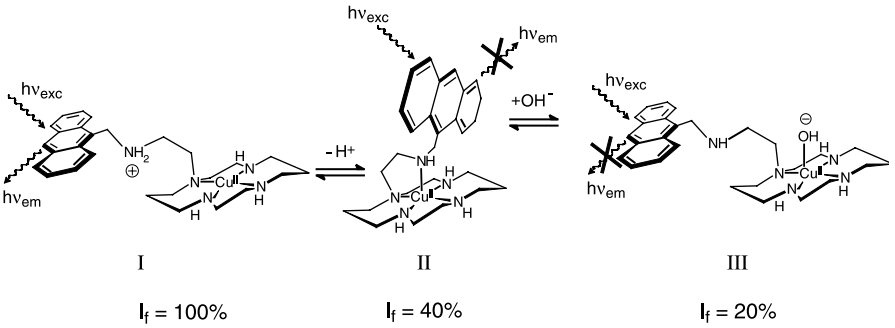

Fig. 6. The mechanism of the pH-controlled variation of the fluorescent intensity of the anthracene subunit in the Cu(II)/**3** system. Binding of the pendant arm to the Cu(II) center, when moving from **I** to **II**, induces a substantial quenching of the fluorescent emission (ascribed to an energy transfer process involving the metal center). In the second step (from **II** to **III**) the pendant arm is displaced by an hydroxide ion: an electron transfer process from the secondary amine group close to the excited anthracene fragment takes place and is responsible for the additional quenching of the fluorescence (to less than 20%)

for the case of the Ni(II)-**3** system (i.e., deprotonation of an already axially bound water molecule). In fact, $[Cu(II)(L)]^{2+}$ neither possesses a coordinated water molecule nor displays any tendency to reach six-coordination by binding an OH^- ion coming from the solution. It is therefore suggested that the OH^- anion replaces in the apical site of the square pyramid the amine group of the pendant arm, which is removed from the coordination sphere. Under such circumstances, an electron transfer process takes place from the uncoordinated secondary amine group to the nearby excited anthracene fragment, quenching the fluorescent emission. Apparently, the N-to-An* electron transfer mechanism is not so efficient as the Ni(II)-to-An* electron transfer process observed in the $[Ni(II)(L)(OH)]^+$ complex, which is able to quench emission almost completely (I_F brought down to less than 2%).

The controlled motion of an arm covalently linked to a ring, a further scorpionand-like system, has been designed also with purely organic systems, in the absence of metal ions. A recent example refers to system **4**, in which a side-chain containing the π-electron rich 1, 5-dioxynaphthalene moiety is covalently linked to a tetracationic cyclophane, containing two π-electron deficient 4, 4′-bipyridinium subunits, as indicated in Fig. 7 [14].

In an MeCN solution, the naphthalene residue is completely threaded inside the cavity of the covalently linked cyclophane ring, in order to profit from donor-acceptor interactions of a π nature. Among the pieces of evidence, self-complexing is demonstrated by the presence of a π-π charge transfer absorption band in the visible region ($\lambda_{max} = 515$ nm, $\varepsilon = 650\ M^{-1} \cdot cm^{-1}$), which is responsible for the intense red color. System **4** undergoes two two-electron reduction steps, at −0.35 and at −0.71 V vs. SCE. The first reduction step is especially relevant from the point of view of the molecular motion. In fact, during this process, one electron goes on each 4, 4′-bipyridinium fragment of the cyclophane ring, drastically reducing its acceptor tendencies.

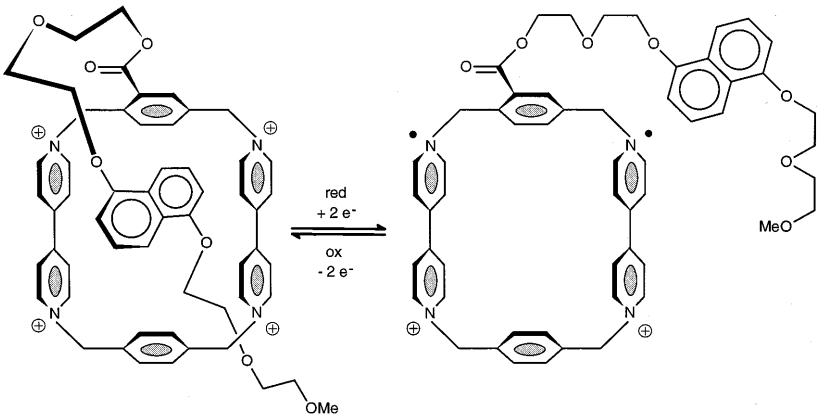

4

Fig. 7. Redox-controlled threading/unthreading of a π-donor pendant arm within a π-acceptor cyclophane ring. The process takes place in an MeCN solution in the course of a controlled potential electrolysis experiment

Thus, the π-π interaction vanishes and the naphthalene containing pendant arm dethreads. Occurrence of the dethreading process could be in principle monitored by looking at the emission of the intrinsically fluorescent 1, 5-dioxynaphthalene fragment. In fact, in the self-complexed system, the fluorescence of the naphthalene containing moiety is fully quenched due to the occurrence of either an energy transfer process (since the tetracationic cyclophane possesses suitable low-energy excited states) or an electron transfer mechanism (from the reducing side-chain to the oxidizing ring). In these circumstances, one would expect that, on dethreading, any quenching mechanism ceases and the intrinsic emission of the 1, 5-dioxynaphthalene fragment is restored. However, when carrying out an exhaustive electrolysis experiment with the potential of the working electrode set at −0.40 V vs. SCE (i.e., a value 50 mV more negative than the $E_{1/2}$ observed for the first two-electron reduction process in the cyclic voltammetry profile), no fluorescence recovery from the naphthalene fragment was seen. This has been ascribed to the fact that the short and flexible polyethoxy chain keeps the naphthalene (naph) moiety close to the reduced cyclophane ring, allowing the occurrence of a high number of encounters within the lifetime of naph* excited state and inducing fluorescence quenching. Notice that fluorescence quenching due to occasional contacts between the ring and the pendant arm was not equally efficient in the protonated form $[M(II)(LH)]^{3+}$ of the previously discussed light-emitting metal scorpionate complexes. This may be due to the existence of rather strong electrostatic repulsions between the ammonium group and the M^{2+} cation, which rigidifies the side-chain and minimizes the encounters between the photo-excited fragment and the metal center (the quantum yield of the $[M(II)(LH)]^{3+}$ complex was about 1/3 of that observed for plain anthracene, under the same conditions). However, occurrence of the redox

induced dethreading process in system **4** is demonstrated by the disappearance of the CT absorption band at 515 nm and by the development of the band of the reduced bipyridinium units. On the other hand, following two-electron oxidation, the tetracationic cyclophane is restored and the side-chain threads again. Oxidation can be carried out either electrochemically or chemically (for instance, by bubbling dioxygen into the MeCN solution).

A unique example of light-driven motion of a side-chain covalently linked to a ring was described by Shinkai in the 1980s and is illustrated in Fig. 8 [15, 16]. In system **5**, the side-chain ends with an ammonium group, which can interact electrostatically with the ethereal oxygen atoms of an 18-crown-6 subunit. The pendant arm contains also an azobenzene fragment, whose light-induced isomerization controls the electrostatic interaction with the crown. In particular, in the thermodynamically stable form, the azobenzene subunit exhibits a *trans* configuration, which forces the ammonium group to stay far away from the ring. Irradiation in the UV region induces π-π^* excitation and rotation around the N—N bond, which brings system **5** to its photostationary state: 80% *cis*, 20% *trans*. In the *cis* isomer, the ammonium group of the pendant arm can interact electrostatically with the polyether ring. Re-isomerization to 100% of the *trans* isomer, which involves the endothermic detachment of the pendant arm from the crown, can be induced photochemically through irradiation with visible light, or can take place thermally, at a much lower rate. In particular, the thermal process at 30 °C is characterized be a lifetime of 5.9 h. It has to be noted that when the pendant arm ends with an amine group (rather than with an ammonium group), which excludes any

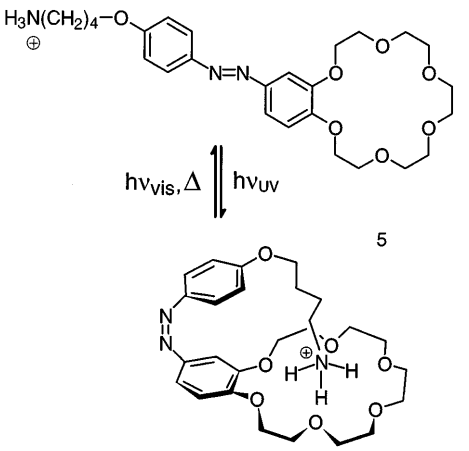

Fig. 8. A light-driven movement of an pendant arm which bears an ammonium group and is covalently linked to a crown ether. UV irradiation induces the *trans*-to-*cis* rearrangement of the azobenzene fragment. The self-complexing process is favored by the establishing of hydrogen bonding interactions between the ammonium group and the oxygen atoms of the crown. Decomplexation (*cis*-to-*trans* re-isomerization) can take place either via irradiation with visible light or thermally

electrostatic interaction with the ring, UV irradiation produces a smaller amount of the *cis* isomer (*cis* 63%, *trans* 37%), while thermal re-isomerization to the *trans* form takes place distinctly faster, the lifetime for the *cis-trans* process at 30 °C being 2.7 h.

The light-induced isomerization of the azobenzene moiety is a classical example of controlled molecular motion and has provided the basis for the construction of some of the first archetypes of molecular machines [17]. In system **5**, the pendant-arm/ring interaction concurs to improve the efficiency of the azobenzene-based engine, which converts photonic energy into a mechanical work, at the molecular level.

3
pH- and Redox-Controlled Translocation of Metal Ions within Two-Compartment Ligands

Classically defined, molecular machines possess a movable part which can be relocated, at will, in two, or more, different sites of either a molecular or supramolecular system, as a consequence of an external input (rotaxanes, catenanes, scorpionates, systems based on the azobenzene moiety). When the mobile portion is displaced with respect to the fixed molecular framework, energy (chemical or photonic) is converted into a mechanical work. However, there exists another way to produce mechanical work at the molecular level: i.e., by taking an ionic particle loosely bound to a given site and displacing it to a different not too distant site, within the same molecular framework. Again, in order to fulfill the typical requirements of an oriented molecular motion, the displacement has to be the consequence of an external perturbation (e.g., variation of the pH or of the redox potential of the solution), and must be reversible. The controlled motion of a particle between two distinct sites, following a defined pathway, is called *translocation*. In the following, we will consider examples of translocation of metal ions (driven by either a pH or redox potential change) and of inorganic anions (induced by a variation of the redox potential).

3.1
pH-Driven Translocation of Metal Ions

Given a molecular system containing two distinct and non-equivalent coordinating compartments, A and B, a metal ion M can be translocated from A to B and vice versa by means of a pH change. pH-controlled translocation requires that one of the compartments, e.g., A, displays Brønsted acid properties, for instance, undergoing the acid-base equilibrium: $AH_n = A^{n-} + nH^+$. An important consequence of deprotonation is that binding tendencies towards M are substantially enhanced. The further significant point for the purposes of metal translocation is that the coordinating tendencies of the other compartment, B, are intermediate between those of A^{n-} and AH_n. In other words, the constants of the complexation equilibrium $M + L = ML$, should decrease along the series:

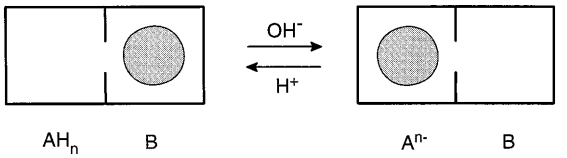

Fig. 9. The model for the pH driven translocation of a metal ion between the two compartments of a heteroditopic ligand. One of the compartment must also display the properties of a Brønsted acid, through the $AH_n = A^{n-} + nH^+$ equilibrium. If the affinity sequence towards the metal center is $A^{n-} > B > AH_n$, the consecutive deprotonation-protonation of compartment A induces the translocation from B to A and vice versa

$A^{n-} \gg B \gg AH_n$ [18]. In these circumstances, when compartment A exists in its protonated form, AH_n, the metal prefers to reside in B. On increasing the pH, compartment A deprotonates and M chooses to move to it in order to profit from more intense metal-ligand interactions. Then, on subsequent addition of standard acid and protonation of A^{n-}, the metal leaves the no longer appealing compartment AH_n and moves back to B. The reversible pH-controlled translocation of M between compartments A and B in a two-box ditopic receptor is pictorially illustrated in Fig. 9.

Quick reversibility requires that the metal ion is substitutionally labile: thus, Cu(II) and Ni(II) are suitable ions for translocation, and Co(III) is not. Moreover, the envisaged system should be flexible enough to bring A and B moieties at occasional contact, in order to allow the metal to be transferred from one compartment to the other.

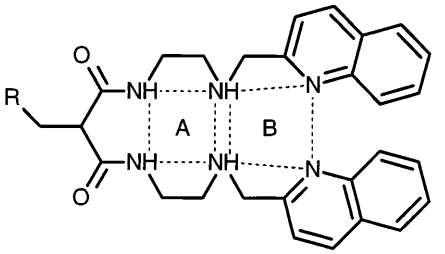

6, R =

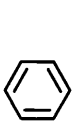

7, R =

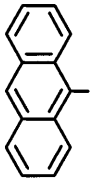

The recently synthesized sexidentate ligand **6** seems to fulfill the prerequisites for hosting the reversible translocation of a transition metal ion under a pH gradient [19]. Compartments A and B are clearly defined: compartment A (in its protonated form AH_2) contains two amine nitrogen atoms and two amide groups. In view of the very poor coordinating tendencies of the amide

nitrogen atoms, the N_4 donor set of the AH_2 compartment is expected to form poorly stable complexes with any kind of metal. In presence of a transition metal late in the 3*d* series [Ni(II), Cu(II)], AH_2 tends to release two H^+ ions, one from each amide group, at a neutral or slightly alkaline pH and, in its deprotonated form, A^{2-}, establishes especially strong metal-ligand interactions. Thus, the doubly deprotonated A^{2-} donor moiety is expected to form particularly stable metal complexes. The donor set of compartment B consists of two amine groups and two pyridine nitrogen atoms. Coordinating tendencies of B are expected to be much higher than those of AH_2, but distinctly lower than those of A^{2-}. This fulfills the stability sequence required for pH-driven metal translocation: $A^{2-} \gg B \gg AH_2$. In particular, the acidity controlled motion of the Ni(II) ion between compartments A and B of the ditopic ligand **6** has been recently described.

The formation of 1:1 complexes between Ni(II) and ligand **6** (indicated in the following as LH_2) in an $MeCN/H_2O$ mixture (4:1, v/v), at varying pH, is illustrated by the distribution diagram shown in Fig. 10. The concentration profiles of the species present at the equilibrium over the 2–12 pH interval were calculated from the pertinent complexation constants, which had been

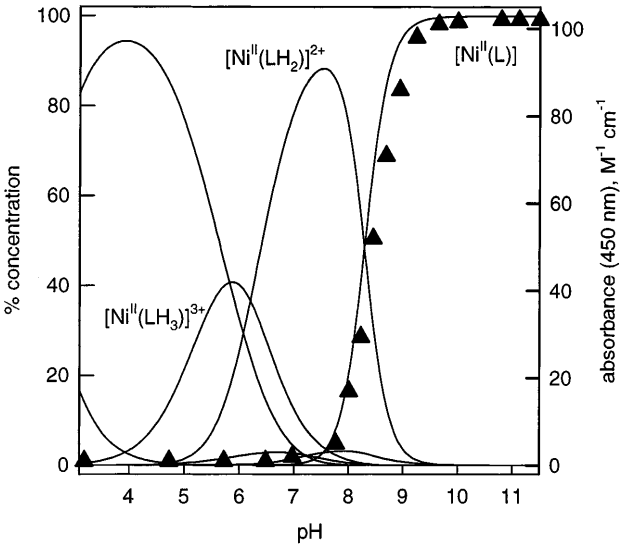

Fig. 10. The distribution diagram of the species present at the equilibrium in a solution containing equimolar amounts of Ni(II) and of the heteroditopic ligand **6** (% concentration in the left vertical axis). Relevant species to the translocation process are:$[Ni(II)(LH_2)]^{2+}$, 90% at pH = 7.5, in which the Ni(II) center occupies compartment B, and [Ni(II)(L)], 100% at pH ≥ 9.5, in which Ni(II) has moved to the doubly deprotonated A^{2-} compartment. When in the A^{2-} compartment, the Ni(II) center shows a square-planar stereochemistry (low-spin, yellow, *d-d* absorption band at 450 nm, $\varepsilon = 103\ M^{-1} \cdot cm^{-1}$): full triangles indicate the variation with pH of the intensity of such an absorption band (molar absorbance on the right vertical axis)

determined through non-linear least-squares treatment of pH-metric titration data. Two main metal complex species are present over the 7–10 pH range: the complex of the neutral ligand, $[Ni(II)(LH_2)]^{2+}$, which is present to 90% at pH 7.5, and the complex of the doubly deprotonated ligand, [Ni(II)(L)], which is present to 100% at pH ≥ 9. It has been suggested that in the dicationic complex $[Ni(II)(LH_2)]^{2+}$ the metal is located in compartment B, whereas in the neutral complex [Ni(II)(L)] the metal stays in the A^{2-} section. This argument is mainly based on the spectral features of the two complex species. The $[Ni(II)(LH_2)]^{2+}$ complex (pale blue solution, adjusted to pH = 7.5) exhibits two weak metal-centered absorption bands, at 606 nm ($\varepsilon = 11\ M^{-1} \cdot cm^{-1}$) and at 820 nm ($\varepsilon = 5\ M^{-1} \cdot cm^{-1}$). These band are typically observed with a high-spin Ni(II) ion in an octahedral stereochemical environment (the two unpaired electrons occupy the $x^2 - y^2$ and z^2 *d* orbitals). This coordinative environment can be provided by the two amine nitrogen atoms, the two quinoline nitrogen atoms and the oxygen atoms of two water molecules. Coordination by the quinoline nitrogen atoms is supported by the fact that the formation of the $[Ni(II)(LH_2)]^{2+}$ complex (when moving from pH 5 to 7.5) is accompanied by the progressive quenching of the weak emission of the quinoline fragments, at 392 nm. On the other hand, the solution of the [Ni(II)(L)] neutral complex is yellow and its absorption spectrum shows a relatively intense *d-d* band ($\varepsilon = 103\ M^{-1} \cdot cm^{-1}$) centered at 450 nm. Such a band is typically observed with Ni(II) complexes of square stereochemistry, which form with quadridentate ligands exerting strong in-plane interactions. This is the case of the tetraaza donor set consisting of two deprotonated amide groups and two amine groups. The extremely strong metal-ligand interactions induce pairing within the z^2 orbital of the two unpaired electrons of the Ni(II) center, which becomes diamagnetic (while its electronic configuration is said to be low-spin). Thus, a pH variation from 7.5 to 9 makes the Ni(II) ion move from compartment B to compartment A, and the translocation process is accompanied by a net change of both the electronic configuration and the magnetic properties of the Ni(II) center: from high-spin (paramagnetic) to low-spin (diamagnetic). Moreover, the occurrence of the translocation can be distinctly perceived both visually (through a sharp color change, from pale blue to yellow) and instrumentally (through the development of the absorption band of the [Ni(II)(L)] complex, centered at 450 nm.

Quite happily, the B-to-A translocation takes place in the time scale of the stopped-flow experiment and can be monitored through the growth of the band at 450 nm, when a solution containing equimolar amounts of Ni(II) and **6**, adjusted to pH 7.5 (thus containing 90% of the $[Ni(II)(LH_2)]^{2+}$ complex, syringe 1) is mixed with a solution buffered at pH 9.5 (CHES buffer, syringe 2). The family of spectra recorded in the course of the experiment is shown in Fig. 11. The lifetime τ associated to the first-order process is 0.25 ± 0.01 s.

On the other hand, when acid is added to the yellow solution adjusted to pH ≥ 9.5, containing 100% of the [Ni(II)(L)] complex, and pH is brought back to 7.5, the pale blue color is quickly restored, indicating that the metal ion has been relocated in the B compartment. The temporal progress of the A-to-B

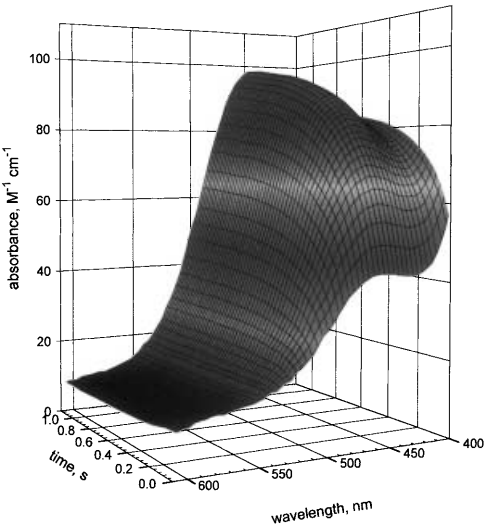

Fig. 11. The translocation of Ni(II) from compartment B to A of the heteroditopic ligand **6**, induced by a pH change from 7.5 to 9.5 and followed by stopped-flow spectrophotometry. The development of the band at 450 nm indicates that the Ni(II) ion has moved to the A^{2-} compartment. The first-order translocation process is characterized by a lifetime τ of 0.25 ± 0.01 s

translocation could be followed by a stopped-flow spectrophotometric technique, by monitoring the decay of the band at 450 nm, in an experiment in which a solution of [Ni(II)(L)], adjusted to pH 9.5 (syringe 1), was mixed with a solution of HEPES buffer (pH = 7.5, syringe 2). Noticeably, the reverse translocation process (A-to-B) was found to be significantly slower than the direct process, being characterized by a lifetime $\tau = 2.2 \pm 0.1$ s. In this connection, one must consider that the preliminary step of each translocation process, either direct or inverse, should involve the dissociation of the coordinative bonds. B-to-AH_2 translocation involves the dissociation of a high-spin Ni(II) ion, whereas the A^{2-}-to-B process involves the dissociation of a low-spin Ni(II) ion. Classical coordination chemistry studies have demonstrated that a low-spin d^8 metal center in a square planar coordinative environment (the case of the [Ni(II)(L)] complex), in view of the rather high value of the Crystal Field Activation Energy, is relatively inert with respect to ligand substitution, much more than a high-spin d^8 center in an octahedral stereochemical arrangement (the situation of the $[Ni(II)(LH_2)]^{2+}$ complex) [20].

Interest in associating molecular motion to the generation of a luminescent signal prompted us to equip the previously described ditopic system with a light-emitting subunit. In particular, an anthracene fragment was linked through a -CH_2- spacer to the middle carbon atoms of the aliphatic chain joining the amide groups of compartment A, to give system **7** [19].

The solution behavior of the Ni(II)/**7** system is very similar to that observed for **6** (which contained a benzyl instead of the anthracenyl substituent). In

particular, the same species were found to be present at the equilibrium over the 2–12 pH range, as indicated by the pertinent distribution diagram shown in Fig. 12. It is of interest for translocation purposes that the dicationic species $[Ni(II)(LH_2)]^{2+}$, in which the high-spin Ni(II) center is located in compartment B (diamine-diquinoline donor set), displays its maximum concentration (80%) at pH 7, whereas the neutral complex [Ni(II)(L)], in which the low-spin Ni(II) cation occupies the A^{2-} compartment (deprotonated diamide-diamine donor set), forms at 100% at pH ≥ 9. Thus, also with system **7**, the Ni(II) ion can be moved back and forth between the two compartments by a moderate pH change (from 7 to 9, and vice versa), i.e., through the addition to the solution of a few drops of standard base or acid. Very conveniently for signaling purposes, $[Ni(II)(LH_2)]^{2+}$ and [Ni(II)(L)] display totally different photophysical behaviors, so that the translocation process can be monitored by looking at the anthracene fluorescence and by recording the corresponding emission spectra. Fig. 12 shows that the intensity of the anthracene (An) emission, I_F (full triangles in the diagram), shows its highest value at pH = 7, i.e., in correspondence with the maximum concentration of the $[Ni(II)(LH_2)]^{2+}$ species. The fluorescence intensity of the solution of the $[Ni(II)(LH_2)]^{2+}$complex is the same as that of a solution of **7** in the absence of metal at the same pH, and is comparable to that of plain anthracene under the same conditions.

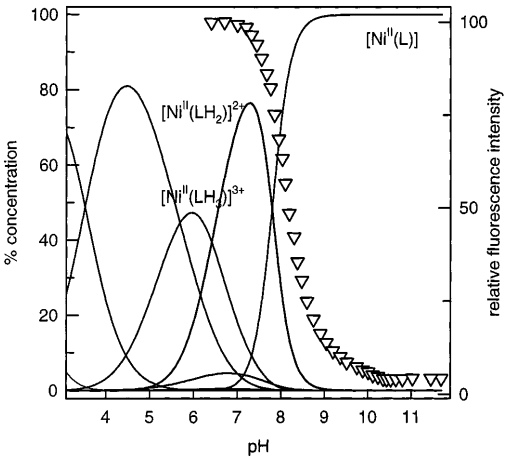

Fig. 12. The distribution diagram of the species present at the equilibrium in a solution containing equimolar amounts of Ni(II) and of the fluorescent heteroditopic ligand **7** (% concentration in the left vertical axis). Relevant species to the translocation process are: $[Ni(II)(LH_2)]^{2+}$, 80% at pH = 7.0, in which the Ni(II) center stays in compartment B, and [Ni(II)(L)], 100% at pH ≥ 8.5, in which Ni(II) has moved to occupy the doubly deprotonated A^{2-} compartment. Open triangles indicate the fluorescence intensity of the anthracene fragment covalently linked to the framework of **7**. When the Ni(II) center stays in compartment B, the anthracene subunit is not perturbed and discloses its full fluorescent emission. When the metal moves to compartment A^{2-}, an electron transfer process takes places from Ni(II) to the excited fluorophore which induces complete fluorescence quenching

This indicates that the Ni(II) center, when in the B compartment, is distant enough from the anthracene subunit for not interfering with its radiative decay. As the pH increases, I_F decreases following a sigmoidal profile, and complete quenching of An fluorescence is observed at pH ≥ 9, where the 100% of the [Ni(II)(L)] form is present (see Fig. 12). Thus, the location of the Ni(II) center within the ditopic system **7** is distinctly signaled by the emission of the anthracene component: when the metal is in compartment B, fluorescence is on; when it is in compartment A^{2-}, fluorescence is off.

Fluorescence quenching in complex [Ni(II)(L)] has to be ascribed to the occurrence of an electron transfer process from Ni(II) to the nearby photoexcited fluorophore An*, a process made possible by the easy oxidation to Ni(III) in the deprotonated diamide-diamine coordinative environment. On acidification to pH = 7.5, the metal is removed from the A^{2-} compartment and brought back to the B compartment, where it profits from much weaker metal-ligand interactions, which do not favor oxidation to the Ni(III) state: as a consequence, the eT mechanism vanishes and fluorescence is fully restored. The mechanism of the Ni(II) translocation, driven by a pH change and signaled through fluorescence quenching-revival is pictorially illustrated in Fig. 13. The process fits quite well to the metaphor of the light switch of the everyday life, as a mechanical act (metal displacement) switches on/off the light emitted by a connected bulb (the anthracene fragment), in a repeatable way.

The translocation processes, both direct and reverse, can be temporally followed, by carrying out spectrofluorimetric stopped-flow experiments and by monitoring the first-order decay development of I_F. The B-to-AH_2 translocation ($\tau = 12 \pm 1$ s) is faster than A^{2-}-to-B back translocation ($\tau = 66 \pm 12$ s), a pattern already observed in the case of system **6**. However, the rates of both direct and reverse processes are remarkably slower for **7** than for **6**. This is probably due to the presence of the bulky anthracene substituent, which slows down the conformational rearrangement to which the ligating backbone is

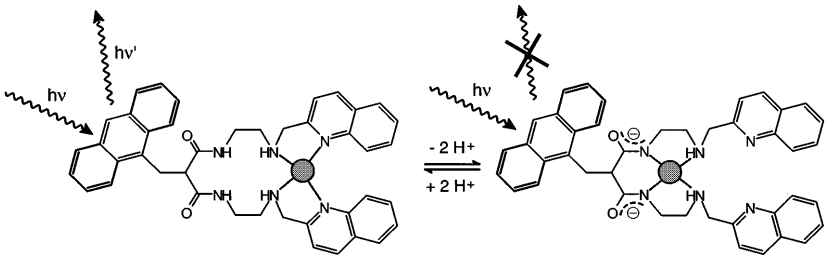

Fig. 13. A pictorial view of the Ni(II) translocation within the heteroditopic ligand **7**. The reversible molecular motion is signaled by quenching/revival of the intense anthracene emission, depending on whether the metal center is close to (fluorescence off) or far away from the fluorophore (fluorescence on). This system fits quite well the metaphor of the light switch, as the light emitted by the bulb (the fluorogenic fragment) is switched on/off through a mechanical operation (the pressure of a finger in the everyday life, the controlled displacement of a metal center in the molecular world)

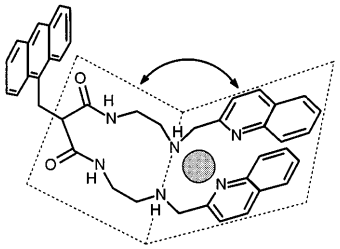

Fig. 14. The 'facing pages' mechanism. It is suggested that the metal translocation process of the type illustrated in Fig. 13 is associated to the occasional folding of the two halves of the heteroditopic ligand (either **6** or **7**). In practice, compartments A and B are laid on two 'facing pages of a book', whose spine passes through the two secondary amine nitrogen atoms. In this situation, it is expected that a bulky substituent (e.g., an anthracene fragment), due to steric repulsive effects, raises the energy of the transition state and slows down the translocation of the metal from one 'page' to the other

subjected during the translocation process. Translocation should be associated with the occasional folding of the ditopic receptor (**6** or **7**) around the ideal line passing through the two amine nitrogen atoms, which acts as a hinge.

This situation is pictorially illustrated in Fig. 14, in which compartments A and B have been laid down on two adjacent pages of a book. Thus, the transition state for the translocation process corresponds to a situation of maximum folding, in which the two halves of the receptor (the two pages of the book) are brought one to face the other at the closest possible distance, an event which precedes the metal transfer. The bulky anthracene substituent raises the energy of such a transition state, thus reducing the rate of both direct and reverse translocation processes.

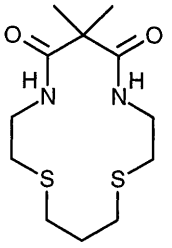

8

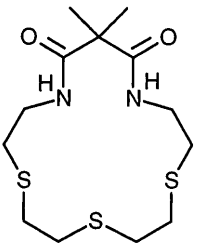

9

Intramolecular coordination rearrangement related to the acidic behavior of the amide group has been observed also in the platinum(II) complex of macrocycles **8** and **9**, which contain two amide groups in one side, and two and three thioether sulfur atoms, respectively, in the opposite side [21]. In an acidic solution, the Pt(II) ion is bound to the sulfur atoms, with two (**8**) or one (**9**) water molecule completing the four-coordination according to a square-planar stereochemistry.

When, in an MeOH/H_2O mixture (4:1 v/v), enough standard base is added to bring the pH to 9, the two amide groups deprotonate and go to coordinate the Pt(II) ion. The metal center adopts again its preferred square stereochemistry, the donor set being provided by the deprotonated amide groups and two sulfur atoms of the polythia moiety of the macrocycle. In the case of **9**, it is the central sulfur atom that remains uncoordinated. The structural aspects of the coordination rearrangement associated to the pH change are sketched in Fig. 15. The stereochemical arrangement of the form stable in basic solution with both **8** and **9** macrocycles has been ascertained through X-ray diffraction studies on crystalline, isolated complexes [21, 22]. Rearrangement is rather slow, with a lifetime of 100 s for **8** and 128 s for **9**, at 35 °C. Sluggishness is to be ascribed to the intrinsic substitutional inertness of the Pt(II) ion. On making the solution strongly acidic (1 M $HClO_4$), each deprotonated amide group uptakes an H^+ ion and the Pt(II) center adopts again the original coordination mode, which involves the thia moiety and water molecule(s).

The acidity driven structural rearrangements illustrated in Fig. 15 involve the movement of a metal ion from a defined portion of the ligand to another, with solvent molecules completing the coordination sphere, when necessary, and must be considered as a translocation processes. Independent of the location of the metal, Pt(II) complexes of both **8** and **9** are colorless and the occurrence of the translocation (which is slow due to metal inertness) has to be followed by monitoring pertinent changes in the UV portion of the absorption spectrum.

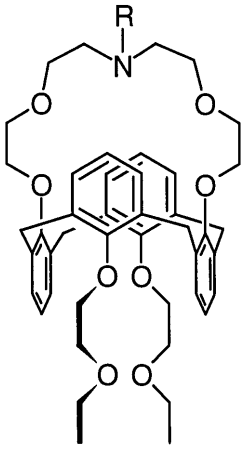

10

A rather sophisticated ditopic ligand, based on a calix[4]arene, suitable for acidity controlled metal translocation has been recently described by Shinkai [23]. The calix-derivative **10** exhibits an 1, 3-alternate conformation and possesses two distinct coordinating compartments: an NO_4-crown-like moiety on one side, and a bis(ethoxyethoxy) chelating subunit on the opposite

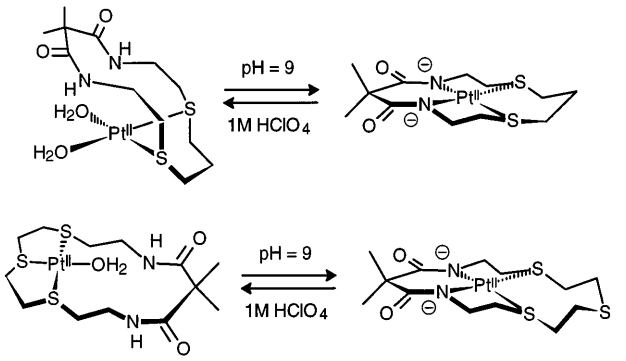

Fig. 15. The translocation of a Pt(II) center between two compartments of a heteroditopic ligand induced by a drastic change of the acidity of the solution. In 1 M $HClO_4$, the metal is coordinated by the thioether sulfur atoms, the square-planar arrangement being completed by water molecule(s). At pH = 9, with both system **8** (upper part) and system **9** (lower part), the metal is coordinated by the two deprotonated amide groups and two sulfur atoms. The translocation to the amide compartment (from 1 M $HClO_4$ to pH = 9) is especially sluggish, due to the typical inertness of the Pt(II) ion

side. The metal ion candidate for the translocation process (which implies tunneling across the aromatic cavity of the 1, 3-alternate conformer) is silver(I). The quinquedentate NO_4 compartment, which in the following will be indicated as B, displays a higher affinity towards Ag(I) than the bis-bidentate tetraoxa compartment, indicated with A. In both compartments A and B, the Ag(I) ion profits from the metal-ligand interaction with four ethereal oxygen atoms and from the cationic π-interactions with the aromatic rings of the calix[4]arene framework; then, the additional interaction with the tertiary amine nitrogen atom present in the crown definitively favors metal binding to B compartment. Moreover, the B compartment, due to the presence of the amine group, displays the behavior of a Brønsted base and can take up a proton to give BH^+. Electrostatic repulsions exerted by the ammonium group drastically reduce the coordinating tendencies of the BH^+ compartment, which are extremely low or zero. This generates an affinity sequence ($B \gg A \gg BH^+$) suitable for the occurrence of a metal translocation process coupled to an acid-base equilibrium.

Indeed, in a CH_2Cl_2/CH_3OH solution (4:1 v/v), containing equimolar amounts of Ag(I) and **10**, the metal goes to occupy the NO_4-crown-like compartment. Here, Ag(I) is not completely happy with the provided coordinating framework: in fact, the NO_4 ring aperture is probably too small to fully encompass the metal and to allow co-planar coordination. Thus, it keeps Ag(I) out of the NO_4 plane and, at room temperature, displays a sort of rope jumping motion, moving from one side to the other with respect to the metal, as shown in Fig. 16. The flip-flop movement slows down with decreasing temperature and stops at −20 °C.

On addition of excess trifluoroacetic acid to the CH_2Cl_2 solution, the amine group of the NO_4-crown is protonated and the Ag(I) ion, in order to escape the electrostatic repulsion, moves to the A compartment, as illustrated in Fig. 17.

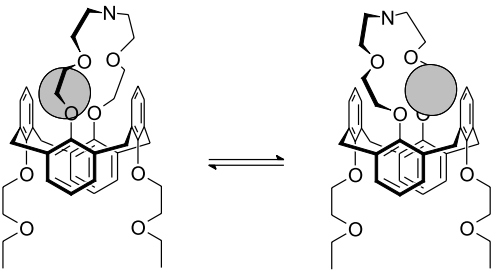

Fig. 16. The rope jumping motion of the NO_4 crown of the functionalized calix[4]arene **10** on the coordinated Ag(I) ion. The flip-flop movement results from the fact that the NO_4 ring has too small an aperture to encompass the metal ion. In a CH_2Cl_2/CH_3OH solution (4:1 v/v, deuterated solvents) the oscillating motion slows down with temperature and stops at −20 °C

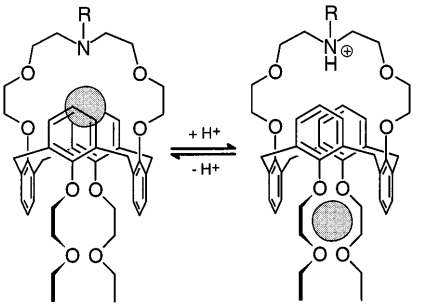

Fig. 17. A molecular 'Pasteur pipette'. On addition of acid, the tertiary amine group of the upper NO_4 crown compartment pushes the Ag(I) ion down to the bis(ethoxyethoxy) chelating compartment, from which the metal is released to the solution. On addition of base, Ag(I) is sucked back to the NO_4 compartment. The reversible process is intramolecular and the metal center travels up and down across the aromatic portion of the 1, 3-alternate calix[4]arene **10**

The intramolecular nature of the translocation process requires that the Ag(I) ion travels across the 'tunnel' represented by the aromatic rings of the 1, 3-alternate calix[4]arene derivative **10**. The occurrence of metal ion tunneling across the aromatic cavity of a 1, 3-alternate calix[4]arene had been previously documented on the basis of dynamic ^{1}H-NMR experiments for Na^+, K^+ and Ag^+ [24, 25]. The authors suggested that system Ag(I)/**10** could be considered as the molecular level version of a Pasteur pipette, in which, on one side, the calix[4]arene moiety and the appended ethoxyethoxy fragments represent the glass tube, and, on the other side, the NO_4-crown is the rubber cap. An external input (addition of acid) pushes out the metal ion through the π-basic cavity to the bis(ethoxyethoxy) compartment. From here, due to the lower energy and higher lability of the metal-ligand interactions, the Ag(I) ion can be released to the solution (in this connection it has to be noted that the complexation constant for the $\{Ag^+ + \mathbf{10}\}$ equilibrium is 5.8×10^9, whereas

that for the $\{Ag^+ + \mathbf{10}H^+\}$ equilibrium is 2.2×10^2). Moreover, the metal can be 'sucked' back to the NO_4-crown compartment on addition of base: excess solid Li_2CO_3, which neutralizes the unreacted trifluoroacetic acid, plus one equivalent of diazabicycloundecene, which deprotonates the ammonium group of the crown moiety. On neutralization, Ag(I) travels back across the aromatic cavity to reach the again appealing amine-containing crown section. The process is fast and reversible, as one would expect when operating a pipette in the macroscopic world.

3.2
Redox-Driven Translocation of Metal Ions

A metal ion M, which is redox active through the $M^{(n+1)+}/M^{n+}$ change, can be translocated within a two-box ligand by taking advantage of a coupled oxidation and reduction process. In particular, one of the two compartments, e.g., A, should display specific affinity for the oxidized form, $M^{(n+1)+}$, whereas the other compartment, B, should give an especially stable complex with the metal in its reduced form, M^{n+}. If the $M^{(n+1)+}$ is added to a solution containing the ditopic ligand A $\sim$ B, according to a 1:1 molar ratio, it will go to occupy compartment A. But, if $M^{(n+1)+}$ is reduced, chemically or electrochemically, the M^{n+}ion which forms will find it thermodynamically convenient to move from A to the nearby soft compartment B. The A-to-B translocation process is pictorially sketched in Fig. 18.

Consecutive oxidation and reduction processes would make the metal center M shuttle back and forth, between A and B, along a determined route. The rate of the translocation process should depend on the nature of the coordinative interactions between M and receptors A and B, whether labile or inert, and on the feasibility of the stereochemical rearrangement which may accompany the metal displacement. Examples of redox-driven metal ion translocation within a two-component system have been recently investigated, and refer to the Fe(III)/Fe(II) and Cu(II)/Cu(I) couples.

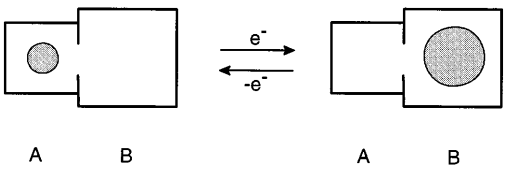

Fig. 18. The model for the redox-driven translocation of a metal ion between a two compartments ligand. The metal center exists in two oxidation states of comparable stability, connected by a fast and reversible one-electron redox change. The two compartments display different coordinating tendencies, e.g., compartment A is *hard*, compartment B is *soft*. In these circumstances, the oxidized metal (the smaller ball) will prefer to stay in compartment A, whereas the reduced form (larger ball) will occupy compartment B. Therefore, it is expected that, following consecutive oxidation/reduction, the metal center will translocate sequentially between A and B

The first example of the translocation of a metal ion driven by the change of metal oxidation state is due to Shanzer and is based on the Fe(III)/Fe(II) change [26]. The chosen compartment for Fe(III) consists of three hydroxamate fragments, -N(O^-)C(=O)-. Tris-hydroxamate complexes are among the most stable Fe(III) complexes in aqueous solution, the corresponding β_3 equilibrium constants being of the order of 10^{30} [27]. The compartment suitable for binding of Fe(II) is made of three 2, 2′-bipyridine (bpy) fragments: the $[Fe(II)(bpy)_3]^{2+}$ complex exhibits an especially high thermodynamic stability ($\log \beta_3 = 17.5$) [28], and is also substitutionally inert, as expected for a d^6 metal center in an octahedral environment. In order to generate the pertinent two-compartment ligand, three strands, each containing a hydroxamate subunit and a bpy subunit, were anchored to a tripodal framework: either the tripodal tetramine tren or a chiral tris-alanyl moiety. A sketch of the triple-stranded ditopic ligand containing tren as a cap is shown in Fig. 19.

On addition of one equivalent of Fe(III) to an aqueous methanol solution of the ditopic triple stranded ligand, the solution turns light-brown, while an intense band develops ($\lambda_{max} = 420$ nm, $\varepsilon = 2400\ M^{-1} \cdot cm^{-1}$). These optical features are typical of Fe(III)-tris-hydroxamate complexes and indicate that the metal goes to occupy the tris-hydroxamate cavity of the ditopic ligand. On treating the solution with a reducing agent (e.g., ascorbic acid), the

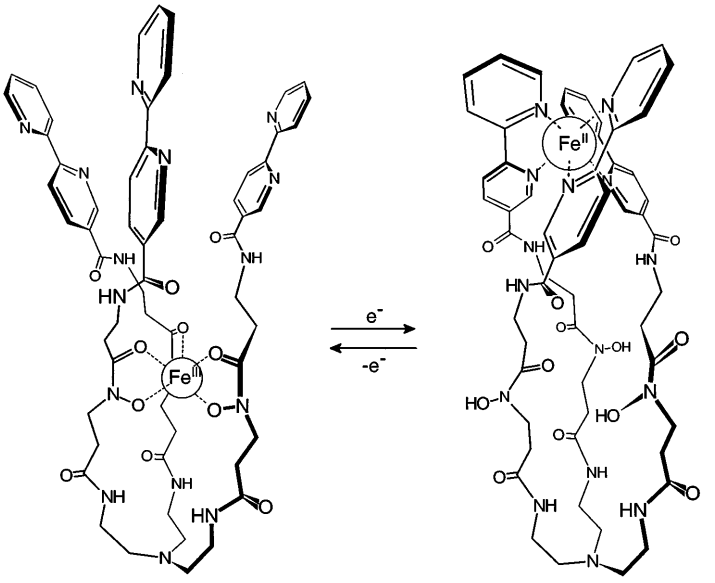

Fig. 19. The redox-driven translocation of an iron center within a heteroditopic ligand containing a *hard* compartment [the tris(hydroxamate) donor set, lower level; preferred by Fe(III)] and a *soft* compartment [tris(2, 2′-bipyridine) donor set, upper level; chosen by the Fe(II) center). Chemical reduction (with ascorbic acid) and oxidation (with peroxydisulfate) make the iron center translocate from one level to the other

color changes to deep purple ($\lambda_{max} = 540$ nm, $\varepsilon = 4700\ M^{-1} \cdot cm^{-1}$), a feature observed with the $[Fe(bpy)_3]^{2+}$ chromophore. Thus, Fe(III)-to-Fe(II) reduction induces the translocation of the metal center from the inner compartment to the external one, as illustrated in Fig. 19. The process is relatively slow, being characterized by a lifetime of $\tau = 22$ s for the system with the tren cap, and of $\tau = 65$ s for the system with the tris-alanyl cap. On the other hand, the way back to the tris-hydroxamate compartment appears beset with difficulties and the journey is much more time-consuming. In fact, the light brown color of the Fe(III) derivative is regenerated in minutes on addition of the strong oxidizing agent $(NH_4)_2S_2O_8$, but the solution must be heated at 70 °C! Sluggishness of the process has to be related to the severe conformational changes associated to metal translocation.

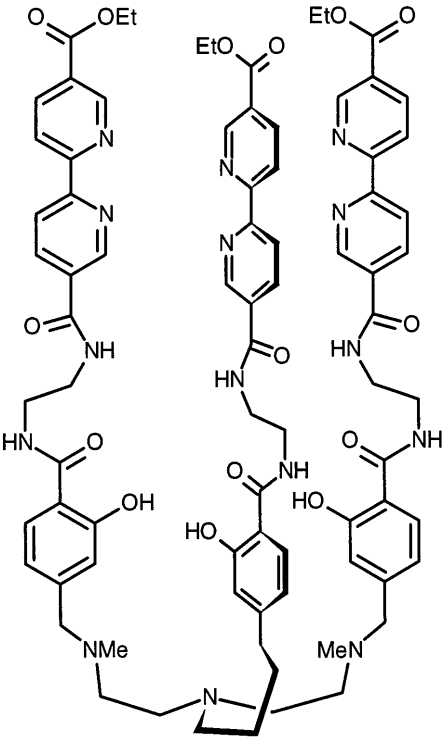

11

A similar ditopic system, **11**, suitable for an iron translocation process based on the Fe(III)/Fe(II) redox couple has been recently designed by Ward [29–31]. Like the ligand illustrated in Fig. 18, system **11** is made of three equivalent strands, held together by a tripodal cap, and contains an internal compartment A and an external compartment B. Compartment A consists of three salicylamide groups: each group behaves as a negatively charged ligand

and offers two oxygen donor atoms. Thus, compartment A exhibits a definitely hard nature and is expected to display a specific affinity towards Fe(III), high-spin. Compartment B, like in the previously considered systems, is made by three 2, 2′-bipyridine fragments and is the perfect host for low-spin Fe(II). The 1:1 complex of Fe(III) and **11**, in a DMF/H_2O solution shows an orange color ($\lambda_{max} = 460$ nm, $\varepsilon = 3200\ M^{-1} \cdot cm^{-1}$), as expected for a tris-salicylamide-Fe(III) complex, thus indicating that Fe(III) resides in compartment A. On addition of a reducing agent (e.g., ascorbic acid), the solution gradually turns violet, while an absorption band develops ($\lambda_{max} = 574$ nm, $\varepsilon = 2300\ M^{-1} \cdot cm^{-1}$, with a shoulder at 543 nm, $\varepsilon = 2250\ M^{-1} \cdot cm^{-1}$). These spectral features pertain to an $[Fe(II)(bpy)]^{2+}$ chromophore, indicating that, on reduction, the metal center has moved to compartment B. The presence of an isosbestic point at 510 nm demonstrates that only two species are present at the equilibrium, thus suggesting the occurrence of an intramolecular process. When treated with an oxidizing agent (H_2O_2) at room temperature, the violet solution of the Fe(II) complex gradually turns orange, eventually affording the Fe(III)-tris-salicylaldimine complex. Hydrogen peroxide is a convenient oxidizing agent, as it provides on reduction hydroxide ions ($H_2O_2 + 2e^- = 2OH^-$), which help the deprotonation of the OH group of each salicylate moiety. Kinetic investigations indicated that translocation processes in either direction take place in the 10 s time scale, i.e., much faster than those observed with Shanzer's derivatives. This may be associated to the greater flexibility of system **11**.

Another redox-driven metal translocation process which profits from the Fe(III)/Fe(II) couple takes place within the ditopic ligand **12,** sketched in Fig. 20 [32]. The ligand consists of a 4-methylphenol platform, with ligating appendances in positions 2 and 6. The appendance at position 2 generates a compartment A, which contains a tertiary amine group and three phenolate oxygen atoms (including that of the central phenol subunit). This compartment has a rather 'hard' nature and is suitable for Fe(III) binding: six-coordination of Fe(III) will be completed by two solvent molecules S (S = MeCN). The appendance in position 6 originates the B compartment, which is made up of a tertiary amine nitrogen atom, two pyridine nitrogen atoms, and the central phenolate oxygen atom (shared with compartment A). Compartment B displays more pronounced 'soft' ligating properties and is designed for Fe(II) binding. Also in the present case, two solvent molecules are required to reach six-coordination. In an MeCN solution, in presence of the base collidine to keep phenolic groups deprotonated, the iron center is translocated from compartment A to compartment B, and vice versa, following the oxidation and reduction processes on the Fe(III)/Fe(II) couple, carried out electrochemically. Structural details of the reversible translocation process are sketched in Fig. 20.

During the electrochemically switched process, the iron center remains bound to the central phenolate oxygen atom, which acts as a hook. On consecutive oxidation and reduction, the hung metal ion swings from one compartment to the other, following a pendular motion. Probably due to the beneficial assistance of the central phenolate oxygen atom, the translocation

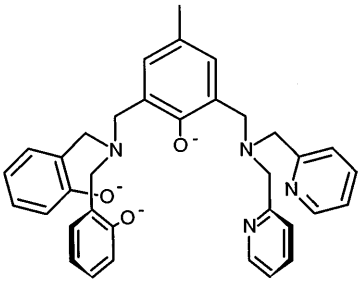

12

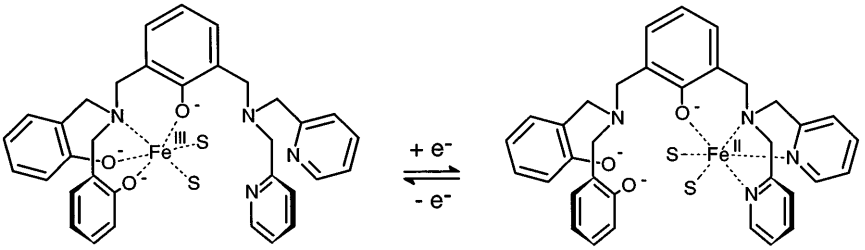

Fig. 20. The electrochemically triggered translocation of an iron center within the two-compartment ligand **12**, based on the Fe(III)/Fe(II) redox couple. Following consecutive oxidation and reduction processes, the iron center oscillates from the left compartment [Fe(III) state] to the right one [Fe(II) state]. The remaining two coordination sites of the metal center in each oxidation state [both Fe(III) and Fe(II) want to be six-coordinate] are occupied by solvent molecules (S = MeCN)

process is very fast, the lifetime for both direct and reverse oscillation being lower than 0.5 s.

A copper center can undergo reversible translocation within a heteroditopic ligand, by taking advantage of the Cu(II)/Cu(I) redox change. The octadentate ligand **13** provides two distinct compartments displaying selective affinity towards Cu(II) and Cu(I) [33]. In particular, the transitional cation Cu(II) is expected to prefer the coordination by the σ-donor compartment A, which consists of an aliphatic tetramine fragment. Indeed, on addition of one

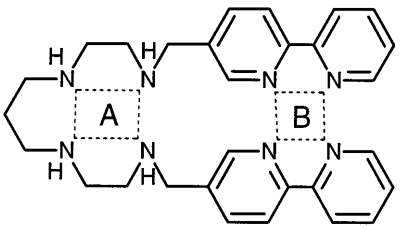

13

equivalent of a Cu(II) salt, an MeCN solution of **13** takes on the violet color typically displayed by Cu(II)-tetramine complexes (*d-d* band: $\lambda_{max} = 548$ nm, $\varepsilon = 120\ M^{-1} \cdot cm^{-1}$). On the other hand, the d^{10} cation Cu(I) strongly wants to be coordinated by the bis-2, 2′-bipyridine set (compartment B), in view of its capability to back-donate electrons to empty π-orbitals of the polypyridine ligand. In fact, on 1:1 addition of $[Cu(I)(CH_3CN)_4]ClO_4$, a solution of **13** takes on the typical brick-red color of the $[Cu(I)(bpy)_2]^+$ chromophore (MLCT band: $\lambda_{max} = 430$ nm, $\varepsilon = 1450\ M^{-1} \cdot cm^{-1}$). Reversible translocation of the copper center between the A and B compartments can be chemically induced, as illustrated in Fig. 21, and visually perceived through a sharp color change of the solution.

When the blue-violet MeCN solution containing equimolar amounts of Cu(II) and **13** is treated with ascorbic acid, the color turns instantaneously brick-red, indicating reduction to Cu(I) and fast translocation from A to B. On the other hand, addition of hydrogen peroxide makes the solution color turn instantaneously from brick-red to blue-violet, which gives evidence for the occurrence of the back translocation from B to A.

Cu(II) and Cu(I) translocation processes within the 'bidimensional' system **13** are much faster processes than those observed for Fe(III) and Fe(II) cations in the 'tridimensional' system **11** and analogues. This may be referred to the higher simplicity of the two-dimensional ligand (which can allow a 'facing pages' mechanism for the translocation of the oxidized/reduced metal center) and to the extremely high substitutional lability of Cu(II) and Cu(I) cations.

Other molecular systems have been reported in which a change of the oxidation state of an incorporated metal center induces a drastic change of the conformation of the ligating framework, thus promoting a controllable molecular motion. In a first example, due to Shanzer, a calix[4]arene, in its cone conformation, had been armed by two 2, 2′-bipyridine and two hydroxamate side-chains, in an alternating fashion [34]: solution-stable 1:1 complexes are formed with both Fe(II) and Fe(III). Fe(II) is coordinated by the two bpy fragments and by two solvent molecules, while Fe(III) achieves six-coordination through the binding of the two hydroxamate arms and two

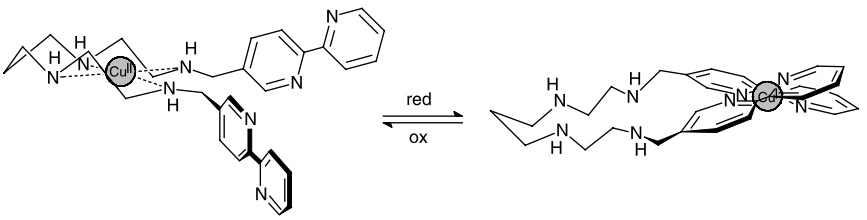

Fig. 21. A redox-driven translocation based on the Cu(II)/Cu(I) change. The Cu(II) ion stays in the tetramine compartment of the heteroditopic ligand **13**, whereas the Cu(I) ion prefers to occupy the bis(2, 2′-bipyridine) compartment. The very fast translocation of the copper center between the two compartments can be induced chemically (reducing agent: ascorbic acid; oxidizing agent: hydrogen peroxide)

solvent molecules. Chemically induced Fe(III)/Fe(II) redox change (by using ascorbic acid and ammonium peroxydisulfate) triggers a conformational rearrangement, in which the side chains, two by two, bind and detach from the metal center.

A second example, due to Canary, is based on the Cu(II)/Cu(I) couple [35]. Here the ligand is a tetraaza tripod, with an amine cap and three quinolyl arms: Cu(II) is fully coordinated by the ligand, with a thiocyanate anion completing a distorted trigonal-bipyramidal sterochemistry. On reduction with ascorbic acid in a methanolic solution, Cu(I) is formed. As Cu(I) prefers four-coordination, a quinolyl arm detaches away from the metal center. Full coordination can be achieved again on oxidation to Cu(II) with ammonium peroxydisulfate. Since the ligating framework possesses a chiral center, the stereochemical rearrangement induces drastic change of the exciton coupled circular dichroism signal and can be conveniently monitored through dramatic changes in the CD spectrum.

The two latter examples do not involve any net displacement of the metal center between two defined distant positions and should not therefore be considered as translocation processes. Nonetheless, they provide further interesting examples of oriented molecular motions promoted by the redox activity of a metal center. It is not coincidental that the involved redox couples [Fe(III)/Fe(II), Cu(II)/Cu(I)) are the same governing the genuine translocation processes described earlier in this Section.

3.3
Redox-Driven Anion Translocation Between Metal Centers

An anion X^- can be made to move between two different transition metal centers M_1 and M_2, by taking advantage of the redox activity of one of them. It is convenient that each metal center is hosted by a given receptor and that the two receptors are covalently linked through a spacer: the length of the spacer determines the length of the route covered by the anion during the translocation process. Moreover, the two metals should fulfill the following requirements:

1) M_2 must undergo a reversible one-electron redox change, $M_2^{(n+1)+}/M_2^{n+}$, at a moderate potential [i.e., $M_2^{(n+1)+}$ and M_2^{n+} should exhibit comparable stability];
2) M_1 and M_2 should be coordinatively unsaturated (thus providing room for X^- coordination) and the affinity toward X^- should decrease along the series: $M_2^{(n+1)+} > M_1 > M_2^{n+}$.

Under these circumstances, the following redox equilibrium is established in solution:

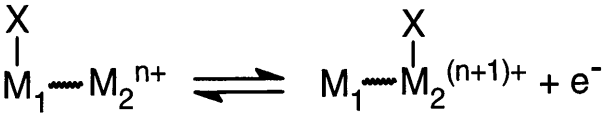

(1)

In particular, when M_2 is in its reduced form, M_2^{n+}, X^- prefers to reside on M_1, but when M_2 is oxidized to $M_2^{(n+1)+}$, X^- moves to the M_2 center. Thus, if the M_1-X and M_2-X coordinative bonds are labile, the X^- anion can be translocated at will, back and forth between M_1 and M_2, by oxidizing and reducing the M_2 center, either chemically or electrochemically.

A suitable redox change is provided by the Ni(III)/Ni(II) couple, when incorporated in a tetramine macrocycle of the type of cyclam. In fact, this redox change induces a drastic variation of the stereochemical features of the metal. In particular, the reduced form, $[Ni(II)(cyclam)]^{2+}$, tends to be square-planar in solution [with the Ni(II) ion in the low-spin state], with the metal showing a very low tendency to bind anions. On the other hand, the oxidized form [Ni(III), low-spin] likes to assume a higher coordination number than 4 and strongly binds anions (e.g., Cl^-) in the axial positions. A good candidate to play the ancillary role of M_1 is the Cu(II) complex of the tripodal tetramine: tris(2-aminoethyl)amine (tren). In fact, the quadridentate tren ligand imposes a trigonal-bipyramidal stereochemistry, thus leaving one of the axial sites of the coordination polyhedron available for anion coordination. Moreover, $[Cu(II)(tren)]^{2+}$ has a defined tendency to bind an anion, much higher than $[Ni(II)(cyclam)]^{2+}$, but substantially lower than $[Ni(III)(cyclam)]^{3+}$. This gives rise to the required sequence of affinity: $[Ni(III)(cyclam)]^{3+} > [Cu(II)(tren)]^{2+} > [Ni(II)(cyclam)]^{2+}$.

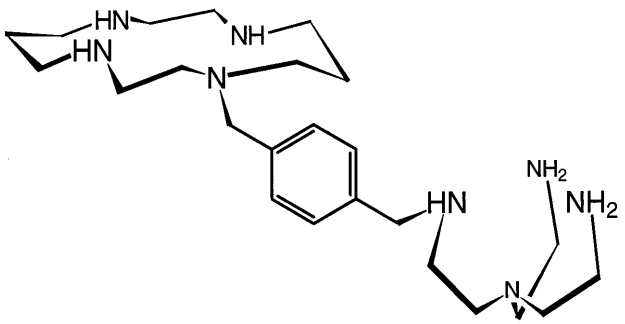

14

Thus, the two tetramine receptors cyclam and tren were linked by a 1, 4-xylyl spacer to give system **14**, tren-cyclam. The heterodimetallic complex $[Cu(II)(tren)\text{-}Ni(II)(cyclam)]^{4+}$ operates chloride anion translocation between copper and nickel centers, through the Ni(II)/Ni(III) couple, in an MeCN solution [36]. In particular, when 1 equivalent of Cl^- is added to an MeCN solution of the heterodimetallic complex [with the nickel center in the Ni(II) state], the anion goes on the Cu(II) ion. In particular, since the log K value for the 1:1 adduct formation equilibrium is 5.7, in a 10^{-3} M solution of the heterodimetallic complex, 95% of the Cl^- ion is bound to Cu(II), while the remaining 5% is dispersed in the solution. The solution has a blue-green color, due to an absorption band centered at 460 nm, pertinent to the $[Cu(II)(tren]^{2+}$ fragment of the heterodimetallic complex [Cl-to-Cu(II) CT transition). If in an

experiment of exhaustive electrolysis, the potential of the working electrode is set at 0.40 V vs. Fc^+/Fc, the color of the solution changes to bright-yellow. This is the color of the $[Ni(III)(cyclam)Cl]^{2+}$ fragment (intense absorption band at 315 nm). The Ni(III)-Cl binding constant is $>10^7$, thus 100% of Cl^- is bound to the trivalent center. Therefore, the blue-green to bright-yellow color change signals the occurrence of the redox-driven chloride translocation illustrated by the half-reaction sketched in Fig. 22.

The process is fully reversible: on setting the potential of the working electrode at 0.00 vs. Fc^+/Fc, Ni(III) is reduced to Ni(II), Cl^- moves back on the Cu(II) center, and the solution takes its original blue-green color. Due to the high stability of both reduced and oxidized form of the heterodimetallic complex, the Cl^- anion can be moved back and forth between copper and nickel centers, at will, by switching the value of the potential of the working electrode at 0.40 and 0.00 V.

Arguments can be raised whether the Cl^- anion moving on Ni(III) comes from the proximate Cu(II) center (through an *intra*-molecular process) or from a Cu(II) center belonging to a different heterodimetallic complex (through an *inter*-molecular process). From a mechanistic point of view, the intramolecular process could involve folding of the two halves of the Cu(II)(Cl) ~ Ni(II) conjugate on the 1, 4-xylyl bridge, followed by anion exchange at the axial positions. On the other hand, the intermolecular process could result from the collision of the Cu(II)(Cl) half of a conjugate with the Ni(III) half of a different conjugate, according to a bimolecular process. The probability for the intramolecular process to occur is very much higher than that of the intermolecular one. Consider, for instance, that the Cu(II)-Cl fragment moves in a sphere whose center is Ni(II) and whose radius is 7.5 Å [i.e., the Cu(II)-Ni(II) distance, as calculated through molecular modeling]. Notice also that a Cu(II)-Cl fragment in a volume of 1766 $Å^3$ (the volume of the sphere) has a concentration 0.94 M, i.e., much higher than the $\leq 10^{-3}$ M

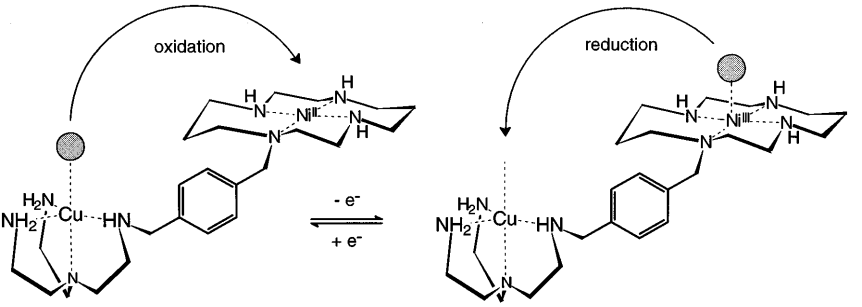

Fig. 22. Chloride ion translocation between a Cu(II) ion and a nickel center, driven by the Ni(II)/Ni(III) redox change. When the nickel center is in its reduced form, Ni(II), Cl^- stays on Cu(II). On oxidation to Ni(III), the anion moves to the nickel center. This behavior derives from the different affinity of the tetramine complexed metal centers towards Cl^-, which decreases along the series: Ni(III) ≫ Cu(II) ≫ Ni(II)

solution used in the spectro-electrochemical experiments. This suggests that the intramolecular anion exchange is much more probable that the intermolecular collision. From a different point of view, one could observe that, in a 10^{-3} M solution, the average distance between two different molecules is 117 Å, to be compared to the 7.5 Å distance which separates Cu(II) and Ni(II) in the heterodimetallic complex. The remarkably lower distance points towards the much more probable occurrence of the intramolecular anion translocation, compared to the intermolecular anion transfer. These considerations have been corroborated by some thermodynamic evidences: the free energy change $\Delta G°$ associated to the chloride translocation process within the $[Cu(II)(tren) \sim Ni(II)(cyclam)]^{4+}$ is substantially more negative (by 7.5 kcal $\cdot$ mol^{-1}) than the anion transfer between the separate fragments $[Cu(II)(tren)]^{2+}$ and $[Ni(II)(cyclam)]^{2+}$. Quite interestingly, the free energy advantage originates from a much more favorable entropy term: this points in favor of the probability effect associated to the intramolecular process.

No other pair of transition metal ions except Cu(II) and Ni(II) allow the redox-driven anion translocation within the tren $\sim$ cyclam conjugate. Even simple swapping of the two metals prevents the process. In fact, Cu(II), when incorporated in the cyclam ring, can have access to the Cu(III) state, even if at a rather positive potential. However, the Cu(III) center, which possesses a d^8 electronic configuration, likes being square planar and does not have any affinity for anion binding, thus altering the required sequence of coordinating tendencies: $M_{2^{(n+1)+}} > M_1 > M_{2^{n+}}$. Moreover, no other anion than Cl^- can be translocated within the $\{[Cu(II)(tren)] \sim [Ni(II)(cyclam)]\}^{4+}$ system. In particular, anions possessing distinctive donor tendencies (NCS^-, Br^-) display also more or less pronounced reducing tendencies and undergo oxidation before or simultaneously with the Ni(II)-to-Ni(III) process. Anions resistant to the oxidation (ClO_4^-, NO_3^-) do not exhibit satisfactorily high binding tendencies towards the $[Cu(II)(tren)]^{2+}$ subunit. Cl^- is a successful compromise, as it is a rather poor reducing agent, but it is also a reasonably good ligand for Cu(II) and Ni(III) tetramine complexes.

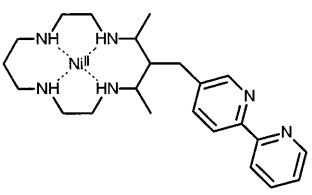

15

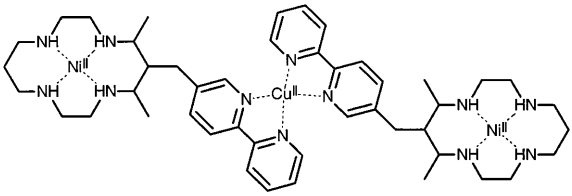

16

The copper-nickel couple works well also in the heterodimetallic system based on molecule **15** [37]. Here, a 2, 2′-bipyridine fragment is covalently linked to the carbon backbone of a $[Ni(II)(cyclam)]^{2+}$ subunit. Two bpy fragments coordinate a Cu(II) center, giving rise to the trimetallic system **16**

which can be considered as a *supramolecule*, because it consists of three defined subunits held together by non-covalent (coordinative) interactions. The trimetallic system **16** fulfills the requirements for the occurrence of a redox driven anion translocation. The redox change driving the anion translocation is again the Ni(II)/Ni(III) couple inside the cyclam ring. The central $[Cu(II)(bpy)_2]^{2+}$ fragment acts as an ancillary subunit, as Cu(II) wants to achieve five-coordination and gives a fairly stable 1:1 adduct in aqueous solution with an inorganic anion X^- (e.g., Cl^-). Thus, when 1 equivalent of Cl^- is added to an aqueous solution of **16** in its reduced form, Ni(II) ∼ Cu(II) ∼ Ni(II), the anion goes on the Cu(II) metal, at the center of the system. Following the Ni(II)-to-Ni(III) electrochemical oxidation (the two metals display independent redox activity and are oxidized at the same potential) the anion moves to the periphery to bind one of the Ni(III)(cyclam) subunits. The stereochemical aspects of the anion translocation process are illustrated in Fig. 23. In conclusion, the covalently linked conjugate complex $[Cu(II)(tren) \sim Ni(II)(cyclam)]^{4+}$ (ligand **14**) and the supramolecular system **16** display a similar behavior. However, translocation in system **16** has a more directional character, as one movement [from Cu(II) to Ni(III)] is divergent and the other is convergent. Moreover, the Cu(II)-to-Ni(III) movement profits from a statistical factor of 2, as the Cl^- anion can choose among two equivalent sites.

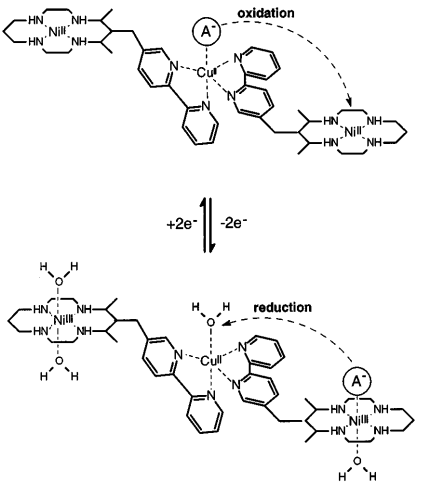

Fig. 23. Anion translocation between Cu(II) and nickel centers in the supramolecular system **16**, controlled by the Ni(II)/Ni(III) redox change. The process is analogous to that illustrated in Fig. 21. In the present case, following Ni(II)-to-Ni(III) oxidation, the anion has the faculty to choose to move from the central Cu(II) ion to one of two equivalent peripheral Ni(III) centers

4 Perspectives

The systems described in the present article share two important properties:

(i) the capability of existing in two states displaying distinct optical properties (light absorption/emission), and
(ii) the fact that each state can be addressed by an external stimulus.

In this sense, the envisaged systems belong to the broad class of molecular switches, thus being susceptible for application in the field of signal processing and data storage at the molecular level. A common feature is that they operate in a fluid medium, being sensitive to the variation of two typical parameters of a solution: pH and redox potential. The development of molecular computers operating in solution has been considered and discussed [38]: it is indisputable that all the two-state systems previously described could represent convenient elemental units for construction of a 'wet' chemical computer. In particular, such an opportunity has been recently discussed in the case of system **7**, in which the pH-driven translocation of a Ni(II) ion between two definite positions of a ditopic ligand switches on/off the fluorescence of a light-emitting fragment covalently linked to the ligating framework [39]. In any case, it has been predicted that computers based on single molecules will take over from silicon chip computers in two decades, thus overcoming the limits of the current technology based on miniaturization [40]. Real applications will probably involve the immobilization of the switchable system on a surface, to give an organized assembly. Under these circumstances, conformational changes associated to the controlled movement of each single molecule could modify drastically the orientation of the entire assembly, thus producing an amplified signal.

However, before application, candidate switching systems need to be optimized in their features and behavior. In particular, for systems undergoing ion translocation, two issues appear especially stringent:

(i) a well established intramolecular nature, and
(ii) a full control of the reversibility of the process.

Requirement (i) can be fulfilled by operating the oriented ion displacement inside a closed (cyclic or polycyclic) coordinating framework. Such a possibility has been explored by Lehn for the redox-driven translocation of a copper center [based on the Cu(II)/Cu(I) couple] within a cylindrical heteroditopic macrocyclic ligand, consisting of an N_2O_3 ring [preferred by the Cu(II) center] and of an N_2S_2 cycle [chosen by the Cu(I) ion] [41s]. As far as point (ii) is concerned, it has been shown in the previous Sections how seriously the translocation rate can by affected by steric factors. In particular, the energy of the transition state associated to the translocation process can be increased/reduced through a fine control of the steric hindrance present in the hosting system: this results in the corresponding enhancement/decrease of the rate. Fast translocation in either directions is recommended, when the system is designed to operate as a switch. On the other hand, a slow rearrangement of

the ligating framework, following the external input, may generate hysteresis, a valuable situation from the point of view of data storage at the molecular level. In principle, translocation rate can be tuned through thoughtful ligand design and careful choice of the metal center(s), either labile or inert. It seems therefore that there exist rich opportunities for transition metals and a stimulating business for coordination chemists in the fascinating field of the design of molecular devices and in the development of a technology based on single molecules.

5 References

1. Bissell RA, Córdova E, Kaifer AE, Stoddart JF (1994) Nature 369: 133
2. Livoreil A, Dietrich-Buchecker CO, Sauvage J-P (1994) J Am Chem Soc 116: 9399
3. Balzani V, Gómez-López M, Stoddart JF (1998) Acc Chem Res 31: 405
4. Sauvage J-P (1998) Acc Chem Res 31: 611
5. Lotz TJ, Kaden TA (1977) J Chem Soc Chem Commun 15
6. Cabbiness DK, Margerum DW (1969) J Am Chem Soc 91: 6540
7. Pallavicini P, Perotti A, Poggi A, Seghi B, Fabbrizzi L (1987) J Am Chem Soc 109: 5139
8. Fabbrizzi L, Licchelli M, Pallavicini P, Parodi L (1998) Angew Chem Int Ed Engl 37: 800
9. Goulle V, Harriman A, Lehn J-M (1993) J Chem Soc Chem Commun 1034
10. Fabbrizzi L, Poggi A (1995) Chem Soc Rev 24: 197
11. De Santis G, Fabbrizzi L, Licchelli M, Mangano C, Sacchi D (1995) Inorg Chem 34: 3581
12. De Santis G, Fabbrizzi L, Licchelli M, Sardone N, Velders AH (1996) Chem Eur J 2: 1243
13. Bergonzi R, Fabbrizzi L, Licchelli M, Mangano C (1998) Coord Chem Rev 170: 31
14. Ashton PR, Ballardini R, Balzani V, Boyd SE, Credi A, Gandolfi MT, Gómez-López M, Iqbal S, Philp D, Preece JA, Prodi L, Ricketts HG, Stoddart JF, Tolley MS, Venturi M, White AJP, Williams DJ (1997) Chem Eur J 3: 152
15. Shinkai S, Ishihara M, Ueda K, Manabe O (1984) J Chem Soc Chem Commun 727
16. Shinkai S, Ishihara M, Ueda K, Manabe O (1985) J Chem Soc Perkin Trans 511
17. Shinkai S, Nakaji T, Nishida Y, Otgawa T, Manabe O (1980) J Am Chem Soc 102: 5860
18. Amendola V, Fabbrizzi L, Licchelli M, Mangano C, Pallavicini P, Parodi L, Poggi A (1999) Coord Chem Rev 190–192: 649
19. Amendola V, Fabbrizzi L, Mangano C, Pallavicini P, Perotti A, Taglietti A (2000) J Chem Soc Dalton Trans 185
20. Basolo F, Pearson RG (1967) Mechanisms of Inorganic Reactions. Wiley, New York
21. Kimura E, Kurogi, Y, Tojo T, Shionoya M, Shiro M (1991) J Am Chem Soc 113: 4857
22. Kimura E, Kurogi, Y, Wada Y, Shionoya M, Shiro M (1989) J Chem Soc Chem Commun 781
23. Ikeda A, Tsudera T, Shinkai S (1997) J Org Chem 62: 3568
24. Ikeda A, Shinkai S (1994) J Am Chem Soc 116: 3102
25. Koh NK, Araki K, Shinkai, S, Asfari Z, Vicens J (1995) Tetrahedron Lett 36: 6095
26. Zelikovich L, Libman J, Shanzer A (1995) Nature 374: 790
27. Anderegg G (1963) Helv Chim Acta 46: 1390
28. Anderegg G (1963) Helv Chim Acta 46: 2397
29. Lutz A, Ward TR, Albrecht M (1996) Tetrahedron 52: 12197
30. Lutz A, Ward TR (1998) Helv Chim Acta 81: 207
31. Ward TR, Lutz A, Parel SP, Ensling J, Gütlich P, Buglyó P, Orvig C (1999) Inorg Chem 38: 5007
32. Belle P, Pierre J-L, Saint-Aman E (1998) New J Chem 1998: 1399
33. Amendola V, Fabbrizzi L, Mangano C, Pallavicini P (2000) submitted for publication

34. Canevet C, Libman J, Shanzer A (1996) Angew Chem Int Ed Engl 33: 2657
35. Zahn S, Canary JW (1998) Angew Chem Int Ed Engl 37: 305
36. Fabbrizzi L, Gatti F, Pallavicini P, Zambarbieri E (1999) Chem Eur J 5: 682
37. De Santis G, Fabbrizzi L, Iacopino D, Pallavicini P, Perotti A, Poggi A (1997) Inorg Chem 36: 827
38. Bradley D (1993) Science 259: 890
39. Milgrom L (2000) New Scientist, 19 February
40. Rouvray D (1998) Chem Br, February, 26
41. Lehn J-M (1995) Supramolecular Chemistry, Concepts and Perspectives. VCH, Weinheim, pp 135–136

Molecular Hysteresis by Linkage Isomerizations Induced by Electrochemical Processes

Mitsuru Sano

School of Informatics and Sciences, Nagoya University, Nagoya 464-8601, Japan
E-mail: sano@info.human.nagoya-u.ac.jp

The redox behavior of $[Ru(NH_3)_5(sulfoxide)]^{2+/3+}$ has been characterized. Kinetic parameters and mechanisms of linkage isomerizations for $Ru^{2+}O \rightarrow S$ and $Ru^{3+}S \rightarrow O$ induced by electrochemical processes are reviewed. The properties of molecules specifically designed to exhibit a hysteresis loop on being addressed electrochemically are described. These molecules comprise a combination of two Ru^{3+}/Ru^{2+} couples, one with the metal attached to an electrochemically reversible group and the other with the metal attached to the sulfoxide by a bridging ligand. Their redox and kinetic behaviors are presented and their memory lives are determined as the rates of the conversions between two isomeric intermediate states. Reading out the memory by intervalence bands is also discussed. Some considerations are also presented for linkage isomerizations and molecular hysteresis.

Keywords: Linkage isomerization, Electrochemical process, Ruthenium sulfoxides, Molecular hysteresis, Memory

1 Introduction 118

2 Linkage Isomerizations Induced by Electrochemical Processes 118

3 Kinetic and Equilibrium Parameters for Linkage Isomerizations of Sulfoxide/Ruthenium Complexes 120

4 Gated Electron Transfer in the Reaction of $[Ru(NH_3)_5(sulfoxide)]^{2+}$ with *cis*-$[Ru(NH_3)_4(pyridine\ 4\text{-}carboxyamide)_2]^{3+}$ 125

5 Hysteresis 127

6 Molecular Hysteresis by Use of Linkage Isomerization by Electrochemical Processes 128

7 Molecular Design of Molecular Hysteresis 130

8 Overview of the Electrochemistry of *cis, cis*-$[(NH_3)_4(py)Ru(pz)Ru(NH_3)_4(dmso)]^{4+}$ Exhibiting Molecular Hysteresis 131

9 The Life Time of Memory in Molecular Hysteresis 132

Structure and Bonding, Vol. 99

10 Reading Out the Memory by Absorption of Light 133

11 Consideration of Linkage Isomerizations and Molecular Hysteresis 136

12 References 138

1 Introduction

Hysteresis as it occurs in a collection of interacting particles is a well-known phenomenon. Magnetic recording devices, such as floppy disks and magnetic tapes, make use of hysteresis phenomena in their magnetization. When elements have the capacity to persist in more than one state under the same values of applied external forces, and their states depend on the directions of the forces, they show hysteresis. Hysteresis was considered by some not to exist at a molecular level [1]. When a molecule shows hysteresis, it can act as an element in an ultra-high-density memory device and is a key building block in every digital electronic device at the molecular level. Further exploration of such behavior is useful for modeling and investigating memory phenomena in nature.

Neumann [2] first used the term "molecular hysteresis" to describe the phenomenon which was hysteresis on precipitation and dissolution of the polymers in pH changes of aqueous solutions. However, because segments of the molecules interact, as do molecules in condensed form, the hysteresis he describes is still a collective phenomenon. Frieden [3] proposed the idea of a "hysteretic enzyme" in 1970 and Hand and Carpenter [4] reported that phosphofructokinase, an important regulatory enzyme, could be a hysteretic enzyme. The concept is of a simple mechanism consisting of two parts; fast binding between the enzyme and a substrate, and a slow conformational change in the complex enzyme. The resulting conformation is retained for a considerable time, behavior that constitutes a memory effect but not hysteresis.

Here we review some simple molecules which have been designed to exhibit important features of a hysteresis loop. Upon species, an electrochemically reversible couple is combined with a couple that shows linkage isomerization on electron transfer.

2 Linkage Isomerizations Induced by Electrochemical Processes

We now describe linkage isomerization that is triggered electrochemically, an essential element of the manifestation of molecular hysteresis which we will be introducing later. A redox process can direct various charges in structure and the reverse (redox switching) and provides a basis for molecular machines and engines.

In the square scheme shown in Fig. 1, the subscript 1 denotes a common structure for the species Z_1 and Z_1^+ which constitute a redox couple, and the

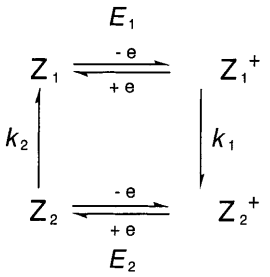

Fig. 1. A square scheme diagram

subscript 2 denotes a different structure common to Z_2 and Z_2^+. Z_1 is a stable state (i.e., more stable than Z_2) but Z_1^+ is unstable to Z_2^+, which has a different structure. Species Z_2, obtained on $1e^-$ reduction of Z_2^+, is unstable and can isomerize to Z_1. When electron transfer is rapid compared to the structural change, reversible potentials E_1 and E_2 can be measured. Application of E_1 generates Z_1^+ from Z_1, which decays to Z_2^+ at a specific rate given by k_1. Application of E_2 generates Z_2 that decays to Z_1 at k_2, completing the cycle. In electrochemical terminology, this kind of behavior is designated as ECEC.

Different kinds of structural changes have been observed as accompanying redox changes, and reviews dealing with them have appeared in 1990 [5], 1992 [6] and 1998 [7]. Here we briefly describe some interesting molecules that exhibit linkage isomerizations induced by electrochemical processes. Shanzer et al. [8] and Ward et al. [9] studied examples of linkage isomerizations of $Fe^{2+/3+}$ between two binding sites in a three-stranded ligand twisting into a helix, as shown in Fig. 2A. By changing the iron oxidation state, translocation of the metal is observed. Stoddart et al. [10] reported a vast family of interlocking and threaded compounds constructed on donor-acceptor aromatic complexes. They demonstrated that molecular movements can be induced in such systems, either by using electrochemical reactions or by irradiating the compounds with light in the presence of other additional reagents, as shown in Fig. 2B. Sauvage et al. reported two interesting systems [11]. One is an electrochemically triggered rearrangement of a [2]-catenate containing two different rings, as shown in Fig. 2C. The Cu^+ four-coordinate complex is oxidized to an intermediate tetrahedral Cu^{2+} species. This compound undergoes a rearrangement to afford the stable five-coordinate Cu^{2+} complex. The other is the electrochemically induced molecular motions in a $Cu^{+/2+}$ complex pseudorotaxane, as shown in Fig. 2D. Other inorganic molecules based on linkage isomerization are also known [12].

In our application to molecular hysteresis accompanying a change in oxidation state, we have exploited linkage isomerization of ruthenium and osmium complexes (oxidation states 2+ and 3+). An early example in this circumscribed field is the linkage isomerization observed for the pentammine ruthenium complex with dimethyl sulfoxide when the oxidation state changes from 2+ (heteroligand attached at S) to 3+ (relocation to oxygen) (Fig. 3A) [13, 14]. The points of attachment have been confirmed by X-ray diffraction

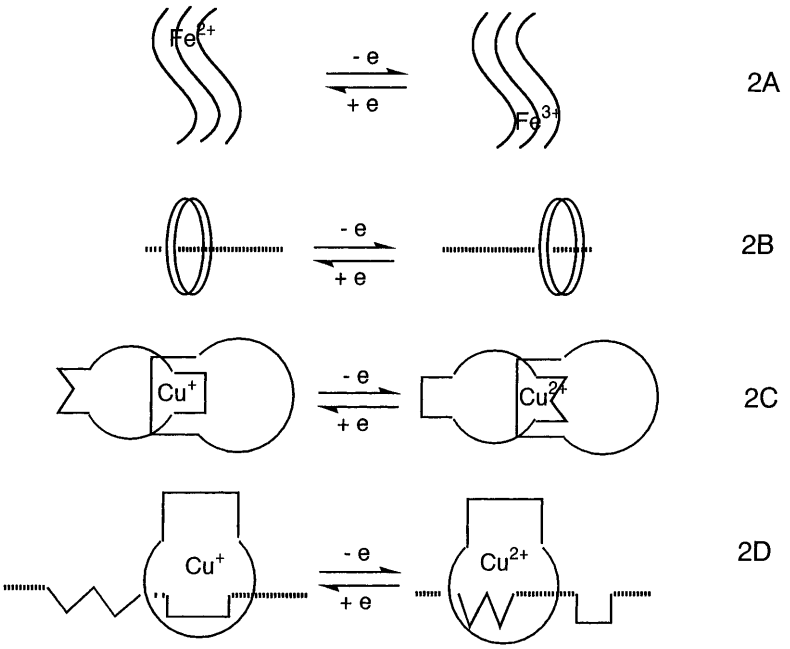

Fig. 2. Some linkage isomerization systems induced by electrochemical processes

studies [15]. This relocation is a result of the much greater back-bonding capacity for the metal atom in the lower oxidation state favoring the π acid character of the sulfur site together with the loss of this capacity on $1e^-$ oxidation coupled with the higher affinity of the higher oxidation state for the oxygen donor site [14]. Another example is the linkage isomerization observed for the acrylate complex of $Ru(NH_3)_5^{3+/2+}$ where the η^2-coordinated Ru^{2+} species isomerizes the O-bound form upon one-electron oxidation (Fig. 3B) [16]. Owing to the superior back-bonding capacity of Os^{2+}, examples are especially abundant when turning to the heavier metal element, two typical examples being illustrated in Fig. 3C and 3D [17, 18]. The complex $[Os(NH_3)_5(C_6H_5N(CH_3)_2)]^{2+}$ undergoes a linkage isomerization from its nitrogen-bound form to one in which the metal center engages the aromatic ring. Upon one-electron oxidation this η^2-coordinated species reverts to the nitrogen isomer. The other is a linkage isomerization between η^1-bound ketone and η^2-arene species of a 2, 2-dimethylpropiophenone complex.

3
Kinetic and Equilibrium Parameters for Linkage Isomerizations of Sulfoxide/Ruthenium Complexes [14]

The first deliberate demonstration of important elements of hysteresis was performed by making use of a couple. Its cyclic voltammetric behavior (as

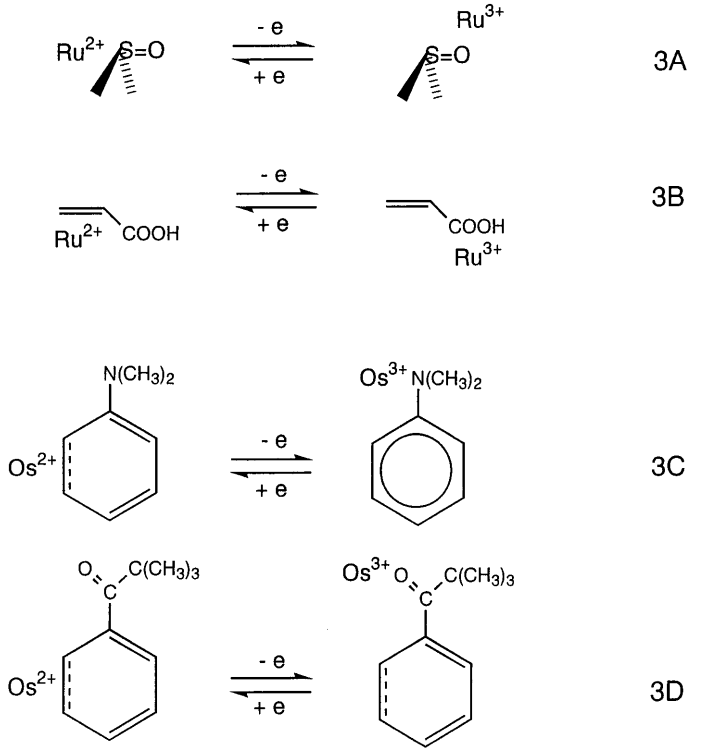

Fig. 3. Some linkage isomerization systems induced by electrochemical processes

shown in Fig. 4) exhibits an oxidation wave at 1.01 V (vs. NHE) corresponding to the reduction of the O-bound form at slow scan rates (<100 mV s^{-1}) and at 20 °C.

A similar response is obtained from the cyclic voltammetry (CV) of $[Ru(NH_3)_5(dmso)]^{3+}$ at slow scan rates (<100 mV s^{-1}) (Fig. 3C). However, at higher scan rates, since the scanning rate of CV is faster than the rates of the linkage isomerizations, both complexes display reversible cyclic voltammograms; for $[Ru(NH_3)_5(dmso)]^{2+}$ at 1 V s^{-1}, a couple is observed at 0.97 V, while for $[Ru(NH_3)_5(dmso)]^{2+}$ at 20 V s^{-1}, a couple is observed at 0.07 V (Fig. 3B and 3D). This linkage isomerization scheme is illustrated in Fig. 5.

Table 1 summarizes the values of the linkage isomerization rate parameters of some sulfoxide/ruthenium complexes at 20 °C. The abbreviations for the ligands are denoted in Fig. 6. The rate constants, k_1, are 0.37 s^{-1} (dmso) < 1.57 (tmso) < 4.3 (*n*-buso) < 16 (benzylso) < 38 (dpso) < 63 (sos) < 5000 (*s*-buso) for S → O isomerization in the series $[Ru(NH_3)_5(sulfoxide)]^{3+}$. Substitution of the bulky *s*-butyl group for the methyl group on the sulfur atom increases the rate by four orders of magnitude for the $Ru^{3+}S \rightarrow Ru^{3+}O$ conversion. Substitution of chlorine for hydrogen on the methyl group and on the phenyl group increases the rate, 0.37 s^{-1} (dmso) <1.9 (Cl-mso) and 38 (dpso) < 44

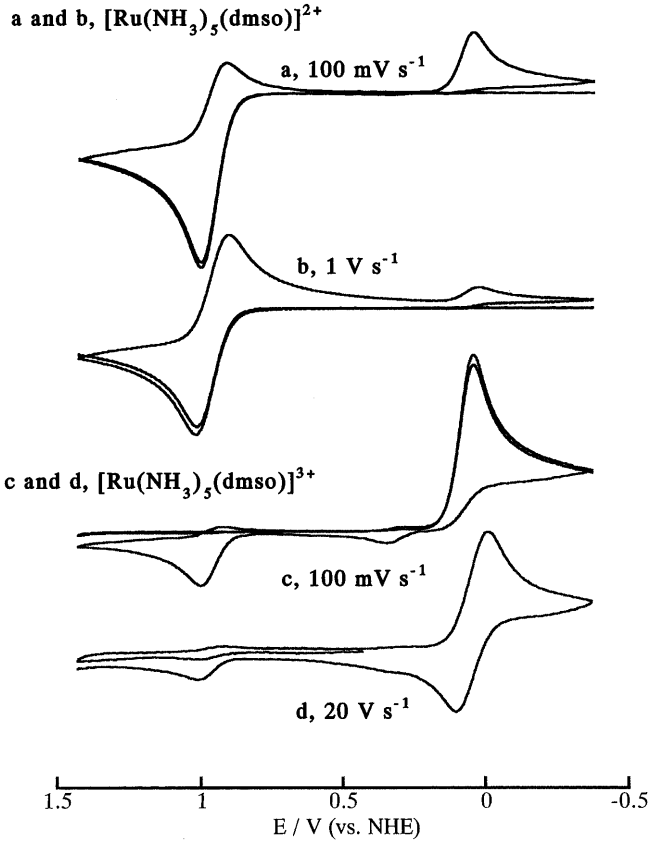

Fig. 4. Cyclic voltammograms in acetone solutions containing $[Ru(NH_3)_5(dmso)]^{2+/3+}$ (10 mM dm^{-3}) and n-$(C_4H_9)_4PF_6$ (0.1 M dm^{-3})

(Cl-pso). The rate for the $Ru^{3+}S \rightarrow Ru^{3+}O$ conversion increases from 0.37 s^{-1} to 3.0 by substituting pyridine for NH_3 in the dmso complex.

The specific rates for O → S isomerization in the $[Ru(NH_3)_5(sulfoxide)]^{2+}$ series remain near 10 s^{-1}, revealing no significant difference between the complexes. However, substitution of pyridine for NH_3 in the dmso complex decreases the rate from 14 to 0.71 s^{-1}. This very large decrease in rate when pyridine replaces NH_3 suggests that the higher affinity of Ru^{2+} for S compared to O is of no help. Bond making is hardly a factor in controlling the rate of reaction.

In *cis*-$[Ru(NH_3)_4(dmso)_2]^{2+/3+}$, rate constants were determined for linkage isomerizations of $Ru^{3+}SS \rightarrow Ru^{3+}SO$ and $Ru^{2+}OO \rightarrow Ru^{2+}SO$ and the values obtained are also shown in Table 1. The isomerization rate for $Ru^{3+}SS \rightarrow Ru^{3+}SO$ is over 1000 s^{-1} at −13 °C and is the fastest among the sulfoxide complexes measured, while the rate for $Ru^{2+}OO \rightarrow Ru^{2+}SO$ is 16 s^{-1}, similar to those for the isomerization of the pentammine/sulfoxide complexes.

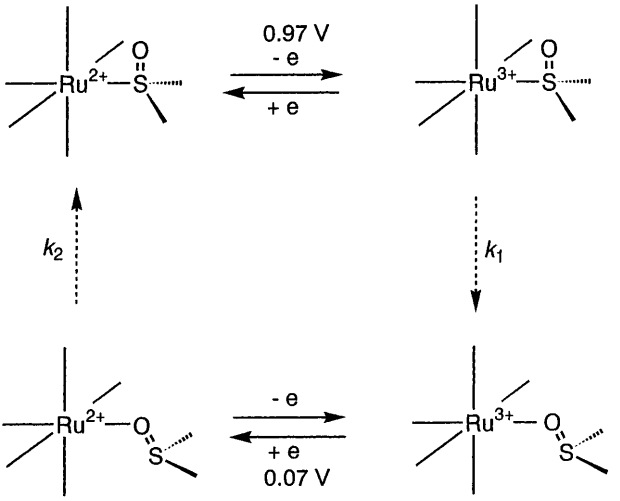

Fig. 5. The square scheme of the linkage isomerization system for $[Ru(NH_3)_5(dmso)]^{2+/3+}$

Table 1. Rate constants and thermodynamics for linkage isomerization of $[Ru(NH_3)_5(sulfoxide)]^{2+/3+}$ and *cis*-$[Ru(NH_3)_4L(sulfoxide)]^{2+/3+}$ in acetone (20 °C)

Ligand	k_1 (s^{-1})	$\Delta H_1^{\ddagger}$ (kJ mol^{-1})	$\Delta S_1^{\ddagger}$ (J K^{-1} mol^{-1})	$\Delta G_1^{\ddagger}$ (kJ mol^{-1})
$Ru^{3+}S \rightarrow Ru^{3+}O$				
dmso	0.37 ± 0.01	78.9 ± 1.0	16 ± 4	74.2
tmso	1.57 ± 0.02	81.0 ± 0.5	35 ± 2	70.7
Cl-mso	1.93 ± 0.01	77.1 ± 0.6	24 ± 2	70.1
n-buso	4.3 ± 0.2	77.4 ± 0.5	32 ± 2	68.0
benzylso	16.0 ± 0.9	72.6 ± 0.9	26 ± 3	65.0
dpso	37.8 ± 1.7	72.1 ± 1.0	31 ± 4	63.0
Cl-pso	43.8 ± 1.8	73.7 ± 0.7	38 ± 2	62.6
sos	62.9 ± 0.7	68.3 ± 0.3	23 ± 1	61.6
s-buso	(5000)	63.3 ± 1.4	42 ± 5	51.0
$>(dmso)_2$	1150 (−13 °C)	–	–	–
(py)(dmso)	3.0 ± 0.1	76.5 ± 0.5	25 ± 2	69.2
	k_2 (s^{-1})	$\Delta H_2^{\ddagger}$ (kJ mol^{-1})	$\Delta S_2^{\ddagger}$ (J K^{-1} mol^{-1})	$\Delta G_2^{\ddagger}$ (kJ mol^{-1})
$Ru^{2+}O \rightarrow Ru^{2+}S$				
dmso	14.3 ± 1.4	55.2 ± 0.7	−35 ± 3	65.5
tmso	10.8 ± 0.2	56.6 ± 1.0	−32 ± 4	66.0
n-buso	9.6 ± 0.6	53.1 ± 0.7	−44 ± 3	66.0
benzylso	15.9 ± 1.1	52.5 ± 1.0	−42 ± 4	64.8
sos	12.6 ± 0.7	51.5 ± 0.7	−48 ± 3	65.6
s-buso	(6.5 ± 0.7)	–	–	–
$(dmso)_2$	16.0 ± 1.9	58.7 ± 1.0	−22 ± 4	65.1
(py)(dmso)	0.71 ± 0.04	61.7 ± 0.9	−38 ± 3	72.8

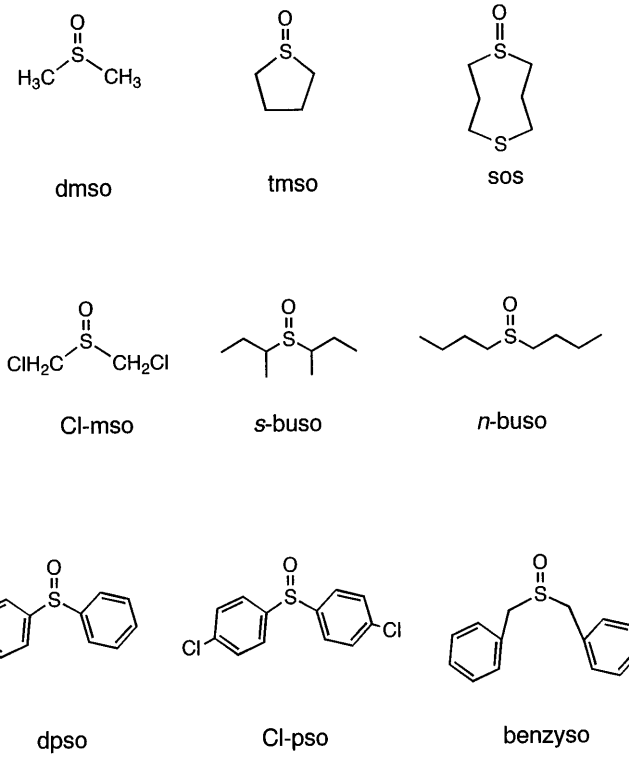

Fig. 6. Abbreviations for sulfoxide ligands

In Table 1, $\Delta H^{\ddagger}$, $\Delta S^{\ddagger}$ and $\Delta G^{\ddagger}$ are summarized for the values of linkage isomerizations at 20 °C for sulfoxide/ruthenium complexes. Those of $\Delta H^{\ddagger}$ range from 81 (tmso) to 63 kJ mol^{-1} (*s*-buso) for $Ru^{3+}S \rightarrow Ru^{3+}O$ and from 62 [(py)dmso] to 52 kJ mol^{-1} (sos) for $Ru^{2+}O \rightarrow Ru^{2+}S$. The $\Delta S^{\ddagger}$ values range from 16 (dmso) to 42 J K^{-1} mol^{-1} (*s*-buso) for $Ru^{3+}S \rightarrow Ru^{3+}O$ and from −22 [$(dmso)_2$] to −48 J K^{-1} mol^{-1} (sos) for $Ru^{2+}O \rightarrow Ru^{2+}S$. The activation entropies are positive for $Ru^{3+}S \rightarrow Ru^{3+}O$ and negative for $Ru^{2+}O \rightarrow Ru^{2+}S$.

A striking result is the reversal of the sign of $\Delta S^{\ddagger}$ for the isomerization on Os^{3+} and Os^{2+} [18], which suggests that an important factor in determining the value of $\Delta S^{\ddagger}$ is the difference in polarity at the two points of attachment. The O site, being more negative, will interact more strongly with the solvent, and solvent disorder will increase when S rather than O is exposed to the solvent. This effect will be reflected, at least in part, in the transition state for $Ru^{3+}S \rightarrow Ru^{3+}O$, hence the positive value of $\Delta S^{\ddagger}$. In the process $Ru^{2+}O \rightarrow Ru^{2+}S$, the reverse is true. Table 2 shows equilibrium parameters for the linkage isomerizations for some complexes.

In the isomerization of Ru^{3+}, the values of ΔG_1 and $\Delta G_1^{\ddagger}$ are different for the dmso, the *n*-buso, and the sos complexes. However, we find that the kinetic free energy barrier to S → O isomerization on Ru^{3+} [this is given by

Table 2. Thermodynamic parameters of $[Ru(NH_3)_5(sulfoxide)]^{2+/3+}$ linkage isomerizations at 20 °C

Ligand	K_1	k_1 (s^{-1})	k_{-1} (s^{-1})	ΔG_1 (kJ mol^{-1})	$\Delta G_1^{\ddagger}$ (kJ mol^{-1})
$Ru^{3+}S \rightarrow Ru^{3+}O$					
dmso	2×10^4	0.37	2×10^{-5}	−24	74
n-buso	4×10^5	4.3	1×10^{-5}	−32	68
sos	3×10^6	63	2×10^{-5}	−37	62
	K_2	k_2 (s^{-1})	k_{-2} (s^{-1})	ΔG_2 (kJ mol^{-1})	$\Delta G_2^{\ddagger}$ (kJ mol^{-1})
$Ru^{2+}O \rightarrow Ru^{2+}S$					
dmso	2×10^{11}	14	1×10^{-10}	−63	66
n-buso	4×10^9	9.6	2×10^{-9}	−54	66
sos	4×10^9	13	3×10^{-9}	−54	66

$(\Delta G_1 - \Delta G_1^{\ddagger})]$ is almost identical for the three complexes. While in the case of Ru^{2+}, O → S isomerization, involving as it does the stable isomer changing to the unstable, is not directly measurable, in the case of Ru^{2+}, O → S isomerization takes the unstable form to the stable. As in the case of Ru^{2+}, we find that for the O → S changes the rates are almost independent of the steric bulk of the substituents on the sulfur atom. In both cases, the relief of strain in the activated complex is measured as the same of that measured on the overall change. A similar pattern has been observed [18] in studying the dynamics of linkage isomerization for $Os(NH_3)_5^{3+/2+}$ in changing between a position on the aromatic ring to the polar groups of NH_2 or $N(CH_3)_2$ as substituents on the ring. However, in these cases, participation in the activated complex by the polar group when $Os(NH_3)_5^{3+}$ is transferring to it from a 2:3 position on the ring is unlikely. In the system we have studied, the two sites are adjacent and, even in this case, in the O → S isomerization, the steric effects of the substituents on the ring are not sensed in the activated complex. The energetics for the two cases are shown schematically in Fig. 7.

4 Gated Electron Transfer in the Reaction of $[Ru(NH_3)_5(sulfoxide)]^{2+}$ with *cis*-$[Ru(NH_3)_4(pyridine\ 4\text{-}carboxyamide)_2]^{3+}$ [19]

A structural change accompanying electron transfer is frequently encountered in biological systems. Although some theoretical considerations have been presented [20], few experimental research programs devoted to a systematic investigation of the effect seem to have been undertaken, despite the importance, because proper systems are limited. Well-characterized linkage isomerization systems on redox provide powerful materials for the study of such gated electron transfer reactions.

When solutions of $[Ru(NH_3)_5(n\text{-buso})]^{2+}$ and *cis*-$[Ru(NH_3)_4(pyridine\ 4\text{-}carboxyamide)_2]^{3+}$ are mixed, the resulting solution gradually turns an intense

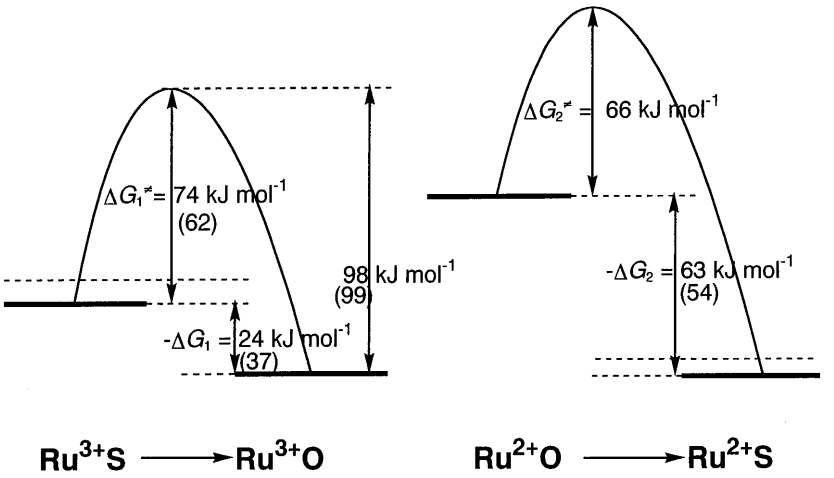

Fig. 7. Energy relationships of the linkage isomerizations for $[Ru(NH_3)_5(dmso)]^{2+/3+}$ and $[Ru(NH_3)_5(sos)]^{2+/3+}$ in acetone at 20 °C. The values in parentheses are for the sos complex

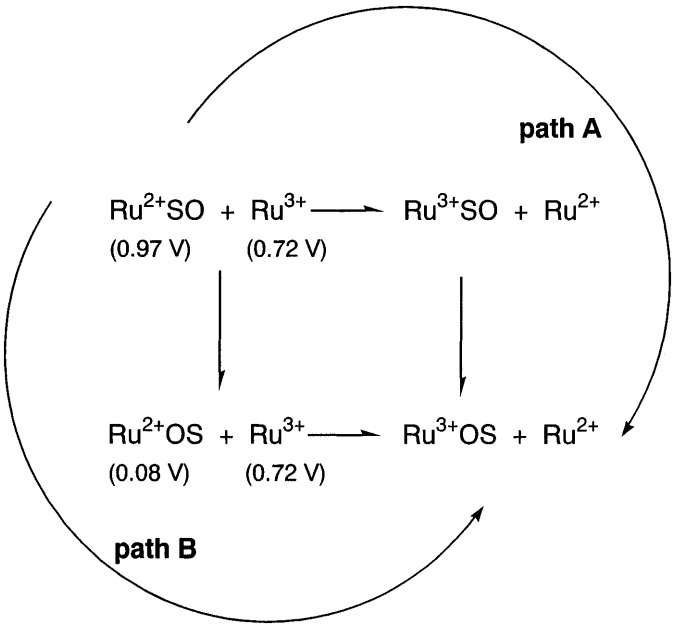

Fig. 8. Two possible reaction paths for the electron-transfer reaction between $[Ru(NH_3)_5(n\text{-buso})]^{2+}$ with *cis*-$[Ru(NH_3)_4(\text{pyridine 4-carboxyamide})_2]^{3+}$

blue, which implies an increase in the concentration of the *cis*-$[Ru(NH_3)_4(\text{pyridine 4-carboxyamide})_2]^{2+}$. In Fig. 8, alternative paths, A and B, are introduced. In path A, the first step is the electron-transfer reaction $Ru^{2+}SO + Ru^{3+} \rightarrow$

$Ru^{3+}SO + Ru^{2+}$ and the second step is the isomerization, $Ru^{3+}S \rightarrow Ru^{3+}O$, while in path B electron transfer takes place only after isomerization.

The kinetic data and the information about linkage isomerization and redox potentials demonstrated that electron transfer takes place by path A, where $[Ru(NH_3)_5(n\text{-buso})]^{2+}$ is first oxidized by *cis*-$[Ru(NH_3)_4$(pyridine 4-carboxyamide)$_2]^{3+}$ against a 24 kJ mol^{-1} up-hill electron transfer with the rate constant over 50 M^{-1} s^{-1} and, in the second step, the $Ru^{3+}SO$ isomerizes to $Ru^{3+}OS$ with a rate constant of 4.3 s^{-1}. This conclusion is interesting to consider as the mechanism not only for biological but also for the gated electron transfer systems.

5 Hysteresis

We now turn to the phenomenon of hysteresis. A ferromagnetic substance becomes magnetized in an applied magnetic field, as shown in Fig. 9. When the substance is placed in a positive magnetic field, it shows magnetization *b*. Reducing the magnetic field decreases the magnetization, but, even on complete removal of the magnetic field, it shows residual magnetization *c*. Application of a negative magnetic field leads to negative magnetization *d* and, on removal of the applied field, a residual magnetization *e* remains. Thus, a ferromagnetic substance has two residual magnetizations, *c* and *e*, and depending on the direction of the applied field, the system retains a memory of its past history.

A brief explanation of the mechanism of hysteresis in a ferromagnetic substance follows. When a ferromagnetic substance is placed in a magnetic field, magnetic domains that are parallel to the applied field are stabilized. On the other hand, magnetic domains that are anti-parallel to the field are destabilized, and the stable domain expands, as shown in Fig. 10b. Although a

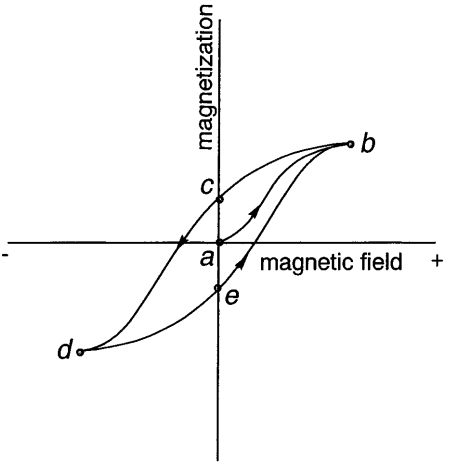

Fig. 9. A magnetic hysteresis curve

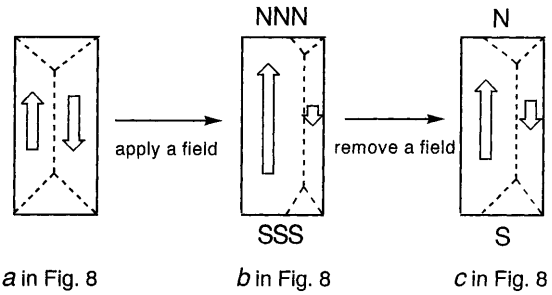

Fig. 10. Extents of magnetic domains in a ferromagnetic substance in a magnetic field

decrease in the field reduces the domain, impurities in the substance prevent its disappearance, as shown in Fig. 10c, and the substance shows residual magnetization even in the absence of a field.

The correlation between residual magnetization and particle size is depicted in Fig. 11. The smaller the particle is, the stronger the magnetization, until the particle size is less than 100 Å, after which the magnetization decreases suddenly. In this size domain (i.e. >100 Å), the magnetization of a substance responds linearly to the applied field, resulting in loss of the residual magnetization [1]. In this example and others, hysteresis occurs in a collection of interacting particles.

6
Molecular Hysteresis by Use of Linkage Isomerization by Electrochemical Processes

The couple $[Ru(NH_3)_5(dimethylsulfoxide)]^{2+/3+}$ has two stable forms as previously described. While two states can be achieved (i.e. a bistable system)

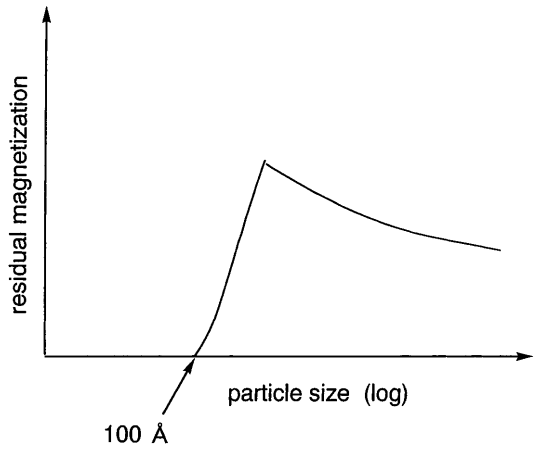

Fig. 11. Residual magnetization vs. particle size of ferromagnetic substances

by changing the direction of the applied field, the system does not exhibit hysteresis because the states differ in composition. However, hysteresis appears when this couple is combined with a reversible couple, such as $[Ru(NH_3)_5]^{2+/3+}$.

In the molecule we offer as an example of hysteresis, a reversible couple is combined with that just described so that there is a possibility of communication between the metal centers in the binuclear species, as shown in Fig. 12. The reversible couple was chosen to have a potential bracketed by the irreversible potentials of the sulfoxide couple. The redox behavior for this binuclear species is described as follows. When the molecule is fully reduced, the form in which Ru^{2+} is attached to the sulfur of the sulfoxide linkage is stable; [Ru^{2+}—Ru^{2+}SO] back-bonding being favored in this isomer. When the

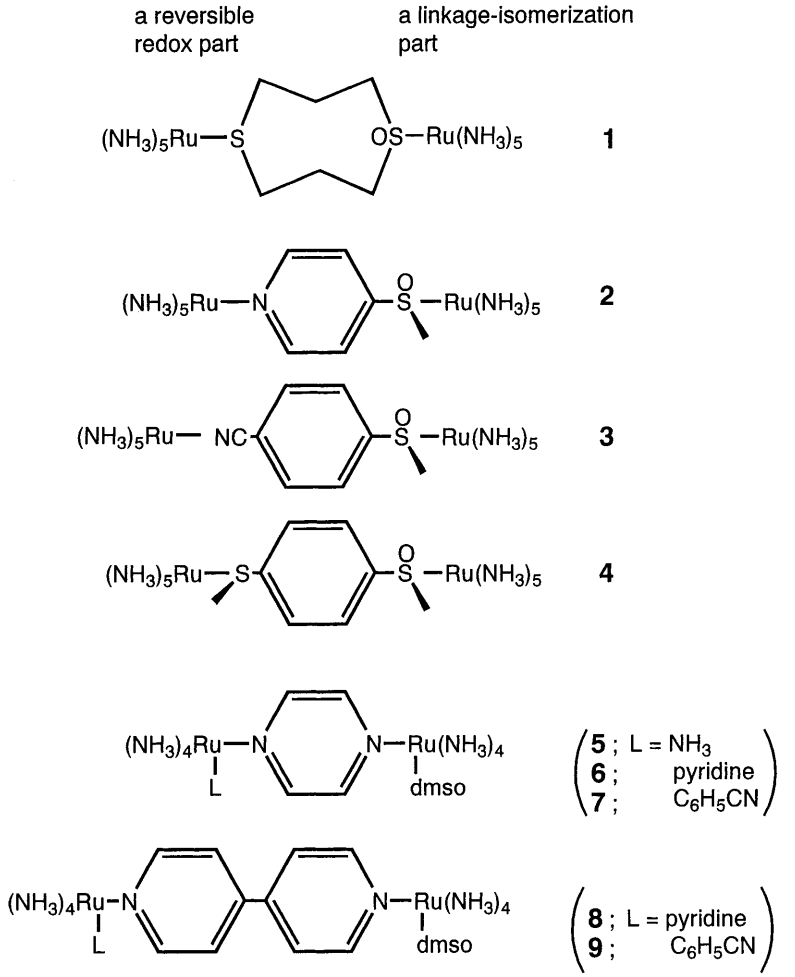

Fig. 12. Prepared binuclear species exhibiting molecular hysteresis

potential is increased, $1e^-$ oxidation takes place first at the reversible couple site, producing $[Ru^{3+}—Ru^{2+}SO]$. Upon a further increase in the potential, $[Ru^{3+}—Ru^{3+}SO]$ is the immediate product of the next $1e^-$ oxidation with the sulfur atom of the sulfoxide being bound to Ru^{3+}. The advantage of back-bonding is now lost, and this isomer rearranges rapidly to $[Ru^{3+}—Ru^{3+}OS]$, where Ru^{3+} is attached to the more negative site of the sulfoxide linkage. Upon a decrease in the applied potential, $[Ru^{2+}—Ru^{3+}OS]$ is formed, and upon a further decrease in potential, $[Ru^{2+}—Ru^{2+}OS]$ is first formed, but this is unstable and rapidly rearranges to $[Ru^{2+}—Ru^{2+}SO]$, completing the cycle.

The above process is illustrated in Fig. 13. The mixed-valence state exists in two forms, **A′** and **B′**, species **A′** accessible only by oxidation of the stable fully reduced form, and species **B′** only by reduction of the stable fully oxidized form. The structures of **A′** and **B′** are different from one another. The structure of **A′** is similar to that of **A**, and **B′** is similar to **B**. Hence, the **A′** and **B′** species remember their former structures. There is a bistability in the system and which bistable state depends on the direction of an external perturbation, constituting hysteresis at the molecular level.

7 Molecular Design of Molecular Hysteresis

The archetypal molecule that exhibits molecular hysteresis made by our group consists of two parts, a reversible redox part and a linkage isomerization part, as shown in Fig. 12. In our first example [21] the linkage isomerization element was fully incorporated into the bridging framework [22]. By using only one of the two bonds to the sulfoxide unit for the bridging group, the opportunities for bringing systematic changes in composition and structure to bear are greatly increased. Some examples of structures that make use of this greater freedom appear in Fig. 12. The variations now made possible include changes in the values of E_f or the reversible couple, the extent of communication between the two couples, and changes in the dynamics of

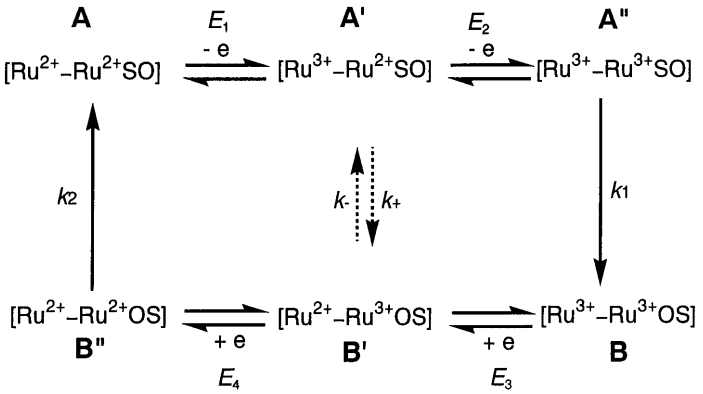

Fig. 13. A double square scheme of redox behavior of the binuclear complexes

the linkage isomerization function; a bridging ligand such as pyrazine [23], bipyridine [24], and cyanopyridine [24], and the isomerization and reversible redox parts such as $Ru(NH_3)_4$(dmso) and $Ru(NH_3)_4L$ (L = NH_3, pyridine, and benzonitrile).

8 Overview of the Electrochemistry of *cis, cis*-$[(NH_3)_4(py)Ru(pz)Ru(NH_3)_4(dmso)]^{4+}$ Exhibiting Molecular Hysteresis

cis, cis-$[(NH_3)_4(py)Ru(pz)Ru(NH_3)_4(dmso)]^{4+}$ (**6**) is one example of a molecule that exhibits molecular hysteresis. Figure 14 shows examples of cyclic voltammetry traces for the fully oxidized and the fully reduced forms together with digital simulations for each.

At a scan rate of 100 mV s^{-1}, the electrochemical behavior of the fully oxidized form (Fig. 14c) is simpler and will be dealt with first. Starting at oxidizing potentials, two reversible couples are observed, one at $E_{1/2}$ = 0.92 V, which is assigned to $[Ru^{3+/2+}—Ru^{3+}OS]$, and the other at $E_{1/2}$ = 0.45 V

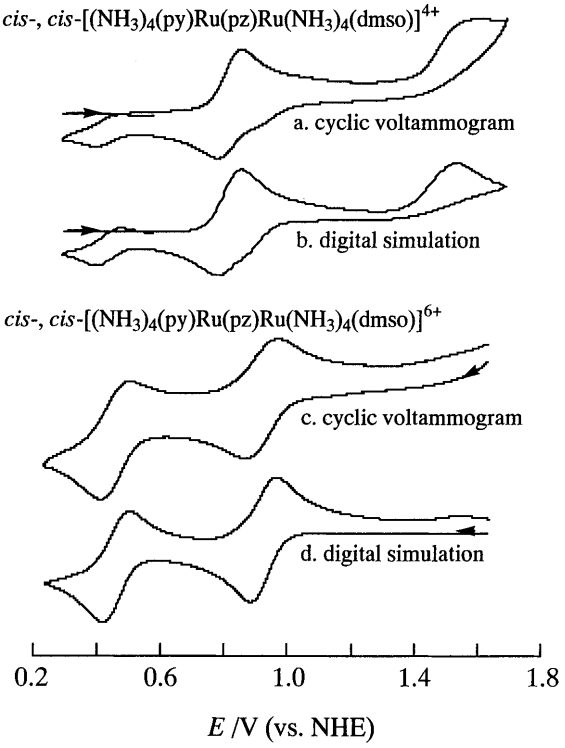

Fig. 14. Cyclic voltammograms and digital simulations at 100 mV s^{-1} in acetone solutions containing species **6**

assigned to [Ru^{2+}—$Ru^{3+/2+}$OS]. The fact that no complications arise shows that isomerization of Ru^{2+}OS to Ru^{2+}SO is slow on the time scale defined by the sweep rate. In starting with the fully reduced form, E_a at 0.87 V is assigned to [Ru^{2+}—Ru^{2+}SO] → [Ru^{3+}—Ru^{2+}SO], close, but not identical, to the corresponding value of E_a = 0.97 V in Fig. 14c. The oxidation [Ru^{3+}—Ru^{2+}SO] → [Ru^{3+}—Ru^{3+}SO] takes place at E_a = 1.55 V with no corresponding reduction wave on reversing the sweep, owing to rapid isomerization of Ru^{3+}SO to Ru^{3+}OS. On the reverse scan, only a small signal of E_c = 0.87 V for the process [Ru^{3+}—Ru^{3+}OS] → [Ru^{2+}—Ru^{3+}OS] is observed, owing to loss by diffusion from the electrode, and a larger signal of E_c = 0.79 V ascribable to [Ru^{3+}—Ru^{2+}SO] → [Ru^{2+}—Ru^{2+}SO]. A wave at about 0.45 V is assigned to [Ru^{2+}—$Ru^{3+/2+}$OS]; it is weak because of loss by diffusion from the electrode.

To extract values of the dynamic parameters, the cyclic voltammograms for the fully reduced and the fully oxidized forms were digitally simulated according to Fig. 13. In these simulations, experimental redox potentials were used, and rates of the isomerization and of heterogeneous electron transfer on electrodes are parameterized, interconversion between **A′** and **B′** being neglected. Figure 14b and 14d shows two examples of the fitting results. Experimental and simulated results are in fair agreement indicating that the proposed scheme is reasonable and the interconversions are so slow as to be negligible.

9 The Life Time of Memory in Molecular Hysteresis

That both of the intermediate states **A′** or **B′** (see Fig. 13) can be characterized constitutes storage of memory. Interconversion between **A′** or **B′** leads to loss of memory, and thus the rate of this interconversion is an important parameter of the system.

An extremely slow rate of conversion can be determined with the use of thin layer cyclic voltammetry (TLCV) [25]. TLCV was performed on 1 mL of acetone solution that was admitted to a compartment (0.08 mm thickness layer) of an electrochemical cell equipped with a platinum-mesh working electrode (Fig. 15). This constitutes bulk electrolysis in the solution. When the potential is increased, $1e^-$ oxidation takes place at 0.83 V, producing **A′**. Upon a further increase in the potential to about 1.48 V, the fully oxidized species **A″** is formed, which isomerizes to **B**. On decreasing the applied potential, two reduction waves are obtained. The simulation (the dotted line in Fig. 15a) of the scheme shown in Fig. 13 without the conversion is in good agreement with the experiment.

When the potential is increased in Fig. 15b, $1e^-$ oxidation takes place at 0.83 V. Upon further increase in the potential up to 1.06 V, the formation of **A′** is completed after which the potential is kept at 1.06 V for specific intervals (0 h, 1.5 h, and 3 h). The applied potential is then decreased and species **A′** is reduced to **A** at 0.83 V. However, during the specific intervals, some of **A′** is converted to **B′** with a rate k_+, and is immediately oxidized to form the species

B. As a result, the amplitudes of two reduction waves at 0.92 V and 0.45 V are proportional to the amount of this conversion. In Fig. 14d, the potential is applied at 1.6 V in the thin layer cell to form the fully oxidized species **B**. When the potential is decreased, $1e^-$ reduction takes place at about 0.9 V. On decreasing the potential to 0.77 V, **A′** is formed completely after which the potential is kept at 0.77 V for specific intervals (0 min, 15 min, and 30 min). During the specific intervals, some of **B′** is converted to **A′** with a rate k_-, then immediately reduced to the species **A**. As a result, the amplitudes of the two oxidation waves at 0.83 V and 1.48 V are proportional to the amount of this conversion.

The TLCV data were simulated with variable parameters of rates k_+ and k_- of forward and reverse reactions. Figure 14c and 14e shows the best fit obtained, yielding for k_+ the value 4.0×10^{-5} s^{-1} and for k_- the value 3.8×10^{-4} s^{-1}. Consequently, the equilibrium constant $K = k_+/k_-$ between the mixed-valence species is 0.11 for complex **6**. The above procedure was also successfully applied to determine the rates and the equilibrium constants of the conversions for the other complexes, and these are given in Table 3.

The approach to equilibrium is governed by $(k_- + k_+)$. We define the half-time for the approach to equilibrium, namely $(\ln 2)/(k_- + k_+)$, as the life time of the memory. These are from $1.1–7.7 \times 10^3$ s for the complexes. It must be emphasized that the life of memory of molecule **1** with the non-conducting bridging ligand is shorter than those of other molecules. It is indispensable to combine some electronic coupling and a longer life of memory for applications of molecules of this kind in high-density memory storage, when light quanta are used to address the system. In our results, the stronger metal–metal interaction is compatible with a longer life of memory in a molecule.

10
Reading Out the Memory by Absorption of Light

Figure 16 shows the absorption spectra covering the near-infrared and visible region for each accessible state based on complex **6**. They were obtained in acetone by use of thin layer electrochemical cells. Only the mixed-valence states **A′** and **B′** show strong absorption in the near-infrared region – the small absorption shown by **B** in this energy region is probably caused by an impurity.

The absorptions of **A′** (λ_{max} = 1010 nm) and **B′** (λ_{max} = 1300 nm) are intervalence transitions assignable to $[Ru^{2+}SO] \rightarrow [Ru^{3+}]$ and $[Ru^{2+}] \rightarrow [Ru^{3+}OS]$, respectively. Their high intensity relative to those of the iso-valent forms, and the difference in λ_{max} for **A′** and **B′**, qualify them as a means of reading out the memory.

The energies of the intervalence (IT) bands for **A′** and **B′** decrease and increase respectively in the order **5**, **6**, and **7**. These trends are in line with the redox potentials of the relevant couples. While the changes in potential for the dmso couples in the series are small – ΔE in the most extreme case is 0.07 V – those for the reversible couple are greater than 0.30 V. This difference in sensitivity is expected because, within the series, only the immediate environment of the metal atom in the reversible couple is changed. This

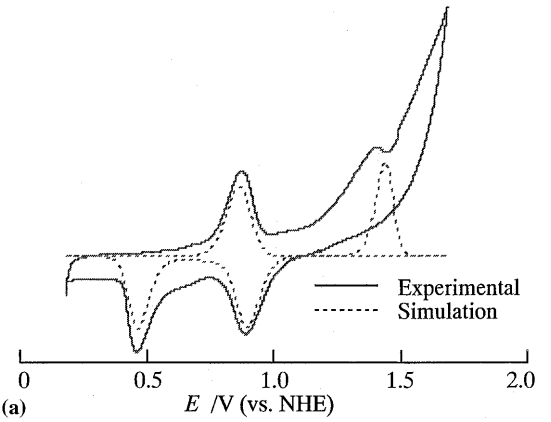

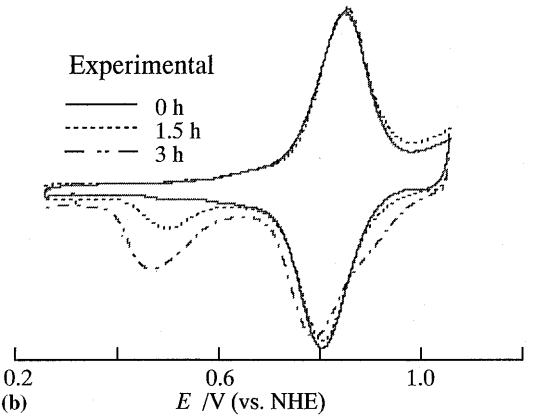

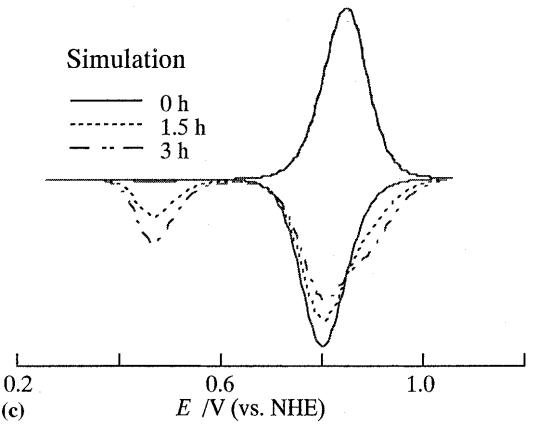

Fig. 15. Thin layer cyclic voltammograms and digital simulations at 1 mV s^{-1} in acetone solutions containing species **6**

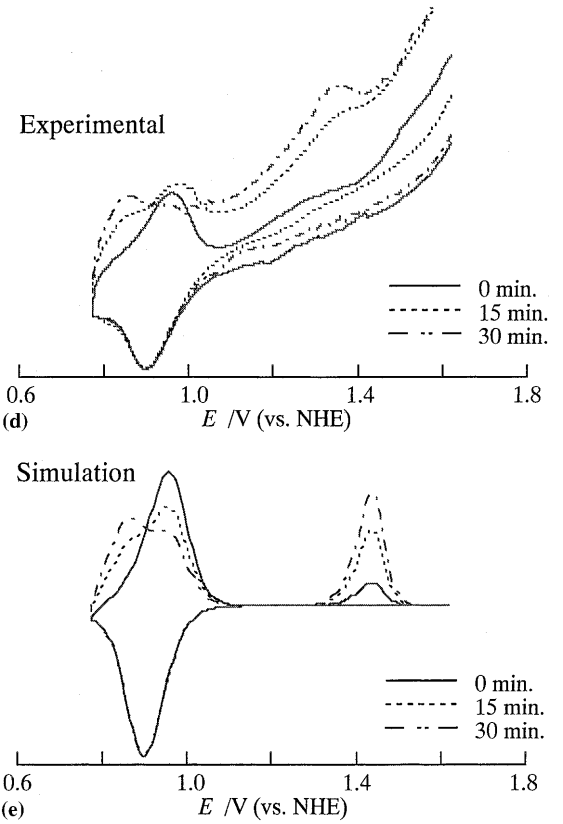

Fig. 15. (Continued)

Table 3. Rate constants for the conversions between **A′** and **B′** in acetone (20 °C)

Complex	k_+ (s^{-1})	k_- (s^{-1})	Life time of the memory (s)
1	2.0×10^{-4}	4.4×10^{-4}	1.1×10^{3}
2	$>1.0 \times 10^{-6}$	3.6×10^{-4}	1.9×10^{3}
3	3.6×10^{-6}	1.4×10^{-4}	4.8×10^{3}
4	2.0×10^{-5}	7.0×10^{-5}	7.7×10^{3}
5	5.0×10^{-6}	4.0×10^{-4}	1.7×10^{3}
6	4.0×10^{-5}	3.8×10^{-4}	1.7×10^{3}
7	2.4×10^{-4}	5.2×10^{-5}	2.4×10^{3}
8	9.5×10^{-5}	6.0×10^{-5}	4.5×10^{3}
9	6.5×10^{-5}	6.2×10^{-5}	5.5×10^{3}

couple becomes more strongly oxidizing in the order **5**, **6**, and **7**, which decreases the energy of the $[Ru^{2+}SO] \rightarrow [Ru^{3+}]$ transition (**A′**), the order being reversed for $[Ru^{2+}] \rightarrow [Ru^{3+}OS]$ (**B′**).

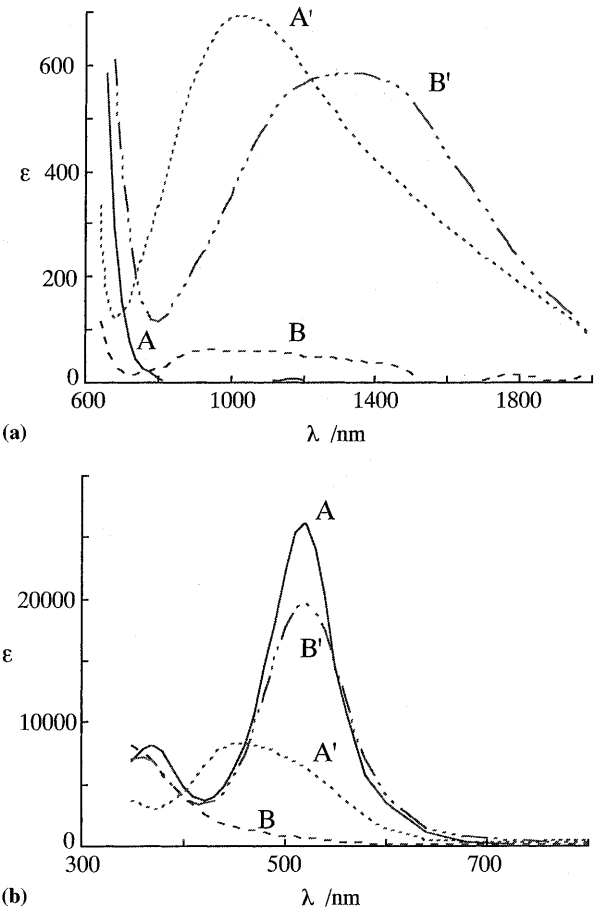

Fig. 16a, b. Absorption spectra of **6** in acetone

In reference to the visible region of the spectrum, we note in Fig. 15b an intense ($\varepsilon = 24700\ M^{-1}\ cm^{-1}$) absorption for **A** [$Ru^{2+}$—$Ru^{2+}SO$] and **B** [$Ru^{3+}$—$Ru^{3+}OS$], but no corresponding bands for **A′** [Ru^{3+}—$Ru^{2+}SO$] and **B′** [Ru^{3+}—$Ru^{3+}OS$]. Thus, the absorption can be assigned to $Ru^{2+} \rightarrow \pi^*$ (pyrazine). Absorption for **A′** in the complex **5** is observed at 450 nm, which is almost the same as those in complexes **6** and **7**, where it is assigned to [$Ru^{2+}SO$] $\rightarrow \pi^*$ (pyrazine).

11
Consideration of Linkage Isomerizations and Molecular Hysteresis

Some interesting applications of redox-switchable linkage isomerizations were discussed previously (see Fig. 2). Some other interesting features are described here. Lehn [26], Beer [6, 27], De Santis et al. [28], and Kaifer [29] reviewed

some metal redox active ligand systems for recognizing guest species, respectively. An interesting application in this field would be to control stereo- and regiospecific reactions by switching of molecular catalysts. Waymouth et al. [30] reported the temperature dependency of the specificity of zirconium compounds that catalyze polymerizations of isotactic and atactic blocks of polypropylene. Another application is as an information processing system built by molecules affected by two or more external perturbations. This primitive application [16] is shown in Fig. 3b, in which linkage isomerization from η^2-ene and η^1-O is switchable by redox and proton.

We now turn our attention to molecular hysteresis which has two essential factors. One is that a system can be expressed a "double square scheme diagram" (or "ladder scheme diagram") [5], as shown in Fig. 17a. **A**, **A′**, **A″**, **B**, **B′**, and **B″** are chemical species or states. These series of **A** and **B** vary reversibly with one another under an external perturbation such as potential, pH, ion concentration, light, etc. With **A** and **B** more stable than **B″** and **A″**, respectively, **A″** and **B″** can be rapidly converted to **B** and **A**. Hence we will obtain a scheme as shown in Fig. 17b. The other important thing is that the conversion is slow between **A′** and **B′**. The slow rate produces a bistability, **A′** and **B′**, which depends on the direction of an external perturbation. This is molecular hysteresis. Some binuclear or multinuclear metal complexes with the double square scheme diagram have been reported [31]. However, because they were not designed to exhibit molecular hysteresis, their hysteresis behaviors in redox are insufficient.

Molecular hysteresis could be possible in metalloproteins. Barker et al. [32] studied cytochrome *c* in which oxidation state was linked with conformational

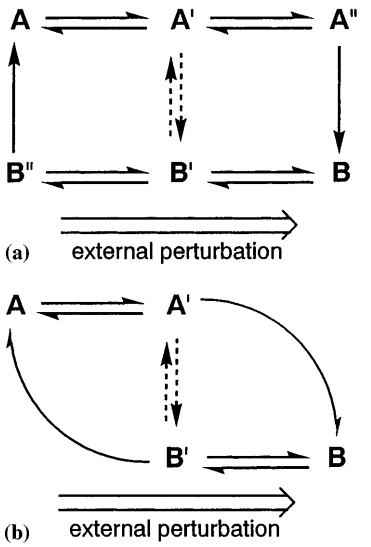

Fig. 17a, b. A double square scheme diagram and scheme of the hysteresis behavior

changes. It is claimed that there could be a possibility of molecular hysteresis in this protein. We also think molecular hysteresis may be seen in modifications of enzymes such as phosphorylation.

Acknowledgements. We are grateful to Prof. H. Taube of Stanford University for his encouragement and for his critical review of the manuscript.

12 References

1. Barra AL, Caneshi A, Cornia A, Fabrizi de Biani F, Gatteschi D, Sangregorio C, Sessoli R, Sorance L (1999) Small molecular clusters exhibiting magnetic hysteresis behavior at extremely low temperatures have recently been reported. J Am Chem Soc 121: 5302 and references cited therein
2. Neumann E (1973) Angew Chem Int Ed Engl 12: 356
3. Frieden C (1970) J Biol Chem 245: 5788
4. Hand SC, Carpenter JF (1986) Am J Physiol 259: R505
5. Evans DH (1990) Chem Rev 90: 739
6. Beer PD (1992) Adv Inorg Chem 39: 79
7. Boulas PL, Gomez-Kaifer M, Echegoyen L (1998) Angew Chem Int Ed Engl 37: 217
8. Zelikovich L, Libman J, Shanzer A (1995) Nature 374: 790; Canevet C, Libman J, Shanzer A (1996) Angew Chem Int Ed Engl 35: 2657
9. Ward TR, Lutz A, Parel SP, Ensling J, Gutlich P, Buglyo P, Orvig C (1999) Inorg Chem 38: 5007
10. Balzani V, Gomez-Lopez M, Stoddart JF (1998) Acc Chem Res 31: 405 and references cited therein
11. Armaroli N, Balzani V, Collin J-P, Gavina P, Sauvage J-P, Ventura B (1999) J Am Chem Soc 119: 4397; Sauvage J-P (1998) Acc Chem Res 31: 611 and references cited therein
12. Field JS, Francis AMA, Haines RJ, Woollam SF (1991) J Organomet Chem 412: 383; Alessio E, Balducci G, Calligaris M, Costa G, Attia WM, Mestroni G (1991) Inorg Chem 30: 609; Powell DW, Lay PA (1992) Inorg Chem 31: 3542; Katz NE, Fagalde F (1993) Inorg Chem 32: 5391; Sanaullah K-k, Glass RS, Wilson GW (1993) J Am Chem Soc 115: 592; Silva DO, Toma HE (1994) Can J Chem 72: 1705; Angus PM, Jackson WG (1994) Inorg Chem 33: 477; Ooyama D, Nagao N, Nagao H, Miura Y, Hasegawa A, Ando K, Howell FS, Mukaida M, Tanaka K (1995) Inorg Chem 34: 6024; Marken F, Bond AM, Colton R (1995) Inorg Chem 34: 1705; Moraczewski J, Sassano CA, Mirkin CA (1995) J Am Chem Soc 117: 11379; Singewald ET, Mirkin CA, Stern CL (1995) Angew Chem Int Ed Engl 34: 1624; Delville-Desbois M-H, Mross S, Astruc D, Linares J, Varret F, Rabaa H, Le Beuze A, Saillard J-Y, Culp RD, Atwood DA, Cowly AH (1996) J Am Chem Soc 118: 4133; Chin TT, Geiger WE, Rheingold AL (1996) J Am Chem Soc 118: 5002; Wytko JA, Boudon C, Weiss J, Gross M (1996) Inorg Chem 35: 4469; Hech M, Schults FA, Speiser B (1996) Inorg Chem 35: 5555; Ooyama D, Nagao N, Kuroda H, Satoh U, Howell FS, Mukaida M, Nagao H, Tanaka K (1996) Bull Chem Soc Jpn 69: 1593; Fairlie DP, Ilan Y, Taube H (1997) Inorg Chem 36: 1029; Ooyama D, Nagao H, Ito K, Nagao N, Howell FS, Mukaida M (1997) Bull Chem Soc Jpn 70: 2141; Zahn S, Canary JW (1998) Angew Chem Int Ed Engl 37: 305; Trujillo HA, Casado CM, Ruiz J, Astruc D (1999) J Am Chem Soc 121: 5674 and references cited therein
13. Yeh A, Scott N, Taube H (1982) Inorg Chem 21: 2542
14. Tomita A, Sano M (1994) Inorg Chem 33: 5825
15. March FC, Ferguson G (1971) Can J Chem 49: 3590; Tomita A (2000) PhD thesis, Nagoya University, Japan

16. Sano M, Itoh Y unpublished work
17. Harman WD, Fairlie DP, Taube H (1986) J Am Chem Soc 108: 8223; Cordone R, Taube H (1987) J Am Chem Soc 109: 8101; Harman WD, Sekine M, Taube H (1988) J Am Chem Soc 110: 2439; Harman WD, Wishart JF, Taube H (1989) Inorg Chem 28: 2411
18. Harman WD, Taube H (1988) J Am Chem Soc 110: 5403
19. Sano M, Sago H, Tomita A (1996) Bull Chem Soc Jpn 69: 977
20. Hoffman BM, Ratner MA (1987) J Am Chem Soc 109: 6237; Klosek-Dygas MM, Hoffman BM, Matkowsky BJ, Nitzan A, Ratner MA, Schuss Z (1989) J Chem Phys 90: 1141
21. Sano M, Taube H (1991) J Am Chem Soc 113: 2327
22. Sano M, Kurauchi T unpublished results for the complexes **2**, **3**, and **4**
23. Tomita A, Sano M (2000) Inorg Chem 39: 200
24. Sano M, Nagai A unpublished results
25. Tomita A, Sano M (1996) Chem Lett 981
26. Lehn J-M (1995) In: Supramolecular chemistry. VCH, Weinheim, chap 8.5
27. Beer PD (1994) In: Fabbrizzi L, Poggi A (eds) Transiton metals in supramolecular chemistry. Kluwer, Dordrecht, p 33
28. De Santis G, Dicasa M, Fabbrizzi L, Licchelli M, Mangano C, Pallavicini P, Perotti A, Poggi A, Sacchi D, Taglietti A (1994) In: Fabbrizzi L, Poggi A (eds) Transiton metals in supramolecular chemistry. Kluwer, Dordrecht, p 133
29. Kaifer AE (1994) In: Fabbrizzi L, Poggi A (eds) Transiton metals in supramolecular chemistry. Kluwer, Dordrecht, p 227
30. Coates GW, Waymouth RM (1995) Science 267: 217
31. Lyons LJ, Tegen MH, Haller KJ, Evans DH, Treichel PM (1988) Organometallics 7: 357; Geiger WE, Salzer A, Edwing J, Philipsborn W, Piantini U, Rheingold AL (1990) J Am Chem Soc 112: 7113; Inomata S, Tobita H, Ogino H (1991) Inorg Chem 30: 3039; Roth T, Kaim W (1992) Inorg Chem 31: 1930
32. Barker PD, Mauk AG (1992) J Am Chem Soc 114: 3619

Switchable Molecular Devices: From Rotaxanes to Nanoparticles

Jian Liu, Marielle Gómez-Kaifer, Angel E. Kaifer

Center for Supramolecular Chemistry and Department of Chemistry,
University of Miami, Coral Gables, FL 33124-0431, USA
E-mail: akaifer@miami.edu

Rotaxanes have been used as molecular frameworks for the preparation of switchable or bistable systems. The properties of a rotaxane that can be switched by electrochemical and chemical means are described in detail and used as an example in this discussion. The advantages of the rotaxane framework compared to systems containing the individual active components mixed together are considered. A series of practical problems hindering the application of single-molecule devices in actual circuits are discussed. Finally, some emerging alternatives to single-molecule devices based on the quickly growing field of metal and semiconductor nanoparticles are briefly described.

Keywords: Electrochemical reactions, Molecular devices, Nanoparticles, Rotaxanes, Switching

1 Introduction 142

2 Rotaxanes and Catenanes as Molecular Devices 142

3 Advantages of Rotaxanes Compared to Multi-Component Systems 149

4 A More Physical View of Switchable Rotaxanes 152

5 Towards Practical Devices: Bumps on the Road 156

5.1 Switching Rates 156
5.2 Miniaturization and Phase Requirements 157
5.3 Miniaturization and Information Scrambling 157
5.4 Miniaturization and Molecular Wires 158
5.5 Device Stability 159

6 Nanoparticle-Based Devices 159

7 Future Developments 160

8 References 161

Structure and Bonding, Vol. 99

1 Introduction

Recent experimental results have raised fundamental concerns regarding the long-sustained, progressive miniaturization of electronic components. The insulator character of silicon oxide, which is crucial for the operation of metal oxide semiconductor field effect transistors (MOSFETs), will break down at layer thicknesses under 1.0 nm, a level of miniaturization that will be reached around 2012 at the current pace [1, 2]. This is a manifestation of what appears to be a fundamental limitation; we simply cannot anticipate that current miniaturization trends will be maintained forever as we approach device dimensions that are about 10 times the size of the atoms composing the materials of choice. Furthermore, the bulk properties (i.e., electronic conductivity) of these materials change or lose their meaning as the device sizes shrink to dimensions equivalent to just a few atoms. Undoubtedly, silicon will still rule in the manufacturing of electronic devices for a few more years, but these fundamental problems appear as serious barriers to the continued technological development that we have come to expect from the microelectronics industry.

The "bottom-up" approach [3] is receiving increasing attention as a group of techniques that may overcome the problems encountered by the traditional "top-down" methods. The central idea of "bottom-up" methodology is that functional devices can be synthesized through the rational assembly of atoms, as the smallest possible building blocks. This idea is indeed one of the basic tenets behind the development of the relatively young field of supramolecular chemistry and has been recognized by a recent report from the U.S. National Science and Technology Council (NSTC) entitled "Nanostructure Science and Technology" [3].

In this chapter we focus our attention on the use of rotaxanes as the framework for the assembly of switchable molecules. This is indeed only one of the many different types of molecules and molecular assemblies that have been proposed in the literature as candidates for the development of novel devices. However, the chemistry of rotaxanes has developed considerably, mostly through the efforts of Professor Stoddart and his coworkers [4]. We will describe some of our own collaborative work with the Stoddart group and venture into some relatively unexplored aspects of the physical chemistry of rotaxanes. We will also address in detail some of the real problems that hamper the practical use of molecular devices in technological applications. Finally, we will discuss the use of metal and semiconductor nanoparticles as a possible new route for the development of new types of molecular devices.

2 Rotaxanes and Catenanes as Molecular Devices

Rotaxanes are molecules consisting of one or more macrocyclic rings (beads) threaded by a linear component with bulky stopper groups at both ends [5]. The sliding motion of the macrocyclic rings is limited by the stopper groups,

which prevent bead-thread dissociation processes. Therefore, a [2]-rotaxane (a rotaxane with only one bead) can be conceptually considered as a trapped inclusion complex. A catenane is composed of two or more interlocked macrocycles. A [2]-catenane (two interlocked rings) is then conceptually similar to a [2]-rotaxane, in the sense that one of the rings can be considered trapped by the second ring. In a [2]-catenane, it is the cyclic nature of the second ring that prevents dissociation, while in a [2]-rotaxane dissociation is precluded by the bulky stopper groups (Scheme 1). In both cases, the net result is the same: the range of sliding motions available to the macrocyclic bead is confined to a spatial region determined by another molecular component. It is precisely this spatial confinement that makes these molecules so attractive as potential molecular devices.

In 1991, Anelli, Spencer, and Stoddart reported the preparation of a novel [2]-rotaxane containing two electron-rich aromatic groups (stations) along the thread and a macrocyclic bead with a marked electron-deficient character [6]. NMR experiments demonstrated that the bead shuttles back and forth between the two equivalent aromatic donor stations at thermally controlled rates. Owing to the bead shuttling process, this rotaxane was termed a "molecular shuttle". These authors suggested the appealing idea of desymmetrizing the molecular shuttle structure, introducing in the thread two aromatic stations with different π-donor character. In such an asymmetric molecular shuttle, the bead would be expected to bind preferentially to the stronger donor station (S). However, the difference in the properties of the donor stations should make it possible to address them individually. Ideally, the application of an external stimulus to the molecule would lead to the 'deactivation' of donor station S ($S \rightarrow S'$), forcing the molecule into a different state in which the bead must move to interact primarily with the weaker donor station, W. If the changes in the nature of the stronger donor station can be reversed (S′ back to

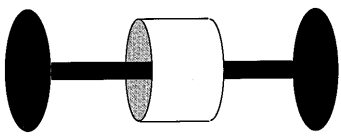

Rotaxane

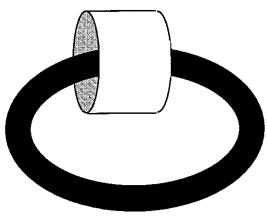

Catenane

Scheme 1. Rotaxanes and catenanes

S), then a mechanism for reversible control on the average position of the bead would be accessible. This class of molecules was dubbed "switchable or controllable molecular shuttles" and they constitute clear examples of bi-stable molecules (Scheme 2). Ideally, one would like to use an easily measurable property to distinguish the two states of the molecule, i.e., to read the molecular state in more digital terms.

Synthetic methodology for the preparation of switchable rotaxanes has been primarily developed by Stoddart and coworkers [4]. In collaboration with Stoddart, the author's group reported in 1994 a molecular shuttle that exhibited a novel feature: dual control. In this rotaxane the average position of the bead could be controlled by both proton- and electron-transfer reactions [7]. We will describe some of the most important properties of this rotaxane here since it will be used as an illustrative example in the remaining sections of this chapter. The basic design features of this rotaxane emerged from previous studies [8] on the complexation of benzidine and biphenol guests by the tetracationic host cyclobis (paraquat-*p*-phenylene) ($\mathbf{1}^{4+}$, see structure in Scheme 3). This electron-deficient host was found to bind benzidine over biphenol with an approximate selectivity of 8:1 in acetonitrile solution. Furthermore, the binding selectivity was not affected significantly by the covalent attachment of ethyleneoxy tethers at both reactive ends of the guests [8]. Finally, the larger stability of the benzidine · $\mathbf{1}^{4+}$ complex (as compared to the biphenol · $\mathbf{1}^{4+}$ complex) can be disrupted by generation of positive charge in the benzidine guest, a process that can be conducted by electrochemical or chemical oxidation as well as by protonation of its basic nitrogen atoms.

The synthesis of the target rotaxane $\mathbf{2}^{4+}$ was achieved in 20% yield by the procedure shown in Scheme 3 [7]. The ^{1}H-NMR spectrum at room temperature of $\mathbf{2}^{4+}$ (400 MHz, CD_3CN) was severely broadened by the fast sliding motion of the bead along the thread. At −40 °C bead sliding was sufficiently slow to allow the observation of the two interconverting translational conformers shown in Scheme 4. In agreement with our previously obtained

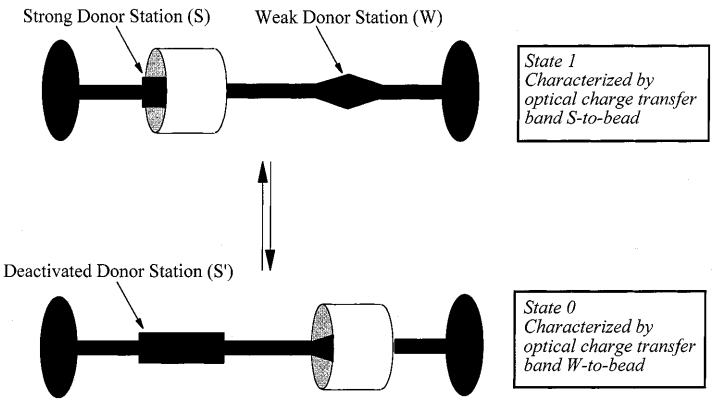

Scheme 2. A switchable molecular device

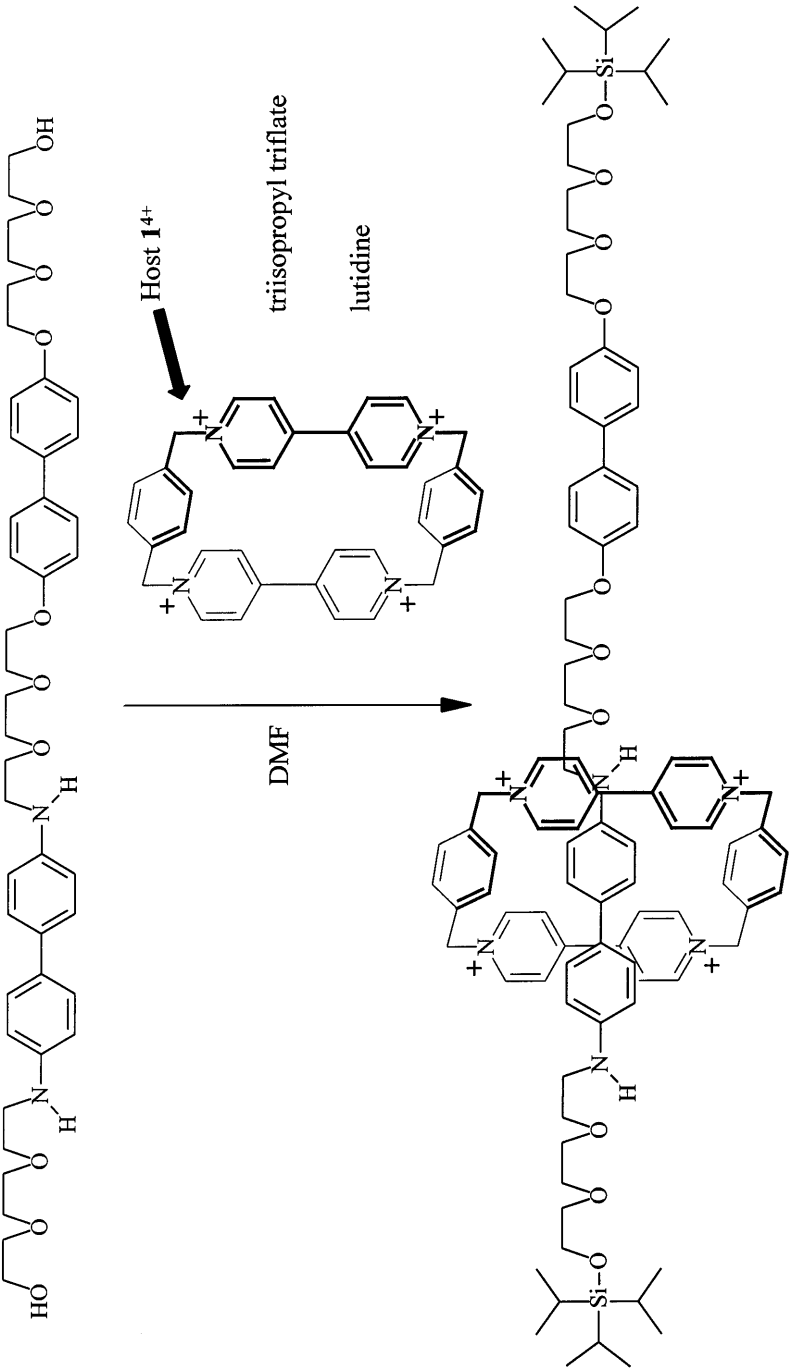

Scheme 3. Synthesis of rotaxane 2^{4+}

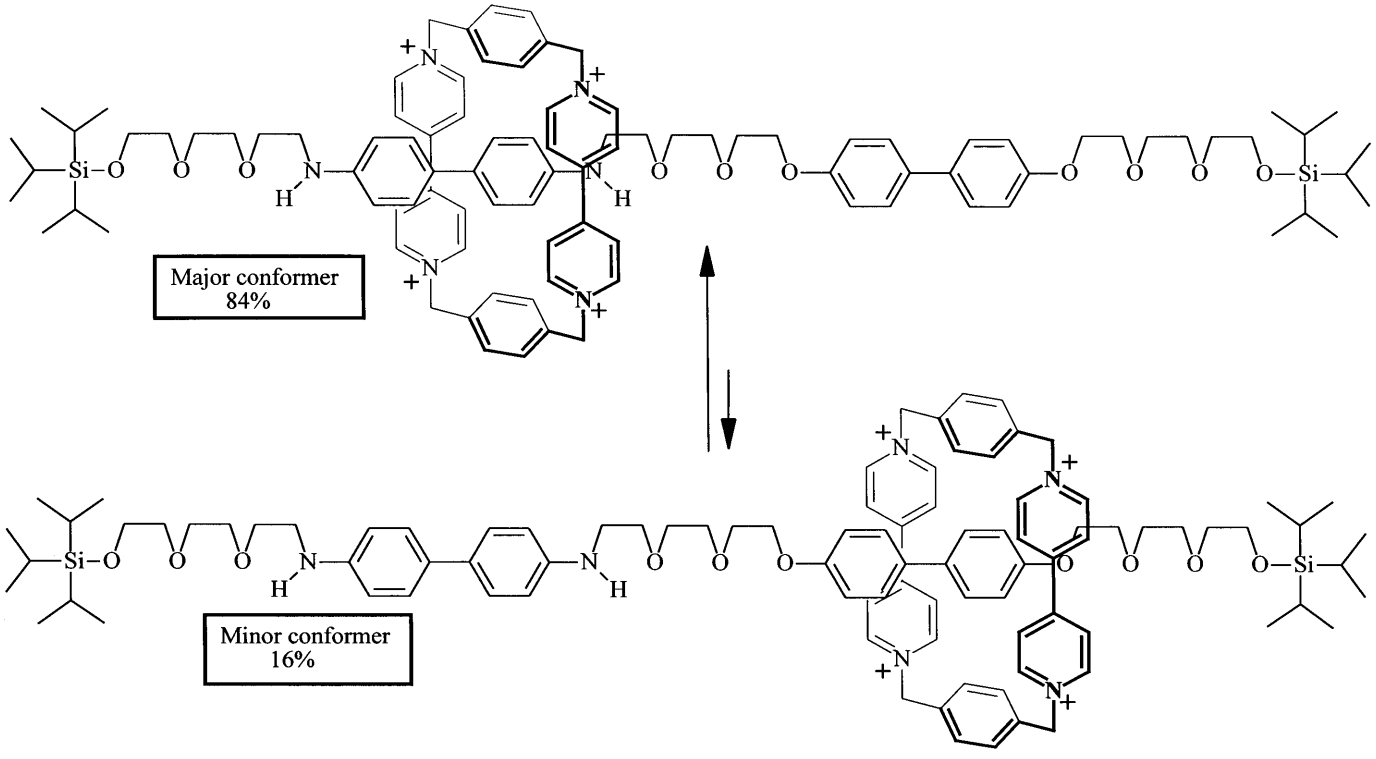

Scheme 4. Conformational equilibrium of rotaxane 2^{4+} in CD_3CN at 299 K

binding data, the conformer in which the tetracationic macrocycle resides on the benzidine station is preferred to that in which the biphenol station is encircled by the bead. The ratio of the two conformers (84:16) at this temperature is also in excellent agreement with the binding selectivity measured with this macrocyclic host.

Electrochemical oxidation of the benzidine guest in $\mathbf{2}^{4+}$ creates a positive charge that forces the tetracationic bead to move over to the biphenol station (Scheme 5). This was clearly verified by the half-wave potential values obtained in cyclic voltammetric experiments with this rotaxane [7]. The reversible character of the one-electron oxidation of the benzidine unit in $\mathbf{2}^{4+}$ provides a useful electrochemical mechanism to control the sliding motion of this rotaxane's bead. Although we did not verify this point experimentally, it should be equally possible to oxidize the benzidine unit using homogeneous

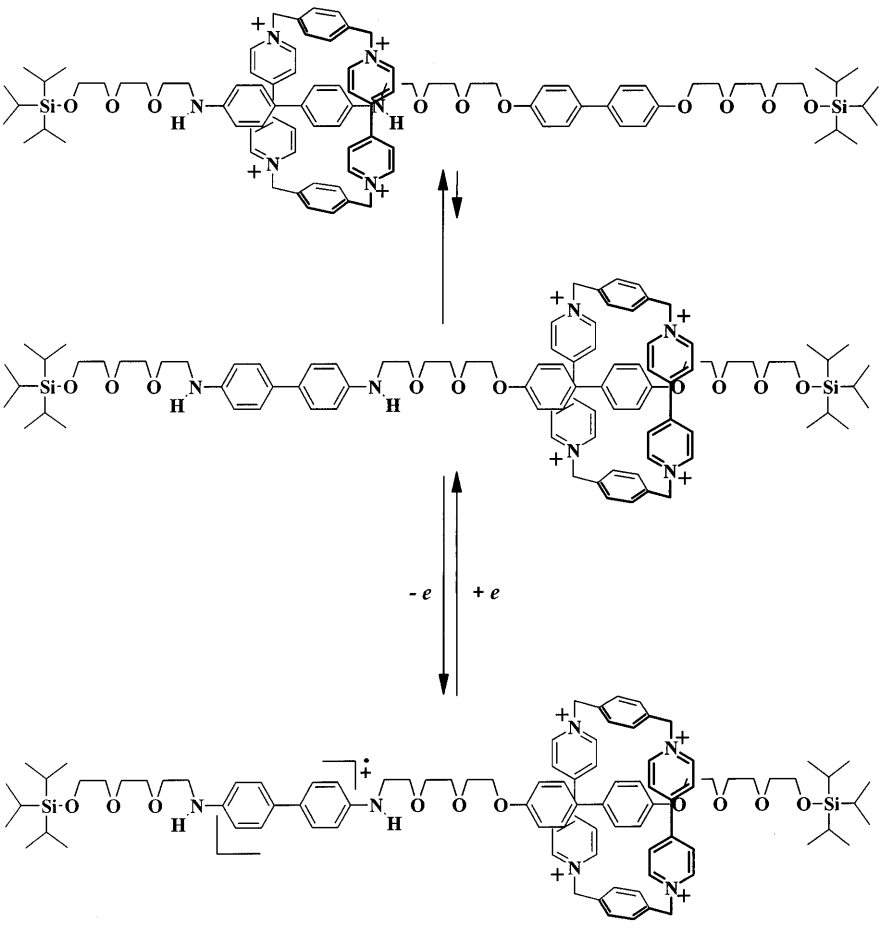

Scheme 5. Electrochemical switching of rotaxane $\mathbf{2}^{4+}$

electron transfer reactions, leading to an alternate (chemical as opposed to electrochemical) mechanism to switch the state of $\mathbf{2}^{4+}$.

The basic character of benzidine affords an alternate mechanism to influence the average position of the bead. Protonation of the amine functional groups by simple addition of trifluoroacetic acid (TFA) to the solution also generates positive charges on the benzidine unit and forces the bead to encircle the biphenol station. Neutralization with base (pyridine) returns the system to its initial state by removing the positive charges on the benzidine station (Scheme 6). These phenomena were verified in careful ^{1}H-NMR spectroscopic experiments [7]. Thus, chemical (proton transfer) reactions are also useful to control the sliding motion of the macrocyclic bead in this rotaxane.

The occupation of each π-donor station in the thread of rotaxane $\mathbf{2}^{4+}$ by the macrocyclic bead gives rise to characteristic charge transfer bands. Therefore,

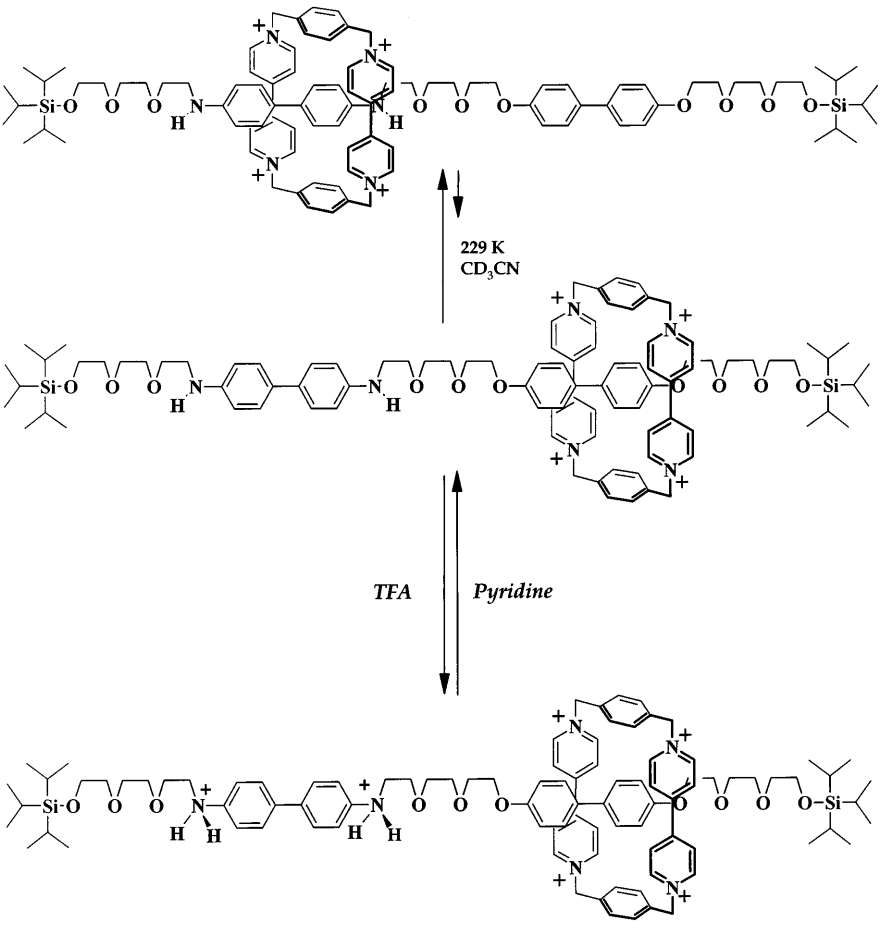

Scheme 6. Protonation of rotaxane $\mathbf{2}^{4+}$

the average bead locations ascertained from the ^{1}H-NMR data can also be independently confirmed by UV-Vis absorption spectroscopy. In this regard, the visible region provided the most useful data because both the bead and the donor stations exhibit intense absorption bands in the UV regions. Before any TFA additions, the visible spectrum of $\mathbf{2}^{4+}$ shows a broad band centered around 690 nm that corresponds to the benzidine-bead charge transfer absorption. Addition of excess TFA eliminates this band and leads to the observation of the biphenol-bead charge transfer band at 480 nm. The original band at 690 nm can be regenerated by neutralization with pyridine. These spectral changes can clearly be seen by the naked eye as a solution of $\mathbf{2}^{4+}$ undergoes dramatic color changes from deep green to light red and back to deep green as acid and base are added [7]. These spectroscopic data are in excellent agreement with the ^{1}H-NMR results and afford further confirmation for the switchable nature of the rotaxane. Conceptually, it can be argued that the spectroscopic properties of $\mathbf{2}^{4+}$ in the visible region can be used to 'read' its molecular state.

A skeptical reader may point out here that molecules whose light absorption patterns change as a result of protonation or oxidation have been known for many decades. While this is obviously true, the criticism misses a very important point: the color changes associated with protonation or oxidation of $\mathbf{2}^{4+}$ are the result of the external control that the experimenter exerts on the movements of the bead along a closed path, i.e., the thread of the rotaxane. Overall, this rotaxane constitutes a remarkable example of a bi-stable or switchable molecule, i.e., a molecule with two well-defined states that can be accessed using chemical or electrochemical stimuli. In this sense, we can conclude that $\mathbf{2}^{4+}$ is a molecular device, using one of the definitions of the word "device" given in the Oxford dictionary ("Something devised or contrived for bringing about some kind of result"). However, the application of $\mathbf{2}^{4+}$ (or similar molecules) to digital electronic circuitry requires the resolution of a number of practical issues that will be addressed in more detail later in this chapter.

3 Advantages of Rotaxanes Compared to Multi-Component Systems

The synthesis of switchable rotaxanes, such as $\mathbf{2}^{4+}$, is laborious, expensive and time-consuming. We should first ask ourselves whether it is worthwhile to go through the trouble of preparing these complicated molecules or can we accomplish similar results with multi-component systems. Specifically, we decided to address this general question by investigating the switching in a tri-molecular system composed of host $\mathbf{1}^{4+}$, a benzidine guest, and a biphenol guest (structures **3** and **4** in Scheme 7). From the behavior of rotaxane $\mathbf{2}^{4+}$ and the known host selectivity exhibited by $\mathbf{1}^{4+}$, we anticipated that, in a solution containing equal concentrations of **3** and **4**, the host (present in lower concentration) will give rise to a concentration of $\mathbf{3} \cdot \mathbf{1}^{4+}$ complex larger than that of $\mathbf{4} \cdot \mathbf{1}^{4+}$ complex. Furthermore, oxidation or protonation of guest **3** will lead to the disappearance of its complex and a subsequent increase of the

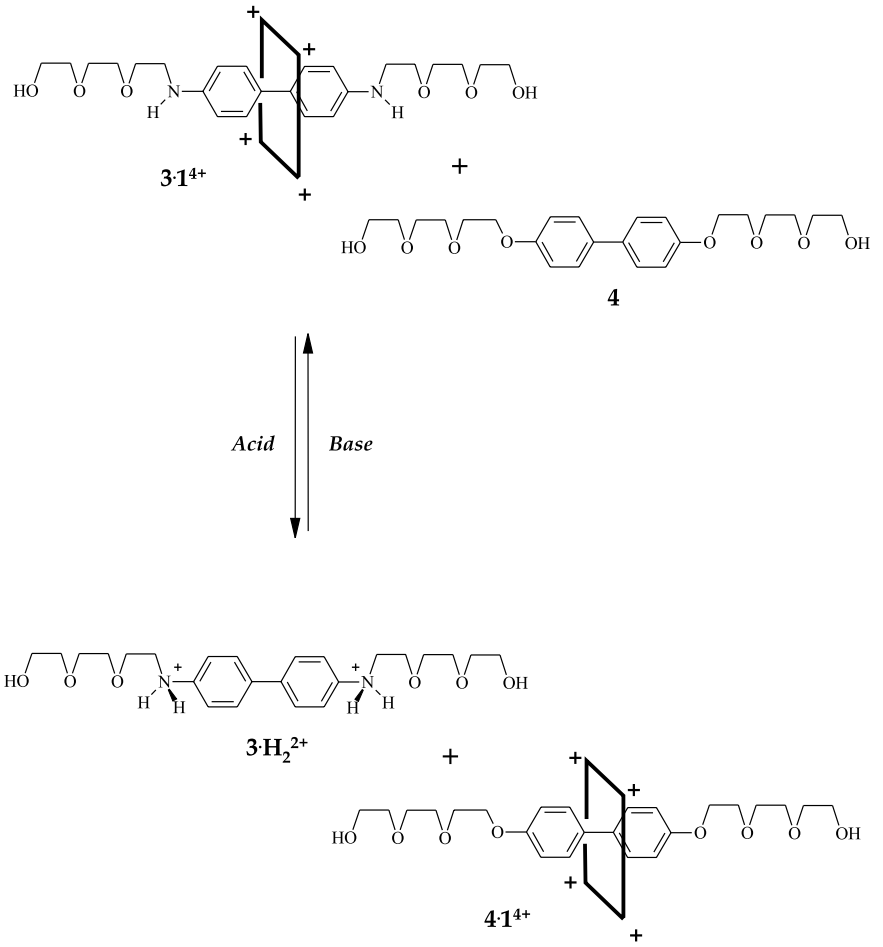

Scheme 7. Protonation-driven switching of the selectivity of host $\mathbf{1}^{4+}$

concentration of $\mathbf{4} \cdot \mathbf{1}^{4+}$ complex. This host switching behavior is schematically represented in Scheme 7.

We performed several series of spectroscopic measurements in acetonitrile solutions containing equimolar solutions of **3** and **4** and a lower concentration of host $\mathbf{1}^{4+}$ and determined the complex concentrations as variable amounts of TFA and pyridine were added to control the extent of protonation of the benzidine derivative **3** [9]. Typical results, obtained with a solution initially containing 2.0 mM of **3**, 2.0 mM of **4**, and 1.0 mM of $\mathbf{1}^{4+}$, are shown in Fig. 1. Clearly, protonation of **3** leads to dissociation of its complex with $\mathbf{1}^{4+}$ and a modest increase of the concentration of complex $\mathbf{4} \cdot \mathbf{1}^{4+}$. To compare in more quantitative terms this switching behavior to that observed with the unimolecular system (rotaxane $\mathbf{2}^{4+}$), it is useful to focus on the molar

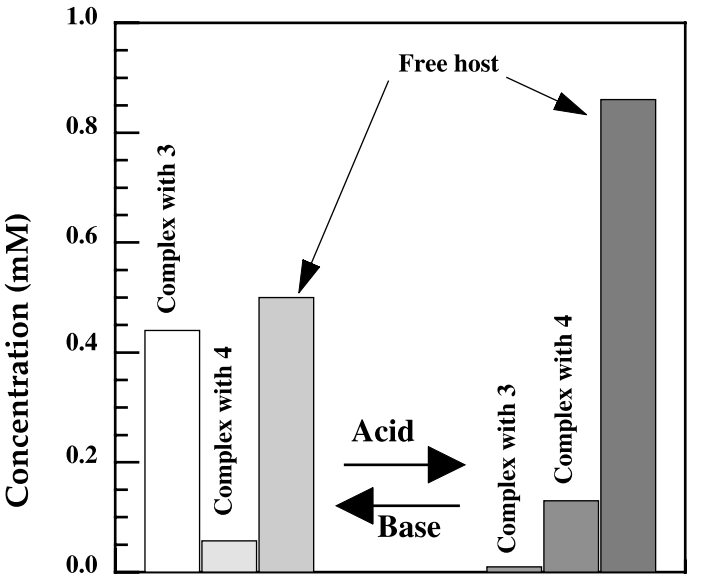

Fig. 1. Bar diagram showing the concentrations of the two complexes and the free host before and after the addition of excess TFA. Initial concentrations: 2.0 mM of **3**, 2.0 mM of **4**, and 1.0 mM of host

fractions of host bound to the secondary guest (the guest with the lower π-donor character) before (X) and after (X') application of the switching stimulus [9]. An ideal switchable system should have values of $X = 0$ and $X' = 1$, reflecting the complete transfer of the host from the primary to the secondary guest upon switching. From the data in Fig. 1, we calculate $X = 0.057$ and $X' = 0.13$ for the trimolecular system at the millimolar concentrations surveyed. Clearly, the main problem observed with this system is that a large fraction of the host remains unassociated, in equilibrium with the complexes. Specifically, the low binding constant between **4** and the host leads to a very low value for X'.

The switching efficiency of a trimolecular binding system can be improved by using complexes with higher binding constants. For instance, if the host binds the primary and secondary guests with binding constants of 10^6 and 10^4 M^{-1}, respectively, equilibrium calculations yield $X = 0.019$ and $X' = 0.916$, values that are much closer to the ideal ones and reveal a much more efficient use of the host in the switching process. However, the binding constants of these types of complexes are usually lower than 10^4 M^{-1}, leading to inherent inefficiencies in trimolecular switching systems. In comparison, our experimental results with rotaxane $\mathbf{2}^{4+}$ lead to $X = 0.16$ and $X' = 1.0$ values. Therefore, we must conclude that the unimolecular system, based on the rotaxane framework, allows more effective switching since the host is transferred from the primary to the secondary guest more efficiently. Of course, this is due to the fact that, in the rotaxane, the macrocyclic bead is not in true equilibrium with the guests. It is

rather confined to slide back and forth between the stopper groups and forced to interact with the π-donor stations inserted along the thread. Thus, the physical confinement of the host in rotaxanes does play a very important role in the expression of efficient switching behavior. Furthermore, another advantage of unimolecular over trimolecular systems must be mentioned here. Unlike the trimolecular systems, the switching behavior of the unimolecular system is not dependent on concentration. In a trimolecular system, the molar fraction of bound host depends on the absolute concentrations of the three components. It should be possible to decrease the fraction of unbound host by increasing all the absolute concentrations in the solution. However, this would be counterproductive as aggregation and formation of higher order complexes may further complicate the system.

In conclusion, these results demonstrate clearly that the rotaxane framework does offer significant performance advantages over multi-component systems for the preparation of switchable molecular assemblies.

4 A More Physical View of Switchable Rotaxanes

Rotaxanes are molecules in which the movement of the macrocyclic component is constrained and limited to a determined physical range. In this regard, it is illustrative to consider this idea in terms of potential energy profiles associated with the movement of the bead along the rotaxane's thread. For the sake of simplicity, let us assume that the thread is rigidly extended and that the macrocycle bead may move anywhere between the two ends defined by the stopper groups. From the structure of rotaxane $\mathbf{2}^{4+}$ and the available binding data, it is reasonable to predict an approximate energy profile of the type sketched in Fig. 2, having two potential wells which represent the relative stabilization afforded by each of the two aromatic donor stations inserted along the thread. In agreement with the known benzidine vs. biphenol selectivity demonstrated by the macrocyclic bead, the benzidine well is deeper than the biphenol well. That is, the benzidine well site constitutes the preferred location for the bead along the rotaxane's thread. Protonation or oxidation will generate positive charges on the benzidine nucleus, introducing pronounced changes in the potential energy profile (see Fig. 2). The benzidine potential well is now replaced by a region with rising potential energy which reflects the coulombic repulsive forces between the positively charged station and the tetracationic bead. As a result of this repulsive potential, the biphenol well becomes the preferred location for the bead after the switching stimulus takes place.

From the standpoint of switchable properties it would be desirable to build a rotaxane capable of more sharply defined "on-off" conversions. Before switching, rotaxane $\mathbf{2}^{4+}$ presents two translational conformers, characterized by either benzidine or biphenol occupation by the bead. Although benzidine occupation is heavily favored (84% vs. 16%), the fraction of systems that show biphenol occupation are conceptually equivalent to a "leak" in the switching device. The selectivity of the bead for one of the two donor stations can be accomplished by one of two approaches:

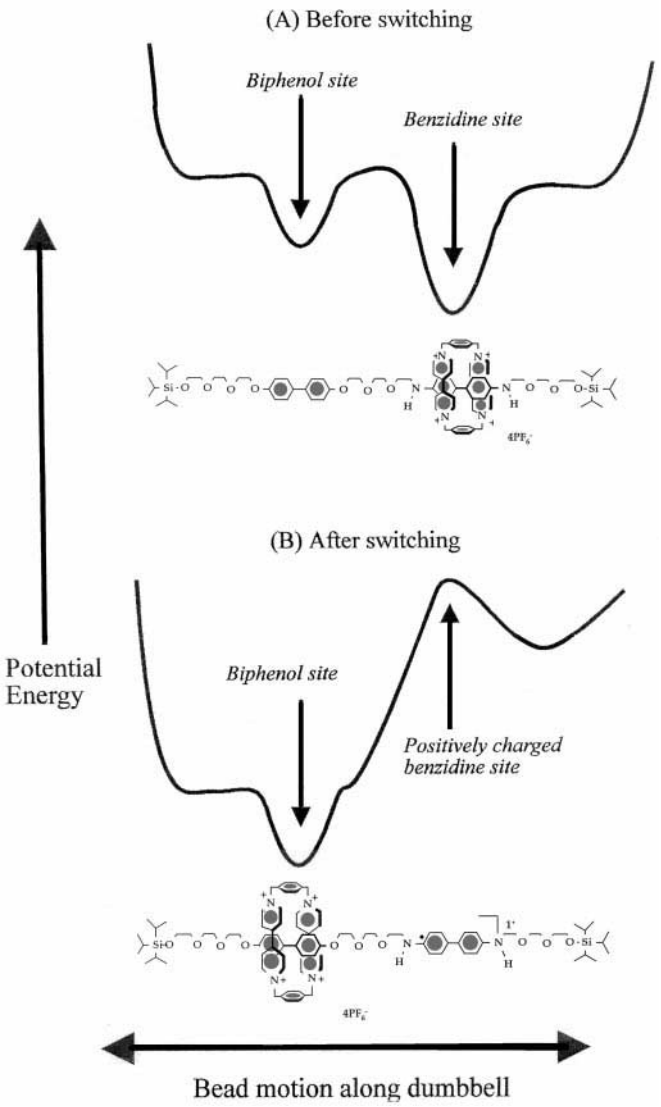

Fig. 2. Potential energy profiles for bead sliding motions in the rotaxane (**A**) before and (**B**) after charge generation on the benzidine station

(i) deepening of the potential well corresponding to the primary donor station (benzidine in this case), or
(ii) flattening of the potential well corresponding to the secondary donor station.

The first approach may not be easy because the binding stabilization achieved with benzidine is already larger than that experienced by most other aromatic

donor guests. On the other hand, replacing biphenol by a poorer aromatic guest may appear as an easy way to improve on the properties of rotaxane $\mathbf{2}^{4+}$. However, some degree of station-bead stabilization is required in the switched state and, therefore, it is not clear how much improvement may be achieved by this approach.

An important property of any switching device is the interconversion or switching rate between its two states. So far, little data has been accumulated on the switching rates of rotaxane $\mathbf{2}^{4+}$ and similar systems. Our ^{1}H-NMR spectroscopic data suggest that the shuttling time between the benzidine and the biphenol stations in this rotaxane is in the millisecond range, similar to that reported for the first symmetric molecular shuttle. Of course, this rate corresponds to the bead motion back and forth between the two stations prior to switching. If we assume that there is no driving force powering the bead movement from station to station and no interactions between the bead and the thread at the beginning, during, and at the end of the bead motion, we can estimate this shuttling rate using a very simple physical model. The movement of the bead along the thread can thus be described by a "random walk" model [10], which is commonly used in diffusional problems in one dimension. Therefore, the average net displacement d after a time t of random unidimensional movements characterized by a diffusion coefficient D is given by Eq. (1):

$$d = (2Dt)^{1/2} \tag{1}$$

If we take the approximate distance between the two donor stations in rotaxane $\mathbf{2}^{4+}$ as 16 Å and approximate the bead diffusion coefficient by a reasonable value (2×10^{-6} cm^2/s), the time required for shuttling between the two stations would be approximately 6 ns. This calculated shuttling time is about six orders of magnitude shorter than the millisecond regime that we detected experimentally. This difference reveals that the interactions between the bead and the two donor stations, as well as those between the bead and the oligoethyleneoxy tethers, play a crucial role at controlling the bead sliding motions. In the absence of more detailed information on these bead-thread interactions, it is reasonable to postulate that the kinetics of the bead-station dissociation process probably determines the overall rate at which the bead can transfer from one station to the other.

Can we reasonably expect that the bead's switching rate will be faster under the effects of the electrostatic field created by the positive charge on the benzidine station? To address this question we have to consider in detail the mechanism of charge generation on the benzidine station. Let us assume that we are generating positive charge through a one-electron electrochemical oxidation of the benzidine residue. In principle, we can visualize switching taking place by either one of two event sequences. In the first sequence, electrochemical oxidation of the benzidine residue in the most stable conformer would then lead to the bead sliding motion over to the biphenol station. In the second possible sequence, electrochemical oxidation of the benzidine station would take place when the bead occupies the biphenol region of the thread, during the thermally driven shuttling process that

equilibrates the two translational conformers. The first sequence of events appears unlikely considering our work with a model rotaxane containing a single benzidine donor station in the thread [11]. We found that the proximity of the tetracationic bead slows considerably the rate of electrochemical oxidation due to the electrostatic effect exerted by the bead. Furthermore, our group has also recently investigated the electrochemistry of other encapsulated redox centers [12, 13]. Our data point to a generalized slowing of the electron transfer rates brought about by the encapsulation of the redox centers. These results are very significant to an understanding of the switching mechanism in rotaxane $\mathbf{2}^{4+}$. They make the first sequence of events described above (electrochemical oxidation followed by bead motion) very unlikely because of the slow rate anticipated for the electrochemical oxidation of benzidine when the tetracationic bead is in its vicinity. Therefore, it follows that the switching of rotaxane $\mathbf{2}^{4+}$ is likely to take place by electrochemical oxidation of the translational conformer in which the bead resides on the biphenol. If this is the case, the rotaxane's electrochemical switching rate must be controlled by the thermally-driven shuttling rate and, according to our ^{1}H-NMR data, it should be in the millisecond regime at room temperature.

Similar arguments can be made for rotaxane switching through proton-transfer reactions. Furthermore, proton-transfer reactions do not appear quite suitable for practical switching applications as they require the addition of reagents (acids and bases) to control the structure of rotaxanes, such as $\mathbf{2}^{4+}$. Although all these arguments are not final and more experiments are needed to determine switching kinetics in this class of molecules, we must conclude that switching rates in rotaxanes, such as $\mathbf{2}^{4+}$, are much slower than the switching rates accessible with MOSFETs [14] and related semiconductor devices (usually larger than 1 MHz).

Unlike all its schematic representations in this chapter, the thread of rotaxane $\mathbf{2}^{4+}$ may not remain in an extended conformation at all times. The oligoethyleneoxy tethers are sufficiently flexible to permit folded conformations that may also tend to slow down the sliding motions of the bead along the thread. In order to speed up the bead motions and the switching rates, it would be desirable to prepare similar rotaxanes having rigid, linear tethers connecting the donor stations and the stopper groups. However, it is questionable that such a synthetic effort will yield substantially faster molecular shuttles. From the random walk calculations of the type performed above, it is clear that, in the diffusion limit, the transfer time between the two stations is determined by the diffusion coefficient of the bead. In order to speed up the shuttling motion, beads with substantially higher diffusion coefficients will be required. In condensed media, small organic molecules exhibit D values rarely higher than 10^{-5} cm^2/s. Therefore, it does not seem feasible to prepare functional macrocyclic beads with substantially larger D values that may foster considerably faster switching rates. In the final analysis, switching in these molecules requires the physical displacement of a rather large molecular component, the macrocyclic bead, and it is unlikely that bead motions will ever occur at rates comparable to those of electrons and holes traveling through semiconductor and metallic components.

Another important parameter that we would like to consider here is the information storage density that can be achieved with rotaxane $\mathbf{2}^{4+}$. Under ideal conditions, we can store one bit of information per rotaxane molecule. In other words, a total of 274 atoms (taking four $[PF_6]^-$ as the counterions for the macrocyclic bead) can hold one bit of information. For comparison purposes, present electronic circuits require more than 10^6 atoms in order to store one bit of information. If digital circuits could be built around this rotaxane, outstanding levels of bit storage density would be within our reach. Unfortunately, the optimism that these figures may generate must be somewhat tempered by the realization that, in real applications, the packing density of rotaxane molecules would have to be substantially decreased. Physical barriers or spacings between neighboring molecules in an array would be required to prevent intermolecular reactions, such as electron-transfer processes between them, that will give rise to data scrambling, i.e., loss or corruption of the stored digital information. Of course this would tend to increase the number of atoms required to store one bit and decrease the information storage density to less spectacular levels.

We have addressed in this section the switching kinetics of rotaxane $\mathbf{2}^{4+}$ and concluded that future improvements on switching rates will be limited by the inherent difficulties associated with achieving fast sliding motions of the bead component along the thread. In the next section we will look at more general problems that hinder the practical development of digital circuits based on single-molecule devices.

5
Towards Practical Devices: Bumps on the Road

The "bottom-up" approach is extremely attractive as it proposes the construction of devices and circuit components through the rational assembly of the smallest set of building blocks (atoms) available to mankind. It can be argued that devices based on subatomic particles may become useful in the future, but their assembly and operation will require the manipulation of huge amounts of energy, a feature that makes them totally inaccessible with our current level of technological development. From the standpoint of chemists, the manipulation of atoms leads naturally to the preparation of molecules and, therefore, the idea of molecular devices has been an important subject of modern research. The key advantage offered by molecular devices is their small size and the fact that they can be prepared in extremely large numbers by chemical synthesis. Their application in actual circuits is currently restricted by a number of technological problems that we intend to summarize briefly in this section of the chapter.

5.1
Switching Rates

We have already discussed the switching kinetics of rotaxane $\mathbf{2}^{4+}$ and the bleak outlook for the development of similar molecules with considerably faster

switching rates. Clearly, as long as switching entails significant molecular motions, the kinetics of the switching steps will not become much faster. Current switching times for molecular devices based on rotaxane and catenane frameworks hover around the millisecond regime, i.e., each molecule could support less than 1,000 switching operations per second. The comparison with a current Pentium® processor (about 1000 MHz) is not appropriate because these processors contain large numbers of individual switching devices in their circuitry. However, semiconductor-based devices switch considerably faster than rotaxane-based devices. For instance, the switching speed of the most commonly used type of MOSFET is limited by device and circuit parasitics rather than by internal physical processes. They can easily operate at switching frequencies of up to 10 MHz (switching times within the nanosecond regime) [14]. In order to develop superior digital circuits based on molecular devices, we must necessarily take advantage from the small size of molecules. In other words, we can perhaps afford to use slower switches if we can reach a much higher device density and the devices operate in parallel fashion.

5.2 Miniaturization and Phase Requirements

In principle, rotaxane $\mathbf{2}^{4+}$ allows the storage of one bit of information using only 274 atoms. The device feature size will approximate an incredibly low value of $\sim$1 nm, suggesting extraordinarily high levels of scale integration and device density. Unfortunately, these figures neglect a fundamental problem. To realize this level of integration we must address (switch and read) individual molecules. The behavior of switchable compounds has been normally demonstrated in the solution phase, using spectroscopic or electrochemical methods that monitor the behavior of a large ensemble of molecules. While these experiments serve as proof-of-concept, they do not guarantee that similar behavior will be retained by a single molecule. Furthermore, the chaotic and fluid nature of a solution makes it impossible to switch a specific molecule, store one bit of information in it, and return later to read it. Information storage and processing requires the assembly of devices in two-dimensional or three-dimensional arrays, where each molecule is characterized by a fixed location. Molecular devices appear feasible if they are set in interfacial monolayers (2D) or solid state arrays (3D). A recent example on the use of rotaxanes as molecular devices in a 2D interfacial array has attracted considerable attention [15].

5.3 Miniaturization and Information Scrambling

Let us assume that we can set up a monolayer (2D array) of switchable rotaxane molecules on an appropriate planar surface and that we have a suitable means to switch individual molecules in known positions. Furthermore, let us assume that switching takes place by an electron-transfer mechanism, such as benzidine oxidation to take a familiar case. In this case, if

we oxidize a rotaxane in a particular surface location, can we anticipate that the molecule will remain in the oxidized state for a long time? The answer depends on the average distance separating the benzidine subunits in adjacent rotaxane molecules. If the average distance between neighboring benzidine groups is not too large, intermolecular electron-transfer processes may readily take place, leading to loss or distortion of the digital information stored in the molecular array. To preclude undesirable electron-transfer reactions ("cross-talk" in electronic jargon), the design must include barriers for electron transfer between adjacent molecules. This means that the molecules have to be separated from one another, or that each active switchable rotaxane must be surrounded by a group of inactive, insulating molecules that will prevent electron transfer between neighboring rotaxanes. In any instance, these arguments reveal that the miniaturization levels suggested at the beginning of this section might not be within reach since intimate contact between switchable molecules will lead to unacceptable levels of information scrambling and storage errors. Exactly how much should we reduce the surface density of switchable rotaxanes to insure that each bi-stable molecule is unaffected by its neighbors is uncertain at this time. However, this practical problem may increase the feature size of molecular devices closer to ~10 nm, substantially decreasing their miniaturization advantages.

5.4 Miniaturization and Molecular Wires

In order to address single sites in an array of molecular devices, some mechanism for contacting the macroscopic world must be employed. The small dimensions of electrochemically switchable molecular devices, for example, would appear to require connections to electrode surfaces via wires of similar dimensions, i.e., molecular wires. The concept of a molecular wire – a long-range path for electron or hole transfer – has been a subject of both theoretical and experimental study for more than a decade. Experimentally, the design of donor-acceptor wire systems has seen much progress in recent years. Recently published systems show effective rates of electron transfer with relatively low attenuation due to increasing distance between the donor and acceptor sites [16]. The theory of current flow and conduction in these systems is still in development. Most theoretical studies have typically been limited to simple molecules such as 1, 4-benzenedithiol [17] or α, α'-xylyldithiol [18], though some studies have addressed conductance in longer or more complex wire structures [19]. The results of these studies appear to suggest that the contact geometry could have substantial effects on conductance [17]. More recently however, work by Ratner and coworkers has suggested that the length of the contact bond in wire systems, i.e., the distance between the electrode and the terminal atom (connection point) on the molecular wire, is the strongest influence on the conductance of the wire [18]. These researchers describe a delicate interplay between the strength of chemisorption of the terminal atom onto the electrode surface and the bonding of the terminal atom to the rest of the wire molecule [18]. On a practical level, more extended, i.e.,

larger, wire structures are likely to exert a greater force on the terminal atom and strain its binding to the electrode surface. Thermal effects on the bonding between the terminal atom and the metal surface may also play a role, e.g., consider the mobility of sulfur atoms on the gold surface in gold-thiolate systems. These are all points for consideration with respect to stable and reproducible conduction via molecular wires when seeking to address single sites for information storage. Electronic cross-talk is also possible between wires, not just devices and, thus, interconnections between devices and the electrode surface becomes a complex issue.

5.5
Device Stability

Finally, although rotaxanes such as $\mathbf{2}^{4+}$ show excellent reversibility in solution, we must question how many operational cycles a bi-stable molecule of this type may endure. In this regard, it seems appropriate to remind the reader that many types of molecular residues that undergo fast and reversible electron-transfer reactions in cyclic voltammetric time scales (millisecond to second regime) undergo significant decomposition reactions at longer time scales. We simply do not have many organic or organometallic redox couples that can be switched between their reduced and oxidized forms numerous times and that can remain in one of their oxidation states for long periods of time without decomposition. Living organisms deal with this problem through renovation mechanisms. We can visualize the same type of correction mechanisms if we could utilize efficient self-assembly schemes to prepare new molecular devices and replace those damaged by freshly prepared ones as the need arises. If these correction mechanisms are not available, durability concerns may become very troublesome for the medium- to long-term operation of circuits based on switchable molecules.

6
Nanoparticle-Based Devices

The problems described in the previous section have led a number of research groups to look for alternatives to single-molecule devices. In this regard, the intense research activity on metal and semiconductor nanoparticles is opening a number of interesting possibilities for their application to information storage and processing circuits. Nanoparticles have been the subject of considerable research activity in the last decade of the Twentieth Century. It is impossible to provide even a reasonable summary of this large body of research work in just one section of this chapter. We will limit ourselves to a brief description of selected research developments with potential applications to the construction of miniature devices.

Metal and semiconductor nanoparticles can be prepared in sizes ranging from a few nanometers to 0.1 μm or larger. Solution (wet chemical) preparation methods are available to produce nanoparticles with fairly monodisperse distributions and sizes that are unreachable with lithographic

procedures (<10 nm). These particles are typically stabilized by surface-bound organic molecules, which prevent particle aggregation and precipitation. The organic surfaces make the particles soluble in a variety of solvents, a feature of interest for nanoparticle processing. Most of the interest in nanoparticles focuses on those with diameters under 10 nm, whose properties deviate from those of the bulk material, showing quantum size effects. Under ideal experimental conditions these nanoparticles acquire electric charge one electron at a time, leading to current-potential responses referred to as 'Coulomb staircases', with current steps separated by voltage plateaus which may span hundreds of mV. Each current step corresponds to the uptake of one electron by the nanoparticle. This behavior constitutes the basis for the operation of single electron transistors (SETs) [20].

The construction of SETs requires the assembly of nanoparticles on solid supports. The organic shells of the particles can play a crucial role for this purpose, as it should be possible to utilize intermolecular forces between the shell molecules to drive the self-assembly of the nanoparticles. Mirkin and coworkers have derivatized gold colloidal particles with thiolated oligonucleotides and taken advantage of complementary base sequences to prepare three-dimensional assemblies of gold nanospheres [21]. They have demonstrated that this system can be effectively adapted for colorimetric polynucleotide sequence assays [22]. We have shown that gold colloidal particles [23] and clusters [24] can be derivatized with thiolated cyclodextrins, which retain their molecular complexation properties on the surface of the nanoparticles. Rotello and coworkers have derivatized gold clusters with molecules terminated on hydrogen bonding residues and have demonstrated their binding to complementary solution partners [25]. Our own group [26] as well as Fitzmaurice and coworkers [27] have shown that intermolecular forces can be utilized to prepare rotaxanes on the surface of nanoparticles. All this work suggests that we are witnessing the early stages of the direct assembly of nanoparticles driven by the properties of their functionalized organic shells. These research avenues have great potential for the controlled placement of nanoparticles on suitably functionalized surface supports and, thus, appear very promising for device fabrication. An SET device made by the assembly of a cadmium selenide nanocrystal between two closely spaced gold leads constitutes a fascinating example of what nanotechnology can accomplish [28].

7 Future Developments

The future of electronic circuits capable of information storage and processing greatly depends on the continued miniaturization trend that we have seen since the invention of the transistor. The long run of semiconductor-based devices fabricated with lithographic techniques seems to be near its end as we are quickly approaching their lowest possible sizes both from intrinsic properties and manufacturing standpoints. In this context, molecular devices appear as an ideal way to overcome these difficulties and continue the circuit

miniaturization trend. However, we have shown here that there are several significant problems hindering the practical use of molecular devices. We propose here that the next generation of miniature devices may utilize metal and semiconductor nanoparticles derivatized with organic shells, which will be responsible for directing their assembly onto functionalized solid supports. These novel manufacturing processes will take advantage of wet chemical methods.

This methodology may allow the preparation of devices with feature sizes around 1–5 nm. Even as future generations enjoy the benefits derived from these astounding levels of information storage densities and computing speeds, the question on how to continue the miniaturization trend will not disappear. In fact, it will become a more open question than it is for us today as it may require a more drastic departure from conventional thinking. Will we ever master the design and construction of atomic and subatomic switching devices? Only time will tell.

8 References

1. Sorsch T, Moccio S, Baumann FH, Evans-Lutterodt K, Timp G, Muller DA (1999) Nature 399: 758
2. Schulz M (1999) Nature 399: 729
3. Hu EL, Shaw DT (1999) Synthesis and assembly. In: Siegal RW, Hu E, Roco MC (eds) Nanostructure science and technology. National Science and Technology Council, Washington, DC, chap 2. To obtain a copy of this report online see *www.nano.gov*
4. Balzani V, Gómez-López M, Stoddart JF (1998) Acc Chem Res 31: 405
5. Schill G (1971) Catenanes, rotaxanes and knots. Academic Press, New York
6. Anelli PL, Spencer N, Stoddart JF (1991) J Am Chem Soc 113: 5131
7. Bissell RA, Córdova E, Kaifer AE, Stoddart JF (1994) Nature 369: 133
8. Córdova E, Bissell RA, Spencer N, Ashton PR, Stoddart JF, Kaifer AE (1993) J Org Chem 58: 6550
9. Bissell RA, Córdova E, Stoddart JF, Kaifer AE (1995) Advantages of the rotaxane framework for the construction of switchable molecular devices. In: Becher J, Schaumburg K (eds) Molecular engineering for advanced materials. NATO ASI Series Kluwer Academic Publishers, chap 2
10. Bard AJ, Faulkner LR (1980) Electrochemical methods: fundamentals and applications. Wiley, New York, chap 4
11. Córdova E, Bissell RA, Kaifer AE (1995) J Org Chem 60: 133
12. Mendoza S, Davidov PD, Kaifer AE (1998) Chem Eur J 4: 864
13. Cardona CM, Mendoza S, Kaifer AE (2000) Chem Soc Rev 29: 37
14. Benda V, Gowar J, Grant DA (1999) Power semiconductor devices. Wiley, New York, chap 10
15. Collier CP, Wong EW, Belohradský M, Raymo FM, Stoddart JF, Kuekes PJ, Williams RS, Heath JR (1999) Science 285: 391
16. Davis WB, Svec WA, Ratner MA, Wasielewski MR (1998) Nature 396: 60
17. Emberly EG, Kirczenow G (1998) Phys Rev B 58: 10911
18. Yaliraki SN, Kemp M, Ratner MA (1999) J Am Chem Soc 121: 3428
19. Magoga M, Joachim C (1997) Phys Rev B 56: 4722
20. Feldheim DL, Keating CD (1998) Chem Soc Rev 27: 1
21. Mirkin CA, Letsinger RL, Mucic RC, Storhoff JJ (1996) Nature 382: 607

22. Storhoff JJ, Elghanian R, Mucic RC, Mirkin CA (1998) J Am Chem Soc 120: 1959
23. Liu J, Mendoza S, Román E, Lynn MJ, Xu R, Kaifer AE (1999) J Am Chem Soc 121: 4304
24. Liu J, Ong W, Román E, Lynn MJ, Kaifer AE (2000) Langmuir 16: 3000
25. Boal AK, Rotello VM (1999) J Am Chem Soc 121: 4914
26. Liu J, Xu R, Kaifer AE (1998) Langmuir 14: 7337
27. Fitzmaurice D, Rao SN, Preece JA, Stoddart JF, Wenger S, Zaccheroni N (1999) Angew Chem Int Ed Engl 38: 1147
28. Klein DL, Roth R, Lim AKL, Alivisatos AP, McEuen PL (1997) Nature 389: 699

Molecular-Level Artificial Machines Based on Photoinduced Electron-Transfer Processes

Roberto Ballardini[1], Vincenzo Balzani[2], Alberto Credi[2], Maria Teresa Gandolfi[2], Margherita Venturi[2]

[1] Istituto FRAE-CNR, via Gobetti 101, 40129, Bologna, Italy
[2] Dipartimento di Chimica "G. Ciamician", Università di Bologna, via Selmi 2, 40126 Bologna, Italy
E-mail: vbalzani@ciam.unibo.it

The concept of macroscopic machine can be extended to the molecular level. A molecular-level machine can be defined as an assembly of a discrete number of molecular components (that is, a supramolecular structure) designed to perform mechanical-like movements (output) as a consequence of appropriate external stimulation (input). Molecular-level machines operate via nuclear rearrangements and, like macroscopic machines, are characterized by (i) the kind of energy input supplied to make them work, (ii) the manner in which their operation can be monitored, (iii) the possibility to repeat the operation at will, i.e., establishing a cyclic process, (iv) the time scale needed to complete a cycle of operations, and (v) the performed function. The extension of the concept of machine to the molecular level is of great interest not only for basic research, but also for the growth of nanoscience and the development of nanotechnology. In this chapter recent examples of molecular-level machines based on pseudorotaxanes, rotaxanes, and catenanes, and operating by means of photoinduced electron-transfer processes are presented.

Keywords: Pseudorotaxanes, Rotaxanes, Catenanes, Photochemistry, Supramolecular chemistry

1 Introduction 164

2 Pseudorotaxanes, Rotaxanes, Catenanes 165

2.1 Pseudorotaxanes 166
2.2 Rotaxanes and Catenanes 166

3 Mechanical Movements 169

4 Photochemically Driven Dethreading/Rethreading of Pseudorotaxanes 173

5 Photochemically Controlled Shuttling Processes in Rotaxanes 179

6 Photochemically Induced Ring Movement in Catenanes 184

7 Conclusions 186

8 References 187

Structure and Bonding, Vol. 99

1 Introduction

In everyday life we make extensive use of macroscopic machines. A machine is "an apparatus for applying mechanical power, having several parts each with a definite function" [1]. When a machine is working, at least some of its components display changes in their relative positions.

The concept of machine can be extended to the molecular level [2]. A *molecular-level* machine can be defined as an assembly of a discrete number of molecular components (that is, a *supramolecular* structure) designed to perform mechanical-like movements (*output*) as a consequence of appropriate external stimuli (*input*).

Molecular-level machines operate via nuclear rearrangements and, like macroscopic machines, are characterized by

(i) the kind of energy input supplied to make them work,
(ii) the manner in which their operation can be monitored,
(iii) the possibility to repeat the operation at will, i.e., establishing a cyclic process,
(iv) the time scale needed to complete a cycle of operations, and
(v) the performed function.

As far as point (i) is concerned, a chemical reaction can be used, at least in principle, as an energy input. In such a case, however, since the machine has to work cyclically [point (iii)], it will need the addition of reactants at any step of the working cycle, and the resulting accumulation of by-products can compromise the operation of the machine. On the basis of this consideration, the best energy inputs to make a molecular machine work are photons (light energy) and electrons (electrochemical energy). With appropriately chosen photochemically and electrochemically driven reactions, it is indeed possible to design very interesting molecular machines [3].

In order to control and monitor the operation of the machine [point (ii)], the electronic and/or nuclear rearrangements of the component parts should cause readable changes in some chemical or physical property of the system. In this regard, photochemical and electrochemical techniques are very useful since both photons [2c] and electrons [4] can play the dual role of energy inputs and information carriers.

The operation time scale of molecular machines [point (iv)] is that of nuclear motions which can range from picoseconds to seconds, depending on the nature of the components involved and the type of motions that are happening.

Finally, as far as point (v) is concerned, molecular-level machines performing various kinds of functions can be imagined, as described here and in other chapters of this volume.

The concept of machine at the molecular level is not new. Our body can be viewed as a very complex ensemble of molecular-level machines that power our motions, repair damage, and orchestrate our inner world of sense, emotion, and thought [5]. The problem of the construction of *artificial* molecular-level

machines was first raised by Richard P. Feynman, Nobel Laureate in Physics, in his famous address "There is plenty of room at the bottom" (American Physical Society, 1959) [6], but research on artificial molecular machines has only begun to develop in the last few years [3, 7]. The extension of the concept of machine to the molecular level is of great interest for the growth of nanoscience and the development of nanotechnology. Indeed, the miniaturization of components for the construction of useful devices, which is an essential feature of modern technology, is currently pursued by the large-downward (top-down) approach. This approach, however, which leads physicists and engineers to manipulate progressively smaller pieces of matter, has its intrinsic limitations. An alternative and promising strategy is offered by the small-upward (bottom-up) approach. Chemists, by the nature of their discipline, are already at the bottom, since they are able to manipulate molecules (i.e., the smallest entities with distinct shapes and properties) and are therefore in the ideal position to develop bottom-up strategies for the construction of nanoscale devices.

For space reasons, in this chapter we will only review recent advances in the field of molecular-level machines operating by means of photoinduced electron-transfer processes. Since such machines are based on pseudorotaxanes, rotaxanes, and catenanes, we will first recall some important features of these kinds of supramolecular systems.

2 Pseudorotaxanes, Rotaxanes, Catenanes

Fig. 1 shows schematically the structures of *pseudorotaxanes*, *rotaxanes*, and *catenanes*. The names of these structures derive from the Latin words *rota* and *axis* for wheel and axle, and *catena* for chain.

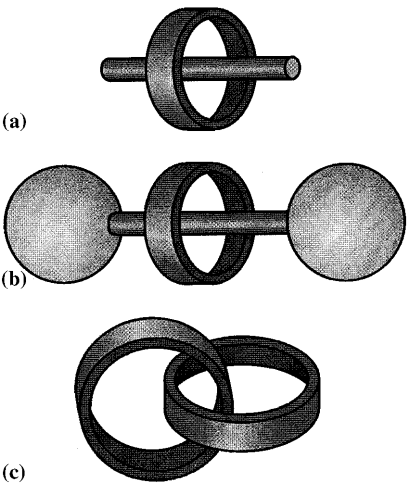

Fig. 1. Schematic representation of a [2]pseudorotaxane **(a)**, a [2]rotaxane **(b)** and a [2] catenane **(c)**. The number in brackets indicates the number of molecular components

2.1 Pseudorotaxanes

Pseudorotaxanes are a particularly interesting family of host-guest systems [2b, 8, 9]. As in the case of any host-guest complex, formation of a pseudorotaxane occurs via a molecular recognition process between two 'instructed' [2b] components. It is a thermodynamically controlled self-assembly process that may occur as a result of a variety of interactions deriving from the size, shape, and electronic properties of the partners. The most important types of interactions are those involving electron-donor/acceptor ability, hydrogen bonding, hydrophobic-hydrophilic character, π-π stacking, coulombic forces and, on the side of the strong interaction limit, metal-ligand bonding. Usually it is not difficult to understand which is the predominant interaction in a given system. It should be noted, however, that in some cases the strongest interaction as far as association is concerned is not that causing the most relevant changes in the properties of the system (e.g., UV-vis absorption, fluorescence and NMR spectra, electrochemical behavior) on going from the separated components to the pseudorotaxane structure.

For the topic of the present chapter, only pseudorotaxanes based on electron donor/acceptor ability are of interest. They can be obtained by threading

(i) a wire-type component containing electron-acceptor units into a macrocycle which comprises electron-donor units, or, vice versa,
(ii) a wire-type component containing electron-donor units into a macrocycle which comprises electron-acceptor units.

Examples are the 1, 1′-dibenzyl-4, 4′-bipyridinium electron-acceptor dication threaded into the 1, 5-dinaphtho-38-crown-10 (Fig. 2a) [10], and the acyclic polyether containing a dioxybenzene electron-donor unit threaded into the electron-acceptor cyclobis(paraquat-*p*-phenylene) tetracationic cyclophane (Fig. 2b) [11]. Although in these cases a large contribution to the association driving force comes from the electron-donor/acceptor (charge-transfer, CT) interactions, hydrogen bonding can also play an important role, as clearly shown in the cases of pseudorotaxanes constituted by 4, 4′-bipyridinium [12a] or 1,2-bis(pyridinium)ethane [12b] threads and crown ethers.

2.2 Rotaxanes and Catenanes

Rotaxanes and catenanes are supramolecular (multicomponent) species [2b, 8, 9, 13, 14] strictly related to, but also very different from, pseudorotaxanes (Fig. 1). Whereas pseudorotaxanes can undergo dissociation into their wire-like and macrocyclic components, rotaxanes and catenanes are interlocked species, whose dissociation requires breaking of a covalent bond. The general strategy to prepare rotaxanes and catenanes with high yields is based on the template effect [15], which relies on the presence of molecular recognition sites in the components to be assembled.

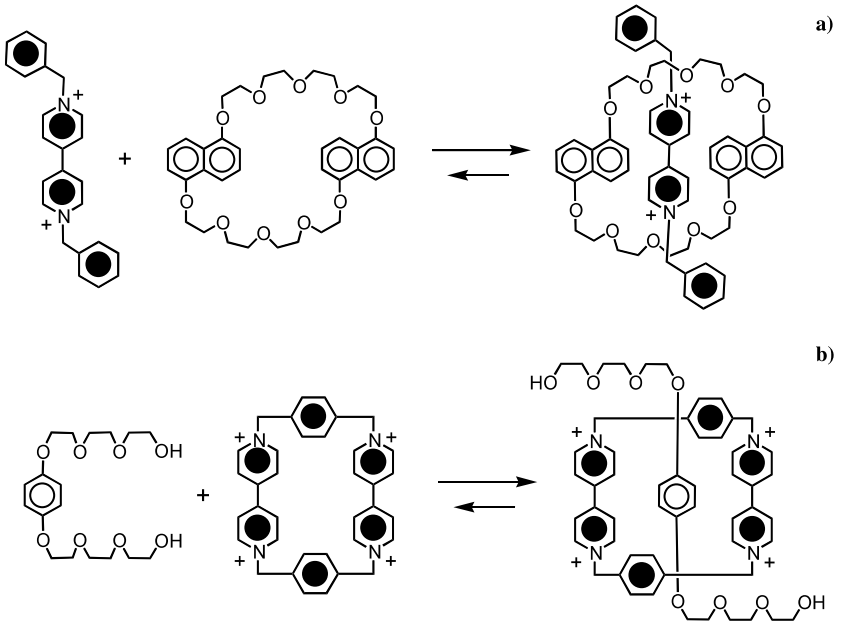

Fig. 2a, b. Two examples of [2]pseudorotaxanes based on charge-transfer interactions [10, 11]

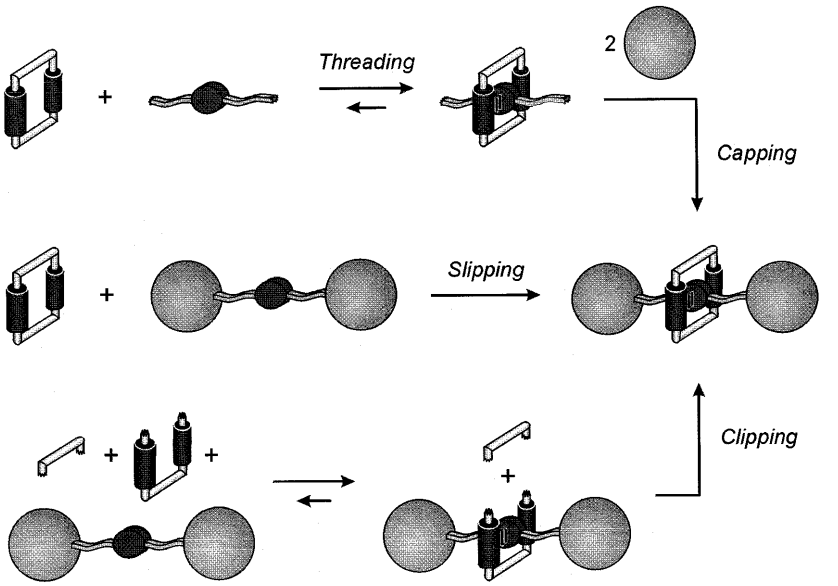

Fig. 3. Routes for the synthesis of [2]rotaxanes

Fig. 3 shows the routes by which components bearing suitable recognition sites lead to the formation of rotaxanes:

(i) *threading* of a molecule through a preformed ring, followed by capping the end(s) of the thread,
(ii) *slipping* of a preformed ring over the stoppers of a preformed dumbbell-shaped component into a thermodynamically favorable site on the rod part of the dumbbell, and

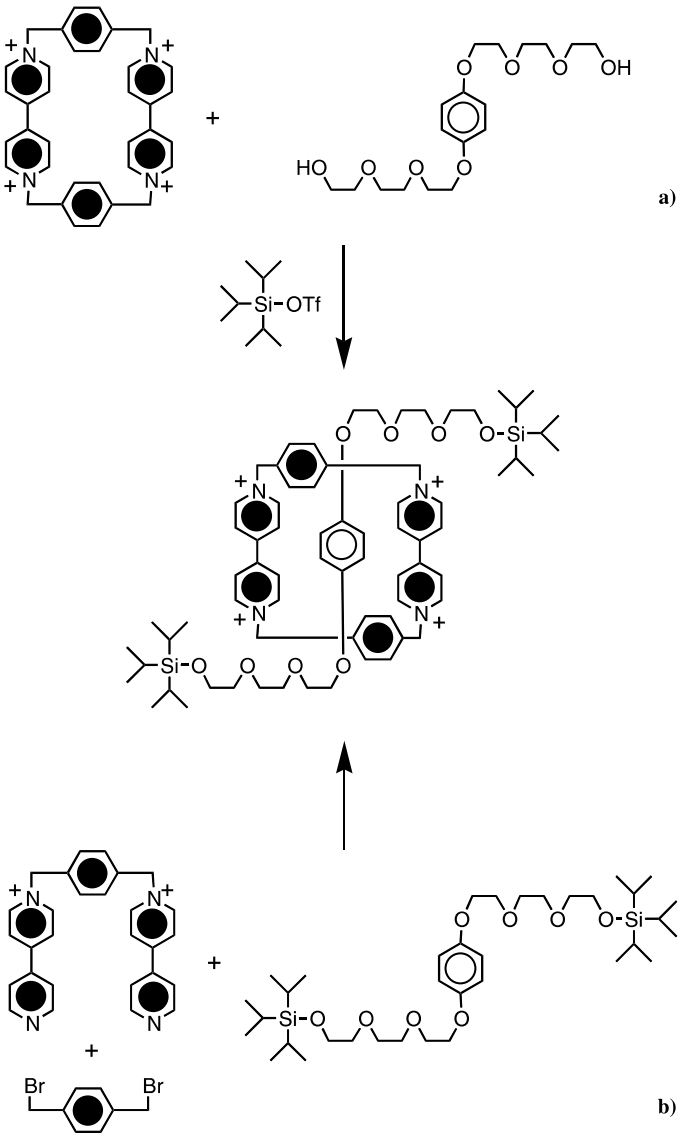

Fig. 4. Synthesis of a [2]rotaxane by the threading **(a)** and clipping **(b)** approaches [11]

(iii) *clipping* of a preformed dumbbell with a suitable U-type component that is subsequently cyclized.

Fig. 4 shows the synthesis of a rotaxane based on donor/acceptor interaction by the threading or the clipping approach [11]. In the first case (Fig. 4a), threading of the electron-acceptor tetracationic cyclophane by a thread containing a hydroquinone electron donating unit yields a pseudorotaxane; then, reaction of the terminal hydroxy groups of the thread with triisopropylsilyl triflate leads to the rotaxane. In the clipping approach (Fig. 4b) the rotaxane is obtained by constructing the electron-acceptor cyclophane around the preformed dumbbell-shaped component.

In the case of catenanes, the most rationale synthetic strategy is the clipping of a macrocycle onto a preformed one (Fig. 5). A double clipping procedure can also be used [16]. Figure 6 shows the synthesis of a catenane templated by donor/acceptor and hydrogen-bonding interactions [11]. Reaction of a dication with a dibromide gives a tricationic intermediate which interacts with bis-*p*-phenylene-34-crown-10 to afford a pseudorotaxane-like, or precatenane, structure. The subsequent cyclization, as a result of nucleophilic displacement of a bromide ion, gives the corresponding catenane.

3 Mechanical Movements

In pseudorotaxanes, rotaxanes, and catenanes, movements of the component parts can take place even in the absence of external energy inputs. For

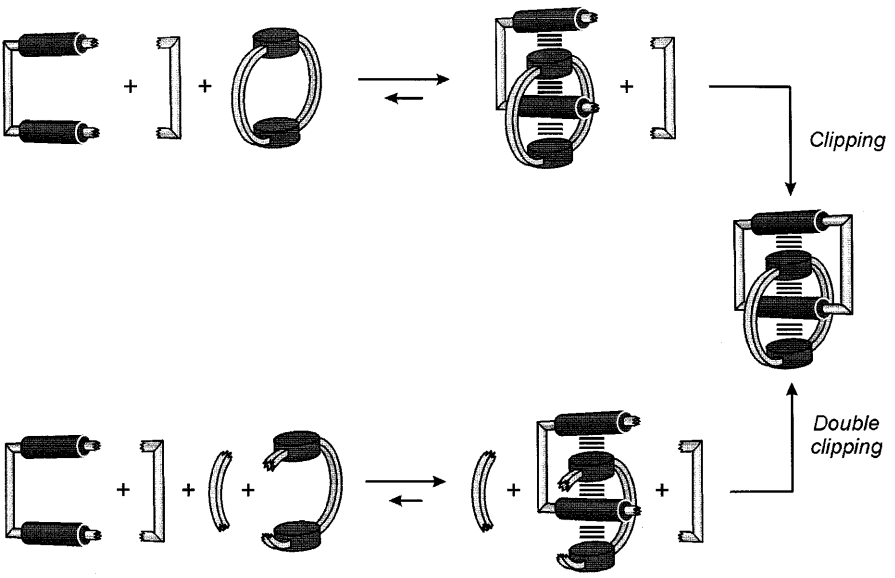

Fig. 5. Routes for the synthesis of [2]catenanes

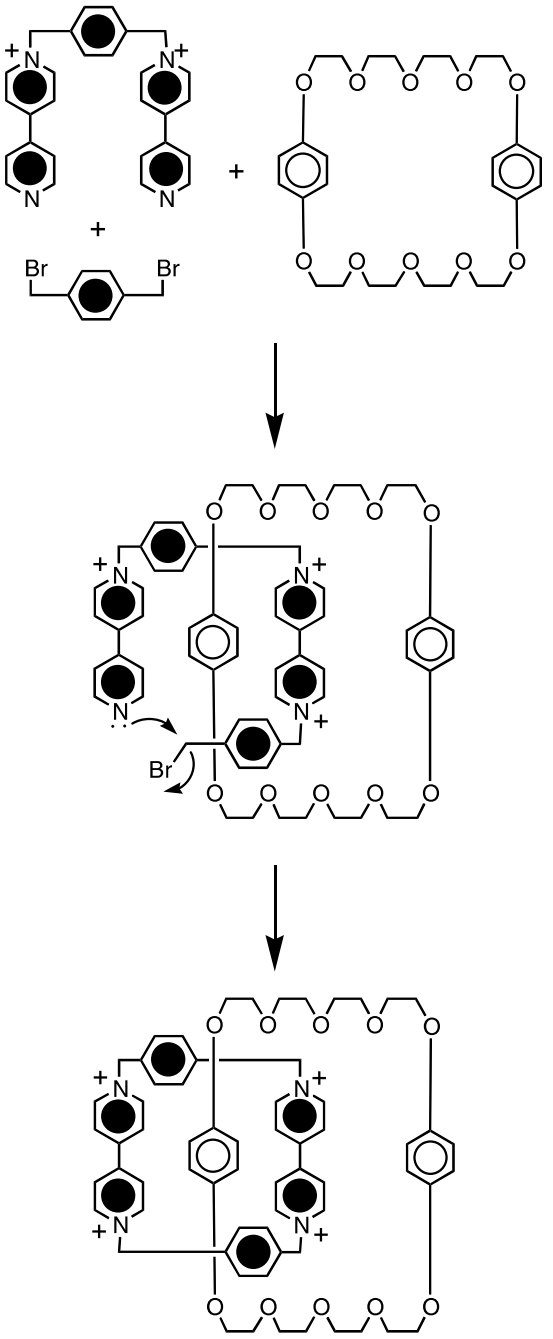

Fig. 6. Synthesis of a [2]catenane templated by donor/acceptor and hydrogen-bonding interactions [11]

example, in pseudorotaxanes the threaded and dethreaded structures are in dynamic equilibrium [17], and in catenanes the two rings can rotate, particularly at high temperature [11, 18, 19]. Such thermal movements, however, have nothing to do with a machine-like behavior, which is related to an input/output relationship. In other words, a machine-like movement

(i) occurs as a consequence of a well defined energy input (i.e., under full control of the operator), and
(ii) changes the state of the system in a well defined way (i.e., transforms a structure into a different one, with monitorable changes in at least one characteristic property of the system).

In a pseudorotaxane, the two different structures involved in a machine-like behavior are simply the threaded and unthreaded ones (Fig. 7a). In order to have a machine-like behavior, one of the two structures of the system must be more stable than the other one, and the energy input has to reverse the initial situation. For example, if the stable structure ('state 0') is the threaded one, the energy input has to cause dethreading ('state 1'). Then, another input has to promote rethreading, and both the dethreading and rethreading processes must cause monitorable changes in at least one property of the system.

In the case of rotaxanes, dethreading cannot occur. Therefore, the two different states related to a machine-like movement are necessarily threaded structures. In principle, there can be many possible situations of this kind [20]. In practice, however, the simplest and most convenient case is that

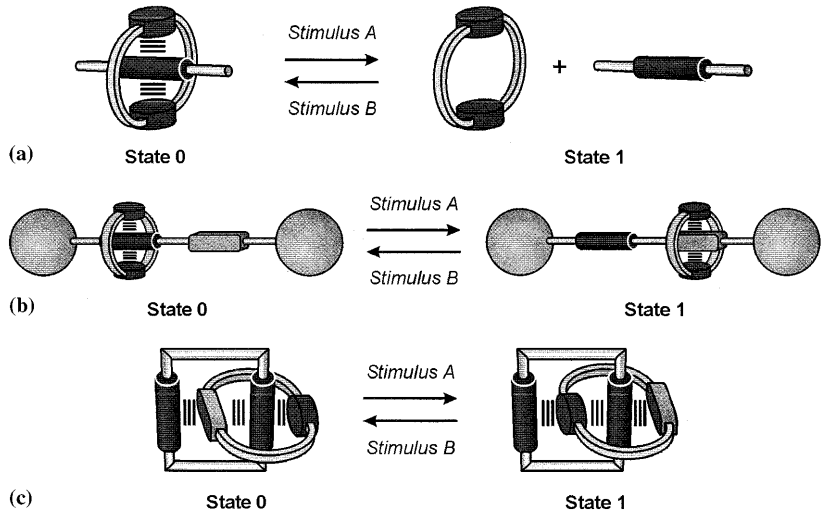

Fig. 7. **(a)** Dethreading/rethreading of a [2]pseudorotaxane; **(b)** switching of the ring component between the two stations of the dumbbell-shaped component of a [2]rotaxane; **(c)** switching between the two structures in a [2]catenane containing a non-symmetrical macrocyclic component

offered by rotaxanes made of a dumbbell-shaped component containing two different recognition sites for the macrocycle. If the two stations of the dumbbell-shaped component are equivalent [20, 21], spontaneous shuttling of the macrocycle component between the two stations can occur. This, however, does not represent a machine-like behavior because the two structures are indistinguishable, and shuttling takes place without a specific external input. When the two stations of the dumbbell-shaped component are not equivalent (Fig. 7b), the macrocycle preferentially resides on one of the two stations (specifically, the one that can interact more strongly with the macrocycle). In appropriately designed rotaxanes, it is possible to destroy this interaction by an external chemical, electrochemical, or photochemical input [3, 7a, f], causing the displacement of the macrocycle to the other station. When an external input, opposite in nature to the first one, allows the original interaction to revive, the macrocycle moves back to the initial position. The forward and back movements are usually related to monitorable changes in at least one property of the system. In the schematic representation shown in Fig. 7b, it has been assumed that the molecular shuttle resides preferentially in 'state 0' until a stimulus is applied that switches off the stronger of the two recognition sites, thus inducing the macrocycle to move to the second weaker recognition site ('state 1'). By switching off and on the recognition properties of one of the two recognition sites, the relative proportions of the two structures can be controlled reversibly (ideally, from 0:100% to 100%:0).

As we have seen above, catenanes are constituted by macrocycles bearing recognition sites. Most often, for synthetic reasons, each macrocycle contains two equivalent functions, i.e., two equivalent electron-donor or two equivalent electron-acceptor units (see, e.g., Fig. 6). In systems of this kind, two equally stable and indistinguishable structures are present, related to rotation of one macrocycle with respect to the other by 180°. Such rotations can take place without a specific external input. In order to obtain a machine-like behavior, at least one of the two macrocycles of a catenane must be non-symmetrical, i.e., it must contain two different recognition sites. In such a case, two clearly different structures are possible (Fig. 7c) [3, 7e, 18]. Initially, the symmetrical macrocyclic component resides preferentially around the stronger of the two different recognition sites incorporated within the non-symmetrical macrocycle ('state 0'). When a suitable stimulus is applied, the stronger recognition site is switched off and the symmetrical macrocycle undergoes rotation in order to obtain the alternative, now more stable, structure ('state 1'). When an external input, opposite in nature to the first one, allows the original interaction to revive, the macrocycle rotates again to the initial position. The forward and back movements are again related to monitorable changes in at least one property of the system.

It can be noted that in all cases (Fig. 7) the machine-like behavior consists in the reversible change of the state of the system (from 'state 1' to 'state 0', and then back to 'state 0'). This shows that such molecular-level machines behave according to binary logic. Therefore, they could be used, in principle, for information processing at the molecular level [22].

In the case of systems based on donor/acceptor interactions, destabilization of the original structure can be achieved by reduction of the electron-acceptor unit(s) or by oxidation of the electron-donor unit(s) as a consequence of chemical, electrochemical, or photochemical electron-transfer processes. The original CT interaction can usually be restored by an opposite redox process, which thus leads back to the original structure. In the case of systems based on metal complexes, the stability of the original structure is related to the compatibility between oxidation state of the metal ion and coordination environment. If the oxidation state of the metal ion is modified as a consequence of a redox process, the original structure is destabilized and the system evolves toward another, more stable structure. Again, an opposite redox process can lead back to the original structure.

For the sake of space, in this chapter we will only discuss examples of molecular-level machines based on photoinduced electron transfer processes. An extensive review on artificial molecular machines [3c] and more detailed discussions on electron-transfer processes involving pseudorotaxanes [23a], and rotaxanes and catenanes [23b] are reported elsewhere.

4 Photochemically Driven Dethreading/Rethreading of Pseudorotaxanes

Intercomponent CT interactions introduce low energy excited states which are responsible for the presence of broad and weak absorption bands in the visible region (and therefore, for the color) exhibited by pseudorotaxanes, rotaxanes, and catenanes based on this kind of interactions. Furthermore, the low energy (non-emissive) CT excited states offer favorable deactivation paths to the potentially luminescent excited states localized on the molecular components, so that this kind of pseudorotaxanes, rotaxanes, and catenanes usually does not exhibit luminescence [11, 18].

Light excitation in the CT absorption bands formally leads to the transfer of an electron from the donor to the acceptor component (optical electron transfer). As a consequence, particularly when this process leads to formation of charges of the same sign in the two components (Fig. 8), one can expect destabilization of pseudorotaxane structures, followed by dethreading. In practice, however, this simple approach does not work because the back electron-transfer process is much faster than the separation of the molecular components, a process which requires extended nuclear motions and solvent rearrangement. In a particular case [24], laser flash photolysis experiments have suggested that a small fraction of the irradiated pseudorotaxane may undergo dissociation.

In order to really achieve photoinduced dethreading, a different approach has been devised [25], based on the use of an external electron-transfer photosensitizer (**P**) and a sacrificial reductant (Red), as illustrated in Fig. 9. The photosensitizer must

(i) be able to absorb light efficiently and
(ii) have a sufficiently long-lived and reductant excited state,

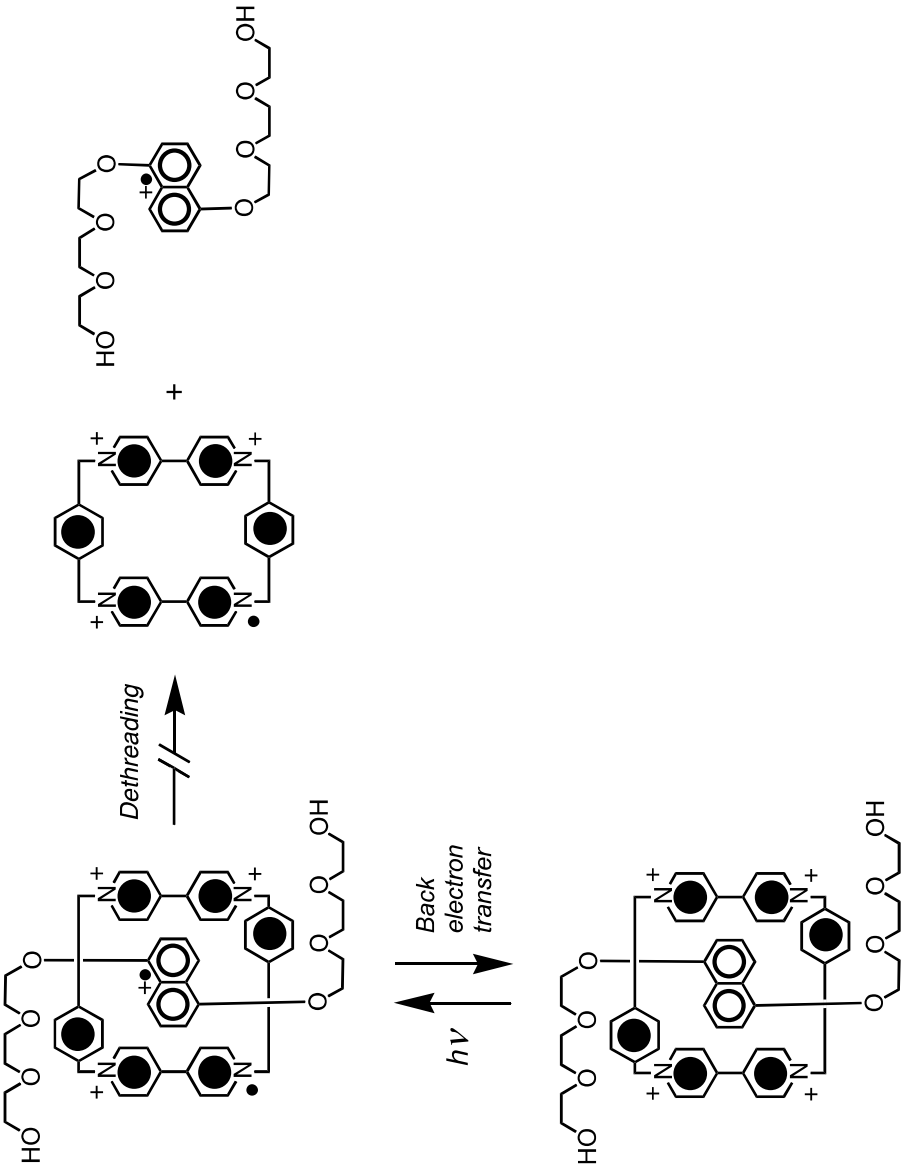
Dethreading
Back electron transfer
hν

Fig. 8. Processes that can occur upon light excitation of a [2]pseudorotaxane in its CT band. Although the original structure is destabilized, dethreading does not occur because it requires nuclear motions that are slower than the back electron-transfer process [25]

so that its excitation (Process 1) in the presence of the pseudorotaxane will lead (Process 2) to the transfer of an electron to a bipyridinium unit of the cyclophane. The relatively fast back electron transfer from the reduced cyclophane component to the oxidized photosensitizer is prevented by the sacrificial reductant which, if present in a sufficient amount, intercepts the oxidized photosensitizer and regenerates (Process 3) the original photosensitizer. Good candidates [25] for the role of photosensitizer are 9-anthracenecarboxylic acid and metal complexes such as $[Ru(bpy)_3]^{2+}$, while efficient reductant scavengers are triethanolamine and polycarboxylate (e.g., oxalate) anions. Under these conditions, in deoxygenated solution, the persistent reduction of a bipyridinium unit of the cyclophane is achieved and the pseudorotaxane dethreads (Process 4), as evidenced by absorption spectral changes and, more importantly, by the increase in the fluorescence intensity of the dioxynaphthalene unit, that can only originate when this unit is not involved in CT interactions. Oxygenation of the solution reoxidizes the cyclophane back (Process 5) to the tetracationic form, thereby promoting rethreading (Process 6), as shown by the absorption and fluorescence spectra.

This strategy has been extended recently to second-generation pseudorotaxanes in which the metal-complex photosensitizer (the 'light-fueled' motor) [26] has been incorporated either into the thread (Fig. 10) [27] or into the ring (Fig. 11) [28] component. The successful operation of these pseudorotaxanes as molecular machines is the result of

(i) the appropriate choice of the functional units and
(ii) their covalent linking into the thread or ring component

in order to achieve the correct integration of the needed functions (e.g., receptor ability, redox features, photophysical properties, etc.), the right sequence of processes, and the lack of interference between the active units. As in the case of the molecular machine shown in Fig. 9, the dethreading and rethreading motions of the pseudorotaxanes represented in Figs. 10 and 11 can be triggered by visible light irradiation and oxygenation of the solution, respectively. The motions can be easily monitored by means of UV-vis absorption and fluorescence spectroscopy. The most important readout signal is the intensity of the dioxynaphthalene fluorescence associated with the free ring (Fig. 10) or free thread (Fig. 11) component. It is worth noting that many deoxygenation-irradiation (dethreading)/oxygenation (rethreading) cycles can be performed on the same solution without any appreciable loss of signal until most of the reductant scavenger is consumed. It should also be stressed that systems which rely on this photosensitizer-scavenger strategy utilize, in addition to light energy, the irreversible decomposition of a reductant scavenger that produces 'waste' species. In this regard, the search for efficient molecular machines exploiting 'clean', reversible photochemical reactions (in

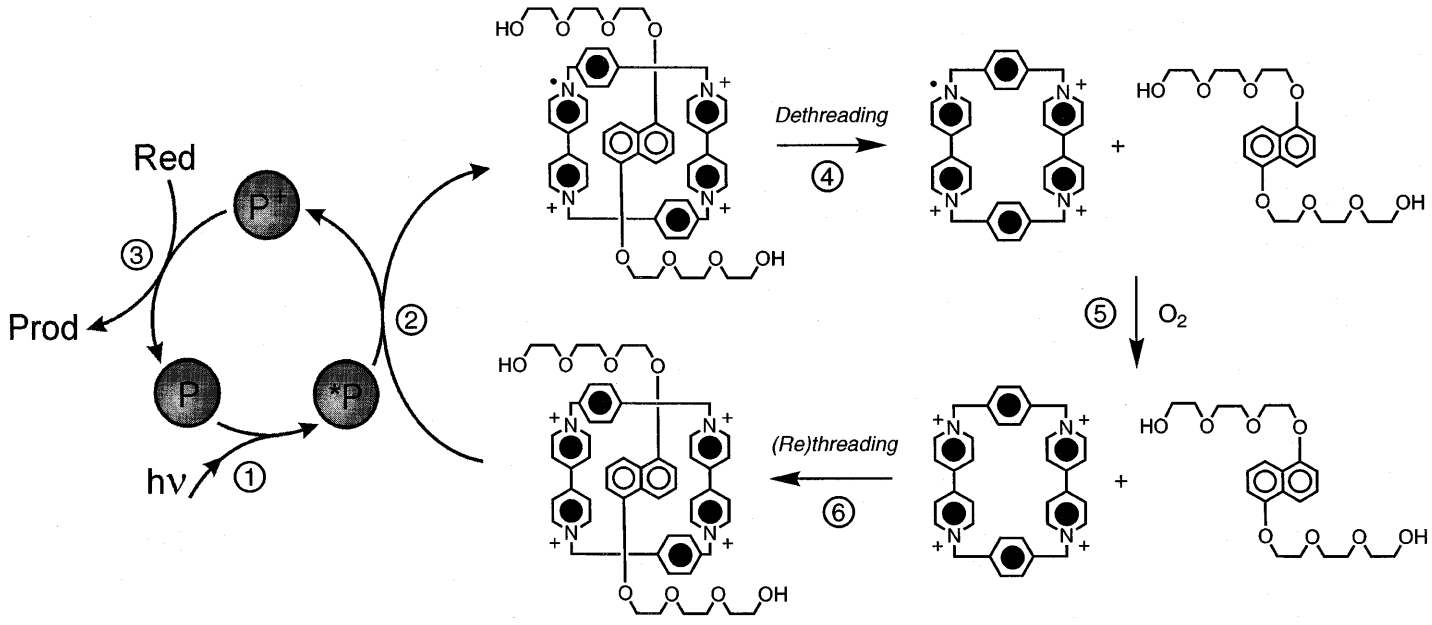

Fig. 9. The photochemically-induced dethreading of a [2]pseudorotaxane based on the use of the external photosensitizer P (9-anthracenecarboxylic acid) and the reductant scavenger Red (triethanolamine). Rethreading occurs upon oxygenation of the solution [25]

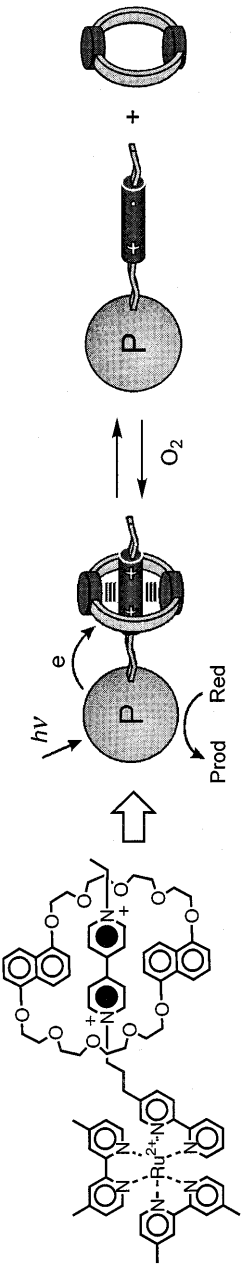

Fig. 10. A photocontrollable molecular machine based on a [2]pseudorotaxane. In this system the 'light-fueled' motor (i.e., the photosensitizer) is part of the wire-type component [27]. Red (triethanolamine) is a reductant scavenger

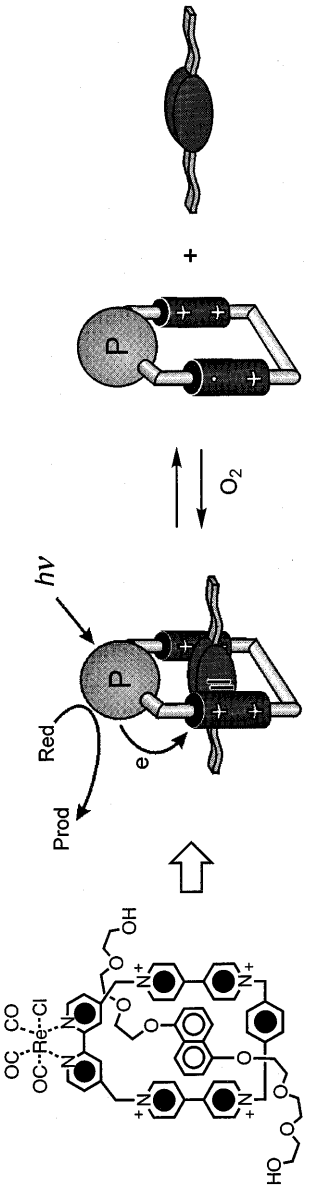

Fig. 11. A photocontrollable molecular machine based on a [2]pseudorotaxane. In this system the 'light-fueled' motor (i.e., the photosensitizer) is part of the macrocyclic component [28]. Red (triethanolamine) is a reductant scavenger

other words, machines which use only light as an energy supply) is of fundamental importance.

5 Photochemically Controlled Shuttling Processes in Rotaxanes

As in pseudorotaxanes, also in the rotaxanes based on electron donor-acceptor interactions there are low energy CT excited states which are responsible for the absorption bands observed in the visible region. As we have seen above, light excitation in these CT absorption bands formally leads to the transfer of an electron from an electron-donor to an electron-acceptor unit (optical electron transfer). As a consequence, one can expect destabilization of the original rotaxane structure, followed by a displacement of the ring along the wire (in pseudorotaxanes, such a destabilization is expected to lead to dethreading, *vide supra*). In practice, however, this simple approach to obtain a photoinduced motion of the ring is not likely to be successful because, as discussed above, the back electron-transfer process is much faster than the extended nuclear motions and solvent rearrangement needed for moving the ring. An attempt along this direction was performed on the rotaxane shown in Fig. 12 [29]. Direct excitation into the CT absorption band results in the transfer of an electron from the central dioxybenzene donor to the cyclophane acceptor. Rapid (τ = 30 ps) back electron transfer occurs, in competition with a minor process involving hole transfer to a ferrocene stopper. The latter process creates a longer lived (τ = 555 ns) excited state, but back electron transfer to form the initial ground state is still much faster than the motion of the ring.

In order to achieve photoinduced shuttling, the carefully designed rotaxane shown in the top of Fig. 13 has been recently synthesized [7f]. This compound is made of the electron-donor macrocycle **R** and a dumbbell-shaped component which contains

(i) a photoactive Ru(II) polypyridine complex (**P**) as one of its stoppers,
(ii) a *p*-terphenyl-type ring system as a rigid spacer (**S**),
(iii) a 4, 4′-bipyridinium unit ($\mathbf{A_1}$) and a 3, 3′-dimethyl-4, 4′-bipyridinium unit ($\mathbf{A_2}$) as electron accepting stations, and
(iv) a tetraarylmethane group as the second stopper (**T**).

The structure of the rotaxane was characterized by mass spectrometry and NMR spectroscopy, which also established, along with cyclic voltammetry, that the stable translational isomer is the one in which the **R** component encircles the $\mathbf{A_1}$ unit, in keeping with the fact that this station is a better electron acceptor than the other one. The electrochemical, photophysical, and photochemical (under continuous and pulsed excitation) properties of the [2] rotaxane, its dumbbell-shaped component, and some model compounds containing electro- and photoactive units (Fig. 13) were investigated. In an attempt to obtain the photoinduced abacus-like movement of the **R** macrocycle between the two stations $\mathbf{A_1}$ and $\mathbf{A_2}$, two strategies were devised: one was fully based on processes involving only the rotaxane components (intramolecular mechanism), while the other one required the help of external reactants (sacrificial mechanism).

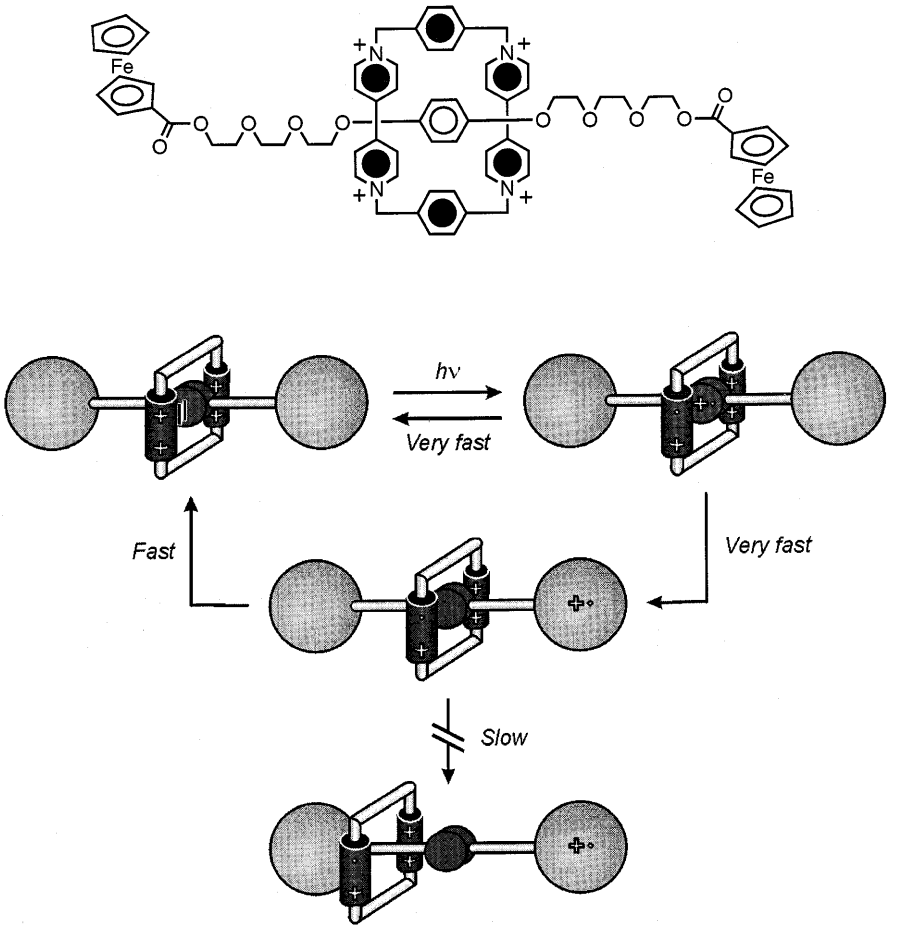

Fig. 12. Optical electron-transfer excitation of a [2]rotaxane [29]. Shuttling does not take place because the direct and ferrocene-mediated back electron-transfer reactions are much faster than the motion of the ring

The intramolecular mechanism, illustrated in Fig. 14, is based on the following four operations [7f]:

(a) *Destabilization of the initial translational isomer.* Light excitation of the photoactive unit **P** (Step 1) has to be followed by the transfer of an electron (Step 2) from the excited state of **P** to the $\mathbf{A_1}$ station, which is encircled by the ring **R**, in order to 'deactivate' this station; such a photoinduced electron-transfer process is in competition with the intrinsic excited-state decay (Step 3).
(b) *Ring displacement.* The ring movement from the reduced station $\mathbf{A_1^-}$ to $\mathbf{A_2}$ (Step 4) has to compete with the back electron-transfer process from $\mathbf{A_1^-}$ (still encircled by **R**) to the oxidized photoactive unit $\mathbf{P^+}$ (Step 5).

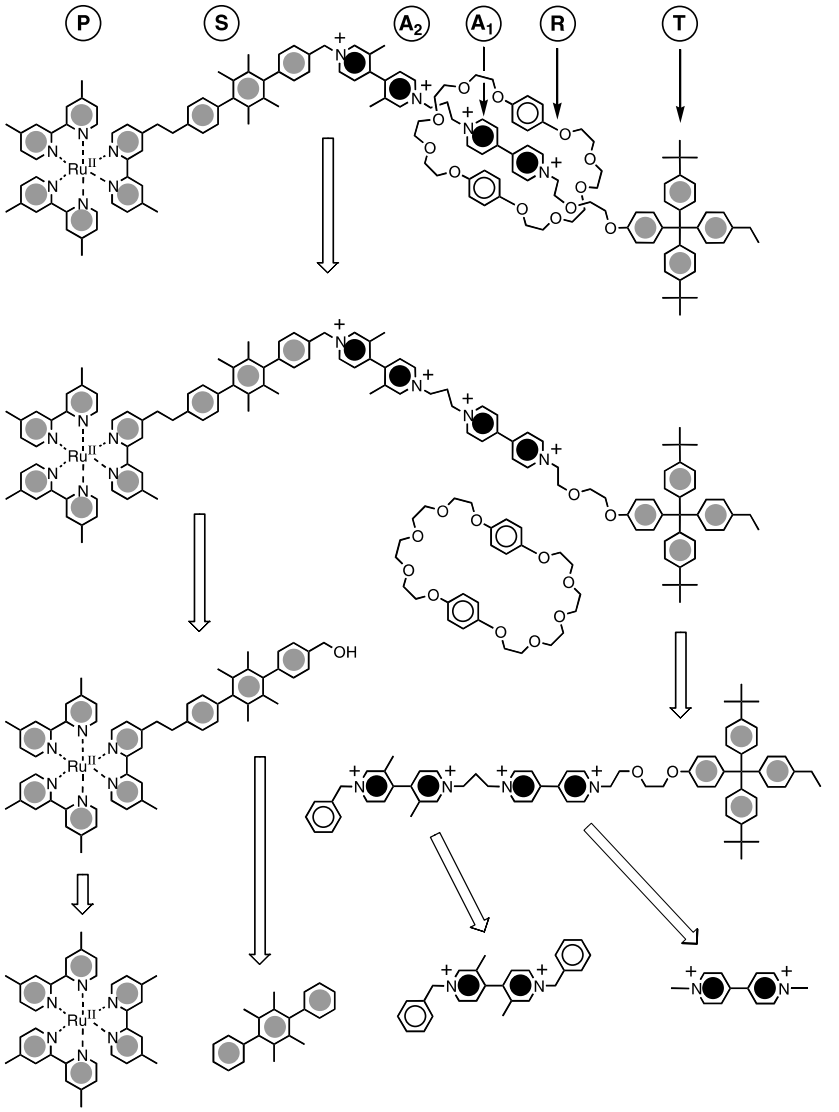

Fig. 13. A [2]rotaxane designed to achieve an abacus-type behavior under light excitation [7f]

(c) *Electronic reset*. A back electron-transfer process from the 'free' reduced station $\mathbf{A_1^-}$ to $\mathbf{P^+}$ has to take place (Step 6), with consequent restoration of the electron-acceptor power to the $\mathbf{A_1}$ station.
(d) *Nuclear reset*. As a consequence of the electronic reset, back movement of the ring from $\mathbf{A_2}$ to $\mathbf{A_1}$ has to occur (Step 7).

The most difficult requirement to meet in such an intramolecular mechanism is the successful competition of Step 4, which involves complex nuclear movements, with Step 5, which only involves the transfer of an electron. The results obtained have shown that Step 2 does occur, so that switching off of the $\mathbf{A_1}$ station can be achieved [7f]. The electronic reset step after light excitation (Step 5 in Fig. 14) occurs with rate constant $8.3 \times 10^5\ s^{-1}$, which likely compares to that of the ring displacement (Step 4) [30]. However, unequivocal evidence for the occurrence of a photochemically-driven switching by the intramolecular mechanism has not yet been obtained.

The alternative, much easier, mechanism to cause the switching process was based on the use of an external sacrificial redox reactant that operates after the photoinduced deactivation of the $\mathbf{A_1}$ station, as illustrated in Fig. 15. Such a sacrificial mechanism is based on the following four operations [7f]:

(a) *Destabilization of the initial translational isomer*. As in the previous mechanism.
(b′) *Ring displacement after scavenging of the oxidized photoactive unit*. If the solution contains a suitable reductant Red, a fast reaction of Red with $\mathbf{P^+}$ (Step 8) competes successfully with the back electron-transfer reaction

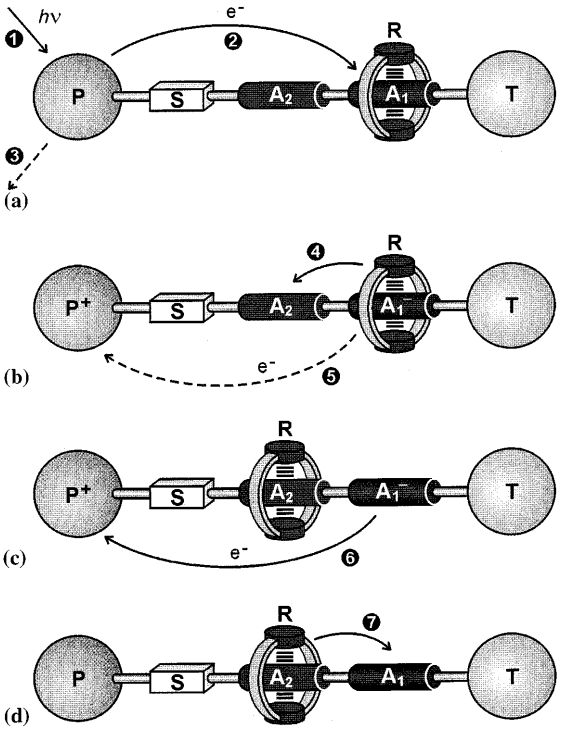

Fig. 14a–d. Intramolecular mechanism for the light-driven switching of the ring **R** between the two stations $\mathbf{A_1}$ and $\mathbf{A_2}$ in the [2]rotaxane represented in Fig. 13 [7f]. The dashed lines indicate processes that are in competition with those needed to perform shuttling

(Step 5); in such a case, the displacement of the ring to A_1 (Step 4), even if it is slow, can take place because the originally occupied station remains in its reduced state A_1^-.
(c′) *Electronic reset.* After an appropriate time, restoration of the electron-acceptor power of the A_1 station can be obtained by oxidizing A_1^- with a suitable oxidant Ox (Step 9).
(d) *Nuclear reset.* As in the previous mechanism (Step 7).

The results obtained showed that the sacrificial mechanism works very well with triethanolamine as Red and dioxygen as Ox [7f].

Of course, the intramolecular switching mechanism (Fig. 14) is much more appealing than the sacrificial one (Fig. 15), principally because the former mechanism implies the conversion of light energy into mechanical energy without using other chemicals and without generation of waste products. Studies in this regard are in progress in our laboratories.

Photochemically controlled shuttling of the macrocycle component by a sacrificial mechanism has also been obtained in a rotaxane containing a phenanthroline and a terpyridine unit in its dumbbell-shaped component, a phenanthroline ligand in the macrocycle, and a Cu(I) center coordinated by

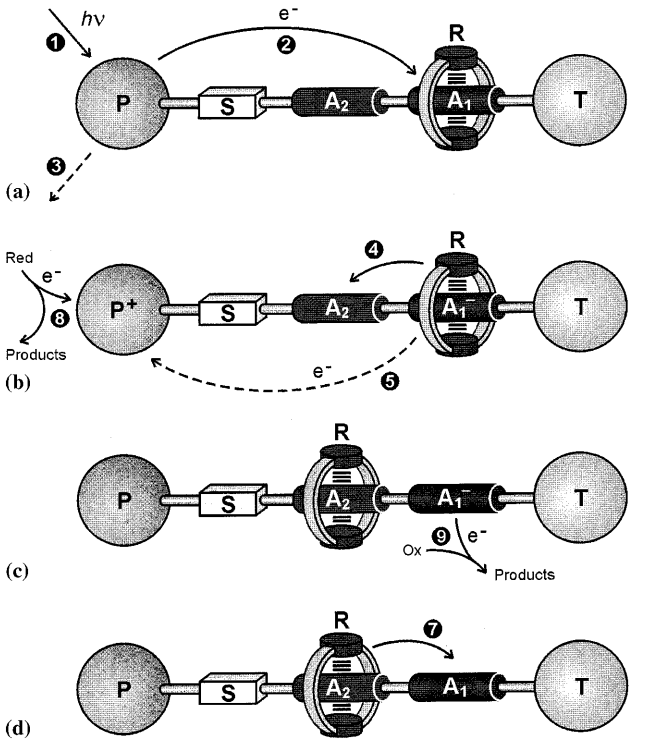

Fig. 15a–d. Sacrificial mechanism for the light-driven switching of the ring **R** between the two stations A_1 and A_2 in the [2]rotaxane represented in Fig. 13 [7f]. The dashed lines indicate the processes that are in competition with those needed to perform shuttling

the phenanthroline ligand of the dumbbell together with the phenanthroline ligand of the macrocycle [31]. The working mechanism of such a system is quite similar to that described below for photoinduced ring movement in a catenane.

6
Photochemically Induced Ring Movement in Catenanes

There are several examples of catenanes where ring movement can be induced by homogeneous or heterogeneous electron-transfer reactions [3]. However, there is only one case in which the electron-transfer process is photoinduced [32].

The catenate (i.e., the metal catenane) shown in Fig. 16 incorporates a terpyridine ligand in one of its two macrocyclic components and a phenanthroline ligand in both of them [33]. As discussed by Raehm and Sauvage in this volume, the stable conformation of such a catenane is that in which the Cu(I) center is tetracoordinated [$Cu(I)N_4$] by the two phenanthroline ligands. Monoelectronic oxidation of the catenate leads to a species containing a tetracoordinated Cu(II) ion. Since Cu(II) prefers a higher coordination number, the terpyridine-containing macrocycle circumrotates through the cavity of the other one (Fig. 16). In this way, the Cu(II) center can adopt a pentacoordination geometry [$Cu(II)N_5$] that is significantly more stable than the original tetracoordination one. Monoelectronic reduction of the latter species transforms the pentacoordinated Cu(II) center into a pentacoordinated Cu(I) ion. In response to the preference of Cu(I) for

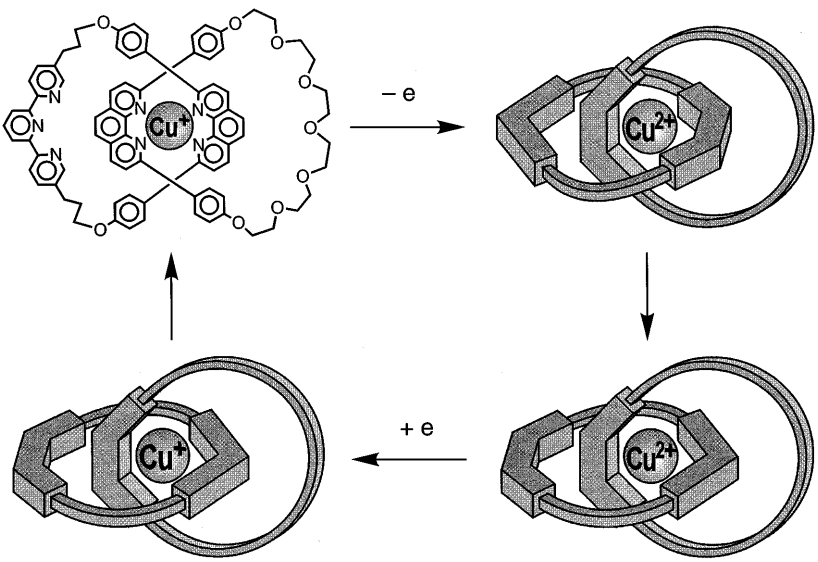

Fig. 16. Ring movements induced by electron-transfer processes in a Cu(I) catenate [32, 33]. As described in the text, the first molecular rearrangement can be caused by a photochemical electron-transfer reaction

tetracoordination, the terpyridine-containing macrocycle circumrotates through the cavity of the other one, affording back the original structure.

The movements illustrated in Fig. 16 can also be induced photochemically [32]. In Cu(I) complexes of polypyridine ligands the lowest triplet metal-to-ligand charge-transfer (MLCT) excited state is luminescent, has a reasonably long lifetime, and can play the role of an electron-transfer reagent [34]. This is also the case of the catenate shown in Fig. 16, that exhibits an MLCT emission band with λ_{max} = 750 nm and τ = 60 ns in aerated acetonitrile solution at 298 K. This first step of the overall swinging process, namely the conversion of $Cu(I)N_4$ into $Cu(II)N_4$, can be induced by light excitation, according to the following mechanism:

$$Cu(I)N_4 + h\nu \rightarrow {}^*Cu(I)N_4 \quad (1)$$

$${}^*Cu(I)N_4 \rightarrow Cu(I)N_4 + \text{heat or } h\nu' \quad (2)$$

$${}^*Cu(I)N_4 + Ox \rightarrow Cu(II)N_4 + Red \quad (3)$$

$$Cu(II)N_4 + Red \rightarrow Cu(I)N_4 + Ox \quad (4)$$

$$Red \rightarrow Products \quad (5)$$

Photoexcitation [Eq. (1)] is followed by an excited state oxidation process in the encounter with a suitable oxidant [Ox, Eq. (3)], which, of course, must not be able to oxidize $Cu(I)N_4$ in the ground state. Such a reaction competes with luminescence [Eq. (2)], which is therefore a useful tool to evaluate whether reaction 3 takes place. The reduction potential of the $Cu(II)N_4/{}^*Cu(I)N_4$ couple can be evaluated by the following equation [35]:

$$E^0[Cu(II)N_4/{}^*Cu(I)N_4] \approx E^0[Cu(II)N_4/Cu(I)N_4] - E' = -1.02\,V \quad (6)$$

where $E^0[Cu(II)N_4/Cu(I)N_4]$ is +0.63 V vs. SCE, in acetonitrile, and E′, the energy of the $^*Cu(I)N_4$ excited state, is about 1.65 eV (as estimated from the maximum of the emission band in the same solvent).

This shows that even a mild oxidant should be capable to oxidize the photoexcited $^*Cu(I)N_4$ catenate [Eq. (3)]. Nevertheless, the choice of the oxidant is not a trivial matter because other important requirements have to be satisfied:

(i) the oxidant should not compete with $Cu(I)N_4$ for light absorption,
(ii) the reaction between $^*Cu(I)N_4$ and the oxidant [Eq. (3)] should be fast enough to compete with the intrinsic excited state decay [Eq. (2)], and
(iii) after reduction, the oxidant should undergo a very fast, irreversible decomposition reaction [Eq. (5)] in order to prevent the occurrence of the back electron-transfer reaction [Eq. (4)].

It was found that *p*-nitrobenzylbromide, $p\text{-}NO_2C_6H_4CH_2Br$, satisfies all the above requirements. The rate constant of the quenching process [Eq. (3)] is $4.1 \times 10^8\ M^{-1}\ s^{-1}$ in acetonitrile solution, so that a sufficiently large fraction of the $^*Cu(I)N_4$ excited states can react with the quencher even using not too high concentrations (10^{-1}–10^{-2} M) of $p\text{-}NO_2C_6H_4CH_2Br$.

Light excitation of the catenate was found to cause spectral changes indicating the disappearance of $Cu(I)N_4$ and the concomitant formation of $Cu(II)N_4$ as the only reaction product. The overall quantum yield of the photoreaction was about 3%. Since only 55% of the $*Cu(I)N_4$ excited states react with the quencher, the fraction of quenching events that give rise to a permanent formation of $Cu(II)N_4$ is ≈5%. The low efficiency of the photoinduced process has to be attributed to the competition between reactions 4 and 5. Under the experimental conditions used, practically complete transformation of $Cu(I)N_4$ into $Cu(II)N_4$ was achieved in about 20 min. The results obtained also showed that $Cu(II)N_4$ is not photosensitive.

At the end of the photoreaction, the irradiated solution was kept in the dark. Spectrophotometric measurements showed that the transformation of $Cu(II)N_4$ into the more stable $Cu(II)N_5$ species was slowly occurring. After about 48 h, no further spectral change was observed and the spectrum of the solution was that of the stable $Cu(II)N_5$ species. In order to complete the cycle (Fig. 16), an excess of ascorbic acid was added to the solution. A gradual reappearance of the spectrum of $Cu(I)N_4$ was observed. After about 30 min, the spectrum was practically coincident with the initial spectrum, showing that the cyclic process (Fig. 16) was completed.

One can wonder whether, besides the oxidation step, the reduction step can also be induced by light. This cannot be the case since in Cu(II) complexes (d^9 electronic configuration) the lowest excited state is a low energy, distorted ligand-field level which undergoes very fast radiationless decay to the ground state [34]. Therefore it is not possible to involve $Cu(II)N_5$ in a bimolecular reaction where an excited state of the complex should play the role of the electron acceptor.

7 Conclusions

In his 1959 address to the American Physical Society, when discussing the possibility of constructing molecular-level machines, R.P. Feynman said [6]: "*An internal combustion engine of molecular size is impossible. Other chemical reactions, liberating energy when cold, can be used instead*". The described examples of molecular machines driven by 'cold' chemical reactions fulfill Feynman's prediction. What Feynman did not predict, however, is the extremely interesting possibility that light can be used as the primary energy input to cause the chemical reactions capable of inducing mechanical movements. This possibility is not surprising, since light is the primary energy source of all the natural molecular machines, and the examples reported in this chapter are important because they open the way to the design of fully light-driven artificial molecular machines.

In the same address, Feynman concluded his reflection on the construction of artificial molecular-scale machines as follows: "*What would be the utility of such machines? Who knows? I cannot see exactly what would happen, but I can hardly doubt that when we have some control of the rearrangement of things on a molecular scale we will get an enormously greater range of possible properties*

that substances can have, and of different things we can do". We believe that these sentences are the most appropriate comment to the work described above. Much progress remains to be made at a fundamental level before the knowledge base reaches that critical threshold which will allow it to be exploited to the full in a technological context. Surely the current high level of research activity surrounding artificial molecular machines demonstrates how new concepts continue to instill new life into chemistry as a scientific discipline.

Acknowledgements. We thank the University of Bologna (Funds for Selected Research Topics), CNR (Italy), and MURST (Supramolecular Devices Project) for financial support.

8 References

1. Hawkins JM (1979) The Oxford Paperback Dictionary. Oxford University Press, Oxford
2. (a) Balzani V, Scandola F (1991) Supramolecular Photochemistry. Horwood, Chichester; (b) Lehn J-M (1995) Supramolecular Chemistry. VCH, Weinheim; (c) Balzani V, Scandola F (1996) In: Atwood JL, Davies JED, MacNicol DD, Vögtle F (eds) Comprehensive Supramolecular Chemistry. Pergamon Press, Oxford, Vol 10, p 687; (d) Balzani V, Credi A, Venturi M (1999) In: Ungaro R, Dalcanale E (eds) Supramolecular Science: Where It Is and Where It Is Going. Kluwer, Dordrecht, p 1
3. (a) Balzani V, Gómez-López M, Stoddart JF (1998) Acc Chem Res 31: 405; (b) Sauvage J-P (1998) Acc Chem Res 31: 611; (c) Balzani V, Credi A, Raymo FM, Stoddart JF (2000) Angew Chem Int Ed 39: 3348
4. Boulas PL, Gómez–Kaifer M, Echegoyen L (1998) Angew Chem Int Ed 37: 216
5. Goodsell DS (1996) Our Molecular Nature: The Body's Motors, Machines, and Messages. Copernicus, New York
6. Feynman RP (1960) Sat Rev 43: 45
7. (a) Ashton PR, Ballardini R, Balzani V, Baxter I, Credi A, Fyfe MCT, Gandolfi MT, Gómez-López M, Martínez-Díaz M-V, Piersanti A, Spencer N, Stoddart JF, Venturi M, White AJP, Williams DJ (1998) J Am Chem Soc 120: 11932; (b) Kelly TR, De Silva H, Silva RA (1999) Nature 401: 150; (c) Koumura N, Zijlstra RWJ, van Delden RA, Harada N, Feringa BL (1999) Nature 401: 152; (d) Raehm L, Kern J-M, Sauvage J-P (1999) Chem Eur J 5: 3310; (e) Balzani V, Credi A, Langford SJ, Raymo FM, Stoddart JF, Venturi M (2000) J Am Chem Soc 122: 3542; (f) Ashton PR, Ballardini R, Balzani V, Credi A, Dress R, Ishow E, Kleverlaan CJ, Kocian O, Preece JA, Spencer N, Stoddart JF, Venturi M, Wenger S (2000) Chem Eur J 6: 3558
8. Atwood JL, Davies JED, Macnicol DD, Vögtle F (eds) (1996) Comprehensive Supramolecular Chemistry. Pergamon Press, Oxford, Vol 2
9. Amabilino DB, Stoddart JF (1995) Chem Rev 95: 2725
10. Credi A, Montalti M, Balzani V, Langford SJ, Raymo FM, Stoddart JF (1998) New J Chem 1061
11. Anelli PL, Ashton PR, Ballardini R, Balzani V, Delgado M, Gandolfi MT, Goodnow TT, Kaifer AE, Philp D, Pietraszkiewicz M, Prodi L, Reddington MV, Slawin AMZ, Spencer N, Stoddart JF, Vicent C, Williams DJ (1992) J Am Chem Soc 114: 193
12. (a) Houk KN, Menzer S, Newton SP, Raymo FM, Stoddart JF, Williams DJ (1999) J Am Chem Soc 121: 1479; (b) Loeb SJ, Wisner JA (1998) Angew Chem Int Ed 37: 2838
13. (a) Schill G (1971) Catenanes, Rotaxanes and Knots. Academic Press, New York (b) Sauvage J-P, Dietrich-Buckecher CO (eds) (1999) Molecular Catenanes, Rotaxanes and Knots. Wiley-VCH, Weinheim

14. (a) Gibson HW, Bheda MC, Engen PT (1994) Progr Polym Sci 19: 843; (b) Jäger R, Vögtle F (1997) Angew Chem Int Ed Engl 36: 931
15. Busch DH, Vance AL, Kolchinski AG (1996) In: Atwood JL, Davies JED, Macnicol DD, Vögtle F (eds) Comprehensive Supramolecular Chemistry. Pergamon Press, Oxford, Vol 9, p 1
16. Amabilino DB, Raymo FM, Stoddart JF (1996) In: Atwood JL, Davies JED, Macnicol DD, Vögtle F (eds) Comprehensive Supramolecular Chemistry. Pergamon Press, Oxford, Vol 9, p 85
17. Ashton PR, Baxter I, Fyfe MCT, Raymo FM, Spencer N, Stoddart JF, White AJP, Williams DJ (1998) J Am Chem Soc 120: 2297
18. Ashton PR, Ballardini R, Balzani V, Credi A, Gandolfi MT, Marquis DJ-F, Menzer S, Pérez-García L, Prodi L, Stoddart JF, Venturi M, White AJP, Williams DJ (1995) J Am Chem Soc 117: 11171
19. Deleuze MS, Leigh DA, Zerbetto F (1999) J Am Chem Soc 121: 2364
20. Anelli PL, Asakawa M, Ashton PR, Bissell RA, Clavier G, Górski R, Kaifer AE, Langford SJ, Mattersteig G, Menzer S, Philp D, Slawin AMZ, Spencer N, Stoddart JF, Tolley MS, Williams DJ (1997) Chem Eur J 3: 1113
21. (a) Anelli PL, Spencer N, Stoddart JF (1991) J Am Chem Soc 113: 5131; (b) Ashton PR, Philp D, Spencer N, Stoddart JF (1992) J Chem Soc Chem Commun 1124; (c) Ashton PR, Ballardini R, Balzani V, Belohradsky M, Gandolfi MT, Philp D, Prodi L, Raymo FM, Reddington MV, Spencer N, Stoddart JF, Venturi M, Williams DJ (1996) J Am Chem Soc 118: 4931; (d) Asakawa M, Ashton PR, Ballardini R, Balzani V, Belohradsky M, Gandolfi MT, Kocian O, Prodi L, Raymo FM, Stoddart JF, Venturi M (1997) J Am Chem Soc 119: 302
22. (a) Credi A, Balzani V, Langford SJ, Stoddart JF (1997) J Am Chem Soc 119: 2679; (b) Ashton PR, Balzani V, Becher J, Credi A, Fyfe MCT, Mattersteig G, Menzer S, Nielsen M, Raymo FM, Stoddart JF, Venturi M, Williams DJ (1999) J Am Chem Soc 121: 3951; (c) Ishow E, Credi A, Balzani V, Spadola F, Mandolini L (1999) Chem Eur J 5: 984
23. (a) Venturi M, Credi A, Balzani V (2001) In: Balzani V (ed) Handbook of Electron Transfer. Wiley-VCH, Weinheim, Vol 3, p 501; (b) Ballardini R, Gandolfi MT, Balzani V (2001) In: Balzani V (ed) Handbook of Electron Transfer, Wiley-VCH, Weinheim, Vol 3, p 539
24. Benniston AC, Harriman A, Yufit DS (1997) Angew Chem Int Ed Engl 36: 2356
25. (a) Ballardini R, Balzani V, Gandolfi MT, Prodi L, Venturi M, Philp D, Ricketts HG, Stoddart JF (1993) Angew Chem Int Ed 32: 1301; (b) Ashton PR, Ballardini R, Balzani V, Boyd SE, Credi A, Gandolfi MT, Gómez-López M, Iqbal S, Philp D, Preece JA, Prodi L, Ricketts HG, Stoddart JF, Tolley MS, Venturi M, White AJP, Williams DJ (1997) Chem Eur J 3: 152
26. Freemantle M (1998) Chem Eng News Oct 26: 38
27. Ashton PR, Ballardini R, Balzani V, Constable EC, Credi A, Kocian O, Langford SJ, Preece JA, Prodi L, Schofield ER, Spencer N, Stoddart JF, Wenger S (1998) Chem Eur J 4: 2411
28. Ashton PR, Balzani V, Kocian O, Prodi L, Spencer N, Stoddart JF (1998) J Am Chem Soc 120: 11190
29. (a) Benniston AC, Harriman A (1993) Angew Chem Int Ed Engl 32: 1459; (b) Benniston AC, Harriman A, Lynch VM (1994) Tetrahedron Lett 35: 1473; (c) Benniston AC, Harriman A, Lynch VM (1995) J Am Chem Soc 117: 5275
30. Ashton PR, Philp D, Spencer N, Stoddart JF (1992) J Chem Soc Chem Commun 1124
31. Armaroli N, Balzani V, Collin J-P, Gaviña P, Sauvage J-P, Ventura B (1999) J Am Chem Soc 121: 4397
32. Livoreil A, Sauvage J-P, Armaroli N, Balzani V, Flamigni L, Ventura B (1997) J Am Chem Soc 119: 12114
33. Cárdenas DJ, Livoreil A, Sauvage J-P (1996) J Am Chem Soc 118: 11980
34. Everly RM, McMillin DR (1991) J Phys Chem 95: 9071 and references cited therein
35. Balzani V, Bolletta F, Gandolfi MT, Maestri M (1978) Top Curr Chem 75: 1

Computing at the Molecular Level

Anthony R. Pease, J. Fraser Stoddart

Department of Chemistry and Biochemistry, University of California Los Angeles, 405 Hilgard Avenue, Los Angeles, CA 90095-1569, USA
E-mail: stoddart@chem.ucla.edu

With the pace of miniaturization of silicon-based computer chips hurtling toward an insurmountable barrier, it has become necessary to envisage a smaller scale on which logic operations can be performed – the molecular scale. This review documents a small fraction of the research currently being undertaken around the globe into the development of systems which, in the solution state, mimic the behavior of switches and logic gates, through the two-dimensional ordering of molecules as a result of the formation of Langmuir films, up to the incorporation of suitably designed molecules into solid-state molecular electronic devices capable of performing useful tasks, such as the retention of memory and the operation of logic gates.

Keywords: Catenane, Molecular device, Molecular logic, Nanocomputer, Rotaxane

1 Introduction 190

2 Molecular Logic 191

2.1 Logic Functions Defined 191
2.2 Luminescent Signaling of Logic Operations 192

3 Co-Conformational and Topological Control of Interlocked and Interpenetrated (Super)Molecules 202

3.1 Rotaxanes 202
3.2 Pseudorotaxanes 205
3.2.1 Pseudorotaxane-Based Switches 207
3.2.2 Pseudorotaxane-Based Logic-Displaying Systems 212
3.3 Catenanes 213

4 Incorporating Switchable Molecules into Devices 220

4.1 Magnetic Memory 220
4.2 Aligning Catenanes in Two Dimensions 222
4.3 Constructing and Testing a Catenane-Based Device 225
4.4 Constructing and Testing a Rotaxane-Based Device 228

5 Wiring Issues 229

5.1 Metal-Nucleated Nanowires 231
5.2 Self-Assembled Nanowires 231

Structure and Bonding, Vol. 99

5.3 Carbon Nanotubes 232
5.4 Conjugated Polymers. 232

6 Concluding Remarks. 232

7 References 234

1 Introduction

We are completely and irrevocably dependent on computers. The insatiable demand for faster, smaller processors has led to breathtaking advances in the design, production, and miniaturization of computer chips. In 1965, Gordon Moore [1], then head of chip manufacturers IBM, predicted that, amongst other things, the number of components on a computer chip would quadruple every 3 years. His prediction – which has proven to be startlingly accurate over the last 35 years – will, however, soon reach an insurmountable barrier if the conventional silicon-based technology is not superceded by a new technology, capable of delivering better performance from other smaller components. Although component miniaturization has proceeded unabated over the last 3 decades, early next decade, the physical limits of silicon as a component in computer chips will have been reached [2]. Vital to the efficacy of silicon in every computer chip is its oxide, SiO_2. With a colossal resistivity, silicon dioxide has proven to be the perfect insulator for use on silicon chips. The state-of-the-art in 1997 reflected the fact that an insulating layer of silicon dioxide on a component was down to as little as 25 silicon atoms thick. If the current rate of component miniaturization proceeds – and there are no indications that it will not – then, by 2012, a layer of silicon dioxide on a chip component will only be five silicon atoms thick. On this miniscule scale, an insulating layer can only just hold back enough current for the oxide layer to function as a working insulator. With four silicon atoms as an insulating barrier, the current leakage through the oxide layer will render any device inoperable [3]. At this point, if silicon alone is considered to be the constituent of microchips, Moore's Law will have reached the only hurdle that it cannot possibly jump, i.e., the physical limits of silicon as a chip component will have been reached.

If miniaturization is to continue, as it surely must, and as the world demands, there is only one scale on which devices can operate – that is, the molecular scale [4]. If a computer could be built from components in which the functions are carried out on a molecular scale [5], the world would undergo a major revolution in computing. These computers – although miniscule – would have the possibility to carry out enormously parallel computations, and, as such, operate at mind-boggling speeds. Although such molecular computers are still many years of hard work away on the part of a vast number of people, their promise is so great that it cannot be ignored. It is the aim of this review to describe the combined efforts that have been made in

a selected number of research groups around the world toward the development of components that could one day find their way into such molecular electronic devices.

2 Molecular Logic

2.1 Logic Functions Defined

Although it is not necessarily the case that the components of a molecular computer [6] will have to operate in ways analogous to those of conventional silicon-based computers, a great deal of effort has been devoted to the design, synthesis, and characterization of molecular systems in which silicon-based logic can, in principle, be mimicked. All silicon chips are based on the operation of logic gates. A logic gate is a collection of individual components – such as transistors and diodes – which have been designed to perform a specific function in response to certain inputs. The three most fundamental types of logic gate are the AND, OR, and NOT ones. Each has been designed to perform according to a set of rules delineated in so-called truth tables, which are a list of outputs that the gate should give, based on certain inputs. All computers operate using binary operations. In this base 2 form of arithmetic, there are only two numbers – namely, 0 and 1 – which correspond quite nicely with electronic operations, insofar as "0" equates with no electronic signal, and "1" translates into a signal.

The truth tables for the three most fundamental types of logic gates are shown in Table 1. The AND gate has a truth table such that it will only give an output of 1 if *both* inputs A *and* B are 1. The OR gate relies on a system in which it will give an output of 1 if *either* input A *or* B is 1. The NOT gate simply *inverts* the signal such that an input of 1 yields an output of 0, and vice versa. However, since these three gates alone are not sufficient to perform all the necessary logic functions, other gates have been designed that obey different

Table 1. Truth tables of **a** an AND, **b** an OR, and **c** an NOT logic gate

I1	I2	O
0	0	0
1	0	0
0	1	0
1	1	1

AND

(a)

I1	I2	O
0	0	0
1	0	1
0	1	1
1	1	1

OR

(b)

I	O
0	1
1	0

NOT

(c)

a The truth table of an AND gate. Both inputs I1 and I2 have to be turned "on" before a positive output is observed. **b** OR Logic decrees that either I1 *or* I2 *or* both inputs have a value of 1 before an output of 1 is recorded. **c** NOT Logic gates have the inverse output to their input, i.e., an input of 0 results in an output of 1, and vice versa.

Table 2. Truth tables for **a** an NAND, **b** an NOR, **c** an XOR, and **d** an XNOR logic gate

I1	I2	O
0	0	1
1	0	1
0	1	1
1	1	0

NAND (a)

I1	I2	O
0	0	1
1	0	0
0	1	0
1	1	0

NOR (b)

I1	I2	O
0	0	0
1	0	1
0	1	1
1	1	0

XOR (c)

I1	I2	O
0	0	1
1	0	0
0	1	0
1	1	1

XNOR (d)

a The truth table for a NAND gate resembles the inverted output from an AND gate, i.e., the output is only equal to 0 when both I1 and I2 are equal to 1. **b** Similarly, NOR logic is the inverse function of OR logic, and the output is 0 if either I1 *or* I2 *or* both are equal to 1. **c** XOR logic has exactly the same truth table as that of an OR function, except in the case when both inputs are equal to 1, in which case the output is 0. **d** The truth table for XNOR logic shows it to be the inverse function of XOR in that, if both inputs are of the same value, the output is equal to 1, and, if the inputs are different, then the output is 0.

truth tables. The first series (Table 2) contains the inverse functions NAND and NOR, which have the same pattern of responses as AND and OR gates, except that ones are replaced by zeroes, and vice versa. The overall effect of generating NOR logic can be imagined as having an OR gate with its output connected to the input of a NOT gate. The second major modifier is the Exclusive function. Exclusive OR (XOR) gates have the same outputs as OR gates, except that the value of the output where both inputs are equal to 1 is inverted.

If molecular computers are to operate within the same architectures as conventional silicon-based processors, then it will be necessary for the molecular chip-builder to have the same array of logic functions that photolithographers currently have at their disposal. With this requirement in mind, many examples have appeared in the literature in which (supra)molecular systems show responses to different stimuli, producing outputs reminiscent of logic operations [7].

2.2 Luminescent Signaling of Logic Operations

The exploitation of photoinduced electron transfer (PET) (Fig. 1) has led to the development of an enormous range of molecules capable of sensing a wide array of analytes [8]. Judicious alteration of these sensors has stimulated the production of molecules capable of displaying characteristics reminiscent of logic operations.

Consider, for example, molecule **1** (Fig. 2), designed in the laboratories of de Silva [9] in Belfast. The fluorescence of anthracene derivatives has been shown, independently, to be quenched by tertiary amines, and also by benzocrown ethers. The rationale behind the design of molecule **1** was such that, in its natural state, fluorescence of the anthracene unit would be quenched by electron transfer from the adjacent tertiary amine, and also from the sodium-

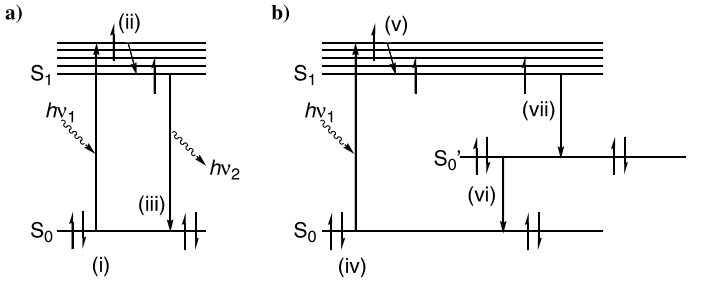

Fig. 1. a The process of fluorescence: *i* Incoming radiation excites an electron from the HOMO of a fluorophore to a high vibrational state of the LUMO, which *ii* relaxes to the lowest LUMO vibronic level. *iii* Decay of the excited electron from the LUMO back to the HOMO occurs radiatively, with the emission of a photon, i.e., fluorescence. **b** In a PET-quenched system, *iv* excitation and *v* vibronic relaxation occur as before. *vi* With an electron-donor present in the system, an electron can be transferred from S_0' of the quencher to S_0 of the fluorophore, preventing fluorescence. *vii* Finally, the excited electron in the fluorophore LUMO decays nonradiatively to the S_0 of the quencher

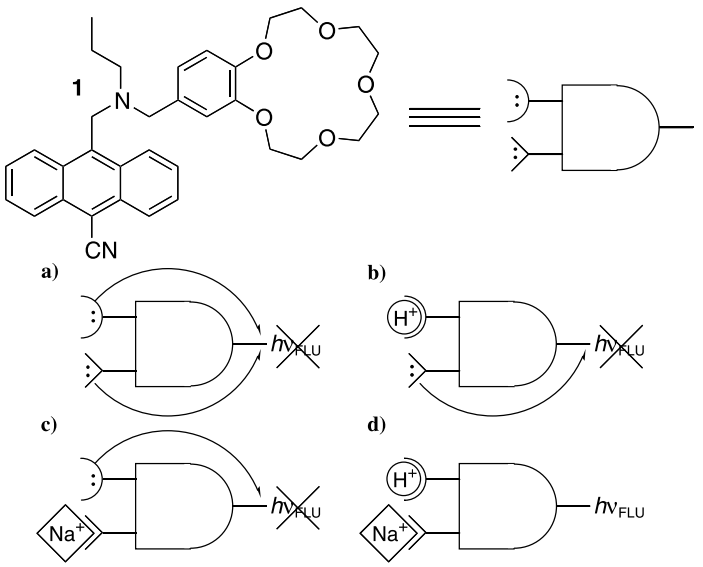

Fig. 2. A molecular AND gate in the shape of compound **1**. Fluorescence of the anthracene unit can be quenched by PET from the tertiary amine (depicted as the circle-receptor), and the benzo-crown ether (the square-receptor). In the absence of **a** both stimuli or **b**, **c** only one stimulus, fluorescence is quenched by PET. **d** Presence of both stimuli removes the possibility of PET, and so the system fluoresces

selective crown ether, benzo-15-crown-5, leading to a low fluorescence output. Upon addition of an excess of acid, the tertiary amine becomes protonated, yielding an ammonium ion, which no longer possesses the lone pair necessary

to quench the fluorescence of the anthracene unit. However, the presence of the fluorescence-quenching benzo-15-crown-5 still leads to a low fluorescent output. In the reverse case, in which an excess of sodium sulfate is added, the electron-donating orbitals of benzo-15-crown-5 are shifted to a lower energy level, from which donation to the anthracene HOMO is impossible, and so quenching is eliminated. The tertiary amine, however, still possesses a lone pair of electrons that can participate in PET quenching of the anthracene, and hence the fluorescence of the system is low. However, when both sodium ions and protons are added to a solution of **1**, neither of the electron donors are capable of donating to the anthracene HOMO and so PET cannot occur, resulting in a large fluorescence output. If one considers the presence (1) or otherwise (0) of H^+ and Na^+ ions to be inputs, and fluorescence to signal an output of 1, then it can be appreciated, by comparing the fluorescence output of **1** in Fig. 2 with the truth table in Table 1, that this molecule exhibits the characteristics of an AND gate in that it only provides a positive response when both inputs are 1.

This system has been improved upon in compound **2** (Fig. 3) in which both receptors are more proximal to the anthracene fluorophore [10]. This compound exhibits a binary response, i.e., in the absence of both, or in the presence of only one of the two stimuli, there is no fluorescence whatsoever, whereas the presence of both inputs results in a bright fluorescence with $\phi_F = 0.24$.

The ingenuity of the design of these PET-based molecules with AND characteristics can be equally well expressed in a molecule which is capable of mimicking the OR logic function [11]. A subtle difference in the design of compound **3** (Fig. 4), compared to that of **1**, gives the former its OR characteristics. In compound **1**, the fluorophore is separated from the proton receptor, which is, in turn, separated from the sodium ion receptor.

The design of an OR molecule demands that the PET quenching be eliminated through addition of either stimulus. This need is reflected in the anthracene derivative **3**, in which the tricarboxylate Group II cation sensor also contains a tertiary amine. Thus, if compound **3** is buffered at pH 7.3, with no metal cations present, the system will not fluoresce, as a consequence of PET from the tertiary amine to the anthracene. If the pH is reduced, the

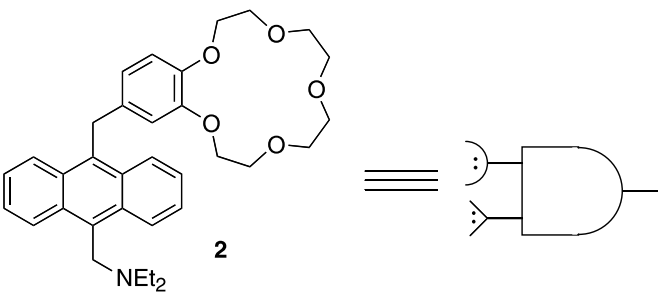

Fig. 3. Compound **2** – a better molecular AND gate

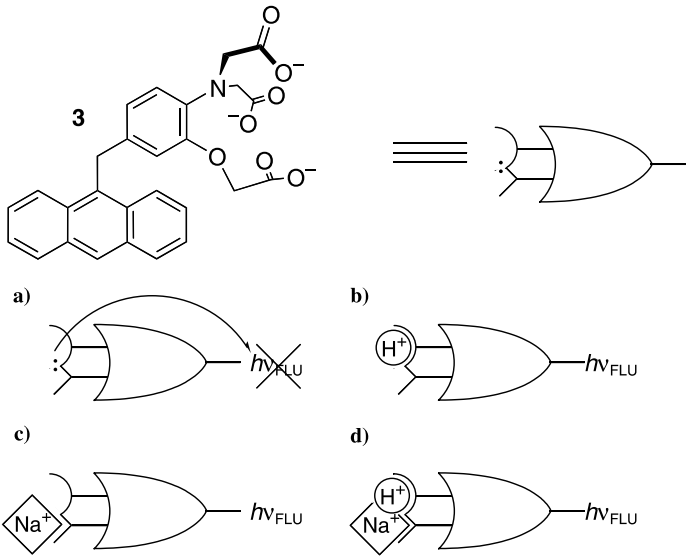

Fig. 4. A molecular OR gate in the shape of compound **3**. With both proton and calcium ion sensitivity, the tertiary amine atom will quench fluorescence of the fluorophore **a** in the absence of both stimuli. The presence of one **b** or **c** the other stimulus reduces the ability of the nitrogen lone pair to participate in PET. The same is true when **d** both stimuli are added to the solution

tertiary amine becomes protonated and, as such, the system fluoresces. If the pH is maintained at 7.3, but calcium or magnesium ions are added, then the lone pair from the tertiary amine becomes involved in coordination to the metal cation and so can no longer participate in quenching. At low pH, and in the presence of Group II cations, the system once again fluoresces strongly, with the tertiary amine competing for occupancy with both metal cations and protons. As before, if the presence or absence of either the metal cation or the proton stimulus is considered as an input, and the output is identified as fluorescence, the overall operation of the compound is reminiscent of OR logic. In the presence of both H^+ and Mg^{2+}, or one of these ions, the system will fluoresce, whereas, in their absence, it will not.

INHIBIT logic, although not frequently employed in chip design, provides two intricate examples of luminescent signaling of logic functions. INHIBIT gates are basically AND gates, with one of the inputs inverted through a NOT function (Table 3). This input is called the INHIBIT input. Truth tables dictate that, if the INHIBIT input is on, the gate cannot possibly yield an output of 1. Phosphorescent systems lend themselves particularly well for use in INHIBIT functions. As phosphorescence (Fig. 5) is a phenomenon involving triplet states, it is particularly vulnerable to quenching by molecular oxygen – a molecule with a triplet ground state.

A two-input INHIBIT gate can be as simple as a receptor-phosphor system. With their inherent sensitivity to molecular oxygen, these systems can be

Table 3. Truth tables for **a** a two-input, and **b** a three-input INHIBIT logic gate

I1	I2	O
0	0	0
1	0	1
0	1	0
1	1	0

Two-input INHIBIT

(a)

I1	I2	I3	O
0	0	0	0
1	0	0	0
0	1	0	0
1	1	0	1
0	0	1	0
1	0	1	0
0	1	1	0
1	1	1	0

Three-input INHIBIT

(b)

a The truth table of a two-input INHIBIT gate decrees that the gate act with AND logic to all inputs except the last. Thus, it can be seen that, with respect to I1, the response is that of a one-input AND gate (a YES gate). However, for any value of I1, there can be no output if the value of I2 is 1. **b** In a similar fashion, a three-input INH gate behaves as an AND gate with respect to I1 and I2 when I3 = 0. A value of 1 from I3 provides an output of zero in any combination of I1 and I2.

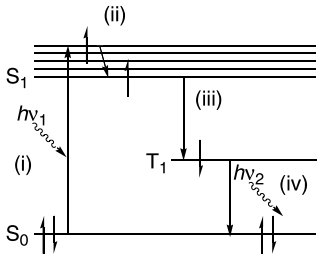

Fig. 5. Phosphorescence occurs when *i* an electron is excited from the singlet HOMO to the singlet LUMO. After *ii* vibronic relaxation, the LUMO-based electron can *iii* decay through intersystem crossing to a vacant triplet orbital. Phosphorescence is *iv* the emissive relaxation of the electron from T_1 to S_0

interpreted as possessing INHIBIT characteristics. Gunnlaugsson's [12] cyclen-quinoline derivative **4**, when complexed to Tb(III), constitutes such a system. The quinoline moiety acts as an antenna for the phosphor Tb(III). Such antenna systems absorb light that is then transferred nonradiatively to an energy level of a fluorophore or phosphor, which is unavailable normally through the phosphor alone. In the presence of protons, but in the absence of molecular oxygen, the quinolinium ion absorbs strongly at the excitation wavelength (330 nm) used in the experiment. The excited-state quinolinium ion then intersystem crosses to its excited-state triplet, which nonradiatively transfers its electron to the terbium trication excited-state triplet, resulting (Fig. 6) in phosphorescence of the terbium trication.

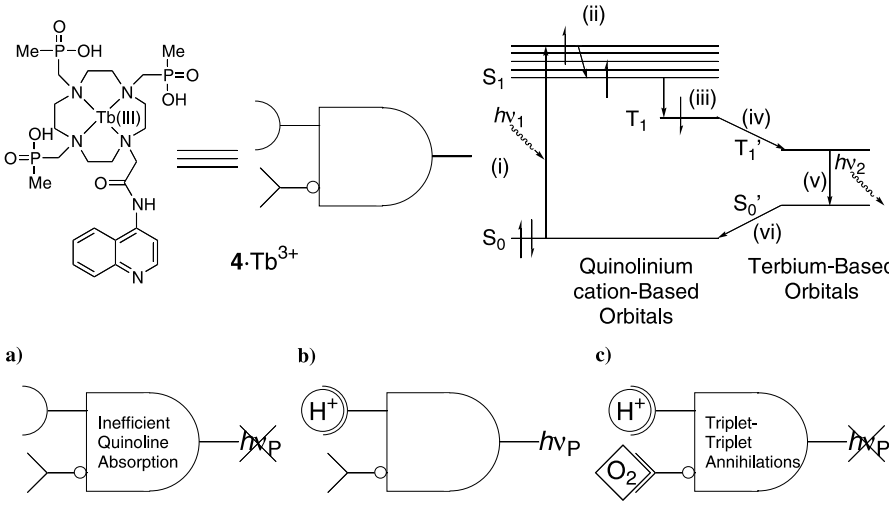

Fig. 6. The antenna effect, as it relates to a two-input INHIBIT gate exemplified by the complex **4**·Tb^{3+}. Whereas the terbium trication cannot absorb light appreciably, the quinolinium ion can do so readily. *i* Photoexcitation from singlet HOMO to LUMO, and *ii* vibronic relaxation occurs as in a fluorescent system. After *iii* the electron intersystem crosses to a quinolinium-based triplet state, it can then *iv* collisionally and therefore nonradiatively transfer to a triplet orbital of the terbium trication. After *v* emissively relaxing to the ground singlet state orbital of the terbium cation, the electron then rapidly neutralizes charge separation by collisionally transferring back to the quinoline radical dication. **a** In the absence of protons, the quinoline antenna absorbs only weakly at the excitation wavelength of 330 nm, and so the terbium phosphoresces poorly. **b** Addition of protons leads to a highly emissive system but, **c** in both the presence and absence of protons, the addition of the INHIBIT stimulus – oxygen – quenches all emission through triplet-triplet annihilations

In the absence of protons and oxygen, the quinoline unit absorption is shifted bathochromically relative to the protonated form, and away from the excitation wavelength. This shift results in a lower population of the quinoline S_1 state, which means that light is not harvested as efficiently by the antenna, and therefore the terbium does not phosphoresce as strongly. With respect to protons only, and in the absence of molecular oxygen, **4**·Tb^{3+} can be seen to act as a YES gate (essentially a one-input AND gate) with an on-off ratio of roughly 50. However, when the INHIBIT input is turned on (solutions are not deoxygenated prior to use), most of the terbium phosphorescence is quenched. The overall effect of this phenomenon is reminiscent of INHIBIT logic.

Arguably the most complex molecular system, showing characteristics of logic functions, is the three-input INHIBIT molecule $\mathbf{5}^{4-}$ (Fig. 7) developed by de Silva [13]. The truth table for a three-input INHIBIT gate (Table 3) can be split into two portions – that where the INHIBIT input is turned off, and that where the INHIBIT input is turned on. With the INHIBIT input in an off state, the system acts as an AND gate with respect to inputs A and B. However, as before, if the INHIBIT input is turned on, all outputs are zero. The output from

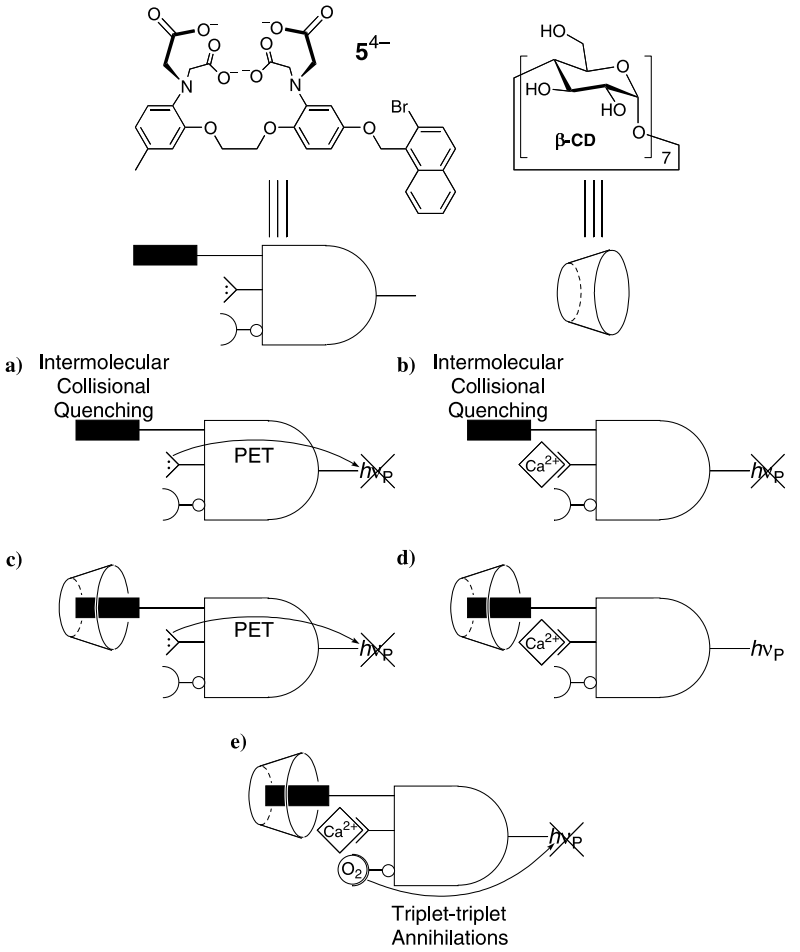

Fig. 7. A three-input INHIBIT gate exemplified by the tetraanion $\mathbf{5}^{4-}$ and β-cyclodextrin (β-**CD**). **a** With neither protons nor β-**CD** present in the solution, phosphorescent output is low, because of both PET from the tertiary amine, and through intermolecular triplet-triplet collisions of the bromonaphthalene phosphor. **b** Addition of calcium ions leads to a reduction in the PET-based quenching of the phosphorescence – however, intermolecular collisions still lead to a low emission. **c** Shielding of the phosphor with β-**CD** reduces intermolecular triplet annihilations, but quenching still occurs via PET. **d** Only with both Ca^{2+} and β-**CD** present does the solution phosphoresce. **e** In any combination of Ca^{2+} and β-**CD**, the solution will yield a low output in the presence of molecular oxygen (the INHIBIT stimulus), as a consequence of triplet-triplet collisions

compound $\mathbf{5}^{4-}$ is measured as phosphorescence from the naphthalene moiety. As with Gunnlaugsson's two-input INHIBIT molecule, the phosphorescent output of this molecule is susceptible to quenching by molecular oxygen and so oxygen acts as the INHIBIT input – any combination of inputs will yield a low output in the presence of oxygen. The tetracarboxylate portion of $\mathbf{5}^{4-}$ is calcium-selective, and, in the absence of Ca^{2+}ions, quenches the S_1 state of the

bromonaphthalene phosphor, reducing phosphorescence intensity. The second input, β-cyclodextrin (β-CD), binds through a hydrophobic effect to the aromatic phosphor, reducing the occurrence of bimolecular collisional triplet-triplet annihilations. As such, **5** will phosphoresce strongly only in the presence of calcium and β-CD, and provided oxygen is absent. This behavior corresponds exactly to the truth table of the three-input INHIBIT gate.

To date, the most conceptually stimulating concept to have arisen in the field of logic-displaying molecules has been the development of a molecular half adder. A half adder is the basic component of computational arithmetic. The function of a half adder is to add two one-digit binary numbers together. A half adder consists of two gates – one an AND and the other an XOR – connected in parallel. The output from the AND gate is the carry digit from the addition, and the output from the XOR gate is the sum digit (Fig. 8).

To transfer the concept of parallel connectivity to the molecular world, one must envisage two logic-displaying molecules that share common stimuli and have different outputs. Therefore, addition of one stimulus will affect both logic-displaying species concurrently, and the molecules can be tailored to provide distinct outputs. de Silva's approach [14] has been to use compounds $\mathbf{6}^{4-}$ and $\mathbf{7}^{4-}$ (Figs. 9 and 10). Compound $\mathbf{6}^{4-}$ – a push-pull chromophore – contains three important features: (i) the tetracarboxylate Ca^{2+} ion receptor, (ii) the styrylquinoline chromophore, and (iii) the quinolino nitrogen atom – a proton receptor. Recognition of the calcium dication shifts the absorbance of the chromophore hypsochromically, whereas protonation of the quinolino nitrogen atom results in a bathochromic shift. Concurrent additions of Ca^{2+} and H^+ ions cancel each other out and the electronic spectrum of the chromophore appears almost unchanged. If the absorbance of the system at 390 nm – the λ_{max} of the parent chromophore – is monitored, with a high absorbance registering as a 1, and a low absorbance as a 0, it can be appreciated that the system behaves with XNOR logic. As a half adder requires use of an XOR gate, the output of the XNOR gate must be inverted. In physical terms, this requirement is reflected by consideration of the UV-Vis spectrum of $\mathbf{6}^{4-}$ in terms of a reciprocal function of absorbance – namely % transmittance (Fig. 9).

AND logic is introduced with the fluorescent molecule $\mathbf{7}^{4-}$. Like the previous PET-based AND systems, the molecule $\mathbf{7}^{4-}$ consists of a fluorophore and two receptors capable of PET (Fig. 10). Vital to the operation of this AND

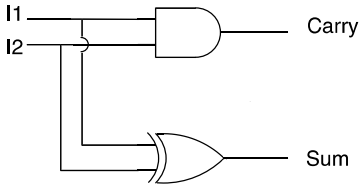

I1	I2	C	S
0	0	0	0
1	0	0	1
0	1	0	1
1	1	1	0

Fig. 8. A half adder consists of an AND and an XOR gate connected in parallel. The AND output represents the carry (C) digit of the addition, and the XOR output indicates the sum (S) digit. Thus, 0 + 0 = 00, 0 + 1 = 1 + 0 = 01, and 1 + 1 = 10

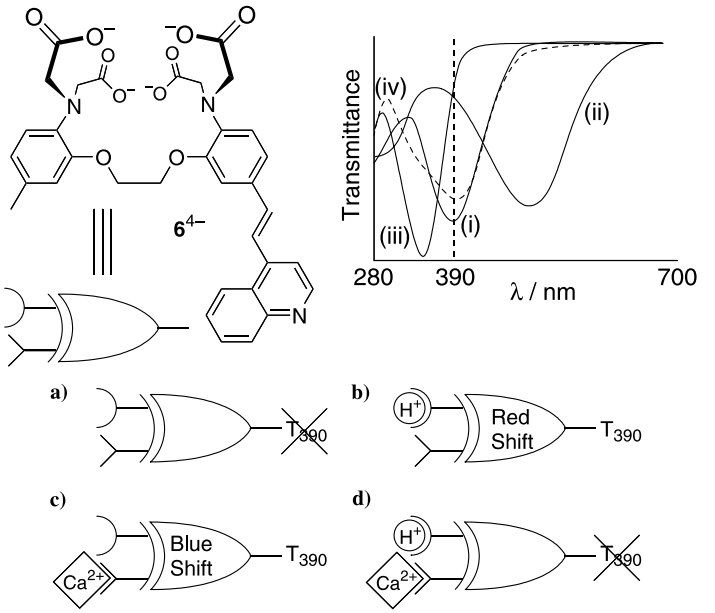

Fig. 9. A proton and calcium ion-sensitive XOR gate exemplified by $\mathbf{6}^{4-}$. The UV transmittance *i* of the styrylquinoline chromophore alone has a minimum at 390 nm. *ii* Addition of protons leads to a bathochromic shift in the transmittance minimum, leading to a high transmittance at 390 nm. *iii* The minimum is shifted hypsochromically through addition of calcium ions, resulting in a high transmittance output at 390 nm. *iv* The position of the minimum is not affected greatly by the presence of both stimuli, leading to a low transmittance output, mimicking the behavior of an XOR gate

molecule, however, is the choice of sensors. Inclusion of a tertiary amine confers proton sensitivity and the tetracarboxylate moiety provides sensitivity to Ca^{2+} ions. These receptors operate using the same stimuli that are used in the XOR molecule $\mathbf{6}^{4-}$. The result of this design is that the two gates can now

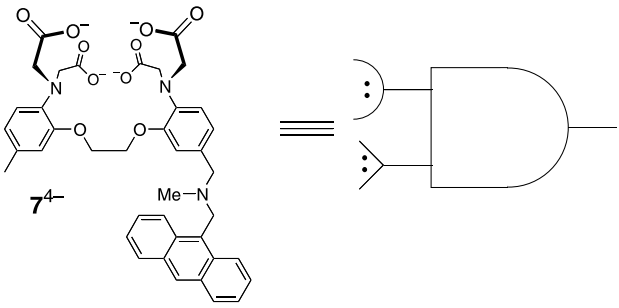

Fig. 10. A proton and calcium dication selective fluorescent AND gate exemplified by $\mathbf{7}^{4-}$. In the absence of both stimuli, or in the presence of only one stimulus, PET can occur from either tertiary amine to quench the fluorescence of the anthracene unit. Only with both protons and calcium dications present will the system fluoresce strongly

be addressed in a parallel sense. The output from the AND gate is the fluorescence of the anthracene unit and the output from the XOR gate is the transmittance of the styrylquinoline chromophore.

In the absence of either stimulus to an equimolar solution of $\mathbf{6}^{4-}$ and $\mathbf{7}^{4-}$, the anthracene fluorescence is quenched and the styrylquinoline has low transmittance at 390 nm, i.e., 0 + 0 = 00. In the absence of Ca^{2+} ions, but at low pH, PET from the nitrogen atoms on the calcium-sensing moiety still prohibits the anthracene unit of $\mathbf{7}^{4-}$ from fluorescing and the minimum in transmittance of the styrylquinoline is blue-shifted, leading to a higher transmittance of $\mathbf{6}^{4-}$ at 390 nm, i.e., 0 + 1 = 01. When Ca^{2+} ions are present at high pH, the transmittance minimum of $\mathbf{6}^{4-}$ is shifted toward the red, resulting in a higher transmittance at 390 nm, and the tertiary amine of $\mathbf{7}^{4-}$ is still quenching the fluorescence – thus, 1 + 0 = 01. In the presence of both stimuli, both receptors of $\mathbf{7}^{4-}$ are complexed, eliminating the possibility of PET, and the batho- and hypsochromic shifts of $\mathbf{6}^{4-}$ cancel each other out, leading to a low transmittance at 390 nm. The result of this state of affairs is that 1 + 1 = 10. The overall effect is that, through analysis of the fluorescence spectrum and the UV transmittance, a pair of rather simple compounds can tell the operator just how many stimuli they have been exposed to during the analysis.

It is obvious that PET-based molecules can be engineered to provide a myriad of systems which provide outputs that can be predicted and described by truth tables. Indeed, adroit design can lead to a system capable of simple binary addition. However, in an electronic circuit, as the name implies, the half adder only does half the job. If a binary number longer than two digits is to be added, a full adder must be constructed [15]. With the circuitry depicted in Fig. 11, a full adder is a three-input device employing two half adders and another XOR gate. Attached, not only in parallel, but also in series with the output of one gate being the input of the next, one finds it very hard to imagine how this scheme can be accomplished in the solution phase and with chemical inputs. It is, therefore, desirable to divert our attention from chemical-input light-output systems toward a regime that can be controlled and monitored electronically, before finally addressing systems that can be operated in a device context.

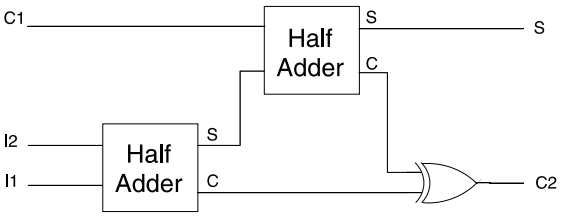

Fig. 11. A full adder for the addition of multi-digit numbers. The three inputs are I1 and I2 – the digits to be added – and C1 – the carry digit from the previous pair of inputs. Through a combination of two half adders and a further XOR gate, connected in both series and in parallel, the sum and carry outputs of the addition are produced

3
Co-Conformational and Topological Control of Interlocked and Interpenetrated (Super)Molecules

Before going on to discuss molecular electronic machines, it will be useful to describe their structural foundation at a molecular level, namely those based on interlocked molecules. Interlocked molecules can take on a variety of forms, the most common being catenanes, rotaxanes, knots [16], and carceplexes [17]. For the purpose of this review, only catenanes, rotaxanes and their geometrically related complexes – pseudorotaxanes [18] – will be discussed. When conferred with the ability to undergo some mechanical motion as a result of an applied stimulus – be it chemical, electrochemical, or photochemical – these interlocked molecular and interpenetrated supramolecular systems often take on the characteristics of molecular machines [19].

3.1
Rotaxanes

A rotaxane is a mechanically interlocked molecule in which one or more cyclic component(s) encircle(s) a dumbbell-shaped component. First made in 1967 by Harrison [20] utilizing a somewhat inefficient statistical approach, rotaxanes are a structurally diverse group of molecules. After Schill's elegant – yet ultimately low yielding – covalently directed syntheses of the late 1960s and early 1970s, the increased understanding of supramolecular chemistry in the late 1980s saw chemists forsaking statistical and covalently directed methods of rotaxane formation for template-directed approaches [21]. Using a wide range of recognition motifs, such as the hydrophobic effect [22], hydrogen bonding [23], metal-ligand coordination [24], and [C—H···O] interactions augmented by π-π interactions [25], rotaxanes can now be synthesized in high yields and on preparative scales. Rotaxanes can be constructed (Fig. 12) in a number of different ways, including stoppering, clipping, and slipping [26].

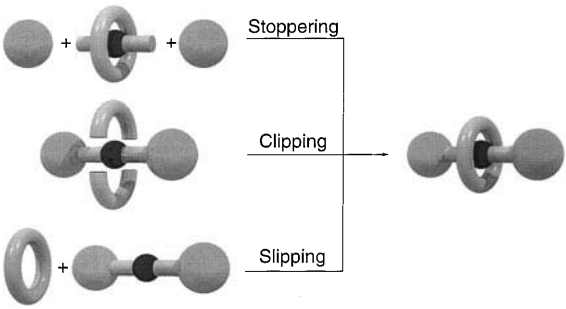

Fig. 12. Three mechanisms of rotaxane formation: stoppering is the addition of bulky end groups to a suitably functionalized pseudorotaxane; clipping is the formation of the macrocyclic component around a preformed dumbbell-shaped compound; slipping is the thermodynamically controlled self-assembly of the macrocycle around the dumbbell-shaped component at elevated temperatures

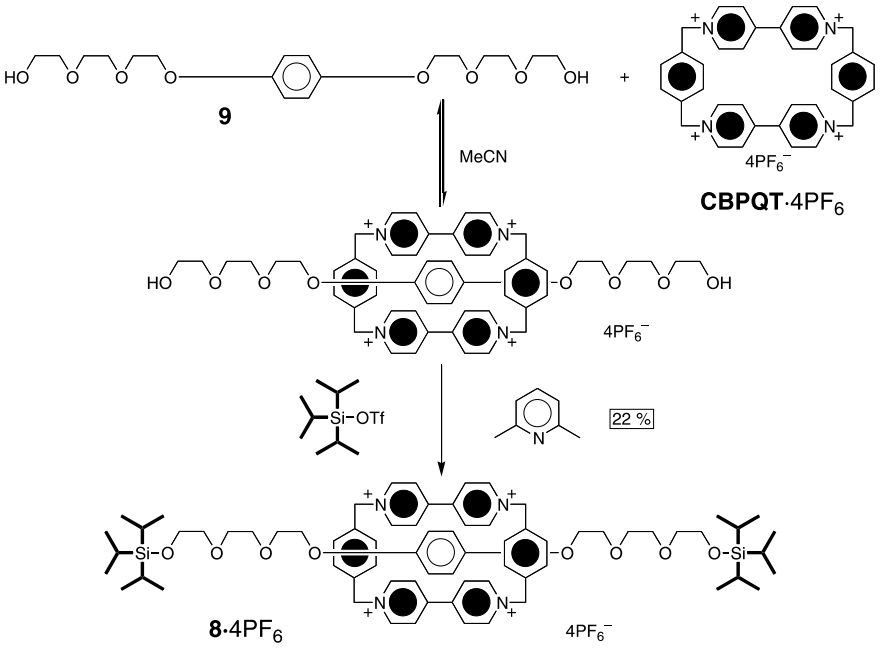

Fig. 13. Formation of the rotaxane **8**·4PF_6 by the stoppering approach. Bulky triisopropyl triflate is added to an equilibrating mixture of the cyclophane **CBPQT**·4PF_6 and linear component **9** in order to put the stoppers in place, resulting in a 22% yield of the desired rotaxane

The first rotaxanes to come out of our laboratories were obtained in moderate yields using the stoppering approach [27]. A mixture of $\mathbf{CBPQT}^{4+}$ and a linear oligoether **9** containing an electron-rich hydroquinone ring (Fig. 13) was treated with bulky triisopropylsilyl triflate (TIPSOTf) and lutidine as a base, resulting in a 22% yield of the corresponding TIPS-stoppered rotaxane $\mathbf{8}^{4+}$. At the time of the initial research, a number of interactions were considered to be responsible for the strong affinity between electron-rich threads and the tetracationic cyclophane – among them π-π stacking, charge-transfer and [C—H$\cdots\pi$] interactions, as well as [C—H$\cdots$O] hydrogen bonding, and electrostatic effects. Recent investigations [28] have shown the most dominant interactions by far are the [C—H$\cdots$O] hydrogen bonds from the protons α to the pyridinium nitrogens on the cyclophane to the oxygen atoms three removed along the polyether chains from the hydroquinone rings (Fig. 14).

Experimental and theoretical investigations on a related [2]rotaxane, which we call a molecular shuttle [29,30], have revealed that the tetracationic cyclophane can shuttle rapidly between two degenerate hydroquinone rings located in the dumbbell component. This discovery paved the way for the development [31] of a [2]rotaxane $\mathbf{10}^{4+}$ in which the recognition sites are different and in which their occupancy can be controlled (Fig. 15) by

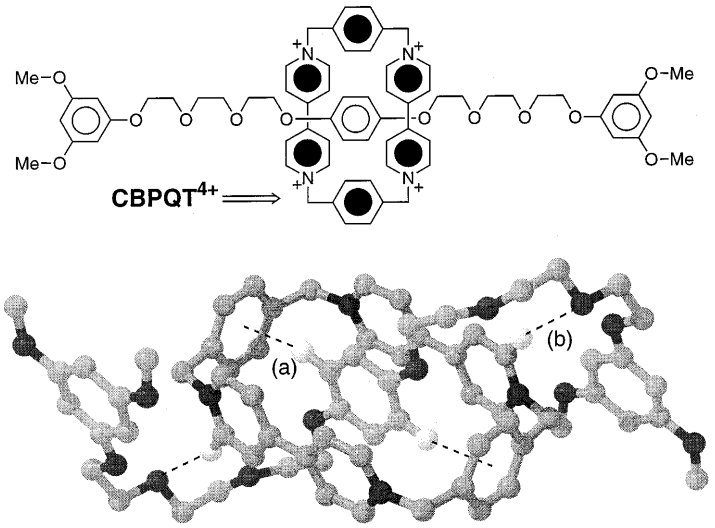

Fig. 14. The importance of [C—H···X] hydrogen bonding is displayed in the crystal structure of a [2]pseudorotaxane in which a polyether chain containing a centrally located hydroquinone ring is terminated by 3,5-dimethoxyphenyl groups and threaded through cyclobis(paraquat-*p*-phenylene) **CBPQT**$^{4+}$. *a* The central hydroquinone ring of the thread forms two [C—H···π] hydrogen bonds, and *b* two of the protons on the α-positions of the bipyridinium unit form strong [C—H···O] hydrogen bonds to the third oxygen atom along the oligoether chain from the hydroquinone ring

electrochemical or chemical means. In the ground state of this molecule, the cyclophane resides preferentially on the benzidine site. However, upon addition of TFA, the benzidine's nitrogen atoms become protonated, resulting in the translation of the cyclophane from this site to the biphenol one. This translational movement of the cyclophane can be envisaged as operating on the basis of electrostatic interactions, insofar as the tetracationic cyclophane resides preferentially on the neutral biphenol site, rather than on the dicationic benzidinium one. It is also, for this reason, that electrochemical oxidation of the benzidine to its radical cation results in the translation of the cyclophane from the benzidine site to the biphenol one. Both of these processes are reversible – the chemical route, by deprotonation with pyridine, and the electrochemical route, by reduction of the benzidine radical cation to its neutral state. This rotaxane **10**$^{4+}$ is therefore deemed to be a chemically and electrochemically controllable molecular switch.

In a recent full paper [32], a molecular switch **11**$^{6+}$, which can be driven either photochemically or electrochemically, has been described. Synthesized in a 59% yield from the corresponding dumbbell compound using the slippage approach, this [2]rotaxane contains (Fig. 16) two chemically distinct recognition sites around which the **BPP34C10** macrocycle can reside. Of the two sites, the unsubstituted bipyridinium unit is the better electron acceptor, and so it is around this site that the macrocycle encircles itself preferentially. However, upon reduction of the bipyridinium site to its radical cation – either

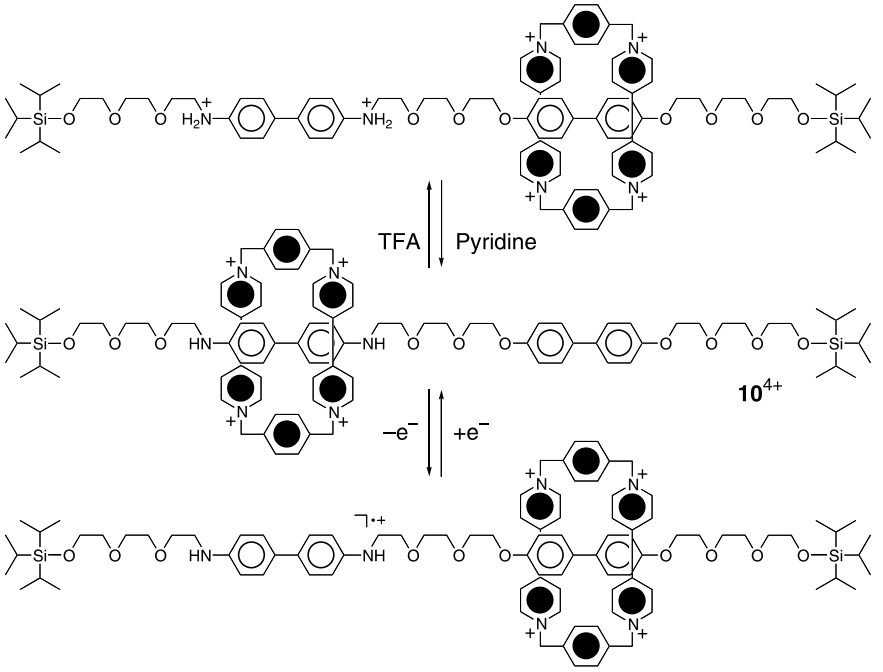

Fig. 15. A chemically and electrochemically controllable molecular shuttle $\mathbf{10}^{4+}$. When the dumbbell is in its unperturbed state, the cyclophane exists in an 84:16 ratio (CD_3CN, –44 °C) encircling preferentially the comparatively more π-electron-rich benzidine site. The cyclophane can be enticed to translate to the biphenol site exclusively either chemically – through protonation of the benzidine nitrogen atoms – or electrochemically – through oxidation of the benzidine unit to its radical cation. Both of these processes are completely reversible, through addition of base, or electrochemical reduction, respectively

electrochemically or via PET from the excited state of the photosensitizing ruthenium-containing stopper – the **BPP34C10** ring moves from the bipyridinium site to the 3,3′-dimethylbipyridinium one. This translational movement is fully reversible by subsequent electrochemical oxidation of the bipyridinium units.

In summary, it is possible to control the co-conformation of suitably designed rotaxanes by employing a number of different inputs. It is not unlikely that those non-transducing components with both electronic input and output could be among the first to be considered for use in a functioning molecular computer.

3.2 Pseudorotaxanes

A pseudorotaxane is defined [18] as a complex in which a linear component is threaded through the cavity of one or more cyclic components in a geometry reminiscent of that of a rotaxane. The difference between rotaxanes and

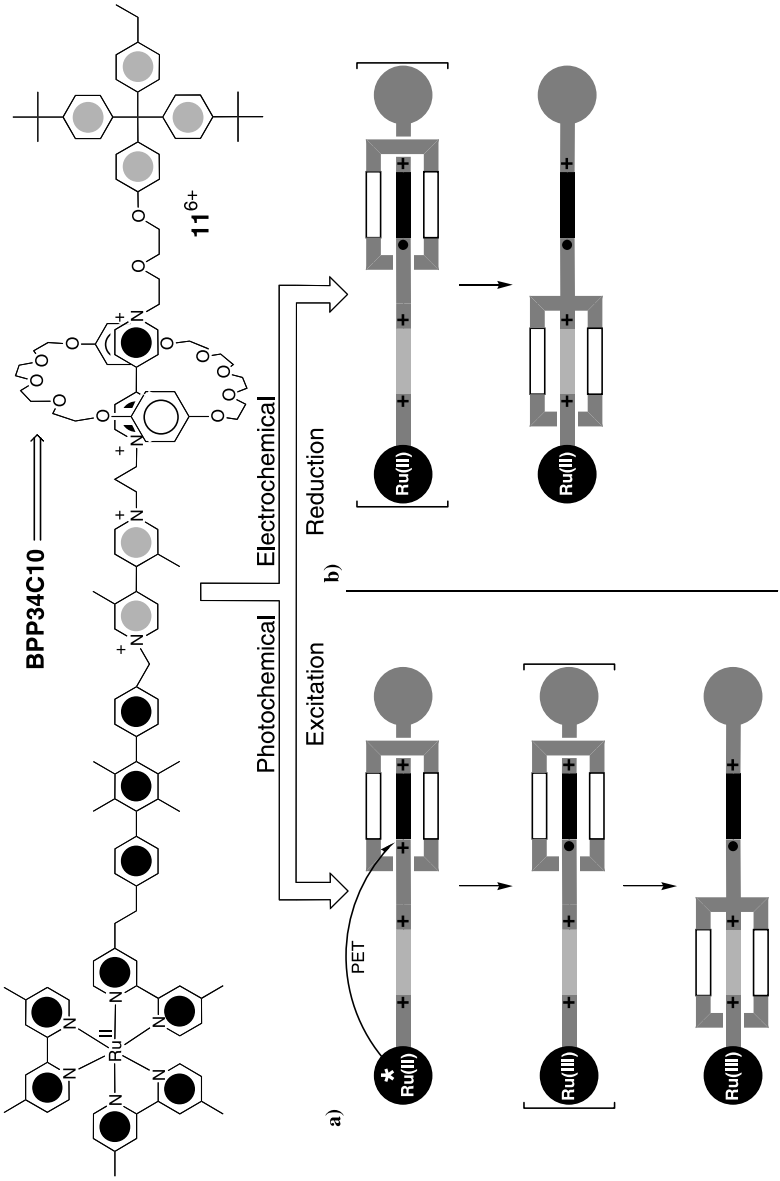
BPP34C10
11^6+
Photochemical
Excitation
Electrochemical
Reduction
PET
Ru(II)
Ru(III)
a)
b)

Fig. 16. A photo- and electrochemically controllable molecular shuttle. The unperturbed rotaxane $\mathbf{11}^{6+}$ exists preferentially in the translational isomer in which the **BPP34C10** crown ether resides around the bipyridinium unit. **a** Photochemical excitation of the $Ru(bipy)_3$ unit results in PET to the bipyridinium site, and consequent translation of the crown ether to the 3,3′-dimethylbipyridinium unit, which is a less efficient recognition site for the cyclophane $\mathbf{CBPQT}^{4+}$ than a bipyridinium system. This process occurs only in the presence of a sacrificial reductant which reduces the Ru(III) center back to its Ru(II) state in order to prevent charge recombination. **b** Conversely, upon electrochemical reduction of the bipyridinium unit, the crown ether takes up residency around the 3,3′-dimethylbipyridinium site. This process is reversed through electrochemical oxidation of the bipyridinium radical cation back to the dication

pseudorotaxanes is that pseudorotaxanes lack at least one of the bulky stoppers possessed by rotaxanes, and so their components are free to dissociate (Fig. 17). Consequently, the switching process now gains another level of complexity, compared to the simpler one-dimensional translational movements witnessed in rotaxane-based molecular machines.

Pseudorotaxanes – although not always the intended target of a synthesis – often surface in synthetic supramolecular chemistry, if only because, when catenanes or rotaxanes are in the process of being synthesized, there is frequently a pseudorotaxane formed somewhere along the synthetic route. When a pseudorotaxane is endowed with a suitably active recognition motif, the supramolecular chemist has the potential to address either the thread or the ring, and to influence the propensity of the system to form pseudorotaxanes or not.

The first publications describing [33] the controlled unthreading and rethreading of pseudorotaxanes from our laboratories appeared in the early 1990s. The pseudorotaxane machines produced to date fall into two distinct classes – one that relates to switches (basic on-off actions in response to an applied stimulus), and the other to gates (responses to two stimuli that mimic the operation of a logic function).

3.2.1
Pseudorotaxane-Based Switches

One of the earliest pseudorotaxane-based switches to emerge from our laboratories relied [34] upon the electrostatic repulsion between the macrocyclic component and a signaling stimulus. In this switch (Fig. 18), the thread

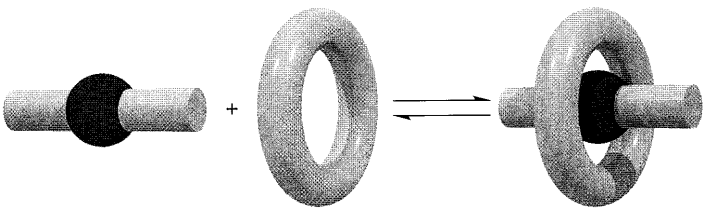

Fig. 17. A pseudorotaxane existing in equilibrium with its constituent linear and cyclic components

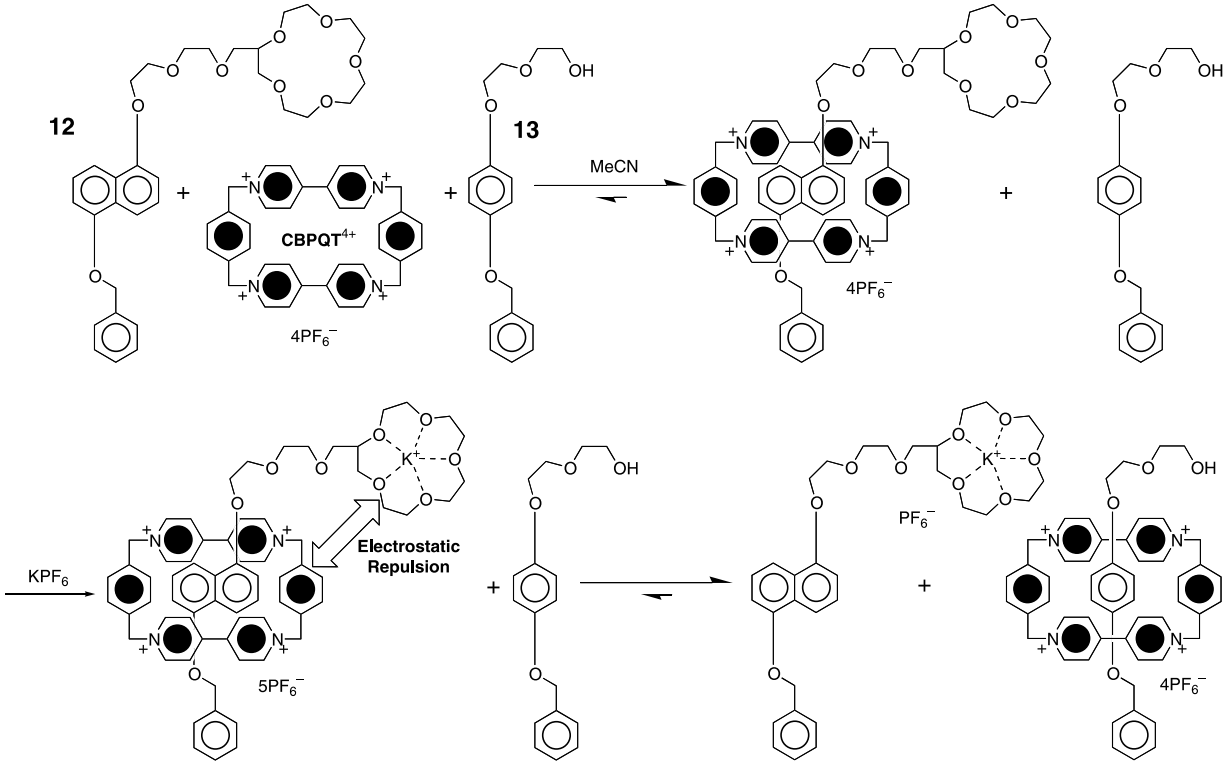

Fig. 18. A chemically driven supramolecular switch. In acetonitrile solution, the cyclophane **CBPQT**$^{4+}$ resides preferentially around the better electron-donating thread **12.** Addition of an excess of potassium ions to the solution results in a strong complex being formed between these cations and the crown ether portion of thread **12.** Electrostatic repulsion between the cyclophane and the thread leads to the cyclophane residing upon the poorer π-electron donating – yet electrically neutral – thread **13**

component **12** of the pseudorotaxane was designed such that it contained a 1,5-dioxynaphthalene recognition site, along with a potassium-responsive 15-crown-5 recognition motif. In acetonitrile solution, the tetracationic cyclophane **CBPQT**$^{4+}$ resides around the thread **12** with a high association constant of 900 M^{-1}. However, upon addition of 10 equivalents of potassium hexafluorophosphate to an equimolar solution of **CBPQT**$^{4+}$, **12**, and **13**, the crown ether moiety of the thread **12** binds a potassium ion. The electrostatic repulsion between the tetracationic cyclophane and the crown ether bound potassium ion forces the cyclophane to relinquish its occupancy of the 1,5-dioxynaphthalene-based site, and take up residency around the less efficient electron-donating hydroquinone-derived thread **13**.

Although this first pseudorotaxane-based switch illustrates quite efficiently that electrostatic repulsion between the metalated thread **12**·K^+ and the cyclophane **CBPQT**$^{4+}$ is a reliable paradigm for inducing the dethreading of a complex, there was no opportunity to demonstrate the reversibility of the system – i.e., the potassium ions cannot be removed from the solution so that the switch can return to its original state. It is clear that any switching system has to be based upon a reversible system, in which the switch can be reset at will. Such a system is portrayed in Fig. 19.

In this supramolecular system, the cyclophane **CBPQT**$^{4+}$ was found [35] to bind strongly to an aniline-terminated thread **14**. The design of this thread included two aniline units so that a relatively basic character could be conferred upon the thread. Addition of TFA to an equimolar mixture of

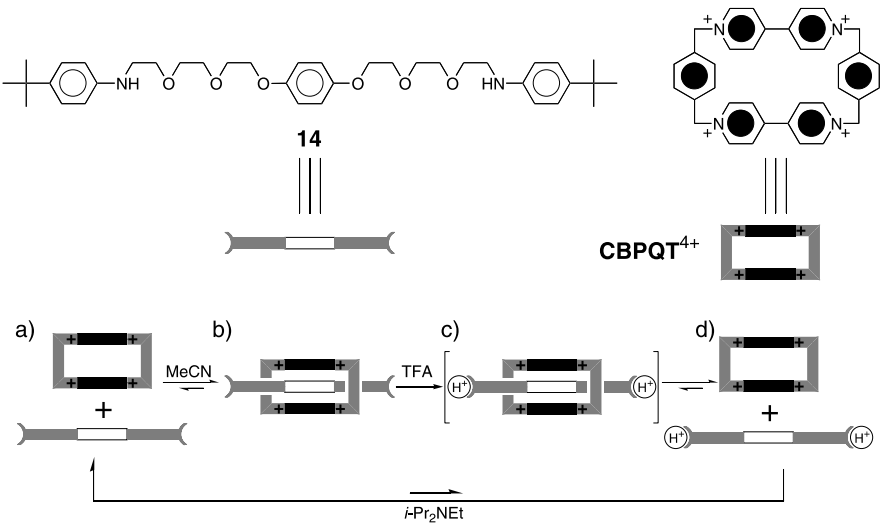

Fig. 19. When the *t*-butylaniline-terminated thread **14** is mixed in acetonitrile solution with the cyclophane **CBPQT**$^{4+}$, a pseudorotaxane is formed. Upon protonation of the anilino nitrogen atoms with trifluoroacetic acid (TFA), electrostatic repulsion leads to dissociation of the pseudorotaxane into its two constituents. Deprotonation of **14**·$2H^+$ leads to the pseudorotaxane being reformed

CBPQT^{4+} and **14** protonated both the anilino nitrogen atoms to give **14**·2H^{+}. This electrostatic repulsion is sufficient to remove the cyclophane from encircling the thread, and the solution changes from its characteristic red color – indicative of CT interactions between the cyclophane and the hydroquinone site – to that of a colorless solution, an observation which implies that the dicationic thread and tetracationic cyclophane now show absolutely no affinity for each other. However, in this supramolecular system, protons can be removed easily – in this case with *i*-Pr$_2$NEt – allowing the reversibility of the switching to be demonstrated. Addition of this base deprotonates the anilinium-derived thread and the cyclophane immediately resumes its occupancy of the thread, an event which is accompanied by the development of a deep red color. This demonstration of acid-base-controlled switching illustrates the potential for engineering reversibility into the dethreading of pseudorotaxanes.

However, with the goal of constructing nanoelectronic machinery in mind, an electrochemically switchable, and electronically readable switching system still had to be developed. The next two examples to be discussed serve to draw attention to the increasing complexity of the pseudorotaxane-based switches that can be constructed.

It is widely known that tetrathiafulvalene (**15**) – commonly known as **TTF** – can be easily oxidized to its radical cation and then on to its dicationic state. Previous research [36] from our laboratories had shown that reduction of the tetracationic cyclophane **CBPQT**$^{4+}$ reduces enormously its binding affinity for π-electron-rich guests. In the light of this knowledge, it was considered possible to develop a pseudorotaxane-based switch in which the switching process is not only controlled and monitored electrochemically, but in which it can be accomplished [37] in one of two ways.

In order to increase the affinity of **TTF** for binding to the cyclophane **CBPQT**$^{4+}$, a short polyether chain was appended to both ends of a **TTF** unit, resulting (Fig. 20) in **16**. Upon mixing the pseudorotaxane components in acetonitrile, the pseudorotaxane **16**⊂**CBPQT**$^{4+}$ formed immediately, as indicated by the appearance of a vivid green color. At sufficiently reducing potentials, the cyclophane can be reduced to its diradical dication. This redox process is accompanied by the dethreading of **16** from the now greatly less accommodating host cyclophane **CBPQT**$^{2+}$. Reoxidation of the cyclophane back to its tetracationic form resulted in the re-location of **16** within the host cavity. Thus, the system had been shown to be an electrochemically controllable switch. However, only one mode of switching has been investigated at this time. What would happen if the **TTF**-based thread **16** was electrochemically oxidized while residing inside the cyclophane cavity? Upon electrochemical oxidation of the thread to its radical cationic form, electrostatic interactions once again dominate and the thread is expelled from the cavity. This second mode of switching is also reversible in that reduction of the **TTF** unit back to its neutral form leads to the reformation of the pseudorotaxane **16**⊂**CBPQT**$^{4+}$. This system – as a consequence of the rich redox chemistry associated with its components – can therefore be said to act as a dual mode switch, i.e., switching from the pseudorotaxane to the free

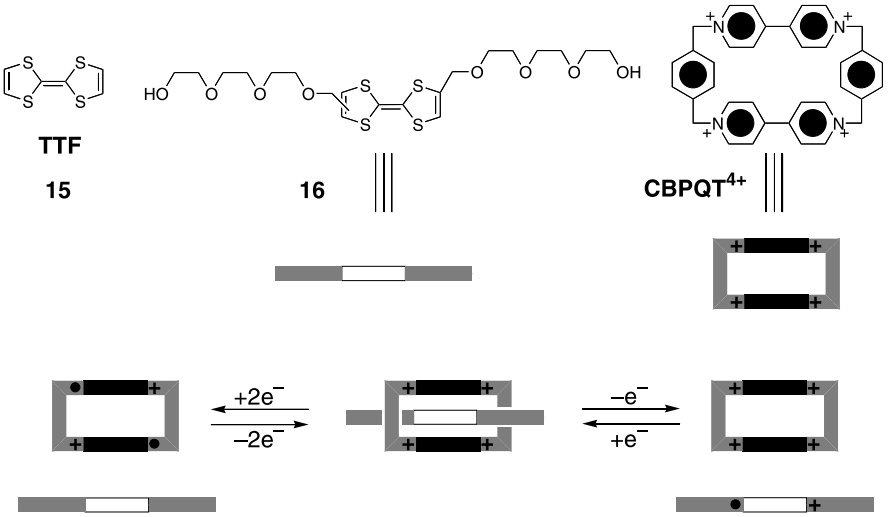

Fig. 20. When the tetrathiafulvalene (**TTF**)-containing thread **16** is mixed in acetonitrile solution with cyclophane **CBPQT**$^{4+}$, a pseudorotaxane is formed. This complex can be dissociated in one of two ways – reduction of the cyclophane to its diradical dication, or oxidation of the **TTF** portion of the thread **16** to its radical cation. Both processes are reversible, by oxidation of the cyclophane and reduction of **16**, respectively

components will occur upon oxidation of the thread or reduction of the cyclophane.

The next incremental step up the ladder of complexity of switching was the development [38] of a three-pole supramolecular switch. Such a switch is one that can be adjusted to any one of three different settings. Bolstered by the success and rich electrochemistry of the dual mode switch, a three-pole switch was designed without delay and investigated.

We knew from the results of previous research [36] that **TTF** is an excellent guest for the cyclophane **CBPQT**$^{4+}$ and that both of its oxidized forms are simply not bound by **CBPQT**$^{4+}$. This observation raises the rather intriguing question – if the cationic forms of **TTF** are not capable of being bound inside the cavity of the π-electron-deficient receptor **CBPQT**$^{4+}$, could they possibly be bound inside a cavity flanked by π-electron-rich ring systems, such as those present in a 1,5-dioxynaphthalene-derived crown ether, 1,5-dinaphtho [38]crown-10 (**1/5DN38C10**)? In order to answer this question, a 1:1:1 solution of **TTF**:**CBPQT**·4PF_6:**1/5DN38C10** was prepared (Fig. 21). The dark green color of the solution confirmed that the **TTF** had assumed its expected occupancy inside the cavity of the tetracationic cyclophane. Electrochemical oxidation of the **TTF** to its radical cation resulted in its predicted expulsion from the cavity of the host. However, as evidenced by the redox potential of the **TTF/TTF**$^{+\bullet}$ couple – in a solution containing **TTF** and **1/5DN38C10** only, this first oxidation potential is unchanged – the radical cation is not sufficiently π-electron-poor to become encircled by the macrocyclic polyether. Only when

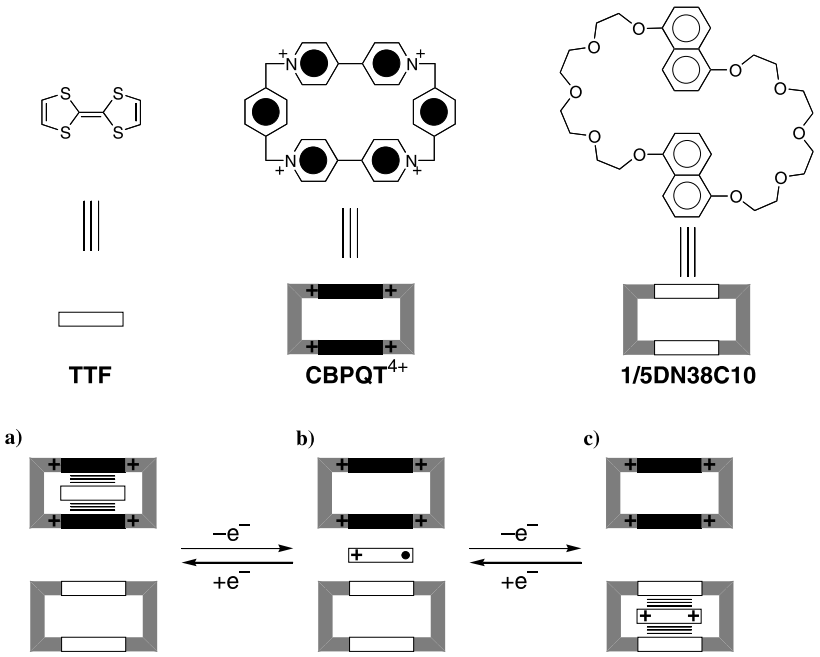

Fig. 21. The three-pole switch can exist in any one of three states. **a** When the three components **TTF**, **CBPQT**$^{4+}$, and **1/5DN38C10** are mixed in solution, **TTF** resides within the cavity of the cyclophane. **b** Oxidation of the **TTF** to its radical cation leads to its expulsion from the tetracationic cyclophane. **c** Further oxidation to the **TTF** dication leads to its encirclement by **1/5DN38C10**

the monocation is oxidized further to its dicationic state does **TTF** assume the occupancy of the cavity within the crown ether molecule. Consistent with previous reports, this redox cycle is completely reversible and recyclable. It is, therefore, reasonable to conclude that this three-component mixture is capable of acting as a three-pole supramolecular switch. Simply by addressing the oxidation state of **TTF**, the solution can be switched reversibly and repeatably between three states: (i) neutral **TTF** encircled by the cyclophane, (ii) a discrete three-component mixture of crown ether, tetracationic cyclophane, and **TTF** radical cation, and (iii) the **TTF** dication residing within the crown ether's cavity.

3.2.2
Pseudorotaxane-Based Logic-Displaying Systems

Although it is not operated by an electrochemical read-and-write regime, the following example serves to illustrate that pseudorotaxanes can be tailored individually to display functions reminiscent of logic gates.

The development of an acid-base-controllable XOR logic gate based upon a pseudorotaxane geometry relied upon a very strict set of guidelines being

adhered to in the process. For example, assuming that a pseudorotaxane geometry predominates in solution, such a complex should be capable of undergoing a reversible change upon the addition of acid – i.e., protons must interact more strongly with one of the discrete pseudorotaxane components than with the complementary component, or they should protonate a vital site in the complex, thus destroying recognition between the thread and the bead. The same has to be true upon addition of base – it must either interact strongly with one of the pseudorotaxane components or it should deprotonate a site vital for binding. In the presence of both stimuli, a simple acid-base reaction will occur and so the pseudorotaxane will remain intact.

In a paper published [39] in 1997, it was the interactions with acid and base that provided the driving force for topological control over the system. When 2,3-dinaphtho[30]crown-10 (**2/3DN30C10**) is mixed with the π-electron-deficient 2,7-dibenzyl-2,7-diazapyrenium ($\mathbf{DAP(Bn)_2}^{2+}$) dication in 9:1 v/v CH_2Cl_2–MeCN solution (Fig. 22), a pseudorotaxane is formed by virtue of a combination of [C—H···O] and π-π interactions. Upon addition of acid, strong hydrogen bonds are formed between the crown ether and protons, forcing the guest to leave the inside of the macrocyclic polyether. Addition of an equivalent of tributylamine results in an acid–base reaction that destroys hydrogen bonding between the free protons and the crown ether, thus allowing the thread to enter the crown ether once again. If the initial pseudorotaxane is treated with tributylamine, then a strong complex is formed between the free base and the diazapyrenium cation [40]. This competing interaction also disfavors formation of a pseudorotaxane, which, once again, for different reasons, is dismembered. Addition of acid destroys the amine complex and both fluorescence and UV-Vis spectroscopy indicate that the pseudorotaxane is reformed. The truth table shown in Fig. 22, when compared with that in Table 2, confirms that this behavior is analogous to that of an XOR logic gate, provided the presence or absence of acid or base is counted as an input of 1 or 0, respectively, and pseudorotaxane formation represents a positive output.

Thus, it has been shown that pseudorotaxanes offer diverse opportunities for the incorporation of switching and gating characteristics – operating under a range of different regimes – into molecular systems.

3.3 Catenanes

Consisting of two or more interlocked rings, catenanes constitute another member of the family of interlocked molecules. First made by Wasserman [41] in 1960 using a statistical approach – the random occurrence of a linear species folding round on itself in a macrocyclization while itself being threaded through another macrocycle – catenanes leapt out of the realm of being little more than scientific curiosities into a world of potentially useful compounds only when the percentage yields associated with their construction were increased beyond single digits, into the high double digit ballpark.

The breakthrough in catenane synthesis occurred when the statistical and covalent template methods were abandoned in favor of approaches that relied

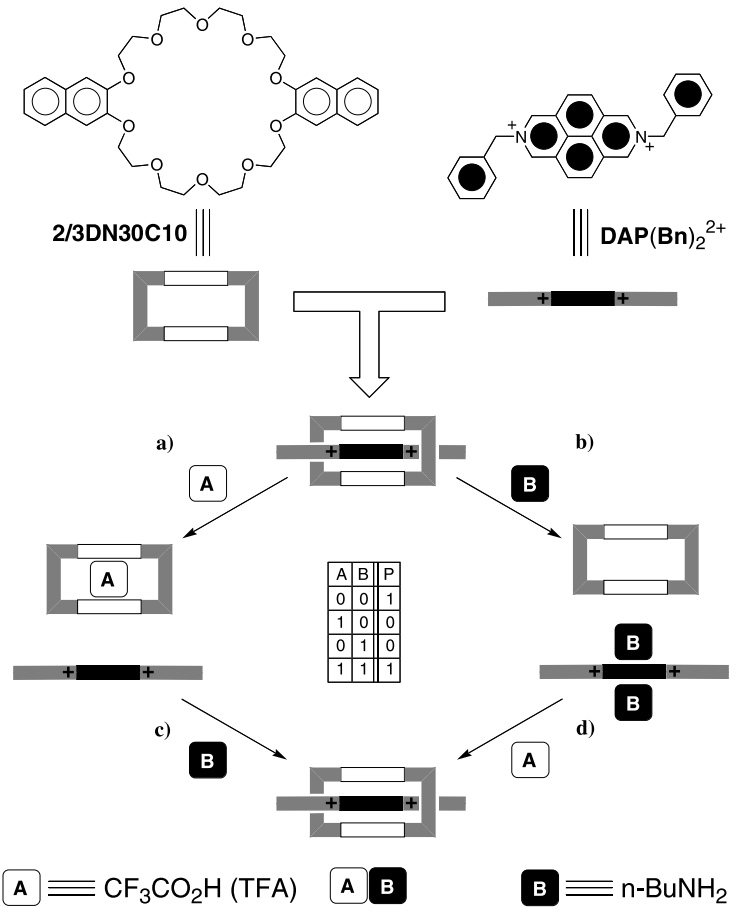

Fig. 22. A binary mixture of **2/3DN30C10** and **DAP(Bn)**$_2^{2+}$ behaves in a manner analogous to an XNOR gate. In the absence of acid or base, a strong complex with pseudorotaxane geometry is formed. **a** Upon addition of trifluoroacetic acid (**A**), by virtue of the formation of a strong complex with the crown ether, protons displace the **DAP(Bn)**$_2^{2+}$ from the cavity of **2/3DN30C10**. **b** Neutralization of the solution with *n*-butylamine (**B**) results in the reformation of the pseudorotaxane. **c** If the initial mixture is treated with base, a strong interaction between *n*-butylamine and **DAP(Bn)**$_2^{2+}$ leads to the destruction of the complex. **d** Neutralization of the solution with TFA leads to a simple acid–base reaction, and pseudorotaxane formation. If the two inputs are acid and base (**A** and **B**), with a 1 signaling presence and a 0 absence, this system behaves as an XNOR gate, if pseudorotaxane formation is represented by an output of 1

upon the propensity of suitably designed and tailored molecules to self-assemble into geometries suitable for catenane formation. This template-directed method – in effect, supramolecular assistance to covalent synthesis – has led to the production of a large number of catenanes being reported in the literature during the 1990s. In particular, the use of amide hydrogen bonding

[23,42], π-π stacking [43], the hydrophobic effect [22], metal-ligand coordination [24, 44], and [C—H···O] interactions augmented by π-π stacking [45], has produced a large number of catenanes with very different properties [25].

The account of the first catenane self-assembled in our laboratories appeared in the literature in 1989. At the time, it was already documented that the tetracationic cyclophane, cyclobis(paraquat-*p*-phenylene) **CBPQT**$^{4+}$, was capable of binding π-electron-rich aromatic rings. The key step in the development of the catenane synthesis was to use a macrocyclic polyether to template the formation of the cyclophane instead of an acyclic polyether. The use of the macrocyclic polyether bis-*para*-phenylene[34]crown-10 (**BPP34C10**) as a template – when the dicationic intermediate **16**$^{2+}$ was reacted with *p*-xylylene dibromide – resulted in the formation (Fig. 23) of the [2]catenane **17**$^{4+}$ in 70% yield. Dynamic ^{1}H NMR experiments revealed the full subtlety and complexity of the relative ring motions in this degenerate [2]catenane. Three different dynamic processes were identified (Fig. 24) – two involving relative circumrotational movements of the rings and one corresponding to a rocking motion of one ring relative to the other. These mechanical processes involving degenerate co-conformers of the catenane led inexorably to the question of whether or not the circumrotational movements could be controlled and possibly even switched.

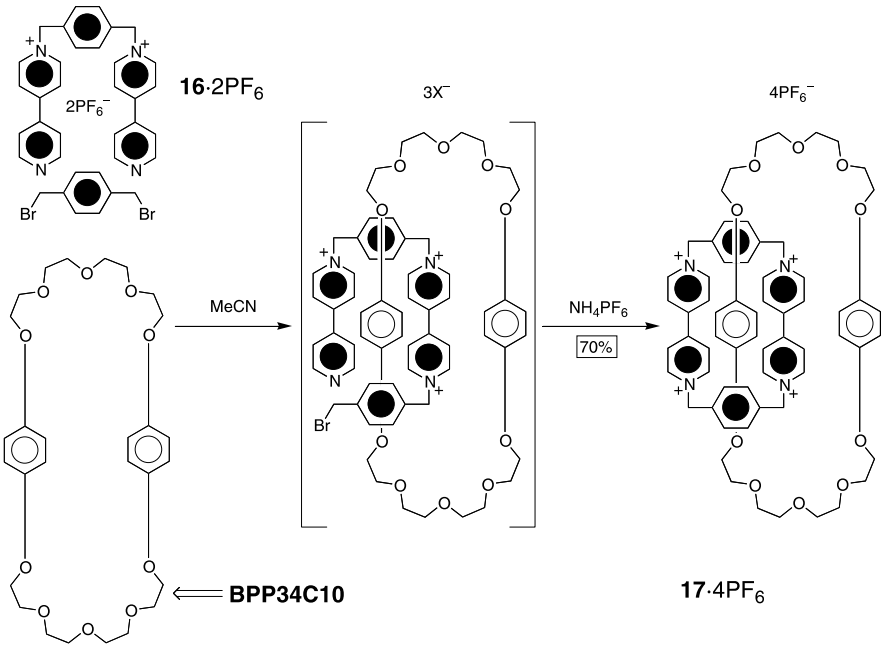

Fig. 23. Reaction of the salt **16**·2PF$_6$ with *p*-xylylene dibromide in the presence of three equivalents of **BPP34C10**, followed by ion exchange to hexafluorophosphate counterions, leads to the formation of [2]catenane **17**·4PF$_6$ in 70% yield

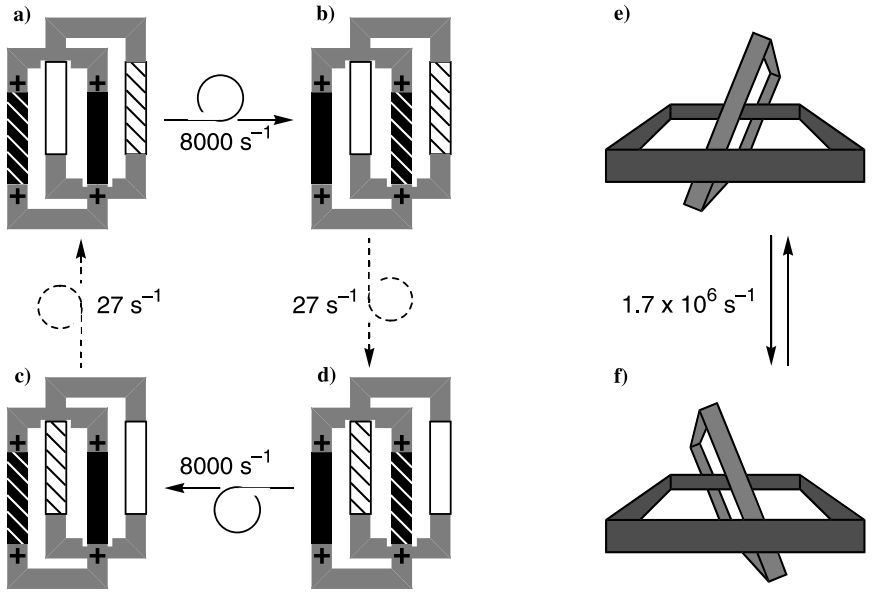

Fig. 24. Three different dynamic processes occur in the [2]catenane $\mathbf{17}^{4+}$. The crown ether circumrotates through the cyclophane (**a** ⇄ **c** and **b** ⇄ **d**) 27 times/s at 298 K, the cyclophane circumrotates through the cavity of the crown ether(**a** ⇄ **b** and **c** ⇄ **d**) 8000 times/s, and the two components rock with respect to each other (**e** ⇄ **f**) nearly 2 million times/s at 298 K

One of the appealing aspects of catenanes that are based upon the interactions between π-electron-rich crown ethers and π-electron-deficient tetracationic cyclophanes is the modularity that can be employed (Fig. 25) in their template-directed syntheses. Virtually any π-electron-rich crown ether with identical or different recognition sites can be introduced into this class of catenanes. Also, by exploiting the different ways in which cyclophanes can be clipped around the preformed ring of a macrocyclic polyether, it is possible to incorporate [46] different π-electron-deficient units into the cyclophanes.

Much of our early research was devoted to determining the co-conformational preferences of unsymmetrical crown ethers containing [47] different π-electron-rich units in catenanes incorporating cyclobis(paraquat-*p*-phenylene). It was only in 1995, when the fourth paper in our Molecular Meccano series was published [48], that the real versatility and potential for the use of "donor-acceptor" catenanes in molecular electronic devices was demonstrated. As a result of an investigation of a large series of catenanes incorporating unsymmetrical cyclophanes, such as that with one bipyridinium unit, and one π-extended (*E*)-1,2-bis(4,4′-bipyridinium)ethylene unit, an electrochemically switchable catenane, based on [C—H···O] interactions augmented by π-π interactions, was obtained. The vinylogous bipyridinium recognition site shows a much lower binding affinity for π-electron-rich ring systems and – crucially – a much higher reduction potential than its bipyridinium cousin.

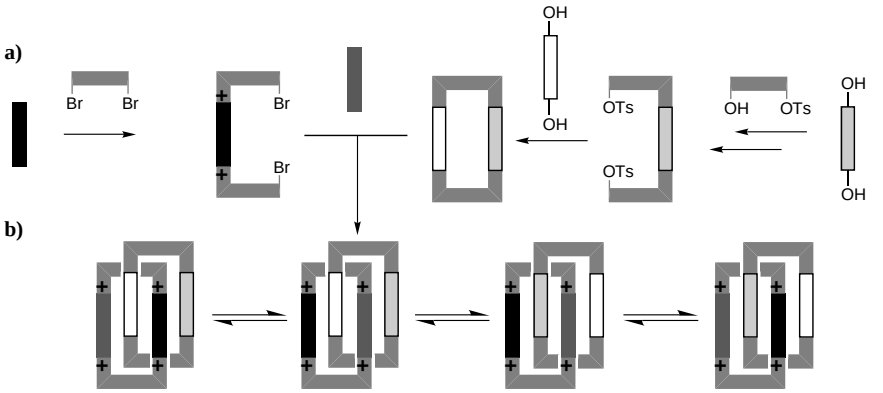

Fig. 25. The modular synthetic scheme outlined in **a** shows how virtually any crown ether containing π-electron-rich units can be catenated with any cyclophane that contains two π-electron-deficient units. **b** When both the crown ether and the cyclophane contain two different recognition sites, then four translational isomers can, in principle, be observed

These happy coincidences meant that, if this unsymmetrical tetracationic cyclophane is concatenated with a symmetrical crown ether, there is every chance that the bipyridinium unit of the cyclophane will reside preferentially inside the cavity of the π-electron-rich macrocyclic polyether. With a lower reduction potential than its extended counterpart, the bipyridinium unit will be reduced first in a voltammetric experiment, and hence it is expected that the cyclophane will circumrotate in order that the vinylogous bipyridinium recognition site – now a much better π-electron-receptor system than the radical cation of the bipyridinium unit – resides within the cavity of the crown ether.

The rationale behind this design was justified upon electrochemical investigation of the [2]catenane $\mathbf{18}^{4+}$. This catenane – synthesized in 43% yield (Fig. 26) from crown ether **BPP34C10**, the bipyridinium dibromide derivative $\mathbf{19}^{2+}$ and (*E*)-1,2-bis(4,4′-bipyridyl)ethylene – was demonstrated to consist, in solution, of mainly "co-conformer" **A**, with the more powerful π-electron-accepting bipyridinium unit located inside the cavity of the crown ether. Upon electrochemical reduction of this bipyridinium unit, the cyclophane undergoes a circumrotational movement with respect to the crown ether such that the profoundly more electron-deficient π-extended bipyridinium unit resides inside the cavity of the crown ether, affording "co-conformer" **B**. When the bipyridinium radical cation is oxidized back down to its dicationic state, the opposite circumrotational process occurs and the system reverts back to "co-conformer" **A**, its ground state [49].

This switching process – although undoubtedly appealing – was not considered at the time for integration into a molecular electronic device for a number of reasons – one of which being that, although "co-conformer" **A** is the most prevalent one in solution, it is not the sole "co-conformer". In acetone solution at 213 K – the highest temperature at which the co-

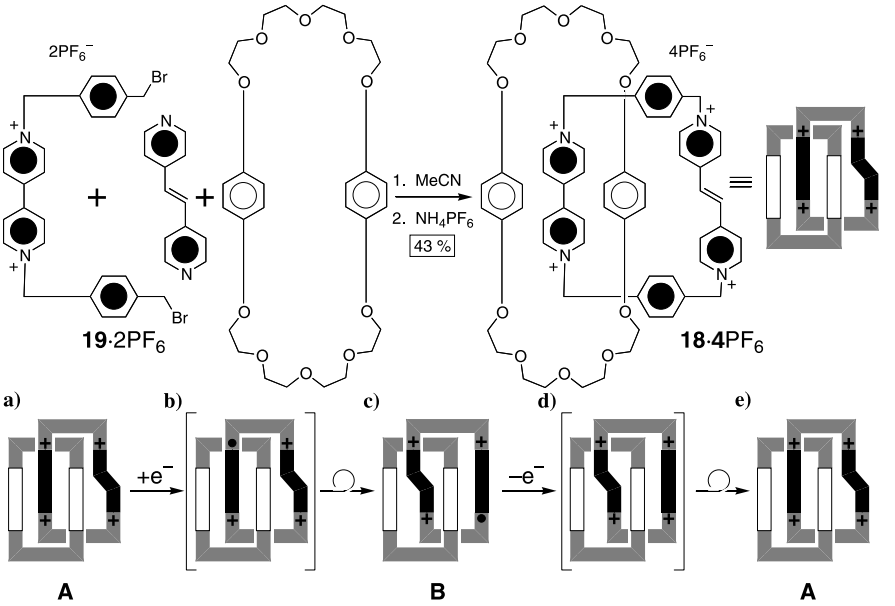

Fig. 26. When the dibromide salt **19**·2PF_6 is reacted with bis(pyridine)ethylene in the presence of **BPP34C10** in acetonitrile, the resultant [2]catenane **18**·4PF_6 is formed in 43% yield. The crown ether resides preferentially around the bipyridinium site in a 92:8 ratio with respect to occupancy around the bis(pyridinium)ethylene site – "co-conformer" **A**. **a** Upon electrochemical reduction, the best electron donor – the bipyridinium site – is reduced first. This reduction leads **b** to the unfavorable situation in which the bipyridinium radical cation is located within the cavity of the crown ether, and so the cyclophane circumrotates **c** to locate the bis(pyridinium)ethylene site within the crown ether cavity – "co-conformer" **B**. This process is reversible, in that **d** reoxidation of the bipyridinium radical cation leads to **e** circumrotation of the cyclophane to yield the [2]catenane in its original state – "co-conformer" **A**

conformational preference of the molecule can be measured – the occupancy is 92:8 in favor of the "co-conformer" (**A**) in which the bipyridinium unit resides inside the cavity of the crown ether. Looking back, however, and with the knowledge that we currently possess, there is no real reason why these phenomena should hamper device operation, and indeed we now intend to investigate the capability of this catenane to perform in a device context.

Armed with the knowledge gained during the design and testing of the three-pole supramolecular switch, we set about fashioning a [2]catenane in which the redox-controllable sites are located within a crown ether ring which is catenated by the tetracationic cyclophane. From previous experiments, it was known (Fig. 27) that the binding constant between the tetracationic cyclophane **CBPQT**$^{4+}$ and **TTF** is in excess of 8000 M^{-1}. However, experience with the dual-mode and three-pole switches reminded us that both of the oxidized forms of **TTF** – the radical cation and the dication – are totally disinclined to bind inside the cyclophane's cavity. Prior experiments on the

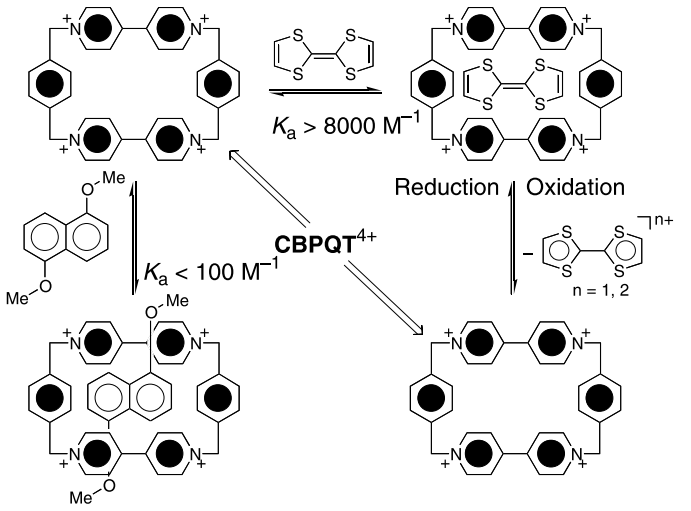

Fig. 27. The rationale behind the design of an electrochemically switchable [2]catenane. The neutral form of **TTF** is bound very strongly within the cyclophane **CBPQT**$^{4+}$. However, when it is oxidized to either of its cationic forms, **TTF** shows no affinity whatsoever for the cyclophane. 1,5-Dimethoxynaphthalene exhibits moderate binding toward the cyclophane. All binding constants K_a were measured in acetonitrile at 298 K

host-guest chemistry of **CBPQT**$^{4+}$ had also revealed that 1,5-dimethoxynaphthalene exhibits a binding constant toward the cyclophane of the order of 100 M^{-1}. This difference led us to ask [50] whether a crown ether could be synthesized in which one of the recognition sites has a 1,5-dimethoxynaphthalene-like constitution while the other one is based on a **TTF** unit. If such a molecule could be constructed, then there is every possibility that it could be catenated by cyclobis(paraquat-*p*-phenylene), yielding a switchable [2]catenane.

Synthesized (Fig. 28) in 32% yield [51,52] starting from 1,5-dihydroxynaphthalene, the macrocyclic polyether **20** contains a 1,5-dioxynaphthalene unit and a bis(methanol)**TTF** ring system, linked in a cyclic fashion by two tetraethylene glycol chains. When this macrocyclic polyether was reacted with the precursors to **CBPQT**$^{4+}$, the resulting [2]catenane **21**$^{4+}$ was formed in 23% yield.

UV-Vis spectroscopy of the [2]catenane **21**$^{4+}$ revealed – by virtue of the presence of a characteristic broad charge-transfer band with a maximum absorbance at 835 nm and the absence of a peak at 515 nm – that the sole co-conformer in a room temperature acetonitrile solution is the one in which the **TTF** unit resides inside the cavity of the tetracationic cyclophane. Upon either chemical or electrochemical oxidation of the **TTF** unit to its radical cationic (or dicationic) state, the Coulombic repulsion between the cyclophane and the positively charged **TTF** unit leads to its expulsion from the cavity of the cyclophane. As the 1,5-dioxynaphthalene site is left untouched by the **TTF** oxidation and has an intermediate affinity for residing within the cyclophane,

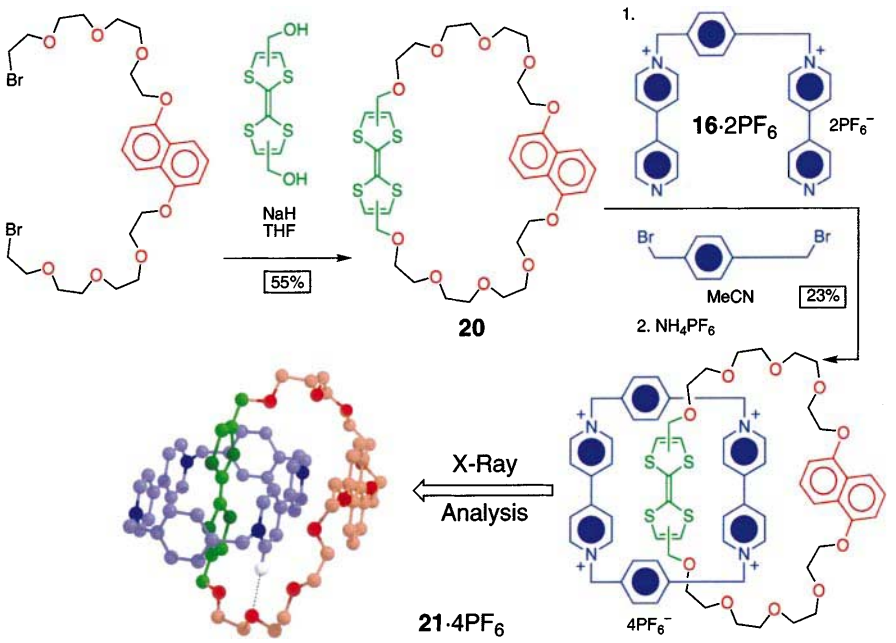

Fig. 28. Synthesis of the electrochemically switchable [2]catenane **21**·4PF_6. Obtained in 55% yield from the naphthalene-containing dibromide and bis(methanol)**TTF**, the crown ether **20** can be catenated under standard conditions to give the [2]catenane **21**·4PF_6 in 23% yield. As well as the expected π-π interactions, a strong [C—H···O] hydrogen bond is also observed

it is this unit which now assumes the occupancy of the cavity. Electrochemical and UV-Vis evidence suggests that this switching process is essentially digital in nature – i.e., the occupancy ratio of the cyclophane switches from 100:0 for **TTF**:1,5-dioxynaphthalene to 0:100 upon oxidation (Fig. 29). The reduction process is swift, quantitative, and totally reversible. Thus, it has been demonstrated that the [2]catenane $\mathbf{21}^{4+}$ acts as a robust molecular switch in the solution phase, where switching can be repeated quite reliably, as well as being controlled and monitored electrochemically.

4
Incorporating Switchable Molecules into Devices

4.1
Magnetic Memory

Before launching into the electronic aspects of the devices built so far, it is prudent to discuss, at a facile level, the basic operation behind magnetic memory storage. When a magnetic bit is written, the dipoles are aligned in a

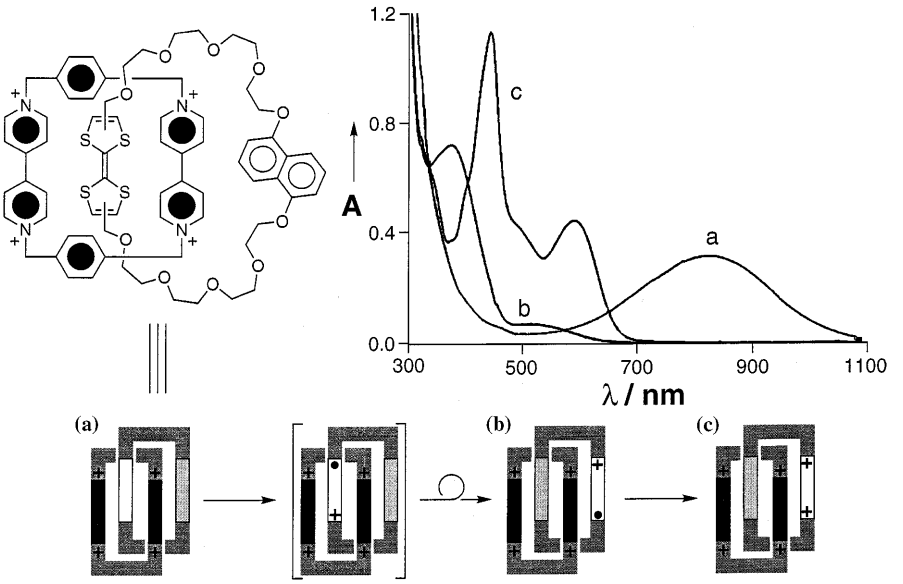

Fig. 29. The UV-Vis spectrum of [2]catenane **21**·4PF_6 shows – **a** by virtue of a strong charge transfer band at 830 nm – exclusive occupancy of the cyclophane cavity by the **TTF** unit. **b** Addition of one equivalent of $Fe(ClO_4)_3$ oxidizes the **TTF** unit to its radical cation, which results in the circumrotation of the crown ether, such that the 1,5-dioxynaphthalene unit resides within the cyclophane's cavity, as indicated by the appearance of a charge-transfer band at 515 nm. **c** Addition of a further equivalent of iron perchlorate yields the **TTF** dication which remains outside the cavity. Chemical reduction of the **TTF** dication back to its neutral form yields the [2]catenane in which the **TTF** resides exclusively within the cyclophane's cavity

certain direction, depending on the information to be encoded therein. Let us imagine (Fig. 30) that, if all the magnetic dipoles are aligned and pointing upwards, the information encoded is a "1" and, if the dipoles point downward,

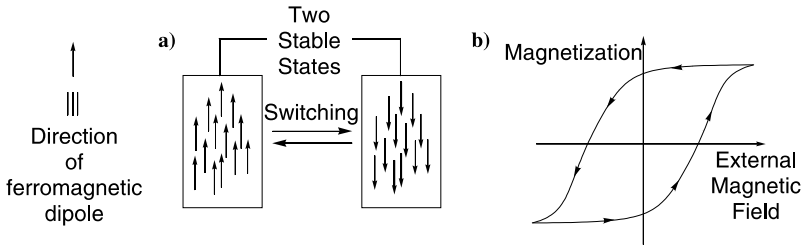

Fig. 30. Representation of information storage using a magnetic bit. **a** The bit can exist in either of two stable states – in this case, with parallel alignments of the individual dipoles, pointing either up or down. **b** The mean dipole direction can be switched repeatedly and reversibly at high and low external magnetic field, and interrogated at zero field, where the bit is not perturbed

then a value of "0" is reported. Because a barrier exists between the two states, it takes an energy input to realign all the magnetic dipoles in the opposite direction, i.e., a threshold external field must be applied before the net magnetization of the magnetic bit is realigned. However, at zero external magnetic field, as a consequence of the large hysteresis between the two dipolar alignments, there are two distinct magnetizations that can be read – positive, corresponding to a "1" and negative, corresponding to a "0". Thus, the magnetic bit can be written at high and low applied magnetic fields and yet can be read at zero applied field where interrogation of the system will not lead to its perturbation.

If any systems we design are to operate as potential electronically controllable molecular-based memory devices, then they must show a similar hysteretic profile, except "Magnetization" has to be replaced by "Current" and "External Magnetic Field" by "Voltage".

4.2 Aligning Catenanes in Two Dimensions

One of the more pressing questions that is asked of the proponents of the molecular computer has been and still is how to organize inherently disordered molecules into potentially useful arrays. It is obvious that solution-based systems – although very satisfying intellectually – are doomed to the realm of scientific curiosity unless they can be incorporated into useful, practical devices in which single, or collections of, molecules can be addressed without influencing each other. One route by which this objective can be achieved, and which corresponds to conventional silicon devices – at least at a conceptual level – is to immobilize the pertinent molecules onto a solid support and then to build up a framework around which the molecules can be addressed.

Fortunately, ordering suitably tailored molecules in two dimensions at interfaces and then transferring them onto surfaces is a very widely used technique. Although the deposition of appropriately functionalized molecules onto metal surfaces provides a reliable method for the formation of self-assembled monolayers, we feel that the most versatile, and easily adaptable, paradigm for the formation of monolayers is to produce a Langmuir film at an air–water interface. With judicious design, bipolar molecules can be programmed to align themselves in a two-dimensional array at the interface between air and water. Thereafter, a number of techniques exist by which monolayers can be transferred onto solid supports.

Initial investigations from the early 1990s onwards have provided [53] a reliable means by which the tetracationic cyclophane **CBPQT**$^{4+}$ and a number of [2]- and [3]catenanes can be self-organized at the air–water interface. Although an amphiphilic character is usually required to obtain a Langmuir monolayer, it is obvious that the catenane **17**$^{4+}$ – when associated with four hexafluorophosphate counterions – possesses few bipolar properties. This realization is reflected in the fact that the hexafluorophosphate (PF_6^-) salt of **17**$^{4+}$ forms brittle monolayers that are difficult to reproduce. The amphi-

philicity – and also the quality and reproducibility of the associated monolayers – of the catenanes was increased enormously by replacing the PF_6^- counterions with dimyristoylphosphatidyl ($DMPA^-$) counterions. The long alkyl chains of the $DMPA^-$ counterion confer a high degree of lipophilicity upon the system. With these counterions aligned in a parallel manner at a surface (Fig. 31), the phosphate portion will clearly be aligned pointing toward the aqueous substrate. In order to balance this high negative charge density, a layer of tetracationic catenanes associates near the surface as a highly ordered monolayer. This "supramolecular amphiphilicity" leads to the formation of robust monolayers that can be readily reproduced.

The tetrakis($DMPA^-$) salt of redox-switchable [2]catenane $\mathbf{21}^{4+}$ was also tested for its ability to form Langmuir films. In its tetracationic form, the Π/A isotherm revealed (Fig. 32) an area per molecule of approximately 120 $Å^2$. This

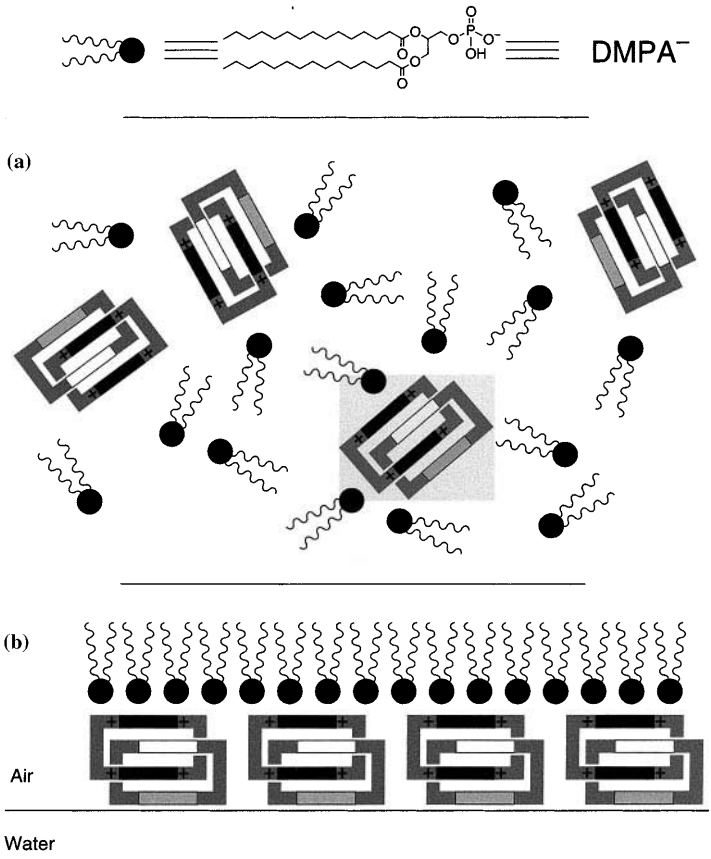

Fig. 31. **a** In the solution phase, the [2]catenane $\mathbf{21}^{4+}$ – as its tetrakis($\mathbf{DMPA}^-$) salt – exists in a totally disordered state. **b** However, upon deposition at an air/water interface, the resultant monolayer consists of a two-dimensional lattice of tetracationic catenanes below a layer of parallel-aligned $\mathbf{DMPA}^-$ counterions

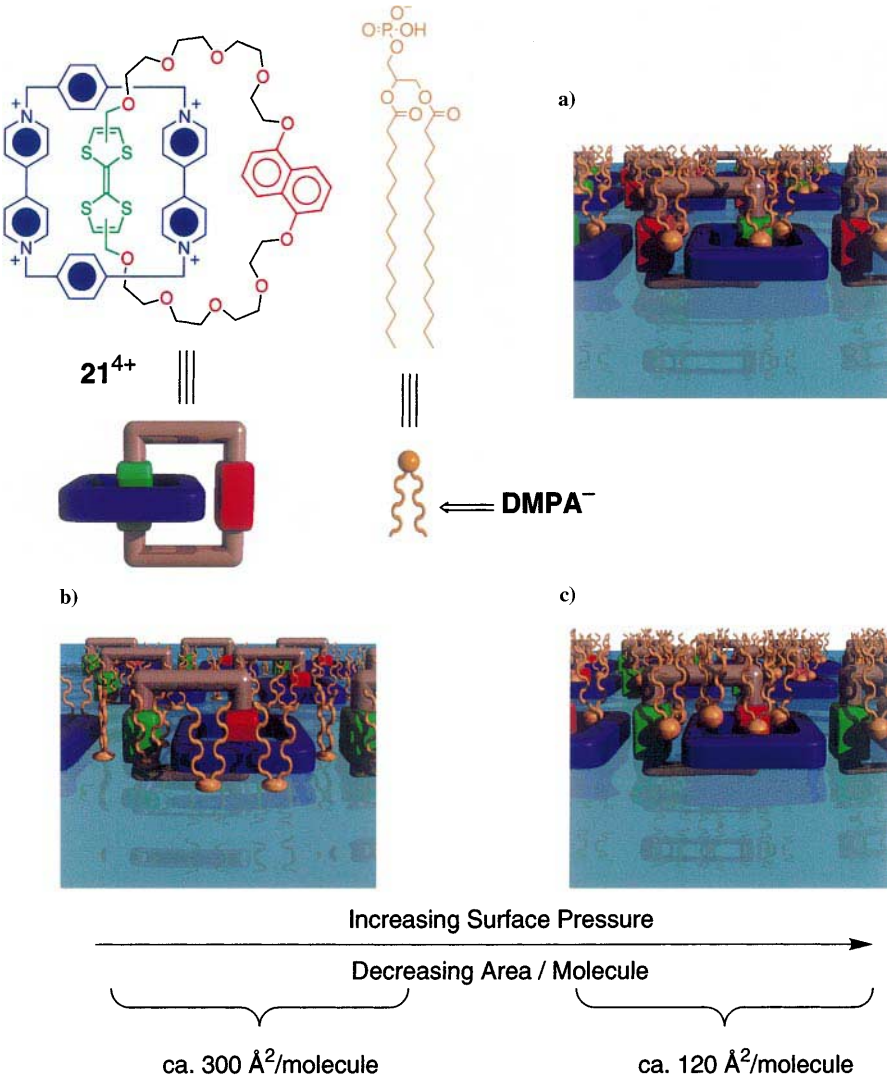

Fig. 32. **a** When the tetracationic [2]catenane **21**·4**DMPA** is deposited as a monolayer, the "alongside" interactions between dioxynaphthalene units and bipyridinium rings in adjacent catenanes augment the close packing of the monolayer with an area per molecule equivalent to one catenane. Therefore, the **DMPA**$^-$ counterions must be lying atop the catenane monolayer. **b** When the **TTF** unit is oxidized, and the monolayer is formed, the first stable monolayer occurs with an observed area per molecule representative of the **DMPA**$^-$ counterions lying between discrete hexacationic [2]catenanes. This arrangement is presumably a consequence of the lack of attractive alongside interactions between adjacent tetracationic [2]catenanes. **c** It is only when the surface pressure is increased that the counterions are forced atop this catenane monolayer

result corresponds to the catenane lying such that the cavity of the cyclophane component is positioned orthogonal to the plane of the air–water interface. The profile of the catenane in this orientation is estimated to be ca. 121 $Å^2$, which corresponds satisfyingly with the observed area per molecule. It follows that the counterions – which in this model do not appear to inhabit any space – must be located (Fig. 32a) on top of the catenane. In this two-dimensional arrangement, there is the distinct possibility of attractive interactions between adjacent catenanes. The 1,5-dioxynaphthalene unit that is forced to reside outside the cavity of the cyclophane can participate in "alongside" interactions with a bipyridinium unit in an adjacent catenane molecule.

If the catenane $\mathbf{21}^{4+}$ is oxidized to its hexacationic state prior to Langmuir film deposition, and then deposited as its hexakis($DMPA^-$) salt, the Π/A isotherm appears markedly different to that of the tetracationic form. Possibly because of a lack of "alongside" interactions between the **TTF** dication and the dicationic bipyridinium unit of an adjacent catenane, the isotherm shows less intermolecular attraction at a given surface pressure. The first of two stable Langmuir films observed in this case occurs with an observed area per molecule of ca. 300 $Å^2$. This result – although not expected – can be explained easily by taking into account the electrostatic, dispersive, alongside interactions that are present between discrete catenane molecules. With there being no real propensity for the catenane molecules to aggregate, the space in between them is occupied (Fig. 32b) by charge-balancing $DMPA^-$ counterions. If the area per molecule of catenane is added to six times the area per $DMPA^-$ ion, the number of 300 $Å^2$ corresponds well with the observed area per molecule. It is only at much higher surface pressures – between two and three times as high as that employed in the case of the tetracation – that a Langmuir film with an area per molecule of ca. 150 $Å^2$ is observed.

If the monolayers are transferred (by a horizontal lifting technique) onto a gold substrate at a surface pressure of 20 mNm^{-1} – a surface pressure at which the tetracationic [2]catenane has an area per molecule of 120 $Å^2$, and the hexacationic form has an area per molecule of ca. 300 $Å^2$ – then the two different film architectures can be examined using tunneling microscopy techniques. A voltage cycling experiment conducted using an STM tip positioned a short way above either of the gold-bound monolayers – essentially a solid-state cyclic voltammogram – showed two very important differences between the two distinct monolayer topologies. The hexacationic form, in which the catenanes are not separated from the gold surface (Fig. 33), shows a virtually ohmic response to applied voltage. The tetracation, however, where the catenanes are insulated from the gold surface, show very little response to the applied potential. In effect, *the DMPA monolayer acts as an electrical insulator*.

4.3
Constructing and Testing a Catenane-Based Device

As soon as the redox-addressable catenane $\mathbf{21}^{4+}$ had been shown to form stable monolayers in both of its "co-conformers", an attempt was made to

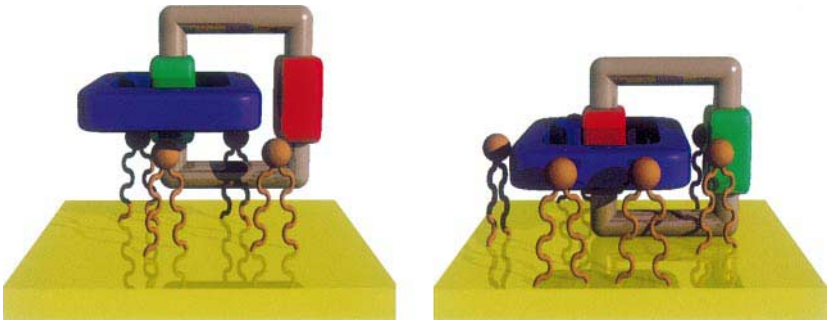

Fig. 33. When the monolayers are transferred onto a gold substrate – at a surface pressure pertaining to the situations evidenced in Fig. 32a and b – by a horizontal lifting technique, **a** the tetracationic [2]catenanes can be seen to form a monolayer insulated from the gold surface by virtue of the aliphatic counterions. **b** The hexacationic [2]catenanes – less insulated from the gold surface – exhibit a linear current/voltage profile upon an applied potential, indicating their coupling to the gold surface

incorporate it into a functioning molecular device. Deposition of the catenane as a Langmuir film was carried out in the manner previously described. The monolayer was then transferred onto a photolithographically patterned polysilicon electrode [54]. The patterning was such that the Langmuir film was deposited along several parallel lines of polysilicon on the electrode. A second set of wires was then deposited on top of the first set, oriented in the orthogonal direction. This second set of electrodes consisted of a 50-Å thick layer of Ti, followed by a 1000-Å thick layer of Al. These electrodes were deposited by the condensation of the appropriate metal vapor through a shadow mask – essentially a very fine stencil. The bottom electrode of the molecular sandwich was 7 μm wide and the top electrode, 10 μm. This approach was used to construct an array of junctions, consisting of a polysilicon electrode, a catenane monolayer, and then a top Ti/Al electrode. Each of these junctions is addressable individually (Fig. 34).

The mechanism for conduction is by electron tunneling through the single-molecule thick layer between the junction electrodes. Thus, any change in the electronic characteristics of the interelectrode medium will affect the tunneling efficiency and so the resistance of the junction will change. It should be emphasized that it is the efficiency of this electron-tunneling process that affects the junction resistance, and hence the magnitude of the current. The current which flows is not capacitive in nature – one in which the measured current is a result of the electron flow associated with oxidation and reduction of the **TTF** units. Because of mirror charge effects, it is important that the catenane molecules are electrically insulated from the electrodes, and, as shown with the gold-based catenane, the DMPA anions fulfil this role admirably.

It was noted that, although the circumrotational motion followed mostly the general mechanism pertaining to the catenane in the solution phase, upon

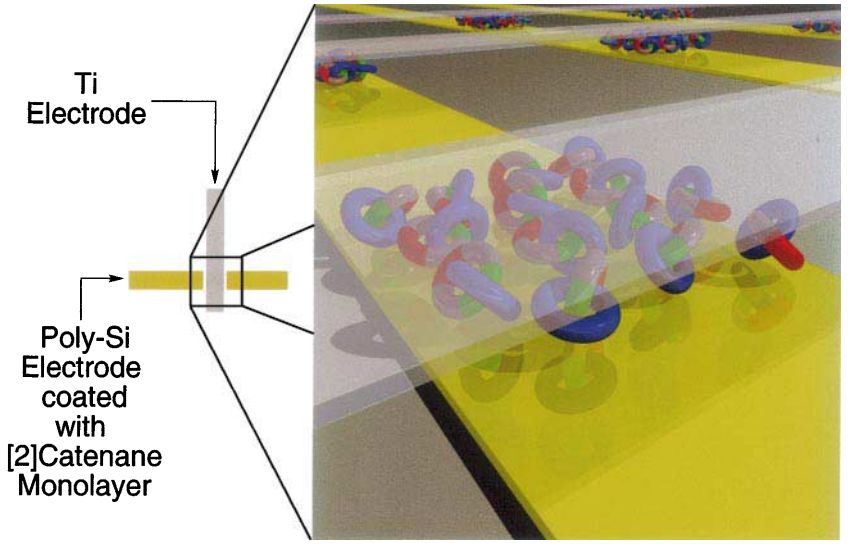

Fig. 34. Deposition of a monolayer of switchable [2]catenane **21**·4**DMPA** is deposited onto a patterned polysilicon substrate, followed by condensation of orthogonal strips of Ti through a layer mask resulting in the formation of a network of junctions, each sandwiching a single layer of redox-active [2]catenanes

reduction of the **TTF** (di)cation, the crown ether did not circumrotate round to give the original "co-conformer" [A^0] (Fig. 35). In fact, "co-conformer" [B^0] is quite stable in the solid state. In order to restore the device to its original state, it is necessary to first turn off the recognition of the cyclophane unit through electrochemical reduction of its bipyridinium units. This redox change presumably leads to expulsion of the 1, 5-dioxynaphthalene ring from the cyclophane cavity – all π-π stacking and supporting [C—H···O] interactions are broken – followed by reinsertion of the **TTF** upon reoxidation of the cyclophane's bipyridinium rings. It is for this reason that the devices are read (the current recorded) at 200 mV, and written (the switch flipped) at ±2 V. The choice of 200 mV as the read voltage is because this is a voltage at which the switch will not be affected, but a high current ratio exists between the two states of the switch, similar to the magnetic memory bit, illustrated in Fig. 36. The voltage profile used to determine the current/voltage characteristics of the junction was a stepped profile, similar to that used in normal pulse voltammetry (Fig. 36). The voltage is written at a certain ramp height, and then read at a set voltage – in this case +200 mV. The current at the read voltage is then plotted as a function of the write voltage. The remnant molecular signature produced can be seen to display a highly hysteretic read current/write voltage profile. Thus, the [2]catenane junction device has been shown to operate as a system with potential for use in random access memory (RAM) storage.

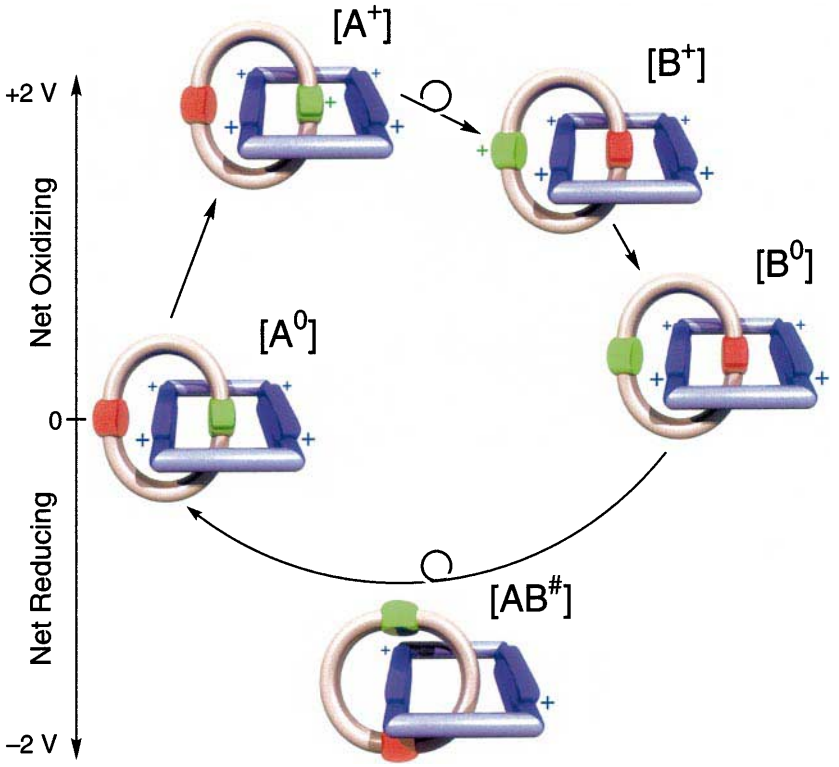

Fig. 35. The device functions in a manner not entirely unlike the solution-state behavior of the catenane, with some subtle differences. The ground state of the device – $[A^0]$ – represents the switch open state, i.e., the switch is "off". Oxidation of the **TTF** unit yields $[A^+]$, which spontaneously circumrotates, resulting in the "co-conformer" $[B^+]$. Subsequent reduction of the **TTF** radical cation yields the stable "co-conformer" $[B^0]$, that represents the closed state of the switch, i.e., the switch is "on". The switch is reset only by (partial) reduction of the bipyridinium units – a reaction which allows the departure of the π-electron-rich unit from the cavity of the cyclophane. Reoxidation of the bipyridinium units completes the closing of the switch, i.e., it is once again "off", on its return to $[A^0]$

4.4 Constructing and Testing a Rotaxane-Based Device

When conferred with a hydrophilic head (in this case a substituted trityl unit), and a hydrophobic (benzylic alcohol) tail, rotaxanes – branched [55] or otherwise – can be formed into Langmuir films in a manner similar to catenanes. Rotaxane $\mathbf{22}^{4+}$ – synthesized from its corresponding thread via the slipping approach – when incorporated into a device in a manner similar to the catenane $\mathbf{21}^{4+}$ also exhibited interesting electron-transport properties [56]. Unlike the catenane-based device, there is no switching element built into the molecule. However, like the switchable catenane, the rotaxane $\mathbf{22}^{4+}$ has electroactive bipyridinium sites, whose presence can mediate the tunneling of

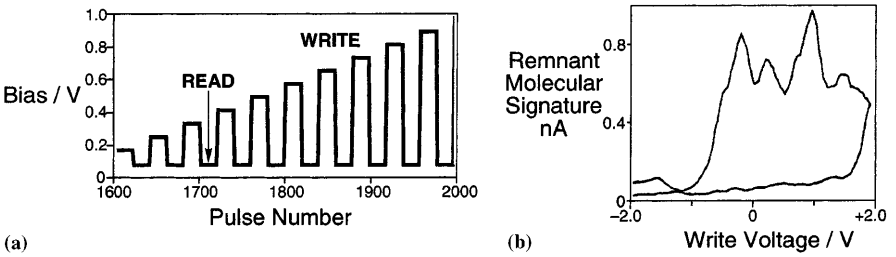

Fig. 36. **a** The pulse profile used to monitor the switching process of the catenane device to generate a remnant molecular signature. A perturbing (WRITE) potential is applied across the device, the state of which is then observed by measuring the current flow at the READ voltage of 200 mV. The WRITE voltage is incremented at each opportunity by ±100 mV (depending on the direction of the scan), to yield a pulse-like waveform. **b** When READ current is plotted as a function of WRITE voltage, a remnant molecular signature is produced. The remnant molecular signature of the catenane device exhibits large hysteresis, with an on-off ratio of roughly 4

electrons through the junction. After a brief period of slightly varying response, the devices yield repeatable responses a short time after fabrication. When a negative bias is applied across the junction, a current is observed to flow (Fig. 37c).

This current profile is highly repeatable and does not vary in magnitude between uses. However, upon a single sweep to positive bias, the system is oxidized, and subsequent scans provide the rather featureless profile recorded in Fig. 37e. This simple, irreversible on-off switching formed the basis for the construction of molecule-based ROM devices. Also, judicious parallel alignment of individual gates leads to electronically addressable, electronically readable AND and OR gates. It is worth mentioning that this observation is a function of the diode behavior of the junctions – by virtue of their possessing two different wiring materials – and not as a result of any logic-displaying properties being designed into the rotaxane.

5 Wiring Issues

The field of molecular electronics is in its embryonic stage. Although many molecular and supramolecular systems have been designed (and synthesized) to work in a solution-phase context, their successful incorporation into functioning devices is hugely dependent not only on the design of the chemical computing element, but also on the nature of the device itself.

In an ideal world in which the perfect computing molecule has been designed, synthesized, and shown to operate reversibly, reliably, and exhibit quick responses to applied stimuli, there remains one major problem for the molecular chip builder to solve – that is, how to wire the molecule into a workable circuit which will take full advantage of the chemical computer's most appealing trait – its miniscule size.

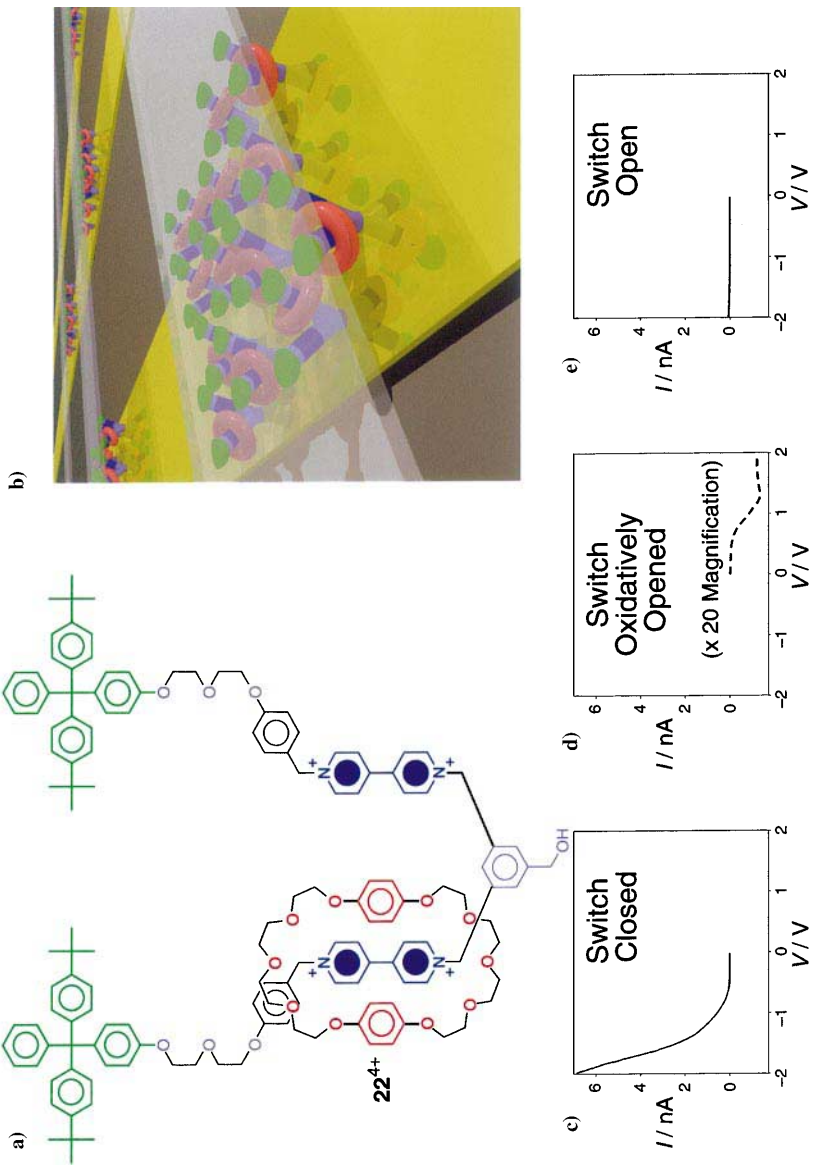
a)
22^{4+}
b)
c)
Switch Closed
I / nA
V / V
d)
Switch Oxidatively Opened
(x 20 Magnification)
I / nA
V / V
e)
Switch Open
I / nA
V / V

Fig. 37. **a** The [2]rotaxane $\mathbf{22}^{4+}$, when **b** deposited between electrodes to yield a network of devices, a singly configurable switch results. **c** Before opening the switch, the device shows a repeatable I/V profile in which there is a large current response to applied voltage. **d** Upon a single oxidative pulse, however, the switch is written to a closed position, in which **e** the resistance of the junction increases dramatically

The smallest functioning device described in this review measures 6×11 μm per junction. Even in terms of today's chip design, this component is gargantuan. There is no point in extolling the virtues of molecular computing if each operation is to be carried out by billions of molecules, all acting in the same manner at the same time. The ultimate goal of the molecular chip designer is to use one molecule per function. Even with the loss taken by the entropic guarantee that not every molecule will sit in its correct junction, in the correct manner, and function appropriately, the Teramac [57] displayed that impressive computational speeds can be obtained by a computer riddled with hundreds of thousands of defects.

The true challenge lies in developing a wiring system which can be functionalized as easily as the polysilicon electrodes in the handful of operating devices in existence today, and connected to terminals, so that, even although the actual computations might be carried out on the molecular scale, the system can still be accessed by macroscopic components. It is no use having a molecular computer if one needs to employ an STM in order to type!

Joking aside, the wiring problem, although probably the most serious omission to date in the molecular chip designer's toolkit, is being pursued actively in many laboratories worldwide. Currently, there are four main trains of thought as to how the future molecular computer will be wired.

5.1
Metal-Nucleated Nanowires

Pioneering work from the research groups of – amongst others – Buhro [58] (Ga, As), Heath [59] (Si, Ge), and Lieber [60] (Si, Ge) has resulted in numerous reported examples of nanowires. Typically grown via vapor-liquid-solid (VLS) growth techniques, or analogies thereof, from metal nucleation sites, these nanowires are typically in the micron length range and can have diameters as low as 6 nm. With semiconducting properties, these wires not only provide an interesting route by which a molecular computer could be wired, but are also very interesting in their own right. Heath et al. [61], for example, have recently reported a field-effect device based upon a silicon nanowire.

5.2
Self-Assembled Nanowires

Williams et al. recently published [62] a paper reporting crystals of erbium disilicide – a compound with high conductivity – that had been grown on a silicon substrate. These nanowires are remarkably straight, and quite uniform

in height and width. They are self-assembled using the underlying silicon crystal lattice as a template. Mismatches between the crystal lattice of the silicon substrate, and that of the growing $ErSi_2$ crystals, encourage the nucleating crystal to grow in only one dimension. This breakthrough is an encouraging start, as crystal-packing studies suggest that erbium is not widely considered to be the most appropriate rare earth element for ensuring the substrate-templated crystal growth.

5.3
Carbon Nanotubes

Some of the more enticing wiring elements, at least to the organic chemist, are undoubtedly the carbon nanotubes. With long aspect ratios, a uniform diameter, and well-defined conductivities, these linear single molecules lend themselves rather nicely for use as the wiring elements in a molecular computer. The problem associated with the use of carbon nanotubes is their very poor solubility, and the lack of any chemistry by which they can be suitably, and regularly, functionalized along the side walls. This area is a very active research topic in our laboratories, and those of many, many others presently.

5.4
Conjugated Polymers

The research group headed by Tour has produced [63] many well-characterized, conducting poly(phenylene-ethynylene) and poly(thiophene-ethynylene) polymers, as well as poly(phenylene-ethynylene)/poly(thiophene-ethynylene) block copolymers, that are precise in their lengths using ingenious iterative synthetic routes. The polymers have been designed and synthesized to exact specifications and their conductivities can be interrogated one molecule at a time. However, the problem with these molecules, as with all other wiring paradigms, is how to attach molecular electronic components to the wires, and how to connect the wires to each other.

As well as their pioneering research into molecular wires, Tour's group has produced a large number of potential components [64] for molecular computers – many of which have been tested and characterized as devices at a single-molecule level [65]. Although it is clear that Tour's contributions to the field of molecular computing has led to a great deal of potentially very important breakthroughs, we have concentrated in this review on resonant tunneling-based devices in which the band gap – and therefore the tunneling current – of a junction is altered as a function of the mechanochemical state of the junction component.

6
Concluding Remarks

The development of potential components for molecular computers started from not so humble beginnings. The enlightening research performed by

A.P. de Silva's research group demonstrated that, without a doubt, the shrewd design of molecules does result in systems that are capable of mimicking logic functions. With the development of a fluorescent AND gate, it has been proven conclusively that molecules can be tailored such that their responses to different stimuli resemble those of ever more complex logic functions. The field of molecular logic quickly embraced such operations as OR, INHIBIT – with two or three inputs – and XOR. The undoubted triumph so far in this field has been the demonstration of a binary mixture of AND and XOR molecules behaving analogously to a half adder. With shared inputs, the individual components can be addressed in parallel, and the fact that the two molecules have different output modes mean that the outputs can be monitored independently of each other. This elegant proof-of-principle demonstrated the versatility of a solution-based approach to molecular logic. However, more complex logic functions remain a goal which – in the solution state at least – remain a much more challenging goal.

Although the development of solid-state, individually addressable functioning molecular devices was a long way off at the time, the nascent field of supramolecular chemistry seemed to hold many possible solutions to the problem of finding a system capable of functioning in a device context. Before the demonstration of an electronically addressable and monitored switching system in a device, many switches and gates were tested in solution by our talented collaborators under the expert supervision of Vincenzo Balzani at the University of Bologna, in which either the relative positions of components of mechanically interlocked molecules – i.e., catenanes and rotaxanes – or the integrity of supramolecular entities – e.g., pseudorotaxanes – could be perturbed and monitored in a number of ways – namely chemically, photochemically, and electrochemically. In the solution phase, rotaxanes, and their supramolecular counterparts pseudorotaxanes, as well as catenanes were demonstrated to provide – through adroit design – properties similar to a number of switches and logic functions.

Although many of these systems proved to be academically interesting, the development of electronically switchable and monitored systems has proved to be the real starting point from which molecular devices can possibly be made. By virtue of the fact that both their inputs and outputs are electronic in nature, these systems lend themselves to relatively easy incorporation into electronic circuitry.

The careful design and delicate synthesis of a number of catenanes and rotaxanes have led to their incorporation into monolayers, and then from these monolayers in the form of Langmuir-Blodgett films onto patterned silicon substrates. This step, followed by the deposition of a second metal layer in the perpendicular direction to form a crossbar, has resulted in the production of an ever-growing number of electrical devices in which the switching is carried out at junctions one molecule thick.

However, if the size advantage of molecular electronic devices is to be exploited in a functioning device, the wires also have to be molecular in their dimensions. A great deal of effort is now being devoted, in a number of different directions simultaneously – namely, using metal nanowires, carbon

nanotubes, and conjugated polymers – toward removing this bottleneck to a new technology.

There is not so much talk these days of *whether or not* molecular electronics will ever become reality. Researchers, funding agencies, large multinational computer firms – and now also governments – are starting to commit large human and financial resources into turning the question to *when* molecular devices will dominate the world of the future as silicon does today.

Acknowledgements. The research presented in this review, which came from our laboratories, was the result of a hugely collaborative effort. The syntheses and spectroscopic characterization have been performed by a team of talented undergraduates, graduate students, and postdoctoral researchers over a period spanning several years in numerous universities. Synthesis alone – however elaborate – is hardly sufficient to characterize molecular devices, and, for this requirement, we have relied heavily over the decades on the combined skills of the research groups of David Williams at Imperial College for X-ray structural and superstructural analysis, Vincenzo Balzani at the University of Bologna for photochemical and electrochemical investigations, and, more recently, on the knowledge and expertise of Jim Heath here at UCLA for the construction of functioning molecule-based electronic devices. Also, none of this research would have been possible without the generous financial support of – amongst others – UCLA and DARPA in the US well as EPSRC and BBSRC in the UK.

7 References

1. Moore GE (1975) IEDM Technical Digest, IEEE Piscataway, New Jersey
2. Schulz M (1999) Nature 399: 729
3. Muller DA, Sorsch T, Moccio S, Baumann FH, Evans-Lutterodt K, Timp G (1999) Nature 399: 758
4. Ball P (2000) Nature 406: 118
5. Goldhaber-Gordon D, Montemerlo MS, Love JC, Opiteck GJ, Ellenbogen JC (1997) Proc IEEE 85: 521
6. Reed MA, Tour JM (2000) Sci Am 282: 86
7. Ghosh P, Bharadwaj PK, Roy J, Ghosh S (1997) J Am Chem Soc 119: 11903; Baytekin HT, Akkaya EU (2000) Org Lett 2: 1725
8. de Silva AP, Gunaratne HQN, Gunnlaugsson T, Huxley AJM, McCoy CP, Rademacher JT, Rice TE (1997) Chem Rev 97: 1515
9. de Silva AP, Gunaratne HQN, McCoy CP (1993) Nature 364: 42
10. de Silva AP, Gunaratne HQN, McCoy CP (1997) J Am Chem Soc 119: 7891
11. de Silva AP, Gunaratne HQN, Maguire GEM (1994) J Chem Soc Chem Commun 1213
12. Gunnlaugsson T, Mac Dónail DA, Parker D (2000) Chem Commun 93
13. de Silva AP, Dixon IM, Gunaratne HQN, Gunnlaugsson T, Maxwell PRS, Rice TE (1999) J Am Chem Soc 121: 1393
14. de Silva AP, McClenaghan ND (2000) J Am Chem Soc 122: 3965
15. Ellenbogen JC, Love JC (2000) Proc IEEE 88: 386
16. Schill G (1971) Catenanes, Rotaxanes, and Knots, Academic Press, New York
17. Cram DJ (1992) Nature 356: 29; Cram DJ, Cram JM (1994) Container Molecules and their Guests, The Royal Society of Chemistry, Cambridge
18. Ashton PR, Philp D, Reddington MV, Slawin AMZ, Spencer N, Stoddart JF, Williams DJ (1991) J Chem Soc Chem Commun 1680
19. Balzani V, Gómez-López M, Stoddart JF (1998) Acc Chem Res 31: 405; Balzani V, Credi A, Raymo FM, Stoddart JF (2000) Angew Chem Int Ed Engl 39: 3348

20. Harrison IT, Harrison S (1967) J Am Chem Soc 89: 5723
21. Stang PJ, Diederich F (eds) (1999) Templated Organic Synthesis, Wiley-VCH, Weinheim
22. Nepogodiev SA, Stoddart JF (1998) Chem Rev 98: 1959
23. Jäger R, Vögtle F (1997) Angew Chem Int Ed Engl 36: 930
24. Sauvage JP (1990) Acc Chem Res 23: 319
25. Amabilino DB, Stoddart JF (1995) Chem Rev 95: 2725
26. Ashton PR, Ballardini R, Balzani V, Belohradsky M, Gandolfi MT, Philp D, Prodi L, Raymo FM, Reddington MV, Spencer N, Stoddart JF, Venturi M, Williams DJ (1996) J Am Chem Soc 118: 4931
27. Anelli P-L, Ashton PR, Ballardini R, Balzani V, Delgado M, Gandolfi MT, Goodnow TT, Kaifer AE, Philp D, Pietraszkiewicz M, Prodi L, Reddington MV, Slawin AMZ, Spencer N, Stoddart JF, Vicent C, Williams DJ (1992) J Am Chem Soc 114: 193
28. Houk KN, Menzer S, Newton SP, Raymo FM, Stoddart JF, Williams DJ (1999) J Am Chem Soc 121: 1479
29. Anelli P-L, Spencer N, Stoddart JF (1991) J Am Chem Soc 113: 5131
30. Grabuleda X, Jaime C (1998) J Org Chem 63: 9635
31. Bissell RA, Córdova E, Kaifer AE, Stoddart JF (1994) Nature 369: 133
32. Ashton PR, Ballardini R, Balzani V, Credi A, Dress R, Ishow E, Kleverlaan CJ, Kocian O, Preece JA, Spencer N, Stoddart JF, Venturi M, Wenger S (2000) Chem Eur J 6: 3558
33. Ashton PR, Ballardini R, Balzani V, Constable EC, Credi A, Kocian O, Langford SJ, Preece JA, Prodi L, Schofield ER, Spencer N, Stoddart JF, Wenger S (1998) Chem Eur J 4: 2413; Asakawa M, Ashton PR, Balzani V, Brown CL, Credi A, Matthews OA, Newton SP, Raymo FM, Shipway AN, Spencer N, Quick A, Stoddart JF, White AJP, Williams DJ (1999) Chem Eur J 5: 860
34. Asakawa M, Iqbal S, Stoddart JF, Tinker ND (1996) Angew Chem Int Ed Engl 35: 976
35. Matthews OA, Raymo FM, Stoddart JF, White AJP, Williams DJ (1998) New J Chem 1131
36. Philp D, Slawin AMZ, Spencer N, Stoddart JF, Williams DJ (1991) J Chem Soc Chem Commun 1584
37. Asakawa M, Ashton PR, Balzani V, Credi A, Mattersteig G, Matthews OA, Montalti M, Spencer N, Stoddart JF, Venturi M (1997) Chem Eur J 3: 1992
38. Ashton PR, Balzani V, Becher J, Credi A, Fyfe MCT, Mattersteig G, Menzer S, Nielsen MB, Raymo FM, Stoddart JF, Venturi M, Williams DJ (1999) J Am Chem Soc 121: 3951
39. Credi A, Balzani V, Langford SJ, Stoddart JF (1997) J Am Chem Soc 119: 2679
40. Ballardini R, Balzani V, Credi A, Gandolfi MT, Langford SJ, Menzer S, Prodi L, Stoddart JF, Venturi M, Williams DJ (1996) Angew Chem Int Ed Engl 35: 978; Balzani V, Credi A, Langford SJ, Raymo FM, Stoddart JF, Venturi M (2000) J Am Chem Soc 122: 3542
41. Wasserman E (1960) J Am Chem Soc 82: 4433
42. Hunter CA (1992) J Am Chem Soc 114: 5303
43. Hamilton DG, Davies JD, Prodi L, Sanders JKM (1998) Chem Eur J 4: 608
44. Fujita M (1999) Acc Chem Res 32: 53
45. Philp D, Stoddart JF (1996) Angew Chem Int Ed Engl 35: 1155; Fyfe MCT, Stoddart JF (1997) Acc Chem Res 30: 393
46. Ashton PR, Boyd SE, Brindle A, Langford SJ, Menzer S, Pérez-García L, Preece JA, Raymo FM, Spencer N, Stoddart JF, White AJP, Williams DJ (1999) New J Chem 23: 587
47. Amabilino DB, Anelli P-L, Ashton PR, Brown GR, Córdova E, Godínez LA, Hayes W, Kaifer AE, Philp D, Slawin AMZ, Spencer N, Stoddart JF, Tolley MS, Williams DJ (1995) J Am Chem Soc 117: 11142; Amabilino DB, Ashton PR, Boyd SE, Gómez-López M, Hayes W, Stoddart JF (1997) J Org Chem 62: 3062
48. Ashton PR, Ballardini R, Balzani V, Credi A, Gandolfi MT, Menzer S, Pérez-García L, Prodi L, Stoddart JF, Venturi M, White AJP, Williams DJ (1995) J Am Chem Soc 117: 11171
49. Whereas the term "co-conformer" is usually reserved for translationally isomeric species, it appears in inverted commas in this instance to signify that the two circumstances in which the catenane can exist are of different oxidation states, and so are not isomeric

50. Asakawa M, Ashton PR, Balzani V, Boyd SE, Credi A, Mattersteig G, Menzer S, Montalti M, Raymo FM, Ruffilli C, Stoddart JF, Venturi M, Williams DJ (1999) Eur J Org Chem 985
51. Asakawa M, Ashton PR, Balzani V, Credi A, Hamers CA, Mattersteig G, Montalti M, Shipway AN, Spencer N, Stoddart JF, Tolley MS, Venturi M, White AJP, Williams DJ (1998) Angew Chem Int Ed Engl 37: 333
52. Balzani V, Credi A, Mattersteig G, Matthews OA, Raymo FM, Stoddart JF, Venturi M, White AJP, Williams DJ (2000) J Org Chem 65: 1924
53. Ahuja RC, Caruso P-L, Möbius D, Wildburg G, Ringsdorf H, Philp D, Preece JA, Stoddart JF (1993) Langmuir 9: 1534; Brown CL, Jonas U, Preece JA, Ringsdorf H, Seitz M, Stoddart JF (2000) Langmuir 16: 1924; Asakawa M, Higuchi M, Mattersteig G, Nakamura T, Pease AR, Raymo FM, Shimizu T, Stoddart JF (2000) Adv Mater 12: 1099
54. Collier CP, Mattersteig G, Stoddart JF, Wong EW, Luo Y, Beverly K, Sampaio J, Raymo FM, Stoddart JF, Heath JR (2000) Science 289: 1172
55. Amabilino DB, Asakawa M, Ashton PR, Ballardini R, Balzani V, Belohradsky M, Credi A, Higuchi M, Raymo FM, Shimizu T, Stoddart JF, Venturi M, Yase K (1998) New J Chem 959
56. Collier CP, Wong EW, Belohradsky M, Raymo FM, Stoddart JF, Keukes PJ, Williams RS, Heath JR (1999) Science 285: 391; Wong EW, Collier CP, Belohradsky M, Raymo FM, Stoddart JF, Heath JR (2000) J Am Chem Soc 122: 5831
57. Heath JR, Keukes PJ, Snider GS, Williams RS (1998) Science 280: 1716
58. Trentler TJ, Hickman KM, Goel SC, Viano AM, Gibbons PC, Buhro WE (1995) Science 270: 1791
59. Chung S-W, Markovich G, Heath JR (1998) J Phys Chem B 102: 6685
60. Morales AM, Lieber CM (1998) Science 279: 208
61. Chung SW, Yu JY, Heath JR (2000) Appl Phys Lett 76: 2068
62. Chen Y, Ohlberg DAA, Medeiros-Ribeiro G, Chang YA, Williams RS (2000) Appl Phys Lett 76: 4004
63. Reed MA, Zhou C, Muller CJ, Burgin TP (1997) Science 278: 252; Tour JM (1996) Chem Rev 96: 537
64. Chen J, Reed MA, Rawlett AM, Tour JM (1999) Science 286: 1550
65. Tour JM, Kozaki M, Seminario JM (1998) J Am Chem Soc 120: 8486; Seminario JM, Zacarias AG, Tour JM (1999) J Phys Chem A 103: 7883

Molecular Memory and Processing Devices in Solution and on Surfaces

Andrew N. Shipway, Eugenii Katz, Itamar Willner

Institute of Chemistry, The Hebrew University of Jerusalem, Jerusalem 91904, Israel
E-mail: willnea@vms.huji.ac.il

Molecular mechanical and supramolecular systems have been with us for some time, but the means for their programmed control have often been lacking. In order to construct useful nanomechanical devices, the structures need not only to have a mechanical function, but this function needs to be addressable. Ideally a nanomechanical system will be 'programmed' for a particular task, that is, it will be sensitive to its environment and contain the processing ability to act appropriately without external control at every step of its operation. Here, we review the developing methods for the integration and interfacing of molecular mechanical components and the solutions that have been found for performing information functions (memory, processing) on a molecular scale. Fundamental units such as photochromic, redox, fluorescent and supramolecular moieties are introduced and their combination into multicomponent covalent or supramolecular systems is discussed. The immobilization of molecular devices on surfaces is given special attention, along with methods for the transduction and amplification of output signals from the devices.

Keywords: Molecular machines, Molecular switches, Molecular memory, Molecular computing, Supramolecular chemistry, Molecular optoelectronics, Command surfaces, Monolayers, Nanotechnology

1 Introduction 238

1.1 Requirements of Molecular Information Devices 238
1.2 Pitfalls of Molecular Information Devices 240

2 Solution-State Molecular Devices 241

2.1 Information Functions of Isomerizable Molecules 241
2.2 Information Functions of Binding Interactions 248
2.3 Mechanically-Switching Molecular Assemblies 253
2.4 Assemblies that Perform Logical Functions 259

3 Surface-Integrated Molecular Devices 260

3.1 Surface-Confined Molecular Optoelectronics 261
3.2 Photoisomerizable 'Command' Surfaces 266
3.3 Surfaces for the Controlled Binding of Photoisomerizable Guests 269
3.4 Mechanically Interlocked Compounds at Interfaces 273

Structure and Bonding, Vol. 99

4 **Outlook and Perspectives** 274

5 **References** 277

1 Introduction

Molecular and supramolecular assemblies have been shown to be capable of many mechanical functions [1]. Working examples of basic mechanical components such as levers, rotors [2] and translational movements [3] are well known, and more complex assemblies have also been reported [4]. What these systems often lack, however, is suitable means for their external control and their integration into larger assemblies capable of carrying out useful functions. In order to realize the nanotechnologist's dreams of molecular-scale computing and machinery [5], it is imperative that these issues of integration and addressability are tackled. Mechanical functions should be controllable and it should be possible to couple the 'output' event to another component. Likewise, systems that perform logical functions should be able to feed the result of their computation into another device. Only by the development of methodologies that allow such integration will the field of nanotechnology realize its confident promises of cheap, powerful and ultraminiaturized devices for computation, technology and medicine. In this work, we will review the current state-of-the-art in the construction of molecular 'switches', 'logic gates' and 'transducers', particularly those that perform mechanical functions, and we will also cover the latest developments in their integration into larger assemblies.

Many of the systems discussed will follow models inspired by nature, and, indeed, nature has provided us with the definitive proof that our goals can be realized [6]. The vision process (in which optical signals are transduced into the electrical signals that activate the neural response), photomorphogenesis (which represents a variety of biological processes where mechanical movements are activated by light), and the light-triggered opening of ion-channels offer examples where nature has gone before us. Extensive interdisciplinary research has utilized biomolecules for the construction of integrated assemblies capable of mechanical and information functions [7]. In this review, however, we will focus on discrete synthetic assemblies, discluding the multitude of systems that have taken advantage of biomaterials to construct functional assemblies.

1.1 Requirements of Molecular Information Devices

In order to act as information devices, molecular architectures must possess some kind of processing functionality, which may arise from a number of origins, such as isomerization, mechanical movement, or optoelectronic activity. Processing is manifested by the conversion of the molecular entity

between two or more states in response to signals such as irradiation, pH or electrochemical potential (Fig. 1). Apart from this function, however, there are a number of other essential and desirable qualities. Most importantly, the unit should have easily addressable input(s) and readable output(s). Without these, its state can neither be controlled nor determined. Ideally, the input and output should be in an identical form so that the output of one device can be channeled into the input of another, as is the case in electronic circuitry. Another requirement is of integration, that is, the ability to constrain the individual units in controlled orientations with respect to the macroscopic world and to each other, and thus to control their influence over each other. Great steps have been taken in this direction by the construction of surface-confined devices. Monolayer and thin film immobilization allows systems to be contacted electrochemically, addressed and read optically, and handled with relative ease [8]. The further possibility of building up multilayer structures allows the construction of integrated assemblies of identical or different units [9]. Other desirable properties for molecular machine components include high chemical stability and reversibility (for the construction of long-lifetime devices), high stability of state (for storage applications), and signal amplification (for sensitive sensing devices and maintaining signal integrity in multicomponent systems).

The chemistry of photochromic materials has been the subject of extensive research in the past few decades, and the use of photoisomers as a route for recording optical information has been thoroughly examined [10]. Here, however, we will concentrate on systems that include an additional dimension to their functionality – either the integration of multiple components or, in particular, devices with a mechanical basis for their behavior. The formation

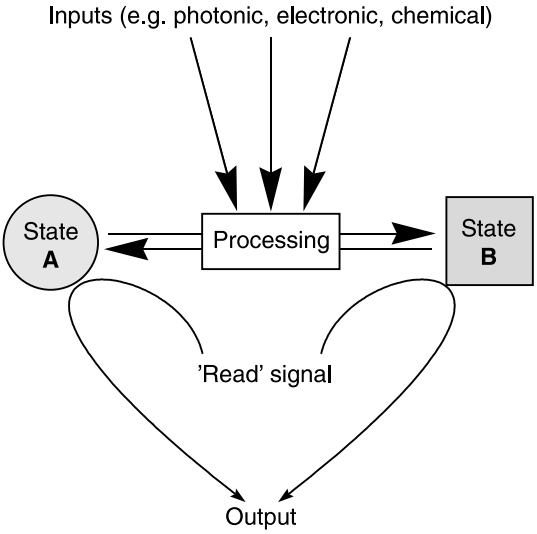

Fig. 1. Schematic representation of a molecular information unit

and dissociation of supramolecular interactions, the structural perturbation of molecular components, and the control of electronic functions represent some possible mechanical functions.

1.2
Pitfalls of Molecular Information Devices

Although the requirements for molecular information device components may seem readily achievable, very few systems have demonstrated commercial viability. Apart from the field's immaturity, this observation can be put down to the numerous pitfalls that await the designer of such systems. Figure 2 gives some examples of very promising systems that are yet to excel because of technical problems. Figure 2A shows the [2]catenane **1** consisting of two interlocking rings whose relative orientation is a function of its microenvironment [11]. Changing the polarity of the solvent causes mechanical

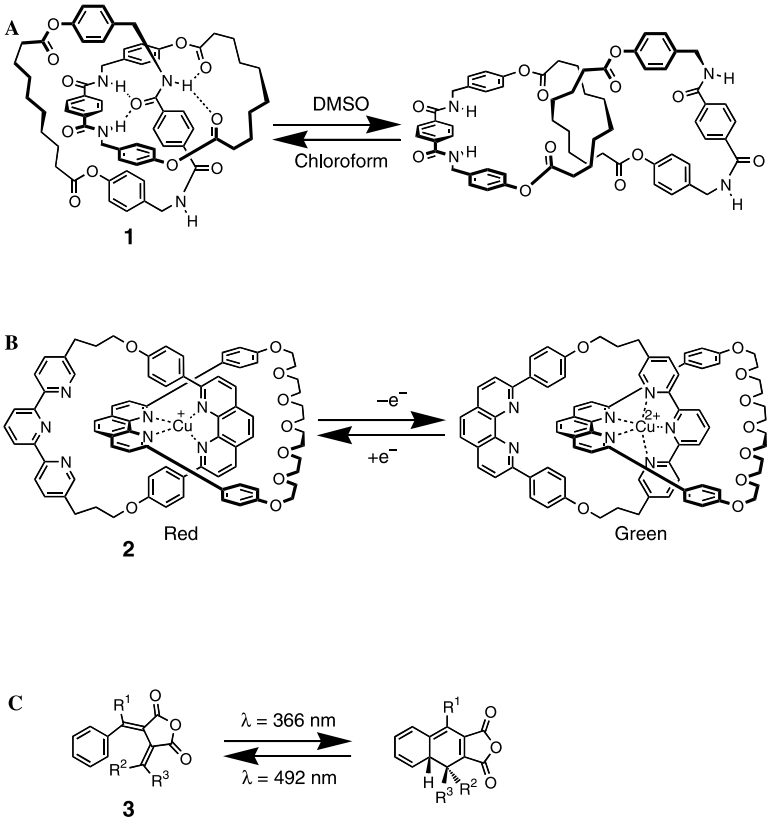

Fig. 2A–C. Some examples of molecular information units: **A** A solvent-switchable [2]catenane. **B** A redox-switchable [2]catenane. **C** A fulgide that undergoes a photoswitchable electrocyclization

switching of the catenane between two distinct states, constituting a 'write' memory function. Unfortunately, no corresponding 'read' function is available – the only way to detect the state of the system is by NMR. Figure 2B shows another [2]catenane **2** [12] (also refer to Sect. 2.3). In this system the orientation of the rings with respect to each other is determined by the oxidation state of the copper ion incorporated in the system, and the state is easily 'read' by examining the color of the solution. The different coordination states of the two conformations result in different absorption spectra. The shortfall of this catenane as an information storage device lies in the time taken for isomerization – several days are required to perform a complete change of state. Fulgides have been developed extensively for molecular switching devices [13]. Figure 2C shows the reversible electrocyclization of the fulgide **3** [14]. Upon appropriate irradiation, the state of the molecule can be switched between 'open' and 'closed' forms, which are easily distinguishable by absorbance spectroscopy. Unfortunately, the changes in the absorbance spectrum coincide with the wavelengths of irradiation for isomerization, and consequently the state cannot be measured without destroying the information. This example demonstrates the importance of compatibility between the 'read' and 'write' signals.

Apart from these shortcomings, there are several other pitfalls to look out for when searching for molecular switching units. The chemical instability of the *cis*-isomer of stilbene, for instance, makes its *trans-cis* isomerization of little practical use, and many switching molecules suffer from incomplete isomerization or thermal back-isomerization to their more thermodynamically stable state.

2
Solution-State Molecular Devices

The construction and study of molecular devices in the solution state offers several advantages over immobilized states. The solution state allows the use of traditional synthetic techniques to produce relatively large quantities of products, which may be analyzed by the highly developed arsenal of analytical techniques that are available to the organic chemist. The three-dimensional freedom of species in solution also means that mechanical movements are unimpaired and the individual units do not need to be specially aligned with respect to a substrate. Very complex mechanical and supramolecular systems have been constructed in solution. Unfortunately, these advantages bring with them a price. The freedom of the solution state makes the integration of units into larger assemblies difficult and the addressing of specific units almost impossible.

2.1
Information Functions of Isomerizable Molecules

Isomerizable molecules may be considered to have a mechanical function based on their transformation between two or more isomeric structures by

means of external stimuli (e.g. photonic, redox, pH). In the simplest case, a molecule is switched between two states upon the application of different signals (e.g. different electrochemical potentials), but often systems may exploit more than one step or more then one type of stimulus to effect isomerization between several states. These different structures can have significantly different properties (e.g. redox, spectroscopic, supramolecular), leading to their use as information storage or processing units.

Perhaps the most important group of isomerizable molecules are photochromic compounds [10]. The state of these units may be controlled by irradiation at specific wavelengths, and their absorbance spectra thus depend on their state. Optical control of state is of great interest for future applications as light may easily be directed to a specific location without the need for complex circuitry. Contemporary technology allows the construction of nanoscale light sources and scanning methodologies, enabling the practical utilization of these systems.

A variety of chemical functionalities undergo photoisomerization, including *trans-cis* isomerization around double bonds, electrocyclic transformations, sigmatropic rearrangements, cycloadditions and bond cleavage. Figure 3

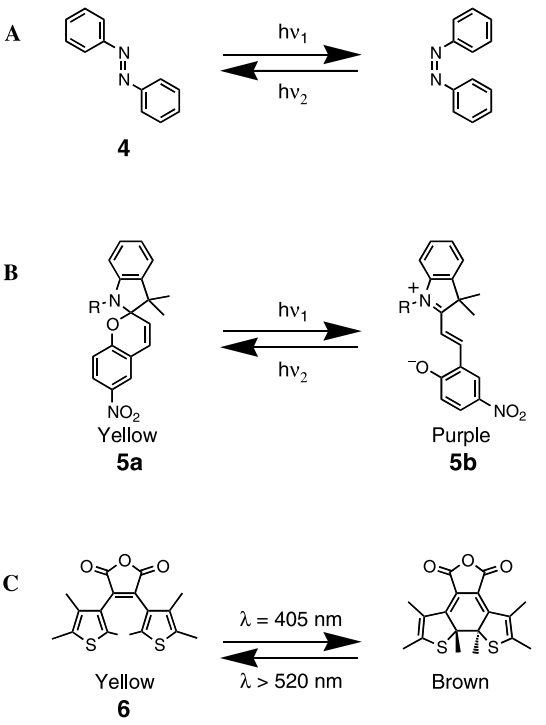

Fig. 3A–C. Some examples of photoisomerizable molecules: **A** *trans-cis* Isomerization around the azobenzene double bond. **B** Isomerization between spiropyran and merocyanine states. **C** The reversible electrocyclic ring closure of diarylethenes

outlines some conceptual examples. Azobenzene (**4**, Fig. 3A) is photochemically isomerizable between the *trans*- and *cis*-configured isomers (with respect to the N=N bond) with an efficiency that is influenced by the substitution of the aromatic rings. The different states are detectable by absorption spectroscopy and can also be utilized for their differences in dipole and steric requirements. Azobenzene has been used in the construction of many simple switching molecules [15]. The spiropyran/merocyanine system is one of the most studied photochromic units [16]. While the spiropyran form, e.g. **5a** (Fig. 3B) [17], is yellow, the zwitterionic merocyanine (**5b**) is purple. At low pH, the phenol of the merocyanine is protonated, and the isomerization is between the neutral and the cationic states, a transformation that can easily be used to influence other functions. Photochemical switching is often achieved by the exploitation of electrocyclic reactions. Diarylalkenes (preferably locked in the *cis*-configuration) can undergo a photochemically activated 6-electron conrotatory ring closure to give a related dihydro species [18]. An early example (**6**) is shown in Fig. 3C [19]. The thermal disrotatory ring closure is sterically excluded by the presence of methyl substituents. The modification of this type of molecule with conjugated substituents allows the 'tuning' or enhancement of the output (redox or fluorescence) [20]. Other photoisomerizable molecules include *trans*/*ana*-quinones [21] and dihydroindolizines [22].

The concepts learned from the examples in Fig. 3 have been used to develop more complex and efficient systems. The idea of *trans-cis* isomerization, for instance, has led to the construction of a molecule that may be converted between its states by the use of circularly polarized light (Fig. 4) [23]. The alkene **7** is forced to adopt a chiral conformation as a consequence of its steric requirements, allowing isomerization between the *trans*- and *cis*-states (**7a** and **7b**) to be accomplished. The state of the system can be monitored easily by measuring the rotation of linearly polarized light. The construction of these 'chiroptical molecular switches' is of great interest because of their ability to be both written to and read by non-interfering photonic means [24].

In many cases, one of the states of a photoisomerizable system is less thermodynamically stable, and a slow thermal isomerization back to the more stable isomer is observed, causing problems for the construction of long-term memory devices. Back-isomerization can also occur as a consequence of the 'read' function or ambient environmental conditions. For these reasons, it can

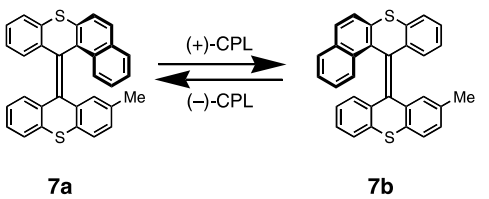

Fig. 4. An alkene-based switching molecule that responds to circularly polarized light (CPL) as the 'write' function

be desirable to add to the binary operation of a molecular switch by the inclusion of a 'locked' state. Data in a 'locked' state is still readable, but has undergone a secondary transformation that removes the possibility of back-isomerization (Fig. 5A). Ideally, it should be possible to 'unlock' the system so that the data can be erased and rewritten. An example of a lockable, erasable molecular memory is given in Fig. 5B [25]. Information may be written to the 'open' molecule **8** by photoisomerization to the 'closed' form **9**, which can also be re-photoisomerized back to **8**. In the 'closed' form (and only in the 'closed' form), a fully conjugated system is created, leading to an electrochemically active hydroquinoid that can be oxidized to the quinoid form **10**. This quinoid is photochemically inactive, and oxidation therefore constitutes the 'lock' function. The 'erase' function can be carried out by the reduction of the quinoid **10** back to the hydroquinoid, which is readily convertible with the 'open' form **8**. Figure 5C shows cyclic voltammograms demonstrating the electrochemical inactivity and activity of **8** and **9**, respectively, and Fig. 5D shows how the entire 'write-lock-unlock-erase' cycle can be followed by absorbance spectroscopy. Other 'locking' cycles based on ion binding to pacify the phenoxy group of merocyanine derivatives [26] and protonation to deactivate a dihydroindolizine [27] have also been developed.

Some molecular components can adopt several different states as a function of several inputs [28]. These compounds are of particular interest for their potential as processing devices. Flavylium salts, for instance, interconvert between a bewildering array of isomers as a result of pH, photonic and thermal inputs [29]. A more elegant example is the interconversion of 5, 6, 7-tri-*tert*-butyl-1, 4-anthraquinone (**11**) between itself and three isomeric states (**12**, **13**, **14**) by photochemical and electrochemical means (Fig. 6) [30]. This system could be considered a dyad of an electrochemically active quinone and a photochemically active tri-*tert*-butyl-substituted polyacene, but, as the conjugation of the entire system is important for its properties, it is treated as a single unit. Each state has a different absorbance spectrum, and the spectral changes for each transformation were measured (Fig. 6). Unfortunately, the conditions required for the electrochemical and photochemical transformations differ, so a single sample cannot be readily interconverted between all four states.

True multicomponent switches are usually based on the model in Fig. 7A [31]. One component performs the 'input' function (e.g. by photoswitching or electroswitching), while the second acts as the 'output'. The 'output' component has a function (e.g. fluorescence, absorbance) that is inhibited by the 'input' component in one of its states. Figure 7B shows a switch (**15**) consisting of a fluorescent difluoroboradiaza-*s*-indacene connected to a tertiary amine through a benzene moiety [32]. In this (unprotonated) state the excited state of the dye is quenched by intramolecular electron transfer from the amine, and no fluorescence is observed (curve a). If the amine is protonated, however, electron transfer is blocked, and fluorescence is clearly observed (curve b). Similarly, the dyad **16** (Fig. 7C) offers the redox switching of luminescence [33]. While the quinone component effectively quenches the

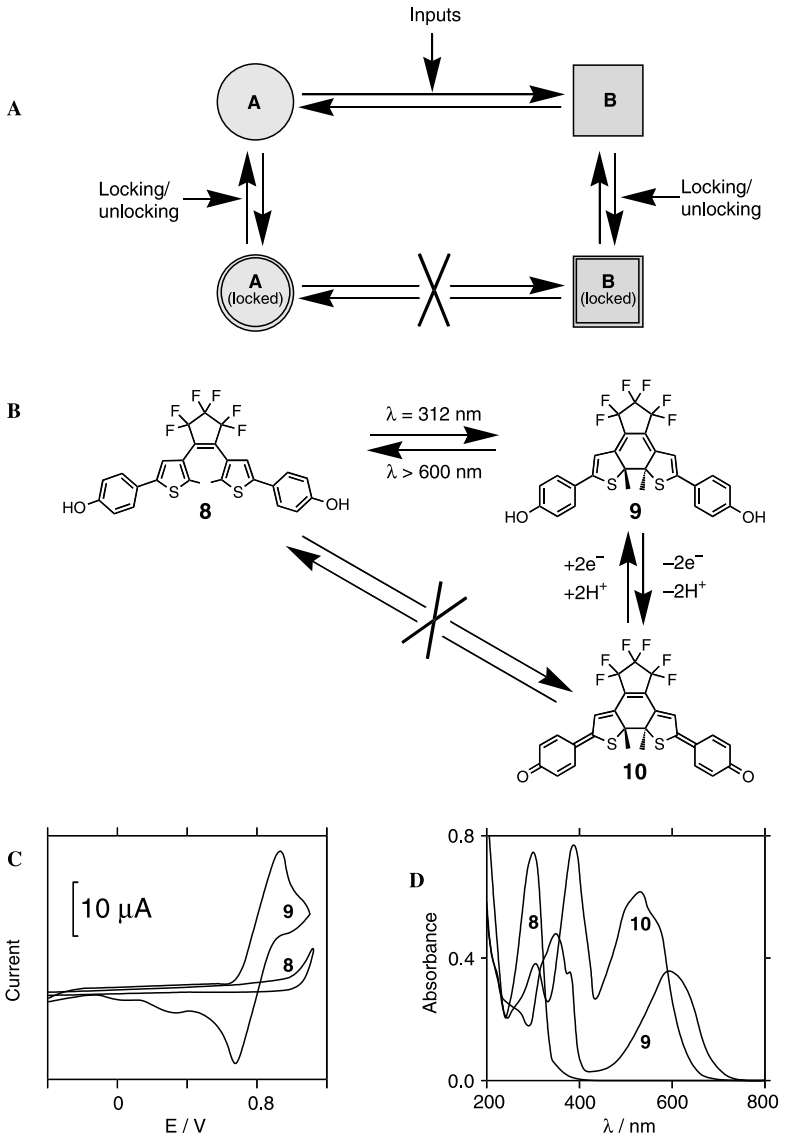

Fig. 5. **A** Schematic representation of a 'locking' molecular memory. **B** A 'locking' molecular memory based on photochemical switching and electrochemical locking. **C** Cyclic voltammograms of the electrochemically inactive 'open'-state **8** and the electrochemically active 'closed'-state **9**, which can be reversibly oxidized to the quinoid 'locked'-state **10**. Recorded in THF with Bu_4NClO_4 (0.1 M) and a potential scan rate of 100 mV s^{-1}. **D** Absorbance spectra of the three states of the lockable molecular memory system. **C** and **D** are adapted from [25] with permission

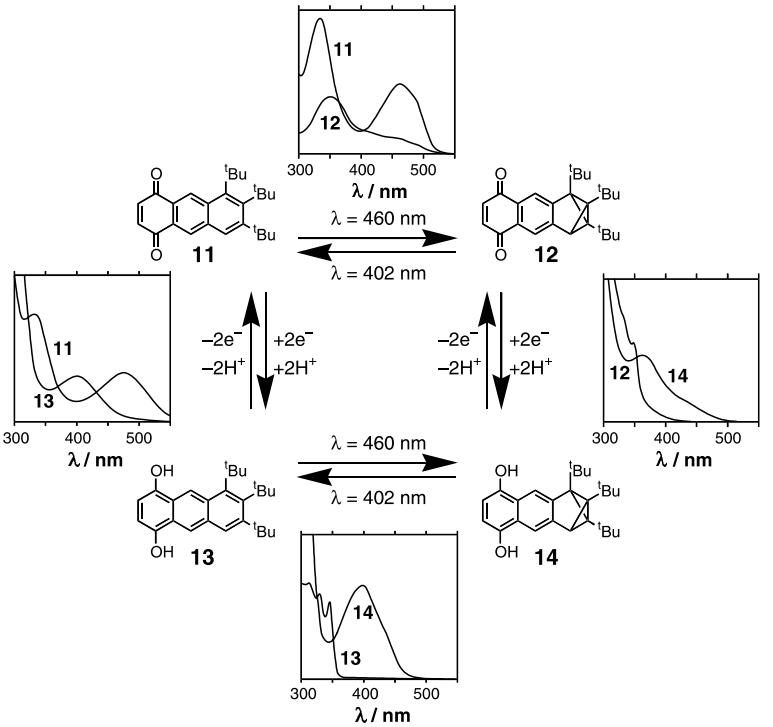

Fig. 6. Interconversion of the four distinct states of an anthraquinone derivative (**11**, **12**, **13** and **14**) by photonic- and redox-switching, and the associated spectral changes. Adapted from [30] with permission

luminescence of the $Ru(bipy)_3^{2+}$ moiety, electroreduction of the quinone to the hydroquinone restores the luminescence as a result of inefficient intramolecular quenching. Finally, a remarkable four-component fluorescence switch is schematically represented in Fig. 7D [34]. This device consists of a difluoroboradiaza-*s*-indacene unit as a photonic 'input', a Zn-porphyrin 'transmission element', a free base porphyrin as a fluorescence output, and a Mg-porphyrin as a redox switch. As the Mg-porphyrin has the lowest oxidation potential, it can be switched between the neutral and the radical cation states (either chemically or electrochemically) without affecting the rest of the assembly. When the Mg-porphyrin is in the neutral (reduced) state, photoexcitation of the 'input' component leads to vectorial energy transfer through the Zn-porphyrin to the free base porphyrin, which emits the energy as fluorescence (curve a). While the neutral Mg-porphyrin has a relatively high-energy absorption, so does not interfere with this energy transfer cascade, its oxidized state (an unstable radical cation) has low-lying energy levels. When an energy input is made to the oxidized assembly, the energy transfer from the Zn-porphyrin to the free base porphyrin is rejected in favor of the more facile energy transfer to the oxidized Mg-porphyrin. Since the excited Mg-porphyrin

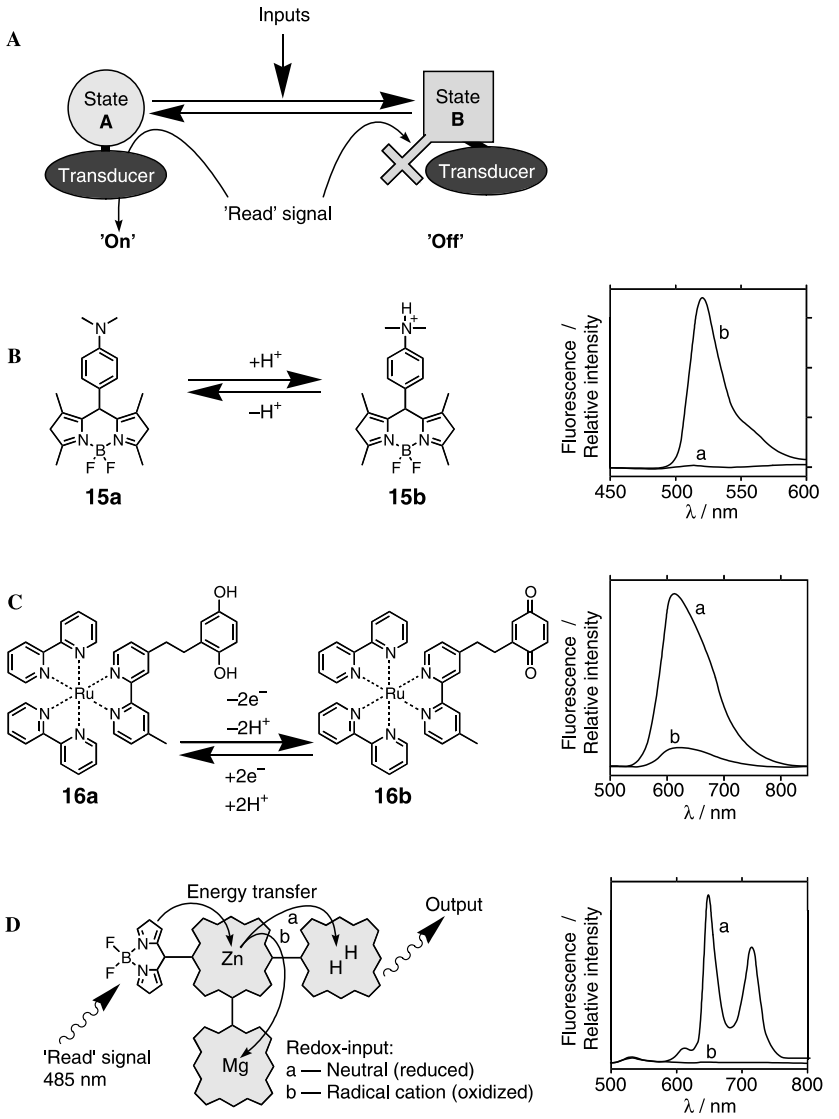

Fig. 7. **A** Schematic representation of a multicomponent system consisting of linked 'input' and 'output' units. **B** A pH-input fluorescence-output molecular switch. **C** A two-component redox-input fluorescence-output molecular switch. **D** A four-component redox-input fluorescence-output molecular switch. The fluorescence spectra in **B**, **C** and **D** are adapted from [32], [33] and [34], respectively, with permission

radical cation does not exhibit any fluorescence, the fluorescence spectrum of the oxidized device is 'switched off' (curve b). Upon re-reduction, the energy transfer pathway to the free base porphyrin is reactivated and the fluorescence is once more 'switched on'.

2.2 Information Functions of Binding Interactions

Reversible and switchable complexation events in solution are widespread in supramolecular chemistry, but do not always constitute useful information functions. Many systems rely on a movement of equilibria rather than true switching, and many more do not possess a practical 'read' function. These systems may be of interest as reversible sensing devices or for the study of supramolecular chemistry, but will not be covered here. Systems where supramolecular binding interactions are triggered by external light or electrochemical signals do provide elements of molecular machinery. Numerous ingenious examples of signal-stimulated binding events have been developed in the last two decades.

Several switches based on the photochemical or electrochemical control of metal ion binding by crown ethers have been constructed (Fig. 8). The binding of the metal cations is highly reliant on the ability of the crown ether to adopt a suitable conformation, and therefore the perturbation of the shape of the host has a marked effect on the binding constant. Figure 8A shows the crown ether **17**, which contains a photochemically isomerizable azobenzene unit [35]. In the *trans*-configuration, the cavity of the crown ether is too extended to accommodate a guest, and hence no ion binding is observed. When it is photoisomerized to the *cis*-isomer, however, very strong complexes are formed between **17** and K^+, Na^+ or Rb^+. The malachite green derivative **18** (Fig. 8B) employs an additional electrostatic interaction to ensure effective switching [36]. Irradiation of **18** (λ = 300–400 nm), which strongly binds Na^+ and K^+, results in both conformational change and the development of a positive charge on the host. This charge helps repel the metal ion, leading to the complete dissociation of the complex. Numerous other photonically and redox-switched crown ethers have been synthesized around diverse switching paradigms [37]. Figure 8C shows the host **19**, which is composed of calix[4]arene and anthraquinone units connected by ethylene glycol spacers to form an ion-binding cavity [38]. The reduction and oxidation of the quinone moiety lead to conformational change in the calixarene component, thus in the binding cavity, and also to an electronic change in the binding cavity. The selectivity of the host **19** towards different ions can therefore be electrochemically switched. Other switchable ion-binding hosts have been used for the transport of ions across membranes [39].

Ion binding may also be used as the signal to switch an 'output'. Figure 9 shows two examples of anthracene-based fluorescence switches. In these cases, the 'input' is the addition or removal of the guest (H^+ for host **20**, and Na^+ or K^+ for **21**) [40]. Neither compound **20** nor compound **21** is fluorescent in this state, as irradiation of the anthracene unit results in quenching of the photoexcited state by the amine donor unit. If the guest ion is added, however, the amine becomes 'tied up', removing the quenching route, and the complexes exhibit strong fluorescence. Similarly, fluorescence quenching can be switched on by the complexation of an amine to a crown ether that is connected to an anthracene unit [41].

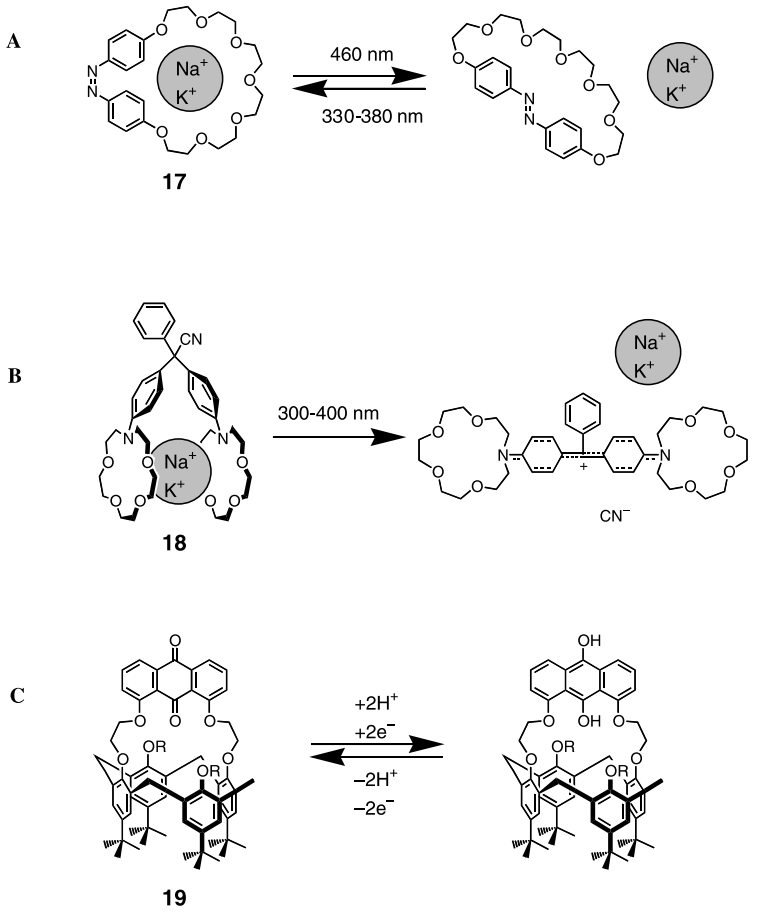

Fig. 8A–C. Molecular switches based on the binding ability of crown ethers. **A** A photoswitchable binding event based on conformational change upon azobenzene isomerization. **B** A photoswitchable binding event based on both conformational and electrostatic changes. **C** A redox-switchable calix[4]arene-crown ether

Supramolecular complexes of two molecules offer many advantages over simple ion-binding systems for the construction of information devices. Often, the binding event causes a strong 'output' (spectroscopic change, electrochemical change) without the need for an extra component. In addition, both the host and the guest are available for modification in order to attach other components or introduce isomerizable groups. A supramolecular system that can incorporate switching in either the host or the guest component is shown in Fig. 10. The tetracationic cyclophane **22** is a π-electron acceptor with a cavity that forms strong complexes with small π-donors such as **23** and **24**. These complexes exhibit charge-transfer bands in the visible region of their absorbance spectra leading to purple and green colors, respectively.

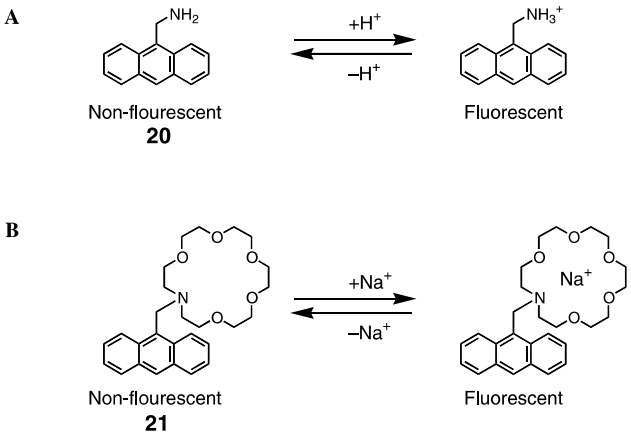

Fig. 9. Molecular switching of fluorescence as a function of ion binding **A** with H^+ ion binding and **B** with Na^+ or K^+ ion binding

Figure 10A shows the effect of reducing the host (**22**) [42]. The reduced host is not a strong π-acceptor, and thus the guest (**23**) is ejected from the cavity, as evidenced by an increase in the fluorescence of the naphthalene unit. Upon exposure to molecular oxygen, the host is re-oxidized, switching the system back to the bound state. The alternative π-donor guest tetrathiafulvalene (TTF) **24** (Fig. 10B) can also act as a redox switch. While it strongly binds **22** in its neutral form, oxidation to the radical cation results in the loss of its π-donor properties and the gain of a positive charge, both of which drive its expulsion from the cavity of the cyclophane [43]. In the unbound state, the system has a light brown color, but the dark-green, complexed state can be recovered by the reduction of **24** back to the neutral molecule. The oxidation and reduction of **24** have been demonstrated chemically and electrochemically, and the reduction of **22** has been shown chemically and photochemically. Ferrocene-based guests may be utilized in a similar manner with an expanded cyclophane [44].

Some other switchable components are shown in Fig. 11. Figure 11A shows a chemically or pH-switching [45] guest molecule (**25**) for the host dibenzo-24-crown-8 (**26**). In dichloromethane, the addition of tetrabutylammonium chloride to a complex of **25** and **26** causes a strong ion pair to form between **25** and chloride [46]. This ion pair cannot function as a guest molecule, so the complex dissociates. If the ion-pair is treated with a suitable base (diisopropylethylamine), the ammonium salt is deprotonated, restoring the complex with the crown ether (**26**). Switching can be followed by changes in the fluorescence spectrum. An interesting photoswitchable saccharide binder (**27**) is shown in Fig. 11B. The host molecule can be photochemically interconverted between 'open' and 'closed' isomers, but only the 'open' form can adopt the correct geometry to bind the substrate [47]. This arrangement constitutes a 'molecular tweezer', of which many other examples exist [48]. Once the

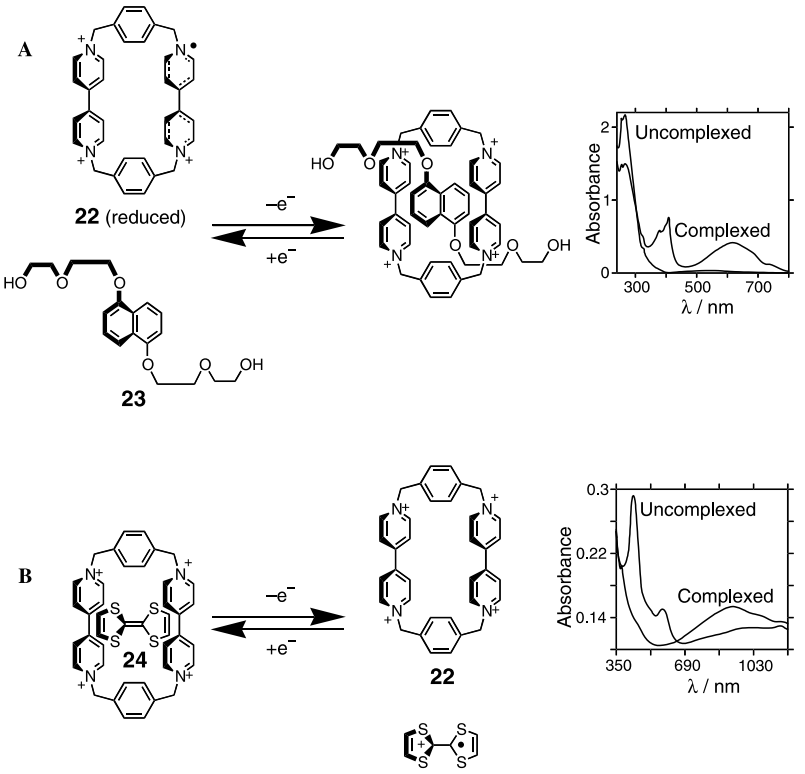

Fig. 10A, B. A redox-switchable supramolecular system based on charge-transfer interactions which can be read by spectroscopic means. **A** Redox switching of the host compound **22**. **B** Redox switching of the guest **24**. The absorbance spectra in **A** and **B** are adapted from [42] and [43], respectively, with permission

complex has formed, its conformational requirements are such that photoisomerization to the closed form is no longer possible. The supramolecular event thus constitutes a 'lock' cycle for the photochemical switch. The saccharide complex can be detected by circular dichroism. Figure 11C schematically shows a complex of cucubituril with a guest that translocates depending on its level of protonation [49], and Fig. 11D shows a flavin-containing cyclophane that changes the shape of its cavity (thus, its binding properties) upon redox-switching [50]. Figure 11E shows a photoswitchable azobenzene-based guest for the cyclophane **22** [51]. While the *trans*-azobenzene unit can associate with the cyclophane through π donor-acceptor interactions, photoisomerization to the *cis* state results in the dissociation of the complex. Switchable units such as azobenzene [52] and pH-sensitive interactions [53] have also been incorporated into cyclodextrins in order to modulate their binding activity.

The use of competing hosts and guests exhibiting various switching, complexation and 'output' functions allows the design of more complicated

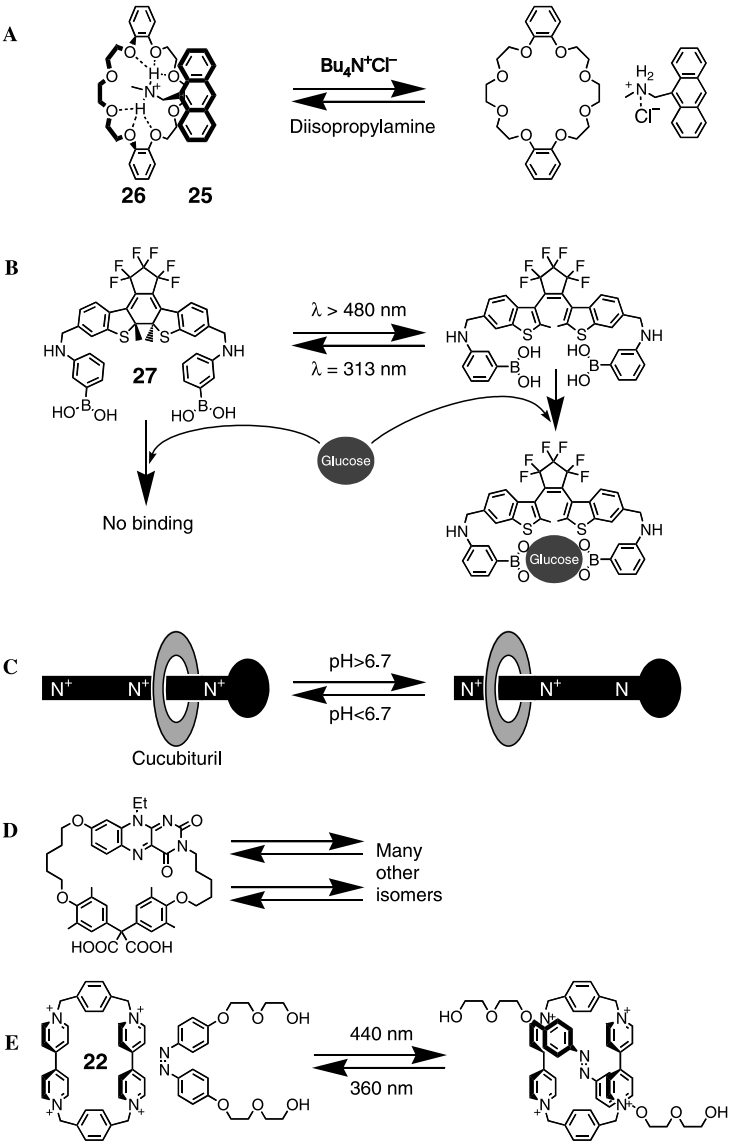

Fig. 11A–E. Some switchable units for supramolecular chemistry. **A** A chemically switchable guest **25** based on an amine. **B** A photoswitchable host for saccharides based on conformational change. **C** A pH-switchable guest for cucubituril. **D** A redox-switchable cyclophane. **E** A photoswitchable azobenzene-based guest for the cyclophane **22**

multicomponent systems [54]. A simple example is given in Fig. 12. This system is composed of the π-electron-rich naphthalene-containing crown ether **28**, 2, 7-dibenzyldiazapyrenium (**29**) and hexylamine (**30**) [55]. The π-electron-deficient dication **29** can form a charge-transfer complex either with

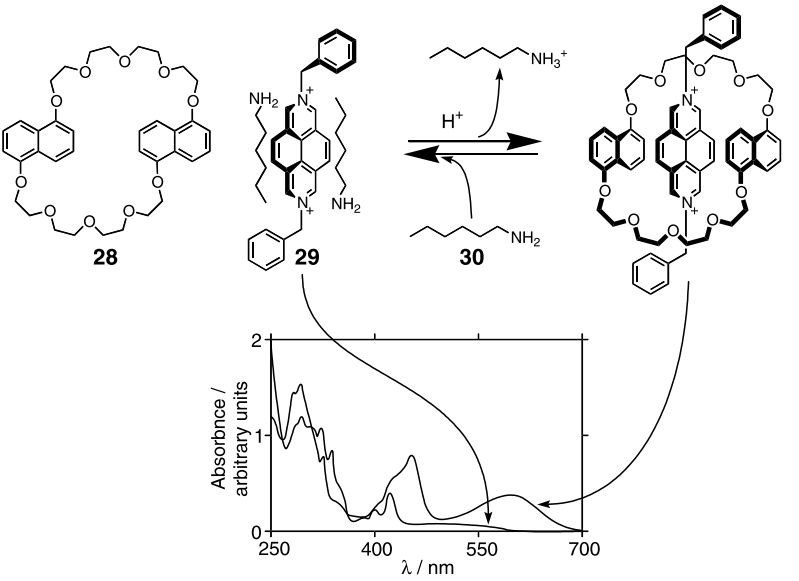

Fig. 12. A multicomponent supramolecular switching system based on competition between the crown ether **28** and hexylamine (**30**) for the binding of **29**. The binding of **30** depends on its protonation state. The absorbance spectra are adapted from [55] with permission

the host **28** or with two molecules of the amine **30**. The addition of trifluoroacetic acid (TFA) causes the protonation of **30**, effectively removing it from the system so that the complex with **28** is favored. The addition of **30** shifts the equilibrium towards the complex between **29** and **30**. The state of the system can be monitored either by absorbance spectroscopy or by examining the fluorescence spectrum of the naphthalene component (in the crown ether **28**), which is quenched when it is complexed with **29**. The same chemical switching concept has been used for the design of a switchable catenane [56].

2.3 Mechanically-Switching Molecular Assemblies

The development of facile synthetic routes to mechanically interlocked rotaxanes and catenanes has allowed the construction of supramolecular interaction-based devices that are fully integrated, rather than a mixture of individual components [57]. These molecules are held together by their topology, so even when there are no interactions between the individual components, they remain integrated. In addition to this advantage, the topological constraining of intercomponent relations allows the design of sophisticated mechanical functions.

The simplest model for mechanical switching is based on the translocation or reorganization of molecular components around a metal ion. Some redox pairs of transition metal ions have markedly different complexation properties,

so a molecule that contains binding sites optimized for each of two redox states of a metal ion will change shape upon the reduction or oxidation of the ion to accommodate the different metal ion redox states. Alternatively, the ions may be translocated between ligation sites upon their electrochemical reduction or oxidation. The different complex states usually have significantly different absorption spectra, so the system can be considered a switch with a redox (chemical or electrochemical) 'write' function and an optical 'read' function.

A switch based on the translocation of an $Fe^{2+/3+}$ ion within a triple helical ligand is shown in Fig. 13A [58]. The three-armed compound **31** contains three 'hard' hydroxamate moieties near its core (suitable for binding the Fe^{3+} ion) and three 'soft' bipyridyl units near its chain ends (suitable for binding the Fe^{2+} ion). Upon complexation with Fe^{3+}, a triple helical structure is formed with the metal ion surrounded by the three hydroxamate units. The ion can then be caused to move to a second binding site, composed of the three bipyridyl units, by its chemical reduction to Fe^{2+} with ascorbic acid. Regeneration of the first structure can be achieved by oxidation with ammonium persulfate. A similar system based on a calix[4]arene bearing alternating hydroxamate and bipyridine substituents around one of its faces (**32**) has also been constructed (Fig. 13B) [59]. In this case, reorganization of the system is achieved by the movement of the coordinating 'arms' of the molecular component upon the reduction and oxidation of the central $Fe^{2+/3+}$ ion. The use of metal ions in switchable supramolecular systems has already been alluded to in Fig. 2B [12]. A series of supramolecular structures with mechanical switching arising from the reduction and oxidation of a copper ion has thus been constructed [12, 60, 61]. In Fig. 13C, the simplest of these systems is presented in the form of a pseudorotaxane [61]. This machine is based on the different preferred coordination numbers of the Cu^{+} and Cu^{2+} ions (4 and 5/6, respectively). The pseudorotaxane consists of a string-like component (**33**) containing bidentate and tridentate ligands, a macrocycle containing a bidentate ligand (**34**), and a copper ion. With the copper ion in the +1 oxidation state, the macrocycle is threaded on the 'string' and resides on the bidentate site, so that the Cu^{+} ion can assume its preferred coordination. If the ion is oxidized to Cu^{2+}, then the macrocycle eventually moves over the tridentate site on the 'string' component so that the metal ion can assume a pentavalent coordination. The system is stable, reversibly switchable, and can be followed easily by absorbance spectroscopy.

One particularly interesting architecture is that of the self-complexing molecule. This is a system where host and guest components are covalently linked, giving the functionality of a multicomponent device with the integration of a covalent assembly. A redox-switched self-complexing molecule with optical 'read' functionality is presented in Fig. 14 [62]. Its structure consists of an electron-rich π-donating dioxynaphthalene residue tethered to an electron-deficient cyclophane. In the oxidized state (**35a**), the naphthalene moiety forms a charge-transfer complex within the cavity of the macrocycle, which brings about a strong absorbance in the visible region. Reduction of the macrocycle to the bis-radical cation (**35b**) results in decomplexation and the loss of the absorbance feature.

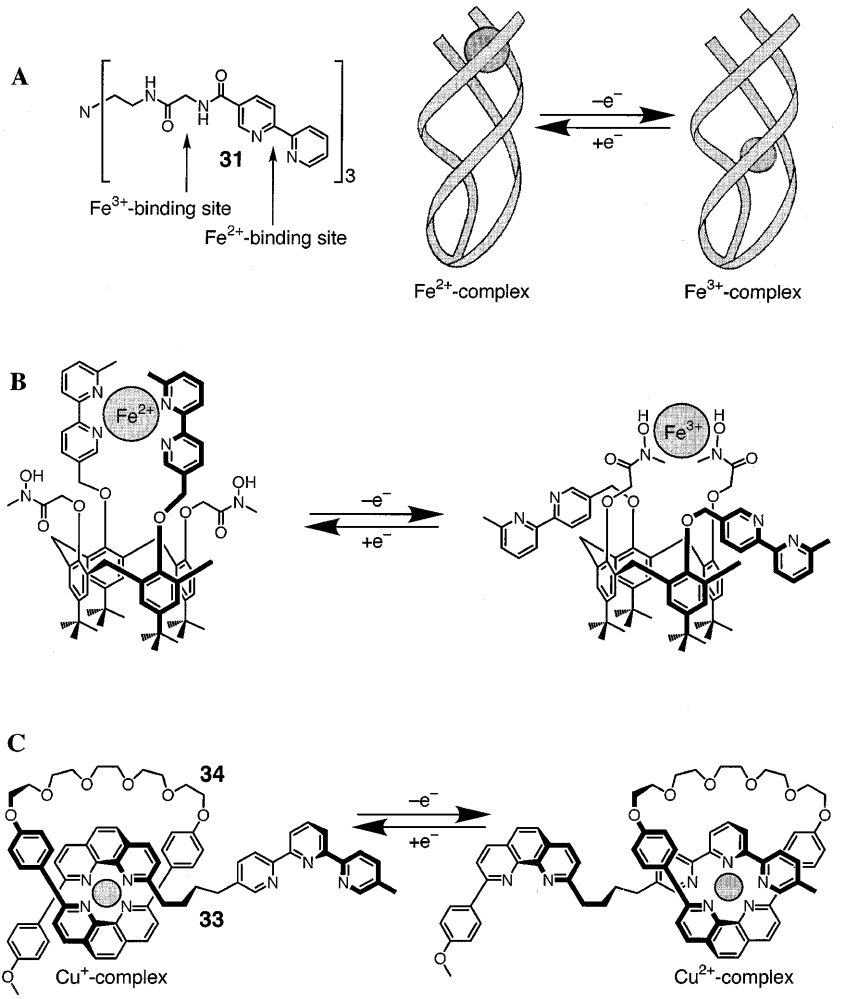

Fig. 13A–C. Topological switching of supramolecular structures by oxidation and reduction on metal ions. **A** The translocation of an $Fe^{2+/3+}$ ion within a triple helical structure. **B** The conformation change of a calixarene in response to the oxidation state of an $Fe^{2+/3+}$ ion. **C** The translocation of a cyclophane upon the change in oxidation state of a $Cu^{+/2+}$ ion

Catenanes are multicomponent systems where the molecular species are integrated by topological rather than covalent constraints. They are composed of two interlocking macrocycles, each a discrete molecule, and may be synthesized by a number of means including self-assembly, a labile linkage between components and statistical threading [63]. Different mechanical states may be accomplished by the rotation of one macrocyclic component through the cavity of the other (Fig. 15A). A redox-switchable catenane functioning on controllable π donor-acceptor interactions is depicted in Fig. 15B [64]. The

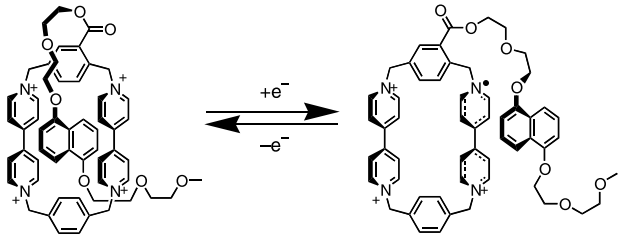

Fig. 14. Redox-switchable complexation in a self-complexing molecule

crown ether component contains both TTF and dioxynaphthalene π-donor sites. In the reduced state, the TTF residue is bound in the cavity of the tetracationic cyclophane component more strongly than is the dioxynaphthalene site, leading to the structure **36a** and a dark-green color (curve a). Chemical or electrochemical oxidation of the TTF residue causes it to lose its high binding affinity for the cavity, leading to its ejection in favor of the dioxynaphthalene donor site (**36b**), which has a maroon color (curve b). The changes in the charge-transfer band of the absorbance spectrum demonstrate reversible changes upon the oxidation and reduction of the TTF radical cation. A similar system based on the selective reduction of bipyridinium over *bis*-pyridyl ethene in the cyclophane component has also been synthesized [65].

Figure 15C shows a pH-switchable catenane that combines ion binding and π donor-acceptor interactions in one system. The two rings of this catenane (**37**) contain complementary *bis*-bipyridine and dioxynaphthalene sites, and they both include ion-binding phenanthroline units [66]. In acetonitrile solution, the catenane adopts a conformation where the dioxynaphthalene residue resides between the two bipyridine units of the other ring component, giving rise to a charge-transfer absorbance in its spectrum. Upon the addition of trifluoroacetic acid, however, a very strong complex can form by the binding of a proton by the two phenanthroline units. The formation of this complex requires a complete reorganization of the catenane with the loss of the charge-transfer complex and its associated optical absorbance. The subsequent addition of pyridine removes the bound proton, regenerating the original structure and spectrum.

Another class of mechanically interlocked molecules are the rotaxanes, which may be synthesized by similar means to the catenanes. These architectures consist of a long string-like component with a macrocycle threaded on it (Fig. 16A). A true rotaxane has 'stoppers' on the ends of the string-like component that prevent the macrocycle from unthreading, while a pseudorotaxane lacks stoppers and the macrocycle remains on the string as a result of binding interactions. Molecular switches may be constructed by taking advantage of the ability of the macrocycle to move along the length of a string to give different translational isomers. The first of these 'molecular shuttles' was modeled around the binding of the cyclophane **22** with benzidine

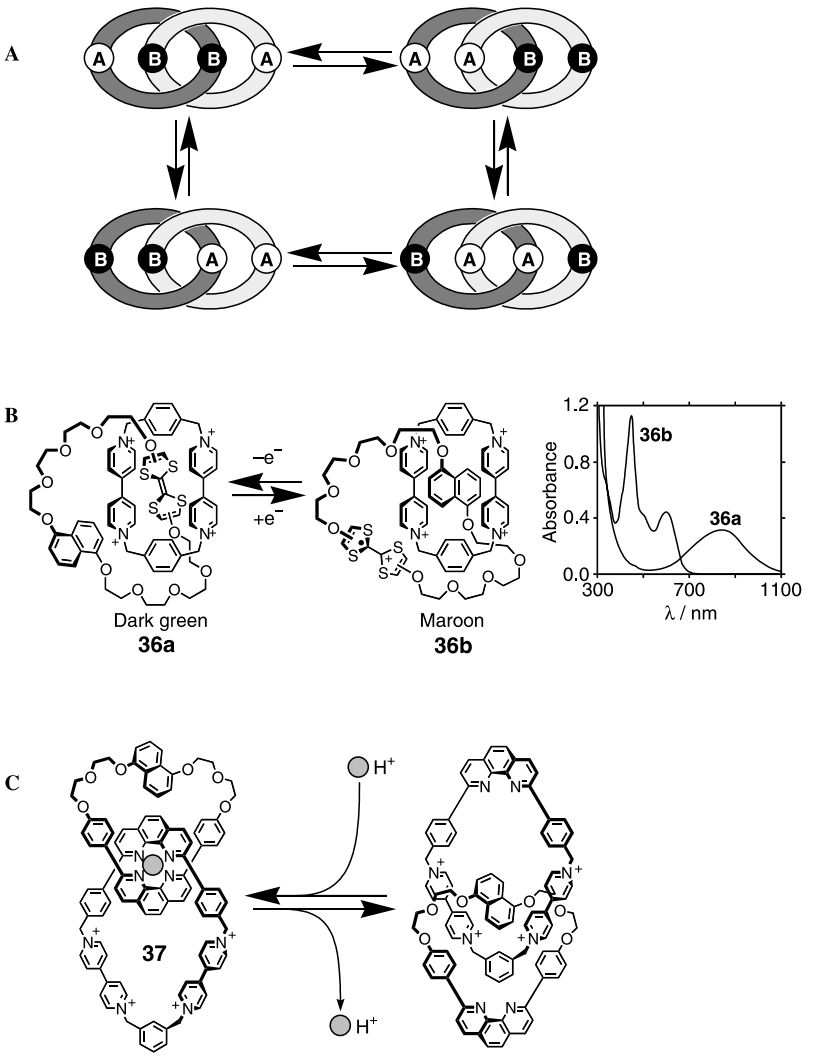

Fig. 15A–C. Mechanical switching in catenanes. **A** The individual rings of catenanes may be unsymmetrical. A [2]catenane with two distinct sites on each ring may exist in four different states. **B** A switchable catenane based on the competitive binding of TTF and dioxynaphthalene residues on one ring inside the cavity of the second ring. The TTF moiety is bound preferentially in the reduced state, but is repelled in the oxidized state and replaced with the dioxynaphthalene unit. **C** A proton-switchable [2]catenane. The phenanthroline units in the rings of 37 form a complex around H^+, but, when H^+ is not present, a charge-transfer complex is formed between the viologen units in one ring and the dioxynaphthalene unit in the other. The absorbance spectra are adapted from [64] with permission

and biphenol sites on a 'string' (**38**, Fig. 16B) [67]. In its native state, the benzidine moiety has the strongest binding affinity for the cyclophane, but, when it is either electrochemically oxidized to a radical cation or protonated

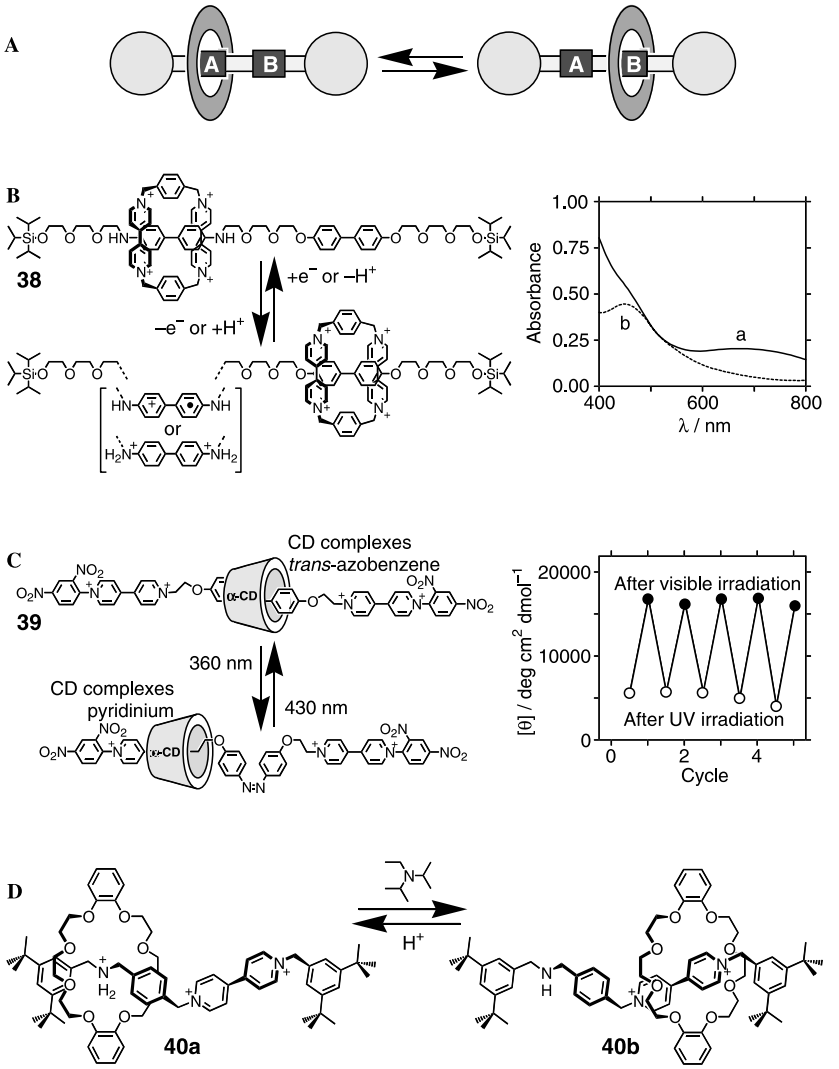

Fig. 16A–D. Mechanical switching in rotaxanes. **A** Rotaxanes may exist in isomeric states by the movement of the ring component between dissymmetric sites on the string component. **B** A redox- or pH-switchable [2]rotaxane. While the cyclophane complexes the native benzidine site (spectrum, curve a), the reduced or protonated benzidine repels the cyclophane, causing it to move to the dioxybiphenylene site (spectrum, curve b). **C** An azobenzene-based switchable [2]rotaxane. The cyclodextrin ring complexes the azobenzene site in the *trans*-state, but it is repelled from the *cis*-azobenzene. The state of the system is measurable by circular dichroism (plot). **D** A pH-switchable rotaxane. When the amine on the string component is protonated, it complexes the crown ether ring by hydrogen-bonding interactions (**40a**). When the amine is deprotonated, however, the ring component moves to the bipyridinium unit, where it is complexed by π donor-acceptor interactions (**40b**). The plots in **B** and **C** are adapted from [67] and [69], respectively, with permission

by TFA, its π-donor properties are weakened and it gains a positive charge. These changes cause the cyclophane to change its preferred binding site to the biphenol moiety, so it translocates accordingly. As with the similar systems discussed previously, this transformation is easily reversed by either reduction or deprotonation and may be followed by absorbance spectroscopy. Similar systems based on the cyclophane **22** and guests containing either TTF (solvent or redox control) [64, 68] or azobenzene (photonic control) [51] have also been constructed.

A photonically driven molecular shuttle consisting of an α-cyclodextrin molecule threaded on an azobenzene-containing string (**39**) has also been developed (Fig. 16C) [69]. Azobenzene binds α-cyclodextrin in the *trans*-conformation, but not in the *cis*-state. Thus, the cyclodextrin molecule moves along the string in response to photoisomerization of the azobenzene unit. The position of the cyclodextrin on the string was confirmed by NMR (by examination of the NOE differential spectrum), and was monitored over several cycles by analysis of the changes in the circular dichroism spectrum (Fig. 16C). Figure 16D shows a pH-switchable shuttle (**40**) where the two states are each stabilized by a different type of binding interaction [70]. In the protonated state (**40a**), the ammonium moiety is strongly bound by the oxygen atoms of the macrocyclic crown ether. Deprotonation of the amine with diisopropylethylamine breaks the ammonium-crown ether complex, after which the dioxybenzene moieties are free to form a charge-transfer complex with the bipyridine unit on the string.

2.4
Assemblies that Perform Logical Functions

A small number of molecular devices that the inventors claim perform logical functions have been synthesized [71, 72]. These systems are extremely important as they offer the basic units required for the construction of information processing devices; nevertheless, the definition of a 'molecular logic gate' is often stretched to its limit. In addition, the devices produced to date only act as stand-alone units. Each input and output is of a different type (e.g. chemical, pH, optical, electrochemical), and chemical inputs are always required. Bearing this in mind, they cannot be used as parts of larger systems until a new concept for component connectivity is developed. A molecular AND gate functioning with chemical inputs and a fluorescence output is shown in Fig. 17A [72]. In its native form, the photoexcited state of the anthracene moiety is quenched by intramolecular photoinduced electron transfer from either the dioxybenzene unit or the amine group. In the presence of Na^+, which binds the crown ether, quenching by the dioxybenzene unit is inhibited, but effective quenching by the amine still occurs. Likewise, protonation of the amine removes the possibility of quenching by the amine donor site, leaving only the dioxybenzene quenching route. Fluorescence from the anthracene moiety is only obtained when both Na^+ and H^+ are associated with **41**, thus the system is described as a molecular AND gate with two chemical inputs (Na^+ and H^+) and a fluorescence output. Figure 17B shows the

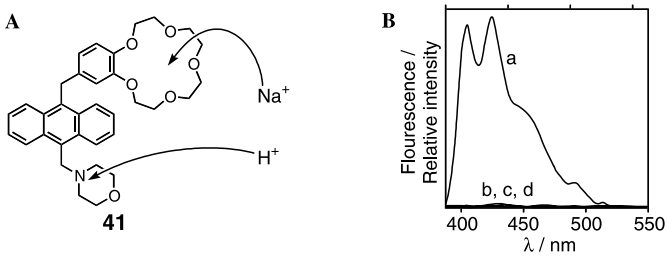

Fig. 17. **A** A molecular 'AND' gate with chemical inputs (H^+ and Na^+) and a fluorescence output. **B** Fluorescence spectra of the 'AND' gate (**a**) in the presence of H^+ and Na^+, (**b**) in the presence of H^+ and the absence of Na^+, (**c**) in the presence of Na^+ and the absence of H^+, and (**d**) in the absence of both H^+ and Na^+. The fluorescence spectra are adapted from [72] with permission

fluorescence spectra of the gate in its four states, demonstrating the striking difference between the AND condition and the other possibilities.

3
Surface-Integrated Molecular Devices

The immobilization of functional units in monolayers or thin films allows the construction of interfaced devices. In recent years, techniques for the construction of these interfaces have become highly developed, and can be broadly categorized into three methodologies – covalent modification [73], self-assembly [74], and Langmuir-Blodgett films [75]. In many cases a combination of these techniques is used to give a desired surface architecture. The surfaces associated with the immobilized devices may be integrated with analytical devices such as piezoelectric crystals (i.e. quartz crystal microbalances, QCMs), electrodes or surface plasmon spectroscopy (SPR) substrates, they may be transparent to facilitate optical and photoelectrochemical studies, and may have a wide range of surface functionalities. Advantage may be taken of units synthesized by classical techniques, and a wide range of immobilization methodologies (e.g. covalent functionalization, immobilization in polymer matrices, Langmuir-Blodgett layers) can be employed. Despite these advantages, however, the construction of surface-integrated devices is fraught with difficulties. The tiny quantities of materials in surface modifications require special characterization techniques, and this difficulty is exacerbated by the inhomogeneity of many surface architectures. If chemical modifications are made on a surface construct, the yield of reaction must either be close to quantitative, or all reactants and side products must be benign, as there is rarely a possibility to purify the sample. The construction of surface-bound mechanical architectures is particularly problematic as the asymmetry provided by the interface, while ultimately of great utility, requires that the individual molecules are specifically aligned on the surface.

The photonic activation of molecular mechanical functions in solution is often limited by its lack of integration. The electrochemical transduction of

photoactivated processes requires relatively high concentrations of the molecular device and is limited by diffusion. The assembly of the molecular devices on surfaces bypasses these problems. Photonic activation of redox functions on surfaces can be easily envisaged as a general methodology for the amperometric transduction of optical signals. Alternatively, the electrochemical switching of chemical functionalities on surfaces may be used for the optical transduction of electronic signals. The assembly of molecular functionalities on electrode supports generates addressable topologies that may lead to the future miniaturization of devices to micro- or nanoscale dimensions.

3.1
Surface-Confined Molecular Optoelectronics

The immobilization of a photoisomerizable material that can be switched by light between redox-active and redox-inactive or conductive and insulating states offers an encouraging route toward integrated molecular memory devices (Fig. 18). In the photoisomer state 'A', the molecular unit is redox-inactive and no electronic signal is transduced. Photoisomerization of the chemical component to state 'B' generates a redox-active assembly, and the electron transfer between the electrode and the chemical interface yields an amperometric (electrochemical) indicator of the state of the system.

The practical construction of such an optoelectronic system was exemplified with a phenoxynaphthacene quinone that exists in two photochemically interchangeable states: the redox-active *trans*-quinone (**42a**) and the redox-inactive *ana*-quinone (**42b**) [76]. A carboxylic acid derivative of the phenoxynaphthacene quinone was assembled as a monolayer on a Au electrode by the coupling of 6-[(4-carboxymethyl)phenyl)oxy]-5, 12-naphthacene quinone to a self-assembled cystamine monolayer (Fig. 19A) [77]. The cyclic voltammogram of the resulting monolayer shows an ill-defined redox wave for **42a** (Fig. 19B, curve a) since a non-densely packed monolayer of the quinone is formed. The random orientation of the quinones relative to the electrode, as well as non-specific adsorption of the quinone to the surface, yields a mixture of quinone units with different electrochemical features, leading to the broad voltammogram. Treatment of the **42a**-functionalized electrode with tetradecane thiol ($C_{14}H_{29}SH$) results in the association of the long-chain hydrophobic thiol to surface pinhole defects, resulting in the formation of a densely packed mixed monolayer consisting of $C_{14}H_{29}S^-$ and **42a**.

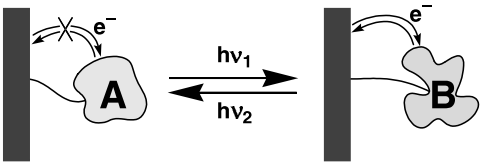

Fig. 18. Schematic representation of an optically switched redox monolayer

Figure 19B shows the effect of the thiol treatment. The quasi-reversible redox wave of the electrode after treatment ($E^\circ = -0.62$ V vs. SCE, curve b) is attributed to the two-electron redox process of **42a** in a rigid, aligned configuration. Coulometric assay of the charge associated with the reduction (or oxidation) of the **42a** component reveals a surface coverage of the quinone of 2×10^{-10} mol cm^{-2}. The electron transfer rate from the electrode to the quinone was estimated to be $k_{et} \approx 2.5$ s^{-1} by following the peak-to-peak separation of the redox wave at different scan rates. Figure 19B shows cyclic voltammograms of the **42**-monolayer in the 'ana' quinone-state (curve c) and 'trans' quinone-state (curve b). In the presence of the **42b**-monolayer, only the

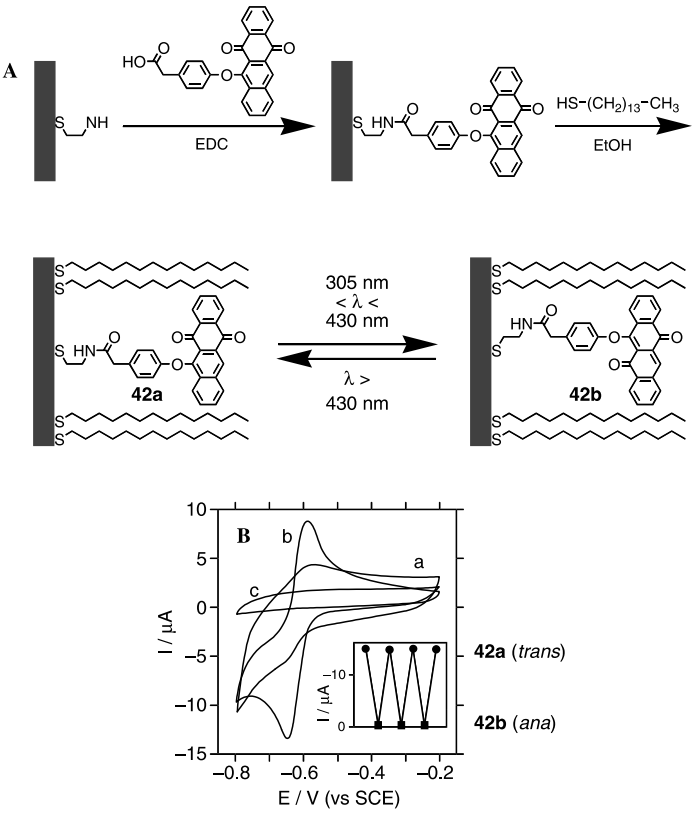

Fig. 19. **A** Assembly of a phenoxynaphthacenequinone 1-tetradecanethiol mixed monolayer on a Au electrode and its photoisomerization. **B** Cyclic voltammograms of the *trans*-quinone monolayer (**42a**) *a* before rigidification with tetradecanethiol and *b* after rigidification with tetradecanethiol. *c* Cyclic voltammogram of the mixed monolayer after photoisomerization of the *trans*-quinone to the *ana*-quinone state. Cyclic voltammograms were recorded in 0.01 M phosphate buffer (pH 7.0) with a potential scan rate of 50 mV s^{-1}. *Inset* Switching behavior of the cathodic peak current in the cyclic voltammogram of the mixed monolayer upon reversible photoisomerization

background current of the electrolyte is observed, implying that this photoisomer monolayer is redox-inactive within this potential range. By the cyclic photoisomerization of the monolayer between the **42a**- and **42b**-states, the transduced current is switched reversibly between 'ON'- and 'OFF'-states, respectively (Fig. 19B, inset).

An important aspect in the development of molecular optoelectronics is the amplification of the electrochemical response to photonic signals. Such systems could find applications in electronic amplifiers for weak light signals or for sensitive actinometers. One way in which amplification can be accomplished is by the coupling of the electroactive component to an electron transfer cascade (Fig. 20A). The mixed monolayer (consisting of $C_{14}H_{29}S^-$ and **42a**) provides an insulating layer, so direct electron transfer from the electrode to a solution-state electron relay is inhibited. Electronic contact between the electrode and solution can only take place using **42** as a relay. In the electrochemically active 'trans' (**42a**)-state, vectorial electron transfer from the redox-active unit to the diffusional relay is possible, stimulating the electrocatalyzed reduction of the solubilized species. The amplification of the electrochemical response to photonic signals can be exemplified by the application of *N, N′*-dibenzyl-4, 4′-bipyridinium (BV^{2+}, **43**) as a secondary electron relay. The reduction potential of BV^{2+} ($E^\circ = -0.58$ V vs. SCE) is pH-independent, while the formal reduction potential of **42a** at pH = 7.5 is $E^\circ = -0.65$ V vs. SCE. The small difference allows the vectorial reduction of

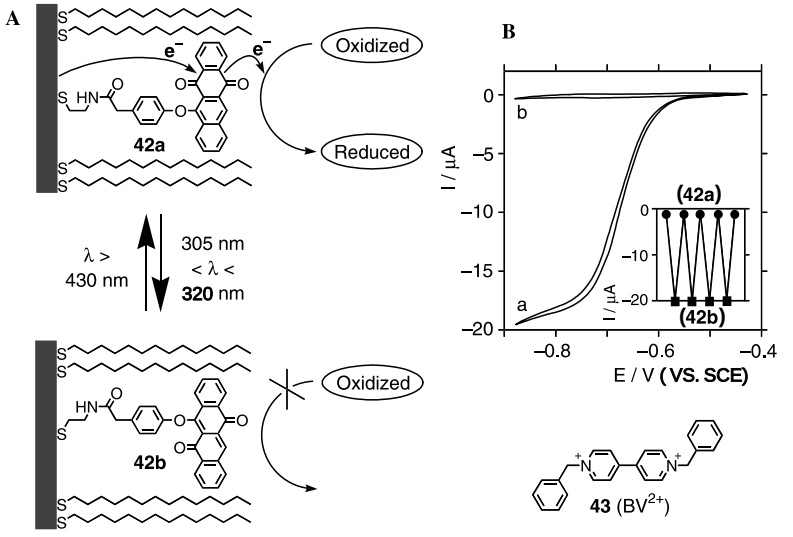

Fig. 20. **A** Use of dibenzylviologen (**43**) to amplify the electrochemical signal of the photoswitchable phenoxynaphthacenequinone/tetradecanethiol mixed monolayer. **B** Cyclic voltammograms of the electrode in the presence of benzyl viologen (1 mM) *a* in the *trans*-quinone state and *b* in the *ana*-quinone state. Recorded at pH 7.5, scan rate 5 mV s^{-1}. *Inset* Photoswitching behavior of the electrocatalytic current

BV^{2+} by the electroactive **42a** monolayer, and thus the activation of an electron transfer cascade. The transduced current is ca. 10-fold enhanced in the presence of the electron relay. Figure 20B shows the cyclic voltammograms of the photoisomerizable electrode in the presence of BV^{2+} and in the **42a**-state (curve a) and the **42b**-state (curve b). While the electrocatalytic current is present in the **42a**-state, photoisomerization of the monolayer to the **42b**-state, 305 nm $< \lambda <$ 320 nm, results in only the background current (curve b), demonstrating that direct electron transfer to BV^{2+} is prohibited.

The reduction potential of the **42a**-monolayer is controlled by the pH of the electrolyte and is positively shifted as the pH decreases (e.g. $E^\circ = -0.65$ V vs. SCE at pH = 7.5 and $E^\circ = -0.51$ V vs. SCE at pH = 5.0). This movement allows the use of pH as an additional controller of the interfacial electron transfer features of the functionalized monolayer. At pH = 5.0, the **42a**-monolayer is thermodynamically prohibited from stimulating electron transfer to BV^{2+} ($E^\circ = -0.58$ V vs. SCE). Only the weak electrical response of the **42a**-monolayer is observed, without the activation of the electron transfer cascade. Thus, the phenoxynaphthacenequinone-functionalized monolayer-electrode can be described as an 'AND' gate with optical and pH inputs that act cooperatively in the activation of an electrochemical output.

The photoisomerizable moiety and the signal transduction moiety in an active molecule can be distinct chemical groups [78]. For example, a Langmuir-Blodgett monolayer composed of molecules with two distinguishable parts: a photoisomerizable azobenzene unit and a TCNQ salt (an organic conductor), was assembled onto a solid support. Lateral conductivity of the monolayer was studied as a function of the photochemically controlled isomerization state of the azobenzene units. The photochemically induced structural changes of the monolayer packing result in the variation of the conductivity, providing optical 'write' and electrical 'read' modes of signal transduction (Fig. 21).

Photoisomerizable properties of azobenzene-functionalized monolayers immobilized onto solid supports by covalent attachment [79], by chemisorption of thiol groups [80] or by the Langmuir-Blodgett method [81] were extensively studied using different spectral techniques and AFM. These monolayers represent other examples of layered assemblies with electrochemical properties controlled by photoisomerization of the layer [82]. For example, 4-octyl-4′-(5-carboxypentamethyleneoxy)azobenzene was deposited in the *trans*-state as a monolayer film onto an SnO_2 electrode using the Langmuir-Blodgett method [82]. The monolayer was reversibly photoisomerized upon appropriate irradiation between *trans*- (**44a**) and *cis*- (**44b**) isomeric states. This monolayer-modified electrode exhibited different cyclic voltammograms for these isomeric states (Fig. 22). Whereas the *cis*-isomer was readily reduced to the hydrozobenzene form (**44c**) (Fig. 22, curve b), the *trans*-isomer was electrochemically inactive in the studied potential range (Fig. 22, curve a). The electrochemical oxidation of the hydrozobenzene returned the monolayer to the thermodynamically favored *trans*-isomer. Thus, the 'write'-optical signal results in the photoisomerization of the **44a**-monolayer to the **44b**-state, but the 'read'-electrochemical procedure 'locks'

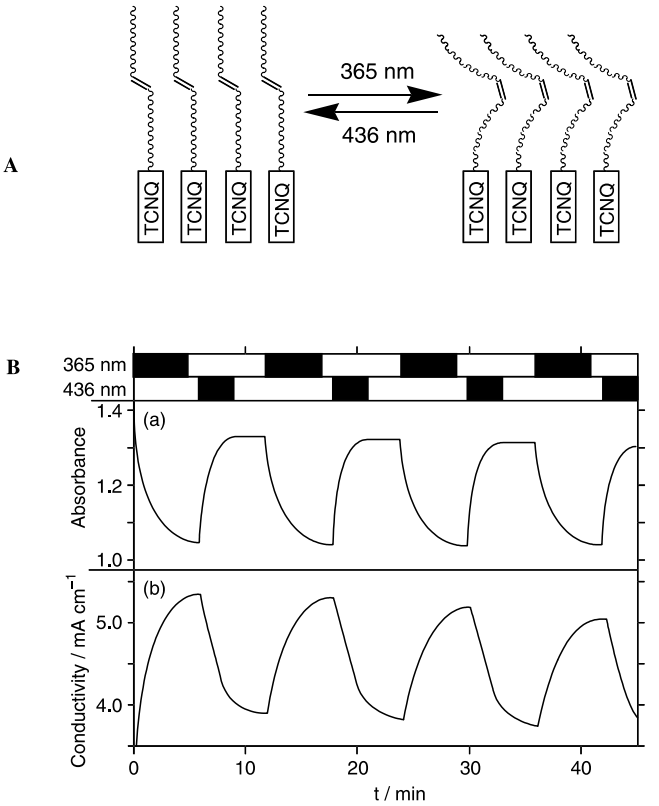

Fig. 21. **A** Schematic representation of a photoisomerizable azobenzene-TCNQ Langmuir-Blodgett monolayer. **B** Changes in *a* absorbance at 356 nm and *b* conductivity of the monolayer upon photoisomerization

the system in the reduced **44c**-state. The stored information can be electrochemically erased upon oxidation of **44c** to the original **44a**-state. Similar results were reported for a self-assembled monolayer of a thiol-functionalized azobenzene derivative [83]. The system has also been applied as an electrochemical actinometer since only one photogenerated isomer is electrochemically detectable [84].

A further system providing photoswitchable redox-activated properties with amplification features via a secondary electrocatalytic vectorial electron transfer reaction has been exemplified by diarylethene (**45**) molecules incorporated into a long-chain thiol monolayer adsorbed on a Au electrode due to hydrophobic interactions [85]. In the 'closed' isomeric state (**45a**), the monolayer demonstrates well-defined reversible cyclic voltammetry, whereas the 'open' (**45b**)-state is completely redox-inactive. The electrochemically active **45a**-state provides electrocatalytic reduction of $Fe(CN)_6^{3-}$, thus enabling a vectorial electron cascade that amplifies the photonic input.

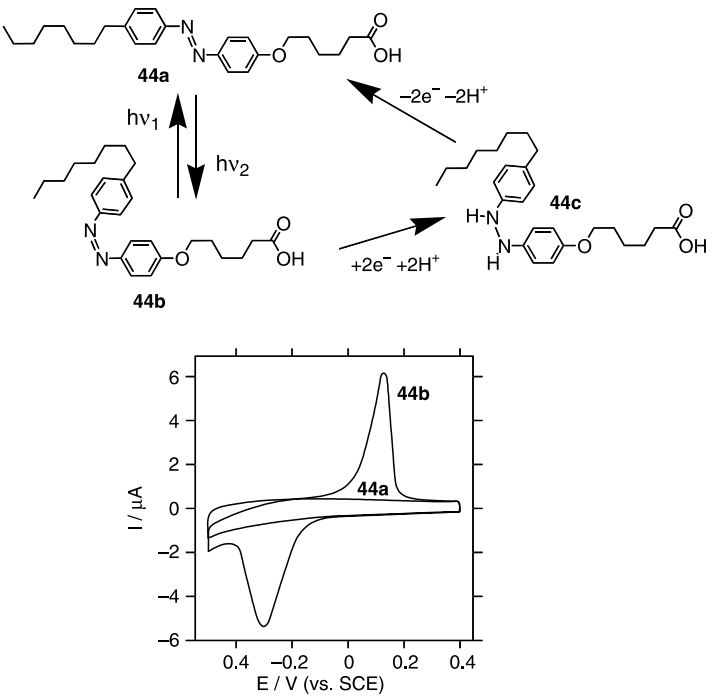

Fig. 22. Isomerization of an azobenzene-based monolayer between the electrochemically inactive *trans*-state and the electrochemically lockable *cis*-state. The cyclic voltammogram shows traces for the *trans*- and *cis*-isomers. Recorded at pH 7.0 at a potential scan rate of 20 mV s^{-1}

3.2 Photoisomerizable 'Command Surfaces'

Another approach to the organization of integrated optoelectronic switches is schematically detailed in Fig. 23, and involves the organization of a photoisomerizable 'command interface' on the solid support [86]. The 'command surface' controls the interfacial electron transfer to a solution-state redox species. In one photoisomeric state, electron transfer to a redox probe solubilized in the electrolyte solution is prohibited (e.g. by repulsive interactions), whereas in the complementary state of the monolayer the interfacial electron transfer is allowed (e.g. because of associative interactions). Various interactions, such as electrostatic interactions, host-guest or donor-acceptor interactions, contribute to the selective contacting of the redox probe to one state of the photoisomerizable monolayer.

Charged monolayers have been successfully employed as active interfaces for controlling electron transfer at electrode supports [87, 88]. Negatively charged monolayers associated with electrodes have been shown to discriminate between the electrochemical reactions of a mixture of positively and

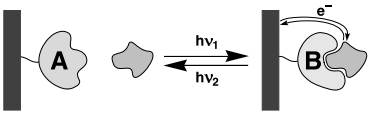

Fig. 23. Schematic representation of a 'command surface'. The response of the surface to an external species is controlled by the state of the interface

negatively charged substrates [89]. Accordingly, a photoisomerizable nitrospiropyran monolayer that alters the electrical charge on the conductive support upon irradiation can be constructed on a Au electrode. In one example, 1-(4-mercaptobutyl)-3, 3-dimethyl-6′-nitrospiro[2′*H*-1-benzopyran-2′, 2-indoline] (mercaptobutylnitrospiropyran) was assembled on a Au electrode (Fig. 24A) [91]. While the nitrospiropyran monolayer (SP-state, **46a**) is neutral, photoisomerization of the monolayer (at pH = 7.0) yields a

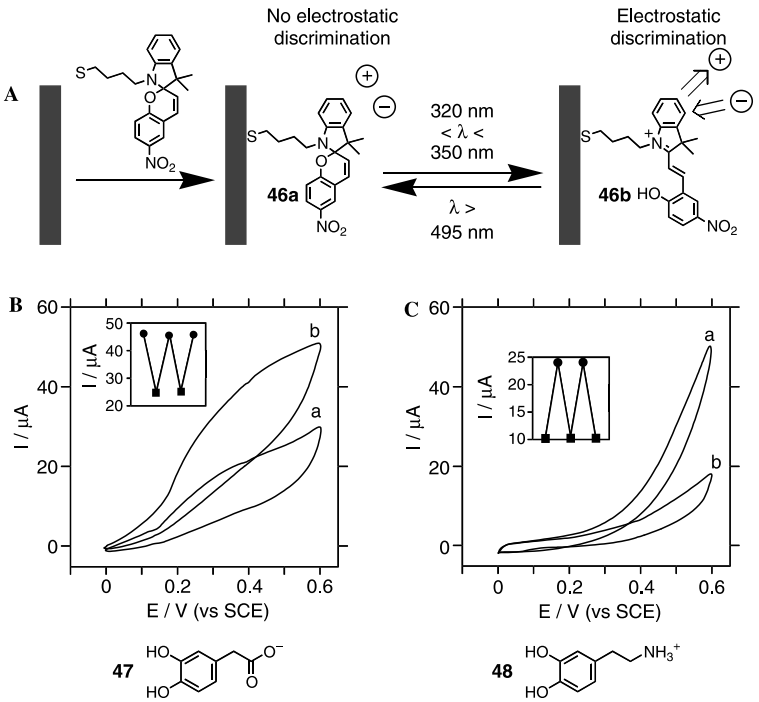

Fig. 24. **A** The assembly and photoswitchable states of a nitrospiropyran monolayer. **B** Cyclic voltammograms of the photoisomerizable electrode in the presence of dihydroxyphenylacetic acid (**47**, 0.5 mM) *a* in the 'spiro' state and *b* in the 'mero' state. *Inset* Photoswitching of the anodic current of the system at +470 mV. **C** Cyclic voltammograms of the photoisomerizable electrode in the presence of dopamine (**48**, 0.5 mM) *a* in the 'spiro' state and *b* in the 'mero' state. *Inset* Photoswitching of the anodic current of the system at +470 mV. Experiments were performed in 0.02 M phosphate buffer (pH 7.0) at a scan rate of 200 mV s^{-1}

protonated nitromerocyanine monolayer (MRH^+-state, **46b**). This cationic monolayer is positively charged and thus the electrochemistry of charged redox substrates can be discriminated. Positively charged redox probes are repelled by the functionalized electrode, while negatively charged species are attracted by the monolayer and display enhanced electron transfer.

The photostimulated oxidation of the negatively charged substrate 3, 4-dihydroxyphenylacetic acid (**47**) and the positively charged substrate 3-hydroxytyramine (dopamine, **48**) at pH 7.0 was examined in the presence of the photoisomerizable monolayer electrode. Figure 24B (curve a) shows the cyclic voltammogram corresponding to the electrochemical oxidation of **47** by the **46a**-functionalized electrode. Photoisomerization of the monolayer to the **46b**-state results in the cyclic voltammogram shown in Fig. 24B, curve b, and photoregeneration of the **46a**-monolayer restores the cyclic voltammogram shown in curve a. By reversible photoisomerization of the monolayer between the **46a**- and **46b**-states, the amperometric responses of the electrode are cycled between low and high values, respectively (Fig. 24B, inset) as a consequence of electrostatic discrimination. With the positively charged electroactive substrate **48**, the direction of the transduced amperometric signals is reversed. Figure 24C shows the cyclic voltammograms of **48** in the presence of the photoisomerizable electrode. With the **46a**-functionalized electrode, a high amperometric response is observed (curve a), but photoisomerization of the monolayer to the protonated nitromerocyanine **46b**-state retards the electrochemical oxidation of **48** (curve b) due to its electrostatic repulsion from the interface. Back-photoisomerization of the **46b**-monolayer to the **46a**-state regenerates the high amperometric response of the electrode (curve a). By reversible photoisomerization of the monolayer between the **46a**- and **46b**-states, the amperometric responses of the electrode are cycled between high and low values, respectively (Fig. 24C, inset).

Thus, the photoisomerization of the monolayer between the **46a**-state and the protonated nitromerocyanine **46b**-state provides a means to control the electrical features of the electrode surface, thereby regulating electron transfer at the electrode interface. The **46a**-monolayer results in a neutral electrode surface while the **46b**-monolayer gives a positively charged surface, causing the formation of an electrical double-layer at the electrode interface. Photoisomerization of the command interface resulting from the different electrochemical kinetics of the soluble redox probe can also be probed by Faradic impedance spectroscopy [90]. A small electron transfer resistance is found for the system when there is an attractive interaction between the charged redox probe and the command interface. Much larger electron transfer resistances are found upon photoisomerization to the state when repulsive interactions exist.

The interactions between the photoisomerizable monolayer and charged substrates may also be controlled by the pH of the system [91]: At pHs below 8.6, the merocyanine form of the monolayer is protonated (i.e. cationic), so negatively charged redox probes are attracted to the electrode and are electrochemically enhanced. At pH values above 8.6, however, the merocyanine is deprotonated (i.e. zwitterionic), so the electrochemistry of the

negatively charged species is not enhanced. The nitrospiropyran form of the electrode is neutral at all values of pH.

In another example, a mixed monolayer composed of a photoisomerizable component and an electrochemical catalyst was applied to switch the electrocatalytic properties of a modified electrode between 'ON'- and 'OFF'-states. A gold electrode surface functionalized with a spiropyran-monolayer and pyrroloquinoline quinone (PQQ) moieties incorporated into the monolayer was applied to control the electrocatalytic oxidation of NADH by light [92]. The positively charged merocyanine-state interface resulted in the repulsion of Ca^{2+} cations (promoters for the NADH oxidation by the PQQ), thus resulting in the inhibition of the electrocatalytic process. In the nitrospiropyran-state the monolayer does not prevent association of the PQQ-catalyst and Ca^{2+}-promoter, so provides efficient electrocatalytic oxidation of NADH. Similar results have been achieved by a combination of the photo- and thermal effects resulting in the isomerization of the spiropyran-monolayer with the incorporated PQQ-catalyst [93]. Other photoisomerizable materials such as an azobenzenealkanethiol derivative mixed with a ferrocene-redox component have also been used to control the electrocatalyzed electron transfer process between a command interface and a dissolved redox probe [94].

Self-assembled monolayers of isomerizable compounds can give rise to surfaces with switchable properties. Different isomeric states of self-assembled monolayers can have different packing densities, thus resulting in different permeabilities for a diffusional redox probe. For example, a self-assembled monolayer of 4-cyano-4′-(10-thiodecoxy)stilbene (**49**) on a gold electrode demonstrated a higher blocking effect for the $Fe(CN)_6^{3-/4-}$ electrochemistry when it was in the *trans*-state (**49a**) [95] than when it was in the *cis*-state (**49b**). In the *cis*-state (**49b**), the monolayer packing was disturbed, giving rise to increased permeability (Fig. 25). Reversible photoisomerization between two isomeric states allowed the electrochemical transduction of the structural changes of the monolayer resulting from the photoisomerization of the monolayer components. The same monolayer displayed markedly different wetting properties in the *trans*- and *cis*-states.

3.3
Surfaces for the Controlled Binding of Photoisomerizable Guests

The third approach to the assembly of molecular optoelectronic switches is shown in Fig. 26, and involves the association of a chemically functionalized surface with a photoisomerizable guest. In configuration 'A' of the molecular component, no affinity interactions with the modified surface exist, and the system is in a mute state. Photoisomerization of the substrate to state 'B' activates the affinity binding of the molecular component to the surface – a process that can be electronically transduced (e.g. to give an amperometric impedance or piezoelectric signal).

This approach for tailoring molecular optoelectronic assemblies has been demonstrated using several photoisomerizable substrates [96, 97]. In one case,

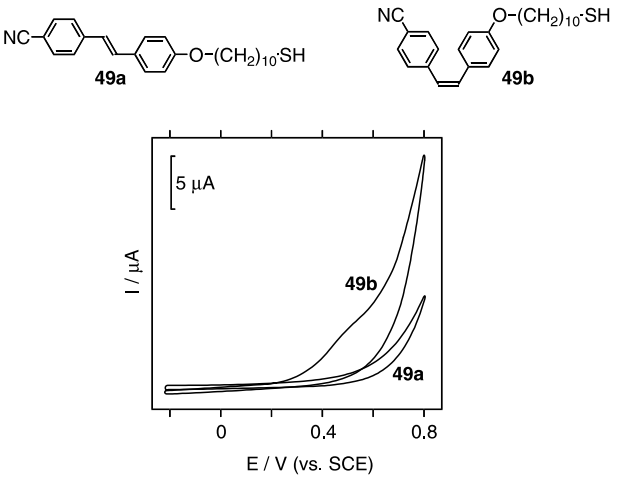

Fig. 25. Cyclic voltammograms of $Fe(CN)_6^{4-}$ (1.2 mM) at electrodes modified by **49a** or **49b**, which exhibit different packing. Recorded in 0.1 M KCl at a potential scan rate of 100 mV s^{-1}

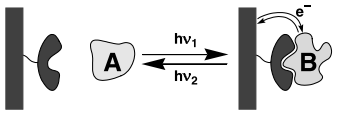

Fig. 26. Interaction of a solution-state species with a receptor-functionalized interface may be controlled by the isomerization of the free component

trans-*N*-methyl-*N*′-[1-phenylazobenzyl]-4,4′-bipyridinium (**50a**) exhibits reversible photoisomerizable properties. Irradiation of **50a** at λ = 355 nm yields the *cis*-isomer (**50b**) and illumination of **50b** at $\lambda > 375$ nm restores the *trans*-substrate, **50a**. The two photoisomers differ substantially in their binding constants with β-cyclodextrin (K_a = 1700 M^{-1} for **50a** and K_a = 180 M^{-1} for **50b**) [98]. Accordingly, amino-β-cyclodextrin (**51**) was synthesized and assembled on a Au electrode [96] (Fig. 27A). The association of **50a** to the β-CD receptor monolayer is reflected by the high amperometric response of the electrode (Fig. 27B, curve a). Photoisomerization of the substrate to the *cis*-isomer state (**50b**) results in a substantially lower amperometric response (curve b). By cyclic photoisomerization of the substrate between the states **50a** and **50b**, high and low current signals are transduced by the β-CD-functionalized electrode, respectively (Fig. 27B, inset). The association of **50a** to the receptor monolayer is supported by the fact that the cathodic (and anodic) peak currents observed in the cyclic voltammogram vary directly with the scan rate ($I_p \propto v$), implying that the redox-active species is confined to the electrode surface. It should be noted that irradiation of *trans*-bipyridinium azobenzene (**50a**) yields a photostationary equilibrium with **50a** and **50b** in a ratio of approximately 1:9. Thus, it was estimated that ca. 40% of the current

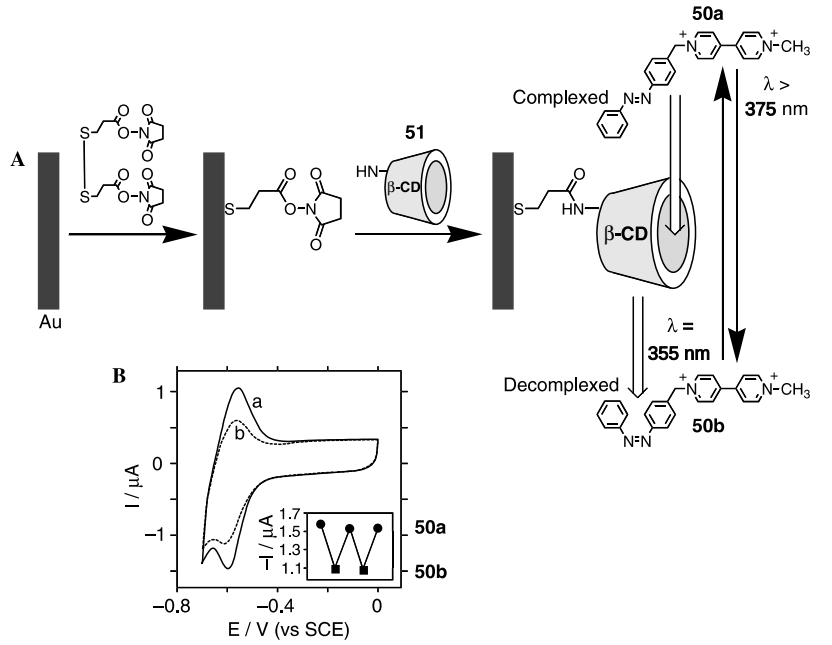

Fig. 27. **A** Assembly of a cylodextrin monolayer on a gold electrode. **B** Cyclic voltammograms of the electrode in the presence of *a* **50a** and *b* **50b** at 1 μM. *Inset* Photoswitching behavior of the cathodic peak current. Experiments were performed in 0.01 M phosphate buffer (pH 10.8), at a scan rate of 100 mV s^{-1}

observed in the presence of **50b** originates from the residual **50a** that is present in the system.

The light-controlled formation and dissociation of donor-acceptor complexes at solid supports provides an alternative to electrostatic or host-guest interactions. The formation of donor-acceptor complexes between bipyridinium salts (electron acceptors) and xanthene dyes (electron donors, e.g. eosin, Rose Bengal) has been studied extensively [99]. The crystal structures of these complexes have been identified and the structural features of the donor-acceptor complexes in solutions have been characterized using NMR spectroscopy. The xanthene dye/bipyridinium donor-acceptor complexes are stabilized by charge-transfer interactions, π-π overlap, and attractive electrostatic interactions between the electron-donor and electron-acceptor units [100]. It has also been demonstrated that the complexation features of photoisomerizable bipyridinium and *bis*-pyridinium electron acceptors to the xanthene dye are controlled by the photoisomeric state of the electron acceptor [97, 101]. The formation and the dissociation of the supramolecular donor-acceptor complex between the xanthene dye and the bipyridinium unit can therefore be triggered by the light-induced transformation of the latter component to photoisomers exhibiting high or low affinities for the electron donor, respectively.

The photoswitchable complexation/dissociation properties of π donor-acceptor complexes between xanthene dyes and photoisomerizable bipyridinium salts have been used to generate an optoelectronic interface [97] (Fig. 28). Eosin isothiocyanate (**52**) was covalently linked to an electrode surface via a thiourea bond (Fig. 28A). The electron acceptor 3, 3′-*bis*(*N*-methylpyridinium)azobenzene **53** was used as the photoisomerizable component. The association constants of the π donor-acceptor complexes generated between eosin and **53a** or **53b** in solution correspond to $K_a = 8.3 \times 10^3\ M^{-1}$ and $K_a = 3.4 \times 10^3\ M^{-1}$, respectively. The analysis of complexation on the functionalized surface was accomplished by quartz crystal microbalance measurements. The frequency change (Δf) of a piezoelectric quartz crystal on which a mass change Δm occurs is given by the Sauerbrey equation (Eqn. 1):

$$\Delta f = -\frac{2f_0^2}{\sqrt{\mu_q \rho_q}} \frac{\Delta m}{A} \tag{1}$$

where f_0 is the base frequency of the crystal, ρ_q is the quartz density, μ_q is the shear modulus of the crystal, and A is the surface area.

The formation of a complex between the eosin-functionalized Au/quartz crystal and **53a** results in a mass increase on the transducer, leading to a decrease in the crystal frequency. Photoisomerization of the electron acceptor to the **53b**-state, Fig. 28B, yields an acceptor of lower affinity for the eosin interface. Thus, dissociation of the π donor-acceptor complex occurs, causing a decrease in the mass on the crystal (i.e. an increase of the crystal's resonant frequency). Figure 28C shows the frequency changes of the eosin monolayer-functionalized Au/quartz crystal upon its interaction with **53a** and **53b**. While the association of **53a** is accompanied by a frequency decrease of $\Delta f = -25$ Hz, the binding of **53b** to the modified surface results in a frequency change of

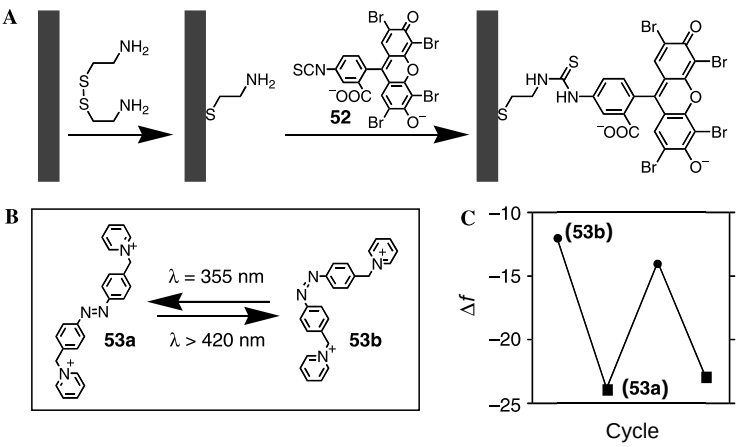

Fig. 28. **A** Assembly of an eosin monolayer on a QCM electrode. **B** Structures of the two states of the photoisomerizable acceptor **53**. **C** Frequency changes of an eosin-modified quartz crystal upon photoisomerization of **53** (at 74 μM) between the *trans*- and *cis*-states

only $\Delta f = -13$ Hz, indicating a lower affinity for the π-donor interface. By the cyclic photoisomerization of the electron acceptor between the states **53a** and **53b**, respectively, their binding to the modified transducers can be switched between low and high affinity interactions, respectively. This effect is transduced by frequency changes of the piezoelectric crystal (Fig. 28C).

The immobilization of photoisomerizable host molecules immobilized onto an electrode surface can be used for the construction of novel ion-selective electrodes. A photoisomerizable calix[4]arene derivative was incorporated into a polymeric membrane on an electrode surface and the two different isomeric states of the host molecule provided responses selective to Li^+ or Na^+ ions depending on the state [102]. Another photoisomerizable host molecule was constructed from spiropyran and crown-ether subunits [103]. Different binding affinities for Li^+ were found depending on the isomeric state of the photoisomerizable component (**54**). The researchers suggested that this effect was caused by the coordination of the Li^+ ion to the O^- of the zwitterionic merocyanine form (Fig. 29). The photocontrolled host molecules were immobilized in a polymeric film onto an electrode surface resulting in a photochemically switchable ion-selective electrode.

3.4
Mechanically Interlocked Compounds at Interfaces

Interlocked compounds have a large potential for both mechanical and information functions. We have already discussed the use of catenanes and rotaxanes as mechanically functioning information storage and processing devices in solution (Sect. 2.3). The immobilization and utilization of these structures on surfaces, although of great interest, is challenging for several reasons. Interlocked molecules tend to be large and complex, making their aligned immobilization difficult and their communication with electrodes problematic. In addition, they need enough spatial freedom to perform their mechanical function unimpeded. Despite these difficulties, however, several examples of immobilized interlocked compounds have been reported in the last year.

The catenane **36** [104] (Fig. 15) as well as a rotaxane [105] have been sandwiched between conductive electrodes. The electrically induced translocations of the internal components of the immobilized molecules result in a change in the resistance of the organic layer. Reversible translocation of the

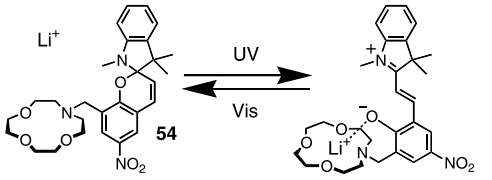

Fig. 29. Photocontrolled binding of Li^+ by the 'crowned spiropyran' **54**

molecular components allows a multiple, reversible change of the electronic properties of the devices between two distinct states, labeled 'ON' and 'OFF'. Several devices were configured together to produce AND and OR logic gates The high and low current levels of these gates were separated by factors of 15 and 30, respectively, which is a significant enhancement over that expected for wired logic gates. The behavior of the solid-state devices can be interpreted on the basis of the redox properties of the interlocked supramolecular components in solution. The similarity of the electronic behavior of the molecules in the solid-state devices to that of molecules in a dilute solution suggests that the device properties are determined largely by molecular properties. Thus, the devices should scale down to molecular dimensions without any change to their fundamental properties.

An optoelectronic surface-bound switchable rotaxane is schematically described in Fig. 30A [106]. The assembly consists of a ferrocene-functionalized cyclodextrin (**55**) molecule threaded on a 'string' containing a photoisomerizable azobenzene unit and a long alkyl chain. The structure was confirmed by electrochemical analyses. When the azobenzene is in the *trans*-configuration it is complexed by **55**, but photoisomerization to the *cis*-state leaves complexation sterically impossible, so that **55** moves to the alkyl component. Back-photoisomerization restores the original state. Spatial separation between the ferrocene redox label and the electrode surface is anticipated to retard the interfacial electron transfer rate. Figure 30B (curve a) shows the chronoamperometric response of the surface-bound **55**-rotaxane in the *trans*-state. A fast current decay, $k_{et}^{(1)} = 65\ s^{-1}$, is observed, implying that the molecular shuttle is close to the electrode surface. Photoisomerization of the monolayer to the *cis*-state ($320 < \lambda < 380$ nm) results in the chronoamperometric transient shown in Fig. 30B, curve b. A substantially lower electron transfer rate constant is observed ($k_{et}^{(2)} = 15\ s^{-1}$) indicating that the redox-active component is located further from the electrode surface. Further photoisomerization of the *cis*-azobenzene unit back to the *trans*-azobenzene configuration ($\lambda > 420$ nm) restores the chronoamperometric response characteristic for the receptor positioned on the *trans*-azobenzene unit. By cyclic photoisomerization of the monolayer between the *trans*- and *cis*-states, the threaded receptor can be reversibly moved between the *trans*-azobenzene site and the alkyl chain (Fig. 30C).

4 Outlook and Perspectives

The construction of molecular devices relies on the chemical synthesis of mechanical and computing components, their supramolecular assembly where necessary, and their integration into interfaced, working devices. In the last two decades, substantial progress has been accomplished in the synthesis of a large arsenal of molecules sensitive to external stimuli such as light, or thermal and electrical energy. Photochromic compounds show spectral (and usually configurational) changes in response to light, energy absorbing and fluorescent components give possibilities for sensitive 'input' and 'output' routes, and

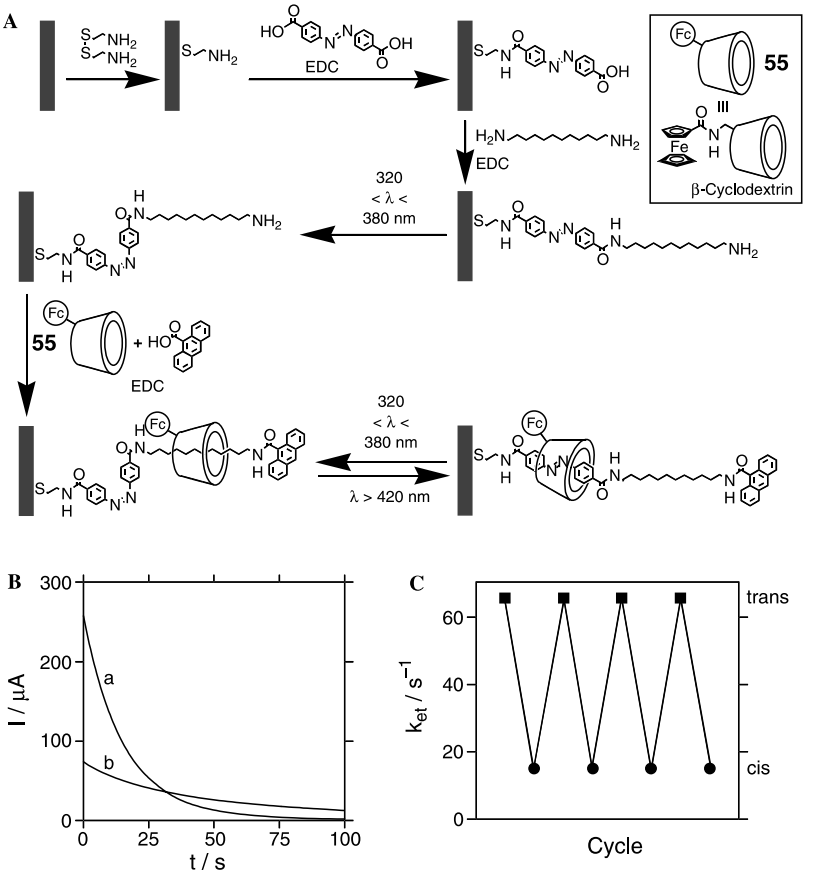

Fig. 30. **A** Assembly and photoisomerization of a switchable rotaxane on a gold electrode. **B** Chronoamperometric response of the monolayer in *a* the *trans*-state and *b* the *cis*-state. **C** Electron transfer rate constant between the electrode and the ferrocene component over four photoisomerization cycles. Electrochemistry was performed in 0.1 M phosphate buffer (pH 7.3)

reversible redox systems can allow the controlled and vectorial transport of charge. In addition, supramolecular concepts have led to the development of non-covalently linked mechanical structures such as catenanes and 'shuttles', as well as other interesting architectures such as rotors (including 'brakes' and 'ratchets') and 'tweezers'.

With all these fundamental building blocks at our disposal, it has become possible to move on to the second part of the nanotechnology puzzle – the combination of building blocks into multicomponent architectures that perform programmed functions. With organic chemistry now mature enough to offer routes for complex synthesis and modern engineering providing the means to create submicron-scale patterning, this kind of research is now becoming possible. The characterization of these systems has been facilitated

by recent advances in extremely sensitive characterization techniques such as Fourier transform infrared spectroscopy (FTIR), scanning probe microscopies (AFM; STM), surface plasmon resonance (SPR), X-ray photoelectron spectroscopy (XPS), ellipsometry, quartz crystal microgravimetry (QCM), and electrochemistry (cyclic voltammetry; impedance spectroscopy).

Supramolecular interactions between different molecules in solution can be used to form very complex multicomponent systems. The self-organization that is provided by recognition events allows unconnected units to interact in a programmed way by simple mixing. These recognition events range from simple ion binding to complex multicomponent host-guest interactions. In future devices, components of these systems may act as chemical messengers between immobilized receptors in systems that mimic the operation of biological systems. As yet, however, these applications are far off, and the systems that exist at present act as statistical mixtures rather than integrated devices.

Many of the problems associated with the solution state can be alleviated by the study of surface-bound species. Molecular components are easily interfaced with solid supports, and multicomponent architectures on surfaces can be built up step by step. The use of modified surfaces with free solution-state species allows the construction of devices such as 'command surfaces'. The organization of molecular memory and processing devices requires the nanoengineering of dense, individually addressable molecular assemblies. Recent advances in nanotechnology provide the means to construct nanometer-sized 'wires', 'dot-junctions' and circuits of higher complexity [107]. Scanning probe microscopy provides 'nanometric pens', where chemical solutions act as 'inks' for the nanoscale patterning of surfaces [108]. Similarly, scanning near-field optical microscopy (SNOM) provides nanometric light sources for the addressing of molecular domains and the dense storage of optical information as well as the means to stimulate molecular outputs such as fluorescence [109]. The further development of the battery of molecular functionalities and nanometer-sized tools for the molecular engineering and construction of programmed arrays on surfaces will pave the way to molecular memory and processing devices of even higher complexity.

The use of molecular species for super-dense information storage in three-dimensional matrices is a very promising prospect [110]. Multilayers and crystals of molecular subunits can theoretically hold orders of magnitude more information than current systems, and could be addressed extremely quickly by means of multiple or focused light beams and CCD arrays. Other 'skeletons' for the construction and immobilization of molecular devices may become important in the future, for instance dendrimers [111], microporous materials [112] and, in particular, nanoparticles, which can be synthesized in controllable shapes from a large number of materials and can be easily organized into two- and three-dimensional superstructures [113]. Similarly, the organization of composite assemblies consisting of organic thin films and inorganic layered materials is anticipated to yield systems of higher functional complexity.

All in all, the construction of molecular machines and computing devices is a field that still faces weighty problems, even at a conceptual level. As further

advances are made, however, we will learn what we can expect from these systems, and ultimately how to control them for the construction of useful devices. In all probability, the mature science of molecular machines will borrow only small parts of what we study today, but without this fundamental research we will never see the full potential of this very new branch of interdisciplinary research.

Acknowledgement. This research is supported by the German-Israeli Project Cooperation (DIP). Dr AN Shipway would like to thank the Valazzi-Pikovsky fellowship trust for financial support.

5 References

1. (a) Balzani V, Gómex-López M, Stoddart JF (1998) Acc Chem Res 31: 405; (b) Gómez-López M, Stoddart JF (2000) In: Nalwa HS (ed) Handbook of nanostructured materials, vol 5. Organics, polymers and biological materials. Academic Press, San Diego, USA, chap 3, p 225; (c) Benniston AC, Mackie PR (2000) In: Nalwa HS (ed) "Handbook of nanostructured materials, vol 5. Organics, polymers and biological materials, Academic Press, San Diego, USA, chap 4, p 277
2. (a) Guenzi A, Johnson CA, Cozzi F, Mizlow K (1983) J Am Chem Soc 105: 1438; (b) Kelly TR, Bowyer MC, Bhaskar KV, Bebbington D, Garcia A, Lang F, Kim MH, Jette MP (1994) J Am Chem Soc 116: 3657; (c) Schoevaars AM, Kruizinga W, Zijlstra RWJ, Veldman N, Spek AL, Feringa BL (1997) J Org Chem 15: 4943; (d) Koumura N, Zijlstra RWJ, van Delden RA, Harada N, Feringa BL (1999) Nature 401: 6749; (e) Kelly TR, Tellitu I, Sestelo JP (1997) Angew Chem Int Ed Engl 36: 1866
3. Philp D, Stoddart JF (1996) Angew Chem Int Ed Engl 35: 1155
4. (a) Menzer S, White AJP, Williams DJ, Belohradsky M, Hamers C, Raymo FM, Shipway AN, Stoddart JF (1998) Macromolecules 31: 295; (b) Ashton PR, Baldoni V, Balzani V, Claessens CG, Credi A, Hoffman HAD, Raymo FM, Stoddart JF, Venturi M, White AJP, Williams DJ (2000) Eur J Org Chem 7: 1121; (c) Amabilino DB, Asakawa M, Ashton PR, Ballardini R, Balzani V, Belohradsky M, Credi A, Higuchi M, Raymo FM, Shimizu T, Stoddart JF, Venturi M, Yase K (1998) New J Chem 22: 959
5. Drexler KE (ed) (1992) Nanosystems, molecular machinery, manufacturing and computation. Wiley, New York
6. (a) Marder E (1998) Annu Rev Neurosci 21: 25; (b) Stephens NL, Seow CY, Halayko AJ, Jiang H (1992) Can J Physiol Pharmacol 70: 515; (c) Namba K (1993) Wear 168: 189
7. (a) Pardo-Yissar V, Katz E, Willner I, Kotlyar AB, Sanders C, Lill H (2000) Faraday Discuss 116: 119; (b) Willner I, Lion-Dagan M, Katz E (1996) Chem Commun 623; (c) Willner I, Doron A, Katz E, Levi S, Frank AJ (1996) Langmuir 12: 946; (d) Willner I, Blonder R, Katz E, Stocker A, Bückmann (1996) J Am Chem Soc 118: 5310; (e) Blonder R, Katz E, Willner I, Wray V, Bückmann AF (1997) J Am Chem Soc 119: 11747
8. Willner I, Katz E (2000) Angew Chem Int Ed 39: 1180
9. (a) Lahav M, Gabriel T, Shipway AN, Willner I (1999) J Am Chem Soc 121: 258; (b) Lahav M, Shipway AN, Willner I (1999) J Chem Soc Perkin Trans 2 1925; (c) Kharitonov AB, Shipway AN, Willner I (1999) Anal Chem 71: 5441; (d) Lahav M, Shipway AN, Willner I, Nielsen MB, Stoddart JF (2000) J Electroanal Chem 482: 217
10. Crano JC, Guglielmetti RJ (eds) (1998) Organic photochromic and thermochromic compounds, Plenum Press
11. Leigh D, Moody K, Smart JP, Watson KJ, Slawin AMZ (1996) Angew Chem Int Ed Engl 35: 306
12. Livoreil A, Dietrich-Buchecker CO, Sauvage J-P (1994) J Am Chem Soc 116: 9399

13. Yokoyama Y (2000) Chem Rev 100: 1717
14. Whittal J (1990) In: Dürr H, Bouas-Laurent H (eds) Photochromism, molecules and systems. Studies in organic chemistry, vol 40. Elsevier, Amsterdam, chap 9, p 467
15. (a) Nakagawa M, Rikukawa M, Watanabe M, Sanui K, Ogata N (1994) Chem Lett 1785; (b) Otsuki J, Sato K, Tsujino M, Okuda N, Araki K, Seno M (1996) Chem Lett 847; (c) Nakagawa M, Rikukawa M, Watanabe M, Sanui K, Ogata N (1997) Bull Chem Soc Jpn 70: 737
16. Berkovic G, Krongauz V, Weiss V (2000) Chem Rev 100: 1741
17. Hirschberg Y (1956) J Am Chem Soc 78: 2304
18. Irie M (2000) Chem Rev 100: 1685
19. (a) Irie M, Mohri M (1988) J Org Chem 53: 803; (b) Irie M, Nakamura S (1988) J Org Chem 53: 6136
20. (a) Tsivgoulis GM, Lehn J-M (1996) Chem Eur J 2: 1399; (b) Tsivgoulis GM, Lehn J-M (1997) Adv Mater 9: 627; (c) Gilat SL, Kawai SH, Lehn J-M (1995) Chem Eur J 1: 275; (d) Fernández-Acebes A, Lehn J-M (1998) Adv Mater 10: 1519
21. (a) Gritsan NP, Klimenko LS (1993) J Photochem Photobiol A 70: 103; (b) Malkin J, Zelichenok A, Krongauz V, Dvornikov AS, Rentzepis PM (1994) J Am Chem Soc 116: 1101
22. (a) Andreis C, Scheidhauer P, Dürr H, Wintgens V, Valat P, Kossanyi J (1997) Chem Eur J 3: 509; (b) Bleisinger H, Scheidhauer P, Dürr H, Wintgens V, Valat P, Kossanyi J (1998) J Org Chem 63: 990
23. (a) Feringa BL, Jager WF, de Lange B (1991) J Am Chem Soc 113: 5468; (b) Feringa BL, Jager WF, de Lange B (1993) J Chem Soc Chem Commun 288; (c) Schoevaars AM, Kruizinga W, Zijlstra RW, Veldman N, Speck AL, Feringa BL (1997) J Org Chem 62: 4943
24. Feringa BL, van Delden RA, Koumura N, Geertsema EM (2000) Chem Rev 100: 1789
25. (a) Gilat SL, Kawai SH, Lehn J-M (1995) Chem Eur J 1: 275; (b) Kawai SH, Gilat SL, Ponsinet R, Lehn J-M (1995) Chem Eur J 1: 285
26. (a) Inouye M, Noguchi Y, Isagawa K (1994) Angew Chem Int Ed Engl 33: 1163; (b) Tanaka M, Kamada K, Ando S, Kitagaki T, Shibutani Y, Yajima S (1999) Chem Commun 1453; (c) Zhou J-W, Li Y-T, Song X-Q (1995) J Photochem Photobiol A 87: 37
27. Weber C, Rustemeyer F, Dürr H (1998) Adv Mater 10: 1348
28. (a) Salbeck J, Komissarov N, Minkin VI, Daub J (1992) Angew Chem Int Ed Engl 31: 1498; (b) Huck NPM, Feringa BL (1995) J Chem Soc Chem Commun 1095
29. (a) Pina F, Roque A, Melo MJ, Maestri M, Belladelli L, Balzani V (1998) Chem Eur J 4: 1184; (b) Pina F, Maestri M, Balzani V (1999) Chem Commun 107
30. Miki S, Noda R, Fukunishi K (1997) Chem Commun 925
31. Daub J, Beck M, Knorr A, Spreitzer H (1996) Pure Appl Chem 68: 1399
32. Kollmannsberger M, Gareis T, Heinl S, Breu J, Daub J (1997) Angew Chem Int Ed Engl 36: 1333
33. Goulle V, Harriman A, Lehn J-M (1993) J Chem Soc Chem Commun 1034
34. Wagner RW, Lindsey JS, Seth J, Palaniappan V, Bocian DF (1996) J Am Chem Soc 118: 3996
35. (a) Shinkai S, Kusano Y, Manabe O, Nakaji T, Nishida Y, Ogawa T (1980) J Am Chem Soc 102: 5860; (b) Shinkai S, Minami T, Kusano Y, Manabe O (1983) J Am Chem Soc 105: 1851
36. Kimura K, Mizutani R, Yokoyama M, Arakawa R, Matsubayashi G, Okamoto M, Doe H (1997) J Am Chem Soc 119: 2062
37. (a) Nabeshima T, Sakiyama A, Yagyu A, Furukawa N (1989) Tetrahedron Lett 30: 5287; (b) Yamashita I, Fujii M, Kaneda T, Misumi S (1980) Tetrahedron Lett 21: 541; (c) Tamaki T, Ichimura K (1989) J Chem Soc Chem Commun 1477; (d) Shinkai S, Inuzuka K, Miyazaki O, Manabe O (1985) J Am Chem Soc 107: 3950; (e) Echegoyen L, Gustowski DA, Gatto VJ, Gokel GW (1986) J Chem Soc Chem Commun 220; (f) Gutowski DA, Delgado M, Gatto VJ, Echegoyen L, Gokel W (1986) J Am Chem Soc 108: 7553; (g) Echegoyen L, Hafez Y, Lawson RC, de Mendoza J, Torres T (1994) Tetrahedron Lett 35:

6383; (h) Kaifer A, Gustowski DA, Echegoyen L, Gatto VJ, Schultz RA, Cleary TP, Morgan CR, Goli DM, Rios AM, Gokel GW (1985) J Am Chem Soc 107: 1958
38. Bethell D, Dougherty G, Cupertino DC (1995) J Chem Soc Chem Commun 675
39. (a) Irie M, Kato M (1985) J Am Chem Soc 107: 1024; (b) Shinkai S, Minami T, Kusano Y, Manabe O (1983) J Am Chem Soc 105: 1851
40. Bissell RA, de Silva AP, Gunaratne HQM, Lynch PLM, Maguire GEM, Sandanayake KRAS (1992) Chem Soc Rev 21: 187
41. de Silva AP, Sandanayake KRAS (1990) Angew Chem Int Ed Engl 29: 1173
42. Ballardini R, Balzani V, Gandolfi MT, Prodi L, Venturi M, Philp D, Ricketts HG, Stoddart JF (1993) Angew Chem Int Ed Engl 32: 1301
43. (a) Philp D, Slawin AMZ, Spencer N, Stoddart JF, Williams DJ (1991) J Chem Soc Chem Commun 1584; (b) Devonport W, Blower MA, Bryce MR, Goldenberg LM (1997) J Org Chem 62: 885
44. Balzani V, Becher J, Credi A, Nielsen MB, Raymo FM, Stoddart JF, Talarico AM, Venturi M (2000) J Org Chem 65: 1947
45. (a) Montalti M, Ballardini R, Prodi L, Balzani V (1996) Chem Commun 2011; (b) Ashton PR, Ballardini R, Balzani V, Baxter I, Credi A, Fyfe MCT, Gandolfi MT, Gómez-López M, Martínez-Díaz M-V, Piersanti A, Spencer N, Stoddart JF, Venturi M, White AJP, Williams DJ (1998) J Am Chem Soc 120: 11932
46. Montalti M, Prodi L (1998) Chem Comm 1461
47. Takeshita M, Uchida K, Irie M (1996) Chem Commun 1807
48. (a) Irie M, Kato M (1985) J Am Chem Soc 107: 1024; (b) Klarner FG, Burkert U, Kamieth M, Boese R, Benet-Buchholz J (1999) Chem Eur J 5: 1700; (c) Meyer S, Louis R, Metz B, Angus Y, Varnek A, Gross M (2000) New J Chem 24: 371
49. Mock WL, Pierpont J (1990) J Chem Soc Chem Commun 1509
50. Seward EM, Hopkins RB, Sauerer W, Tam S-W, Diederich F (1990) J Am Chem Soc 112: 1783
51. Asakawa M, Ashton PR, Balzani V, Brown CL, Credi A, Matthews OA, Newton SP, Raymo FM, Shipway AN, Spencer N, Quick A, Stoddart JF, White AJP, Williams DJ (1999) Chem Eur J 5: 860
52. Ueno A, Tomita Y, Osa T (1983) Tetrahedron Lett 24: 5245
53. Nagai K, Ukai S, Hayakawa K, Kanematsu K (1985) Tetrahedron Lett 26: 1735
54. (a) Plenio H, Aberle C (1998) Angew Chem Int Ed Engl 37: 1397; (b) Asakawa M, Iqbal S, Stoddart JF, Tinker ND (1996) Angew Chem Int Ed Engl 35: 967; (c) Credi A, Montalti M, Balzani V, Langford SJ, Raymo FM, Stoddart JF (1998) New J Chem 1061
55. (a) Ballardini R, Balzani V, Credi A, Gandolfi MT, Langford SJ, Menzer S, Prodi L, Stoddart JF, Venturi M, Williams DJ (1996) Angew Chem Int Ed Engl 35: 978; (b) Ashton PR, Chrystal EJT, Glink PT, Menzer S, Schiavo C, Spencer N, Stoddart JF, Tasker PA, White AJP, Williams DJ (1996) Chem Eur J 2: 709; (c) Glink PT, Schiavo C, Stoddart JF, Williams DJ (1996) Chem Commun 1843
56. Balzani V, Credi A, Langford SJ, Raymo FM, Stoddart JF, Venturi M (2000) J Am Chem Soc 122: 3542
57. (a) Benniston AC (1996) Chem Soc Rev 427; (b) Ashton PR, Ballardini R, Balzani V, Boyd SE, Credi A, Gandolfi MT, Gómez-López M, Iqbal S, Philp D, Preece JA, Prodi L, Ricketts HG, Stoddart JF, Tolley MS, Venturi M, White AJP, Williams DJ (1997) Chem Eur J 3: 152
58. Zelikovich L, Libman J, Shanzer A (1995) Nature 374: 790
59. Canevet C, Libman J, Shanzer A (1996) Angew Chem Int Ed Engl 35: 2657
60. (a) Sauvage J-P (1998) Acc Chem Res 31: 611; (b) Livoreil A, Sauvage J-P, Armaroli N, Balzani V, Flamigni L, Ventura B (1997) J Am Chem Soc 119: 12114; (c) Collin J-P, Gaviña P, Sauvage J-P (1997) New J Chem 21: 525
61. Collin J-P, Gavinã P, Sauvage J-P (1996) Chem Commun 2005
62. Ashton PR, Ballardini R, Balzani V, Boyd SE, Credi A, Gandolfi MT, Gómez-López M, Iqbal S, Philp D, Preece JA, Prodi L, Ricketts HG, Stoddart JF, Tolley MS, Venturi M, White AJP, Williams DJ (1997) Chem Eur J 3: 152

63. Amabilino DB, Stoddart JF (1995) Chem Rev 95: 2725
64. (a) Asakawa M, Ashton PR, Balzani V, Credi A, Hamers C, Mattersteig G, Montalti M, Shipway AN, Spencer N, Stoddart JF, Tolley MS, Venturi M, White AJP, Williams DJ (1998) Angew Chem Int Ed 37: 333; (b) Balzani V, Credi A, Mattersteig G, Matthews OA, Raymo FM, Stoddart JF, Venturi M, White AJP, Williams DJ (2000) J Org Chem 65: 1924
65. (a) Ashton PR, Pérez-García L, Stoddart JF, White AJP, Williams DJ (1995) Angew Chem Int Ed Engl 34: 571; (b) Ashton PR, Ballardini R, Balzani V, Credi A, Gandolfi MT, Menzer S, Pérez-García L, Prodi L, Stoddart JF, Venturi M, White AJP, Williams DJ (1995) J Am Chem Soc 117: 11171
66. Amabilino DB, Dietrich-Buchecker CO, Livoreil A, Pérez-García L, Sauvage J-P, Stoddart JF (1996) J Am Chem Soc 118: 3905
67. Bissell RA, Córdova E, Kaifer AE, Stoddart JF (1994) Nature 369: 133
68. (a) Ashton PR, Bissell RA, Spencer N, Stoddart JF, Tolley MS (1992) Synlett 923; (b) Anelli P-L, Asakawa M, Ashton PR, Bissell RA, Clavier G, Górski R, Kaifer AE, Langford SJ, Mattersteig G, Menzer S, Philp D, Slawin AMZ, Spencer N, Stoddart JF, Tolley MS, Williams DJ (1997) Chem Eur J 3: 1113
69. Murakami H, Kawabuchi A, Kotoo K, Kunitake M, Nakashima N (1997) J Am Chem Soc 119: 7605
70. Martínez-Díaz M-V, Spencer N, Stoddart JF (1997) Angew Chem Int Ed Engl 36: 1904
71. (a) de Silva AP, Dixon IM, Gunaratne HQN, Gunnlaugsson T, Maxwell PRS, Rice TE (1999) J Am Chem Soc 121: 1393; (b) de Silva AP, Gunaratne HQN, McCoy CP (1993) Nature 364: 42; (c) de Silva AP, Gunaratne HQN, Maguire GEM (1994) J Chem Soc Chem Commun 1213; (d) Credi A, Balzani V, Langford SJ, Stoddart JF (1997) J Am Chem Soc 119: 2679
72. de Silva AP, Gunaratne HQN, McCoy CP J Am Chem Soc (1997) 119: 7891
73. (a) Murray RW (1980) Acc Chem Res 13: 135; (b) Abruña HD (1988) Coord Chem Rev 86: 135
74. (a) Finklea HD (1996) In: Bard AJ, Rubinstein I (eds) Electroanalytical chemistry. Marcel Dekker, New York 19: 109; (b) Delamarche E, Michel B, Biebuyck HA, Gerber C (1996) Adv Mater 8: 719; (c) Xu J, Li H-L (1995) J Colloid Sci 176: 138; (d) Knoll W (1996) Curr Opin Colloid Interface Sci 1: 137; (e) Zhong C-J, Porter MD (1995) Anal Chem 67: 719A; (f) Mandler D, Turyan I (1996) Electroanalysis 8: 207
75. Ulman A (1991) An introduction to ultrathin organic films: from Langmuir-Blodgett to self-assembly. Academic Press, Boston, USA
76. (a) Zelchenok A, Buchholz F, Fisher E, Ratner J, Krongauz V, Anneser H, Bräuchle C (1993) J Photochem Photobiol A 76: 135; (b) Fang Z, Wang S, Yang Z, Chen B, Li F, Wang J, Xu S, Jiang Z, Fang T (1995) J Photochem Photobiol A 88: 23; (c) Tajima MM, Keat LE, Matsunaga K, Yamashita T, Tokoro M, Inoue H (1993) J Photochem Photobiol A 74: 211; (d) Gritsan NP, Klimenko LS (1993) J Photochem Photobiol A 70: 103
77. (a) Doron A, Portnoy M, Lion-Dagan M, Katz E Willner I (1996) J Am Chem Soc 118: 8937; (b) Doron A, Katz E, Portnoy M, Willner I (1996) Angew Chem Int Ed Engl 35: 1535
78. (a) Tachibana H, Nakamura T, Matsumoto M, Komizu H, Manda E, Niino H, Yabe A, Kawabata Y (1989) J Am Chem Soc 111: 3080; (b) Tachibana H, Azumi R, Nakamura T, Matsumoto M, Kawabata Y (1992) Chem Lett 173; (c) Tachibana H, Nishio Y, Nakamura T, Matsumoto M, Manda E, Niino H, Yabe A, Kawabata Y (1992) Thin Solid Films 210/211: 293; (d) Tachibana H, Manda E, Azumi R, Nakamura T, Matsumoto M, Kawabata Y (1992) Appl Phys Lett 61: 2420
79. (a) Sekkat Z, Wood J, Geerts Y, Knoll W (1995) Langmuir 11: 2856; (b) Siewierski LM, Brittain WJ, Petrash S, Foster MD (1996) Langmuir 12: 5838
80. (a) Caldwell WB, Campbell DJ, Chen K, Herr BR, Mirkin CA, Malik A, Durbin MK, Dutta P, Huang KG (1995) J Am Chem Soc 117: 6071; (b) Wang R, Iyoda T, Tryk DA, Hashimoto K, Fujishima A (1997) Langmuir 13: 4644

81. (a) Vélez M, Mukhopadhyay S, Muzikante I, Matisova G, Vieira S (1997) Langmuir 13: 870; (b) Liu Z, Zhao C, Tang M, Cai S (1996) J Phys Chem 100: 17337; (c) Sato T, Ozaki Y, Iriyama K (1994) Langmuir 10: 2363
82. Liu ZF, Hashimoto K, Fujishima A (1990) Nature 347: 658
83. Yu H-Z, Wang Y-Q, Cheng J-Z, Zhao J-W, Cai S-M, Inokuchi H, Fujishima A, Liu Z-F (1996) Langmuir 12: 2843
84. Liu Z-F, Kazuhito M, Fujishima A (1992) Anal Chem 64: 134
85. Nakashima N, Nakanishi T, Nakatani A, Deguchi Y, Murakami H, Sagara T, Irie M (1997) Chem Lett 591
86. (a) Katz E, Willner B, Willner I (1997) Biosens Bioelectr 12: 703; (b) Willner I, Willner B (1998) J Mater Chem 8: 2543; (c) Willner I (1997) Acc Chem Res 30: 347; (d) Willner I, Willner B (1997) Bioelectrochem Bioenerg 42: 43
87. Lane RT, Hubbard AT (1973) J Phys Chem 77: 1411
88. Takehara K, Ide Y (1992) Bioelectrochem Bioenerg 27: 207
89. Malem F, Mandler D (1993) Anal Chem 65: 37
90. Patolsky F, Filanovsky B, Katz E, Willner I (1998) J Phys Chem B 102: 10359
91. Doron A, Katz E, Tao G, Willner I (1997) Langmuir 13: 1783
92. Katz E, Lion-Dagan M, Willner I (1995) J Electroanal Chem 382: 25
93. Katz E, Willner I (1995) Electroanalysis 7: 417
94. Walter DG, Campbell DJ, Mirkin CA (1999) J Phys Chem B 103: 402
95. Wolf MO, Fox MA (1995) J Am Chem Soc 117, 1845
96. Lahav M, Ranjit KT, Katz E, Willner I (1997) Chem Commun 259
97. (a) Marx-Tibbon S, Ben-Dov I, Willner I (1996) J Am Chem Soc 118: 4717; (b) Ranjit KT, Marx-Tibbon S, Ben-Dov I, Willner B, Willner I (1996) Isr J Chem 36: 407; (c) Ranjit KT, Marx-Tibbon S, Ben-Dov I, Willner I (1997) Angew Chem Int Ed Engl 36: 147
98. Lahav M, Ranjit KT, Katz E, Willner I (1997) Isr J Chem 37: 185
99. Willner I, Eichen Y, Rabinovitz M, Hoffman R, Cohen S (1992) J Am Chem Soc 114: 637
100. Willner I, Eichen Y, Doron A, Marx S (1992) Isr J Chem 32: 53
101. Willner I, Marx S, Eichen Y (1992) Angew Chem Int Ed Engl 31: 1243
102. Deng G, Sakaki T, Kawahara Y, Shinkai S (1993) Supramolecular Chem 2: 71
103. Kimura K, Yamashita T, Yokoyama M (1992) J Phys Chem 96: 5614
104. Collier CP, Mattersteig G, Wong EW, Luo Y, Beverly K, Sampaio J, Raymo FM, Stoddart JF, Heath JR (2000) Science 289: 1172
105. (a) Collier CP, Wong EW, Belohradsky M, Raymo FM, Stoddart JF, Kuekes PJ, Williams RS, Heath JR (1999) Science 285: 391; (b) Wong EW, Collier CP, Behloradsky M, Raymo FM, Stoddart JF, Heath JR (2000) J Am Chem Soc 122: 5831
106. Willner I, Pardo-Yissar V, Katz E, Ranjit KT (2001) J Electroanal Chem 497: 172
107. (a) Seeman NC (1997) Acc Chem Res 30: 357; (b) Coffer JL (1997) J Cluster Sci 8: 159; (c) Mucic RC, Storhoff JJ, Mirkin CA, Letsinger RL (1998) J Am Chem Soc 120: 12674
108. (a) Piner RD, Zhu J, Xu F, Hong S, Mirkin CA (1999) Science 283: 661; (b) Hong S, Zhu J, Mirkin CA (1999) Science 286: 523; (c) Piner RD, Mirkin CA (1997) Langmuir 13: 6864
109. (a) Barbara PF, Adams DM, O'Connor DB (1999) Ann Rev Mater Sci 29: 433; (b) Dunn RC (1999) Chem Rev 99: 2891
110. Kawata S, Kawata Y (2000) Chem Rev 100: 1777
111. (a) Matthews OA, Shipway AN, Stoddart JF (1998) Prog Polym Sci 23: 1; (b) Newkome GR, Moorefield CN, Vögtle F (1996) Dendritic molecules. VCH, Weinheim, Germany
112. (a) Cheetham AK, Ferey G, Loiseau T (1999) Angew Chem Int Ed 38: 3269; (b) Aoyama Y (1998) Design Organic Solids 198: 131
113. (a) Shipway AN, Katz E, Willner I (2000) ChemPhysChem 1: 18; (b) Shipway AN, Lahav M, Willner I (2000) Adv Mater 12: 993

Author Index Volumes 1–99

Abolmaali B, Taylor HV, Weser U (1998) Evolutionary Aspects of Copper Binding Centres in Copper Proteins. *91*: 91–190

Adam W, Mitchell CM, Saha-Möller CR, Weichhold O (2000) Structure, Reactivity and Selectivity of Metal-Peroxo Complexes Versus Dioxiranes. *97*: 237–286

Aegerter MA (1996) Sol-Gel Chromogenic Materials and Devices. *85*: 149–194

Ahrland S (1966) Factors Contributing to (b)-behavior in Acceptors. *1*: 207–220

Ahrland S (1968) Thermodynamics of Complex Formation between Hard and Soft Acceptors and Donors. *5*: 118–149

Ahrland S (1973) Thermodynamics of the Stepwise Formation of Metal-Ion Complexes in Aqueous Solution. *15*: 167–188

Aisen P, see Doi K (1980) *70*: 1–26

Alcock NW, see Leciejewicz J (1995) *82*: 43–84

Allan CB, see Maroney MJ (1998) *92*: 1–66

Allen GC, Warren KD (1971) The Electronic Spectra of the Hexafluoro Complexes of the First Transition series. *9*: 49–138

Allen GC, Warren KD (1974) The Electronic Spectra of the Hexafluoro Complexes of the Second and Third Transition Series. *19*: 105–165

Alonso JA, Balbas LC (1993) Hardness of Metallic Clusters. *80*: 229–258

Alonso JA, Balbás LC (1987) Simple Density Functional Theory of the Electronegativity and Other Related Properties of Atoms and Ions. *66*: 41–78

Amendola V (2001) Molecular Movements and Translocations Controlled by Transition Metals and Signalled by Light Emission. *99*: 79–115

Andersson LA, Dawson JH (1991) EXAFS Spectroscopy of Heme-Containing Oxygenases and Peroxidases. *74*: 1–40

Antanaitis BC, see Doi K (1988) *70*: 1–26

Ardon M, Bino A (1987) A New Aspect of Hydrolysis of Metal Ions: The Hydrogen Oxide Bridging Ligand (H_3O_2). *65*: 1–28

Arendsen F, see Hagen WR (1998) *90*: 161–192

Armstrong FA (1990) Probing Metalloproteins by Voltammetry. *72*: 137–221

Athanassopoulou MA, see also Haase W (1999) *94*: 139–197

Augustynski J (1988) Aspects of Photo-Electrochemical and Surface Behavior of Titanium(IV) Oxide. *69*: 1–61

Auld DS (1997) Zinc Catalysis in Metalloproteases. *89*: 29–50

Averill BA (1983) FE—S and Mo—Fe—S Clusters as Models for the Active Site of Nitrogenase. *53*: 57–101

Babel D (1967) Structural Chemistry of Octahedral Fluorocomplexes of the Transition Elements. *3*: 1–87

Bacci M (1984) The Role of Vibronic Coupling in the Interpretation of Spectroscopic and Structural Properties of Biomolecules. *55*: 67–99

Baekelandt BG, Mortier WJ, Schonheydt RA (1993) The EEM Approach to Chemical Hardness in Molecules and Solids: Fundamentals and Applications. *80*: 187–228

Baker EC, Halstead GW, Raymond KN (1976) The Structure and Bonding of 4*f* and 5*f* Series Organometallic Compounds. *25*: 21–66
Balbás LC, see Alonso JA (1987) *66*: 41–78
Balbás LC, see Alono JA (1993) *80*: 229–258
Baldwin AH, see Butler A (1997) *89*: 109–132
Ballardini R (2001) Molecular-Level Artificial Machines Based on Photoinduced Electron-Transfer Processes. *99*: 163–188
Balsenc LR (1980) Sulfur Interaction with Surfaces and Interfaces Studied by Auger Electron Spectrometry. *39*: 83–114
Balzani V, see Ballardini R (2001) *99*: 163–188
Banci L, Bencini A, Benelli C, Gatteschi D, Zanchini C (1982) Spectral-Structural Correlations in High-Spin Cobalt(II) Complexes. *52*: 37–86
Banci L, Bertini I, Luchinat C (1990) The ^{1}H NMR Parameters of Magnetically Coupled Dimers – The Fe_2S_2 Proteins as an Example. *72*: 113–136
Banse F, see Girerd JJ (2000) *97*: 145–178
Baran EJ, see Müller A (1976) *26*: 81–139
Bartolotti LJ (1987) Absolute Electronegativities as Determined from Kohn-Sham Theory. *66*: 27–40
Bates MA, Luckhurst GR (1999) Computer Simulation of Liquid Crystal Phases Formed by Gay-Berne Mesogens. *94*: 65–137
Bau RG, see Teller R (1981) *44*: 1–82
Baughan EC (1973) Structural Radii, Electron-cloud Radii, Ionic Radii and Solvation. *15*: 53–71
Bayer E, Schretzmann P (1967) Reversible Oxygenierung von Metallkomplexen. *2*: 181–250
Bearden AJ, Dunham WR (1970) Iron Electronic Configuration in Proteins: Studies by Mössbauer Spectroscopy. *8*: 1–52
Bencini A, see Banci L (1982) *52*: 37–86
Benedict C, see Manes L (1985) *59/60*: 75–125
Benelli C, see Banci L (1982) *52*: 37–86
Benfield RE, see Thiel RC (1993) *81*: 1–40
Bergmann D, Hinze J (1987) Electronegativity and Charge Distribution. *66*: 145–190
Bernadou J, see Meunier B (2000) *97*: 1–36
Berners-Price SJ, Sadler PJ (1988) Phosphines and Metal Phosphine Complexes: Relationship of Chemistry to Anticancer and Other Biological Activity. *70*: 27–102
Bernt I, see Uller E (2000) *96*: 149–176
Bertini I, see Banci L (1990) *72*: 113–136
Bertini I, Ciurli S, Luchinat C (1995) The Electronic Structure of FeS Centérs in Proteins and Models. A Contribution to the Understanding of Their Electron Transfer Properties. *83*: 1–54
Bertini I, Luchinat C, Scozzafava A (1982) Carbonic Anhydrase: An Insight into the Zinc Binding Site and into the Active Cavity Through Metal Substitution. *48*: 45–91
Bertrand P (1991) Application of Electron Transfer Theories to Biological Systems. *75*: 1–48
Bill E, see Trautwein AX (1991) *78*: 1–96
Bino A, see Ardon M (1987) *65*: 1–28
Blackman AG, see Tolman WB (2000) *97*: 179–210
Blanchard M, see Linares C (1977) *33*: 1
Blasse G, see Powell RC (1980) *42*: 43–96
Blasse G (1991) Optical Electron Transfer Between Metal Ions and its Consequences. *76*: 153–188
Blasse G (1976) The Influence of Charge-Transfer and Rydberg States on the Luminescence Properties of Lanthanides and Actinides. *26*: 43–79
Blasse G (1980) The Luminescence of Closed-Shell Transition Metal-Complexes. New Developments. *42*: 1–41
Blauer G (1974) Optical Activity of Conjugated Proteins. *18*: 69–129
Bleijenberg KC (1980) Luminescence Properties of Uranate Centres in Solids. *42*: 97–128

Boca R, Breza M, Pelikán P (1989) Vibronic Interactions in the Stereochemistry of Metal Complexes. *71*: 57–97
Boeyens JCA (1985) Molecular Mechanics and the Structure Hypothesis. *63*: 65–101
Bögge H, see Müller A (2000) *96*: 203–236
Böhm MC, see Sen KD (1987) *66*: 99–123
Bohra R, see Jain VK (1982) *52*: 147–196
Bollinger DM, see Orchin M (1975) *23*: 167–193
Bominaar EL, see Trautwein AX (1991) *78*: 1–96
Bonnelle C (1976) Band and Localized States in Metallic Thorium, Uranium and Plutonium and in some compounds, Studied by X-ray Spectroscopy. *31*: 23–48
Bose SN, see Nag K (1985) *63*: 153–197
Bowler BE, see Therien MJ (1991) *75*: 109–130
Bradshaw AM, Cederbaum LS, Domcke W (1975) Ultraviolet Photoelectron Spectroscopy of Gases Adsorbed on Metal Surfaces. *24*: 133–170
Braterman PS (1972) Spectra and Bonding in Metal Carbonyls. Part *A*: Bonding. *10*: 57–86
Braterman PS (1976) Spectra and Bonding in Metal Carbonyls. Part *B*: Spectra and Their Interpretation. *26*: 1–42
Bray RC, Swann JC (1972) Molybdenum-Containing Enzymes. *11*: 107–144
Brec R, see Evain M (1992) *79*: 277–306
Brese NE, O'Keeffe M (1992) Crystal Chemistry of Inorganic Nitrides. *79*: 307–378
Breza M, see Boca R (1989) *71*: 57–97
Briggs LR, see Kustin K (1983) *53*: 137–158
Brooks MSS (1985) The Theory of 5f Bonding in Actinide Solids. *59/60*: 263–293
Brown DG, see Wood JM (1972) *11*: 47–105
Bruce DW, see also Donnio B (1999) *95*: 193–247
Buchanan BB (1966) The Chemistry and Function of Ferredoxin. *1*: 109–148
Bucher E, see Campagna M (1976) *30*: 99–140
Buchler JW, Dreher C, Künzel FM (1995) Synthesis and Coordination Chemistry of Noble Metal Porphyrins. *84*: 1–70
Buchler JW, Kokisch W, Smith PD (1978) Cis, Trans, and Metal Effects in Transition Metal Porphyrins. *34*: 79–134
Bulman RA (1978) Chemistry of Plutonium and the Transuranics in the Biosphere. *34*: 39–77
Bulman RA (1987) The Chemistry of Chelating Agents in Medical Sciences. *67*: 91–141
Burdett JK (1987) Some Structural Problems Examined Using the Method of Moments. *65*: 29–90
Burdett JK (1976) The Shapes of Main-Group Molecules: A Simple Semi-Quantitative Molecular Orbital Approach. *31*: 67–105
Burger RM (2000) Nature of Activated Bleomycin. *97*: 287–304
Burgmayer SJN (1998) Electron Transfer in Transition Metal–Pteridine Systems. *92*: 67–119
Butler A, Baldwin AH (1997) Vanadium Bromoperoxidase and Functional Mimics. *89*: 109–132

Campagna M, Wertheim GK, Bucher E (1976) Spectroscopy of Homogeneous Mixed Valence Rare Earth Compounds. *30*: 99–140
Capozzi F, Ciurli S, Luchinat C (1998) Coordination Sphere Versus Protein Environment as Determinants of Electronic and Functional Properties of Iron-Sulfur Proteins *90*: 127–160
Carr AJ, see Melendez RE (2000) *96*: 31–62
Carter RO, see Müller A (1976) *26*: 81–139
Cauletti C, see Furlani C (1978) *35*: 119–169
Cederbaum LS, see Bradshaw AM (1975) *24*: 133–170
Cederbaum LS, see Schmelcher PS (1996) *86*: 27–62
Ceulemans A, Vanquickenborne LG (1989) The Epikernel Principle. *71*: 125–159
Chandrasekhar V, Thomas KR, Justin KR (1993) Recent Aspects of the Structure and Reactivity of Cyclophosphazenes. *81*: 41–114
Chandrashekar TK, see Ravikanth M (1995) *82*: 105–188

Chang J, see Therien MJ (1991) *75*: 109–130
Chapman SK, Daff S, Munro AW (1997) Heme: The Most Versatile Redox Centre in Biology? *88*: 39–70
Chasteen ND (1983) The Biochemistry of Vanadium. *53*: 103–136
Chattaraj PK, Parr RG (1993) Density of Functional Theory of Chemical Hardness. *80*: 11–26
Cheh AM, Neilands JP (1976) The γ-Aminoevulinate Dehydratases: Molecular and Environmental Properties. *29*: 123–169
Chimiak A, Neilands JB (1984) Lysine Analogues of Siderophores. *58*: 89–96
Christensen JJ, see Izatt RM (1973) *16*: 161–189
Ciampolini M (1969) Spectra of 3d Five-Coordinate Complexes. *6*: 52–93
Ciurli S, see Bertini I (1995) *83*: 1–54
Ciurli S, see Capozzi F (1998) *90*: 127–160
Clack DW, Warren KD (1980) Metal-Ligand Bonding in 3d Sandwich Complexes. *39*: 1–141
Clark SJ, see also Crain J (1999) *94*: 1–39
Clarke MJ, Fackler PH (1982) The Chemistry of Technetium: Toward Improved Diagnostic Agents. *50*: 57–58
Clarke MJ, Gaul JB (1993) Chemistry Relevant to the Biological Effects of Nitric Oxide and Metallonitrosyls. *81*: 147–181
Clarke RJH, Stewart B (1979) The Resonance Raman Effect. Review of the Theory and of Applications in Inorganic Chemistry. *36*: 1–80
Codling K, Frasinski LJ (1996) Molecules in Intense Laser Fields: an Experimental Viewpoint. *86*: 1–26
Cohen IA (1980) Metal-Metal Interactions in Metalloporphyrins, Metalloproteins and Metalloenzymes. *40*: 1–37
Connett PH, Wetterhahn KE (1983) Metabolism of the Carcinogen Chromate by Cellular Constituents. *54*: 93–124
Cook DB (1978) The Approximate Calculation of Molecular Electronic Structures as a Theory of Valence. *35*: 37–86
Cooper SL (2001) Optical Spectroscopic Studies of Metal–Insulator Transitions in Perovskite-Related Oxides. *98*: 161–220
Cooper SR, Rawle SC (1990) Crown Thioether Chemistry. *72*: 1–72
Corbett JD (1997) Diverse Naked Clusters of the Heavy Main-Group Elements. Electronic Regularities and Analogies. *87*: 157–194
Corbin PS, see Zimmerman SC (2000) *96*: 63–94
Cotton FA, Walton RA (1985) Metal–Metal Multiple Bonds in Dinuclear Clusters. *62*: 1–49
Cox PA (1975) Fractional Parentage Methods for Ionisation of Open Shells of d and f Electrons. *24*: 59–81
Cox MC, see Sun H (1997) *88*: 71–102
Crabtree RH, see Siegbahn PEM (2000) *97*: 125–144
Crain J, Clark SJ (1999) Calculation of Structure and Dynamical Properties of Liquid Crystal. *94*: 1–39
Cras JA, see Willemse J (1976) *28*: 83–126
Credi A, see Ballardini R (2001) *99*: 163–188
Cremer D, see Frenking G (1990) *73*: 17–96
Crichton RR (1973) Ferritin. *17*: 67–134

Daff S, see Chapman SK (1997) *88*: 39–70
Dance J-M, see Tressaud A (1982) *52*: 87–146
Darriet J, see Drillon M (1992) *79*: 55–100
Daul C, Schläpfer CW, von Zelewsky A (1979) The Electronic Structure of Cobalt(II) Complexes with Schiff Bases and Related Ligands. *36*: 129–171
Davidson G, see Maroney MJ (1998) *92*: 1–66
Davidson P (1999) Selected Topics in X-Ray Scattering by Liquid-Crystalline Polymers. *95*: 1–39

Dawson JH, see Andersson LA (1991) *74*: 1–40
Deeth RJ (1995) Computational Modelling of Transition Metal Centres. *82*: 1–42
Degen J, see Schmidtke H-H (1989) *71*: 99–124
Dehnicke K, Shihada A-F (1976) Structural and Bonding Aspects in Phosphorus Chemistry – Inorganic Derivates of Oxohalogeno Phosphoric Acids. *28*: 51–82
Demleitner B, see Uller E (2000) *96*: 149–176
Denning RG (1992) Electronic Structure and Bonding in Actinyl Ions. *79*: 215–276
Dhubhghaill OMN, Sadler PJ (1991) The Structure and Reactivity of Arsenic Compounds. Biological Activity and Drug Design. *78*: 129–190
Diehn B, see Doughty MJ (1980) *41*: 45–70
Diemann E, see Müller A (1973) *14*: 23–47
Dirken MW, see Thiel RC (1993) *81*: 1–40
Dobiás B (1984) Surfactant Adsorption on Minerals Related to Flotation. *56*: 91–147
Doi K, Antanaitis BC, Aisen P (1998) The Binuclear Iron Centers of Uteroferrin and the Purple Acid Phosphatases. *70*: 1–26
Domcke W, see Bradshaw AM (1975) *24*: 133–170
Donnio B, Bruce DW (1999) Metallomesogens *95*: 193–247
Dophin D, see Morgan B (1987) *64*: 115–204
Doughty MJ, Diehn B (1980) Flavins as Photoreceptor Pigments for Behavioral Responses. *41*: 45–70
Drago RS (1973) Quantitative Evaluation and Prediction of Donor–Acceptor Interactions. *15*: 73–139
Dreher C, see Buchler JW (1995) *84*: 1–70
Drillon M, Darriet J (1992) Progress in Polymetallic Exchange-Coupled Systems, some Examples in Inorganic Chemistry. *79*: 55–100
Duffy JA (1977) Optical Electronegativity and Nephelauxetic Effect in Oxide Systems. *32*: 147–166
Dunham WR, see Bearden AJ (1970) *8*: 1–52
Dunn MF (1975) Mechanisms of Zinc Ion Catalysis in Small Molecules and Enzymes. *23*: 61–122

Ealtough DJ, see Izatt RM (1973) *16*: 161–189
Egami T (2001) Local Atomic Structure of CMR Manganites and Related Oxides. *98*: 115–160
Eller PG, see Ryan RR (1981) *46*: 47–100
Emmerling A, see Fricke J (1991) 77: 37–88
Emsley E (1984) The Composition, Structure and Hydrogen Bonding of the β-Diketones. *57*: 147–191
Englman R (1981) Vibrations in Interaction with Impurities. *43*: 113–158
Epstein IR, Kustin K (1984) Design of Inorganic Chemical Oscillators. *56*: 1–33
Ermer O (1976) Calculations of Molecular Properties Using Force Fields. Applications in Organic Chemistry. *27*: 161–211
Ernst RD (1984) Structure and Bonding in Metal-Pentadienyl and Related Compounds. *57*: 1–53
Erskine RW, Field BO (1976) Reversible Oxygenation. *28*: 1–50
Evain M, Brec R (1992) A new Approach to Structural Description of Complex Polyhedra Containing Polychalcogenide Anions. *79*: 277–306

Fabbrizzi L, see Amendola V (2001) *99*: 79–115
Fackler PH, see Clarke MJ (1982) *50*: 57–58
Fajans K (1967) Degrees of Polarity and Mutual Polarization of Ions in the Molecules of Alkali Fluorides, SrO and BaO. *3*: 88–105
Fan M-F, see Lin Z (1997) *87*: 35–80
Fee JA (1975) Copper Proteins – Systems Containing the "Blue" Copper Center. *23*: 1–60
Feeney RE, Komatsu SK (1966) The Transferrins. *1*: 149–206
Fehlner TP (1997) Metalloboranes. *87*: 111–136

Felsche J (1973) The Crystal Chemistry of the Rare-Earth Silicates. *13*: 99–197
Ferreira R (1976) Paradoxical Violations of Koopmans' Theorem, with Special Reference to the 3d Transition Elements and the Lanthanides. *31*: 1–21
Fichtinger-Schepman AMJ, see Reedijk J (1987) *67*: 53–89
Fidelis IK, Mioduski T (1981) Double-Double Effect in the Inner Transition Elements. *47*: 27–51
Field BO, see Erskine RW (1976) *28*: 1–50
Figlar J, see Maroney MJ (1988) *92*: 1–66
Fischer J, see Mathey F (1984) *55*: 153–201
Fischer S, see Tytho KH (1999) *93*: 125–317
Follmann H, see Lammers M (1983) *54*: 27–91
Fonticella-Camps JC (1998) Biological Nickel. *91*: 1–30
Fournier JM, Manes L (1985) Actinide Solids. 5f Dependence of Physical Properties. *59/60*: 1–56
Fournier JM (1985) Magnetic Properties of Actinide Solids. *59/60*: 127–196
Fraga S, Valdemoro C (1968) Quantum Chemical Studies on the Submolecular Structure of the Nucleic Acids. *4*: 1–62
Frasinski LJ, see Codling K (1996) *85*: 1–26
Fraústo da Ailva JJR, Williams RJP (1976) The Uptake of Elements by Biological Systems. *29*: 67–121
Frenking G, see Jørgensen CK (1990) *73*: 1–16
Frenking G, Cremer D (1990) The Chemistry of the Noble Gas Elements Helium, Neon, and Argon – Experimental Facts and Theoretical Predictions. *73*: 17–96
Frey M (1998) Nickel-Iron Hydrogenases: Structural and Functional Properties. *90*: 97–126
Fricke B (1975) Superheavy Elements. *21*: 89–144
Fricke J, Emmerling A (1991) Aerogels-Preparation, Properties, Applications. *77*: 37–88
Friebel C, see Reinen D (1979) *37*: 1–60
Friedrich H (1996) Field Induced Chao and Chaotic Scattering. *86*: 97–124
Friesen C, see Keppler BK (1991) *78*: 97–128
Fuhrhop J-H (1974) The Oxidation States and Reversible Redox Reactions of Metalloporphyrins. *18*: 1–67
Fujii H, see Watanabe Y (2000) *97*: 61–90
Fujita M (2000) Molecular Paneling Through Metal-Directed Self-Assembly. *96*: 177–202
Furlani C, Cauletti C (1978) He(1) Photo Electron Spectra of d-metal Compounds. *35*: 119–169

Gani D, Wilkie J (1997) Metal Ions in the Mechanism of Enzyme Catalysed Phosphate Monoester Hydrolyses. *89*: 133–176
Gallagher TF (1996) Microwave Multiphoton Exitation and Ionization. *86*: 125–148
Galland P, see Russo VEA (1980) *41*: 71–110
Galván M, see Gázquez JL (1987) *66*: 79–98
Gandolfi MT, see Ballardini R (2001) *99*: 163–188
Gatteschi D, see Banci L (1982) *52*: 37–86
Gaul JB, see Clarke MJ (1993) *81*: 147–181
Gavezzotti A, see Simonetta M (1976) *27*: 1–43
Gázquez JL, Vela A, Galván M (1987) Fukui Function, Electronegativity and Hardness in the Kohn-Sham Theory. *66*: 79–98
Gazquéz JL (1993) Hardness and Softness in Density Functional Theory. *80*: 27–44
Gerloch M, Harding JH, Woolley RG (1981) The Context and Application of Ligand Field Theory. *46*: 1–46
Ghijsen J, see Naegele JR (1985) *59/60*: 197–262
Gilert TR, see Kustin K (1983) *53*: 137–158
Gillard RD, Mitchell PR (1970) The Absolute Configuration of Transition Metal Complexes. *7*: 46–86
Gimzewski J, see Joachim C (2001) *99*: 1–18

Girerd JJ, Banse F, Simaan AJ (2000) Characterization and Properties of Non-Heme Iron-Peroxo Complexes. *97*: 145–178
Gleitzer C, Goodenough JB (1985) Mixed-Valence Iron Oxides. *61*: 1–76
Gliemann G, Yersin H (1985) Spectroscopic Properties of the Quasi One-Dimensional Tetracyanoplatinate(II) Compounds. *62*: 87–153
Golovina AP, Zorov NB, Runov VK (1981) Chemical Luminescence Analysis of Inorganic substances. *47*: 53–119
Gómez-Kaifer M, see Liu J (2001) *99*: 141–162
Goodby JW (1999) Twist Grain Boundary (TGB) Phases. *95*: 83–147
Goodenough JB, see Gleitzer C (1985) *61*: 1–76
Goodenough JB (2001) General Considerations. *98*: 1–16
Goodenough JB (2001) Transport Properties. *98*: 17–114
Grätzel M, see Kiwi J (1982) *49*: 37–125
Gray HB, see Therien MJ (1991) *75*: 109–130
Green JC (1981) Gas Phase Photoelectron Spectra of d- and f-Block Organometallic Compounds. *43*: 37–112
Grenier JC, Pouchard M, Hagenmuller P (1981) Vacancy Ordering in Oxygen-Deficient Perovskite-Related Ferrites. *47*: 1–25
Grice ME, see Politzer P (1993) *80*: 101–114
Griffith JS (1972) On the General Theory of Magnetic Susceptibilities of Polynuclear Transitionmetal Compounds. *10*: 87–126
Grisham CM, see Mildvan AS (1974) *20*: 1–21
Gubelmann MH, Williams AF (1984) The Structure and Reactivity of Dioxygen Complexes of the Transition Metals. *55*: 1–65
Güdel HU, see Ludi A (1973) *14*: 1–21
Guilard R, Lecomte C, Kadish KM (1987) Synthesis, Electrochemistry, and Structural Properties of Porphyrins with Metal–Carbon Single Bonds and Metal–Metal Bonds. *64*: 5–268
Guillaumont R, see Hubert S (1978) *34*: 1–18
Guillon D (1999) Columnar Order in Thermotropic Mesophases. *95*: 41–82
Gütlich P (1981) Spin Crossover in Iron(II)-Complexes. *44*: 83–195
Gutmann V, see Mayer U (1972) *12*: 113–140
Gutmann V, Mayer U (1973) Redox Properties: Changes Effected by Coordination. *15*: 141–166
Gutmann V, Mayer U (1972) Thermochemistry of the Chemical Bond. *10*: 127–151
Gutmann V, Mayer H (1976) Application of the Functional Approach to Bond Variations Under Pressure. *31*: 49–66

Haase W, Athanasspoulou MA (1999) Crystal Structure of LC Mesogens. *94*: 139–197
Häder D-P, see Nultsch W (1980) *41*: 111–139
Hagen WR, Arendsen AF (1998) The Bio-Inorganic Chemistry of Tungsten. *90*: 161–192
Hagenmuller P, see Grenier JC (1981) *47*: 1–25
Hale JD, see Williams RJP (1966) *1*: 249–281
Hale JD, see Williams RJP (1973) *15*: 1 and 2
Halet J-F, Saillard J-Y (1997) Electron Count Versus Structural Arrangement in Clusters Based on a Cubic Transition Metal Core with Bridging Main Group Elements. *87*: 81–110
Hall DI, Ling JH, Nyholm RS (1973) Metal Complexes of Chelating Olefin-Group V Ligands. *15*: 3–51
Halstead GW, see Baker EC (1976) *25*: 21–66
Hamilton AD, see Meléndez RE (2000) *96*: 31–62
Hamstra BJ, see Slebodnick C (1997) *89*: 51–108
Hanack M, see Schultz H (1991) *74*: 41–146
Harding JH, see Gerloch M (1981) *46*: 1–46
Harnung SE, Schäffer CE (1972) Phase-fixed 3-G Symbols and Coupling Coefficients for the Point Groups. *12*: 257–255

Harnung SE, Schäffer CE (1972) Real Irreducible Tensorial Sets and their Applications to the Ligand-Field Theory. *12*: 257–295
Harris WR (1998) Binding and Transport of Nonferrous Metal by Serum Transferrin. *92*: 121–162
Hathaway BJ (1984) A New Look at the Stereochemistry and Electronic Properties of Complexes of the Copper(II) Ion. *57*: 55–118
Hathaway BJ (1973) The Evidence for "Out-of-the Plane" Bonding in Axial Complexes of the Copper(II) Ion. *14*: 49–67
Hawes JC, see Mingos DMP (1985) *63*: 1–63
Hellner EE (1979) The Frameworks (Bauverbände) of the Cubic Structure Types. *37*: 61–140
Hemmerich P, Michel H, Schung C, Massey V (1982) Scope and Limitation of Single Electron Transfer in Biology. *48*: 93–124
Henry M, Jolivet JP, Livage J (1991) Aqueous Chemistry of Metal Cations: Hydrolysis, Condensation and Complexation. *77*: 153–206
Herrmann WA, see Kühn FE (2000) *97*: 213–236
Hider RC (1984) Siderophores Mediated Absorption of Iron. *57*: 25–88
Hill HAO, Röder A, Williams RJP (1970) The Chemical Nature and Reactivity of Cytochrome P-450. *8*: 123–151
Hilpert K (1990) Chemistry of Inorganic Vapors. *73*: 97–198
Hinze J, see Bergmann D (1987) *66*: 145–190
Hoffman BM, Natan MJ, Nocek JM, Wallin SA (1991) Long-Range Electron Transfer Within Metal-Substituted Protein Complexes. *75*: 85–108
Hoffmann BM, see Ibers JA (1982) *50*: 1–55
Hoffmann DK, Ruedenberg K, Verkade JG (1977) Molecular Orbital Bonding Concepts in Polyatomic Molecules – A Novel Pictorial Approach. *33*: 57–96
Hogenkamp HPC, Sando GN (1974) The Enzymatic Reduction of Ribonucleotides. *20*: 23–58
Housecroft CE (1997) Clusters with Interstitial Atoms from the p-Block: How Do Wade's Rules Handle Them? *87*: 137–156
Huber R, see Ramao MJ (1998) *90*: 69–96
Hubert S, Hussonois M, Guillaumont R (1978) Measurement of Complexing Constants by Radiochemical Methods. *34*: 1–18
Hudson RF (1966) Displacement Reactions and Concept of Soft and Hard Acids and Bases. *1*: 221–223
Hulliger F (1968) Crystal Chemistry of Chalcogenides and Pnictides of the Transition Elements. *4*: 83–229
Hussonois M, see Hubert S (1978) *34*: 1–18
Hyde BG, see Makovicky E (1981) *46*: 101–170
Hyde BG, see O'Keeffe M (1985) *61*: 77–144

Ibers JA, Pace LJ, Martinsen J, Hoffmann BM (1982) Stacked Metal Complexes: Structures and Properties. *50*: 1–55
Imrie CT (1999) Liquid Crystal Dimers. *95*: 149–192
Ingraham LL, see Maggiora GM (1967) *2*: 126–159
Iqbal Z (1972) Intra- and Inter-Molecular Bonding and Structure of Inorganic Pseudohalides with Triatomic Groupings. *10*: 25–55
Izatt RM, Eatough DJ, Christensen JJ (1973) Thermodynamics of Cation–Macrocyclic Compound Interaction. *16*: 161–189

Jain VK, Bohra R, Mehrotra RC (1982) Structure and Bonding in Organic Derivatives of Antimony(V). *52*: 147–196
Jerome-Lerutte S (1972) Vibrational Spectra and Structural Properties of Complex Tetra cyanides of Platinum, Palladium and Nickel. *10*: 153–166
Joachim C (2001) Single Molecular Rotor at the Nanoscale. *99*: 1–18
Johnston RL (1997) Mathematical Cluster Chemistry. *87*: 1–34
Johnston RL, see Mingos DMP (1987) *68*: 29–87

Jolivet JP, see Henry M (1991) *77*: 153–206
Jørgensen CK, see Müller A (1973) *14*: 23–47
Jørgensen CK, see Reisfeld R (1982) *49*: 1–36
Jørgensen CK, see Reisfeld R (1988) *69*: 63–96
Jørgensen CK, see Reisfeld R (1991) *77*: 207–256
Jørgensen CK, Frenking G (1990) Historical, Spectroscopic and Chemical Comparison of Noble Gases. *73*: 1–16
Jørgensen CK, Kauffmann GB (1990) Crookes and Marignac – A Centennial of an Intuitive and Pragmatic Appraisal of "Chemical Elements" and the Present Astrophysical Status of Nucleosynthesis and "Dark Matter". *73*: 227–254
Jørgensen CK, Reisfeld R (1982) Uranyl Photophysics. *50*: 121–171
Jørgensen CK (1976) Deep-Lying Valence Orbitals and Problems of Degeneracy and Intensitities in Photo-Electron Spectra. *30*: 141–192
Jørgensen CK (1966) Electric Polarizability, Innocent Ligands and Spectroscopic Oxidation States. *1*: 234–248
Jørgensen CK (1990) Heavy Elements Synthesized in Supernovae and Detected in Peculiar A-type Stars. *73*: 199–226
Jørgensen CK (1996) Luminescence of Cerium(III) Inter-Shell Transitions and Scintillator Action. *85*: 195–214
Jørgensen CK (1976) Narrow Band Thermoluminescence (Candoluminescence) of Rare Earths in Auer Mantles. *25*: 1–20
Jørgensen CK (1975) Partly Filled Shells Constituting Anti-bonding Orbitals with Higher Ionization Energy than Their Bonding Counterparts. *22*: 49–81
Jørgensen CK (1975) Photo-Electron Spectra of Non-Metallic Solids and Consequences for Quantum Chemistry. *24*: 1–58
Jørgensen CK (1978) Predictable Quarkonium Chemistry. *34*: 19–38
Jørgensen CK (1966) Recent Progress in Ligand Field Theory. *1*: 3–31
Jørgensen CK (1967) Relationship Between Softness, Covalent Bonding, Ionicity and Electric Polarizability. *3*: 106–115
Jørgensen CK (1981) The Conditions for Total Symmetry Stabilizing Molecules, Atoms, Nuclei and Hadrons. *43*: 1–36
Jørgensen CK (1973) The Inner Mechanism of Rare Earths Elucidated by Photo-Electron Spectra. *13*: 199–253
Jørgensen CK (1969) Valence-Shell Expansion Studied by Ultra-violet Spectroscopy. *6*: 94–115
Justin KR, see Chandrasekhar V (1993) *81*: 41–114

Kadish KM, see Guilard R (1987) *64*: 205–268
Kahn O (1987) Magnetism of the Heteropolymetallic Systems. *68*: 89–167
Kaifer AE, see Liu J (2001) *99*: 141–162
Kalyanasundaram K, see Kiwi J (1982) *49*: 37–125
Kato T (2000) Hydrogen-Bonded Liquid Crystals – Molecular Self-Assembly for Dynamically Functional Materials. *96*: 95–146
Katz E, see Shipway AN (2001) *99*: 237–281
Kauffmann GB, see Jørgensen CK (1990) *73*: 227–254
Keijzers CP, see Willemse J (1976) *28*: 83–126
Kelly JM, see Moucheron C (1998) *92*: 163–216
Kelly TR (2001) Rotary Motion in Single-Molecule Machines. *99*: 19–53
Kemp TJ, see Leciejewicz J (1995) *82*: 43–84
Keppler BK, Friesen C, Moritz HG, Vongerichten H, Vogel E (1991) Tumor-Inhibiting Bis (β-Diketonato) Metal Complexes. Budotitane, cis-Diethoxybis (1-phenylbutane-1, 3-dionato) titanium(IV). *78*: 97–128
Kimura E, Koike T, Shionoya M (1997) Advances in Zinc Enzyme Models by Small, Mononuclear Zinc(II) Complexes. *89*: 1–28

Kimura T (1968) Biochemical Aspects of Iron Sulfur Linkage in Non-Heme Iron Protein, with Special Reference to "Adrenodoxin". *5*: 1–40
Kirsch-De Mesmaekar A, see Moucheron C (1998) *92*: 163–216
Kitagawa T, Ozaki Y (1987) Infrared and Raman Spectra of Metalloporphyrins. *64*: 71–114
Kiwi J, Kalyanasundaram K, Grätzel M (1982) Visible Light Induced Cleavage of Water into Hydrogen and Oxygen in Colloidal and Microheterogeneous Systems. *49*: 37–125
Kjekshus A, Rakke T (1974) Considerations of the Valence Concept. *19*: 45–83
Kjekshus A, Rakke T(1974) Geometrical Considerations on the Marcasite Type Structure. *19*: 85–104
Klabunde T, Krebs B (1997) The Dimetal Center in Purple Acid Phosphatases. *89*: 177–198
Kögerler P, see Müller A (2000) *96*: 203–236
Koike T, see Kimura E (1997) *89*: 1–28
Kokisch W, see Buchler JW (1978) *34*: 79–134
Komatsu SK, see Feeney RE (1966) *1*: 149–206
Komorowski L (1993) Hardness Indices for Free and Bonded Atoms. *80*: 45–70
König E (1991) Nature and Dynamics of the Spin-State Interconversions in Metal Complexes. *76*: 51–152
König E (1971) The Nephelauxelic Effect. Calculation and Accuracy of the Interelectronic Repulsion Parameters 1. Cubic High-Spin d_2, d_3, d_7 and d_8 Systems. *9*: 175–212
Köpf H, see Köpf-Maier P (1988) *70*: 103–185
Köpf-Maier P, Köpf H (1988) Transition and Main-Group Metal Cyclopentadienyl Complexes: Preclinical Studies on a Series of Antitumor Agents of Different Structural Type: *70*: 103–185
Koppikar DK, Sivapullaiah PV, Ramakrishnan L, Soundararajan S (1978) Complexes of the Lanthanides with Neutral Oxygen Donor Ligands. *34*: 135–213
Kóren B, see Valach F (1984) *55*: 101–151
Krause R (1987) Synthesis of Ruthenium (II) Complexes of Aromatic Chelating Heterocycles: Towards the Design of Luminescent Compounds. *67*: 1–52
Krebs B, see Klabunde T (1997) *89*: 177–198
Krische MJ, Lehn JM (2000) The Utilization of Persistent H-Bonding Motifs in the Self-Assembly of Supramolecular Architectures. *96*: 3–30
Krumholz P (1971) Iron(II) Diimine and Related Complexes. *9*: 139–174
Kühn FE, Herrmann WA (2000) Rhenium-Oxo and Rhenium-Peroxo Complexes in Catalytic Oxidations. *97*: 213–236
Kubas GJ, see Ryan RR (1981) *46*: 47–100
Kuki A (1991) Electronic Tunneling Paths in Proteins. *75*: 49–84
Kulander KC, Schafer KJ (1996) Time-Dependent Calculations of Electron and Photon Emission from an Atom in an Intense Laser Field. *86*: 149–172
Künzel FM, see Buchler JW (1995) *84*: 1–70
Kurad D, see Tytko KH (1999) *93*: 1–64
Kustin K, see Epstein IR (1984) *56*: 1–33
Kustin K, McLeod GC, Gilbert TR, Briggs LR (1983) Vanadium and Other Metal Ions in the Physiological Ecology of Marine Organisms. *53*: 137–158

Labarre JF (1978) Conformational Analysis in Inorganic Chemistry: Semi-Empirical Quantum Calculation vs. Experiment. *35*: 1–35
Lammers M, Follmann H (1983) The Ribonucleotide Reductases: A Unique Group of Metallo-enzymes Essential for Cell Proliferation. *54*: 27–91
Le Brun NE, Thomson AJ, Moore GR (1997) Metal Centres of Bacterioferritins or Non-Heam-Iron-Containing Cytochromes b_{557}. *88*: 103–138
Leciejewicz J, Alcock NW, Kemp TJ (1995) Carboxylato Complexes of the Uranyl Ion: Effects Ligand Size and Coordinat. Geometry Upon Molecular and Crystal Structure. *82*: 43–84
Lecomte C, see Guilard R (1987) *64*: 205–268
Lee YJ, see Scheidt WR (1987) *64*: 1–70

Lehmann H, see Schultz H (1991) *74*: 41–146
Lehn J-M (1973) Design of Organic Complexing Agents. Strategies Towards Properties. *16*: 1–59
Lehn JM, see Krische MJ (2000) *96*: 3–30
Li H, see Sun H (1997) *88*: 71–102
Lioccia S, Paolesse R (1995) Metal Complexes of Corroles and Other Corrinoids. *84*: 71–134
Lin Z, Fan M-F (1997) Metal–Metal Interactions in Transition Metal Clusters with π-Donor Ligands. *87*: 35–80
Linarés C, Louat A, Blanchard M (1977) Rare-Earth Oxygen Bonding in the $LnMO_4$ Xenotime Structure. *33*: 179–207
Lindskog S (1970) Cobalt(II) in Metalloenzymes. A Reporter of Structure–Function Relations. *8*: 153–196
Ling JH, see Hall DI (1973) *15*: 3–51
Linton BR, see Meléndez RE (2000) *96*: 31–62
Liu A, Neilands JB (1984) Mutational Analysis of Rhodotorulic Acid Synthesis in Rhodotorula philimanae. *58*: 97–106
Liu J (2001) Switchable Molecular Devices: From Rotaxanes to Nanoparticles *99*: 141–162
Livage J, see Henry M (1991) *77*: 153–206
Livorness J, Smith T (1982) The Role of Manganese in Photosynthesis. *48*: 1–44
Llinás M (1973) Metal–Polypeptide Interactions: The Conformational State of Iron Proteins. *17*: 135–220
Louat A, see Linarés C (1977) *33*: 179–207
Luchinat C, see Banci L (1990) *72*: 113–136
Luchinat C, see Bertini I (1982) *48*: 45–91
Luchinat C, see Bertini I (1995) *83*: 1–54
Luchinat C, see Capozzi F (1998) *90*: 127–160
Lucken EAC (1969) Valence-Shell Expansion Studied by Radio-Frequency Spectroscopy. *6*: 1–29
Luckhurst GR, see also Bates MA (1999) *94*: 65–137
Ludi A, Güdel HU (1973) Structural Chemistry of Polynuclear Transition Metal Cyanides. *14*: 1–21
Lutz HD (1988) Bonding and Structure of Water Molecules in Solid Hydrates. Correlation of Spectroscopic and Structural Data. *69*: 125
Lutz HD (1995) Hydroxide Ions in Condensed Materials – Correlation of Spectroscopy and Structural Data. *82*: 85–104

Maaskant WJA (1995) On Helices Resulting from a Cooperative Jahn-Teller Effect in Hexagonal Perovskites. *83*: 55–88
Maggiora GM, Ingraham LL (1967) Chlorophyll Triplet States. *2*: 126–159
Magyar B (1973) Salzebullioskopie III. *14*: 111–140
Makovicky E, Hyde BG (1981) Non-Commensurate (Misfit) Layer Structures. *46*: 101–170
Manes L, see Fournier JM (1985) *59/60*: 1–56
Manes L, Benedict U (1985) Structural and Thermodynamic Properties of Actinide Solids and Their Relation to Bonding. *59/60*: 75–125
Mangano C, see Amendola V (2001) *99*: 79–115
Mann S (1983) Mineralization in Biological Systems. *54*: 125–174
March NH (1993) The Ground-State Energy of Atomic and Molecular Ions and Its Variation with the Number of Electrons. *80*: 71–86
March NH (1996) Semiclassical Theory of Atoms and Ions in Intense External Fields. *86*: 63–96
Maroney MJ, Davidson G, Allan CB, Figlar J (1998) The Structure and Function of Nickel Sites in Metalloproteins. *92*: 1–66
Martinsen J, see Ibers JA (1982) *50*: 1–55
Mason SF (1980) The Ligand Polarization Model for the Spectra of Metal Complexes: The Dynamic Coupling Transition Probabilities. *39*: 43–81

Massey V, see Hemmerich P (1982) *48*: 93–124
Mathey F, Fischer J, Nelson JH (1984) Complexing Modes of the Phosphole Moiety. *55*: 153–201
Mauk AG (1991) Electron Transfer in Genetically Engineered Proteins. The Cytochrome c Paradigm. *75*: 131–158
Mayer U, see Gutman V (1972) *10*: 127–151
Mayer U, see Gutman V (1973) *15*: 141–166
Mayer H, see Gutman V (1976) *31*: 49–66
Mayer U, Gutman V (1972) Phenomenological Approach to Cation-Solvent Interactions. *12*: 113–140
Mazumdar S, Mitra S (1993) Biomimetic Chemistry of Hemes Inside Aqueous Micelles. *81*: 115–145
McGrady JE, see Mingos DMP (1992) *79*: 1–54
McLendon G (1991) Control of Biological Electron Transport via Molecular Recognition and Binding: The "Velcro" Model. *75*: 159–174
McLeod GC, see Kustin K (1983) *53*: 137–158
Mehmke J, see Tytko KH (1999) *93*: 1–64
Mehmke J, see Tytko KH (1999) *93*: 125–317
Mehrotra RC, see Jain VK (1982) *52*: 147–196
Mehrotra RC (1991) Present Status and Future Potential of the Sol-Gel Process. *77*: 1–36
Meier PC, see Simon W (1973) *16*: 113–160
Meléndez RE, Carr AJ, Linton BR, Hamilton AD (2000) Controlling Hydrogen Bonding: From Molecular Recognition to Organogelation. *96*: 31–62
Melnik M, see Valach F (1984) *55*: 101–151
Messerschmidt A (1998) Metal Sites in Small Blue Copper Proteins, Blue Copper Oxidase and Vanadium-Containing Enzymes. *90*: 37–68
Meunier B, Bernadou J (2000) Active Iron-Oxo and Iron-Peroxo Species in Cytochromes P-450 and Peroxidases; Oxo-Hydroxo Tautomerism with Water-Soluble Metalloporphyrins. *97*: 1–36
Michel H, see Hemmerich P (1982) *48*: 93–124
Mildvan AS, Grishan CM (1974) The Role of Divalent Cations in the Mechanism of Enzyme Catalyzed Phosphoryl and Nucleotidyl. *20*: 1–21
Mingos DMP, Hawes JC (1985) Complementary Spherical Electron Density Model. *63*: 1–63
Mingos DMP, Johnston RL (1987) Theoretical Models of Cluster Bonding. *68*: 29–87
Mingos DMP, McGrady JE, Rohl AL (1992) Moments of Inertia in Cluster and Coordination Compounds. *79*: 1–54
Mingos DMP, Zhenyang L (1990) Hybridization Schemes for Coordination and Organometallic Compounds. *72*: 73–112
Mingos DMP, Zhenyang L (1989) Non-Bonding Orbitals in Coordination Hydrocarbon and Cluster Compounds. *71*: 1–56
Mioduski T, see Fidelis IK (1981) *47*: 27–51
Mitchell CM, see Adam W (2000) *97*: 237–286
Mitchell PR, see Gillard RD (1970) *7*: 46–86
Mitra S, see Mazumdar S (1993) *81*: 115–145
Moody DC, see Ryan RR (1981) *46*: 47–100
Moore GR, see Le Brun NE (1997) *88*: 103–138
Moreau-Colin ML (1972) Electronic Spectra and Structural Properties of Complex Tetracyanides of Platinum, Palladium and Nickel. *10*: 167–190
Morf WE, see Simon W (1973) *16*: 113–160
Morgan B, Dophin D (1987) Synthesis and Structure of Biometric Porphyrins. *64*: 115–204
Moritz HG, see Keppler BK (1991) *78*: 97–128
Morris DFC (1968/1969) An Appendix to Structure and Bonding. *4*; 6: 157–159
Morris DFC (1968) Ionic Radii and Enthalpies of Hydration of Ions. *4*: 63–82
Mortensen OS (1987) A Noncommuting-Generator Approach to Molecular Symmetry. *68*: 1–28

Mortier JW (1987) Electronegativity Equalization and its Application. *66*: 125–143
Mortier WJ, see Baekelandt BG (1993) *80*: 187–228
Moucheron C, Kirsch-De Mesmaeker A, Kelly JM (1998) Photophysics and Photochemistry of Metal Polypyridyl and Related Complexes with Nucleic Acids. *92*: 163–216
Moura I, see Xavier AV(1981) *43*: 187–213
Moura JJG, see Xavier AV (1981) *43*: 187–213
Mullay JJ (1987) Estimation of Atomic and Group Electronegativities. *66*: 1–25
Müller A, Baran EJ, Carter RO (1976) Vibrational Spectra of Oxo-, Thio-, and Selenometallates of Transition Elements in the Solid State. *26*: 81–139
Müller A, Diemann F, Jørgensen CK (1973) Electronic Spectra of Tetrahedral Oxo, Thio and Seleno Complexes. Formed by Elements of the Beginning of the Transition Groups. *14*: 23–47
Müller A, Kögerler P, Bögge H (2000) Pythagorean Harmony in the World of Metal Oxygen Clusters of the $\{MO_{11}\}$ Type: Giant Wheels and Spheres both Based on Pentagonal Type Unit. *96*: 203–236
Müller U (1973) Strukurchemie der Azide. *14*: 141–172
Müller W, Spirlet J-C (1985) The Preparation of High Purity Actinide Metals and Compounds. *59/60*: 57–73
Munro AW, see Chapman SK (1997) *88*: 39–70
Murray JS, see Politzer P (1993) *80*: 101–114
Murrell JM (1977) The Potential Energy Surfaces of Polyatomic Molecules. *32*: 93–146

Naegele JR, Ghijsen J (1985) Localization and Hybridization of 5f States in the Metallic and Ionic Bond as Investigated by Photoelectron Spectroscopy. *59/60*: 197–262
Nag K, Bose SN (1985) Chemistry of Tetra- and Pentavalent Chromium. *63*: 153–197
Nalewajski RF (1993) The Hardness Based Molecular Charge Sensitivities and Their Use in the Theory of Chemical Reactivity. *80*: 115–186
Natan MJ, see Hoffman BM (1991) *75*: 85–108
Neilands JB, see Liu A (1984) *58*: 97–106
Neilands JB, see Chimiak A (1984) *58*: 89–96
Neilands JB (1972) Evolution of Biological Iron Binding Centres. *11*: 145–170
Neilands JB (1984) Methodology of Siderophores. *58*: 1–24
Neilands JB (1966) Naturally Occurring Non-Porphyrin Iron Compounds. *1*: 59–108
Neilands JP, see Cheh AM (1976) *29*: 123–169
Nelson JH, see Mathey F (1984) *55*: 153–201
Nickerson DP, see Wong L-L (1997) *88*: 175–208
Nieboer E (1975) The Lanthanide Ions as Structural Probes in Biological and Model Systems. *22*: 1–47
Nieter Burgmeier SJ (1998) Electron Transfer in Transition Metal-Pteridine Systems. *92*: 67–120
Nocek JM, see Hoffman BM (1991) *75*: 85–108
Nomoto K, see Sugiura Y (1984) *58*: 107–135
Novack A (1974) Hydrogen Bonding in Solids. Correlation of Spectroscopic and Crystallographic Data. *18*: 177–216
Nultsch W, Häder D-P (1980) Light Perception and Sensory Transduction in Photosynthetic Prokaryotes. *41*: 111–139
Nyholm RS, see Hall DI (1973) *15*: 3–51

O'Keeffe M, see Brese NE (1992) *79*: 307–378
O'Keeffe M, Hyde BG (1985) An Alternative Approach to Non-Molecular Crystal Structures with Emphasis on the Arrangements of Cations. *61*: 77–144
O'Keeffe M (1989) The Prediction and Interpretation of Bond Lengths in Crystals. *71*: 161–190
Odom JD (1983) Selenium Biochemistry. Chemical and Physical Studies. *54*: 1–26
Oehme I, see Wolfbeis OS (1996) *85*: 51–98

Oelkrug D (1971) Absorption Spectra and Ligand Field Parameters of Tetragonal 3d-Transition Metal Fluorides. *9*: 1–26
Oosterhuis WT (1974) The Electronic State of Iron in Some Natural Iron Compounds: Determination by Mössbauer and ESR Spectroscopy. *20*: 59–99
Orchin M, Bollinger DM (1975) Hydrogen-Deuterium Exchange in Aromatic Compounds. *23*: 167–193
Ostrovskii PI (1999) Packing and Molecular Conformation, and Their Relationship with LC Phase Behaviour. *94*: 199–240
Ozaki Y, see Kitaagawa T (1987) *64*: 71–114

Pace LJ, see Ibers JA (1982) *50*: 1–55
Padhye SB, see West DC (1991) *76*: 1–50
Pallavicini P, see Amendola V (2001) *99*: 79–115
Paolesse R, see Licoccia S (1995) *84*: 71–134
Parr RG, see Chattaraj PK (1993) *80*: 11–26
Patil SK, see Ramakrishna VV (1984) *56*: 35–90
Peacock RD (1975) The Intensities of Lanthanide $f \leftrightarrow f$ Transitions. *22*: 83–122
Pearson RG (1993) Chemical Hardness – An Historial Introduction. *80*: 1–10
Pease AR (2001) Computing at the Molecular Level. *99*: 189–236
Pecoraro VL, see Slebodnick C (1997) *89*: 51–108
Pelikán P, see Boca R (1989) *71*: 57–97
Penfield KW, see Solomon EI (1983) *53*: 1–56
Penneman RA, Ryan RR, Rosenzweigh A (1973) Structural Systematics in Actinide Fluoride Complexes. *13*: 1–52
Penner-Hahn JE (1998) Structural Characterization of the Mn Site in the Photosynthetic Oxygen-Evolving Complex. *90*: 1–36
Pereira IAC, Teixeira M, Xavier AV (1998) Hemeproteins in Anaerobes. *91*: 65–90
Perlman ML, see Watson RE (1975) *24*: 83–132
Politzer P, Murray JS, Grice ME (1993) Charge Capacities and Shell Structures of Atoms. *80*: 101–114
Pouchard M, see Grenier JC (1981) *47*: 1–25
Powell AK (1997) Polyiron Oxides, Oxyhydroxides and Hydroxides as Models for Biomineralisation Processes. *88*: 1–38
Powell RC, Blasse G (1980) Energy Transfer in Concentrated Systems. *42*: 43–96

Que Jr. L (1980) Non-Heme Iron Dioxygenases. Structure and Mechanism. *40*: 39–72

Raehm L (2001) Molecular Machines and Motors Based on Transition Metal-Containing Catenanes and Rotaxanes *99*: 55–78
Rakke T, see Kjekshus A (1974) *19*: 45–83
Rakke T, see Kjekshus A (1974) *19*: 85–104
Ramakrishna VV, Patil SK (1984) Synergic Extraction of Actinides. *56*: 35–90
Ramakrishnan L, see Koppikar DK (1978) *34*: 135–213
Rao VUS, see Wallace WE (1977) *33*: 1–55
Raphael AL, see Therien MJ (1991) *75*: 109–130
Ravikanth M, Chandrashekar TK (1995) Nonplanar Porphyrins and Their Biological Relevance: Ground and Excited State Dynamics. *82*: 105–188
Rawle SC, see Cooper SR (1990) *72*: 1–72
Raymond KN, see Baker EC (1976) *25*: 21–66
Raymond KN, Smith WL (1981) Actinide-Specific Sequestering Agents and Decontamination Applications. *43*: 159–186
Reedijk J, Fichtinger-Schepman AMJ, Oosterom AT van, Putte P van de (1987) Platinum Amine Coordination Compounds as Anti-Tumour Drugs. Molecular Aspects of the Mechanism of Action. *67*: 53–89
Rein M, see Schultz H (1991) *74*: 41–146

Reinen D, Friebel C (1979) Local and Cooperative Jahn-Teller Interactions in Model Structures. Spectroscopic and Structural Evidence. *37*: 1–60
Reinen D (1970) Kationenverteilung zweiwertiger 3dn-lonen in oxidischen Spinell-, Granat und anderen Strukturen. *7*: 114–154
Reinen D (1969) Ligand-Field Spectroscopy and Chemical Bonding in Cr3+-Containing Oxidic Solids. *6*: 30–51
Reisfeld R, see Jørgensen CK (1982) *50*: 121–171
Reisfeld R, Jørgensen CK (1988) Excited States of Chromium(III) in Translucent Glass-Ceramics as Prospective Laser Materials. *69*: 63–96
Reisfeld R (1996) Laser Based on Sol-Gel Technology. *85*: 215–234
Reisfeld R, Jørgensen CK (1982) Luminescent Solar Concentrators for Energy Conversion. *49*: 1–36
Reisfeld R (1996) New Materials for Non-linear Optics. *85*: 99–148
Reisfeld R, Jørgensen CK (1991) Optical Properties of Colorants or Luminescent Species in Sol-Gel Classes. *77*: 207–256
Reisfeld R (1976) Excited States and Energy Transfer from Donor Cations to Rare Earths in the Condensed Phase. *30*: 65–97
Reisfeld R (1975) Radiative and Non-Radiative Transitions of Rare Earth Ions in Glasses. *22*: 123–175
Reisfeld R (1973) Spectra and Energy Transfer of Rare Earths in Inorganic Glasses. *13*: 53–98
Reisfeld R, see Wolfbeis OS (1996) *85*: 51–98
Reslova S, see Thomson AJ (1972) *11*: 1–46
Röder A, see Hill HAO (1970) *8*: 123–151
Rohl AL, see Mingos DMP (1992) *79*: 1–54
Romao MJ, Huber R (1998) Structure and Function of the Xanthine-Oxidase Family of Molybdenum Enzymes. *90*: 69–96
Rosenzweig A, see Pennemen RA (1973) *13*: 1–52
Rüdiger W (1980) Phytochrome, a Light Receptor of Plant Photomorphogenesis. *40*: 101–140
Ruedenberg K, see Hoffmann DK (1977) *33*: 57–96
Runov VK, see Golovina AP (1981) *47*: 53–119
Russo VEA, Galland P (1980) Sensory Physiology of Phycomyces Blakesleeanus. *41*: 71–110
Ryan RR, see Penneman RA (1973) *13*: 1–52
Ryan RR, Kubas GJ, Moody DC, Eller PG (1981) Structure and Bonding of Transition Metal-Sulfur Dioxide Complexes. *46*: 47–100

Saalfrank RW, see Uller E (2000) *96*: 149–176
Sadler PJ, see Berners-Price SJ (1988) *70*: 27–102
Sadler PJ, see Dhubhghaill OMN (1991) *78*: 129–190
Sadler PJ, see Sun H (1997) *88*: 71–102
Sadler PJ (1976) The Biological Chemistry of Gold: A Metallo-Drug and Heavy-Atom Label with Variable Valency. *29*: 171–214
Saha-Möller CR, see Adam W (2000) *97*: 237–286
Saillard J-Y, see Halet J-F (1997) *87*: 81–110
Sakka S, Yoko T (1991) Sol-Gel-Derived Coating Films and Applications. *77*: 89–118
Sakka S (1996) Sol-Gel Coating Films for Optical and Electronic Application. *85*: 1–50
Saltman P, see Spiro G (1969) *6*: 116–156
Sando GN, see Hogenkamp HPC (1974) *20*: 23–58
Sankar SG, see Wallace WE (1977) *33*: 1–55
Sano M (2001) Molecular Hysteresisby Linkage Isomerizations Induced by Electrochemical. *99*: 117–139
Sauvage JP, see Raehm L (2001) *99*: 55–78
Schäffer CE, see Harnung SE (1972) *12*: 201–255
Schäffer CE, see Harnung SE (1972) *12*: 257–295
Schäffer CE (1968) A Perturbation Representation of Weak Covalent Bonding. *5*: 68–95

Schäffer CE (1973) Two Symmetry Parameterizations of the Angular-Overlap Model of the Linda-Field. Relation to the Crystal-Field Model. *14*: 69–110
Scheidt WR, Lee YJ (1987) Recent Advances in the Stereochemistry of Metallotetrapyrroles. *64*: 1–70
Schläpfer CW, see Daul C (1979) *36*: 129–171
Schmelcher PS, Cederbaum LS (1996) Two Interacting Charged Particles in Strong Static Fields: A Variety of Two-Body Phenomena. *86*: 27–62
Schmid G (1985) Developments in Transition Metal Cluster Chemistry. The Way to Large Clusters. *62*: 51–85
Schmidt H (1991) Thin Films, the Chemical Processing up to Gelation. *77*: 115–152
Schmidt PC, see Sen KD (1987) *66*: 99–123
Schmidt PC (1987) Electronic Structure of Intermetallic B 32 Type Zintl Phases. *65*: 91–133
Schmidt W (1980) Physiological Bluelight Reception. *41*: 1–44
Schmidtke H-H, Degen J (1989) A Dynamic Ligand Field Theory Vibronic Structures Rationalizing Electronic Spectra of Transition Metal Complex Compounds. *71*: 99–124
Schneider W (1975) Kinetics and Mechanism of Metalloporphyrin Formation. *23*: 123–166
Schoonheydt RA, see Baekelandt BG (1993) *80*: 187–228
Schretzmann P, see Bayer E (1967) *2*: 181–250
Schröder D, Schwarz H, Shaik S (2000) Characterization, Orbital Description, and Reactivity Patterns of Transtition-Metal Oxo Species in the Gas Phase. *97*: 91–124
Schubert K (1977) The Two-Correlations Model, a Valence Model for Metallic Phases. *33*: 139–177
Schug C, see Hemmerich P (1982) *48*: 93–112
Schultz H, Lehmann H, Rein M, Hanack M (1991) Phthalocyaninatometal and Related Complexes with Special Electrical and Optical Properties. *74*: 41–146
Schutte CJH (1971) The Ab-Initio Calculation of Molecular Vibrational Frequencies and Force Constants. *9*: 213–263
Schwarz H, see Schröder D (2000) *97*: 91–124
Schweiger A (1982) Electron Nuclear Double Resonance of Transition Metal Complexes with Organic Ligands. *51*: 1–122
Scozzafava A, see Bertini I (1982) *48*: 45–91
Sen KD, Böhm MC, Schmidt PC (1987) Electronegativity of Atoms and Molecular Fragments. *66*: 99–123
Sen KD (1993) Isoelectronic Changes in Energy, Electronegativity, and Hardness in Atoms via the Calculations of <r-1>. *80*: 87–100
Sestelo JP, see Kelly TR (2001) *99*: 19–53
Shaik S, see Schröder D (2000) *97*: 91–124
Shamir J (1979) Polyhalogen Cations. *37*: 141–210
Shannon RD, Vincent H (1974) Relationship Between Covalency, Interatomic Distances, and Magnetic Properties in Halides and Chalcogenides. *19*: 1–43
Shihada A-F, see Dehnicke K (1976) *28*: 51–82
Shionoya M, see Kimura E (1997) *89*: 1–28
Shipway AN (2001) Molecular Memory and Processing Devices in Solution and on Surfaces. *99*: 237–281
Shriver DF (1966) The Ambident Nature of Cyanide. *1*: 32–58
Siegbahn PEM, Crabtree RH (2000) Quantum Chemical Studies on Metal-Oxo Species Related to the Mechanisms of Methane Monooxygenase and Photosynthetic Oxygen Evolution. *97*: 125–144
Siegel FL (1973) Calcium Binding Proteins. *17*: 221–268
Sima J (1995) Photochemistry of Tetrapyrrole Complexes. *84*: 135–194
Simaan AJ, see Girerd JJ (2000) *97*: 145–178
Simon A (1979) Structure and Bonding with Alkali Metal Suboxides. *36*: 81–127
Simon W, Morf WE, Meier PCh (1973) Specificity of Alkali and Alkaline Earth Cations of Synthetic and Natural Organic Complexing Agents in Membranes. *16*: 113–160

Simonetta M, Gavezzotti A (1976) Extended Hückel Investigation of Reaction Mechanisms. *27*: 1–43
Sinha SP (1976) A Systematic Correlation of the Properties of the f-Transition Metal Ions. *30*: 1–64
Sinha SP (1976) Structure and Bonding in Highly Coordinated Lanthanide Complexes. *25*: 67–147
Sivapullaiah PV, see Koppikar DK (1978) *34*: 135–213
Sivy P, see Valach F (1984) *55*: 101–151
Sjöberg B-M (1997) Ribonucleotide Reductases – A Group of Enzymes with Different Metallosites and Similar Reaction Mechanism. *88*: 139–174
Slebodnick C, Hamstra BJ, Pecoraro VL (1997) Modeling the Biological Chemistry of Vanadium: Structural and Reactivity Studies Elucidating Biological Function. *89*: 51–108
Smit HHA, see Thiel RC (1993) *81*: 1–40
Smith DW, Williams RJP (1970) The Spectra of Ferric Haems and Haemoproteins. *7*: 1–45
Smith DW (1978) Applications of the Angular Overlap Model. *35*: 87–118
Smith DW (1972) Ligand Field Splittings in Copper(II) Compounds. *12*: 49–112
Smith PD, see Livorness J (1982) *48*: 1–44
Smith WL, see Raymond KN (1981) *43*: 159–186
Solomon EI, Penfield KW, Wilcox DE (1983) Active Sites in Copper Proteins. An Electric Structure Overview. *53*: 1–56
Somorjai GA, Van Hove MA (1979) Adsorbed Monolayers on Solid Surfaces. *38*: 1–140
Sonawane PB, see West DC (1991) *76*: 1–50
Soundararajan S, see Koppikar DK (1978) *34*: 135–213
Speakman JC (1972) Acid Salts of Carboxylic Acids, Crystals with some "Very Short" Hydrogen Bonds. *12*: 141–199
Spirlet J-C, see Müller W (1985) *59/60*: 57–73
Spiro G, Saltman P (1969) Polynuclear Complexes of Iron and Their Biological Implications. *6*: 116–156
Steggerda JJ, see Willemse J (1976) *28*: 83–126
Stewart B, see Clarke MJ (1979) *36*: 1–80
Stoddart JF, see Pease AR (2001) *99*: 189–236
Strohmeier W (1968) Problem und Modell der homogenen Katalyse. *5*: 96–117
Sugiura Y, Nomoto K (1984) Phytosiderophores – Structures and Properties of Mugineic Acids and Their Metal Complexes. *58*: 107–135
Sun H, Cox MC, Li H, Sadler PJ (1997) Rationalisation of Binding to Transferrin: Prediction of Metal–Protein Stability Constant. *88*: 71–102
Swann JC, see Bray RC (1972) *11*: 107–144
Sykes AG (1991) Plastocyanin and the Blue Copper Proteins. *75*: 175–224

Takita T, see Umezawa H (1980) *40*: 73–99
Tam S-C, Williams RJP (1985) Electrostatics and Biological Systems. *63*: 103–151
Taylor HV, see Abolmaali B (1998) *91*: 91–190
Teller R, Bau RG (1981) Crystallographic Studies of Transition Metal Hydride Complexes. *44*: 1–82
Teixeira M, see Pereira IAC (1998) *91*: 65–90
Telser J (1998) Nickel in F430. *91*: 31–64
Therien MJ, Chang J, Raphael AL, Bowler BE, Gray HB (1991) Long-Range Electron Transfer in Metalloproteins. *75*: 109–130
Thiel RC, Benfield RE, Zanoni R, Smit HHA, Dirken MW (1993) The Physical Properties of the Metal Cluster Compound Au55(PPh3)12C16. *81*: 1–40
Thomas KR, see Chandrasekhar V (1993) *81*: 41–114
Thompson DW (1971) Structure and Bonding in Inorganic Derivatives of β-Diketones. *9*: 27–47
Thomson AJ, Reslova S, Williams RJP (1972) The Chemistry of Complexes Related to cis-$Pt(NH_3)_2Cl_2$. An Anti-Tumor Drug. *11*: 1–46

Thomson AJ, see Le Brun NE (1997) *88*: 103–138
Tofield BC (1975) The Study of Covalency by Magnetic Neutron Scattering. *21*: 1–87
Tolman WB, Blackman AG (2000) Copper-Dioxygen and Copper-Oxo Species Relevant to Copper Oxygenases and Oxidases. *97*: 179–210
Trautwein AX, Bill E, Bominaar EL, Winkler H (1991) Iron-Containing Proteins and Related Analogs-Complementary Mössbauer, EPR and Magnetic Susceptibility Studies. *78*: 1–96
Trautwein AX (1974) Mössbauer-Spectroscopy on Heme Proteins. *20*: 101–167
Tressaud A, Dance J-M (1982) Relationships Between Structure and Low-Dimensional Magnetism in Fluorides. *52*: 87–146
Tributsch H (1982) Photoelectrochemical Energy Conversion Involving Transition metal d-States and Intercalation of Layer Compounds. *49*: 127–175
Truter MR (1973) Structures of Organic Complexes with Alkali Metal Ions. *16*: 71–111
Tytko KH, Mehmke J, Kurad D (1999) Bond Length-Bond Valence Relationships, with Particular Reference to Polyoxometalate Chemistry. *93*: 1–64
Tytko KH (1999) A Bond Model for Polyoxometalate Ions Composed of MO_6 Octahedra (Mok Polyhedra with $k > 4$). *93*: 65–124
Tytko KH, Mehmke J, Fischer S (1999) Bonding and Charge Distribution in Isopolyox-o-metalate Ions and Relevant Oxides – A Bond Valence Approach. *93*: 125–317

Uller E, Demleitner B, Bernt I, Saalfrank RW (2000) Synergistic Effect of Serendipity and Rational Design in Supramolecular Chemistry. *96*: 149–176
Umezawa H, Takita T (1980) The Bleomycins: Antitumor Copper-Binding Antibiotics. *40*: 73–99

Vahrenkamp H (1977) Recent Results in the Chemistry of Transition Metal Clusters with Organic Ligands. *32*: 1–56
Valach F, Kóren B, Sivý P, Melnik M (1984) Crystal Structure Non-Rigidity of Central Atoms for Mn(II), Fe(II), Fe(III), Co(II), Co(III), Ni(II), Cu(II) and Zn(II) Complexes. *55*: 101–151
Valdemoro C, see Fraga S (1968) *4*: 1–62
Valentine JS, see Wertz DL (2000) *97*: 37–60
van Bronswyk W (1970) The Application of Nuclear Quadrupole Resonance Spectroscopy to the Study of Transition Metal Compounds. *7*: 87–113
van de Putte P, see Reedijk J (1987) *67*: 53–89
van Hove MA, see Somorjai GA (1979) *38*: 1–140
van Oosterom AT, see Reedijk J (1987) *67*: 53–89
Vanquickenborne LG, see Ceulemans A(1989) *71*: 125–159
Vela A, see Gázquez JL (1987) *66*: 79–98
Venturi M, see Ballardini R (2001) *99*: 163–188
Verkade JG, see Hoffmann DK (1977) *33*: 57–96
Vincent H, see Shannon RD (1974) *19*: 1–43
Vogel E, see Keppler BK (1991) *78*: 97–128
von Herigonte P (1972) Electron Correlation in the Seventies. *12*: 1–47
von Zelewsky A, see Daul C (1979) *36*: 129–171
Vongerichten H, see Keppler BK (1991) *78*: 97–128

Wallace WE, Sankar SG, Rao VUS (1977) Field Effects in Rare-Earth Intermetallic Compounds. *33*: 1–55
Wallin SA, see Hoffman BM (1991) *75*: 85–108
Walton RA, see Cotton FA (1985) *62*: 1–49
Warren KD, see Allen GC (1974) *19*: 105–165
Warren KD, see Allen GC (1971) *9*: 49–138
Warren KD, see Clack DW (1980) *39*: 1–141
Warren KD (1984) Calculations of the Jahn-Teller Coupling Constants for d_x Systems in Octahedral Symmetry via the Angular Overlap Model. *57*: 119–145

Warren KD (1977) Ligand Field Theory of f-Orbital Sandwich Complexes. *33*: 97–137
Warren KD (1976) Ligand Field Theory of Metal Sandwich Complexes. *33*: 97–137
Watanabe Y, Fujii H (2000) Characterization of High-Valent Oxo-Metalloporphyrins. *97*: 61–90
Watson RE, Perlman ML (1975) X-Ray Photoelectron Spectroscopy. Application to Metals and Alloys. *24*: 83–132
Weakley TJR (1974) Some Aspects of the Heteropolymolybdates and Heteropolytungstates. *18*: 131–176
Weichhold O, see Adam W (2000) *97*: 237–286
Weissbluth M (1967) The Physics of Hemoglobin. *2*: 1–125
Wendin G (1981) Breakdown of the One-Electron Pictures in Photoelectron Spectra. *45*: 1–130
Wertheim GK, see Campagna M (1976) *30*: 99–140
Wertz DL, Valentine JS (2000) Nucleophilicity of Iron-Peroxo Porphyrin Complexes. *97*: 37–60
Weser U (1967) Chemistry and Structure of some Borate Polyol Compounds. *2*: 160–180
Weser U (1968) Reaction of some Transition Metals with Nucleic Acids and Their Constituents. *5*: 41–67
Weser U (1985) Redox Reactions of Sulphur-Containing Amino-Acid Residues in Proteins and Metalloproteins, and XPS Study. *61*: 145–160
Weser U (1973) Structural Aspects and Biochemical Function of Erythrocuprein. *17*: 1–65
Weser U, see Abolmaali B (1998) *91*: 91–190
West DC, Padhye SB, Sonawane PB (1991) Structural and Physical Correlations in the Biological Properties of Transitions Metal Heterocyclic Thiosemicarbazone and S-alkyl-dithiocarbazate Complexes. *76*: 1–50
Westlake ACG, see Wong L-L (1997) *88*: 175–208
Wetterhahn KE, see Connett PH (1983) *54*: 93–124
Wilcox DE, see Solomon EI (1983) *53*: 1–56
Wilkie J, see Gani D (1997) *89*: 133–176
Willemse J, Cras JA, Steggerda JJ, Keijzers CP (1976) Dithiocarbamates of Transition Group Elements in "Unusual" Oxidation State. *28*: 83–126
Williams AF, see Gubelmann MH (1984) *55*: 1–65
Williams RJP, see Fraústo da Silva JJR (1976) *29*: 67–121
Williams RJP, see Hill HAO (1970) *8*: 123–151
Williams RJP, see Smith DW (1970) *7*: 1–45
Williams RJP, see Tam S-C (1985) *63*: 103–151
Williams RJP, see Thomson AJ (1972) *11*: 1–46
Williams RJP, Hale JD (1973) Professor Sir Ronald Nyholm. *15*: 1 and 2
Williams RJP, Hale JD (1966) The Classification of Acceptors and Donors in Inorganic Reactions. *1*: 249–281
Williams RJP (1982) The Chemistry of Lanthanide Ions in Solution and in Biological Systems. *50*: 79–119
Willner I, see Shipway AN (2001) *99*: 237–281
Wilson JA (1977) A Generalized Configuration - Dependent Band Model for Lanthanide Compounds and Conditions for Interconfiguration Fluctuations. *32*: 57–91
Wilson MR (1999) Atomistic Simulations of Liquid Crystals. *94*: 41–64
Winkler H, see Trautwein AX (1991) *78*: 1–96
Winkler R (1972) Kinetics and Mechanism of Alkali Ion Complex Formation in Solution. *10*: 1–24
Wolfbeis OS, Reisfeld R, Oehme I (1996) Sol-Gels and Chemical Sensors. *85*: 51–98
Wong L-L, Westlake ACG, Nickerson DP (1997) Protein Engineering of Cytochrome $P450_{cam}$. *88*: 175–208
Wood JM, Brown DG (1972) The Chemistry of Vitamin B_{12} - Enzymes. *11*: 47–105
Woolley RG, see Gerloch M (1981) *46*: 1–46
Woolley RG (1982) Natural Optical Activity and the Molecular Hypothesis. *52*: 1–35

Wüthrich K (1970) Structural Studies of Hemes and Hemoproteins by Nuclear Magnetic Resonance Spectroscopy. *8*: 53–121

Xavier AV, Moura JG, Moura I (1981) Novel Structures in Iron-Sulfur Proteins. *43*: 187–213
Xavier AV, see Pereira IAC (1998) *91*: 65–90

Yersin H, see Gliemann G (1985) *62*: 87–153
Yoko T, see Sakka S (1991) *77*: 89–118

Zanchini C, see Banci L (1982) *52*: 37–86
Zanello P (1992) Stereochemical Aspects Associated with the Redox Behaviour of Heterometal Carbonyl Clusters. *79*: 101–214
Zanoni R, see Thiel RC (1993) *81*: 1–40
Zhenyang L, see Mingos DMP (1989) *71*: 1–56
Zhenyang L, see Mingos DMP (1990) *72*: 73–112
Zhou JS, see Goodenough JB (2001) *98*: 17–114
Zimmerman SC, Corbin PS (2000) Heteroaromatic Modules for Self-Assembly Using Multiple Hydrogen Bonds. *96*: 63–94
Zorov NB, see Golovina AP (1981) *47*: 53–119
Zumft WG (1976) The Molecular Basis of Biological Dinitrogen Fixation. *29*: 1–65

Printing (Computer to Film): Saladruck, Berlin
Binding: Stürtz AG, Würzburg